WP3 - Deliverable 3.2

Report on static modelling with uncertainties

Release Status: Public
Date: February 2024
Filename and Version: v3.0
Project ID Number: 101022664

PilotSTRATEGY (H2020- Topic LC-SC3-NZE-6-2020 - RIA)

Editor: Sarah Bouquet

Contributing authors:

France: Alina-Berenice Christ, Luca Mattioni

Poland: Tomasz Urych, Jarosław Chećko, Krzysztof Stańczyk

Portugal: Pedro Pereira, Maria Helena Caeiro, , Júlio Carneiro, Karwan Khudhur, Carlos Ribeiro, Ana Mafalda Lopes, Mário Santos, Daniel Marques da Silva

Spain: J. García, I. Moreno, J. F. Mediato, P. Fernández-Canteli

The PilotSTRATEGY project has received funding from the European Union's Horizon 2020 research and innovation programme under grant agreement No. 101022664

Document History

Location

This document is stored in the following location:

Filename	PilotSTRATEGY_D3-2_StaticModelling_and_uncertainties
Location	https://pilotstrategy.eu/about-the-project/work-packages/simulation

Revision History

This document has been through the following revisions:

Version No.	Revision Date	Filename/Location stored:	Brief Summary of Changes
V1	January 2024	Drafts folders by region in D3.2	Review from WP leader
V2	31 January 2024	PilotSTRATEGY_D3-2_StaticModelling_and_Uncertainties_V2.docx	Modifications, validations and merge of the regions files
V3	February 2024	PilotSTRATEGY_D3-2_StaticModelling_and_Uncertainties_V3.docx	Last modifications for Portugal

Authorisation

This document requires the following approvals:

AUTHORISATION	Name	Signature	Date
WP Leader	Sarah Bouquet	ok	07/02/24
Project Coordinator	Fernanda de Mesquita Lobo Veloso	ok	28/02/24

Distribution

This document has been distributed to:

Name	Title	Version Issued	Date of Issue
		PUBLIC	00/00/0000

The PilotSTRATEGY project has received funding from the European Union's Horizon 2020 research and innovation programme under grant agreement No. 101022664

Bouquet, S. 2024. Report on static modelling with uncertainties. Deliverable D3.2. EU H2020 PilotSTRATEGY project 101022664, report, pp 275.

Disclaimer

The information and views set out in this report are those of the author(s) and do not necessarily reflect the official opinion of the European Union. Neither the European Union institutions and bodies nor any person acting on their behalf may be held responsible for the use which may be made of the information contained therein.

The PilotSTRATEGY project has received funding from the European Union's Horizon 2020 research and innovation programme under grant agreement No. 101022664

Executive summary

This report summarizes the work that has been performed in the WorkPackage 3, "WP3, Static and Dynamic modelling", task 3.1, "Static modelling and Uncertainties".

The objective of this task was to build a 3D geological model covering all the targeted area as defined in WorkPackage 2 ("WP2, Geo-characterization") for the choice of the pilot location. The domain contains the storage complex zone (reservoir and caprock), and the underburden and overburden to fit the purposes of the related tasks (3.2, 3.3 and 3.4). Static models are a crucial step for the upcoming dynamic modelling to estimate storage capacity and provide the basis for the risk analysis. While pursuing the efforts on this task, regular knowledge-sharing sessions were committed between partners involved in this WP3.1, and all benefited support from AspenTech on best practices for modelling, in particular for using Aspen Skua software.

This task relied heavily on data that were collected and processed in WP2. Thus, the quality of this work results also from a strong involvement, communication, and data exchange between WP2 and WP3.

All partners followed the same general workflow for static modelling, including collecting available data, data processing, grid modelling, subsurface properties modelling and uncertainties study.

The first step was the construction of a geological grid covering all the area. Horizon interpretations tied to well data are input for this task, and when relevant, from seismic data, as well as the fault model combined into a structural framework coming from the work of WP2. A refinement of the grid was performed for the reservoir and seal intervals to more precisely characterize geological features that would impact the storage complex behaviour while injecting CO_2.

Then, available well data with logs were loaded into the model and discretized (well log upscaling) to assign property values to the cells which are penetrated by wells. This led to input data for property modelling. Property modelling was performed to populate the grid with petrophysical data. Petrophysical modelling took into account the data from plug analysis obtained in WP2. The 3D grid was populated with petrophysical properties using geostatistical modelling. When relevant, this was conditioned by a facies model. Generated petrophysical properties are VShale, porosity and permeability. Uncertainties analysis were conducted on this petrophysical parameters. Due to the encompassed uncertainties in stochastic process (when populating grid properties), the final model, used for the following WP3 tasks, will be some selected quantiles (P10, P50, P90) simulations to end up with several scenarios for the CO_2 injection simulations. The last task of this work was also to consider upscaling and refinement of the grid to fit the purpose and computational limitation to dynamic simulation of the CO_2 injection.

Paris basin

In a first step, structural elements resulting from seismic interpretation and stratigraphic well analysis are used as the basis for the static model construction. Structural elements are seismic horizons after time depth-conversion and well markers, which allow the subdivision of studied intervals. Based on them, the external and internal architecture of the studied reservoir intervals is created in the form of structural model composed of a grid.

In a second step, the cells of the structural model are populated with facies and porosity based on geostatistical modelling techniques. Input data are electrofacies defined at the well level as well as effective porosity from quantified well log interpretation. Permeability is determined from ϕ/K relations and Net-To-Gross based on the facies model.

In a next step, uncertainties about net porous volume available for CO_2 storage are addressed probabilistically in Aspen SKUA using the Jacta module. P10, P50 and P90 scenarios are generated representing best, medium and worst scenarios.

Some layers of the grid were grouped together to create a reservoir mesh used for flow simulations. Vertical and horizontal upscaling was performed. In a next step, two finer meshed grids were produced inside the coarse scale grid which will be used in the dynamic flow simulations and well placement scenarios.

Upper Silesia (Poland)

Based on the initial screening of multiple storage sites completed in STRATEGY CCUS from an initial portfolio of eight European regions in seven countries, three regions were selected for full characterization of the storage complex, and two (including Upper Silesia region in Poland) for enhancement of knowledge on the existing storage capacity.

Building on those results, PilotSTRATEGY aims at increasing the maturity and readiness assessment of storage resources in the Upper Silesia region. The concrete objective of PilotSTRATEGY project for Poland is to increase the maturity and confidence level of storage resources to start planning as Contingent resources, based on new available data, reprocessing of old data and new dynamic simulation studies.

Within the framework of assessment of the Upper Silesia region actions in the WP2 included an exhaustive analyses and re-interpretation of available data of the Dębowiec layers (Skoczów DSA) and Ładzice Fm (Ładzice DSA). Polish team is also currently working in the WP3 and building static and dynamic models.

An exhaustive review of existing data allowed the development of a conceptual geological model and the construction of a static model. The first step in static modelling was to build a geological grid covering the area. Input for this task were horizon interpretations tied to well data (already in depth) as well as the fault model combined into a structural framework coming from the work of WP2. In order to start the construction of the geological model, input from the WP2 (characterization) was needed in the form of geological horizons and faults. The top and base of the reservoir were provided, the top of the seal and other horizons in the overburden and underburden, fault and fracture framework were provided from the WP2. A geological grid was constructed by taking the horizons and faults into account.

The next step of work was facies and petrophysical modelling. Data for petrophysical properties come also from the WP2 (Geo-characterization) in the form of plug analysis from the wells that have cores in the surrounding. This data was loaded into the project in form of a well log. The created facies models were used as conditioning data for the petrophysical model.

The PilotSTRATEGY project has received funding from the European Union's Horizon 2020 research and innovation programme under grant agreement No. 101022664

In the case of Skoczów DSA there were observed lack of permeability data in log files for east part of model (available only porosity and VShale data). Data for porosity and shale volume were loaded into the project in the form of well logs or point attributes.

The permeability estimation was done using the Zawisza formula due to the lack of proper data from the east part of the site. In the Zawisza model, permeability depends on porosity and shale content. The output of this task for the model of Skoczów DSA are the following properties: porosity, VShale (shale volume) and permeability.

In the case of Ładzice DSA there were observed lack of VShale (shale volume) data in log files (available only porosity and permeability). Modelling of porosity and shale volume was performed separately for individual sequences using the control procedure of the previously developed lithological model (petrophysical properties linked to lithofacies). The output of this task for the model of Ładzice DSA are the following properties: facies, porosity and permeability.

Geological models with the results of modelling of petrophysical properties will be adapted to the simulation objectives in next tasks of WP3.

Lusitanian Basin (Portugal)

The static geological model for the Portuguese region, including uncertainties, was conducted in the aim of task 3.1 of the "WP3 – Static and Dynamic Simulation". It focuses on the offshore setting of the northern sector of the Lusitanian Basin, covering the Q4-TV1 prospect, which is the previously selected site for the CO_2 injection and storage pilot. The building of the model was based on the dataset provided from the seismic interpretation elements of the WP2, namely eight structural maps and six fault surfaces, and the four wells (Do-1C, Mo-1, 13E-1, and Ca-1) with the corresponding stratigraphic markers and a set of petrophysical evaluation logs, including effective porosity (PHIE) and volume of clay (Vshale). Based on this information, both the stratigraphic context and the regions of the static model for the study area were defined. The models contemplate not only the Torres Vedras Group (TVG) reservoir (Lower Cretaceous siliciclastics) and the Upper Cretaceous seals (carbonates of the Cacém Formation and siliciclastics of Aveiro Group) but also the geological formations composing the full potential storage complex from the underburden units of the top of the Lower Jurassic Salt (Dagorda Formation) to the overburden units towards the top of the Paleogene-Neogene (Seabed).

A wider geological static model and a smaller reservoir model for dynamic simulation purposes were created. The total area of the static model is approximately 1925 km^2 and covers about three times of the total area of the reservoir model, which includes the full potential of Q4-TV1 prospect.

The structural model for the seven stratigraphic regions was created, including the fault network interpreted in WP2. However, as the reservoir and seals are the main units of the CO_2 storage complex, the vertical refinement of the geological model grid (203x289x225 cells) was only performed for these regions. The dimensions of the vertical cell thickness are: 2m (reservoir), 5m (primary seal) and 10m (secondary seal); and 200x200m of areal cell extension. Due to the lack of detailed knowledge of the conceptual geological model to apply object-based simulation algorithms, the Sequential Indicator Simulation (SIS) and Sequential Gaussian Simulation (SGS) pixel-based algorithms were used to simulate the lithofacies and petrophysical properties, respectively.

The simulated models of TVG reservoir consist of approximately 65% sandstone and 35% clay lithofacies, with mean Vshale at 44%, mean PHIE at 14%, and permeability values of 852mD (mean)

The PilotSTRATEGY project has received funding from the European Union's Horizon 2020 research and innovation programme under grant agreement No. 101022664

and 116mD (median). Simulated models honoured main lithofacies and petrophysical statistics from well data, replicating vertical and lateral heterogeneities and the conceptual geological information.

The final task of the static modelling was accomplished by performing uncertainty analyses based on: (i) the structural elements, to evaluate the impacts of the displacement of faults and horizons in the reservoir gross-rock volumes; (ii) the reservoir properties, to evaluate the spatial distribution of rock properties; and (iii) the integration of the uncertainty of several parameters simultaneously in the same geo-modelling workflow, to estimate the porous-rock volumes of the reservoir region of the static model.

Ebro basin (Spain)

The Ebro basin (NE Spain) has an underground reservoir that shows potential for CO2 storage. This reservoir is the so called Buntsandstein Formation that is composed of fluvial deposits, sealed by impermeable formations called Rané member, Muschelkalk M2 and Keuper (regional sealing formation) from bottom to top. The reservoir in the area is about 1850m below the ground surface. This reservoir has been divided in three sections, from bottom to top: B1, B2 and B3, due to the different properties of each one.

In order to characterize this reservoir, first it was reported a Geological Conceptual model (Deliverable 2.7) that explains the geology of the Zone of Interest (ZOI), in this case that zone is the Lopín Area (about s40Km SE from Zaragoza-Spain).

In this report it is described the procedure used to build the static model, that comprise the present reservoir geometry and the facies distribution inside it. The model includes the parameters needed for reservoirs evaluations (for instance the calculated porosities and permeabilities).

To do so Aspen SKUA software has been used. The software has allowed us to include previous oil exploration data of the Ebro Basin like legacy wells and seismic sections, as well as other data acquired by IGME for this project like gravimetric surveys, passive seismic, field studies and laboratory analysis.

To model the geological structure of the area old seismic data and new data from the gravimetric and passive seismic surveys were especially useful. Finally, we were able to outline a structure that is defined by normal faults streaking NW-SE that isolated large portions of the reservoir on top of faulted blocks (Horst). The seals are extended throughout the whole area and only some inverse faults seem to have affected the regional seal at the SW corner of the ZOI.

The fluvial deposits of the Buntsandstein reservoir are modelled using a dedicated tool of the Aspen SKUA software call FLUVSIM. It is designed to model channelized facies using the data we have collect from the offset wells, field studies, laboratory data and some analogous models from the literature. Accordingly, the Buntsandstein model contain wide channelized formations oriented to the NE. These channelized bodies are more abundant in the B1 member of the Buntsandstein meanwhile B2 has less channels and the B3 is considered a primary seal of the reservoir. Obviously, the net thickness is much bigger in B1 (around 60%) than in B2 (40% in best case).

The reservoir model includes some properties essential for further project developments, summarized in the next table:

Formation	Gross Vol. (Mm^3)	Porosity[1] (%)	Vsh (%)
B1	28,471.15	11%	13.08
B2	15,178.57	9.7%	77.18
B3	9,422.19	-	Seal fm.

[1] Only for channel facies

The PilotSTRATEGY project has received funding from the European Union's Horizon 2020 research and innovation programme under grant agreement No. 101022664

Table of Contents

The PilotSTRATEGY project has received funding from the European Union's Horizon 2020 research and innovation programme under grant agreement No. 101022664

The PilotSTRATEGY project has received funding from the European Union's Horizon 2020 research and innovation programme under grant agreement No. 101022664

The PilotSTRATEGY project has received funding from the European Union's Horizon 2020 research and innovation programme under grant agreement No. 101022664

The PilotSTRATEGY project has received funding from the European Union's Horizon 2020 research and innovation programme under grant agreement No. 101022664

3 Paris Basin Region (France)

3.1 Geomodel database

3.1.1 Available Data

Data for the construction of the static model was mainly compiled during the tasks 2.6 (Petrophysics, D2.6 - Fleury et al., 2023 and Conceptual Geological Models, D2.7 - Wilkinson, 2023). It was further enriched and completed in this task D3.1 (Static Model).

The following data was used for the modelling (loaded into the Aspen SKUA project):

- 13 seismic horizons in depth from task D2.6.
- 6 additional seismic horizons in depth added in this task to characterize better over-and underburden.
- 13 wells (position, trajectory, raw logs, 2 interpreted logs for facies (depositional environment and electrofacies).
- 4 additional wells outside the model area containing plug data.
- Plug data with porosity and permeability measurements.
- Stratigraphic markers at wells.

Additional data was created as input for this model:

- The marker Top Marnes de Massingy was interpreted.
- A facies log for the Oolithe Blanche.
- 3 effective porosity logs based on NPHI and RHOB logs.
- A Vshale log based on the Gamma Ray log.

In total 20 markers at the wells have been imported. The focus was laid on the markers between Top_Oxfordian_Sup and Bj-1, as they define the storage complex (seal plus reservoir). The markers and the horizons used in the construction of the model are listed in the table below.

System	Horizon	Formation	Reservoir Unit	Data type	Workpackage	Definition Stratigraphic context Aspen SKUA
	Topography			3D horizon	WP3	baselap
Cretaceous	Top Upper Cretaceous			3D horizon	WP3	eroded
	Top_Cenomanian			Well Marker	WP2	conformable
	Top_Alb. Clay			Well Marker	WP2	conformable
	Top_Alb. Sand			Well Marker	WP2	Baselap
	Top_Albo-Aptian			Well Marker		Eroded at top
	Top_Barremian			Well Marker, 3D horizon	WP2	Baselap

The PilotSTRATEGY project has received funding from the European Union's Horizon 2020 research and innovation programme under grant agreement No. 101022664

Jurassic	Top_Purbeckian			Well Marker, 3D horizon	WP2	Eroded at top
	Top_Portlandian			Well Marker, 3D horizon	WP2	Conformable
	Top_Kimmeridgian			Well Marker, 3D horizon	WP2	Conformable
	Top_Oxfordian_Sup	Oxfordian Limestone	Top Caprock 2	Well Marker, 3D horizon	WP2	Conformable
	Top_Oxfordian-Inf	Callovo Oxfordian Marls	Top Caprock 1	Well Marker, 3D horizon	WP2	Conformable
	Top_Callovian-Upper			Well Marker	WP2	Conformable
	Top_Callovian-Lower			Well Marker	WP2	Conformable
	Ca26_vf	Dalle Nacrée	Top Reservoir 2	Well Marker, 3D horizon	WP2	Conformable
	Ca24_vf	Comblanchien, top Bathonian		Well Marker, 3D horizon	WP2	Conformable
	Sb-Comb_vf	Oolithe Blanche	Top Reservoir 1	Well Marker	WP2	Conformable
	Bt10_vf			Well Marker, 3D horizon	WP2	Conformable
	Bj1_vf	Top Bajocien	Base Reservoir 1	Well Marker, 3D horizon	WP2	Baselap
	Top_Aalenian			Well Marker, 3D horizon	WP2	Eroded at top
	Top_Toarcian			Well Marker, 3D horizon	WP2	Conformable
	Top_Lias-Middle			Well Marker, 3D horizon	WP2	Conformable
Trias	Top_Trias			3D horizon	WP3	baselap
	Top Carnian			3D horizon	WP3	eroded
	Top Middle Trias			3D horizon	WP3	conformable
	Basement			3D horizon	WP3	eroded

Table 3.1 Markers and horizons used in the construction of the model

3.1.2 Horizons & Well Markers

In an earlier phase of PilotSTRATEGY in France, a 3D seismic campaign of 10x10 km was shot. Task 2.3 interpreted 13 horizons on the seismic and converted them to depth. 5 horizons were added additionally in WP3 to further discretize the over- and underburden (current topography, top Upper Cretaceous, top Carnian, top Middle Trias and top basement). One additional marker was interpreted in this task D3.1, the Top_Marnes_de_Massingy to better discretize the sealing unit. This data was used in the construction of the structural framework of the static model.

The depths of all horizons at the well marker level are listed in table 7.1 in the appendix. The calculated thicknesses based on well marker information are listed in table 7.1 in the appendix.

The PilotSTRATEGY project has received funding from the European Union's Horizon 2020 research and innovation programme under grant agreement No. 101022664

3.1.3 Well log data

Task 2.3 provided data from 13 wells located inside the model area (30x30 km), of which 4 wells are located inside the area of the 3D seismic. The wells came with the information about the well head, well path and log data. More details regarding which logs were available for each well in the reservoir section can be found in table 7.1 in the appendix.

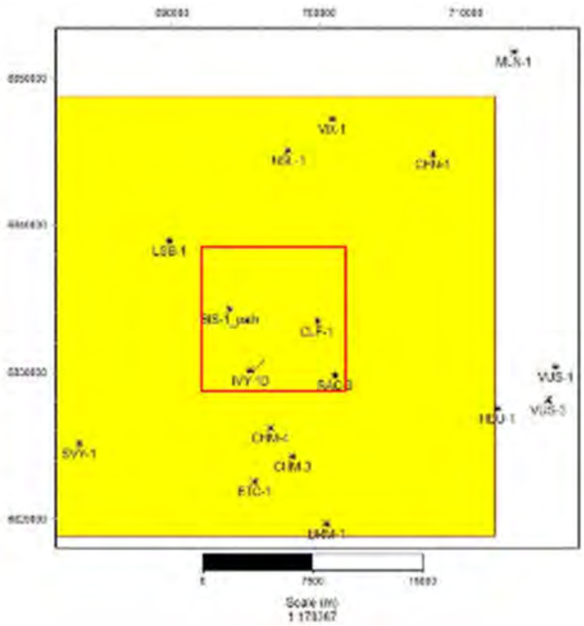

Figure 3.1 position map of static model (yellow box) with well locations. The area covered by 3D seismic is highlighted in red.

3.1.4 Plug data

Task 2.3 provided in total 12 petrophysical measurements from cores of two wells, one inside the 3D model area (CHM-4) and one well outside the model area (VUS-1). From the investigated parameters, porosity and water permeability are used for this modelling. Details can be found in the report D2.6 (Fleury et al., 2023).

Task 2.3 also provided 444 historical measurements for porosity/permeability on core data from the wells inside the model area and 4 additional wells near by the model area. The data comes from the time of the hydrocarbon exploration phase of the area. See table 3.2 for a summary of available plug data.

		CHM-3	CHM-4	CHN-1	HEU-1	IVY-1D	MLN-1	VIX-1	VUS-1	VUS-3
Inside model area		yes	yes	yes		yes		yes		
Inside 3D seismic area						yes				
Outside model area					yes		yes		yes	yes
Plug data porosity	Dalle nacree		Yes	yes	yes		yes	yes	yes	
	Comblanchien	yes	yes	yes	yes	Yes	yes	yes	yes	yes
	Oolithe Blanche		yes			Yes	yes	yes	yes	
Plug data permeability	Dalle nacree		yes	yes	yes		yes	yes	yes	
	Comblanchien		yes	yes	yes	Yes	yes	yes	yes	yes
	Oolithe Blanche		yes			yes	yes	yes	yes	
Measurements D2.7			yes						yes	

Table 3.2 Available plug data for the model

The PilotSTRATEGY project has received funding from the European Union's Horizon 2020 research and innovation programme under grant agreement No. 101022664

3.1.5 Top Marnes de Massingy

An additional well marker to better discretize the seal was interpreted in this task. The well marker is for the top of the Marnes de Massingy, a marly layer, and situated above Top_Callovian_Upper and Top_Oxfordian_Inf. The marker was added as the two other available markers are not located at the top of the marls, which are the primary seal. Instead, the available markers are below and above.

The marker top Marnes de Massingy was interpreted based on the publication Delmas et al. (2012) at the top of the unit described as Marnes Blanches de Épargnes. The GR signal was used for the interpretation in the data. A well pickable peak in the GR just below the Marnes Blanches de Épargnes was used for the interpretation.

The interpretation result can be seen in figures 3.1 – 3.3 in the appendix 7.1.

The thickness of the marls fluctuates between 28 – 45m (table 3.2 in the appendix 7.1). Delmas et al. (2012) measured 35m in the well SMB-17 40km east of the study area.

3.2 Mesh construction

The mesh of the static model was constructed based on seismic and well marker data. Seismic information was available in a 10x10 km area. Stratigraphic information from marker data was available in the seismic area and in wells around. To better account for boundary conditions in the dynamic modeling in task 3.2 it was decided to extend the model outside the 10x10 km area to a size of 30x30 km with the information from well markers.

No faults are present in the model area.

The construction of the geomodel is composed of 3 main steps in Aspen SKUA (Figure 3.2).

- First the construction of the structural/stratigraphic model which creates a horizon model. The horizons serve to vertically limit the model and define the main divisions.
- Second is the construction of the reservoir grid which discretizes the model in individual grid cells to prepare for geostatistical modeling and for the dynamic flow model.
- The third and final step is the filling of the reservoir grid with properties.

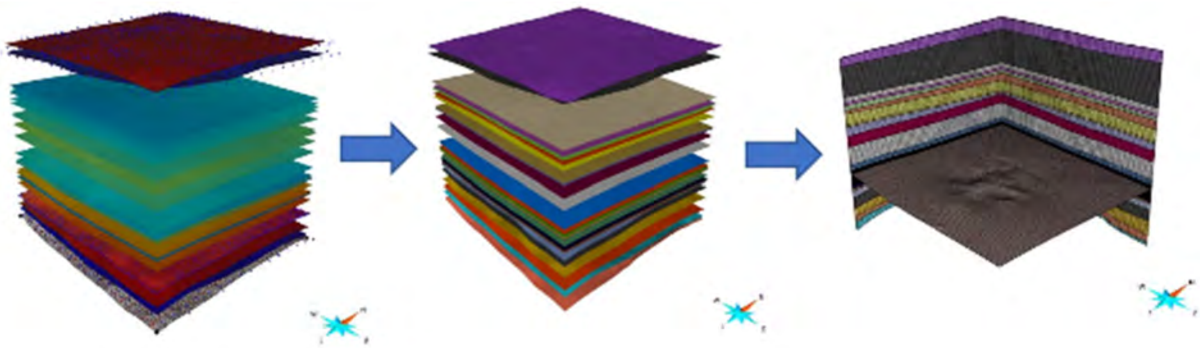

Figure 3.2 Workflow in Aspen SKUA for the mesh construction. The horizon model (left), structural/stratigraphic model based on horizon data (center), and the reservoir grid (right)

3.2.1 Data preparation for structural/stratigraphic model

Data needed to be preprocessed to be usable in the structural/stratigraphic model. Spikes needed to be removed and the horizons extended to cover the area of 30 x 30 km^2.

The PilotSTRATEGY project has received funding from the European Union's Horizon 2020 research and innovation programme under grant agreement No. 101022664

3.2.1.1 Horizon Postprocessing

Task 2.3 provided 13 3D seismic horizons in an area covering 10x10 km. The horizons were already in true vertical depth (TVD). They were smoothed with a 55 voxel radius to overcome stair stepped artifacts visible on the time depth conversion model (details in report D2.7 (Wilkinson, 2023)).

Additional postprocessing was done in task 3.1 to further remove artifacts in form of spikes on the horizons. Spikes were visible on the borders of the horizons, especially a large spike in the Southeast (figure 3.3). They are most likely artifacts from the time depth conversion. It was important to remove spikes along the borders of the horizons to prevent emphasis of nonexistent structures during the horizon extension.

The area where spikes were deleted was interpolated when the horizons were extended to cover an area of 30x30 km (figure 3.4).

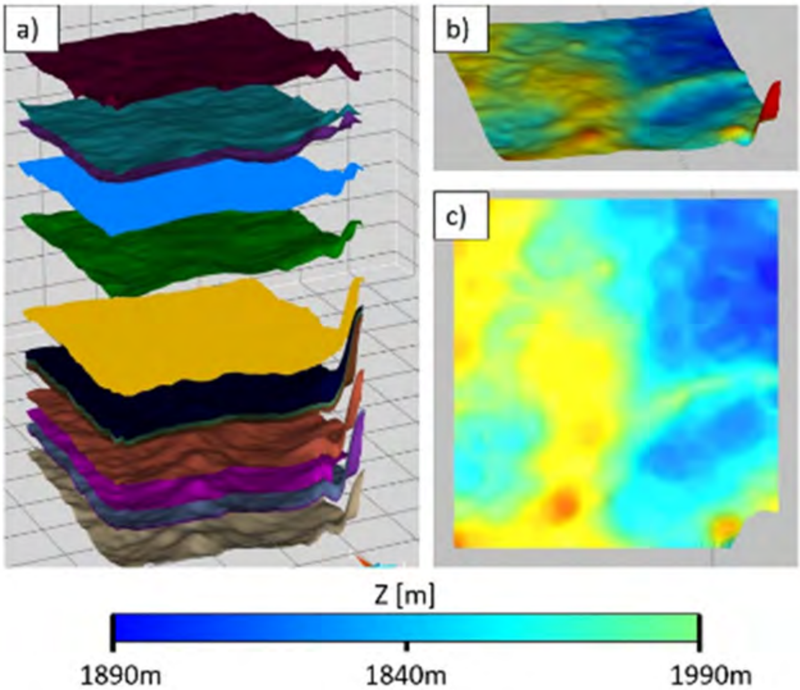

Figure 3.3 Spikes were present on the data for all horizons, especially in the Southeast corner (a). (b) Example of the horizon Bj1 (top Bajocian), at a 10 times vertical exaggeration. (c) The horizon Bj1 (top Bajocian) after the removal of the spike.

3.2.1.2 Horizon extension

The horizons were extended using the information from the well marker data. Well marker data was converted to points and then assigned to the same horizon feature. In a next step, the gaps between the high-resolution horizon data and the marker point data were filled using the surface interpolation functionality in the Aspen SKUA software package (figure 3.4).

It is important to emphasize that the extended horizons have a higher resolution around the 3D seismic and low resolution around the point data from well markers, which makes this area very smooth. The total surface area of the model is 900 km^2 and only in ca 100 km^2 detailed seismic info is available. The rest was interpolated with information from only 8 points. Care should be taken in the structural interpretation of the interpolated area, as the point information from the well markers can only show tendencies.

The PilotSTRATEGY project has received funding from the European Union's Horizon 2020 research and innovation programme under grant agreement No. 101022664

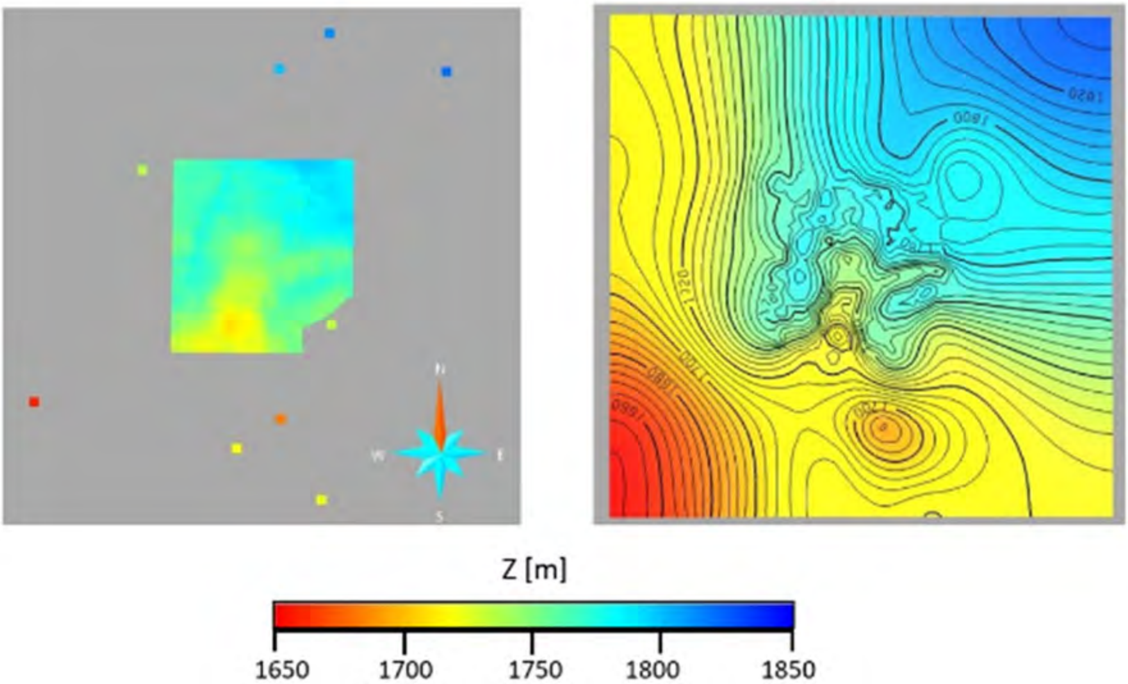

Figure 3.4 Example of the horizon extension process for the horizon top Oolithe blanche

3.2.1.3 Stratigraphic context creation

The extended horizon data was used to build a stratigraphic context in Aspen SKUA, which is a prerequisite to build a structural/stratigraphic model. The stratigraphic context defines the geologic order of the horizons and rules in case horizons are crossing. For the static model, 24 geologic units were defined with 6 orogenic events, based on the unconformities in the Paris Basin (figure 3.5).

The PilotSTRATEGY project has received funding from the European Union's Horizon 2020 research and innovation programme under grant agreement No. 101022664

Horizon name	Layering style	Orogenic event
Topography	baselap	Laramide phase
Top Upper Cretaceous	eroded	
Top Cenomanian	conformable	
Top Albian Clays	conformable	
Top Albian Sands	baselap	Austrian phase
Top Albo Aptian	eroded	
Top Barremian	conformable	
Top Purbeckian	conformable	Lower Cimmerian phase
Top Portlandian	eroded	
Top Kimmeridgian	conformable	
Top Oxfordian Superior	conformable	
Top Oxfordian Inferior	conformable	
Top Dalle Nacree	conformable	
Top Comblanchien	conformable	
Top Oolithe Blanche	conformable	
Top Bt10 internal flooding surface	conformable	
Top Bajocian	baselap	Middle Cimmerian phase
Top Aalenian	eroded	
Top Toarcian	conformable	
Top Lias Middle	conformable	
Top Trias	baselap	Early Cimmerian phase
Top Carnian	eroded	
Top Middle Trias	conformable	Palatinian phase
Top Basement	eroded	

Figure 3.5 Stratigraphic context used in Aspen SKUA. The layering style (middle column) reflects the orogenic events (right column).

3.2.2 Reservoir grid creation

For the reservoir grid a cell size of 250m was chosen as a good tradeoff between capturing the geological heterogeneity and keeping the simulation time reasonable.

Regarding the vertical layering, only one layer per geological unit was chosen for the under- and overburden. For the caprock and the reservoir, the vertical resolution was increased. For the caprock and the formation below the principal reservoir, the vertical resolution is around 5m and for the reservoir units around 3m (figure 3.6 & table 3.3).

In total, the grid has 1.238.400 cells.

The PilotSTRATEGY project has received funding from the European Union's Horizon 2020 research and innovation programme under grant agreement No. 101022664

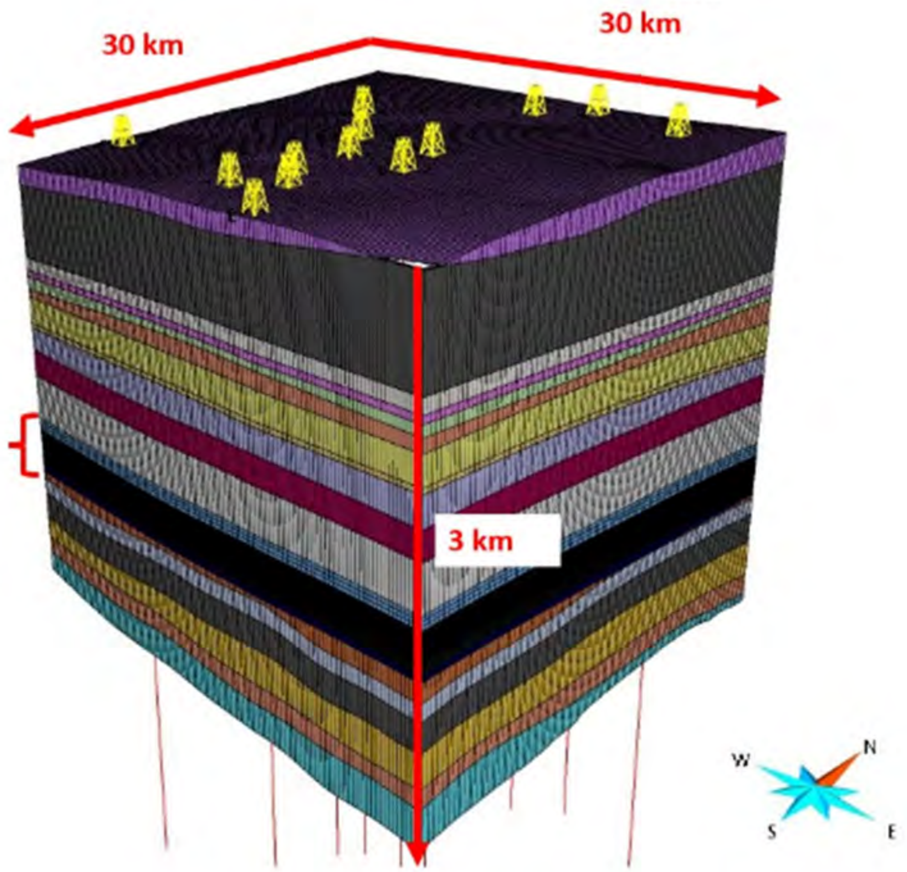

Figure 3.6 The final reservoir grid. Higher cell size resolution in the reservoir section. Reservoir and seal complex highlighted by the red braces. The final model has dimensions of 30x30km in horizontal direction and 3km in depth.

3.3 Petrophysics

3.3.1 Log interpretation

3.3.1.1 Lithology

The neutron porosity (NPHI) and density logs (RHOB) have been plotted on comparable scales to help with the identification of lithology (figure 3.7 (this report) & figure 3.4 (in the appendix 7.1). Both curves superimpose for a large part of the reservoir, notably for the Comblanchien and Oolithe Blanche formations. The superposition indicates limestone as lithology filled with brine.

Towards the top of the reservoir, in the Dalle Nacrée formation, the curves start to separate, NPHI being larger than RHOB, which is an indicator of increased clay content in the formation. This trend continues up into the Marnes de Massigny formation. Below the marker Bt10, the curves separate in the same fashion, indicating a marlier lithology.

The Gamma ray log (GR) shows very low values for most of the reservoir units, which is also a typical indicator of limestones. Towards the top of the Dalle Nacrée, the GR increases, which is correlated with the separation of the NPHI / RHOB curves. This is an indicator of increasing clay content. The same observation can be made below the marker Bt10.

The GR curve is increasing slightly in the Comblanchien formation, but the curves NPHI and RHOB still superimpose. The increase of radioactivity is therefore not related to an increase in clay material, and

The PilotSTRATEGY project has received funding from the European Union's Horizon 2020 research and innovation programme under grant agreement No. 101022664

therefore is not an indicator for a decrease in reservoir quality. This information needs to be considered when calculating the Shale Volume.

The Photoelectric Factor log (PEF) shows values of around 4.5 for the Oolithe Blanche and Comblanchien formations, which is typical for a limestone made of calcite of about 10-20% porosity. The PEF drops to about 3 at the formation boundary of the Dalle Nacrée to the Marnes de Massingy formation. A value of around 3 is typical for clay minerals, such as smectite and illite. The PEF also drops from 4 to 3 in the interval from the marker Bt10 to Bj10 (top Bajocian).

Horizon	Unit number	Number of Layers	Unit Thickness	Cell Thickness
Topo	1	1	197.318	197.318
Top_Upper_Cretaceous	2	1	622.839	622.839
Top_Cenomanian	3	1	86.59	86.59
Top_Alb_Clay	4	1	44.5011	44.5011
Top_Alb_Sand	5	1	83.4344	83.4344
Top_Albo-Aptian	6	1	134.52	134.52
Top_Barremian	7	1	170.466	170.466
Top_Purbeckian	8	1	33.7423	33.7423
Top_Portlandian	9	1	179.609	179.609
Top_Kimmeridgian	10	1	164.023	164.023
Top_Oxf_Sup	11	1	271.897	271.897
Top_Oxf_Inf	12	1	79.7971	79.7971
Top_Marnes_Massigny	13	7	34.5718	4.93883
Top_Dalle_Nacree_Ca26	14	5	15.5039	3.10078
Top_Comblanchien_Bathonian_Ca24	15	6	16.9053	2.81755
Top_Oolithe_Blanche_SBComb	16	36	108.677	3.01881
Bt10_internal_flooding_surface_Bathonian	17	13	65.1448	5.01114
Top_Bajocian	18	1	59.3975	59.3975
Top_Aalenian	19	1	121.117	121.117
Top_Toarcian	20	1	102.871	102.871
Top_Lias_Middle	21	1	180.933	180.933
Top_Trias	22	1	263.11	263.11
Top_Carnian	23	1	190.031	190.031
Top_Middle_Trias	24	1	53.7874	53.7874
Top_Basement				

Table 3.3 Summary of the reservoir grid resolution (thicknesses are averaged values over the area and layer)

The PilotSTRATEGY project has received funding from the European Union's Horizon 2020 research and innovation programme under grant agreement No. 101022664

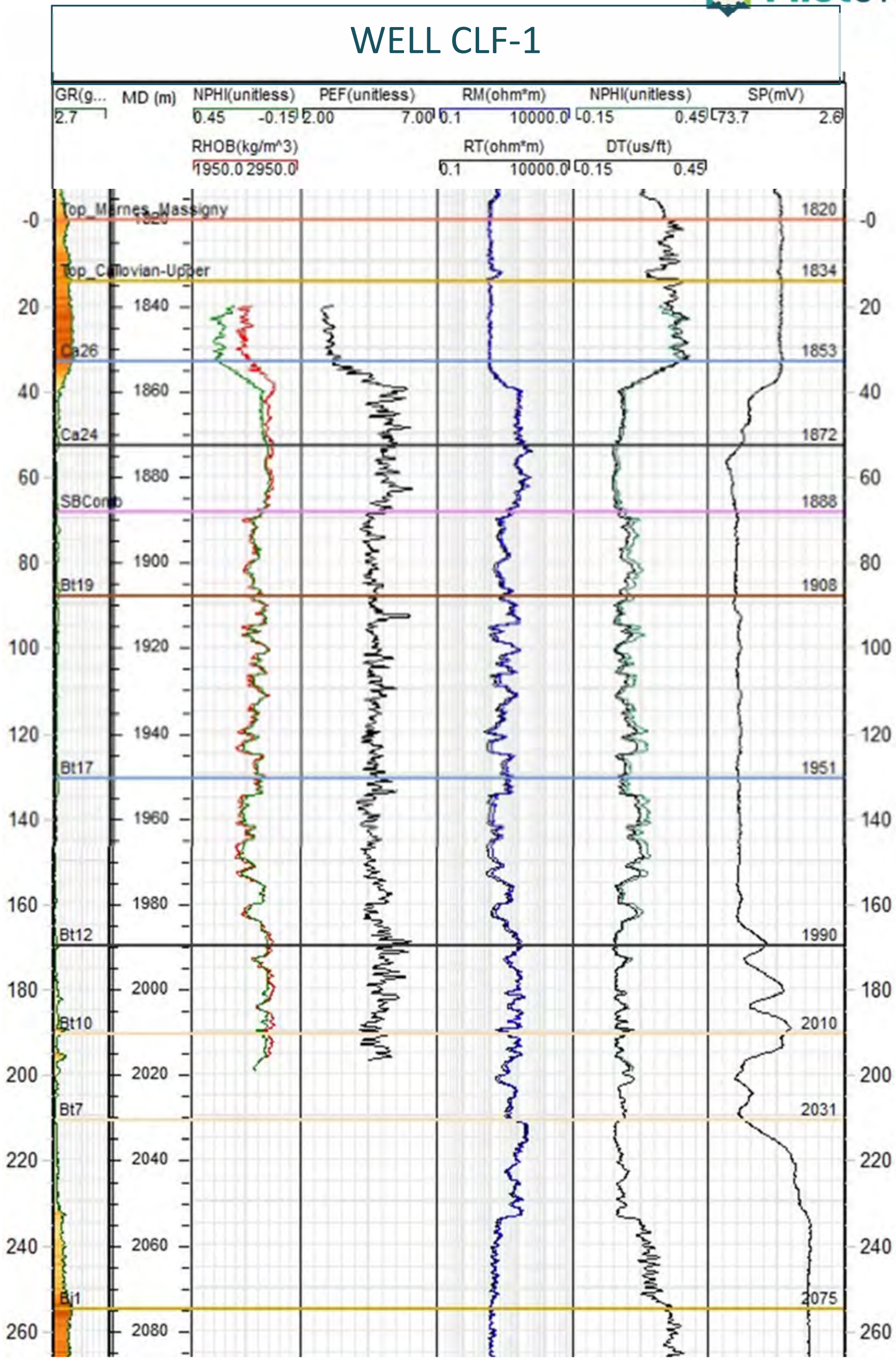

Figure 3.7 Petrophysical log set used for interpretation, example well CLF-1.

3.3.1.2 Diagenesis

Diagenesis from calcite to dolomite can be determined when superimposing the neutron porosity (NPHI) and density logs (RHOB). If the reservoir is shale free and the logs overlay perfectly, it is an

The PilotSTRATEGY project has received funding from the European Union's Horizon 2020 research and innovation programme under grant agreement No. 101022664

indication of clean calcite ($CaCO_3$). A diagenesis of calcite to dolomite ($CaMg(CO_3)_2$) would be visible with a separation of both logs. Dolomites have a lower density porosity, because the grain density is higher than of calcite due to the Mg content in the dolomite. The neutron reading for dolomites is relatively high due to the neutron moderating character of dolomite compared to calcite.

In the clean reservoir intervals, the neutron and density logs superimpose, meaning no trace of diagenesis can be inferred from the log data. This observation is also supported by the reading of the Photoelectric Factor log (PEF). The PEF is fluctuating around a mean value of 4.5 in the reservoir interval, and dolomite would have a lower reading of around 3 in zones with no shale present.

3.3.1.3 Fractures

No modern image logs are available for the wells present in the area. Such logs were specifically designed to identify fractures in borehole images. Due to the lack of adapted logs, porosity was calculated from the sonic log (DT) and compared to neutron porosity (NPHI) to identify fractures. The NPHI log is measuring the total porosity, which includes the fractures. The DT log is only measuring the porosity without the fractures, as they are avoided by the acoustic waves. The factures are avoided if they have a preliminary vertical orientation. Therefore, the DT log will underestimate the porosity if fractures are present. Superimposing the NPHI and porosity calculated from DT can therefore help to identify the presence of fractures. The porosity was calculated from the sonic using the equation below and the following parameters after Carmichael. (https://petrowiki.spe.org/File:Vol5_Page_0174_Image_0001.png)

$$\varphi = \frac{\Delta t - \Delta t_{ma}}{\Delta t_f - \Delta t_{ma}}$$

ϕ = fractional porosity of the rock
Δt = acoustic transit time (µsec/ft)
Δt_f = acoustic transit time of interstitial fluids (µsec/ft)
Δt_{ma} = acoustic transit time of the rock matrix (µsec/ft)

	acoustic transit time (µsec/ft)
Δt_f	189 (value for water with 20 NaCl)
Δt_{ma}	49 (value typical for limestone)

A slight separation of the DT porosity and NPHI log can be observed for the reservoir interval (see well CLF-1, figure 3.7). The DT porosity and NPHI curves show the same features, and the separation diminishes in intervals with higher clay content, such as towards the top of the Dalle Nacrée.

The deep and shallow resistivity logs also show a separation in the reservoir interval and a superposition in clay rich intervals. The separation indicates the infiltration of mud into the formation, which is more distinct in the porous reservoir intervals.

The separation of the DT porosity log and the NPHI log is also larger in intervals with high porosities and therefore not an indication of fractures, but a phenomenon caused by mud invasion.

3.3.1.4 Mud invasion

In intervals where the GR is elevated, deep and shallow resistivity superimpose (see well CLF-1 above marker Bt10, figure 3.7). Further up in the well, where the clay content is lower, the curves start to

The PilotSTRATEGY project has received funding from the European Union's Horizon 2020 research and innovation programme under grant agreement No. 101022664

separate. This means that drilling fluid has entered the formation. Where the formation is less porous, for example in the intervals the GR is elevated, the drilling fluid can't enter the formation.

The curves for NPHI and the DT porosity calculation are also superimposing in the intervals rich with clay. Where clay content is lower, they separate. This could be interpreted as fractures, as the DT porosity is lower than NPIE porosity, but this could also be only a phenomenon due to mud invasion.

3.3.2 Plug data analysis

The reservoir complex was differentiated into two principal reservoirs (Oolithe Blanche & Dalle Nacrée), a semi-permeable reservoir (Comblanchien) and caprock (Callovo Oxfordian Marls) due to different depositional environments and lithologies. The same division was later kept for the petrophysical modeling, and each formation was analyzed separately.

Plug data for porosity and permeability of 8 wells were taken for this analysis. 4 wells are within the modeled area (CHM-4, CHN-1, IVY-1D, VIX-1) and 4 wells near the modeled area (HEU-1, MLN-1, VUS-1, VUS-3). 444 values were available of which 99 are of the Dalle Nacrée formation, 278 for the Comblanchien formation and 67 for the Oolithe Blanche formation (figure 3.8). 4 values are available from task D2.6 for the caprock (see report from this work package).

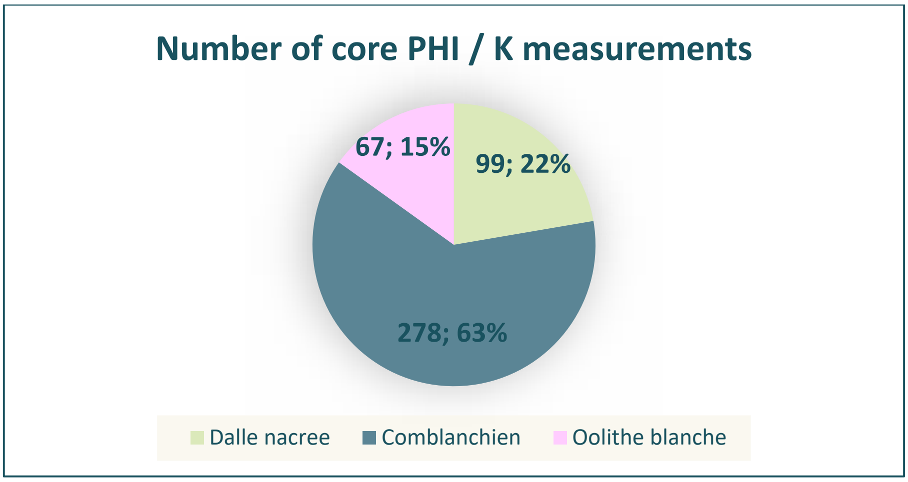

Figure 3.8 Distribution of plug data for PHI / K measurements by formation

The Comblanchien is the most cored formation with all 8 wells crossing the formation (4 crossing completely). The Dalle Nacrée is cored in 6 wells and 1 well is crossing it completely. The Oolithe Blanche formation is cored by 4 wells, but it is not cored completely (figure 3.9).

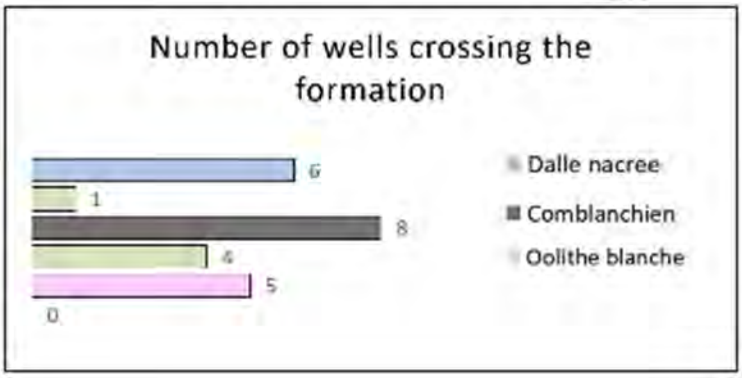

Figure 3.9 Number of wells crossing the formation. In green number of wells crossing the complete formation

The Oolithe Blanche formation is considered the principal reservoir unit for the CO_2 storage. Ranging from the marker SBComb (Top Oolithe Blanche) to Bj1 (Top Bajocian) it measures between 175 – 208 m in the wells which have core measurements. The core measurements available for this study are situated at the top of the Oolithe Blanche and core only 3 – 4m (see Figure 3.10). Little hard data measurements are available of this formation. This is due to the reusage of historical data from oil and gas exploration which had as principal target the overlaying formations Dalle Nacrée and Comblanchien.

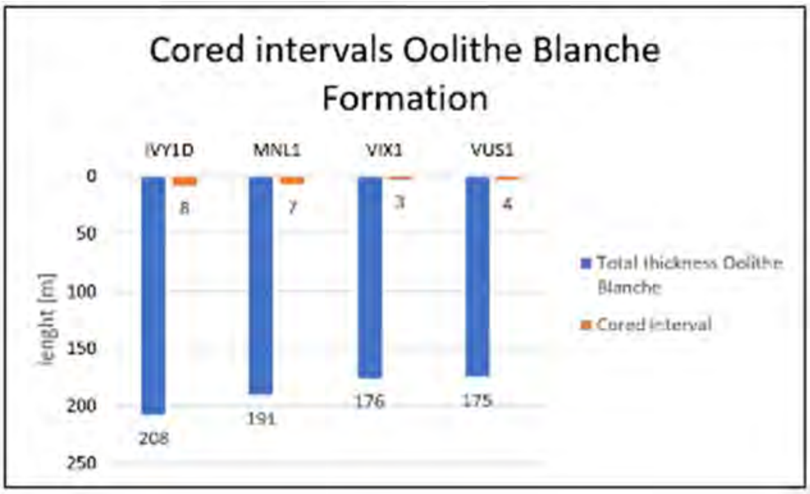

Figure 3.10 Formation thickness vs cored interval length of Oolithe Blanche formation

Analysis of the plug porosity values showed a unimodal distribution for the Comblanchien and Dalle Nacrée formations and a bi-modal distribution for the Oolithe Blanche formation (figure 3.11). This is an indicator that two types of facies are present which should be modeled apart. The cutoff is at 11%.

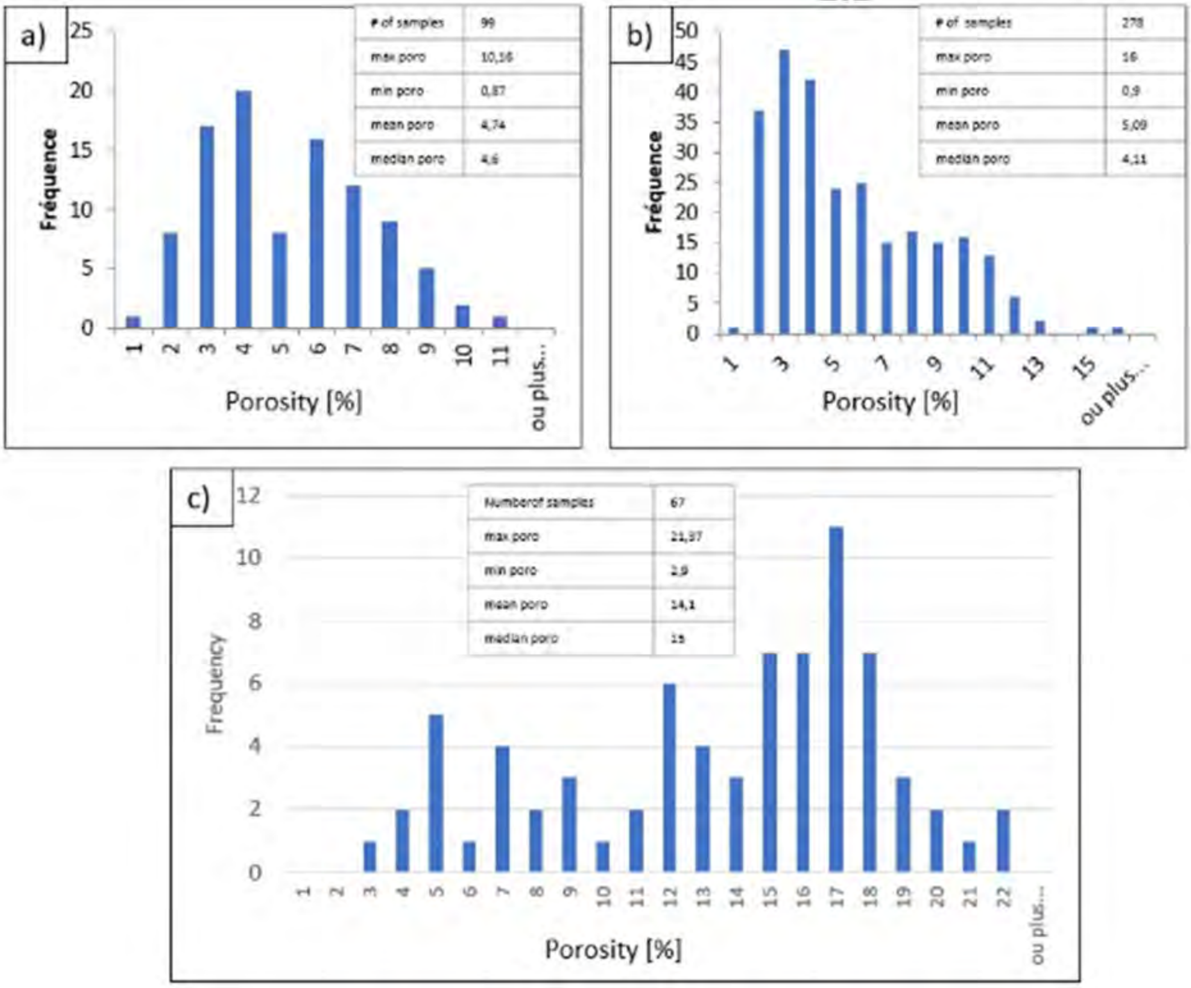

Figure 3.11 Plug porosity distribution of the formation Dalle Nacrée (a), Comblanchien (b), and Oolithe Blanche (c)

3.3.3 Log calculation

3.3.3.1 Shale Volume

Shale volume (Vsh) was calculated as a function from the gamma ray (GR) log for a shaliness indicator using the formula presented in Figure 3.12. The GR response was read for a clean interval to determine GRmin and a shale interval to determine GRmax. As clean interval the top of the calcareous reservoir formation Oolithe Blanche was used and the Toarcien formation (Lower Jurassic) was taken as shale interval. Respective GR max and GR min values for each well are listed in table 3.4 in the appendix 7.1.

$$V_{clay} = \frac{GR_{log} - GR_{min}}{GR_{max} - GR_{min}}$$

Figure 3.12 Vsh calculation from the GR based on a linear function (Rider, M. & Kennedy, M. 2011).

Higher GR values were observed in the Comblanchien formation compared to the Oolithe Blanche formation. Analysis of NPHI and RHOB logs showed when superposed, that both formations are clean of shale and pure calcite. The source of the elevated GR is radioactive elements but are not associated with shale. Radioactive elements can also occur naturally in limestone, but at a much lower concentration than in shales. However, they can reach a higher concentration due to condensation. Concentration might be higher in the Comblanchien formation due to continuous evaporation in the

The PilotSTRATEGY project has received funding from the European Union's Horizon 2020 research and innovation programme under grant agreement No. 101022664

lagoonal environment during deposition. For this reason, the Vsh was corrected for the Comblanchien formation and a Vsh of 0 was assigned in all wells.

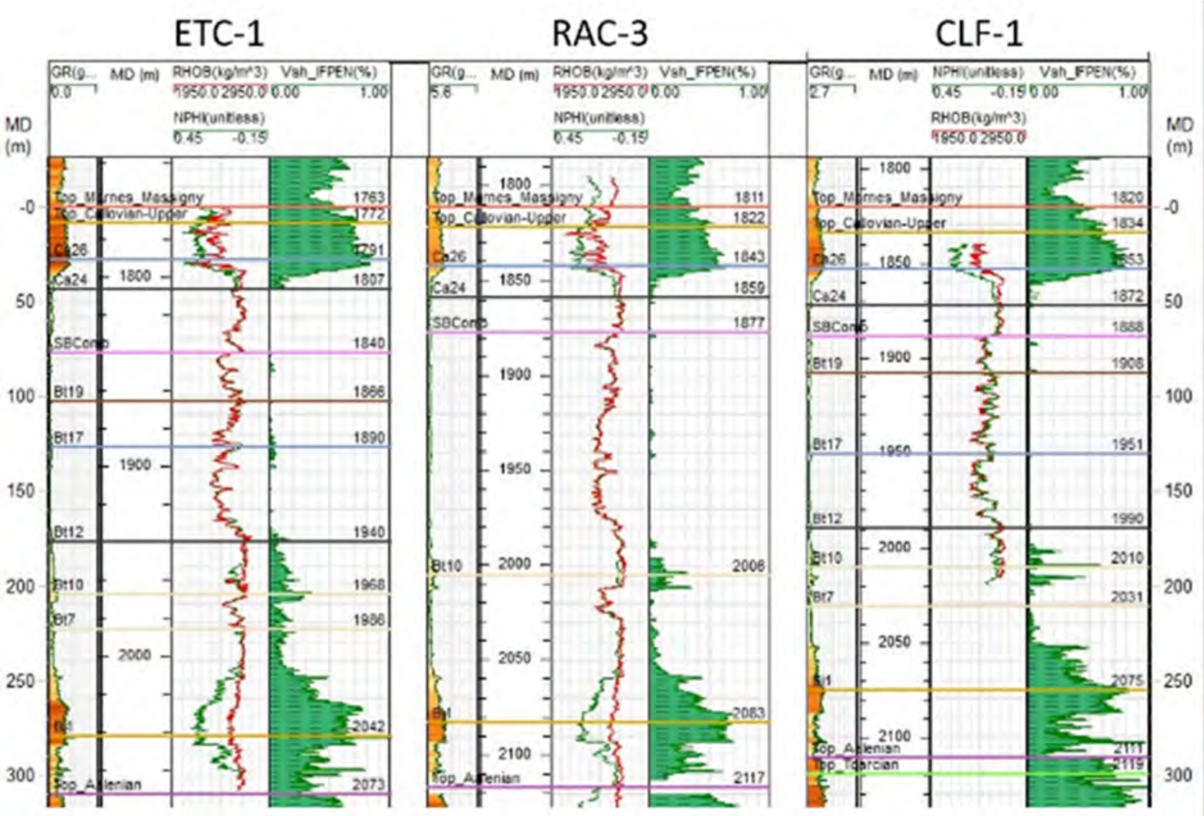

Figure 3.13 Figure 14 Examples of Vshale calculated logs

3.3.3.2 Effective Porosity

Effective porosity was calculated based on NPHI as well as RHOB plus an average of both calculations was taken.

The bulk density is a mixture of the volume weighted average of the components which make up the rock, which makes it a perfect measure to calculate porosity. To calculate porosity, it is necessary to know the density of all the materials involved. The tool measuring the density sees bulk (global) density which is the sum of the both the grains and the fluids enclosed in the pores. In a simple and clean reservoir, the interpretation model is (Rider, M. & Kennedy, M. 2011):

$$\rho_b = \phi \rho_{fl} + (1 - \phi)\rho_{ma}$$

Solved for porosity the equation is:

$$\phi_T = \frac{\rho_{ma} - \rho_b}{\rho_{ma} - \rho_{fl}}$$

The calculated porosity is the total porosity, as no distinction between pore fluid and fluid bound in shales is made. The term is turned into effective porosity when corrected for shale, which requires an additional term:

The PilotSTRATEGY project has received funding from the European Union's Horizon 2020 research and innovation programme under grant agreement No. 101022664

$$\rho_b = \phi_e \rho_{fl} + (1 - \phi_e - V_{sh})\rho_{ma} + V_{sh}\rho_{sh}.$$

ρ_b = bulk density [kg/m^3]
Φ_e = effective porosity [%]
ρ_{fl} = fluid density [kg/m^3]
ρ_{ma} = matrix density [kg/m^3]
ρ_{sh} = shale density [kg/m^3]
Vsh = shale volume [%]

	Density [kg/m^3]
ρ_{fl}	1000
ρ_{ma}	2710 (value typical for calcite)
ρ_{sh}	2200 (value typical for clay)

The effective porosity was also derived from the NPHI log following the equation (Rider, M. & Kennedy, M. 2011).:

$$NPIE = \Phi e + NPIE_{\underset{shale}{max}} * Vsh$$

Φ_e = effective porosity [%]
NPHI_max_shale = value at maximum shale interval
Vsh = shale volume [%]

A shale cutoff value of 0.5 or 0.4 was additionally added to the calculation to remove high porosity values in the shalier intervals, for example in the caprock interval of the Marnes de Massingy (see table 3.5 in the appendix 7.1 for Vshale cutoff values and NPHI max values for each well).

Finally, the effective porosity was calculated by taking the average value of both approaches.

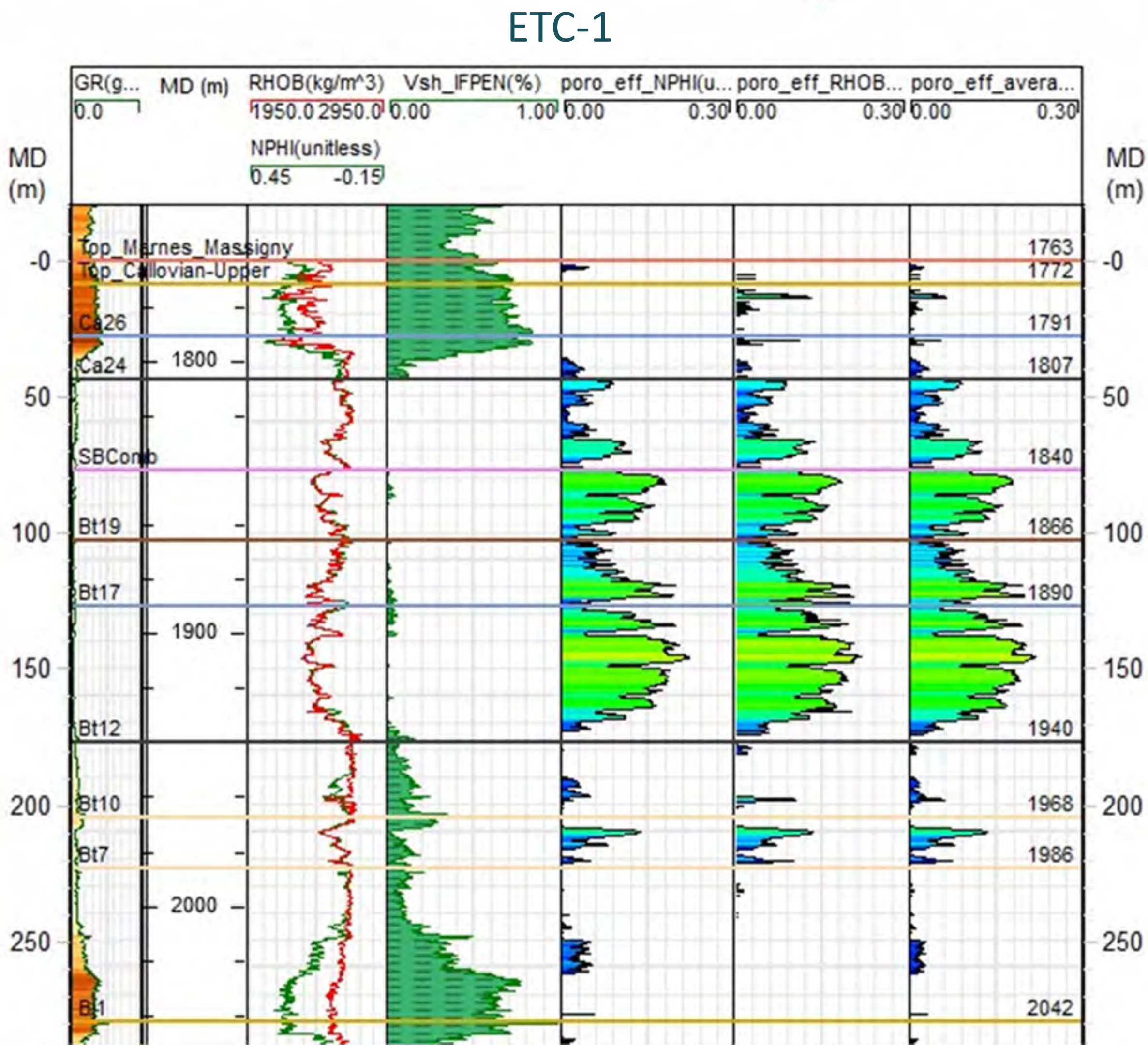

Figure 3.15: Examples of effective porosity logs based on NPHI (left) and RHOB (middle) and then averaging both methods (right)

In a next step the calculated effective porosity was compared to the porosity data for two wells in the model area, IVY-1D and CHM-4. The core data from IVY-1D was historical data from oil and gas exploration and for CHM-4 the data was acquired in WP2 (D2.6).

For the well IVY-1D, data were available for the Comblanchien and Oolithe Blanche formation. The calculated effective porosity fit very well to the measured porosity on the plug data (correlation coefficient 0.97, figure 3.16). At 10% core porosity, the calculated log porosity is 9%, at 19% core porosity, the calculated log porosity is 17%. The larger the porosities, the more the correlation is diverging. This behavior is expected as the core data is not measured at reservoir conditions. The higher the porosities the more the rock can be compressed at reservoir conditions.

The PilotSTRATEGY project has received funding from the European Union's Horizon 2020 research and innovation programme under grant agreement No. 101022664

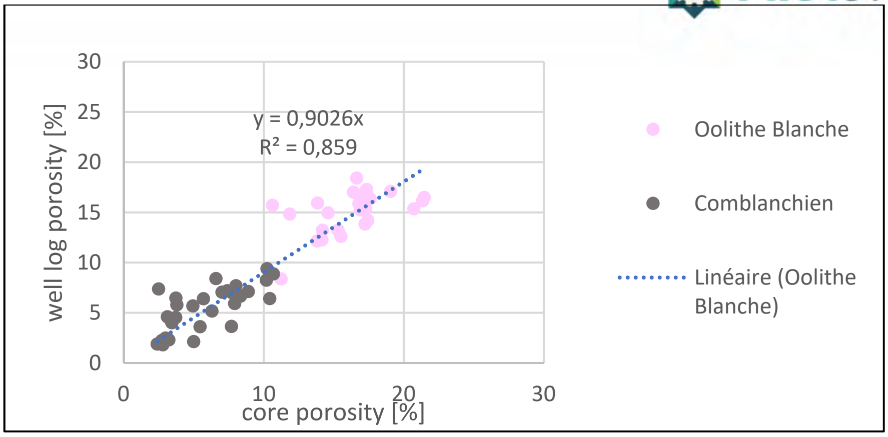

Figure 3.16: Log/core plug porosity comparison IVY-1D well

For the well CHM-4 only 6 plug samples are available. Compared to the calculated effective porosity in the highly porous areas the core data is 15% vs 13.8% on the calculated log data and for the less porous areas 7% on the core data vs 6% on the calculated log data (see figure 3.17).

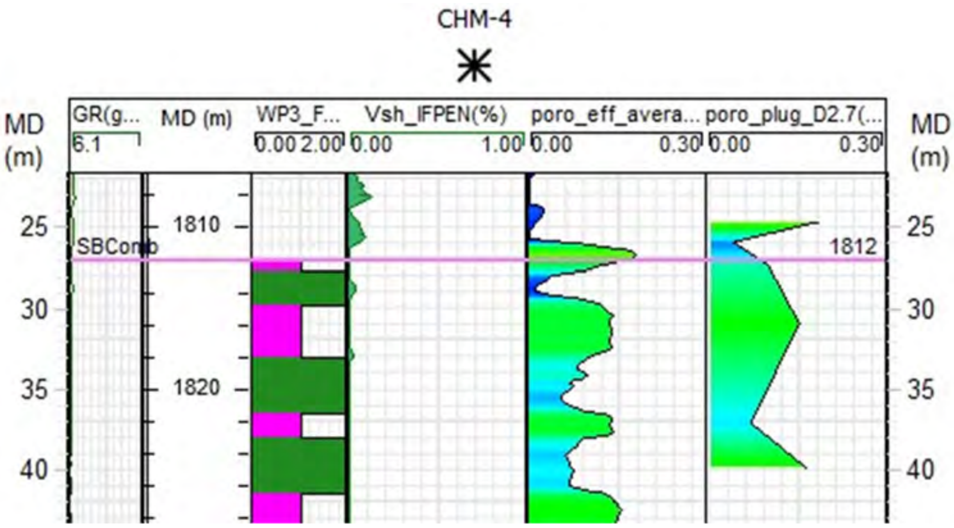

Figure 3.17: Comparison of the calculated porosity with plug porosity data in well CHM-4

3.3.3.3 Facies log Oolithe Blanche formation

WP2 delivered two different facies logs. One has 7 classes and is based on the depositional environment the other one is a classification based on electrofacies with 6 classes in total.

In a workshop on 1st of August 2023 it was decided with the colleagues working in WP2 to simplify those two existing facies models and combine them into one model, which is used in this work. In general, it is preferred to not have not too many different facies types and each facies type should have a spatial predictive power to reduce the uncertainty (Deutsch, C. 2002). Therefore, it was decided to treat the formation Dalle Nacrée as one reservoir unit to be modeled apart and the same was applied to the Comblanchien formation. For the Oolithe Blanche formation it was decided to distinguish two facies classes, one with a low porosity and one with high porosity. This classification enables to separate the high porosity Oolithic bodies from the less porous intervals of the Oolithe Blanche formation. This separation makes sense when looking at the effective porosity log for the Oolithe Blanche formation where individual geological bodies with high porosity stand out.

Analyzing the porosity also from plug data for the Oolithe Blanche formation, it showed a bimodal distribution, which is an indicator that two facies are present (see 3.1.4 section). The cutoff was found to be at 11% for the bimodal distribution. With the help of a script, a facies log was created for the Oolithe Blanche formation which, based on the cutoff at 11% porosity, divides the formation in two facies classes (see figure 3.18).

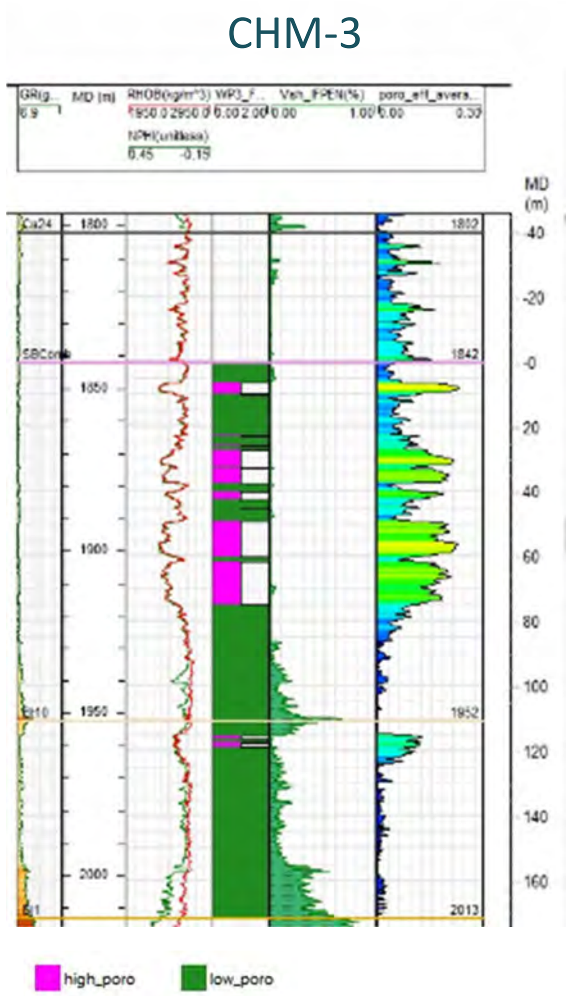

Figure 3.18 Example of the facies log calculation by script based on the effective porosity log.

3.4 Grid filling

The simulation of properties is the step of filling in the 3D grid with the data available on an ad hoc basis (log data, plug data, etc.). This simulation is based on a workflow ranging from facies properties to reservoir properties needed for volume calculation and reservoir engineering.

3.4.1 Facies

A facies log was calculated for the Oolithe Blanche formation to separate into a lower porosity and a higher porosity facies (see section 3.3.3.3). A cutoff was applied at 11% for the effective porosity honoring the information from the plug analysis (figure 3.11).

The modeling of the facies in the Oolithe Blanche reservoir is done using the algorithm of Sequential Indicator Simulation or short SIS.

This flexible method is based on:

- The information of facies upscaled at wells, this information is always respected.
- The variogram models defined in the variogram analyzer.
- Vertical trend curves (VTC) calculated from well data. They constrain layer by layer the proportion of the simulated facies.
- 2D trend maps calculated from well data. They constrain laterally the proportions of the simulated facies.
- 3D trends constructed from VTC and 2D trend maps.

All these elements will guide and constrain the realization of facies. The porosity will then be modeled by facies.

3.4.1.1 Discretization of facies in the grid

To be able to use the log information at the scale of the simulation grid, the first step is to discretize this information on the grid cells. This is done using Aspen SKUA's Data and Trend analysis module by what is called "blocking the data". One value of facies is assigned to each cell passed through a well with facies information. Since each cell can carry only one value, the log information must be averaged, which is done using the "Largest proportion" method. By considering all the log values of facies that fall geometrically into a cell, we assign to this cell the code of the most present facies.

The quality of the results is controlled using histograms (see figure 3.19) comparing the proportions of the facies before and after upscaling.

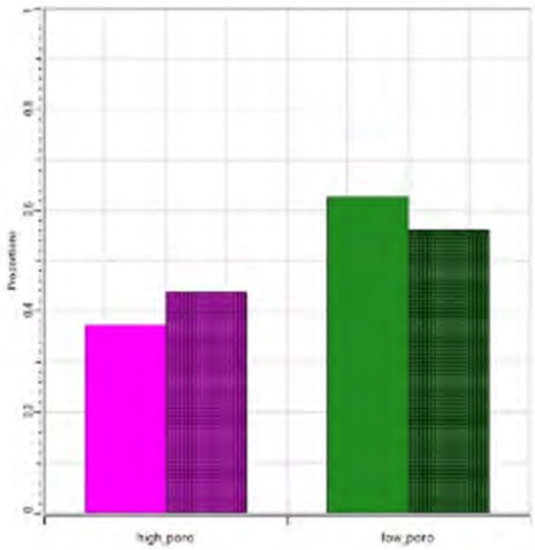

Data	High porosity facies [%]	Low porosity facies [%]
Log data	37.3	62.7
Blocked data	43.8	56.2

Figure 3.19 Result of blocking facies log. Shaded bars represent the blocked data.

The results are also controlled with sections at the level of the wells (see figure 3.20). The results are of very good quality for all intervals. The proportions and vertical heterogeneities of facies are well represented at the scale of the grid. No statistical bias is introduced during this operation.

This step also serves as a quality control for the vertical layering of the simulation grid: if the heterogeneities of facies had not been well represented after upscaling, it would have been necessary to review the vertical layering to define a more appropriate one.

The PilotSTRATEGY project has received funding from the European Union's Horizon 2020 research and innovation programme under grant agreement No. 101022664

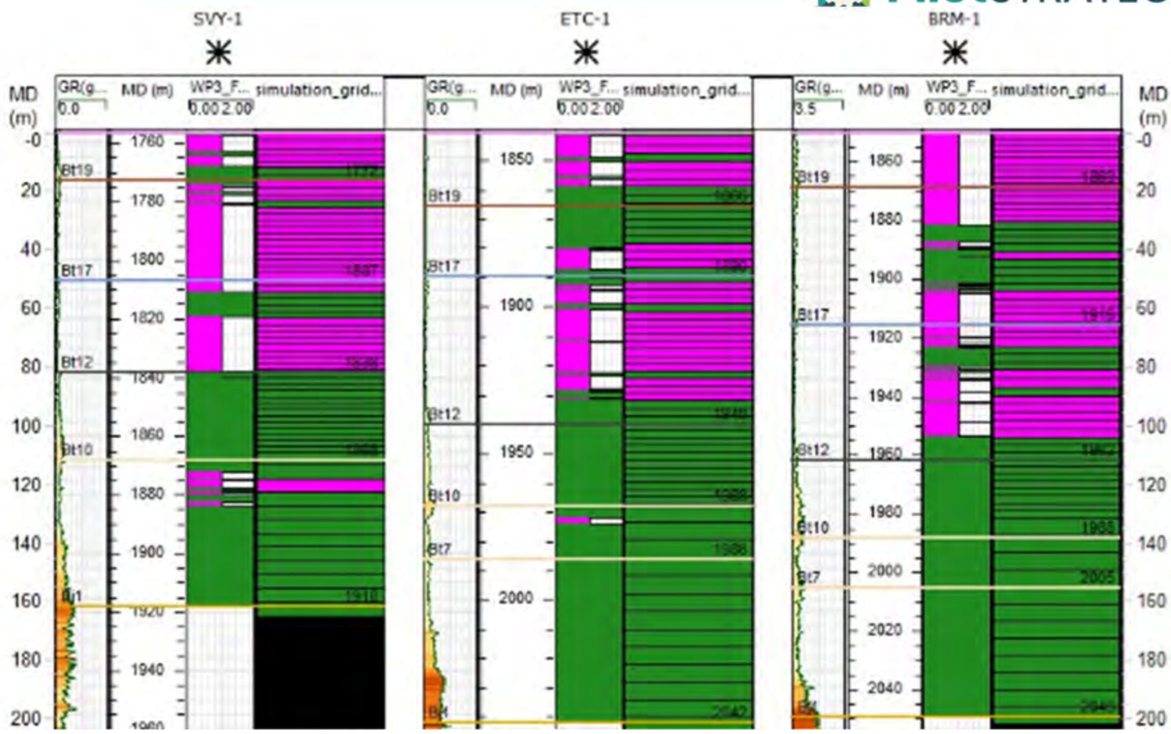

Figure 3.20 Well section window showing on the left log the original facies log and the upscaled log on the right side.

3.4.1.2 Variography

The variogram is used to analyze and model the spatial structure of the data. It thus allows to define in a way the typical three-dimensional shape of a facies. The size and orientation of the modelled geological bodies are directly related to the defined parameters. The parameters of variogram models are mainly:

- The type of variogram model (which also characterizes the behavior at the origin, i.e., for short distances).
- The major range (length in m).
- The minor range (width in m) if anisotropy is present.
- The vertical range (thickness in m).
- The azimuth (orientation in °).

These parameters are defined from the wells at the grid scale. The more wells and therefore the more measuring points, the more accurate and reliable a variogram will be. Vertical accuracy is generally more important because sampling is that of logging. On the other hand, horizontal accuracy will generally be less because it depends heavily on the concentration of wells and their number.

Variogram parameters were established with peak-to-peak correlations for the high porosity bodies visible on the effective porosity log. Correlations were found from well ETC-1 to CHM-3 and bodies with 10-15m thickness identified. Since the wells are 3000m apart, a minimum extension of 3000m in Northeast to Southwest direction was taken. No correlation was possible from SVY-1 to BIS-1 (also Northeast to Southwest direction), so the maximum extension is <13.5 km. No correlation was possible from ETC-1 to BRM-1 in the perpendicular direction (Northwest to Southeast direction), so maximum extension is < 5000m. See figures 3.5-3.7 in the appendix for the peak-to-peak correlation.

Comparison with analog data from Morocco confirmed the thickness range and the lateral extension of several kilometers (personal communication, BRGM).

The PilotSTRATEGY project has received funding from the European Union's Horizon 2020 research and innovation programme under grant agreement No. 101022664

The same variography of oolithic bodies in the Paris basin at the same time of Middle Jurassic was also described in the literature by Brigaud et al. (2014) with azimuth 45N, vertical range 2m, major range 2000m, minor range 1500m. Based on the well data in this project, selected variography parameters are azimuth 45N, vertical range 15m, major range 3000m, minor range 1000m. An elongated variogram was chosen as it best matches the perceived depositional environment of diverging tidal channels with elongated ooid shoal / barrier islands. The slope of the ramp was tilting towards the Southeast to the Sillon Marneux.

The same experimental variograms were used for both facies, the high porosity facies and the low porosity facies in the principal reservoir Oolithe Blanche.

3.4.1.3 Vertical proportion curves

Vertical proportion curves of facies or VPCs are tools that give an estimate of the facies proportions for each layer. The proportions are represented in the form of bars, stacked on top of each other. The proportions are calculated from the facies upscaled at the wells. They are used then to constrain later, either the construction of a 3D constraints for a given facies, or directly the realization of facies. In the latter case, it is the proportions of the VPC that are respected and not the proportions of the wells. The figure 3.22 illustrates the VPCs for the reservoir Oolithe Blanche.

3.4.1.4 Construction of 3D constraints

The DTA module in Aspen SKUA allows to produce 2D proportion maps per facies. In the same module they can be combined into a 3D cube of probability of facies, which will finally serve as a trend in the algorithm of facies simulation.

The data used for the construction of such constraints are:

- The information of facies high porosity / low porosity upscaled on the grid.
- The overall proportions of facies.
- The property of volume proportion in the grid

We thus obtain as output two 3D properties of probability, high porosity, and low porosity. These properties are eventually used as a trend in the facies simulation algorithm.

The figure 3.21 shows the probability of occurrence for the high porosity facies at the top part of reservoir Oolithe Blanche.

The PilotSTRATEGY project has received funding from the European Union's Horizon 2020 research and innovation programme under grant agreement No. 101022664

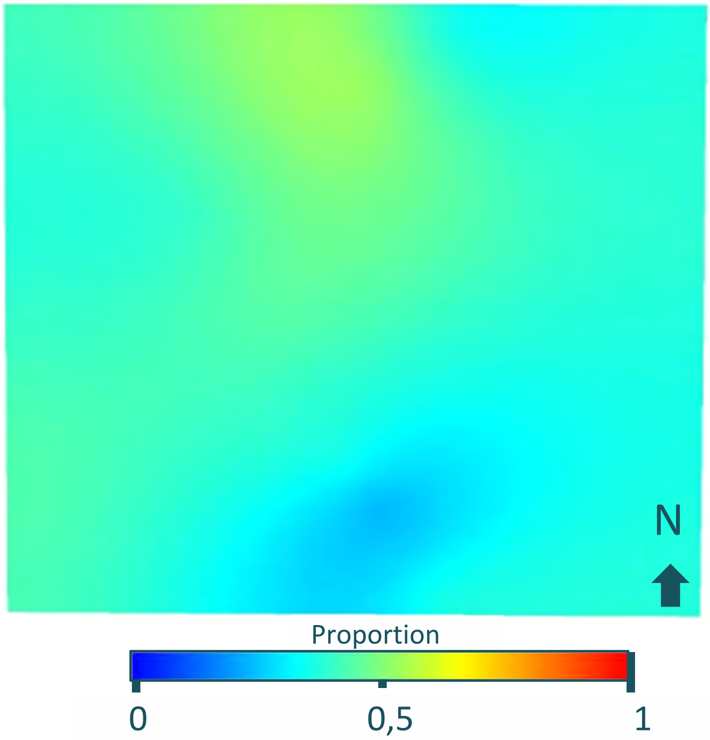

Figure 3.21 2D proportion map for the high porosity facies of the Oolithe blanche.

3.4.1.5 Results analysis

The quality control of the results is done using maps and sections to visualize the spatial variability of the simulated facies and histograms to quantitatively verify the percentages of simulated facies compared to upscaled facies.

One result of the facies simulation is illustrated in the figure 3.22 for a layer of the reservoir and on a cross-section (figure 3.23). The VPC and variography is well respected in the result. One has to keep in mind that this result represents just one equiprobable stochastic realisations among many.

The PilotSTRATEGY project has received funding from the European Union's Horizon 2020 research and innovation programme under grant agreement No. 101022664

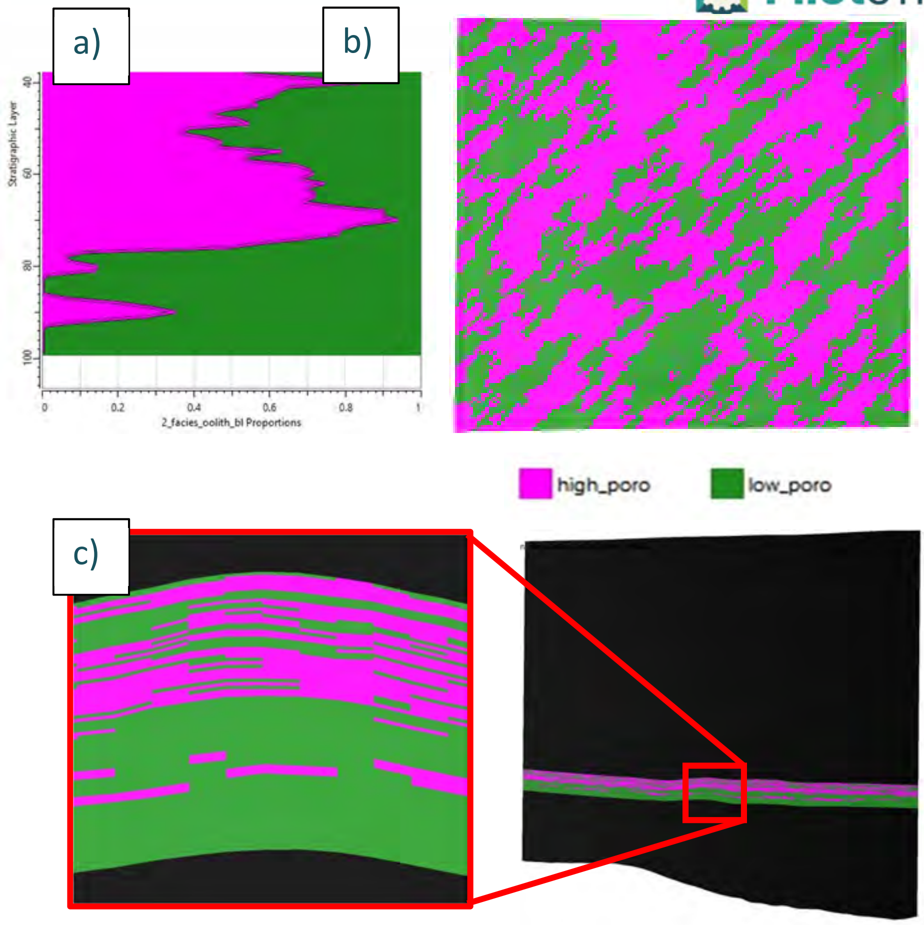

*Figure 3.22 Results of **one realization** of the facies simulation with SIS algorithm. The vertical proportion curve gets well respected as well as the variography. (a) Vertical proportion curve, (b) facies simulation at layer K = 38, (c) cross section at J = 74*

The PilotSTRATEGY project has received funding from the European Union's Horizon 2020 research and innovation programme under grant agreement No. 101022664

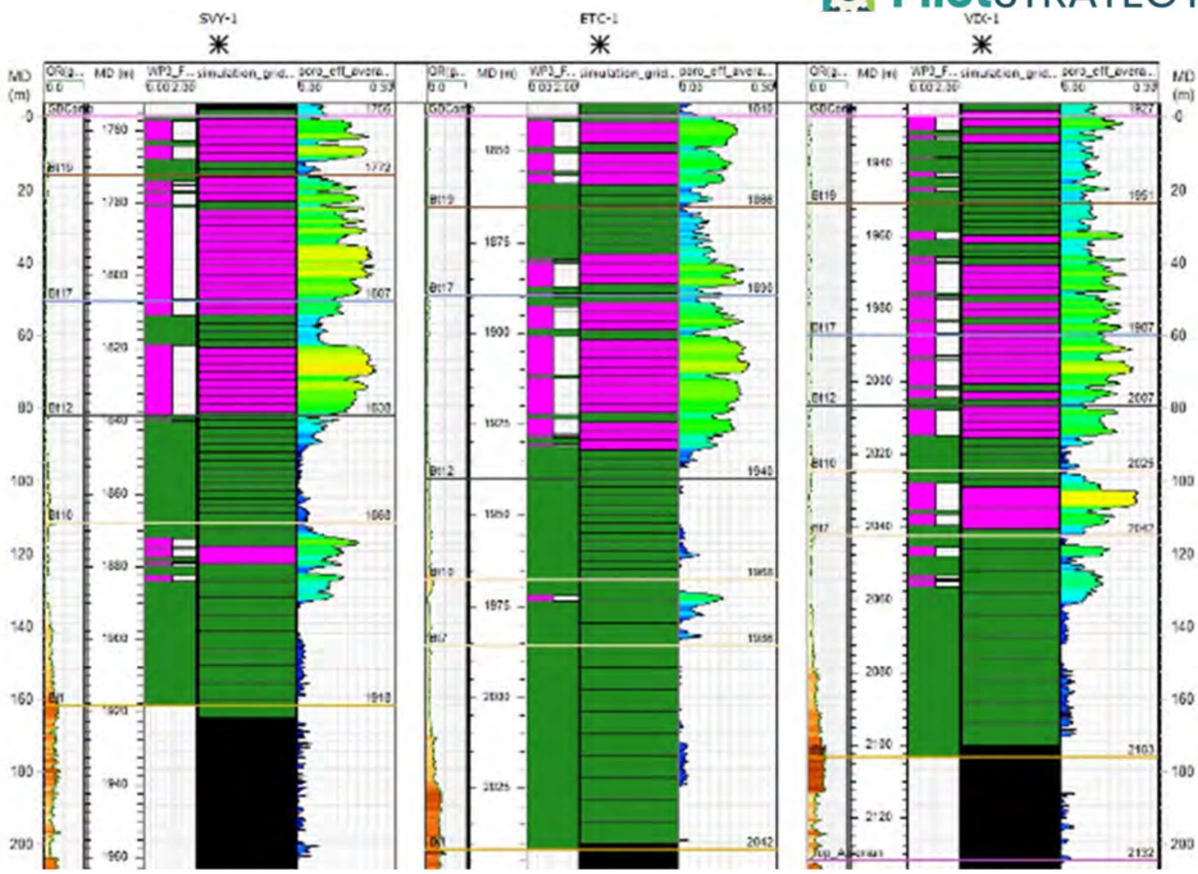

Figure 3.23 Result of the facies modelling on a well section window. The 2 facies classes distinguish well the intervals with high porosity, which are of interest for the CO2 injection.

3.4.2 Porosity filling

The Sequential Gaussian Simulation is used to distribute the porosity in the 3D grid. In the Oolithe Blanche formation this is done by facies, in the other formations it is just done per formation.

The mandatory data are:

- The well log porosity information discretized in the grid. This data is always respected.
- The distribution of porosity for each formation and facies.
- Variogram models of porosity by formation and facies.

SGS is a stochastic simulation which can capture extreme values better in a heterogenous reservoir than for example kriging. Multiple realizations can be run which will each be slightly different but present the same statistics and are equiprobable. In this algorithm, global features and statistics are more honored that local accuracy and randomness is introduced in the modeling (compared to kriging). For simplicity reasons, only one simulation result is presented here. Uncertainty is quantified in a later step regarding uncertainty analysis.

3.4.2.1 Discretization of porosity in the grid

The porosity logs are upscaled on the grid using an arithmetic mean.

Upscaled facies are used as a constraint in the calculation for the Oolithe Blanche formation. The use of facies contain ensures that the porosity assigned to each cell is in accordance with the facies value of that cell. In this way, the discretized porosity on the grid is consistent with the discretized facies.

The PilotSTRATEGY project has received funding from the European Union's Horizon 2020 research and innovation programme under grant agreement No. 101022664

The results are controlled with histogram and sections at the wells (see figure 3.24, figure 3.27, figure 3.28, figure 3.29).

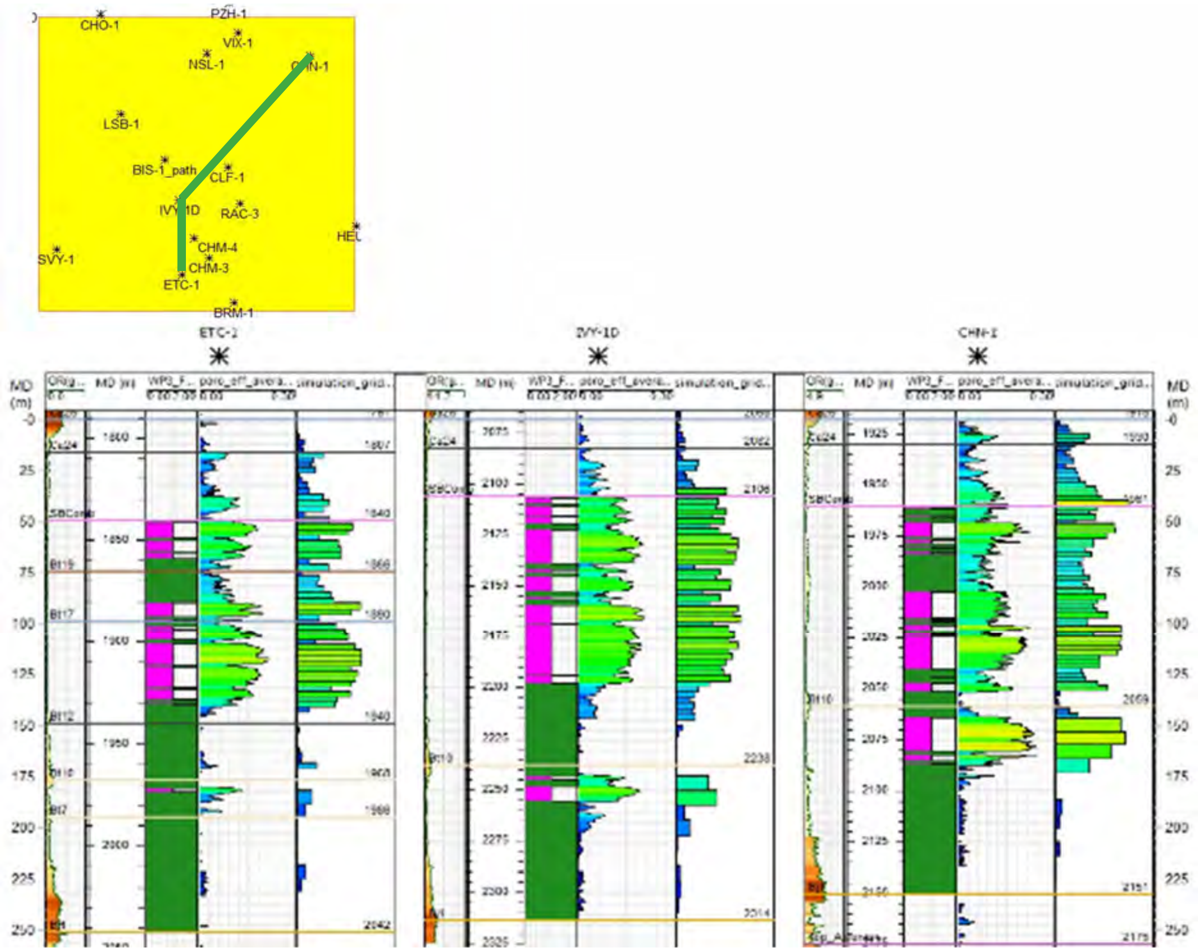

Figure 3.24 Well cross section through the reservoir showing the final simulation of porosity. Comparison of porosity logs before (left) and after (right) upscaling (example of section with 3 wells)

The results are of very good quality for all intervals. The proportions and vertical heterogeneities of porosity are well represented at the scale of the grid. No statistical bias is introduced during this operation.

This step also serves as a quality control for the vertical layering of the simulation grid. If the heterogeneities of porosities had not been well represented after upscaling, it would have been necessary to review the vertical layering to define a more appropriate one.

3.4.2.2 Variographic analysis

Experimental variograms of porosity by facies and for each formation were calculated. Before the variogram analysis, 1D trends were removed from the data and analysis only carried out on the residual.

Vertical variograms were calculated and could be fitted with confidence for each formation and facies. However, it was difficult to calculate robust horizontal variograms (only 13 wells for 900 km^2) and possible anisotropies.

For the Oolithe Blanche the same horizontal variogram parameters were used as during the facies characterization. For the Dalle Nacrée, information from Vermillion was used: no reservoir

The PilotSTRATEGY project has received funding from the European Union's Horizon 2020 research and innovation programme under grant agreement No. 101022664

communication above several hundred of meters is found in the reservoirs operated by Vermillion in proximity in the same formation. Therefore, an omnidirectional variogram with a horizontal range of 300m was used. For the Comblanchien, no other info was available. As the formation is a lagoonal depositional environment, larger horizontal variogram ranges were assumed and an omnidirectional variogram with 1000m as range was chosen.

It was possible to calculate the vertical ranges based on the data (figure 3.8 in the appendix).

The table below lists the calculated and estimated variogram ranges used for each formation and facies:

Formation	Direction	Vertical range [m]	Major direction [m]	Minor direction [m]
Dalle Nacrée	omnidirectional	7	300	300
Comblanchien	omnidirectional	5	1000	1000
Oolithe Blanche – high porosity facies	45 N	7.8	3000	1000
Oolithe Blanche – low porosity facies	45 N	9.5	3000	1000

Table 3.4 Variogram parameters for the porosity distribution

3.4.2.3 Vertical trend curves

Vertical trend curves or VTCs are tools that give an estimate of the porosity for each layer. The proportions are represented in the form of bars, stacked on top of each other. The proportions are calculated from the porosity upscaled at the wells. They are used then to constrain later, either the construction of a 3D constraints for a given formation, or directly the modeling of porosity.

The VTC used for the formations in the model are shown in figure 3.25.

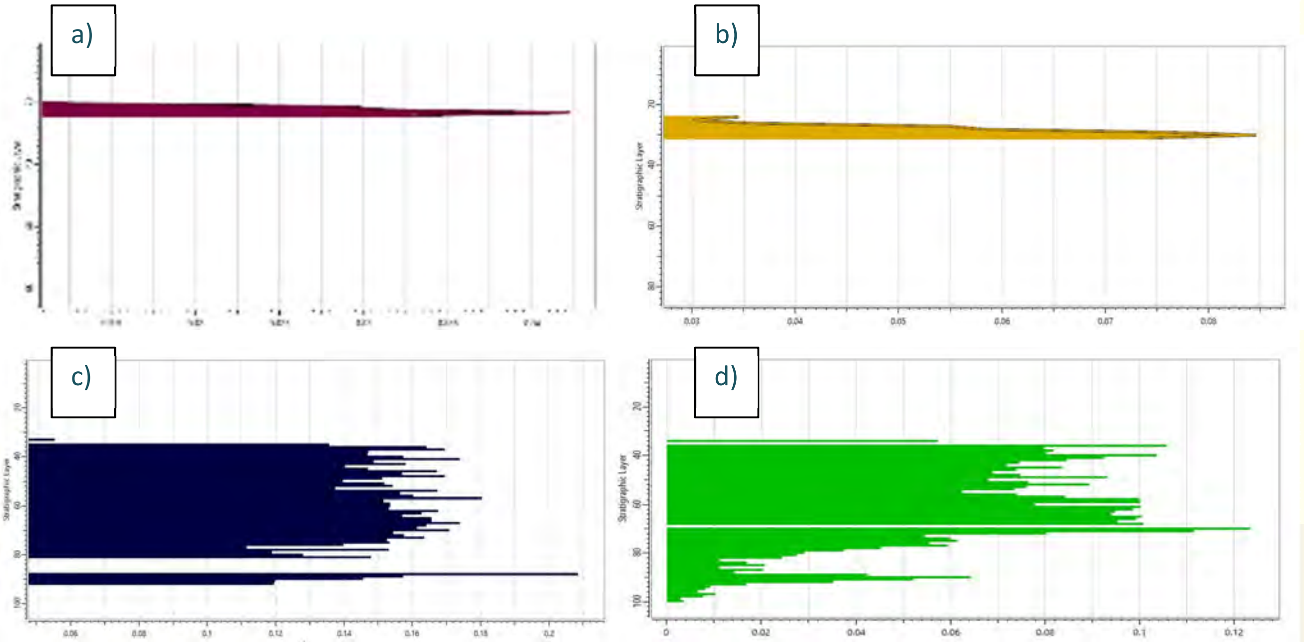

Figure 3.25 VTCs for the formations (a) Dalle Nacrée (b) Comblanchien (c) Oolithe blanche high porosity facies (d) Oolithe blanche low porosity facies

The PilotSTRATEGY project has received funding from the European Union's Horizon 2020 research and innovation programme under grant agreement No. 101022664

3.4.2.4 2D trend maps

2D trend maps are tools that give an estimate of the porosity spatially. The proportions are calculated from the porosity upscaled at the wells (figure 3.26). They are used then to constrain later, either the construction of a 3D constraints for a given formation, or directly the modeling of porosity.

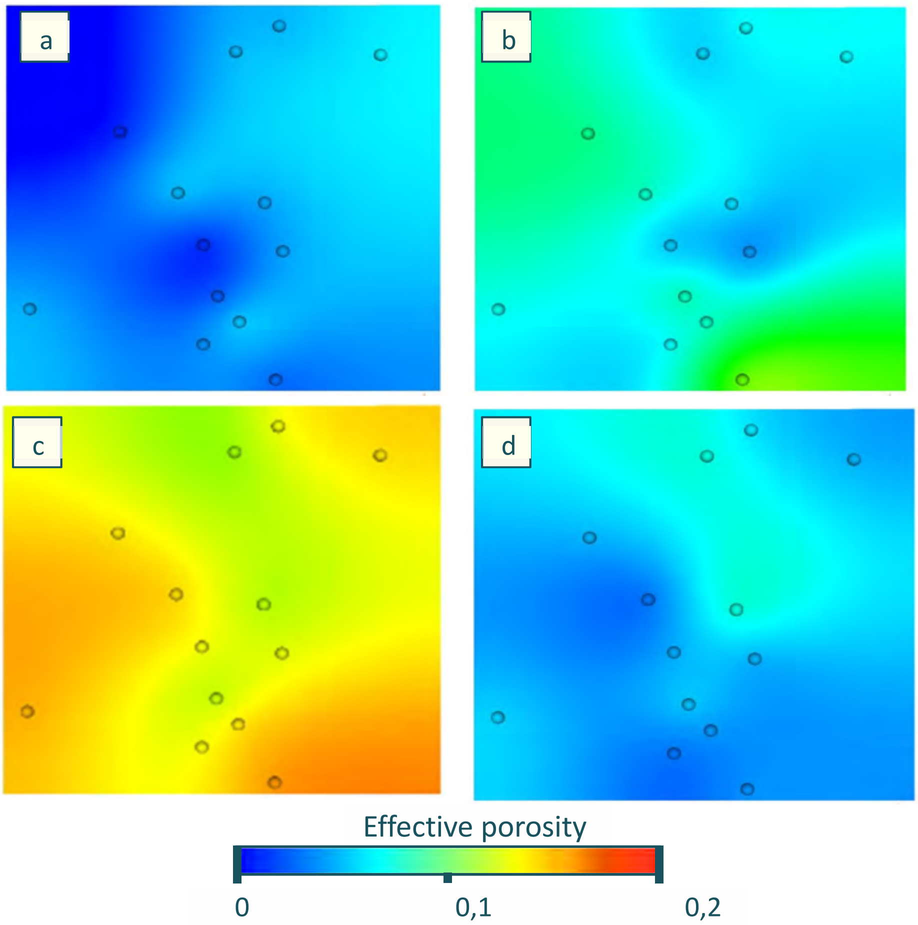

Figure 3.26 2D trends found in the data for effective porosity per formation, (a) Dalle Nacrée (b) Comblanchien (c) Oolithe blanche high porosity facies (d) Oolithe blanche low porosity facies.

3.4.2.5 Construction of 3D trends

The DTA module in Aspen SKUA allows to combine 1D and 2D trends into a 3D trend of porosity, which will serve as a trend in the algorithm of porosity modeling.

3D trends were used to model the porosity.

3.4.2.6 Result analysis

The distribution of porosity simulated by formation (figures 3.30 and 3.31) respects the porosity distributions imposed as input.

3.4.2.6.1 Oolithe Blanche formation

The porosity for the Oolithe Blanche formation was simulated by facies (high porosity / low porosity) which was defined with a cutoff at 11%.

The PilotSTRATEGY project has received funding from the European Union's Horizon 2020 research and innovation programme under grant agreement No. 101022664

For both facies, the global porosity distribution from the log data was honored and reproduced globally and at the well location. Statistical values of the literature were reproduced. For the spatial distribution, hard data at well location and variography data was honored (figure 3.27 and table 3.5).

	High porosity facies			
	Log data	**Blocked data**	**Simulated results**	*Delmas et al 2012*
Samples:	5479	351	367818	
Minimum:	0.110	0.053	0.055	
Median:	0.155	0.153	0.160	0.145
Maximum:	0.312	0.312	0.312	0.268
Mean:	0.157	0.155	0.163	
	Low porosity facies			
Samples:	9313	427	522119	
Minimum:	0	0	0	
Median:	0.02	0.038	0.014	
Maximum:	0.109	0.109	0.109	
Mean:	0.035	0.043	0.035	

Table 3.5 Statistical comparison of the modelling results for porosity of the Oolithe Blanche Formation

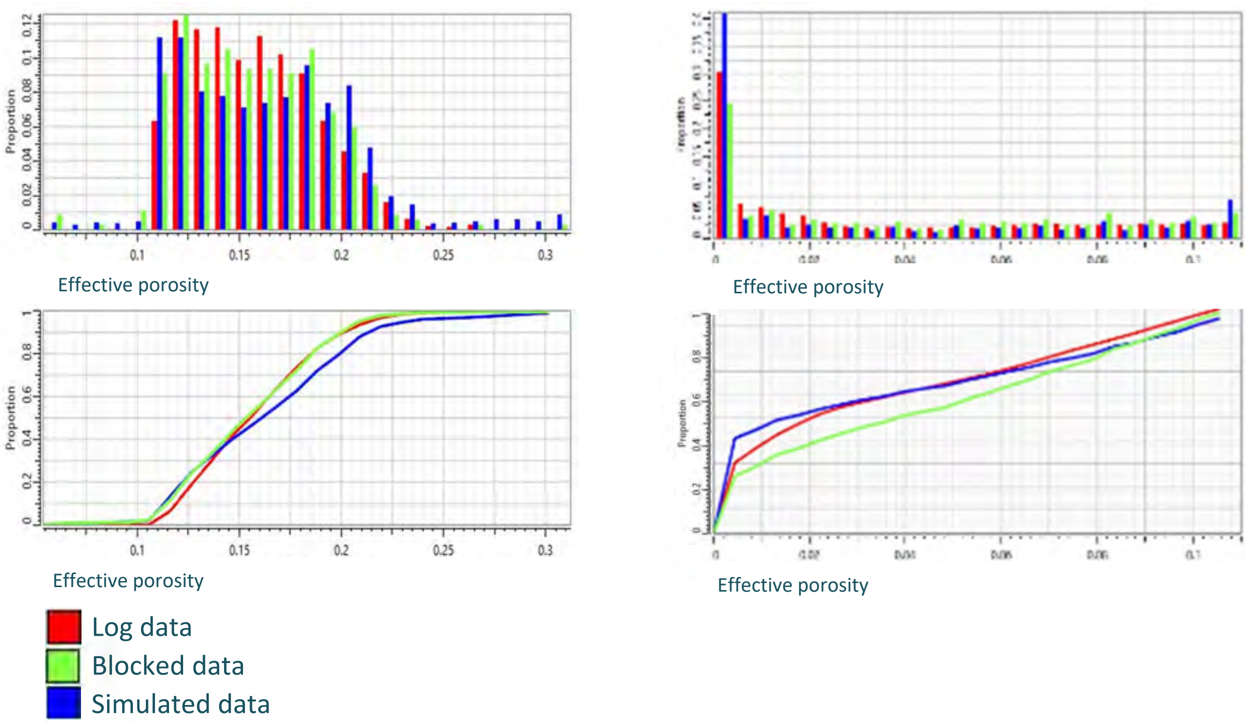

Figure 3.27 Porosity distribution for the Oolithe blanche formation of the log data (red), blocked data (green) and one simulated result (blue). Left high porosity facies, right low porosity facies.

3.4.2.6.2 Comblanchien formation

For the Comblanchien formation, the distribution of the simulated porosity respects the porosity distribution imposed as input from the log data and blocked data. The overall statistics are well respected. For the spatial distribution hard data at well location and variography data was honored (figure 3.28 and table 3.6).

	Log data	**Blocked data**	**Simulated results**	*Delmas et al 2012*
Samples:	1974	104	115200	
Minimum:	0	0.002	0	
Median:	0.045	0.046	0.049	
Maximum:	0.199	0.207	0.207	0.22
Mean:	0.054	0.057	0.059	0.06

Table 3.6 Statistical comparison of the modelling results for porosity of the Comblanchien Formation

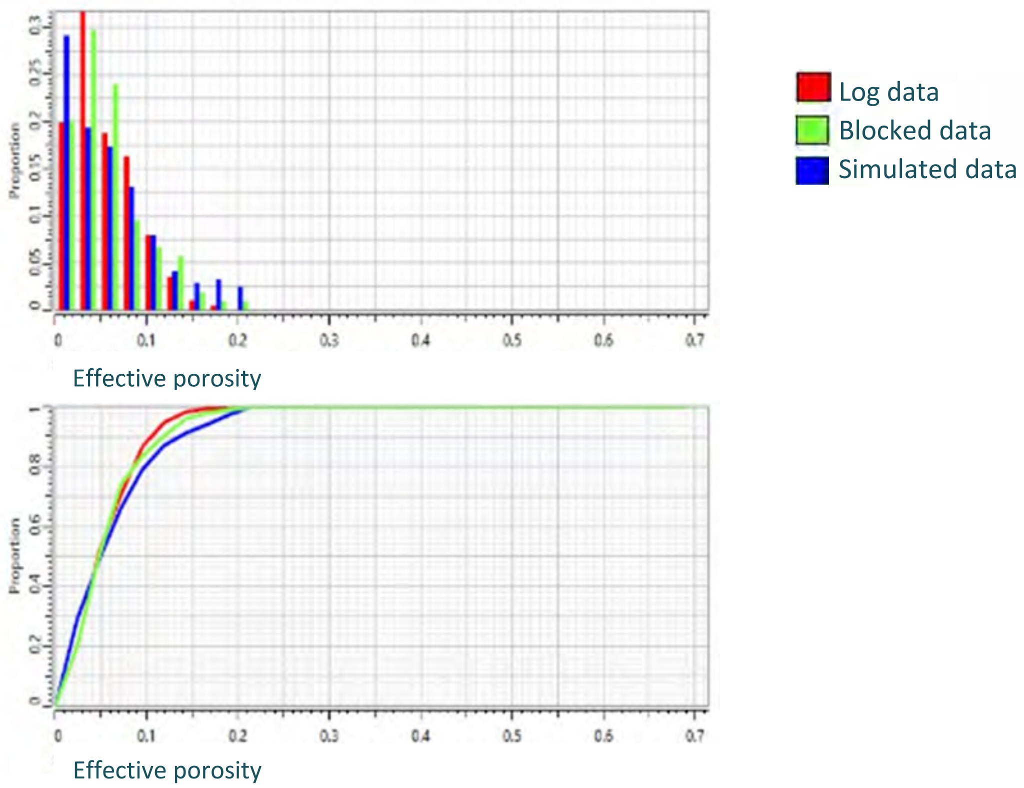

Figure 3.28 Porosity distribution for the Comblanchien formation of the log data (red), blocked data (green) and one simulated result (blue).

3.4.2.6.3 Dalle Nacrée formation

For the Dalle Nacrée formation the distribution of the simulated porosity respects the porosity distribution imposed as input from the log data and blocked data. The overall statistics are well respected. Maximum values as seen in the log data of 23% were not captured in the blocked data neither in the simulation data. Looking at the histogram distribution the amount of such high values is very small (<1%) and therefore not captured in the upscaling process to produce the blocked data. Delmas et al (2012) found a higher mean value of the formation that this study. The reason is a difference at where the marker Top_Dalle_Nacrée is positioned. In Delmas et al (2012), it is below the shaly interval of the Callovo Oxfordian Marls, in this study the marker was positioned inside the marly interval, therefore the mean porosity value is lower.

The PilotSTRATEGY project has received funding from the European Union's Horizon 2020 research and innovation programme under grant agreement No. 101022664

For the spatial distribution hard data at well location and variography data was honored (figure 3.29, table 3.7).

	Log data	Blocked data	Simulated results	*Delmas et al 2012*
Samples:	1230	104	115200	
Minimum:	0	0	0	
Median:	0.017	0.025	0.025	0.02
Maximum:	0.231	0.1	0.101	0.19
Mean:	0.026	0.029	0.031	0.055

Table 3.7 Statistical comparison of the modelling results for porosity of the Dalle Nacrée Formation

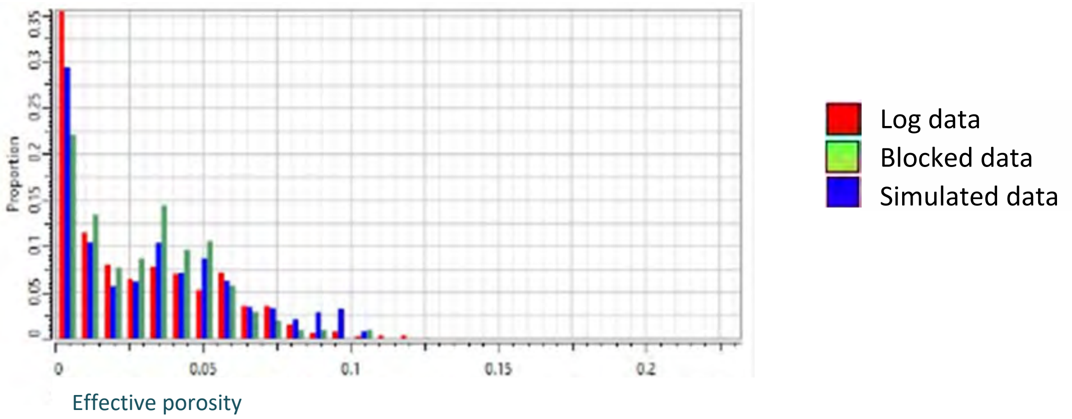

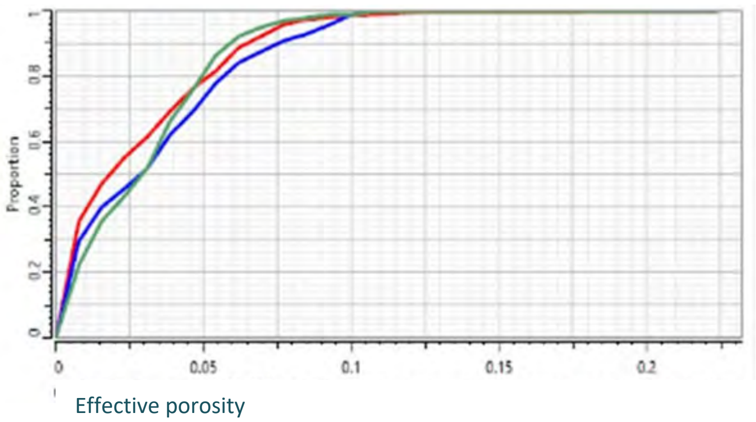

Figure 3.29 Porosity distribution for the Dalle Nacrée formation of the log data (red), blocked data (green) and one simulated result (blue).

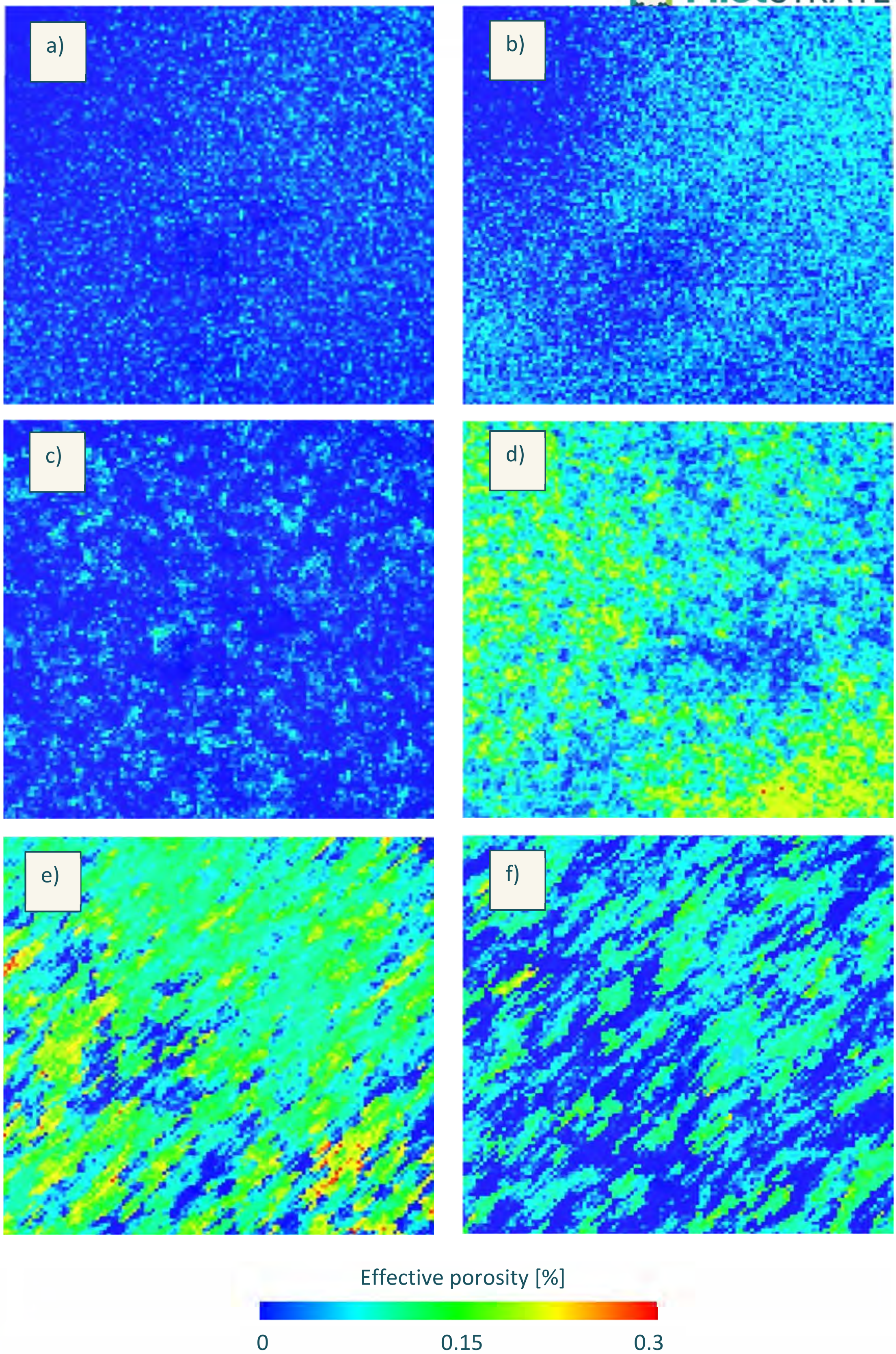

*Figure 3.30 Result of **one realization** of porosity field with SGS algorithm. Dalle Nacrée formation (a K= 22, b K=29), Comblanchien formation (c K=30, d K=37), Oolithe blanche formation (e K=38, f K=91)*

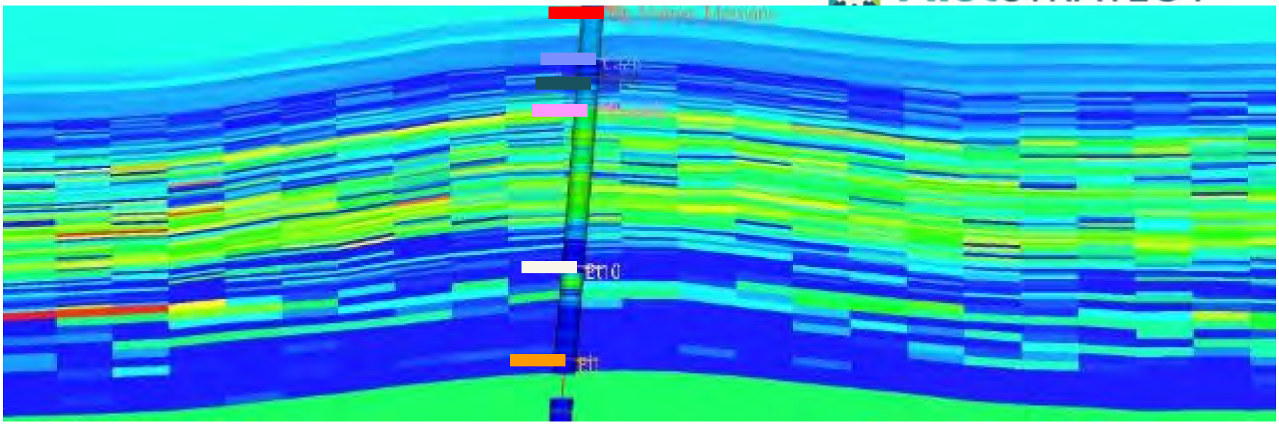

Figure 3.31 Result of one realization of the porosity field with SGS algorithm, cross section at the well IVY-1D (I=74). Well tops indicated with bars: red = top Marnes de Massingy, purple = top Dalle Nacrée, black = top Comblanchien, pink = top Oolithe blanche, white = top Bt10, orange = top Bajocian

3.4.2.6.4 Seal – Marnes de Massingy

The Marnes de Massingy represent the caprock. Only minimal data was available from this formation in form of plugs. The formation is brittle which makes sample taking challenging.

Concerning the porosity, 4 samples were taken in D2.6 from 2 wells. One well is in the extension of the model area (CHM-4) and one close by (VUS-1).

	Name	Well	Depth (m)	Porosity (%)	Kw (µD)	PE (bar)
4856	CHM4_C1_1800,5	Charmottes 4	1800.5	8%	0.4	~ 0,5
4857	CHM4_C1_1803,25	Charmottes 4	1803.25	4%	0.8	~ 1
4866	VUS1_c6_1843,45	Vulaines 1	1843.45	4%	0.007	42 - 46
4867	VUS1_c6_1844,05	Vulaines 1	1844.05	5%	5	1.0 – 1.5

Table 3.8 Results of water permeability Kw and entry pressure PE measurements on caprock samples from Charmottes 4 and Vulaines 1 wells. Data from WP2 task D2.6

Minimum, maximum, and mean values for porosity were calculated from those 4 samples (min = 4%, max = 8%, mean = 5.25%).

The porosity distribution for the Marnes de Massingy was calculated by creating a distribution using a random function for the well log. A normal law was defined with a mean of 5% and a standard deviation of 1% (to avoid samples with too low values).

The porosity was populated in the grid using the SGS algorithm. Input data was the created log, and property distribution curve and a variogram. The Marnes de Massigny formation represents transgressive interval producing a very homogenous marly geological layer which can be followed over long distances in the Paris Basin. Therefore, an omni direction was chosen. A vertical range of 36m was chosen, which represents the average thickness of the seal. Major and minor direction are 15.000m, which represents half of the model size and the maximum range possible for the variogram

The PilotSTRATEGY project has received funding from the European Union's Horizon 2020 research and innovation programme under grant agreement No. 101022664

parameters. A high range was selected for both vertical and horizontal variogram parameters, as the Marnes de Massingy represent a uniform layer.

Formation	Direction	Vertical range [m]	Major direction [m]	Minor direction [m]
Marnes de Massingy	omnidirectional	36	15000	15000

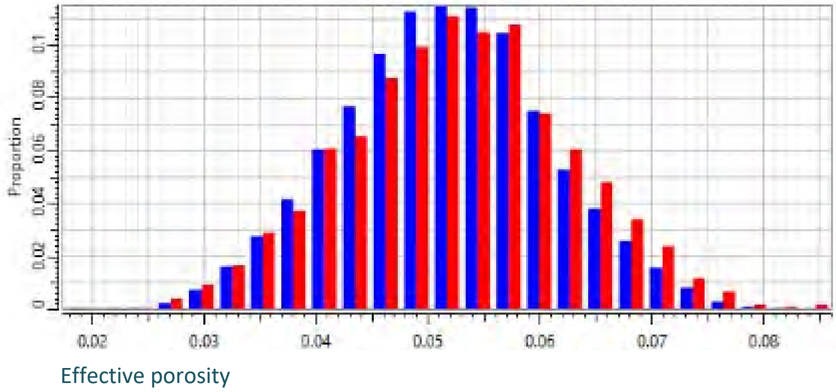

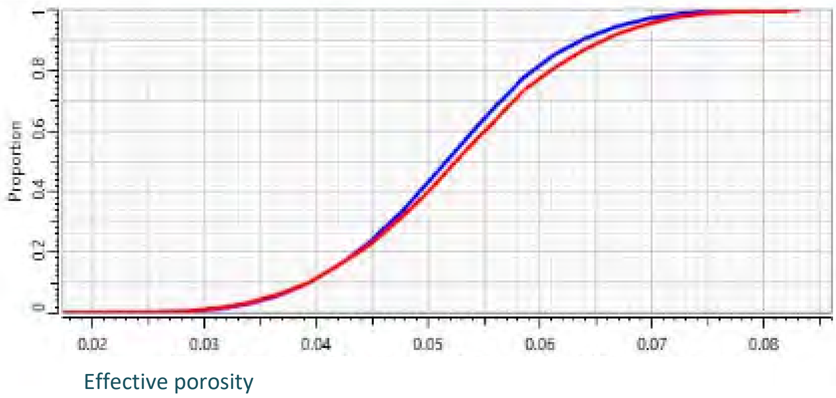

Figure 3.32 Simulated effective porosity for the Marnes de Massingy formation. Log data in red, simulated results in blue.

	Log data	**Simulated results**
Samples:	2405	100800
Minimum:	0.017	0.017
Median:	0.052	0.051
Maximum:	0.086	0.085
Mean:	0.052	0.051

Table 3.9 Statistical comparison of the modelling results for porosity of the Marnes de Massingy Formation

The PilotSTRATEGY project has received funding from the European Union's Horizon 2020 research and innovation programme under grant agreement No. 101022664

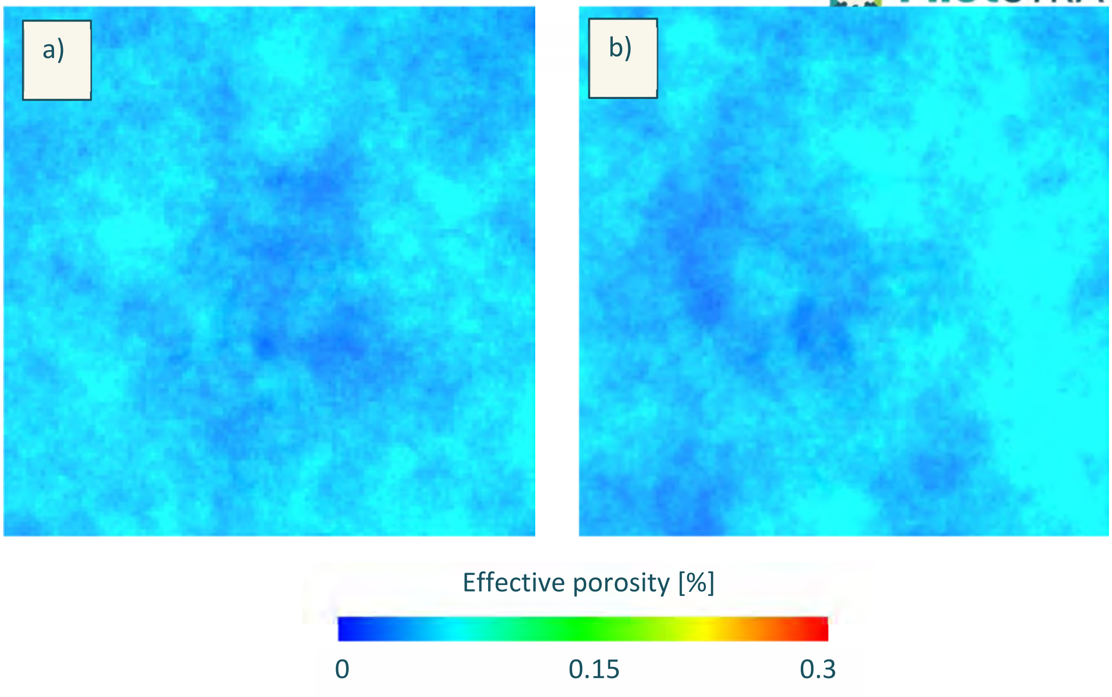

Figure 3.33 Result of one realization of the porosity field with SGS algorithm. Marnes de Massingy formation (a K= 15, b K=22).

3.4.3 Permeability modeling

K-Φ laws were determined to model the 3D permeability property based on the available plug samples. It must be noted that all the available samples were used, also from wells which are not inside the grid. This decision was taken as there were not enough available samples from wells inside the model area.

The K-Φ laws, used in Aspen SKUA, are as follows (see Figure 3.34):

- Oolithe Blanche (high porosity facies): $K = 0.8226e^{0.2009(\Phi)}$ $\log_{10} \mathrm{K} = 20.4332*\varphi - 0.75797$
- Oolithe Blanche (low porosity facies): $K = 0.0261e^{0.5305(\Phi)}$ $\log_{10} \mathrm{K} = 20.4332*\varphi - 0.75797$
- Comblanchien: $K = 0.1047e^{0.334(\Phi)}$
- Dalle Nacrée: $K = 0.2305e^{0.1852(\Phi)}$

Data on K-Φ plots are largely dispersed for all the formations (see figure 3.34). For example, in the Dalle Nacrée formation for a porosity of 2.5% permeability can reach values between 0.1 and 80 mD. In the Comblanchien formation plug samples of 10% porosity can have permeability values ranging from 0.5 – 100 mD. In the Oolithe Blanche formation for a porosity of 15% the permeability can be between 1 – 1000 mD. This large heterogeneity in permeability is explained by diagenesis in the Dogger carbonate reservoir and a known issue in the Paris Basin (Delmas et al 2012). The permeability calculation based on the K-Φ laws can only represent average values but will not capture the great variability. Due to limited amount of data in the Zone of Interest, a linear approach to calculate permeability seems like the best compromise.

The PilotSTRATEGY project has received funding from the European Union's Horizon 2020 research and innovation programme under grant agreement No. 101022664

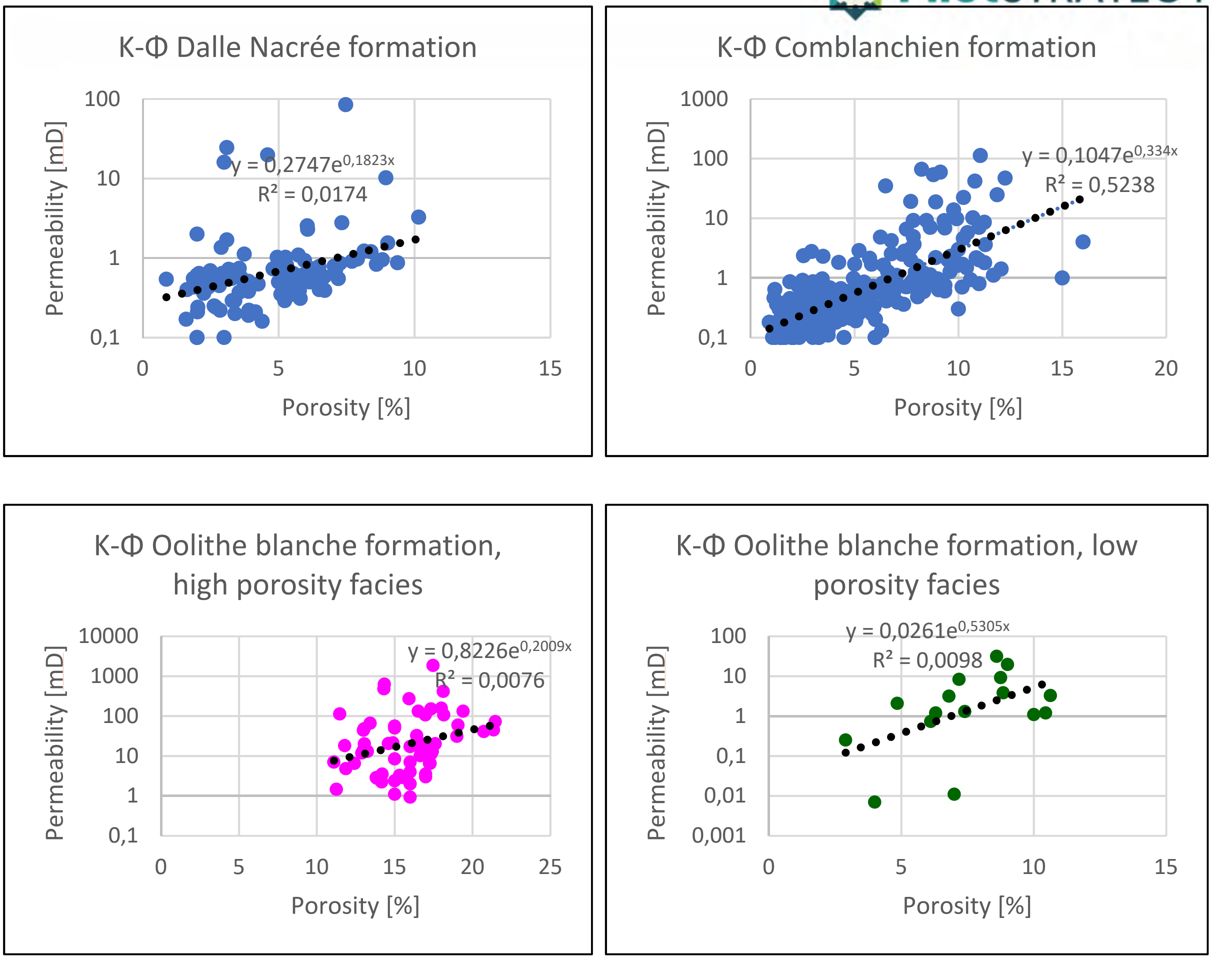

Figure 3.34 K-Φ scatter plots for the Dalle Nacée, Comblanchien and Oolithe blanche formations

We compared the simulation made with the used K-Φ laws to the plug data present in the grid. Wells inside the grid with plug data are CHM-4, CHN-1, IVY-1D and VIX-1.

The statistics show that for the whole reservoir (Dalle Nacrée, Comblanchien and Oolithe Blanche both facies) the K-Φ laws were able to reproduce the distribution seen on the plug data. However, the K-Φ laws tend to underestimate permeabilities between 0.1 – 1 mD and overestimate permeabilities around 100mD over the whole scale of the reservoir (table 3.10 and figure 3.35, also figure 3.9 in appendix).

It must be kept in mind that the reservoir is carbonates and that they underwent diagenesis leading to heterogeneities of the permeabilities. Despite long lasting efforts since the pioneer work of Purser 1972 of the first model of the Dogger carbonate platform, there is no existing model available to statistically deducing reservoir properties from sediment description in carbonates. This is not only true for the Paris Basin, but for most carbonate series. Carbonate rocks resist analytical methods compared to siliciclastic rocks do to two causes: the importance of biogenic processes and environmental parameters in their edification as well as deposition and the strong effects of diagenesis on the mineral composition and therefore on reservoir properties (Delmas et al 2012).

The PilotSTRATEGY project has received funding from the European Union's Horizon 2020 research and innovation programme under grant agreement No. 101022664

	Permeability plug data (mD)	Simulated permeability (mD)
Samples:	157	1221137
Minimum:	0.02	0.070
Median:	1.7	2.225
Maximum:	1855.31	1180.6
Mean:	26.249	31.424

Table 3.10 Comparison of permeability plug data and one simulated permeability realization for the wells present in the model area (CHM-4, CHN-1, IVY-1D and VIX-1).

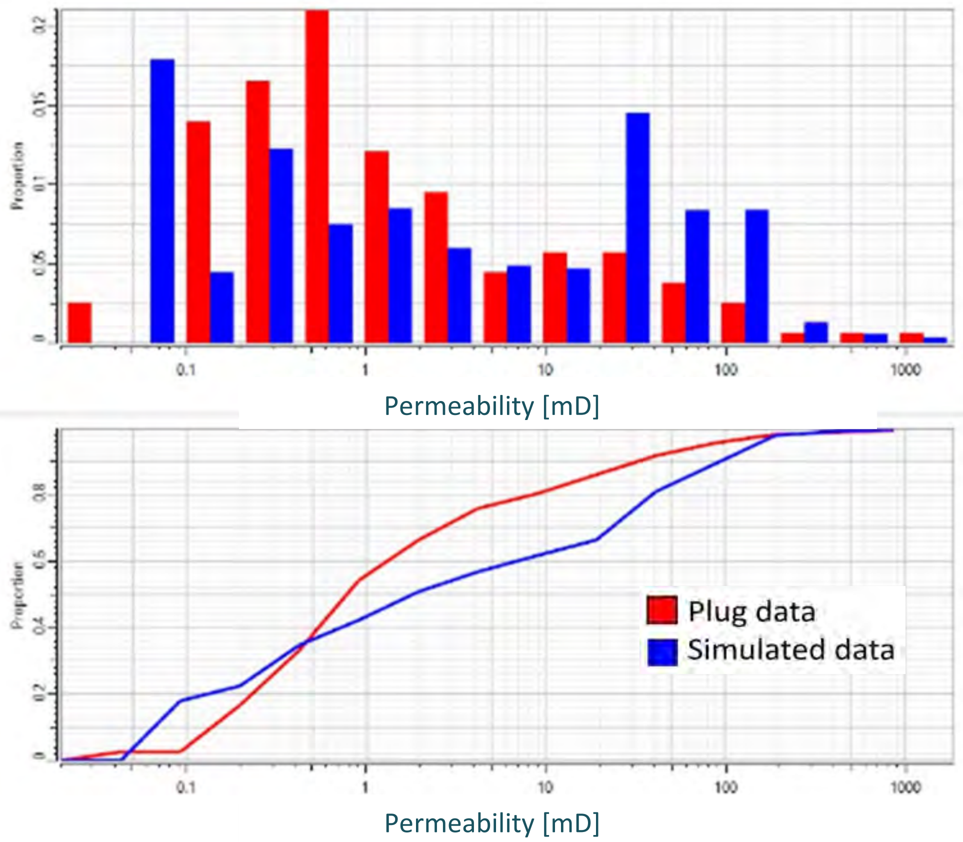

Figure 3.35 Comparison from plug data inside the model area (wells CHM-4, CHN-1, IVY-1D, VIX-1) and one simulated result of permeability field with the K-Φ laws

The PilotSTRATEGY project has received funding from the European Union's Horizon 2020 research and innovation programme under grant agreement No. 101022664

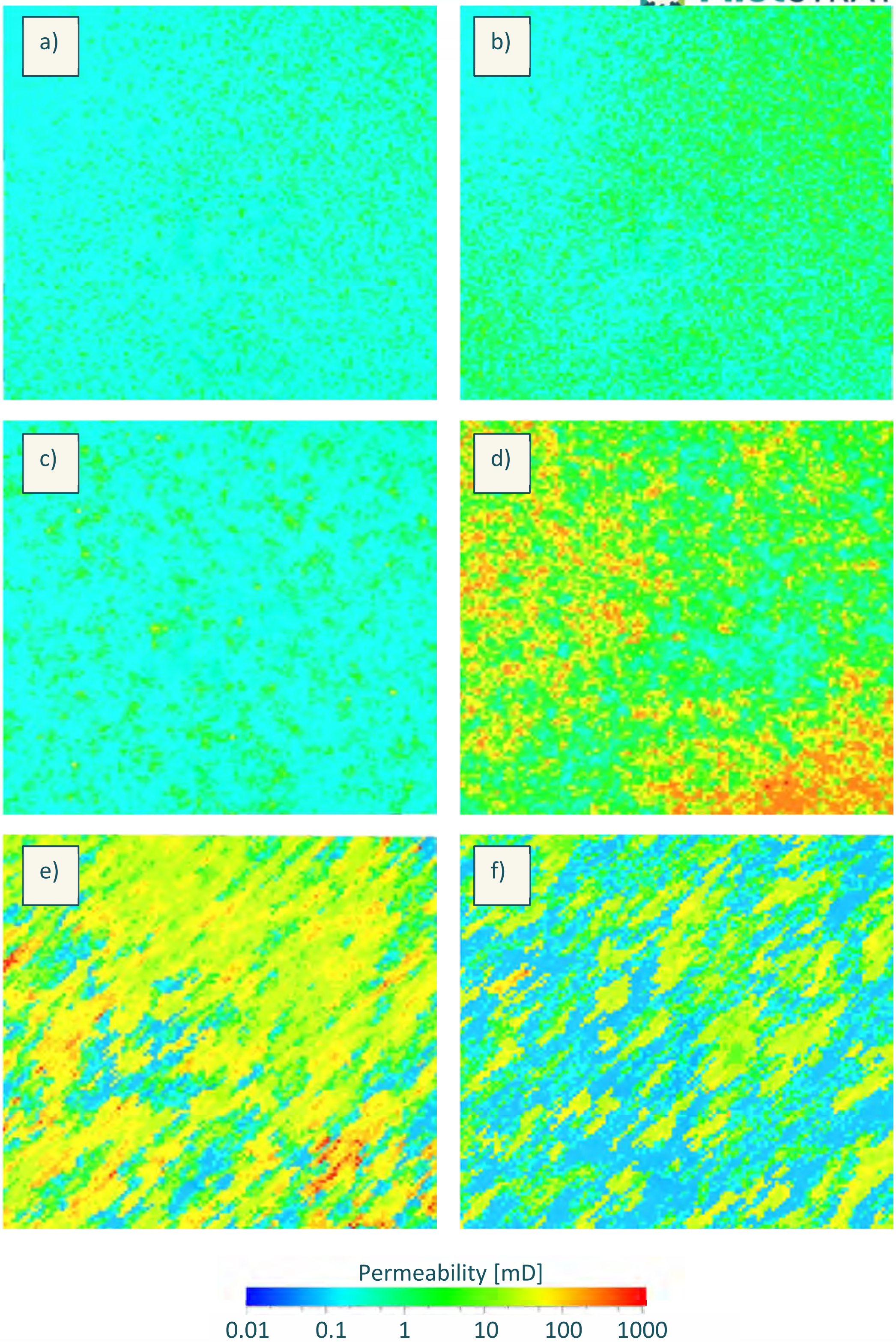

Figure 3.36 Result of one realization of the permeability field based on the K-Φ laws. Dalle Nacrée formation (a K= 22, b K=29), Comblanchien formation (c K=30, d K=37), Oolithe blanche formation (e K=38, f K=91)

The PilotSTRATEGY project has received funding from the European Union's Horizon 2020 research and innovation programme under grant agreement No. 101022664

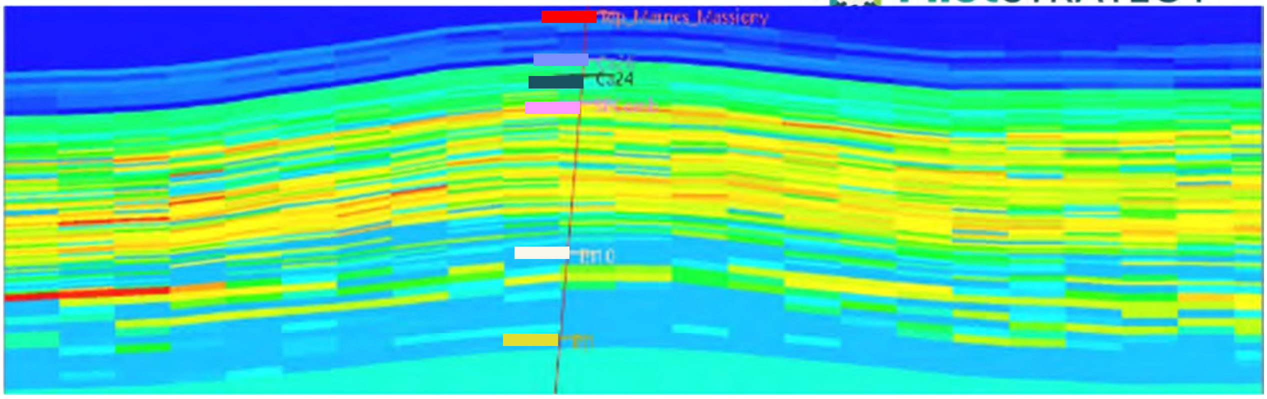

Figure 3.37 Result of one realization the permeability field based on K-Φ laws, cross section at the well IVY-1D (I=74). Well tops indicated with bars: red = top Marnes de Massingy, purple = top Dalle Nacrée, black = top Comblanchien, pink = top Oolithe blanche, white = top Bt10, orange = top Bajocian

3.4.3.1 Oolithe Blanche formation

For the high porosity facies, the distribution of the simulated permeability values, following the K-Φ law, is in the same order of magnitude compared to one of the 28 samples of plug data in the studied area. However, permeabilities below 10mD seem to be underrepresented. When looking at the original K-Φ distribution with plug data also from outside the studied area, also high permeability values seem to be underrepresented (table 3.11).

	Oolithe blanche high porosity facies	
	Permeability plug data (mD)	**Simulated permeability (mD)**
Samples:	28	367818
Minimum:	2.07	6.792
Median:	19.748	56.130
Maximum:	630.08	1180.6
Mean:	64.811	94.281

Table 3.11 Comparison of permeability plug data and one simulation of permeability values for the Oolithe blanche high porosity facies for the wells present in the model area (CHM-4, CHN-1, IVY-1D and VIX-1).

Only 4 plug samples for the low porosity facies in the Oolithe Blanche were available in the grid area from wells IVY-1D and VIX-1 which makes it challenging to extract meaningful statistical information. The mean value for the permeability was well represented in the simulation with the K-Φ law (table 3.12).

	Oolithe blanche low porosity facies	
	Permeability plug data (mD)	**Simulated permeability (mD)**
Samples:	4	522119
Minimum:	2.86	0.070
Median:	3.297	0.155
Maximum:	4.81	24.198
Mean:	3.615	3.603

Table 3.12 Comparison of permeability plug data and one simulation of permeability values for the Oolithe blanche low porosity facies for the wells present in the model area (CHM-4, CHN-1, IVY-1D and VIX-1).

The PilotSTRATEGY project has received funding from the European Union's Horizon 2020 research and innovation programme under grant agreement No. 101022664

3.4.3.2 Comblanchien formation

For the Comblanchien formation, the permeability simulation following the K-Φ law reproduced statistically the values in the same order of magnitude compared to the 88 samples of plug data in the grid. The maximum value of 1855mD in the plug data seems to be not right for the Comblanchien formation. It is situated at 1926.95 MD just above the marker for the Top Oolithe Blanche which is at 1927 MD. In the analysis to establish the K-Φ law this value was selected to be in the Oolithe Blanche formation. Overall, there seems to be a slight underrepresentation by simulation of the permeability values below 0.1mD (table 3.13).

	Comblanchien formation	
	Permeability plug data (mD)	**Simulated permeability (mD)**
Samples:	88	115200
Minimum:	0.02	0.284575
Median:	1.43724	1.94894
Maximum:	1855.31	289.004
Mean:	24.615	13.9763

Table 3.13 Comparison of permeability plug data and one simulation of permeability values for the Comblanchien formation for the wells present in the model area (CHM-4, CHN-1, IVY-1D and VIX-1).

3.4.3.3 Dalle Nacrée formation

For the Dalle Nacrée formation the permeability simulation following the K-Φ law produced a permeability distribution which is between 1 and 10 mD. However, the heterogeneity of the Dalle Nacrée formation could not be captured but instead is represented with a mean value in the same order of magnitude than the plug samples (table 3.14).

	Dalle Nacrée formation	
	Permeability plug data (mD)	**Simulated permeability (mD)**
Samples:	36	115200
Minimum:	0.03	0.746
Median:	0.557	1.206
Maximum:	84.47	4.707
Mean:	3.449	1.552

Table 3.14 Comparison of permeability plug data and one simulation of permeability values for the Dalle Nacrée formation for the wells present in the model area (CHM-4, CHN-1, IVY-1D and VIX-1).

3.4.3.4 Seal - Marnes de Massingy

Permeability data were available from the task D2.6 with 4 values, of which 2 are from a well outside the zone (see Table 3.8). An average value for the well SOU 101 was also available (0.05 mD).

A synthetic well log was created for the permeability using a random function based on a uniform law between min (0.00001) and max (0.05) values. Here the permeability and porosity are not correlated, also due to the lack of available hard data points. Next, the permeability was distributed in the grid using the SGS algorithm. Input data were the log data, the external distribution and the variogram. The same variogram as for the porosity modeling was used.

The PilotSTRATEGY project has received funding from the European Union's Horizon 2020 research and innovation programme under grant agreement No. 101022664

	Seal Marnes de Massingy formation	
	Permeability log data (mD)	Simulated permeability (mD)
Samples:	2857	100800
Minimum:	0.0001	0.001
Median:	0.024	0.03
Maximum:	0.049	0.049
Mean:	0.024	0.028

Table 3.15 Comparison of permeability log data created with a random uniform simulation and the simulated permeability for the Marnes de Massingy formation.

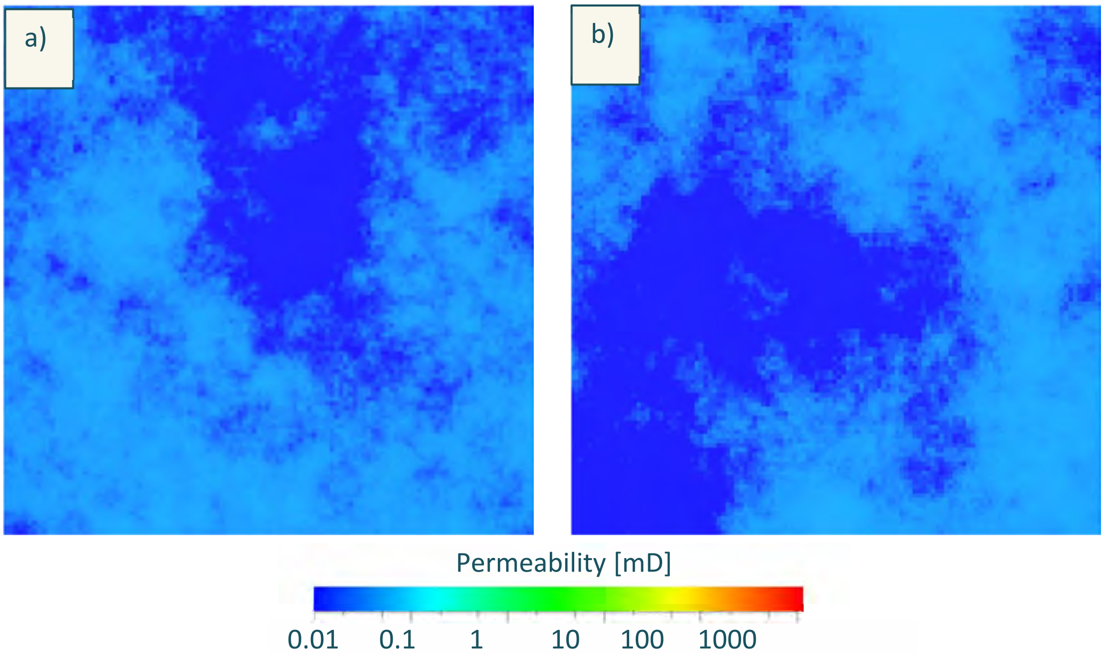

Figure 3.38 Modelling result for permeability field (one realization) using SGS algorithm in the Marnes de Massingy formation (a K= 15, b K=21).

3.4.4 Net-to-Gross

The Net-To-Gross (NtG) property has been modelled to distinguish the parts of the reservoir with the best potential for CO_2 storage in terms of available storage volume. NtG was calculated for the Oolithe blanche reservoir, which is the principal target for CO_2 injection.

NtG was originally developed in the oil- and gas industry to eliminate nonproductive parts of the reservoir to quantify hydrocarbons-in-place and flow calculations. In the oil- and gas industry the hydrocarbons are extracted from the reservoir but in CO_2 storage, the CO_2 is injected into the reservoir. This changes the mechanisms and therefore the calculations of how much pore space is considered 'net-pay'. Due to the injection process of CO_2, pore space is available to CO_2 storage which would not be considered net-pay in oil and gas. At depths below 800m the CO_2 is in supercritical state and has a liquid like density which provides high potential for efficient utilization and storage in the pore space of the saline aquifer (IPCC, 2005). The CO_2 can be stored underground using a variety of mechanisms. It can be trapped under a confining layer using the pore space between grains. It can also be retained as an immobile space between pore spaces and be dissolved in the reservoir fluids.

The PilotSTRATEGY project has received funding from the European Union's Horizon 2020 research and innovation programme under grant agreement No. 101022664

Here, the whole reservoir is considered Net and the whole pore space of the reservoir considered as accessible for the injected CO_2.

3.4.5 Over – and underburden

To correctly represent geomechanical behavior of the system, over – and underburden need to be taken into consideration. Over-and underburden were modeled also for this model in a simplified way. One K-Φ value per geological layer was assigned for the over- and the underburden. They are issue form a thermal basin model of the Paris Basin made with the software Temis Flow (https://www.beicip.com/temisflow). Temis Flow is a software for basin and petroleum systems modeling developed by IFP Energies Nouvelles and Beicip-Franlab. The details of the used K-Φ values can be found in table 3.6 in the appendix.

3.5 Uncertainty analysis

Uncertainty is addressed using the Jacta module in Aspen SKUA. This module is run on the stratigraphic grid containing the reservoir and various parameter sets can be selected.

The uncertainty was quantified by the workflow outlined below:

1. Identification of the uncertain parameter to quantify.
2. Identification of the stratigraphic target layer.
3. Selection of the parameters going into the uncertain analysis.
4. Final risk analysis with determination of deciles P10, P50, P90.

In this uncertainty analysis, the Net Porous Volume was selected as the targeted property/output that will be affected by the uncertainties in model properties. This Net Porous Volume indicates the volume available for CO_2 storage.

The Oolithe blanche formation was selected as the stratigraphic target unit. It has elevated porosity and largest thickness of the reservoir complex and is therefore selected as the principal storage unit.

Uncertainty analysis focuses on the facies percentage in the model and the mean for the porosity distribution.

The final risk analysis followed a Monte Carlo approach to determine the Net Porous Volume distribution and the deciles P10, P50 and P90.

3.5.1 3D facies distribution

For the 3D facies distribution, a modeling approach with SIS modeling algorithm was chosen. The same variogram parameters were chosen as used for the facies modeling. Uncertainty was put on the facies proportion with an uncertainty of 0.05. For the facies with the high porosity proportion is 0.45 and for low porosity facies is 0.55 based on the proportions of the facies modeling result (see section 3.4.1).

3.5.2 Net-to-Gross distribution

The full reservoir is considered as Net in the model. As the CO2 gets injected as supercritical fluid, the whole pore space is considered as available for CO2 storage. Therefore, the Net was set to 1 for the Oolithe blanche reservoir, meaning no cutoff for available pore space is applied.

The PilotSTRATEGY project has received funding from the European Union's Horizon 2020 research and innovation programme under grant agreement No. 101022664

3.5.3 Porosity distribution

The mean porosity for the high porosity facies is 15.6% and 4.4% for the low porosity facies. Uncertainty was modeled with a gaussian distribution for the high porosity facies using the above-mentioned mean value and a standard deviation of 0.02. The porosity was constrained to hard data and boundaries were set (min=11%, max=30%). For the low porosity facies, a uniform distribution was chosen for the mean with a minimum value of 0.01 and a maximum value of 0.043 (see Figure 3.39).

To model the porosity distribution an approach with collocated SGS was chosen to incorporate the 3D trend visible on the effective porosity distribution in the Oolithe Blanche formation. The correlation coefficient between the 3D trend and the hard data (blocked well data) was set to 0.76 a seen on the data (Figure 3.40)

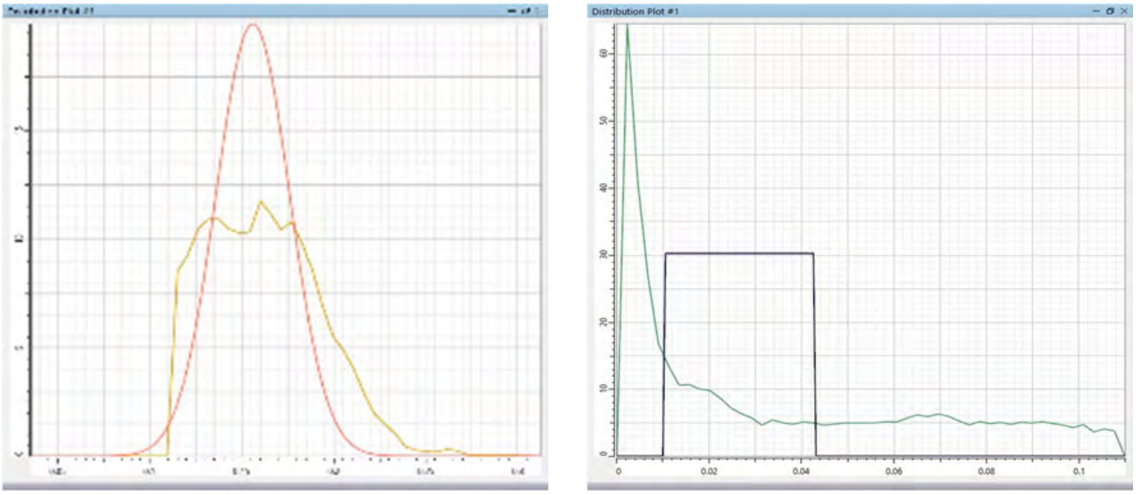

Figure 3.39 On the left-side high porosity facies: porosity distribution of the original data (red) and the uncertainty distribution (brown). On the right-side low porosity facies: porosity distribution of the original data (green) and the uncertainty distribution (blue)

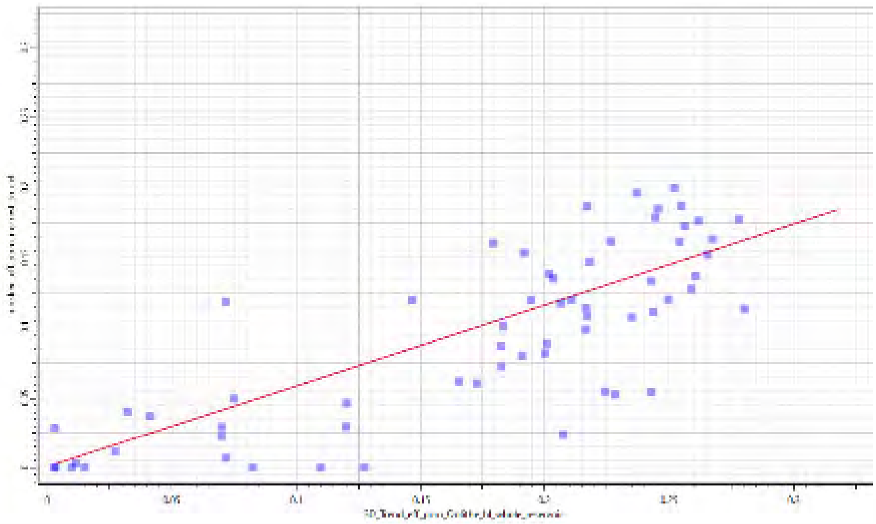

Figure 3.40 Correlation between 3D trend for effective porosity (x-axis) and blocked well data for effective porosity (y-axis) in the Oolithe Blanche formation. Correlation coefficient is 0.76.

The PilotSTRATEGY project has received funding from the European Union's Horizon 2020 research and innovation programme under grant agreement No. 101022664

Oolithe blanche formation Uncertainty Parameters					
	Distribution	**Min**	**Mean**	**Max**	**Sigma**
R1 Major range variogram	constant		3000		
R2 Minor range variogram	constant		1000		
R3 Vertical range variogram	constant		15		
Azimuth	Constant		45		
Mean porosity (high porosity facies)	Gaussian	0.11	0.156		0.02
Mean porosity (low porosity facies)	Uniform	0.01		0.043	

Table 3.16 Summary of uncertainty parameters Oolithe blanche formation

3.5.4 Results analysis

200 simulations were launched with the Jacta tool in the software Aspen SKUA to determine the Net Porous Volume range for percentiles P10, P50, P90. After about 150 simulations the distribution reaches a plateau (see figure 3.43), so 200 simulations have been judged enough simulations to have a reliable statistical robustness. The net porous volume is calculated in Jacta using the formula:

$$Net\ porous\ volume = Gross\ rock\ volume * Net - to - Gross * Porosity$$

Since the NtG is equal to 1 for the whole formation Oolithe Blanche, it can be removed from the formula.

Net porous volume varies between 8665 $10^6 m^3$ (P10) and 10562 $10^6 m^3$ (P90) in the 30x30 km^2 zone. Net porous volume varies between 1123 $10^6 m^3$ (P10) and 1369 $10^6 m^3$ (P90) in the 10x10 km^2 zone. The net porous volume distribution follows a gaussian distribution (see figure 3.10 appendix).

For the P90 scenario, the proportion of high porosities is higher compared to the P50 and P10 scenarios, leading to higher available net porous volume (see Figure 3.41). The same is true for permeabilities (see figure 3.42), as the permeabilities have been calculated using the same laws as described in section 3.4.3.

The PilotSTRATEGY project has received funding from the European Union's Horizon 2020 research and innovation programme under grant agreement No. 101022664

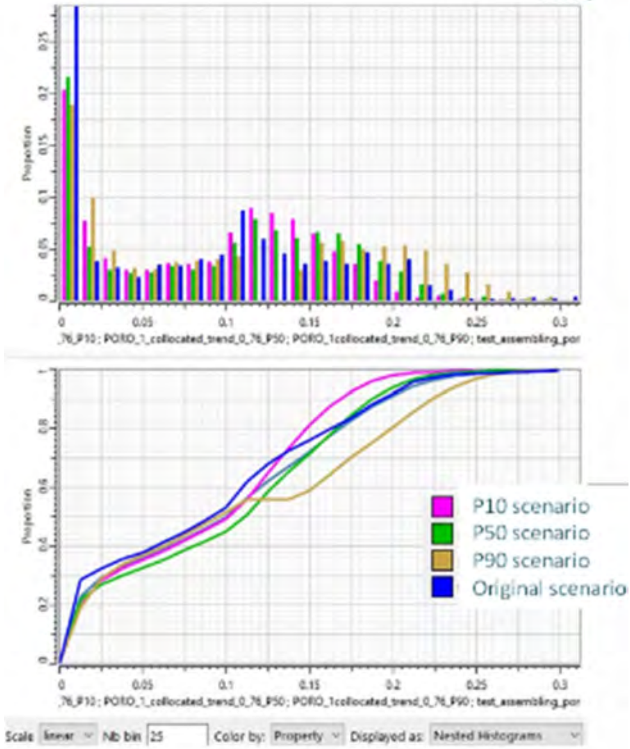

Figure 3.41 Porosity distribution for Oolithe blanche. Uncertainty scenarios compared to the original case.

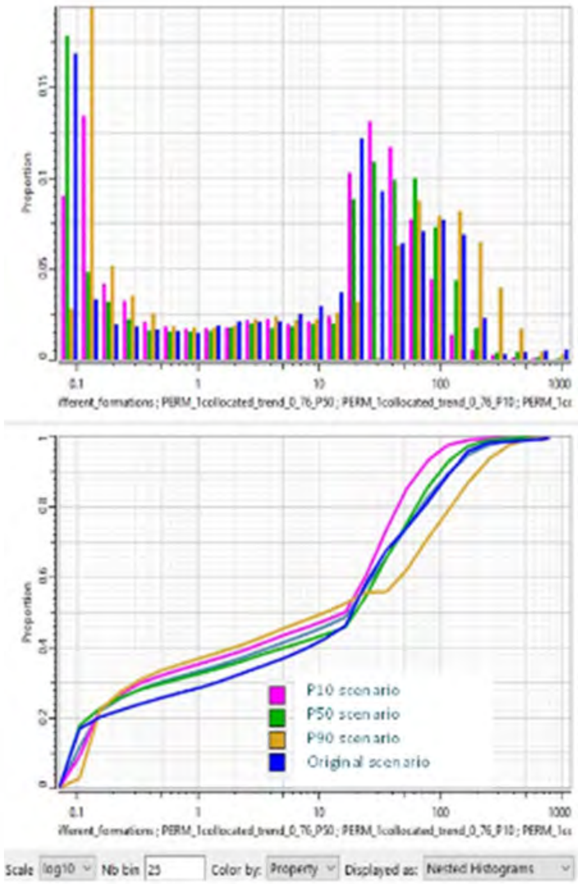

Figure 3.42 Permeability distribution for Oolithe blanche formation. Uncertainty scenarios compared to the original case.

The PilotSTRATEGY project has received funding from the European Union's Horizon 2020 research and innovation programme under grant agreement No. 101022664

		P10	P50	P90
Net porous volume 30x30 km² area [10^6 m³]		8665	9572	10562
Net porous volume 10x10 km² area [10^6 m³]		1123	1246	1369
Porosity Oolithe blanche (both facies together)	**Samples**	s	720000	720000
	Minimum	0.005	0.001	0.007
	Median	0.102	0.112	0.095
	Maximum	0.282	0.300	0.300
	Mean	0.089	0.099	0.109
	Std. deviation:	0.063	0.071	0.085
	Variance	0.004	0.005	0.007
Porosity Oolithe Blanche (high porosity facies)	**Samples**	336961	372144	317759
	Minimum	0.110	0.110	0.145
	Median	0.143	0.155	0.194
	Maximum	0.282	0.300	0.300
	Mean	0.147	0.158	0.196
	Std. deviation:	0.028	0.034	0.034
	Variance	0.001	0.001	0.001
Porosity Oolithe Blanche (high porosity facies)	**Samples**	383039	347856	402241
	Minimum	0.005	0.001	0.007
	Median	0.022	0.018	0.023
	Maximum	0.110	0.110	0.110
	Mean	0.038	0.035	0.039
	Std. deviation:	0.034	0.036	0.034
	Variance	0.001	0.001	0.001
Permeability Oolithe blanche (both facies together)	**Samples**	720000	720000	720000
	Minimum	0.095	0.073	0.104
	Median	16.069	21.672	11.120
	Maximum	640.823	926.682	926.683
	Mean	26.117	37.628	67.626
	Std. deviation:	41.911	62.076	111.111
	Variance	1756.500	3853.410	12345.600
Permeability Oolithe Blanche (high porosity facies)	**Samples**	336961	372144	317759
	Minimum	20.399	20.399	41.384
	Median	39.192	50.041	110.400
	Maximum	640.823	926.682	926.683
	Mean	52.448	70.199	149.414
	Std. deviation:	49.143	72.335	126.334
	Variance	2415.080	5232.380	15960.300
Permeability Oolithe Blanche (low porosity facies)	**Samples**	383039	347856	402241
	Minimum	0.095	0.073	0.104
	Median	0.225	0.185	0.241
	Maximum	24.276	24.276	24.276
	Mean	2.954	2.782	3.016
	Std. deviation:	5.541	5.388	5.598
	Variance	30.703	29.031	31.335

Table 3.17 Statistical analysis of P10, P50 and P90 scenarios for Porosity and Permeability

The PilotSTRATEGY project has received funding from the European Union's Horizon 2020 research and innovation programme under grant agreement No. 101022664

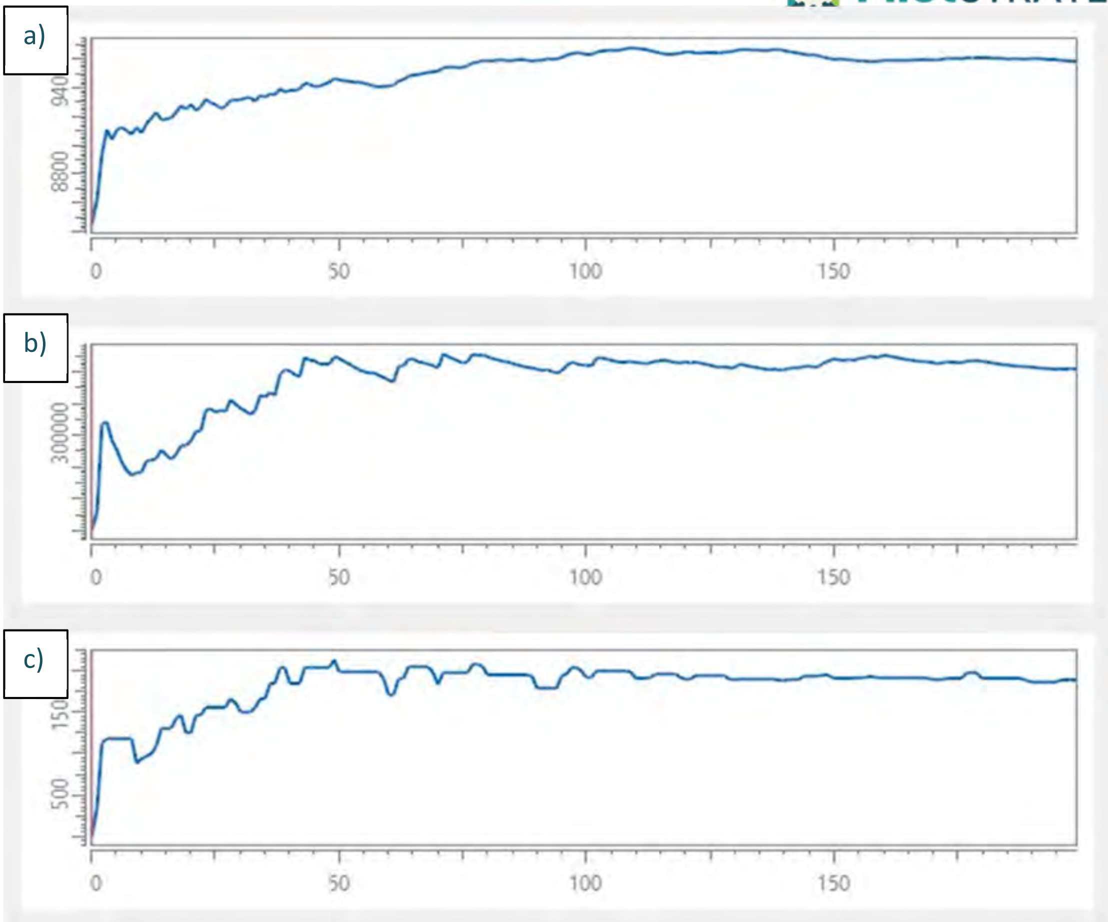

s

Figure 3.43 Distribution of the net porous volume in terms of Mean (a), Variance (b), P90-P10 (c)

3.6 Grid refinement and upscaling

To optimize computational time for dynamic simulations of CO_2 injection scenarios, the grid was reduced to 20 x 20 km. The grid was also upscaled in the area not covered by the 3D seismic. Local grid refinement (LGR) was performed in the area of the 3D seismic to improve the accuracy in this region during reservoir simulation. Two nested LGRs were added (see figure 3.45).

The upscaling and LGR process was done for each of the scenarios P10, P50, P90.

3.6.1 Vertical grid coarsening

Vertical coarsening was performed for the caprock (Marnes de Massingy), the reservoir interval, and the Lower Bathonian (Bt10). In the reservoir interval, vertical coarsening was performed by increasing the thickness by a factor of 2. In the caprock and below the reservoir, the vertical layers are finer towards the reservoir (see figure 3.44). This is done to best capture the effects during the CO_2 injection simulation.

- ***Lower Callovian (Marnes)***
    - **3** layers (top to bottom) (finer towards interface with reservoir)
        - ~25m
        - 5m
        - 5m

The PilotSTRATEGY project has received funding from the European Union's Horizon 2020 research and innovation programme under grant agreement No. 101022664

- ***Dalle Nacrée***
    - **4** layers ~4m (multiplying layer thickness by factor 2)
- ***Comblanchien***
    - **3** layers ~5.6 m (multiplying layer thickness by factor 2)
- ***Oolithe Blanche***
    - **18** layers ~6m (multiplying layer thickness by factor 2)
- ***Lower Bathonian***
    - **4** layers (finer towards interface with reservoir)
        - 5m
        - 5m
        - 20m
        - 35m

The following table 3.18 describes which K layer corresponds to which formation top in the different grids:

K Layer	**Original fine grid**	**Vertical upscaled grid**	**LGR 125m**	**LGR 62,5 m**
Top Oxfordian Inf	12-14 (sum layers 3)	12-14 (sum layers 3)	1-3 (sum layers 3)	-
Top Marnes Massingy	15-21 (sum layers 7)	15-17 (sum layers 3)	4-6 (sum layers 3)	1-3 (sum layers 3)
Top Dalle Nacrée	22-30 (sum layers 9)	18-21 (sum layers 4)	7-10 (sum layers 4)	4-7 (sum layers 4)
Top Comblanchien	31-37 (sum layers 8)	22-24 (sum layers 3)	11-13 (sum layers 3)	8-10 (sum layers 3)
Top Oolithe Blanche	38-87 (sum layers 50)	25-41 (sum layers 17)	14-30 (sum layers 17)	11-27 (sum layers 17)
Top Lower Bathonian (Bt 10)	88-99 (sum layers 12)	42-45 (sum layers 4)	31-34 (sum layers 4)	-

Table 3.18 Vertical layering for all grids

The PilotSTRATEGY project has received funding from the European Union's Horizon 2020 research and innovation programme under grant agreement No. 101022664

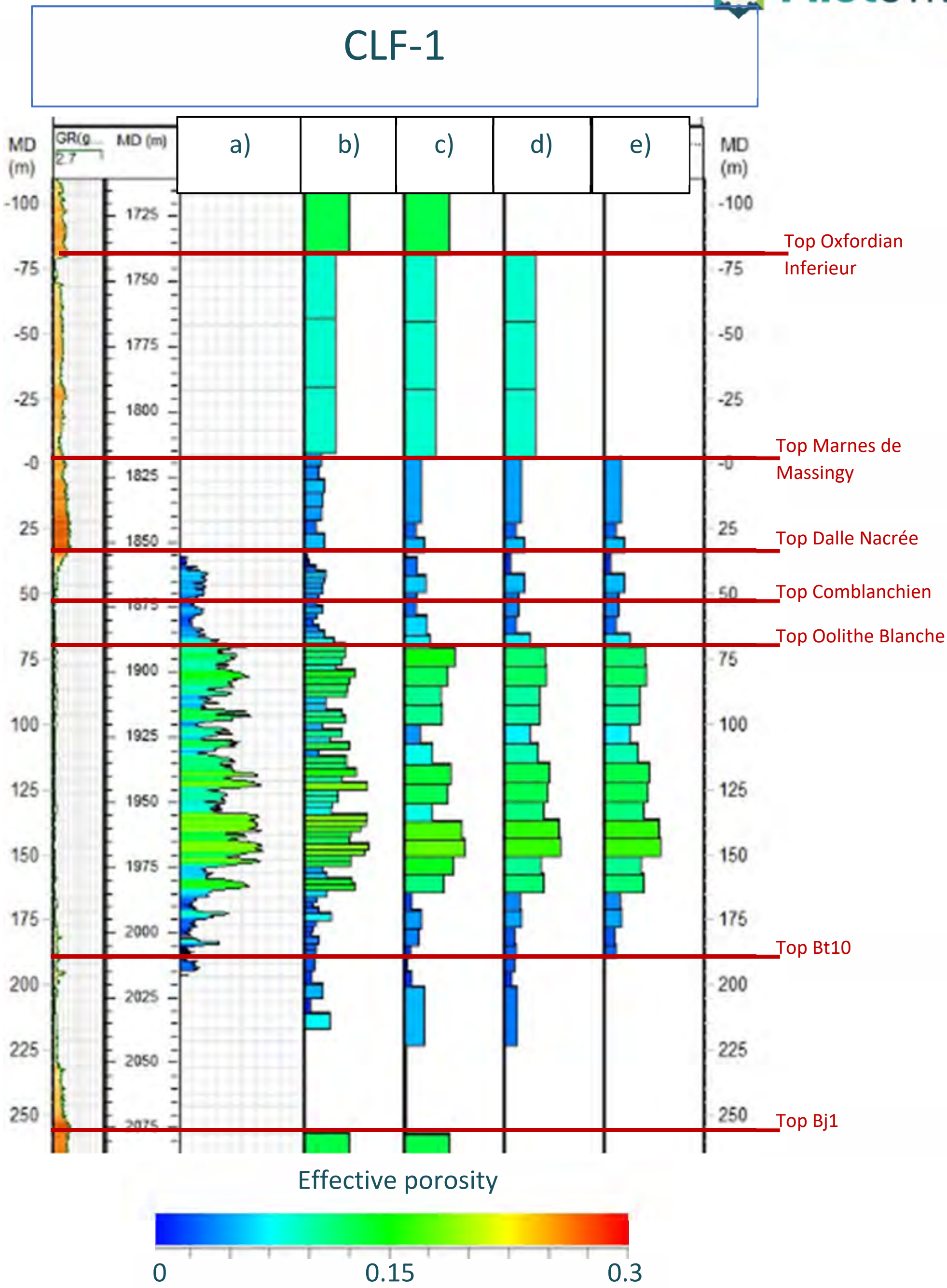

Figure 3.44 Result of vertical coarsening. a) original log for effective porosity, b) original fine grid, c) vertical upscaled grid and 500m cell resolution, d) LGR 125m, e) LGR 62,5 m. All for the P50 scenario

3.6.2 Horizontal grid coarsening and LGR

The grid has been coarsened in the horizontal direction and locally refined in the center. Two LGRs are added with are embedded in each other. This workflow has been done for the P10, P50 and P90 scenario.

From 0 to 5 km & 15 to 20 km (X- & Y- direction)

- Horizontal grid resolution 500 x 500 m
- Contains all layers in vertical direction

From 5 to 6 km & 14 to 15 km (X- & Y- direction)

- Horizontal grid resolution 125 x 125 m
- Vertical extension from top Oxfordian Inferieur to top Bathonian (not including the Bathonian)

From 6 to 14 km (X- & Y- direction)

- Horizontal grid resolution 62.5 x 62.5 m
- Vertical extension from top Marnes de Massingy to top Bt 10 (not including the Bt10)

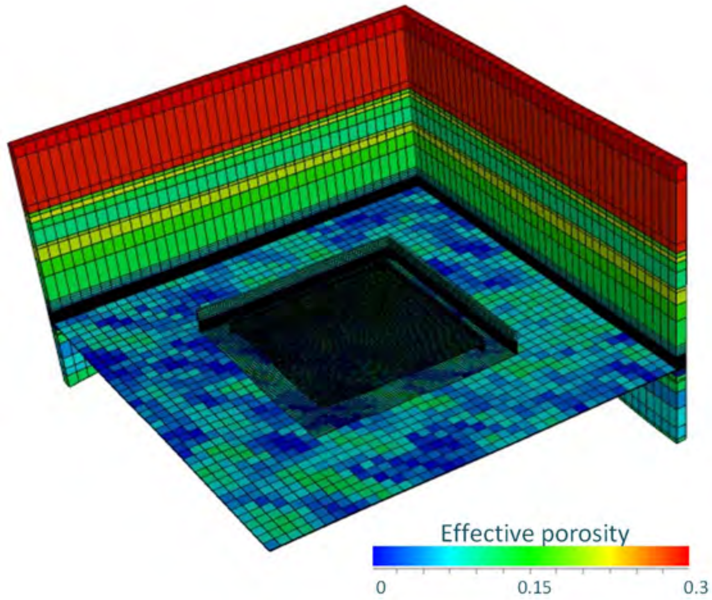

Figure 3.45 Reservoir grid showing the example of the P50 scenario. One large 20x20km grid with cell resolution 500m holds two embedded LGRs. First LGR has a resolution of 125m, second LGR resolution of 62.5m

3.6.3 Property upscaling

The porosity, facies, and permeability properties have been upscaled for the grid with the 500m grid resolution. For both LGRs, the properties were copied from the vertical upscaled grid and pasted in the LGR grids.

In the 500m resolution grid, the properties were upscaled using different methods depending on whether they were continuous or discrete and dynamic or static. The recommended methods in the Aspen SKUA software were used for upscaling.

A statistical summary for upscaling and LGR process for the case P50 for properties porosity and permeability can be seen in table 3.19. It also includes the statistics for the two LGRs (125m and 62.5m resolution).

A statistical summary and comparison for porosity and permeability upscaling is given in table 3.7 in the appendix and figures 3.11 – 3.13 in the appendix.

3.6.3.1 Porosity

Porosity is a continuous and static property. Static means that the values are not a function of flow rate. Porosity scales linearly, so an arithmetic mean method was chosen for upscaling. Porosity is defined by pore volume, which is a function of cell volume and NtG. Therefore, the arithmetic mean

The PilotSTRATEGY project has received funding from the European Union's Horizon 2020 research and innovation programme under grant agreement No. 101022664

was weighted by the cell volume. The weighting by the cell volume ensures the correct preservation of the net pore volume between the fine and coarse grid. It was not weighted by NtG because in this case the whole reservoir is assumed to have NtG=1.

$$Net\ Porous\ Volume = \Sigma\,(\varphi\ x\ NtG\ x\ Gross\ Cell\ Volume)$$

The result of the upscaling process for porosity showing the case P50 as example can be seen in figure 3.46.

3.6.3.2 Facies

Facies, like other discrete properties, is not additive. Therefore, the Most Probable method was chosen to ensure that the most common facies value occurs in the coarse cell. The result of the upscaling process for facies showing the case P50 as example can be seen in figure 3.46.

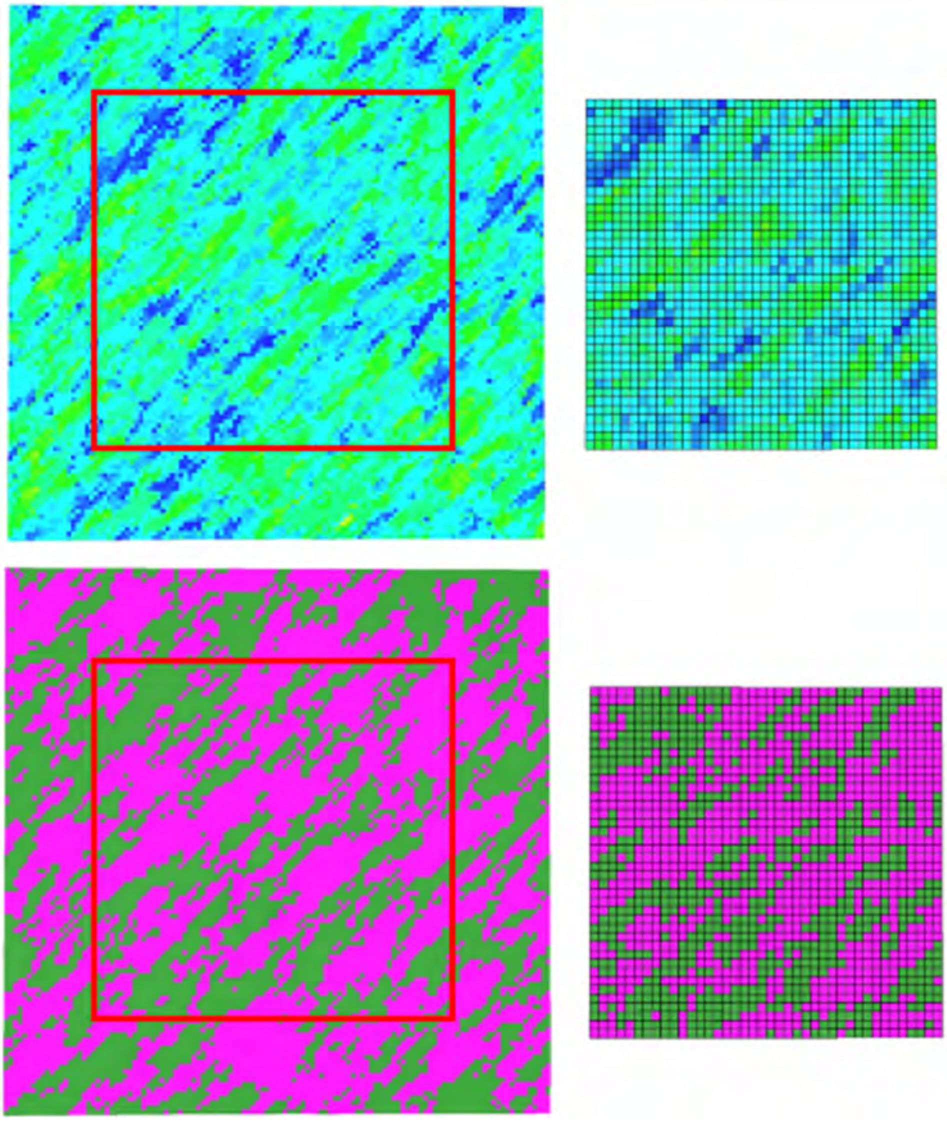

Figure 3.46 Upscaling for the porosity and facies property of the scenario case P50. Shown is the top of the Oolithe Blanche formation. Left is the scenario with 250m cell resolution, right 500m cell resolution.

The PilotSTRATEGY project has received funding from the European Union's Horizon 2020 research and innovation programme under grant agreement No. 101022664

3.6.3.3 Permeability

Permeability is a continuous and highly anisotropic property based on flow. Upscaling of these properties requires the ability to generate properties with three directional components regardless of the number of fine-scale values. Sensitivity to the direction and orientation of the fine-scale values is also required.

To account for the effect of anisotropy, a pressure-filled solution was chosen. An average of upper and lower bounds was chosen to ensure that the upscaled permeability field preserves the behaviour of the fine-scale property.

A confined boundary condition was chosen to best represent the reservoir. The flow is assumed to be completely parallel and in one direction only. This boundary condition imposes a constant pressure on one face of the block and a different constant pressure on the opposite face of the block. The other four sides of the block are assumed to have no flow.

The result of the upscaling process for permeability showing the case P50 as an example can be seen in figure 3.47.

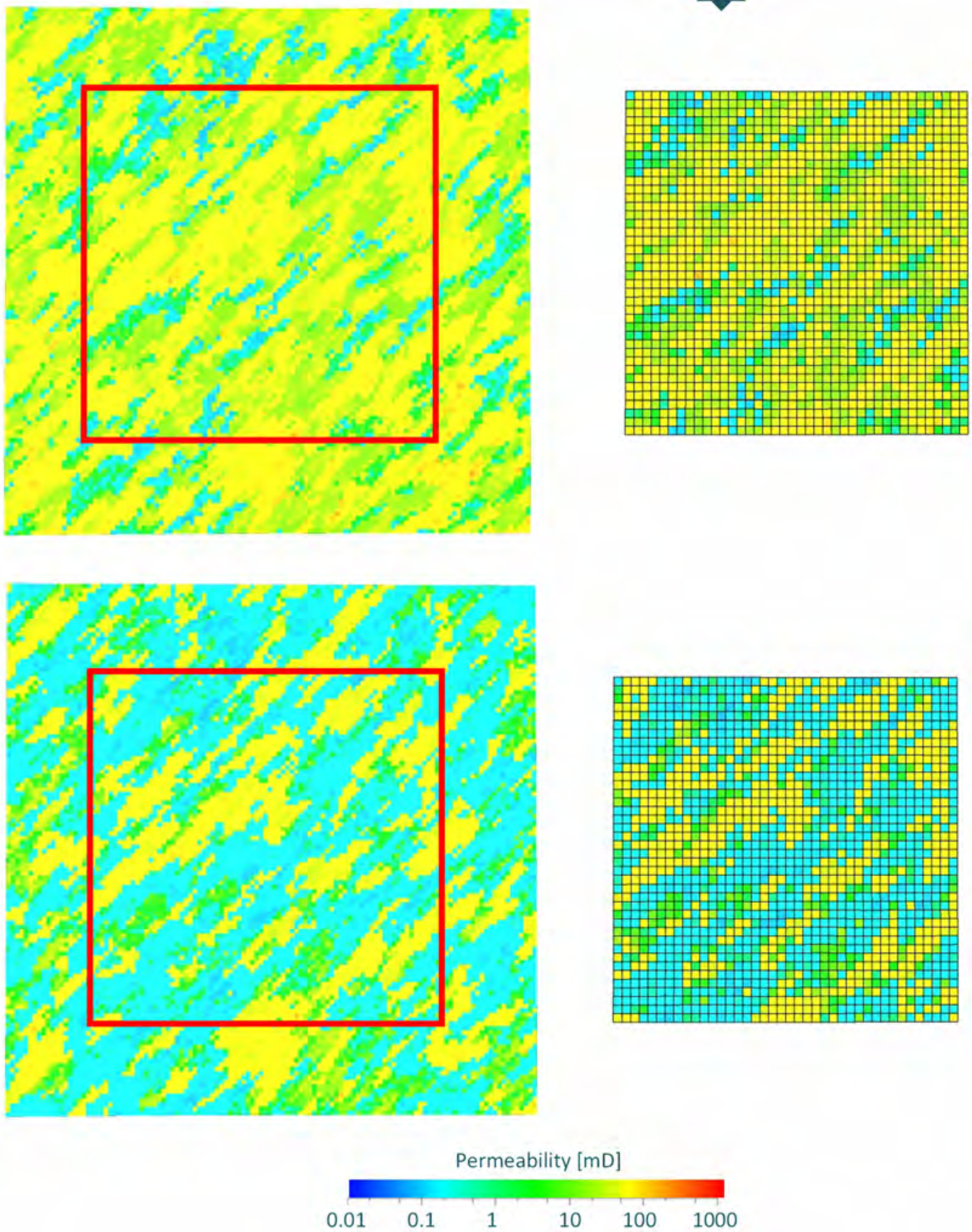

Figure 3.47 Upscaling for the permeability in X direction (top) and permeability in Z direction for the case P50. Shown is the top of the Oolithe Blanche formation. Left is the scenario with 250m cell resolution, right 500m cell resolution.

3.6.4 Results analysis

With an increase in cell size in vertical and horizontal direction, the heterogeneity and trends of the reservoir are still well captured after the upscaling process. The statistics of the upscaling scenarios show a very similar mean for the porosity of the Oolithe Blanche formation. The upscaling process is penalizing the extreme high and low values (see figure 3.48), a behaviour expected from upscaling. The porosity distribution is smoother after the upscaling process.

The PilotSTRATEGY project has received funding from the European Union's Horizon 2020 research and innovation programme under grant agreement No. 101022664

After the upscaling, permeability is separated in X, Y and Z direction. Permeability is higher in X and Y direction compared to Z direction, due to confined boundary conditions (see figures 3.12 and 3.13 in appendix).

		P50 scenario fine resolution	P50 scenario after vertical upscaling, 250m horizontal resolution	P50 scenario after vertical upscaling and horizontal upscaling to 500m cell resolution	P50 scenario 62,5m LGR	P50 scenario 125m LGR
Porosity (whole Oolithe Blanche formation)	**Samples**	720000	244800	27200	278528	108800
	Minimum:	0.001	0.001	0.001	0.000	0.000
	Median	0.112	0.098	0.094	0.094	0.094
	Maximum	0.300	0.288	0.264	0.295	0.295
	Mean	0.099	0.098	0.095	0.093	0.093
	Std. deviation:	0.071	0.047	0.042	0.046	0.046
	Variance	0.005	0.002	0.002	0.002	0.002
Permeability X (whole Oolithe Blanche formation)	**Samples**	720000	244800	27200	278528	108800
	Minimum:	0.073	0.073	0.073	0.071	0.071
	Median	21.672	24.569	23.864	23.679	23.413
	Maximum	926.682	885.283	715.204	839.052	839.052
	Mean	37.628	38.695	35.312	33.095	32.782
	Std. deviation:	62.076	51.608	43.990	37.861	37.422
	Variance	3853.410	2663.390	1935.130	1433.430	1400.420
Permeability Z (whole Oolithe Blanche formation)	**Samples**	720000	244800	27200	278528	108800
	Minimum:	0.073	0.073	0.073	0.071	0.071
	Median	21.672	1.424	1.147	1.080	1.079
	Maximum	926.682	885.105	714.344	839.052	839.052
	Mean	37.628	20.569	18.810	17.955	17.555
	Std. deviation:	62.076	40.491	35.666	32.450	31.670
	Variance	3853.410	1639.520	1272.070	1053.010	1002.980

Table 3.19 Statistical analysis of the Porosity and Permeability before and after upscaling for the P50 scenario. The original P50 scenario with the fine resolution doesn't have a differentiation of Permeability in x, y and z direction but just one permeability.

The PilotSTRATEGY project has received funding from the European Union's Horizon 2020 research and innovation programme under grant agreement No. 101022664

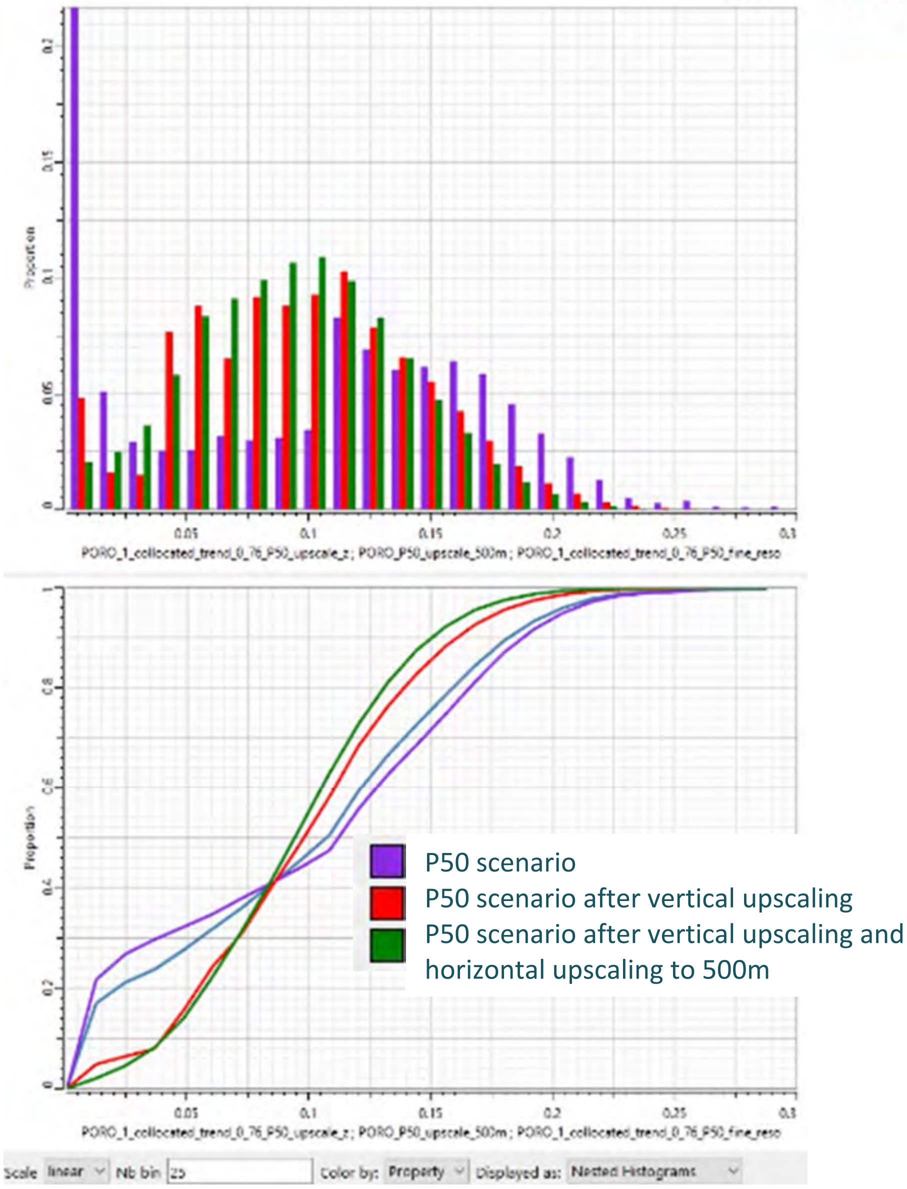

Figure 3.48 Comparison of the porosity distribution for the Oolithe blanche formation. Purple is the P50 scenario in the fine grid, Red porosity distribution after the vertical upscaling, Green is the porosity distribution after the horizontal upscaling to 500m

3.7 Conclusion

In the Paris Basin, the saline aquifer hosted by the Jurassic Oolithe Blanche Formation is the principal reservoir for the pilot CO_2 injection. This formation consists of a Jurassic oolithic carbonate ramp with an average porosity of around 10%, locally reaching up to 30% porosity. The Oolithe Blanche formation is capped by the Dalle Nacrée and the Comblanchien formations with less favourable porosities. The reservoir complex is capped by a continuous 120m thick marly seal, the Marnes de Massingy. According to the existing literature, the Oolithe Blanche Formation is laterally and vertically heterogeneous in lithology and petrophysical properties. The complexity in geometry and spatial distribution of reservoir properties must be considered when injecting CO_2.

The PilotSTRATEGY project has received funding from the European Union's Horizon 2020 research and innovation programme under grant agreement No. 101022664

The grid of our model was constructed based on seismic and well marker information. Emphasis has been placed on the characterization of the lithology, facies and porosity distributions of the target reservoir rocks. Our work is based on an exhaustive interpretation of well data (logs and cores) of 13 wells in the study area and 4 additional wells outside the study area. The well data set used in our study included various types of standard well logs (bulk density, gamma ray, neutron-density), marker data and 444 plug samples.

In addition, Vshale and Effective Porosity logs were calculated from the standard raw well logs. Analysis of the well logs indicated variable reservoir quality and an overall decline in quality from top to bottom. Porosity values from the plug data showed a bimodal distribution, indicating the presence of two facies in the reservoir. By applying a cut-off of 11%, one facies with more favorable petrophysical properties and a second facies with less favorable petrophysical properties were defined. Peak-to-peak correlation of the effective porosity log revealed the presence of elongated 45°N oriented ooidal shoals with lengths between 3000 and 13500 meters and vertical thicknesses between 10 and 15 meters. Minor extension of these shoal geobodies was found to be about 1/3 of the major extension.

The results of this integrated study provided an extended input to the construction of the stochastic 3D geological reservoir model. It describes the reservoir architecture and captures all its petrophysical heterogeneities between and beyond well control. The model includes the overburden and underburden from the topographic surface to the basement with a detailed characterization of the reservoir and sealing formations. The entire 3D model was populated with facies properties using Sequential Indicator Simulation (SIS) geostatistical algorithm. Variogram parameters were determined based on peak-to-peak correlation. 3D porosity modeling was conditioned by the facies model and was populated in the grid with geostatistics using Sequential Gaussian Simulation algorithm (SGS). Permeability was correlated with porosity using a K-Φ law derived from laboratory measurements of plug data. It has to be kept in mind that each geostatistical realization is an equiprobable realization of the reservoir heterogeneity.

Uncertainty analysis was performed with a Monte Carlo approach calculating deciles of P10, P50, P90. The Net Porous Volume was selected as the targeted property that will be affected by the uncertainties in model properties. Net Porous Volume indicates the volume available for CO_2 storage. Considered uncertain parameters were facies proportions and porosity distributions. Uncertainty analysis revealed Net Porous Volume in the Oolithe Blanche formation ranging from 8665 to 10562 10^6 m3 in the 30x30 km^2 area, and 1123 – 1369 10^6 m3 in the 30x30 km^2 area.

Upscaling and LGR were performed for the P10, P50 and P90 cases including a vertical and horizontal upscaling. Two embedded LGRs targeting the reservoir zone were created with 125m and 62,5 m resolution.

Recommendations to improve the model for a later coming operational phase is acquisition of additional data for the Oolithe Blanche formation in the form of core data and plug analysis.

For this current model only plug samples for the top of the Oolithe Blanche formation are available, which don't capture the complete heterogeneity of the formation. Therefore, the acquisition and interpretation of additional core data and analysis of plug data of the Oolithe blanche formation would be of importance.

The PilotSTRATEGY project has received funding from the European Union's Horizon 2020 research and innovation programme under grant agreement No. 101022664

A second recommendation would be to improve horizontal variogram analysis using a secondary data source. For the current model, only information from well data was used. There is a known correlation between porosity (PHIE) and Acoustic impedance (AI). An AI 3D property derived from the acquired seismic cube in an earlier phase of the project could be of help to get the variogram information (minor and major directions) over the whole area.

3.8 References

Brigaud, B., Vincent, B., Durlet, C., Deconinck, J. F., Jobard, E., Pickard, N., & Landrein, P. (2014). Characterization and origin of permeability–porosity heterogeneity in shallow-marine carbonates: From core scale to 3D reservoir dimension (Middle Jurassic, Paris Basin, France). *Marine and Petroleum Geology*, *57*, 631-651.

Delmas, J., Brosse, E., & Houel, P. (2010). Petrophysical properties of the middle Jurassic carbonates in the PICOREF sector (South Champagne, Paris Basin, France). *Oil & Gas Science and Technology–Revue de l'Institut Français du Pétrole*, *65*(3), 405-434.

Deutsch, C. V. (2002). *Geostatistical reservoir modeling*. Oxford University Press, USA.

Fleury, M. et al. (2023). Deliverable D2.6. Pertophysics report of all regions. PilotSTRATEGY project, Grant Agreement: 101022664

IPCC, 2005: IPCC Special Report on Carbon Dioxide Capture and Storage. Prepared by Working Group III of the Intergovernmental Panel on Climate Change [Metz, B., O. Davidson, H. C. de Coninck, M. Loos, and L. A. Meyer (eds.)]. Cambridge University Press, Cambridge, United Kingdom and New York, NY, USA, 442 pp.

Rider, M. & Kennedy, M. (2011). The geological interpretation of well logs. Rider-French Consulting, Scotland

Wilkinson, M. (2023). Deliverable 2.7 – Conceptual Geological Models ofs Portugal, Spain and France. PilotSTRATEGY project, Grant Agreement: 101022664

The PilotSTRATEGY project has received funding from the European Union's Horizon 2020 research and innovation programme under grant agreement No. 101022664

4 Upper Silesia (Poland)

4.1 Available data presentation

4.1.1 Introduction

Within the framework of assessment of the Upper Silesia region actions in the WP2 included an exhaustive analyses and re-interpretation of available data of the Dębowiec layers (Skoczów DSA) and Ładzice Fm (Ładzice DSA) – Figure 4.1. A review of existing data allowed to feed the conceptual geological model and to start building the static model.

Two possible storage places have been identified in the region in deep saline aquifers with potential CO_2 storage capacity of 0.1 Gt:

- Skoczów DSA - Upper Silesian Coal Basin (n° 3),
- Ładzice DSA - Jurassic Czestochowa District (n°4).

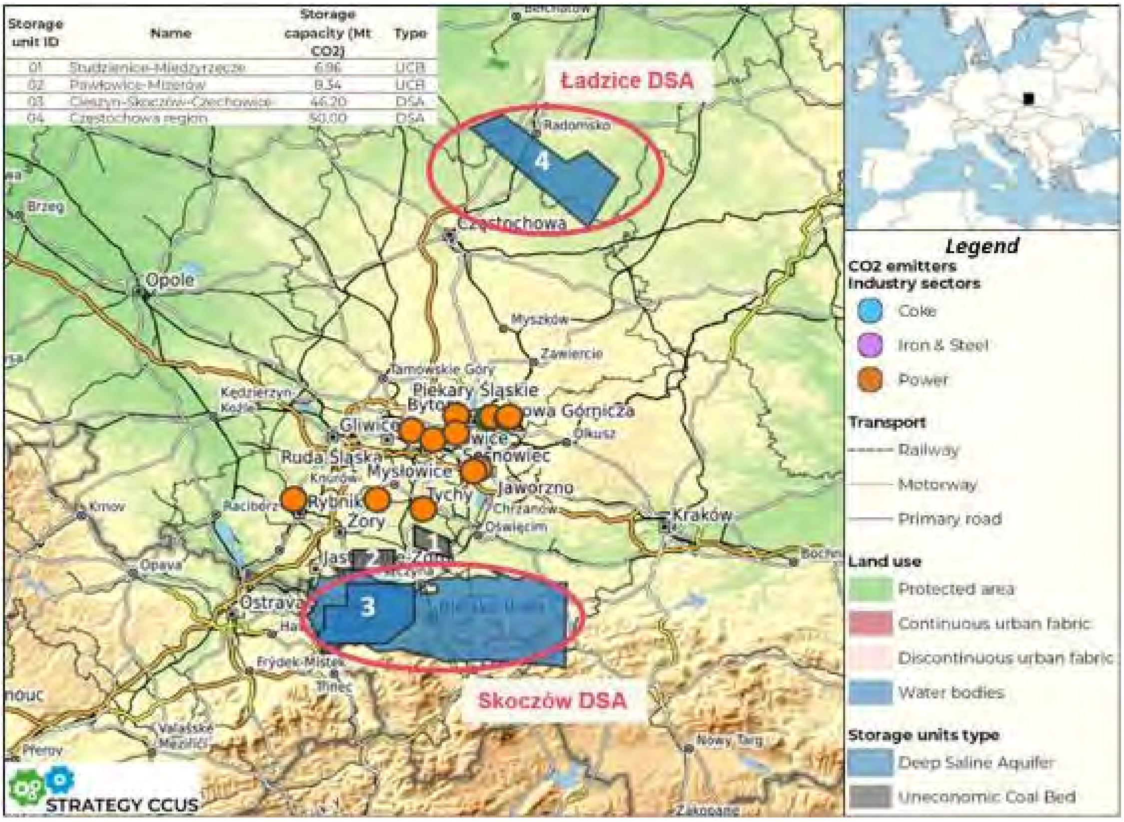

Figure 4.1: Location of the main potential storage units in Upper Silesia (STRATEGY CCUS, 2020)

The objective of PilotSTRATEGY project for Poland is to increase the maturity and confidence level of storage resources to start planning as Contingent resources, based on new available data, reprocessing of old data (WP2) and new dynamic simulation studies (WP3). The research in relation to the analysis of the potential to CCUS development in the Upper Silesia region were focused on enhancing the maturity and confidence level of CO_2 storage resources by studying new data, reprocessing current data within the framework of WP2 (Geo-characterization, Task 2.1 Compilation of existing data and choice of pilot locations, and Task 2.8 Storage potential of Upper Silesia).

The PilotSTRATEGY project has received funding from the European Union's Horizon 2020 research and innovation programme under grant agreement No. 101022664

Within the framework of task 2.1. for the Upper Silesia region, data has been acquired and re-interpreted in order to advance the understanding of the prospects for CO_2. Progress was made in the study of two deep saline aquifers and work included:

1. Upper Silesian Coal Basin (Skoczów DSA) progress:
   - Compilation of additional well data:
   - lithologies in the boreholes;
   - hydrogeological parameters (porosity, permeability);
   - digital Well Log data (Log ASCII Standard - LAS).
   - Works included preparing data regarding parameters of reservoir fluids such as properties of reservoir water, mineralization and other in order to providing inputs for reservoir modeling.
2. Jurassic Częstochowa District (Ładzice DSA) progress:
   - Compilation of additional well data:
   - compilation of lithologies in 10 boreholes
   - part of wells with petrophysical data
   - part of wells with porosity (effective), permeability,
   - mineralization data, properties of reservoir water.

Within the framework of the first part of task 2.8 (Storage potential of Upper Silesia), structural surfaces in the area of the Jurassic Częstochowa District/Ładzice DSA reservoir have been developed including the analysis of the depth, thickness and structural framework of reservoir deposits.

Two candidate areas were identified for the Jurassic Ładzice formation. Based on data availability and parameters values of reservoir layers, the area named "Pągów-Milianów" with an area of approximately 190 km^2 was selected for further work. A detailed characterization of reservoir formations and sealing layers in the selected area was prepared. Additional well data were analyzed and prepared for the needs of 3D static modelling (Task 3.1).

The range and distribution of petrophysical parameters of the reservoir were analyzed in the area of the maximum range of Miocene deposits in Dębowiec layers. An additional area named "Kęty" with the highest potential for CO_2 storage was identified. The selected area, of approximately 115 km^2, is being analyzed in detail for storage of carbon dioxide within the framework of tasks 2.8 and 3.1.

Regarding the methodology used in geo-characterization of Upper Silesia region, firstly works were focused on understanding of REGIONAL GEOLOGY OF SEDIMENTARY BASINS (Figure 4.2). The next step was WELL DATA ANALYSIS which included mainly:

a. Compilation of existing data,
b. Well petrophysics,
c. Well log data analysis.

The final step of work was preparation of ELEMENTS OF GEOLOGICAL CONCEPTUAL MODELS based on the results of previous works. All collected data will be used for creating static reservoir models and dynamic simulations in WP3. The same steps of analysis were used for both selected DSA.

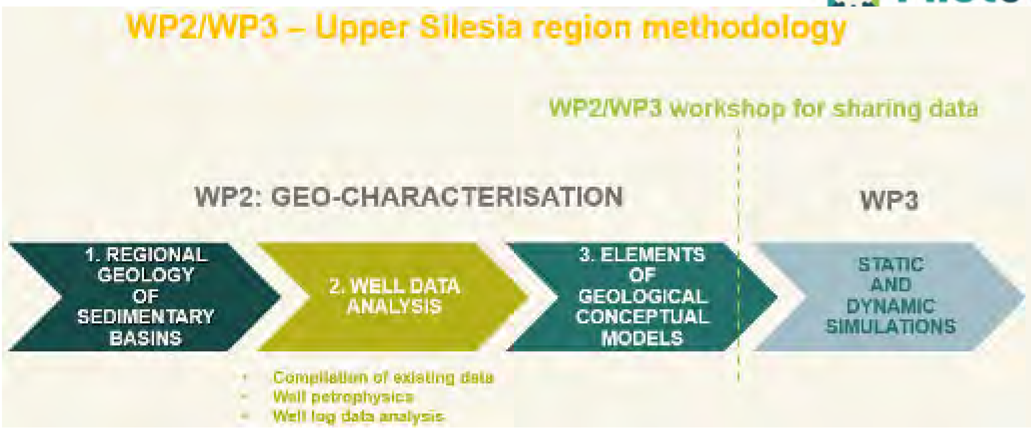

Figure 4.2: WP2/WP3 Upper Silesia region methodology

4.1.2 Upper Silesian Coal Basin (Skoczów DSA)

4.1.2.1 REGIONAL GEOLOGY OF SEDIMENTARY BASINS

4.1.2.1.1 Storage potential of Upper Silesia

Based on stratigraphic and hydrogeological analysis, the most prospective conditions for potential storage of CO_2 are present in deep saline aquifers in the Miocene deposits of the Dębowiec Beds which is located in the southern part of Upper Silesia region (Figure 4.3).

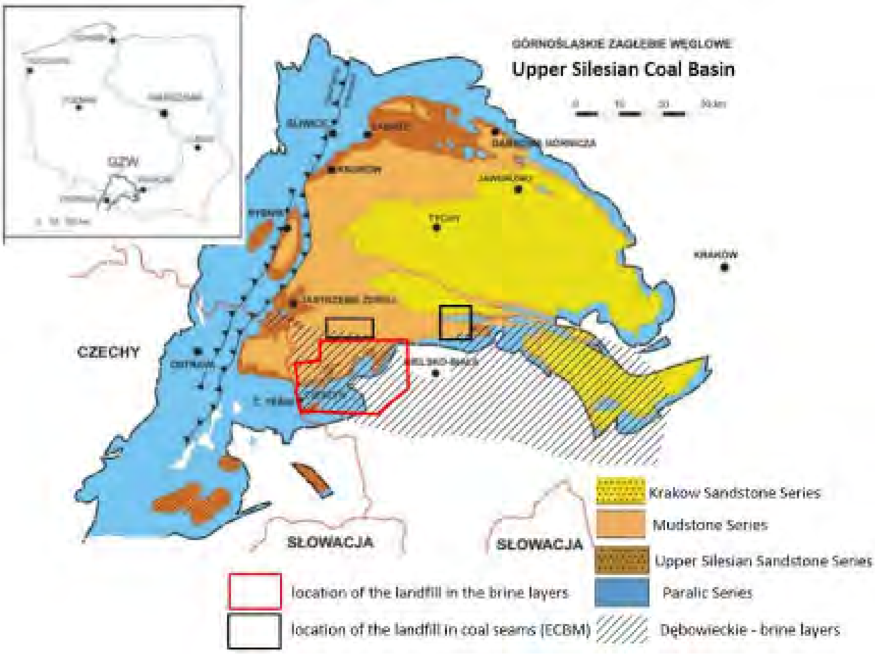

Figure 4.3: The Miocene deposits of the Dębowiec Beds located in the southern part of Upper Silesia Coal Basin

The Dębowiec formation is a Miocene macroclastic molasse composed of four lithofacies: olistostromes, boulders, conglomerates and sandstones (Figure 4.1 and Figure 4.2 in Appendix 7.2). Potential geological structures for carbon dioxide storage in the USCB region also include the top part of the carbonate series (lower Carboniferous) and terrigenous series of the Lower Devonian and Cambrian; however, these series are located at great depths (usually significantly exceeding 2000 m) and are very poorly recognized.

The PilotSTRATEGY project has received funding from the European Union's Horizon 2020 research and innovation programme under grant agreement No. 101022664

4.1.2.1.2 Extend the area of analysed Miocene aquifer to identify the possibility of increasing storage capacity

An important work is done to extend the area of the analyzed aquifer to the maximum range of Miocene deposits in the area of Dębowiec layers (Figure 4.4) in order to identify the maximum storage capacity. This is based on the compilation of existing data with data location using maps and analysis of data uncertainty and of different degree of geological exploration (Figure 4.5, Figure 4.6)

Figure 4.4: The maximum range area of the Dębowiec layers

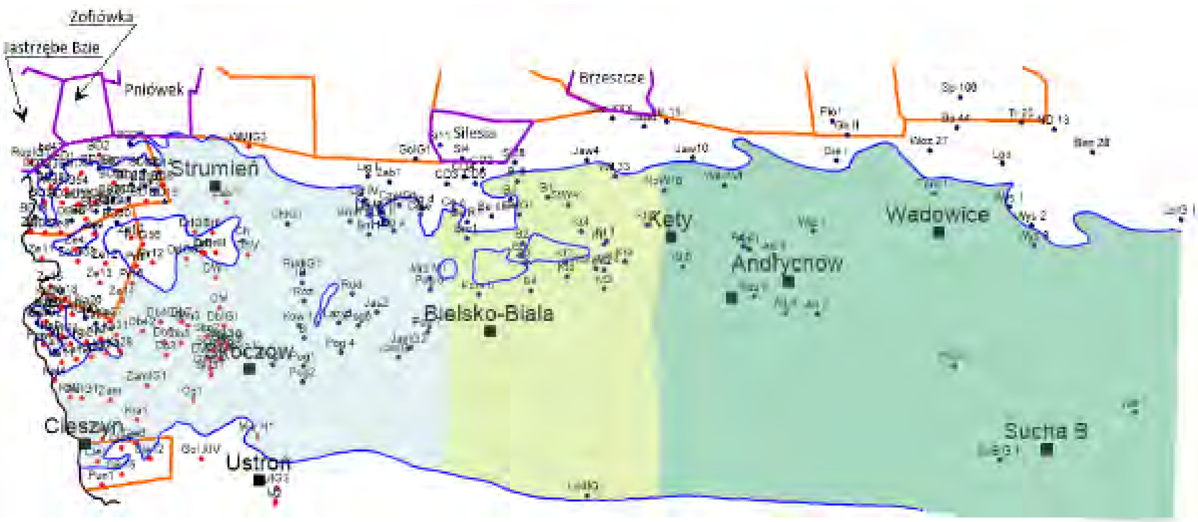

Figure 4.5: Different degree of geological exploration in the maximum range area of the Dębowiec layers

4.1.2.2 WELL DATA ANALYSIS

For the Dębowiec formation, in the Skoczów reservoir site, data from new boreholes have been acquired and all data have been re-interpreted in order to advance the understanding of the prospects for CO_2 storage.

Location of new boreholes and example of the borehole profiles with lithological, petrophysical (porosity, permeability) and hydrogeological data are presented in figures 4.3 and 4.4 in Appendix 7.2.

Moreover, compilation of petrophysical parameters from east part of Dębowiec layers analysed earlier also has been prepared.

The PilotSTRATEGY project has received funding from the European Union's Horizon 2020 research and innovation programme under grant agreement No. 101022664

Works included preparing data regarding parameters of reservoir fluids such as properties of reservoir water, mineralization and other in order to provide inputs for reservoir modeling within the framework of WP3.

4.1.2.2.1 Available data shared in LAS files

Examples of available digital well log data (Log ASCII Standard - LAS) are presented in Figure 4.7 (and Figure 4.5 in Appendix 7.2).

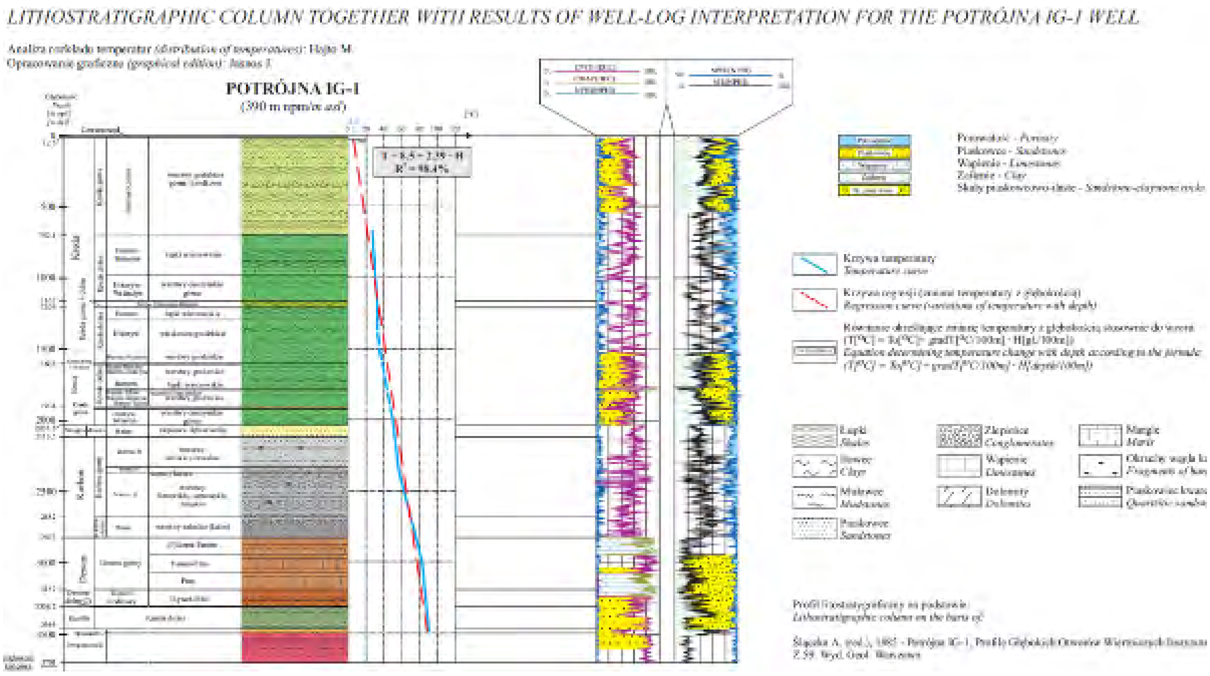

Figure 4.7: Lithostratigraphic column with results of well-log interpretation for the Potrójna IG-1 well (Ślączka, 1985)

Stratigraphic inter-well correlations developed in previous works were also prepared (Figure 4.6 and 4.7 in Appendix 7.2).

4.1.2.2.2 Source of other data:

- Database of Polish Geological Institute – National Research Institute;
- Other available data from literature, reports, scientific papers, websites and other reputable sources.

4.1.2.3 ELEMENTS OF GEOLOGICAL CONCEPTUAL MODELS

4.1.2.3.1 Geo-characterization of the storage complex zone (reservoir, caprock and structural elements)

To characterize the geological aspects of the storage complex (Figure 4.8), data analysis and re-interpretation for the maximum range area of the Dębowiec layers lead to the following maps:

- map of the thickness in the area of the maximum range of the Dębowiec layers (Figure 4.9),
- structural map of the top of the Dębowiec layers (Figure 4.8 in Appendix 7.2.),
- structural map of the top of the Paleozoic formations (Figure 4.9, 4.10 in Appendix 7.2.).

The PilotSTRATEGY project has received funding from the European Union's Horizon 2020 research and innovation programme under grant agreement No. 101022664

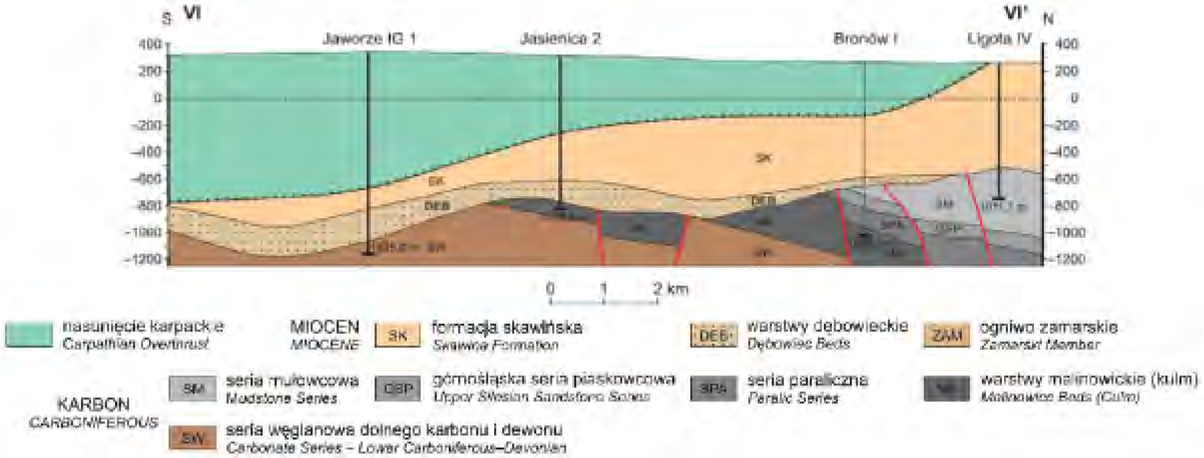

Figure 4.8: Geological cross-sections in the area of the maximum range of the Dębowiec layers (Jureczka et al., 2012)

The average thickness of the Dębowiec layers is 100-150 m (max: 265 m).

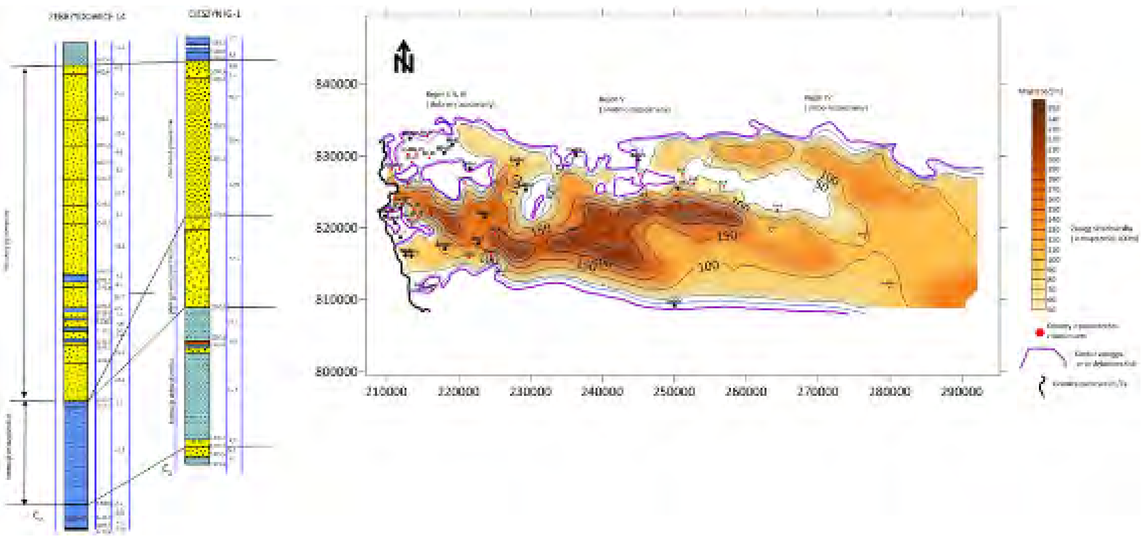

Figure 4.9: Map of the thickness in the area of the maximum range of the Dębowiec layers

4.1.3 Jurassic Czestochowa District (Ładzice DSA)

4.1.3.1 REGIONAL GEOLOGY OF SEDIMENTARY BASINS

Storage capacity has also been identified in DSAs in marine deposits of the Jurassic Radomsko District (Ładzice DSA). This potential CO_2 storage reservoir, about 100 km away from the main emitters is treated as the second possible option for CO_2 storage in the Upper Silesia region (see Figure 4.1).

Reservoir formations of Ładzice (DSA) are associated with water-saturated sediments of the Lower Jurassic and the lower stages of the Middle Jurassic (Figure 4.10). The aquifer is made up of sandstones with a fine- to coarse-grained structure as well as sandstones of various grains. The top of the water-saturated sediments is located at a depth of 1000 to 1500 m. The overburden is formed by a continuous layer of poorly permeable Middle and Upper Jurassic formations (marls, clays, claystones and mudstones) are 350 - 620 m thick. The area of the potential reservoir is relatively poorly explored in terms of hydrogeology. Test results indicated porosity from 7.69 to 22.1% and permeability from 16 to 1478 mD.

The PilotSTRATEGY project has received funding from the European Union's Horizon 2020 research and innovation programme under grant agreement No. 101022664

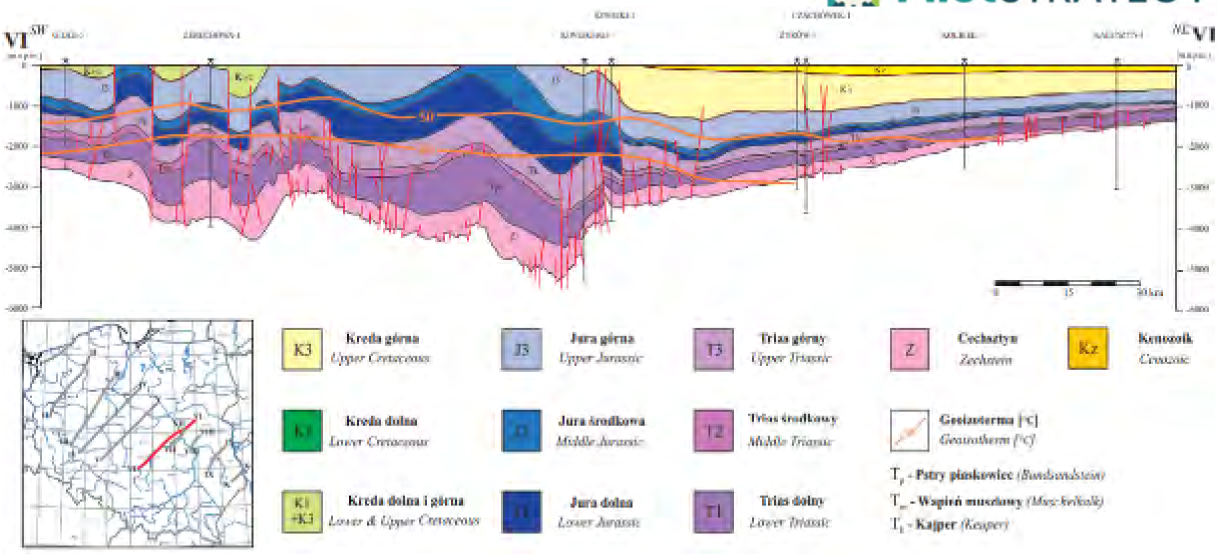

Figure 4.10: Geological cross-sections in the area of the Jurassic structure

4.1.3.2 WELL DATA ANALYSIS

Location of boreholes and example of the borehole profiles with facies data are presented in Figure 4.11 (and Figure 4.11 in Appendix 7.2).

Location of boreholes with petrophysical (porosity, permeability) data are presented in figure 4.12 in Appendix 7.2. Works included preparing data regarding parameters of reservoir fluids such as properties of reservoir water, mineralization (Figure 4.13 in Appendix 7.2) and other in order to providing inputs for reservoir modeling.

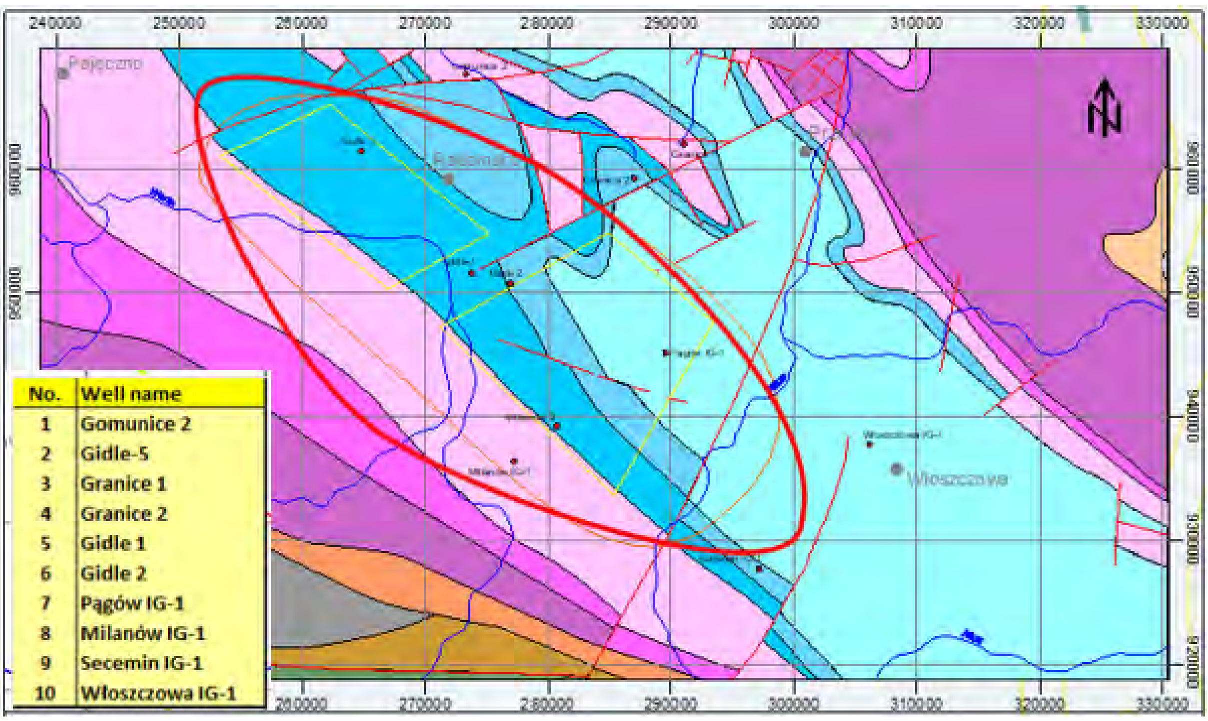

Figure 4.11: Geological map with location of boreholes

The PilotSTRATEGY project has received funding from the European Union's Horizon 2020 research and innovation programme under grant agreement No. 101022664

4.1.3.3 *ELEMENTS OF GEOLOGICAL CONCEPTUAL MODELS*

Based on chronostratigraphy and litostratigraphy borehole data, well data correlation and analysis of geological cross-sections (Figure 4.14 in Appendix 7.2), 21 structural surfaces were developed in the area of the Jurassic structure.

Structural surfaces were developed in the area of the Jurassic Częstochowa District/Ładzice DSA reservoir, taking into account the depth, thickness and structural framework of the selected area of reservoir deposits - maps of top and base of reservoir layers (Figure 4.15 in Appendix 7.2).

Structural geology analysis and fault models were conducted to develop a structural framework model (Figure 4.16, 4.17 in Appendix 7.2).

4.2 Modelling

4.2.1 Introduction

The objective of task 3.1 (Static modelling with uncertainties) is building of two 3D geological models for two potential storage reservoirs (see Figure 4.1). Geological models of the storage complex zone consist of reservoir, caprock and structural elements. Static geological models are being built based on the results obtained from WP2 Geo-characterization. Geological models will be adapted to the simulation objectives in next tasks of WP3.

Regarding the methodology used in task 3.1, firstly works were focused on CONSTRUCTION OF GEOLOGICAL GRID (Figure 4.12), which included mainly: 1) Fault modelling, 2) Well data analysis, 3) Interpretation of geological horizons and 4) Structural framework of geological model. The next step was WELL LOGS UPSCALING. The final step of work was CONSIDERING THE GEOLOGICAL UNCERTAINTIES based on the results of previous works. All collected data have been used for creating static reservoir models. The same steps of analysis were used for both selected DSA. Static 3D models were carried out using the Schlumberger Petrel software (Schlumberger Information Solutions, 2010) with Geoscience Core and Reservoir Engineering Core.

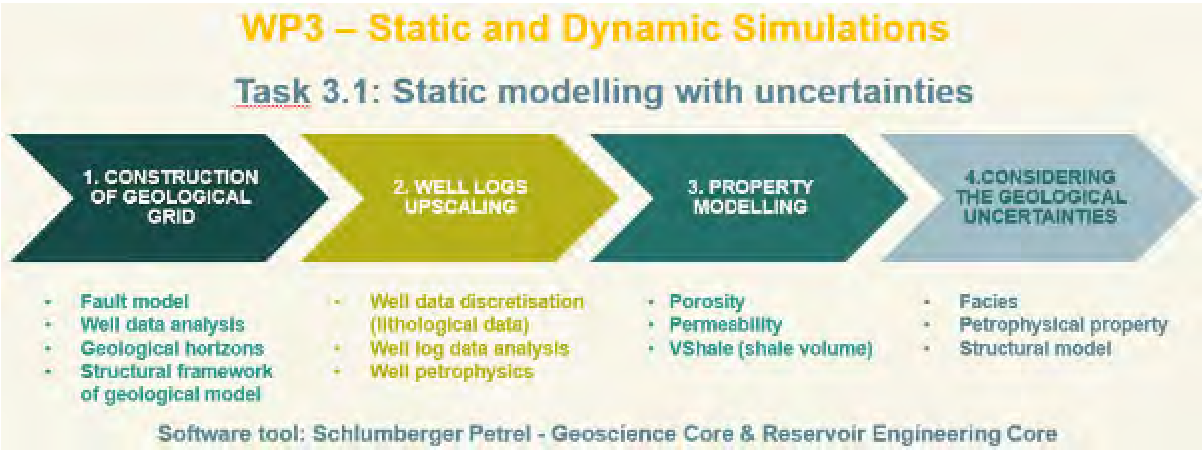

Figure 4.12: WP3 Upper Silesia region methodology

4.2.2 Upper Silesian Coal Basin (Skoczów DSA)

4.2.2.1 *CONSTRUCTION OF GEOLOGICAL GRID*

The first step of static modelling was the construction of a geological grid covering the area. Input for this task were horizon interpretations tied to well data (already in depth) as well as the fault model

The PilotSTRATEGY project has received funding from the European Union's Horizon 2020 research and innovation programme under grant agreement No. 101022664

combined into a structural framework coming from the work of WP2. In order to start the construction of the geological model, input from the WP2 (characterization) was needed in the form of geological horizons and faults. The top and base of the reservoir were provided, the top of the seal and other horizons in the overburden and underburden, fault and fracture framework were provided from the WP2. A geological grid was constructed by taking the horizons and faults into account.

4.2.2.1.1 Fault modeling

Based on stratigraphic and hydrogeological analysis, the most prospective conditions for potential storage of CO_2 are present in deep saline aquifers in the Miocene deposits of the Dębowiec Beds which is located in the southern part of Upper Silesia region.

Faults occurs only in deep layers underlying the reservoir - faults does not continue in the layers of reservoir nor above the reservoir (Figure 4.13, 4.14).

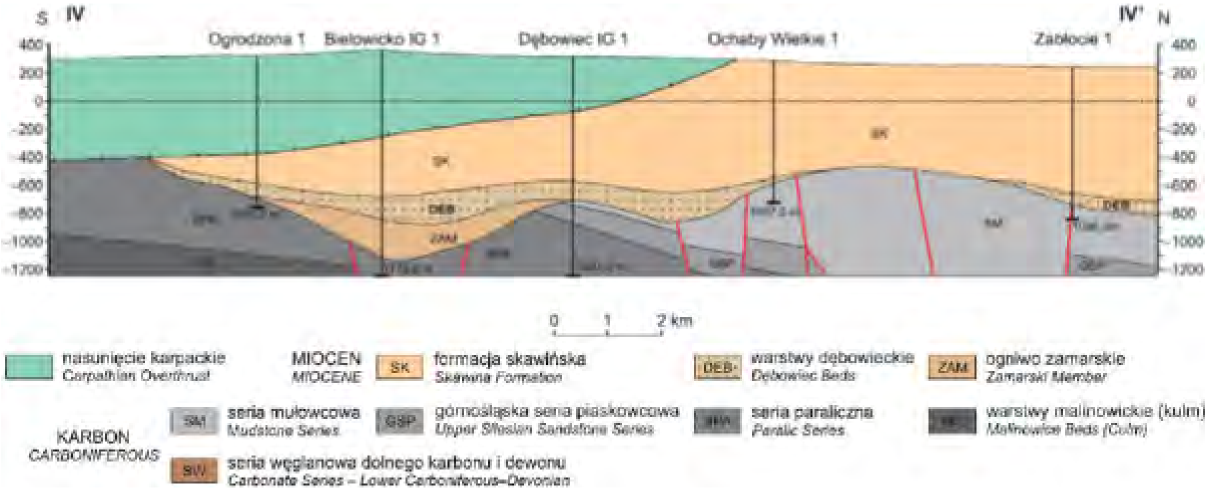

Figure 4.13: Geological cross-sections in the area of the maximum range of the Dębowiec layers (Jureczka et al., 2012)

Figure 4.14: Fault and fracture framework (fault model)

4.2.2.1.2 Interpretation of geological horizons

Geological models of the storage complex zone consist of reservoir, caprock and structural elements. Structural model consists of the main geological horizons for this area including:

The PilotSTRATEGY project has received funding from the European Union's Horizon 2020 research and innovation programme under grant agreement No. 101022664

- structural maps of the top and the bottom of the Dębowiec layers (Figure 4.15),
- other horizons in the overburden of the reservoir (units in the zone of the Carpathian overthrust) - Figure 4.16.

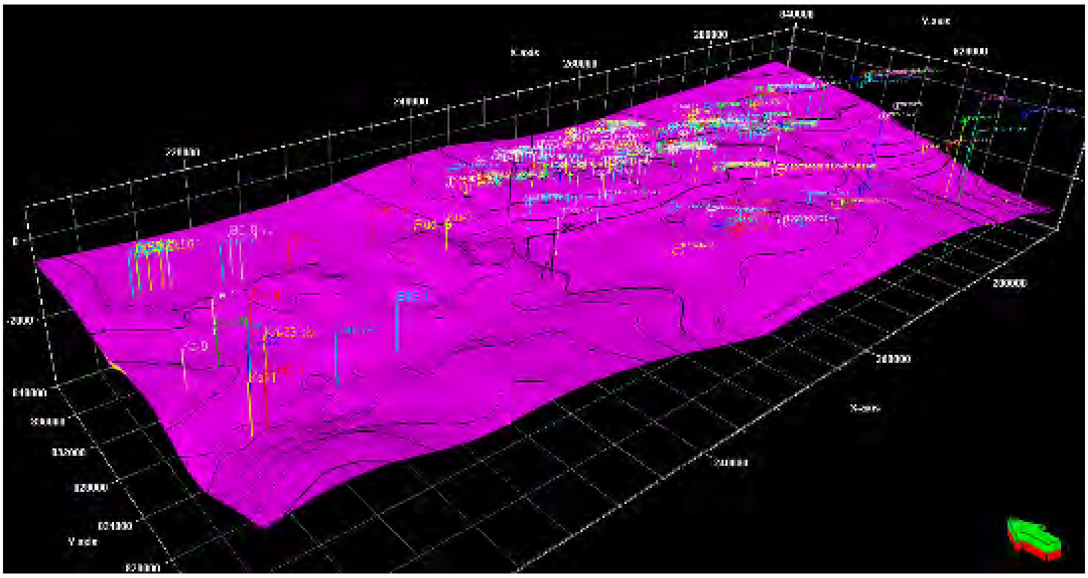

Figure 4.15: Structural maps of the top of the Dębowiec layers

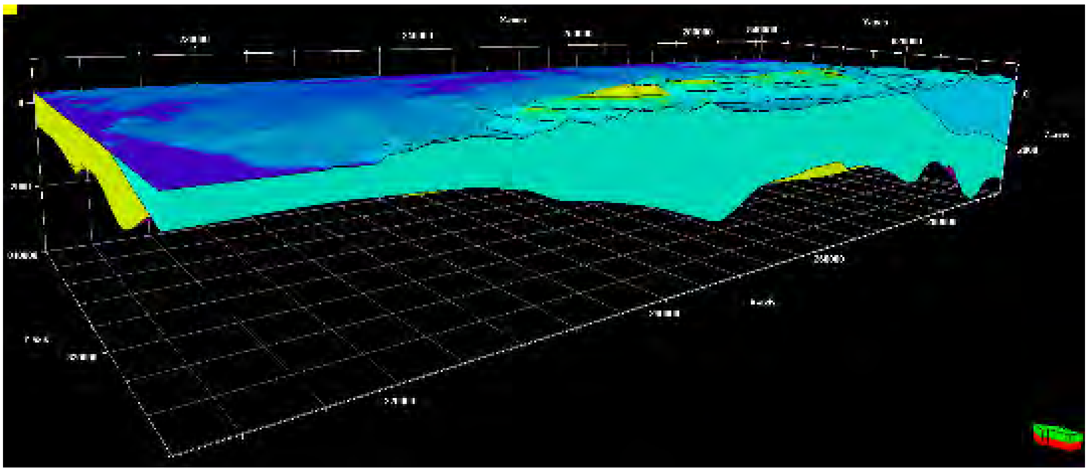

Figure 4.16: Model of the overburden layers

4.2.2.1.3 Structural framework of geological model

The developed static model includes the top and base of the reservoir, the top of the seal and other horizons in the overburden of potential reservoir for CO_2 storage in the area of the maximum range of the Dębowiec layers (Figure 4.17, 4.18).

The PilotSTRATEGY project has received funding from the European Union's Horizon 2020 research and innovation programme under grant agreement No. 101022664

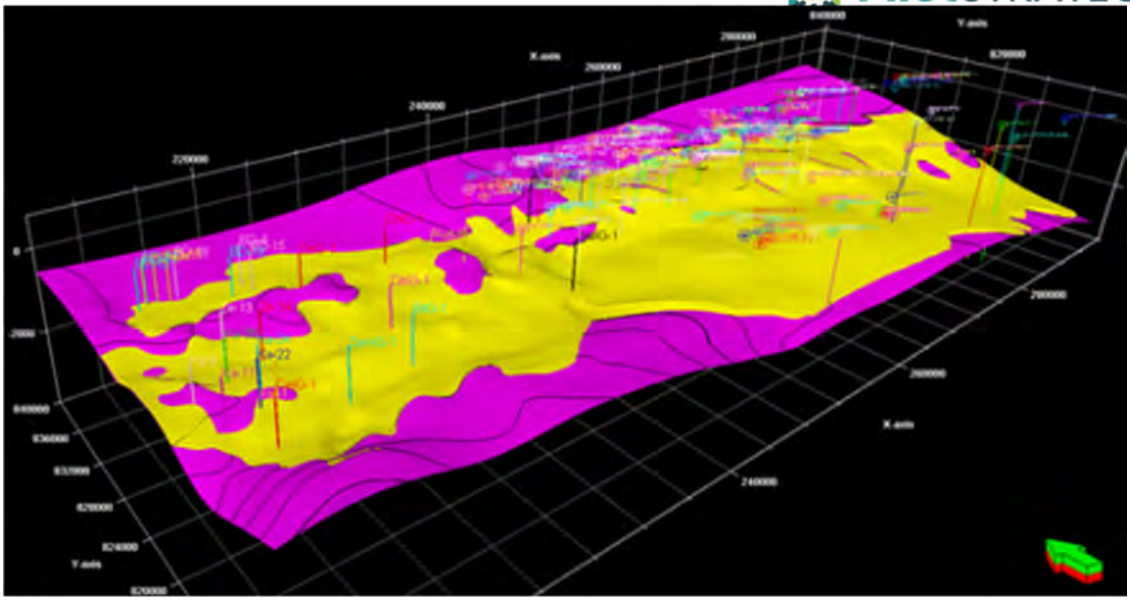

Figure 4.17: Geological grid of the Dębowiec layers

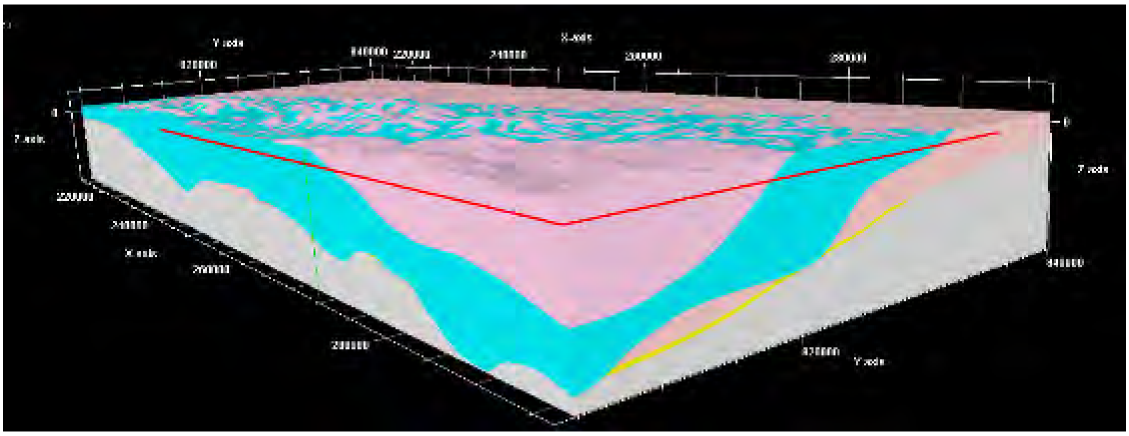

Figure 4.18: Geological grid of the overburden and underburden

4.2.2.2 PROPERTY MODELLING

The next step of work was petrophysical modelling. Data for petrophysical properties come also from the WP2 (Geo-characterization) in the form of plug analysis from the wells that have cores in the surrounding. These data were loaded into the project in form of a well log.

In the area of the Upper Silesian Coal Basin (USCB) the Dębowiec beds (lower Miocene sandstones) were chosen as prospective formation for the purposes of CO_2 storage in deep saline aquifers. The coverage of the study area with wells penetrating Miocene and its basement is relatively dense, but only for a few wells cores were preserved. Virtually, in all deep boreholes, well logging data are available, but only for the few the interpretation of lithology and petrophysical parameters was conducted, because the area was explored rather in order to assess hard coal resources in the Upper Carboniferous than, for example, to determine the properties of the Miocene caprock. In the vertical profile of the Dębowiec layers, gradation is observed, from the thickest in the bottom part (boulders, coarse-grained conglomerates) to fine in the top (fine-grained sandstones). The thickness of the Dębowiec Beds is variable and is usually in the range from 50 to 200-250 m.

The PilotSTRATEGY project has received funding from the European Union's Horizon 2020 research and innovation programme under grant agreement No. 101022664

In the case of the sandstone and conglomerate formations of Dębowiec beds, the average effective porosity is only slightly higher than 10% (the minimum for geological storage) and average permeability of about 40 mD. Similar properties are characteristic for Zamarskie beds (of a small thickness) occurring locally underneath (see Figure 4.1 in Appendix 7.2).

Based on previous research regarding the CO_2 storage potential in the Dębowiec Beds (Śliwińska et al., 2022; Koteras et al., 2020; Urych, Smoliński, 2019; Jureczka et al., 2012), the most suitable conditions exist in deep saline aquifers in the Miocene sediments of the Dębowiec Beds, located west of Bielsko-Biała (the area marked in Figure 4.19 as 'Expected area').

However, the work currently underway as part of the PilotSTRATEGY project focuses on determining the possibility of increasing the CO_2 storage potential in the Dębowiec layers through a detailed geological analysis of the area located east of Bielsko-Biała (the area marked in Figure 4.19 with a red rectangle as 'Maximum area').

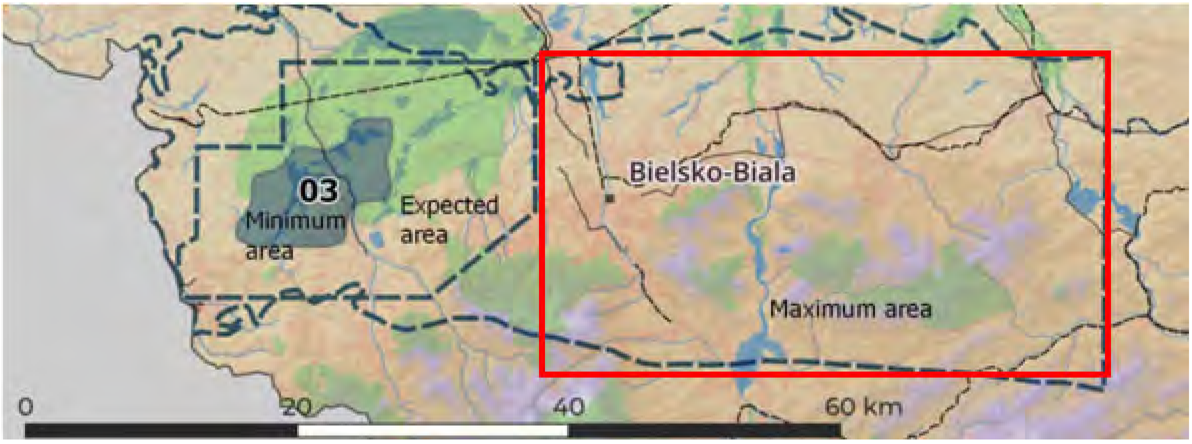

Figure 4.19: The maximum range area of the Dębowiec layers

Analysis of structural model of the storage formations based on data from 14 additional wells and updating of structural model in the area of the maximum range of the Dębowiec layers (updating the main zones in the area of east part of the model) was done (Figure 4.20).

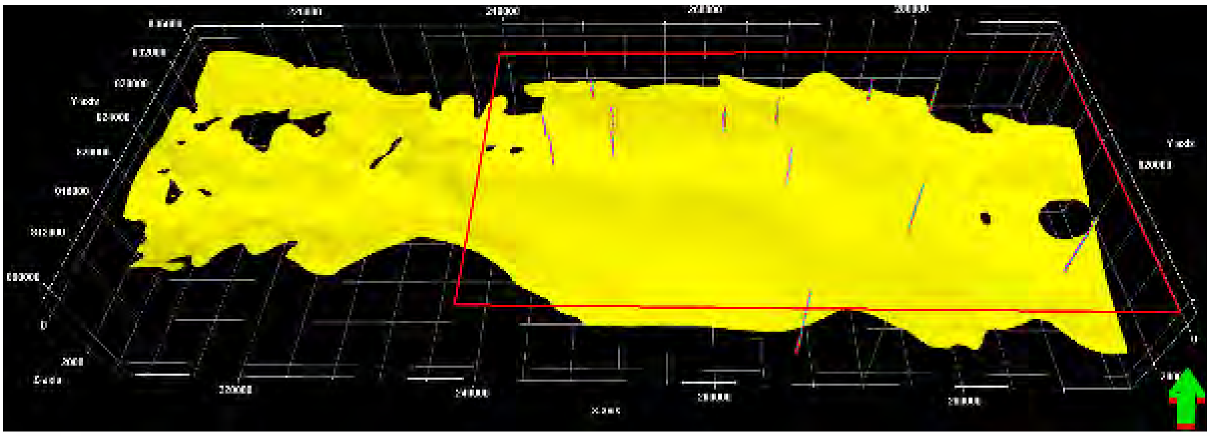

Figure 4.20: The east part of the model with additional wells

Available well data were loaded into the model and discretized (well log upscaling) in order to assign properties to the cells which are penetrated by wells. 14 additional LAS format log files with porosity

The PilotSTRATEGY project has received funding from the European Union's Horizon 2020 research and innovation programme under grant agreement No. 101022664

and shale content (Vshale) data were loaded into the model in order to perform upscaling and petrophysical modelling (Figure 4.21).

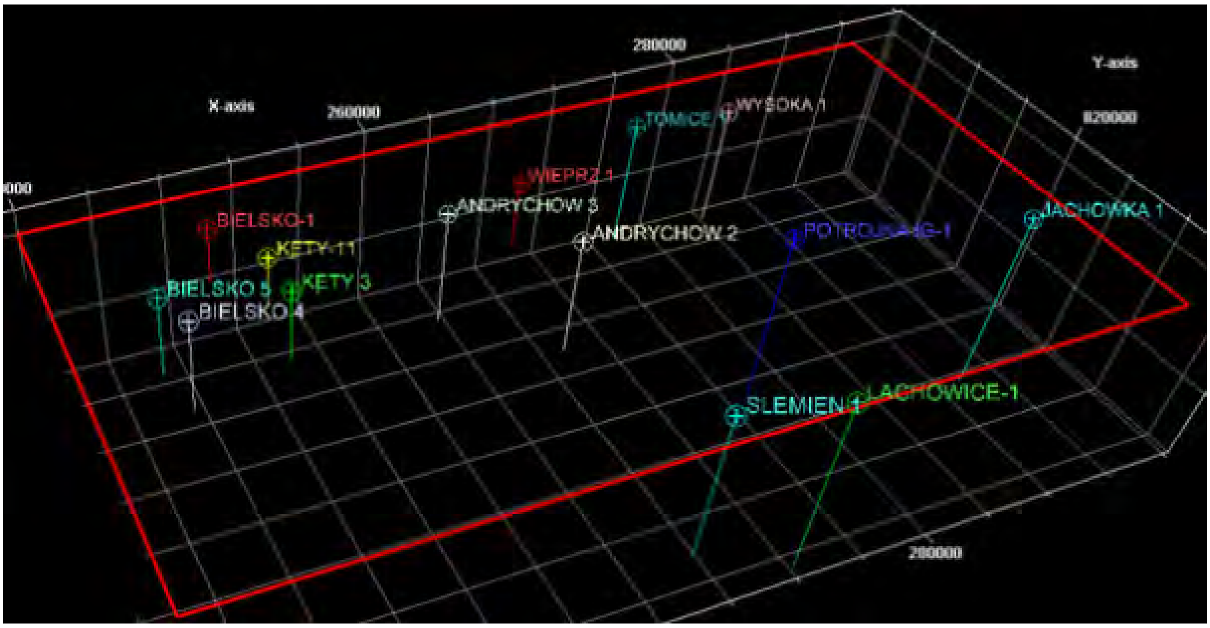

Figure 4.21: Additional wells in the area of east part of the model

4.2.2.2.1 Petrophysical modelling

There were observed lack of permeability data in log files for the east part of model (available only porosity and VShale data).

Data for porosity and shale volume were loaded into the project in form of well logs or point attributes with the results of laboratory tests on samples of cores from boreholes.

Based on the available data, borehole models were calculated, i.e., borehole data regarding reservoir parameters were subjected to averaging (upscaling). In the case of upscaling the effective porosity, arithmetic averaging was used, and permeability - geometric mean.

Petrel data analysis enables interactive analysis of distributions and trends and their relationships across all data types. Histogram, function, and stereonet windows - as well as the Petrel data analysis process - are provided for analyzing upscaled well data and grid properties.

In this case, the interactive variogram analysis included options for initial search-cone parameter suggestions and fitting the variogram to the regression curve, with the ability to also build nested variograms. Detailed analyses were saved for each property for direct use in the modeling processes.

The normalized well data populations were subjected to variography analysis in order to estimate the regional nature of the anisotropy of the analyzed parameters. The azimuths determining the directions with the highest correlation in a plane close to the horizontal and the range of correlation (variogram range) in the horizontal and vertical directions were determined. Based on well profiles, the starting points of variograms (nugget) were determined, reflecting the variability of a given parameter for a scale corresponding to distances smaller than the distances between the points for which data were available.

The PilotSTRATEGY project has received funding from the European Union's Horizon 2020 research and innovation programme under grant agreement No. 101022664

Results from variogram analysis with variogram modelling parameters for petrophysical modelling of Dębowieckie layers are presented in Figures 4.18-4.25 in Appendix 7.2.

Developed experimental variograms were used in porosity and shale volume modelling processes.

Modelling of porosity and shale volume was performed using Sequential Gaussian Simulation (SGS) algorithm separately for each individual sequences (zones).

Moreover, *Data analysis* module of Petrel was used to prepare input data using transformation sequences prior to petrophysical modeling. The input data were transformed to normal distributions due to the requirements of Sequential Gaussian Simulation algorithm.

The results of porosity modeling of the reservoir are presented in Figures 4.22-4.24 and Figure 4.24 in Appendix 7.2. The results of shale content (Vshale) modeling of the reservoir are presented in Figures 4.25-4.26 and Figure 4.25 in Appendix 7.2.

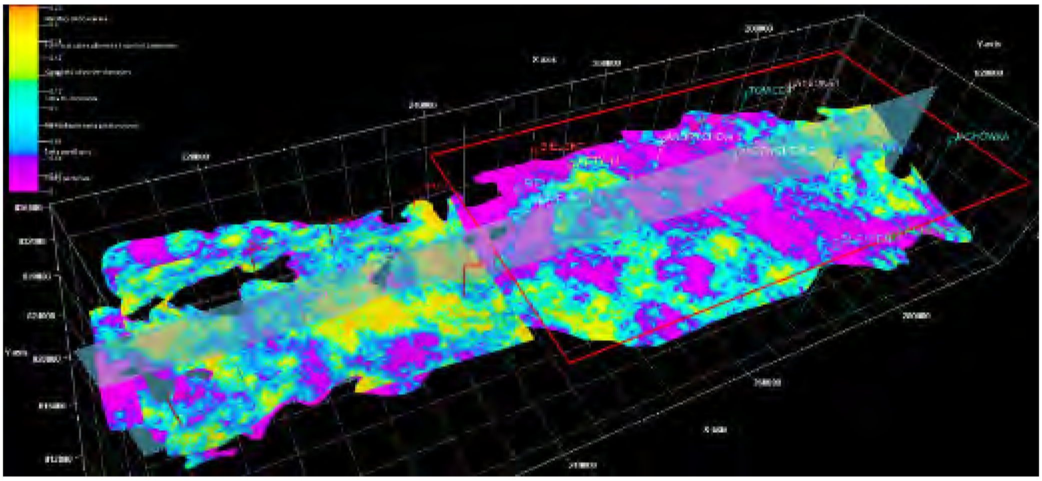

Figure 4.22: XY-Cross-section of Porosity field (one realization, SGS algorithm)

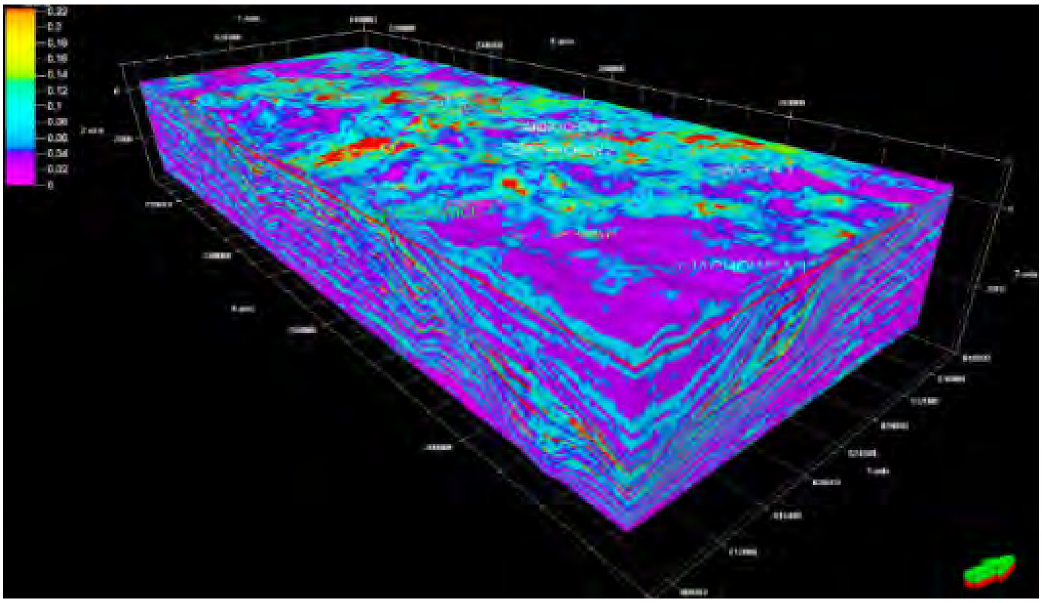

Figure 4.23: Porosity model (one realization, SGS algorithm)

The PilotSTRATEGY project has received funding from the European Union's Horizon 2020 research and innovation programme under grant agreement No. 101022664

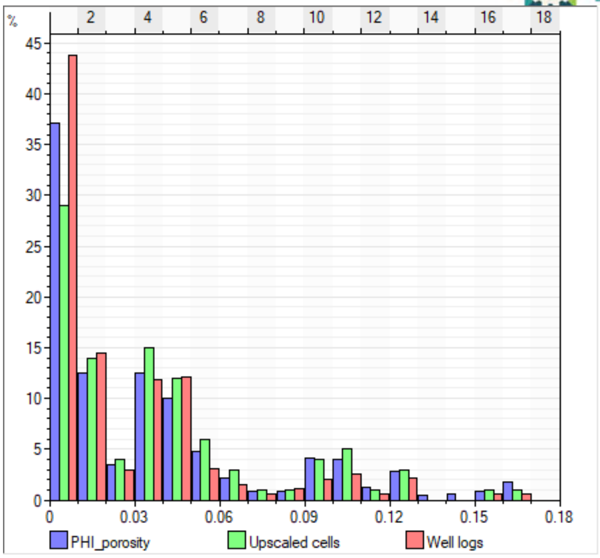

Figure 4.24: Results of porosity modelling of the reservoir layer from one realization of the SGS algorithm

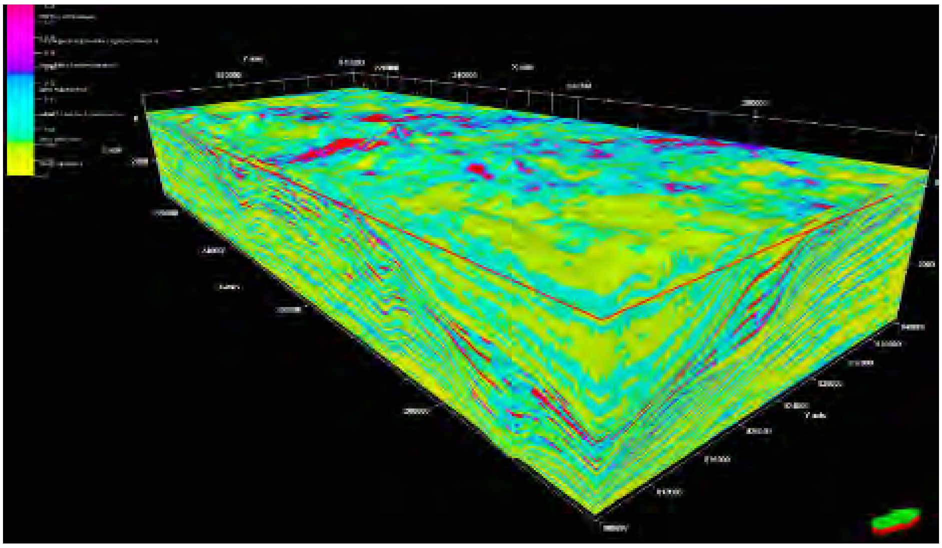

Figure 4.25: Model of shale content (Vshale) (one realization, SGS algorithm)

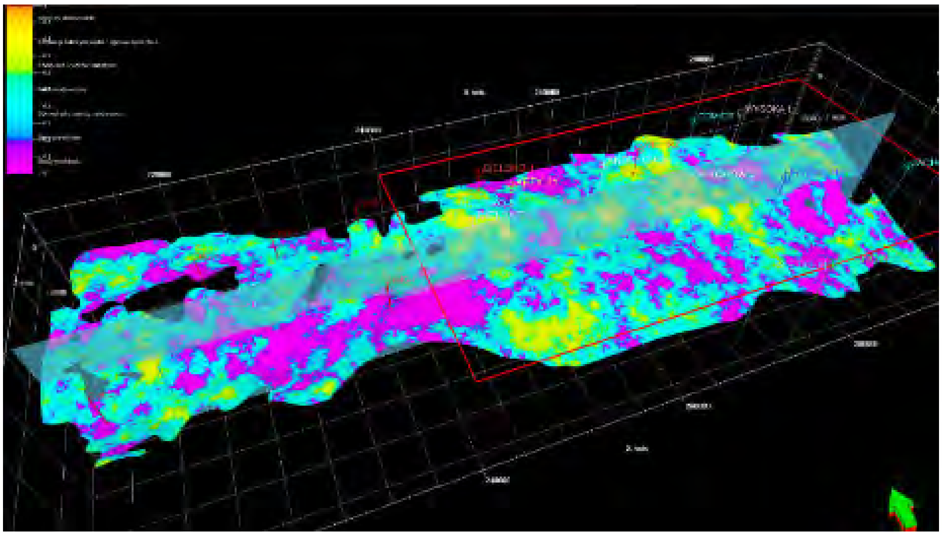

Figure 4.26: XY-cross-section of Shale content (Vshale) (one realization, SGS algorithm)

The PilotSTRATEGY project has received funding from the European Union's Horizon 2020 research and innovation programme under grant agreement No. 101022664

Furthermore, for additional analysis of porosity distribution in the model, the deterministic kriging method was used. As a result of porosity modelling, an area with porosity above 10% and dimensions of 9 km by 13 km was identified in the area of wells: KĘTY-11 and BIELSKO-1 (Figure 4.27-4.28).

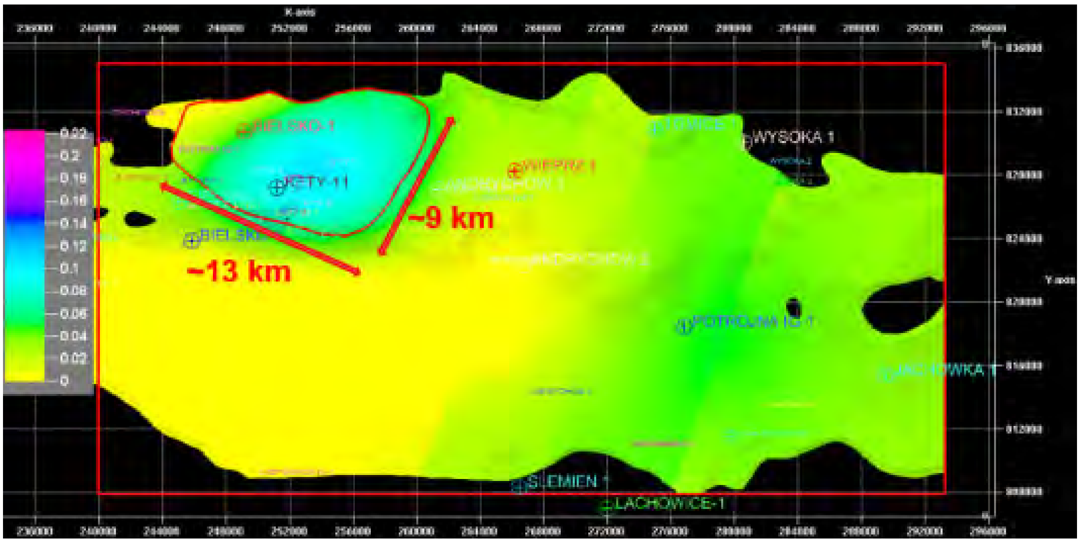

Figure 4.27: Selected part of the model with the highest values of porosity (from kriging algorithm)

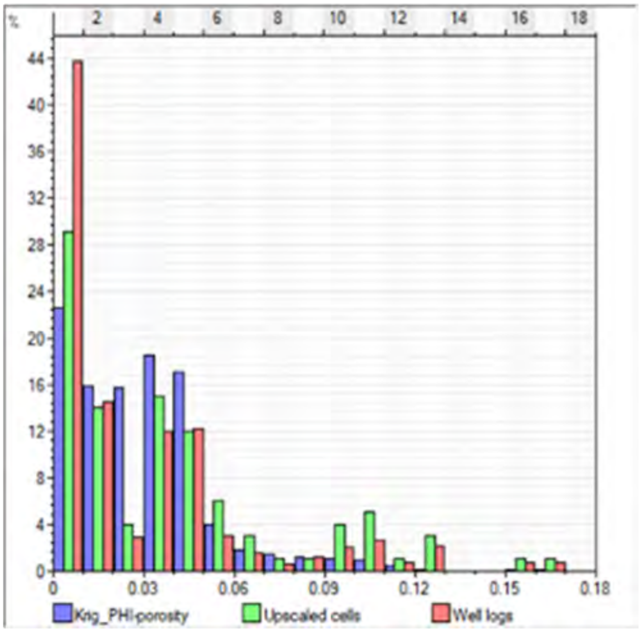

Figure 4.28: Porosity distribution – result from kriging

Due to lack of permeability data in log files for the east part of model (available only porosity and VShale data), the permeability estimation was done using the Zawisza formula (Equation 4.1):

$$K_{xy} = 195000 * \varphi^{3.15} * [1 - {V_{sh}}^{0.61}(1 - \varphi)^{3.18}]^2 \qquad (4.1)$$

where:
K_{xy} – permeability,
φ – porosity,
V_{sh} – volume of shale content.

The PilotSTRATEGY project has received funding from the European Union's Horizon 2020 research and innovation programme under grant agreement No. 101022664

In the Zawisza model, permeability depends on porosity and shale content (Zawisza L., 1993). As a result of permeability modelling, an area with permeability from ~10 mD to ~80 mD was identified in the area of wells: KĘTY-11 and BIELSKO-1 (Figure 4.29-4.30).

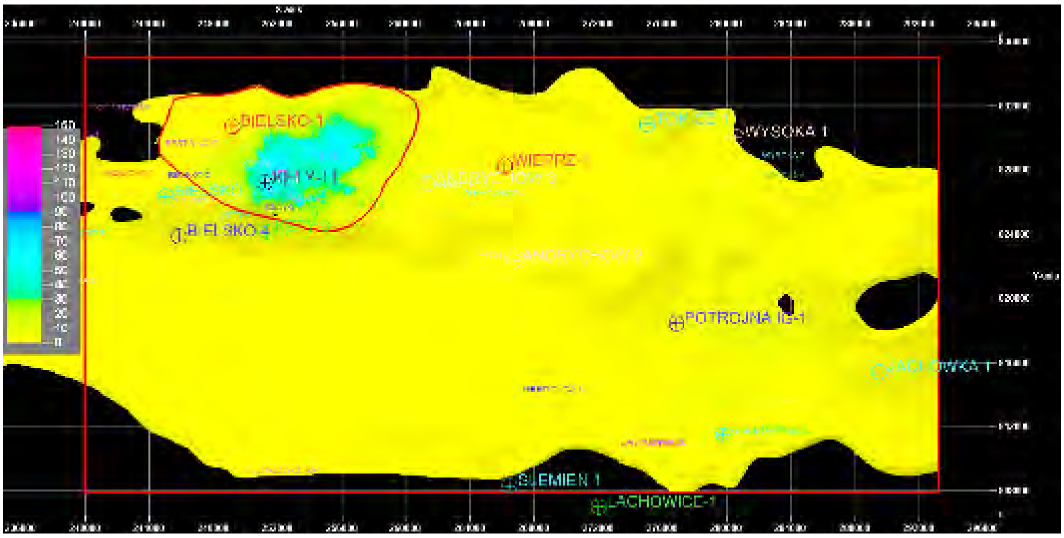

Figure 4.29: Permeability field (based on the Porosity model - Kriging interpolation (fig.2.54), using the Zawisza formula (eq. 4.1)

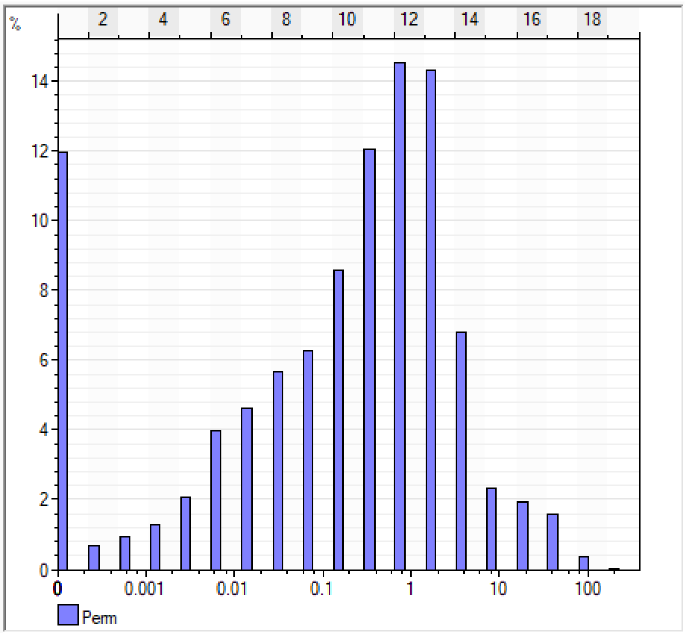

Figure 4.30: Permeability distribution (mD), inferred from the porosity field and using the Zawisza formula (eq.4.1)

The PilotSTRATEGY project has received funding from the European Union's Horizon 2020 research and innovation programme under grant agreement No. 101022664

4.2.3 Jurassic Czestochowa District (Ładzice DSA)

4.2.3.1 CONSTRUCTION OF GEOLOGICAL GRID

4.2.3.1.1 Fault modelling

Fault model was built based on the results obtained from WP2 Geo-characterization including geological maps, cross-sections, and other data. Location of part of faults are confirmed but some parts of faults are only hypothetical (supposed). We implemented it for the purposes of uncertainty and risk analysis (Figure 4.31). Location, range and grid orientation were assumed. The length of the model is about 62 km and its width is about 24 km (Figure 4.32).

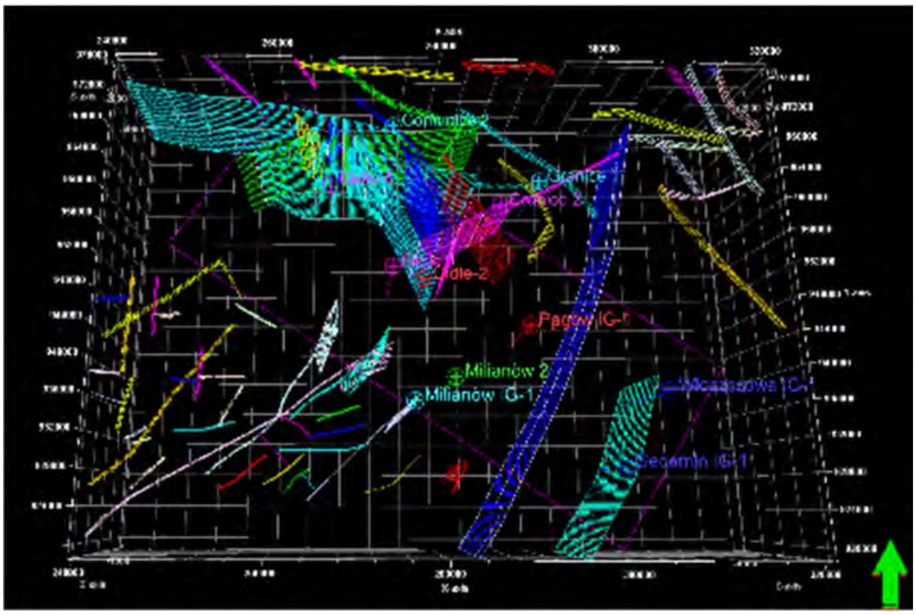

Figure 4.31: Fault and fracture model

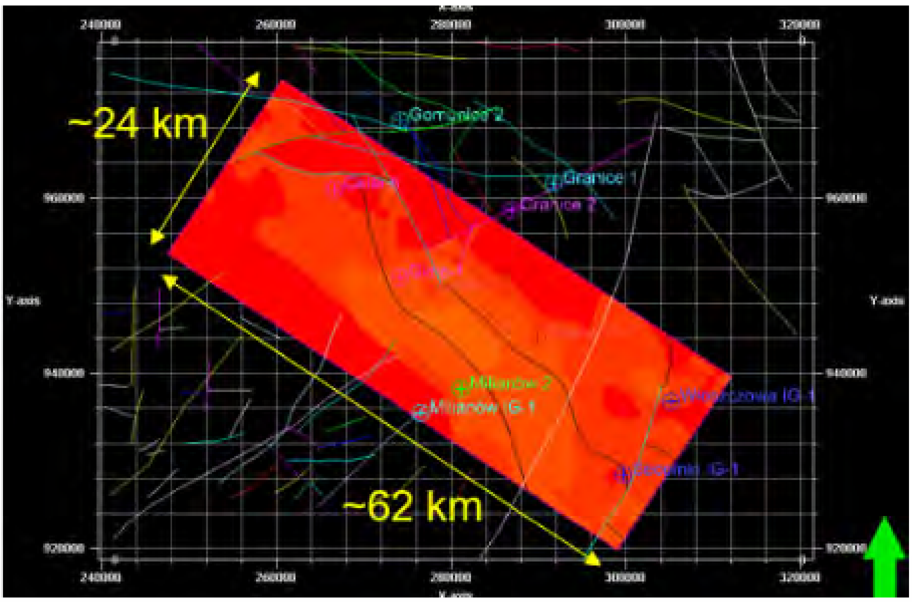

Figure 4.32: Location, range and grid orientation of the model

4.2.3.1.2 Interpretation of geological horizons

Geological models of the storage complex zone consist of reservoir, caprock and structural elements.

The PilotSTRATEGY project has received funding from the European Union's Horizon 2020 research and innovation programme under grant agreement No. 101022664

Horizon interpretations has been made based on on chronostratigraphy and litostratigraphy borehole data, well data correlation and analysis of geological cross-sections (Figure 4.26 in Appendix 7.2). Based on the data obtained, the analysis of the depth and thickness of reservoir deposits was carried out, and then the necessary modifications and corrections were introduced in the structural model.

4.2.3.1.3 Structural framework of geological model

Geological grid has been constructed by taking into account the horizons and faults. The modeling works were focused on depth, thickness and structural framework of the reservoir deposits (Figure 4.27 in Appendix 7.2).

The developed static model includes the top and base of the reservoir, the top of the seal and other horizons in the overburden and underburden of the reservoir, faults, and fracture framework (Figure 4.33).

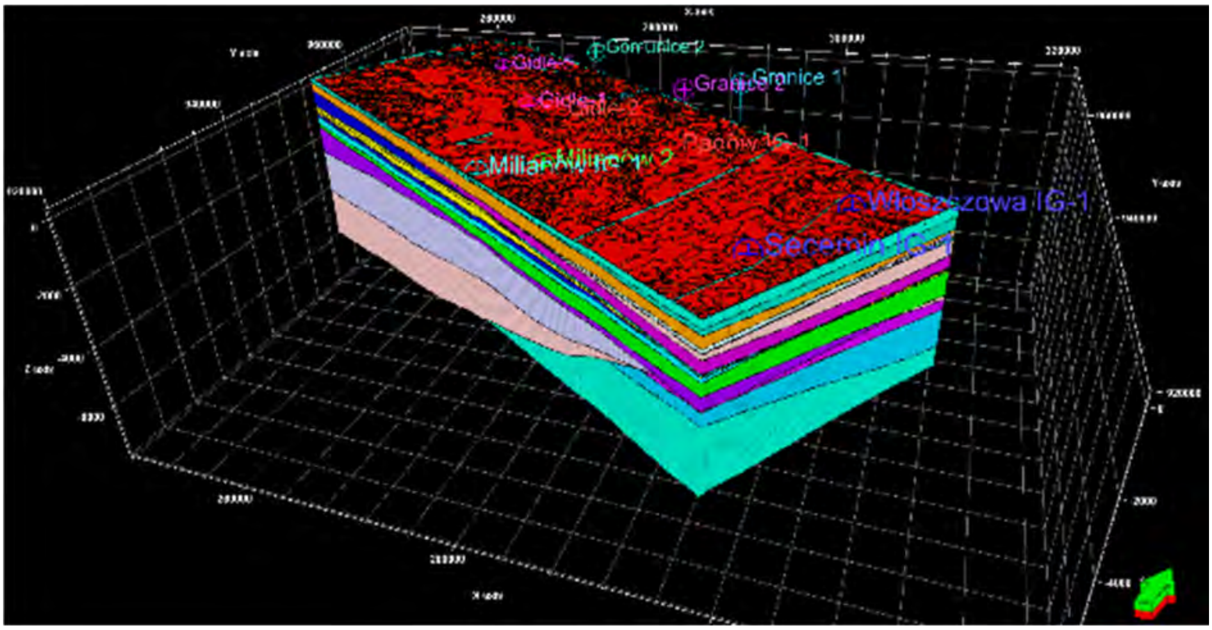

Figure 4.33: The model of reservoir layers with the overburden and underburden of the reservoir

4.2.3.2 PROPERTY MODELLING

The next step of work was petrophysical modelling. Data for petrophysical properties also come from the WP2 (Geo-characterization) in the form of plug analysis from the wells that have cores in the surrounding. Data were loaded into the project in form of well logs.

The output of this task for the model of Ładzice DSA are the following properties: facies, porosity and permeability calculated and interpolated for the whole grid area.

4.2.3.2.1 Characteristics of reservoir formations and sealing layers in the Częstochowa area

The reservoir formations are associated with water-saturated sediments of the Lower Jurassic and the Lower Middle Jurassic. The aquifer is composed of sandstones with a structure ranging from fine to coarse-grained and various-grained.

Within its range, the top of water-saturated formations lies at elevations ranging from -550 m to -1400 m (depth: 780-1600 m), the thickness is 30-390 m, and the overburden is formed by a continuous layer of poorly permeable Middle and Upper Jurassic formations (marls, clays, claystones and mudstones) with a thickness of 350 - 620 m.

The PilotSTRATEGY project has received funding from the European Union's Horizon 2020 research and innovation programme under grant agreement No. 101022664

The area of the potential CO_2 storage reservoirs is relatively poorly explored in terms of hydrogeology. The test results showed porosity from 7.69 to 22.1% and permeability from 16 to 1478 mD.

4.2.3.2.2 Facies modelling

To build a lithological model, Sequential Indicator Simulation (SIS) algorithm, belonging to a group of stochastic algorithms (Deutsch, Journel 1992), was applied. Initial facies modeling was performed for reservoir layers with the primary caprock layers for an area of 62 km by 24 km (Figure 4.34).

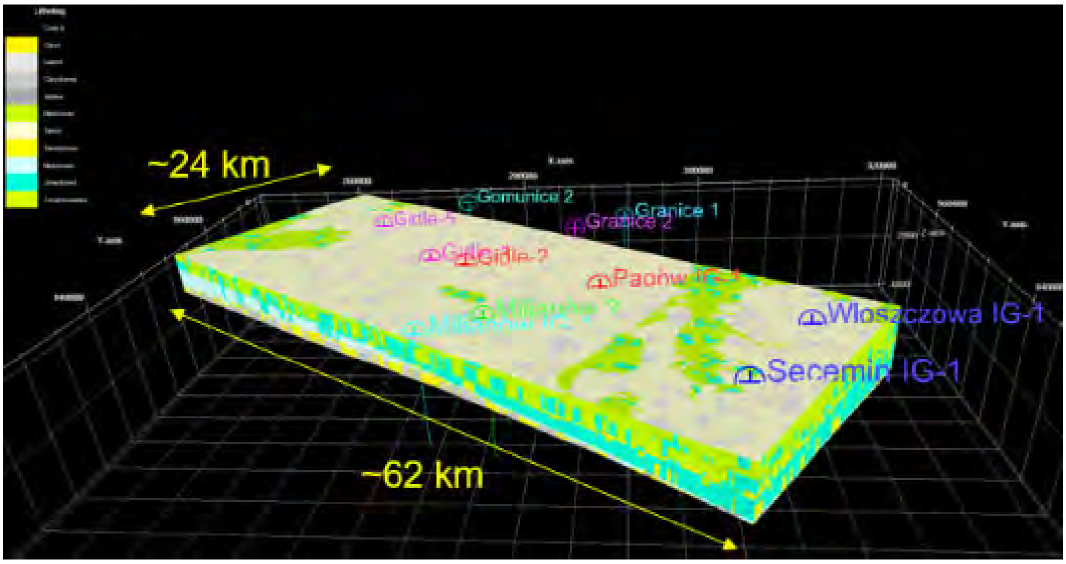

Figure 4.34: Facies model of reservoir layers with the primary caprock layers

Basic input material applied to build a 3D lithological model of the deposit included lithological data from boreholes. The lithofacies from the available core profiles has been given numerical codes (Figure 4.35). Such processed data has been implemented in the structural model prepared earlier.

Code	Name	Color
0	clays	
1	loams	
2	claystones	
3	shales	
4	marlstones	
5	sands	
6	sandstones	
7	mudstones	
8	limestones	
9	conglomerates	

Figure 4.35: List of lithofacies encoded in numerical form

Then, analysis of data availability was performed, and, on this basis, two potential storage areas have been indicated (Figure 4.36):

- Area No. 1 - wells: Pągów IG-1, Milianów 2, Milianów IG-1 - all wells with data for porosity and permeability (lack of VSHALE data);

The PilotSTRATEGY project has received funding from the European Union's Horizon 2020 research and innovation programme under grant agreement No. 101022664

- Area No. 2 - wells: Gidle-1, Gidle-2, Gidle-5 – all wells with data only for porosity (lack of VSHALE and permeability data).

However, only Area no. 1 with dimensions of 10 km by 19 km (Figure 4.36) was selected for further analysis.

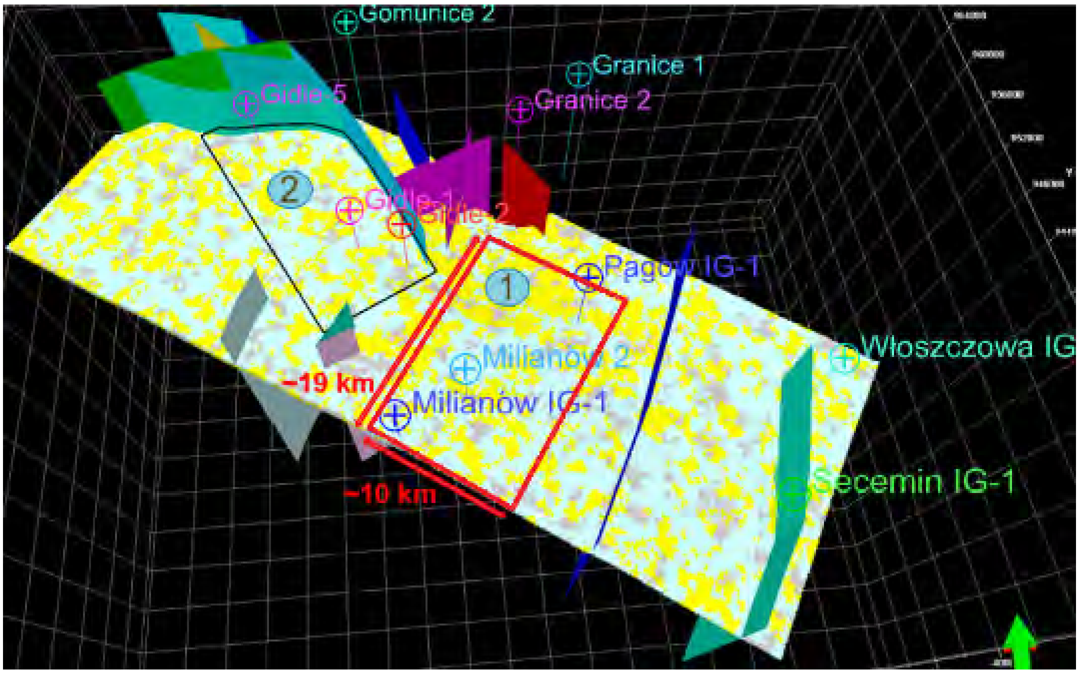

Figure 4.36: Two potential storage areas indicated based on analysis of data availability and part of the model selected for further analysis (in red)

Modelling for selected Area No. 1 has been carried out for the storage complex zone: reservoir, caprock and structural elements (Figure 4.28 in Appendix 7.2).

Additional data on lithology in the entire storage complex zone, including the overburden in three wells (Pągów IG-1, Milianów 2, Milianów IG-1) were implemented into the model. The results of well logs, in discrete form, were scaled up (Scale up well logs procedure). Upscaling algorithm which assigns a given interval to a lithological type which is the most common in the averaging interval, was applied for the lithological data. Accuracy of matching the average data in the model depends mainly on the vertical resolution of the model, i.e., its division into litho-stratigraphic layers. As a result, updated facies model of the storage complex includes (Figure 4.37):

- the reservoir layer with the thickness of about 50 m (Lower Jurassic and the Lower Middle Jurassic - J1/J2 sandstones);
- the primary sealing layer with the thickness of about 30 m (claystones, mudstones) and overburden.

The PilotSTRATEGY project has received funding from the European Union's Horizon 2020 research and innovation programme under grant agreement No. 101022664

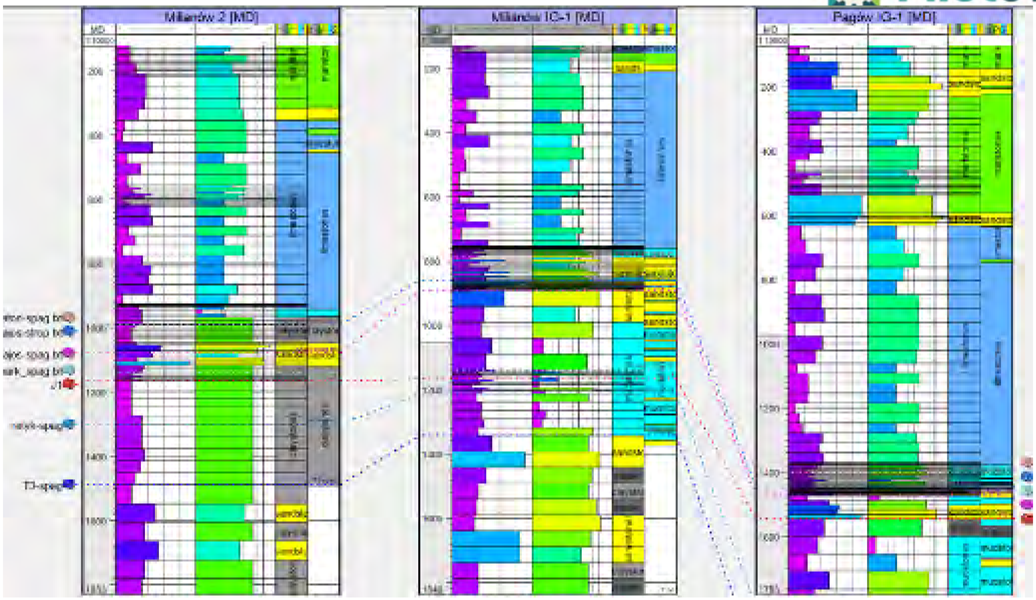

Figure 4.37: Facies model - results of scale up well logs

The next stage of statistical analysis included:

a) calculation of vertical proportion curves which give an estimation of the facies proportions for each layer of the model
b) analysis of variograms which are used to analyze and model the spatial structure of the data.

The variograms and the vertical proportion curves were made in the *Data analysis* module of Petrel.

The vertical proportion curves were calculated from the facies upscaled at the wells are shown in Figure 4.38.

The results from the variogram analysis are variogram functions for the major, minor and vertical directions. These can be used directly as input to the property modelling.

Variogram parameters are of key importance at the stage of calculating spatial distributions, because they determine the spatial correlation of the modeled parameters, and thus the method of extrapolation and interpolation of well data and the scale of their impact on the simulation/estimation result between and outside wells. The size and orientation of the modelled facies are directly related to the defined parameters of parameters of variogram models (see Figure 4.29-4.32 in Appendix 7.2).

To build a facies model, Sequential Indicator Simulation (SIS) algorithm, belonging to a group of stochastic algorithms (Deutsch, Journel 1992), was applied. The lithological model was developed using the calculated variography parameters of available borehole data and using the developed curves of facies proportions in the vertical direction as an element of the optimization of spatial models. Facies modeling has been done both for overburden and reservoir layers (Figure 4.39). A statistical summary of the facies modeling results is presented in Figure 4.40 and Tables 4.1-4.2 in Appendix 7.2.

The PilotSTRATEGY project has received funding from the European Union's Horizon 2020 research and innovation programme under grant agreement No. 101022664

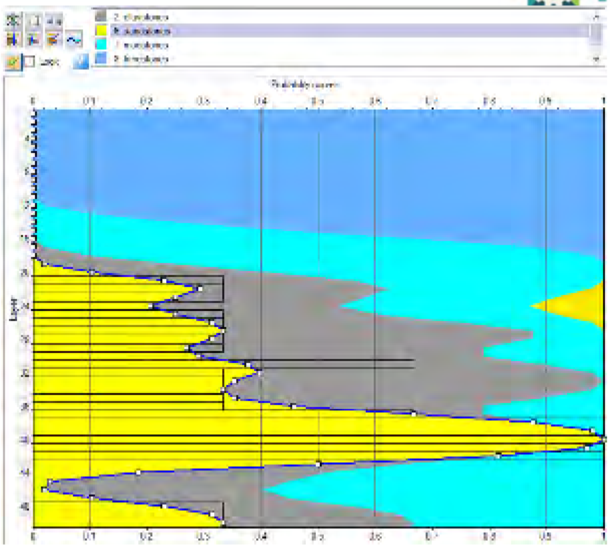

Figure 4.38: Vertical proportion curves of facies

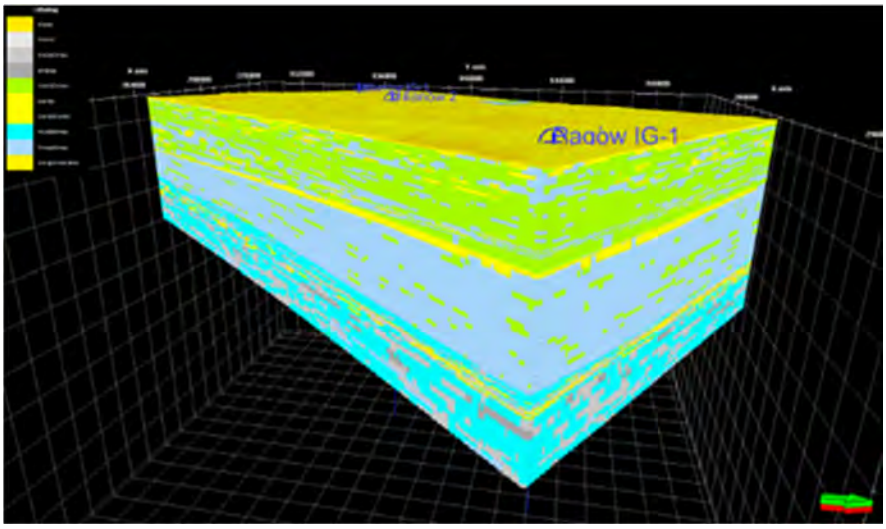

Figure 4.39: Facies model of the storage complex (reservoir and overburden with sealing layers)

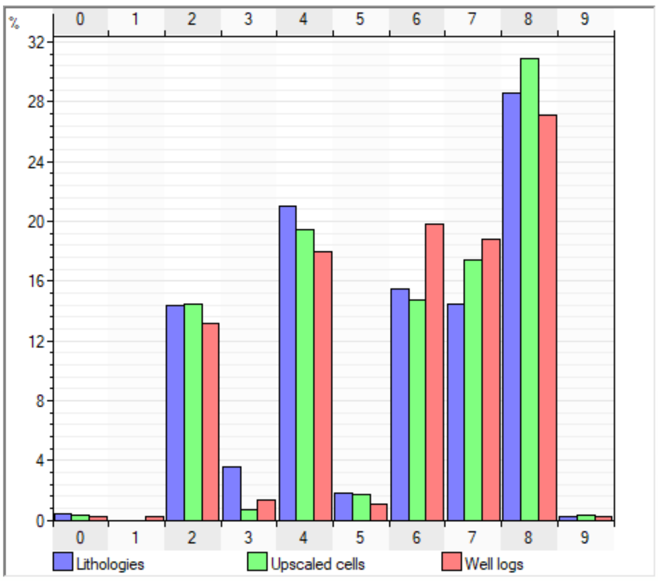

Figure 4.40: Statistical characteristics of the facies model

The PilotSTRATEGY project has received funding from the European Union's Horizon 2020 research and innovation programme under grant agreement No. 101022664

4.2.3.2.3 Petrophysical modelling

In the case of Ładzice DSA, there were observed lack of VShale (shale volume) data in log files (available only porosity and permeability). The created facies model was used as conditioning for the petrophysical model.

Modelling of porosity and permeability was performed using *Sequential Gaussian Simulation (SGS)* algorithm separately for individual sequences using the control procedure of the previously developed lithological model (petrophysical properties linked to lithofacies). *Data analysis* module of Petrel was used to preparation input data using transformation sequences and analysis of variograms prior to petrophysical modeling. The input data were transformed to normal distributions due to the requirements of *Sequential Gaussian Simulation* algorithm.

In the case of porosity model, variograms were used (Figures 4.33-4.36 in Appendix 7.2), whenever possible for each stratigraphic sequence - this enabled a fairly good estimation of the porosity distribution.

The results from the variogram analysis of permeability data are presented in Figures 4.37-4.38 in Appendix 7.2). Permeability modeling was performed in co-kriging with porosity, which further increased the accuracy of the permeability distribution in the model. Permeability is a typical logarithmic property, so in this case, data were transformed to logarithmic distribution and then to normal distribution. Additionally in modelling of permeability, porosity was used as the secondary variable.

The results of petrophysical modeling of the reservoir layer are presented in Figures 4.41-4.43 and the results of petrophysical modeling of the reservoir layer with the overburden are presented in Figures 4.44-4.45.

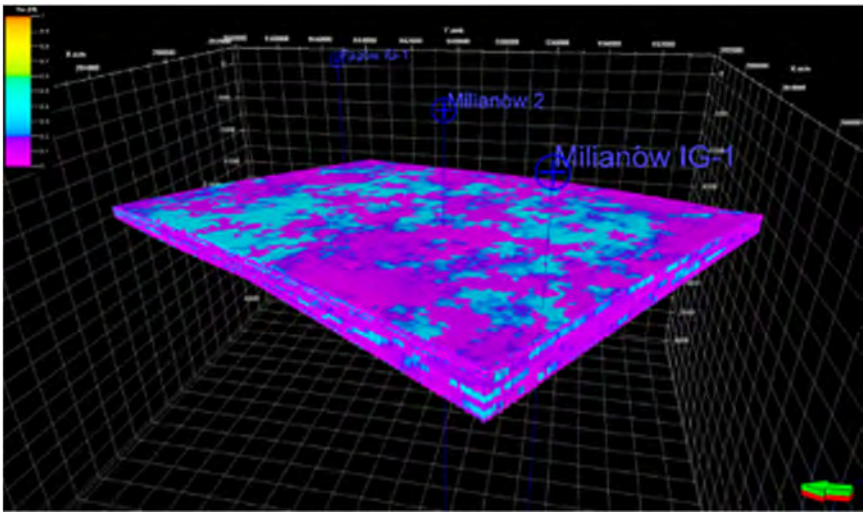

Figure 4.41: Porosity field of the reservoir (one realization from SGS)

The PilotSTRATEGY project has received funding from the European Union's Horizon 2020 research and innovation programme under grant agreement No. 101022664

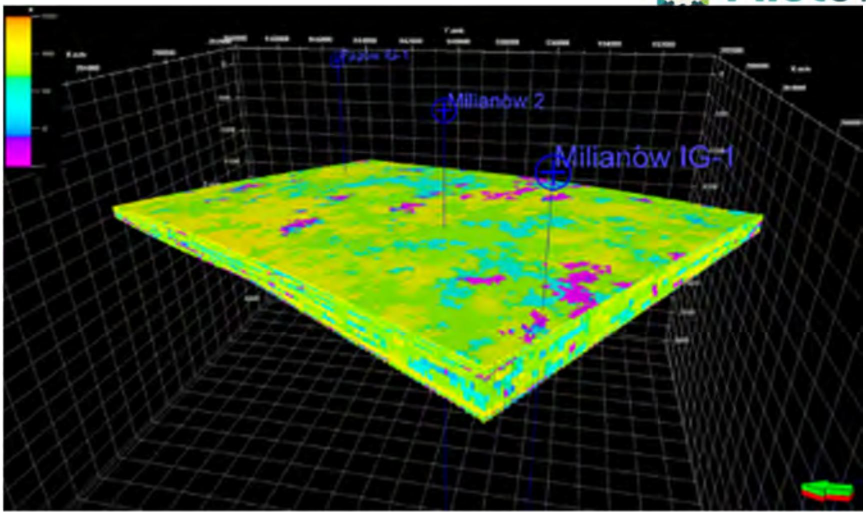

Figure 4.42: Permeability field of the reservoir (one realization from SGS)

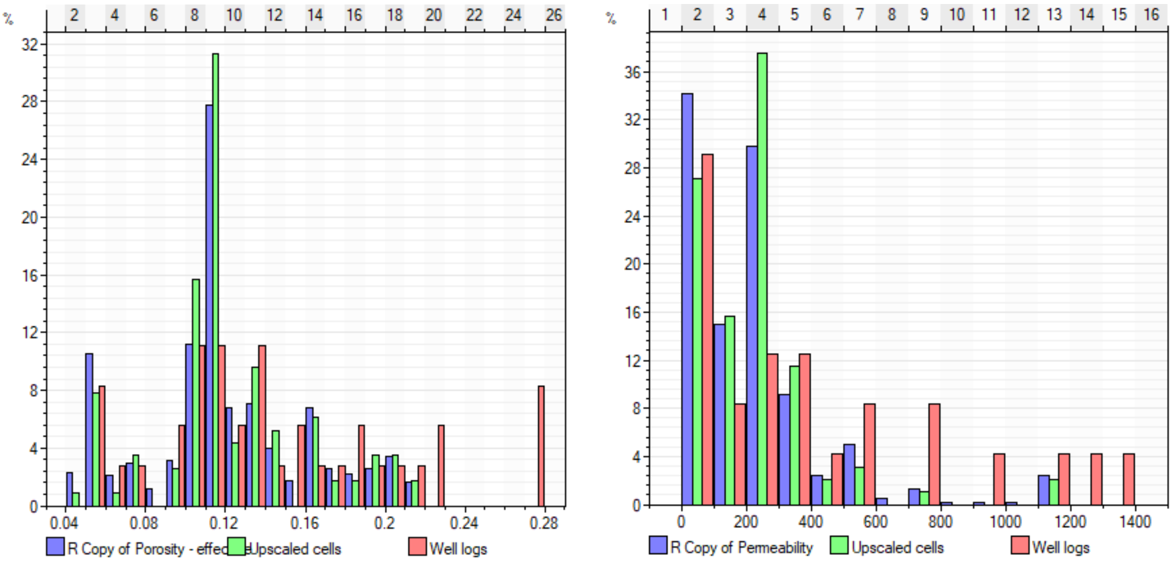

Figure 4.43: Results of petrophysical modelling of the reservoir layer: (left) porosity distribution [-], (right) permeability distribution [mD], from one realization of the SGS algorithm

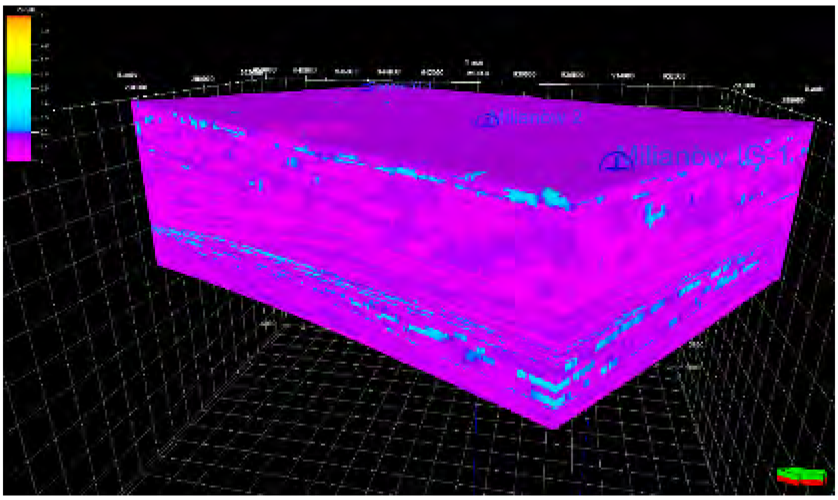

Figure 4.44: Porosity field of the reservoir and the overburden, from one realization of the SGS algorithm

The PilotSTRATEGY project has received funding from the European Union's Horizon 2020 research and innovation programme under grant agreement No. 101022664

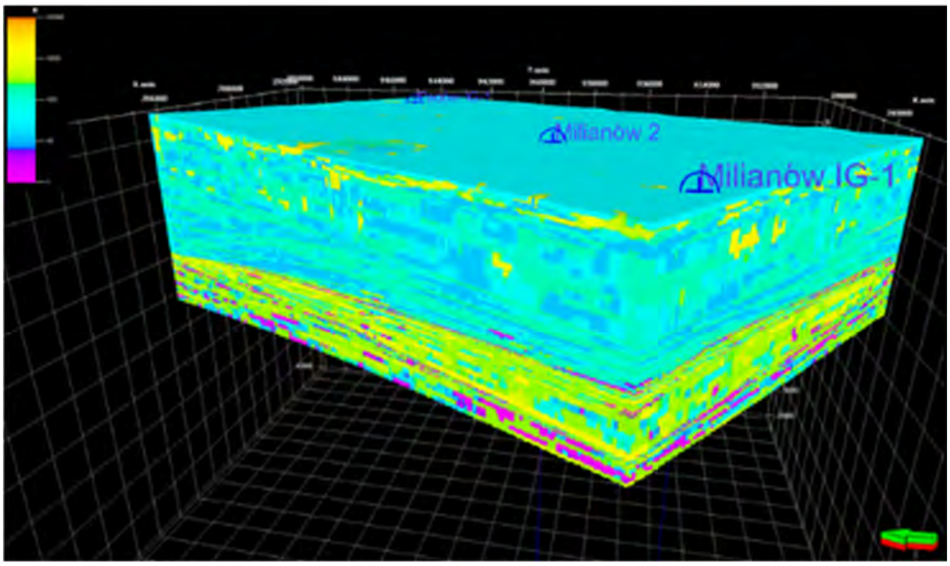

Figure 4.45: Permeability field of the reservoir and the overburden, from one realization from the SGS algorithm

4.3 Considering the geological uncertainties

The uncertainty study, including the risk analysis of modeling structural surfaces as well as comprehensive uncertainty analysis of facies and petrophysical properties, was performed only for the Ładzice DSA in Jurassic Czestochowa District.

4.3.1 Risk analysis of modeling structural surfaces

The risk assessment of the quality of the 3D model in the Petrel software is performed with the module: *Uncertainty and optimization* (task *Uncertainty*). This is used to calculate alternative, stochastic variants of the structural surfaces included in the 3D model (horizons). The stochastically assessed risk is calculated using the following Equation 4.2:

$$S_r = S_{bc} + U_{1s} * U_{sgs} \qquad (4.2)$$

where:
S_r - surface realization,
S_{bc} - the base case surface (deterministic),
U_{1s} - one standard deviation error on the base case, can be a surface or a constant,
U_{sgs} - sequential gaussian simulation (SGS) surface (stochastic) with 0 value at control points (i.e. at wells).

Simulated models are characterized by full compliance with the input data (wells), while in zones not controlled by data, they show a deviation from the structural model closing within the standard deviation. The stratigraphic horizons modeled in this work were generated using the convergent interpolation gridding algorithm of the Schlumberger Petrel software. This algorithm uses an iterative technique to minimize the curvature of the grid using a constrained, biharmonic operator. The convergent interpolation gridding technique preserves general trends in areas with few well log tops, while details are included in areas where more tops exist (Dommisse, 2022).

The PilotSTRATEGY project has received funding from the European Union's Horizon 2020 research and innovation programme under grant agreement No. 101022664

Surfaces of the base of Lower Jurassic (the base of reservoir layer) and the top of Middle Jurassic (the top of main caprock layer) in the form of a cross-section are shown in Figure 4.46 (and Figure 4.39 in Appendix 7.2).

The analysis reveals that the deterministic variant of the structural surface used creates a surface approximately constituting the average of the used stochastic variants, however, the significant probability of deviations of the mapped structural surface from the model is observed. Full compliance of the deterministic model and stochastic variants is achieved at the point of intersection of the cross-section line with the boreholes.

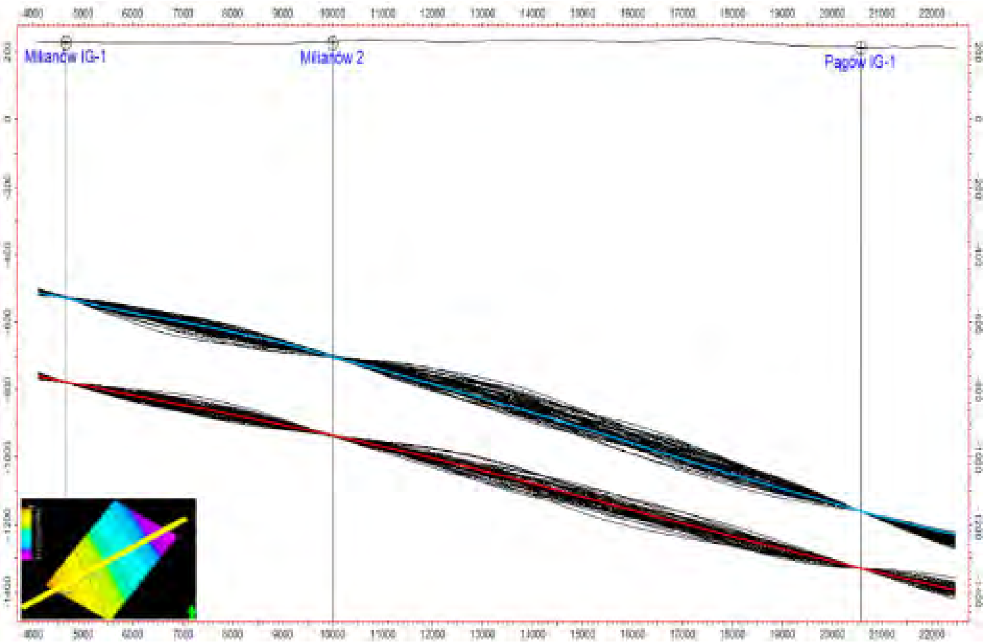

Figure 4.46: Surfaces of the Lower Jurassic floor (red line) and Middle Jurassic top (blue line) and 50 stochastic variants (black lines) on cross-section

4.3.2 Comprehensive uncertainty analysis

The comprehensive uncertainty (facies and petrophysical properties) assessments is used to determine the pore volumes based on the *Uncertainty and optimization* module (Petrel) with 300 simulations of facies and petrophysical models. More precisely, it included 300 simulations of model with facies, porosity and permeability realizations. These 300 samples come from stochastic sampling (without uncertainty ranges on model parameters). The aim of this analysis was to determine to what extent the use of stochastic methods influences volumetric calculations. Based on each model, volumetric calculations representing the pore volume were performed.

To model facies, porosity and permeability distributions, the same methods, parameters and the results of statistical analysis were used as described in the *Facies modeling* section and in the *Petrophysical modelling* section, including the calculated variography parameters of available borehole data, etc. As previously, we used Sequential Indicator Simulation (SIS) algorithm for facies modelling, Sequential Gaussian Simulation (SGS) algorithm for porosity and permeability modelling with a facies conditioning for porosity and a co-simulation with porosity for permeability.

Pore volume distribution resulting from this comprehensive uncertainty analysis is presented in the final histogram (Figure 4.47). The P10, P50 and P90 percentiles values are extracted from this distribution. The median (P50) value of pore volume, the most probable one, is 5640 million rm^3. The

The PilotSTRATEGY project has received funding from the European Union's Horizon 2020 research and innovation programme under grant agreement No. 101022664

P90 value, *i.e.*, the optimistic value in this case, can be considered 5810 million m^3, and the pessimistic value (P10) is 5483 million m^3 (Table 4.1).

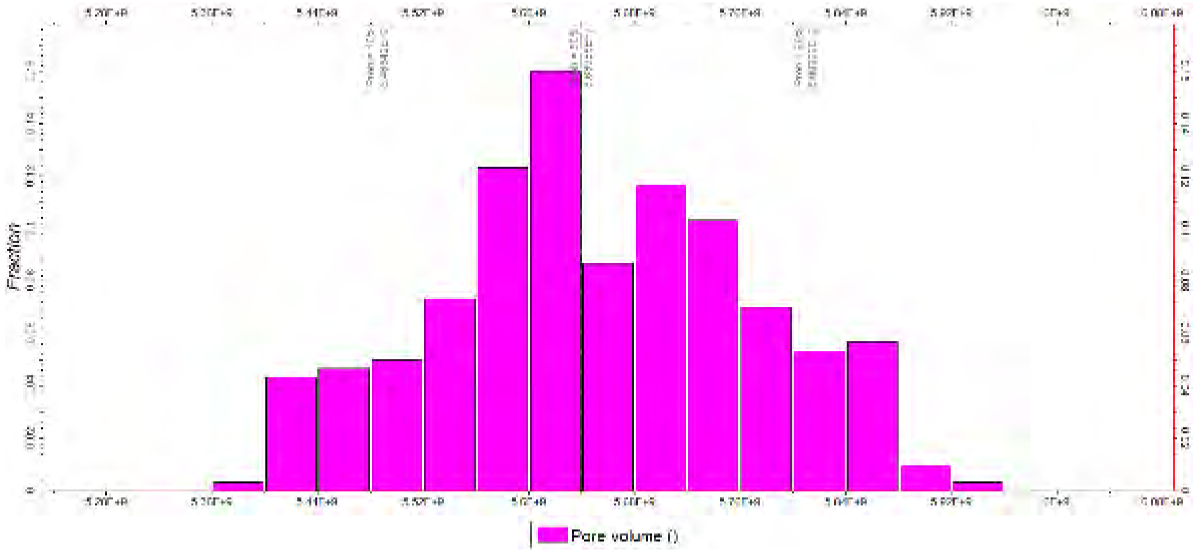

Figure 4.47: Summary histogram of comprehensive uncertainty analysis with marked P10, P50, P90 percentiles (Pore volume - 300 scenarios)

Table 4.1: The parameters of uncertainty analysis for the values of P10, P50 and P90 percentiles

Probability	Case name	Simulation numer ($LOOP)	Pore volume [*10^6 rm^3]
P10	END_82	50	5483
P50	END_271	239	5640
P90	END_118	86	5810

Knowing the values of P10, P50 and P90, it is possible to indicate the realizations that are the closest to the values corresponding to the low, mid and high case pore volumes (Figure 4.48).

a) 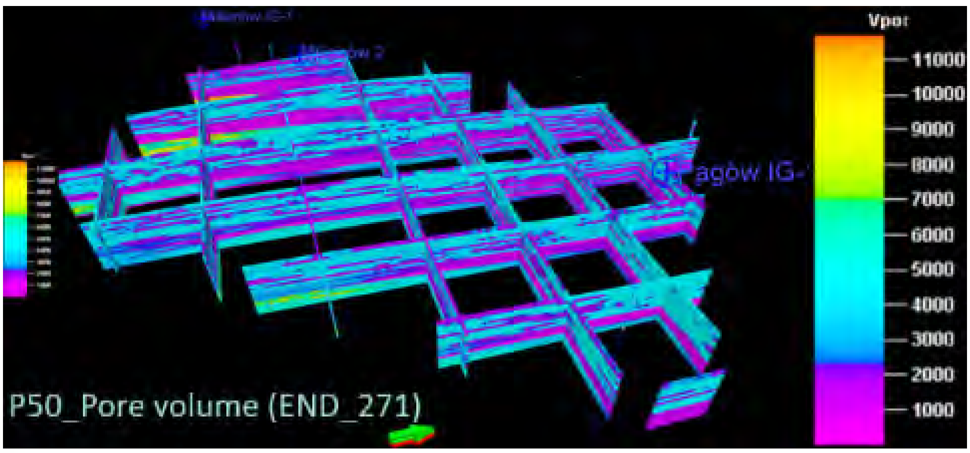

The PilotSTRATEGY project has received funding from the European Union's Horizon 2020 research and innovation programme under grant agreement No. 101022664

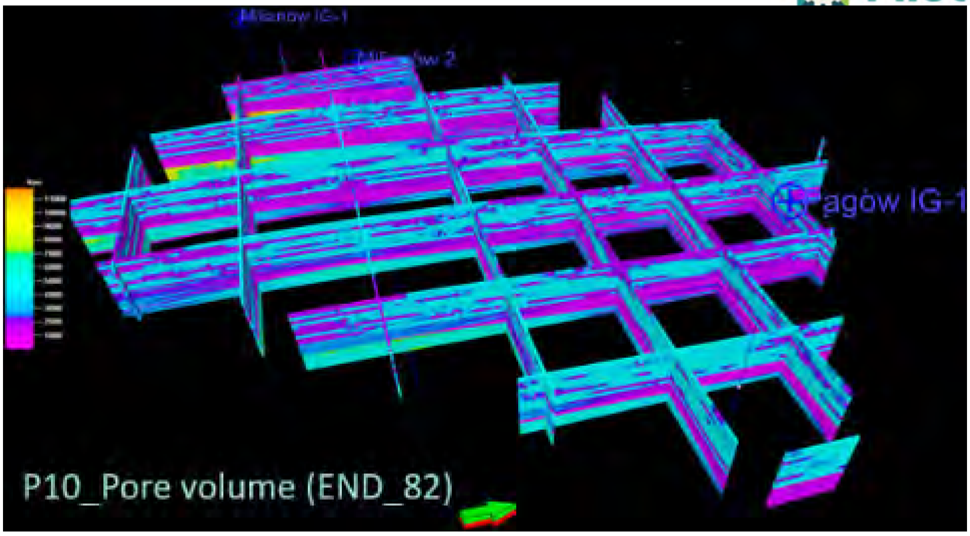

b)

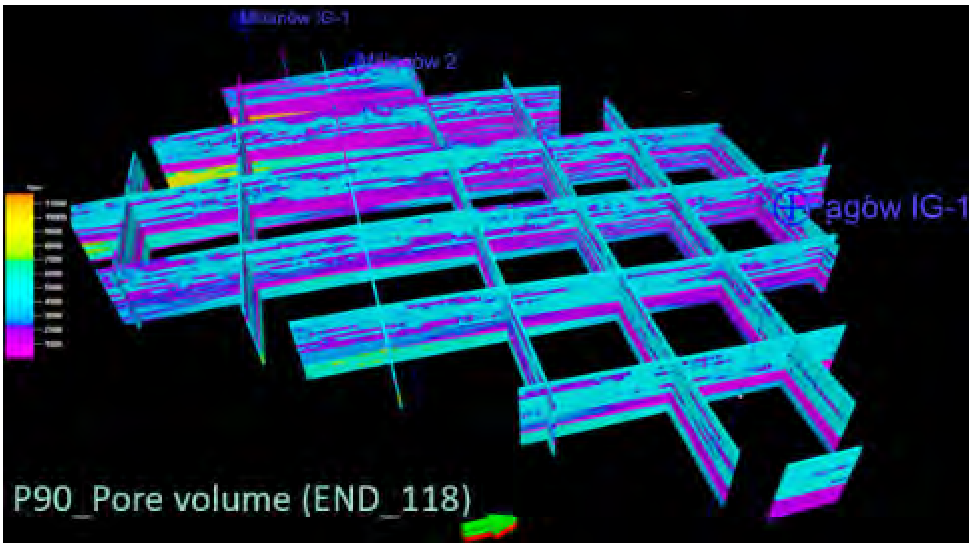

c)

Figure 4.48: Workflow results for uncertainty assessments (facies and petrophysical properties) to determine the pore volumes using Uncertainty and optimization module (Petrel). The models corresponding to a) P10, b) P50, c) P90.

The porosity field of the stochastic realizations closest to the P10, P50, P90 percentiles of the pore volume model are shown in Figures 4.49-4.51. The permeability field of those realizations are shown in Figures 4.52-4.54

The PilotSTRATEGY project has received funding from the European Union's Horizon 2020 research and innovation programme under grant agreement No. 101022664

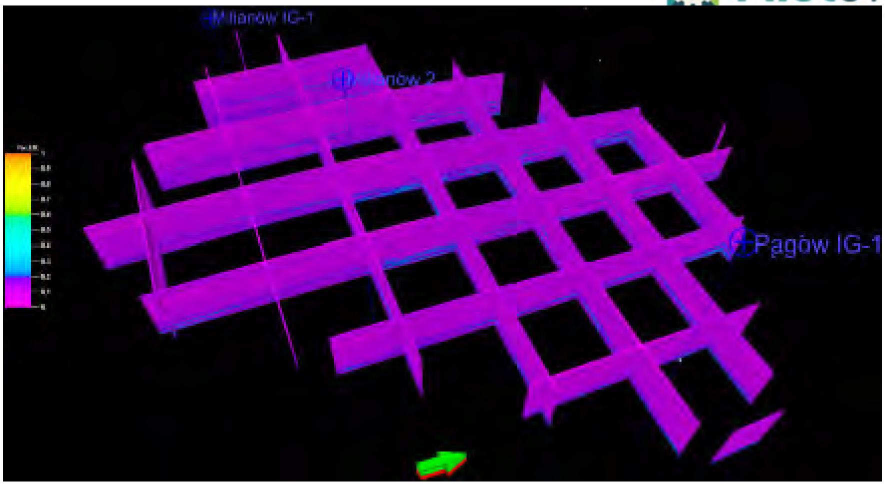

Figure 4.49: Stochastic realization of porosity closest to P10 model of pore volume

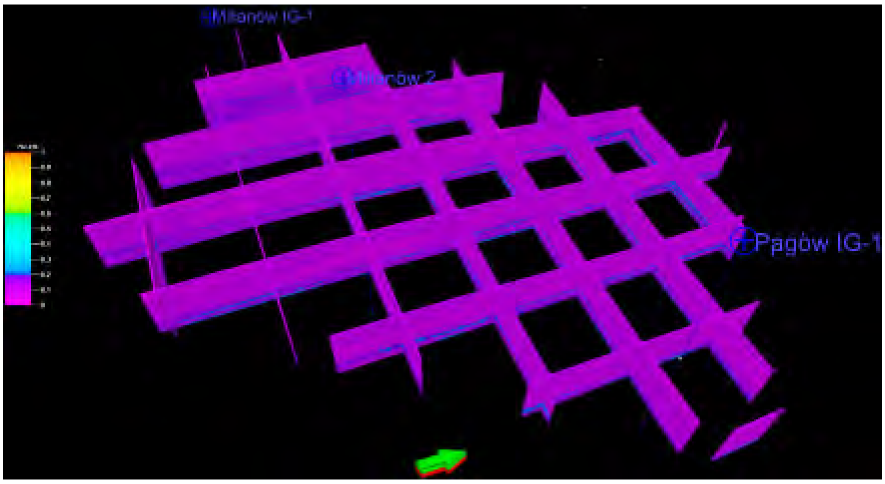

Figure 4.50: Stochastic realization of porosity closest to P50 model of pore volume

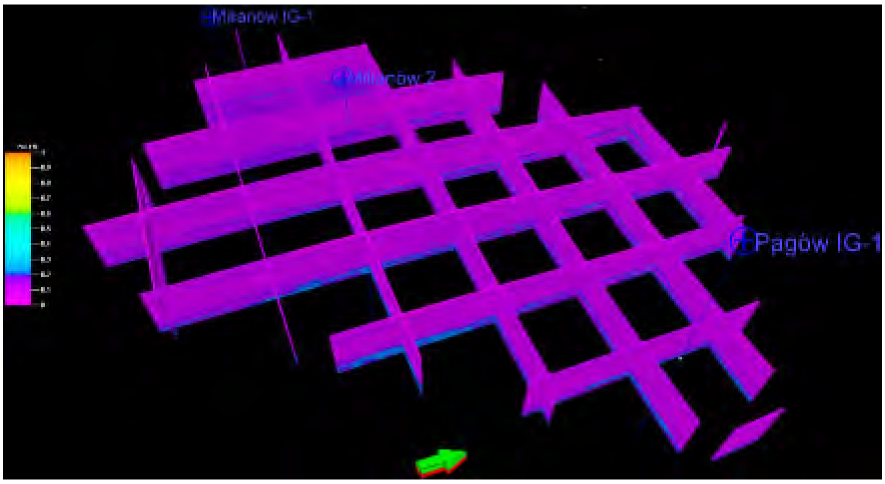

Figure 4.51: Stochastic realization of porosity closest to P90 model of pore volume

The PilotSTRATEGY project has received funding from the European Union's Horizon 2020 research and innovation programme under grant agreement No. 101022664

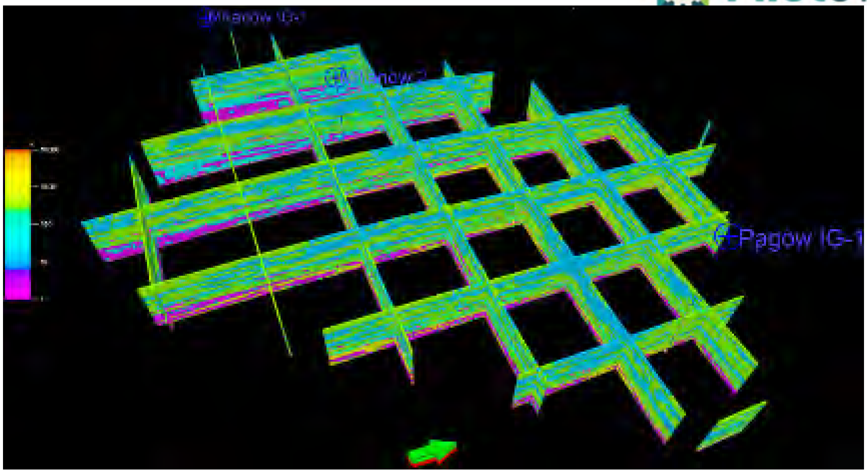

Figure 4.52: Stochastic realization of permeability closest to P10 model of pore volume

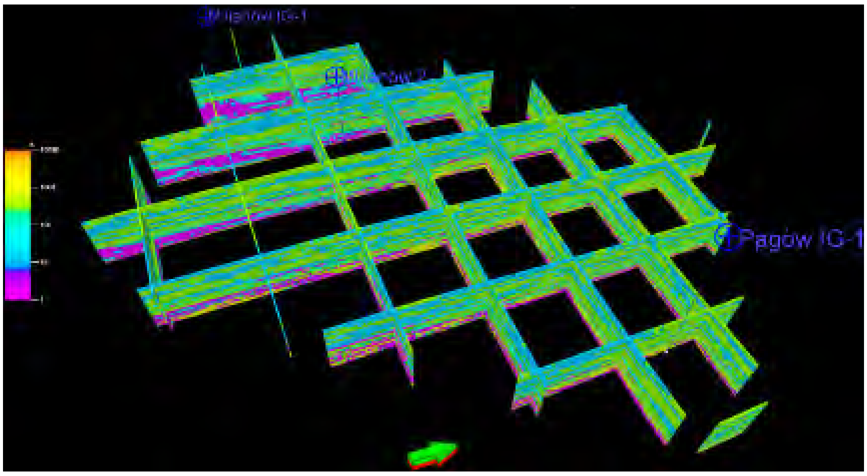

Figure 4.53: Stochastic realization of permeability closest to P50 model of pore volume

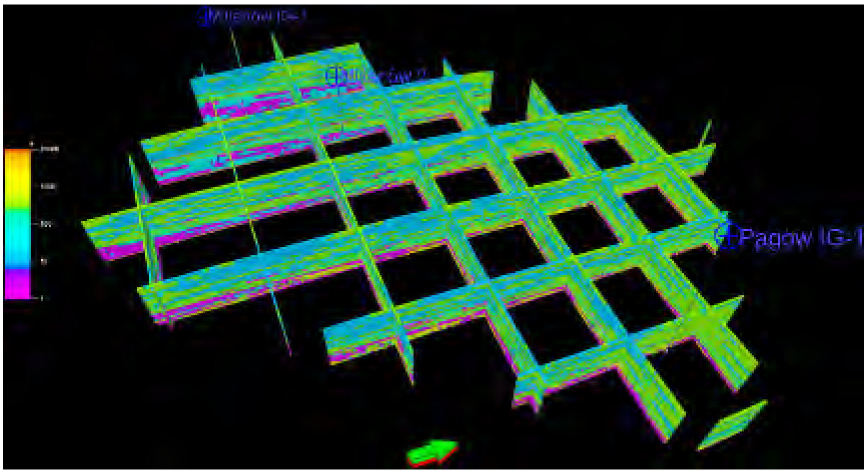

Figure 4.54: Stochastic realization of permeability closest to P90 model of pore volume

The PilotSTRATEGY project has received funding from the European Union's Horizon 2020 research and innovation programme under grant agreement No. 101022664

4.4 Summary and conclusions

The objective of task 3.1 (Static modelling with uncertainties) was building of two 3D geological models for two potential storage reservoirs identified in Upper Silesia region in deep saline aquifers: Skoczów DSA with Miocene deposits in Dębowiec layers and Ładzice DSA with Jurassic deposits in reservoir layers. Developed geological models of the storage complex zone consist of reservoir, caprock and structural elements. Static geological models were developed based on the results obtained from WP2 Geo-characterization.

In the case of Skoczów DSA, there were observed lack of permeability data in log files for east part of model (available only porosity and VShale data). Data for porosity and shale volume were loaded into the project in the form of well logs or point attributes. The permeability estimation was done using the Zawisza formula due to the lack of proper data from the east part of the site. In the Zawisza model, permeability depends on porosity and shale content. The output of this task for the model of Skoczów DSA are the following properties: porosity, VShale (shale volume) and permeability. The range and distribution of petrophysical parameters of the reservoir were analyzed in the area of the maximum range of Miocene deposits in Dębowiec layers. An area named "Kęty" with the highest potential for CO_2 storage was identified. The selected area of approximately 115 km^2 will be analyzed in detail for storage of carbon dioxide within the framework of Task 2.8, including *e.g.,* estimation of static CO_2 storage capacity in saline aquifers of selected area applying the volumetric equation.

In the case of second selected region, two candidate areas were identified for the Jurassic Ładzice formation. Based on data availability and parameters values of reservoir layers, the area named "Pągów-Milianów" with an area of approximately 190 km^2 was selected for further work. A detailed characterization of reservoir formations and sealing layers in the selected area was prepared. Additional well data were analyzed and prepared for the needs of 3D static modelling. There were observed lack of VShale (shale volume) data in log files (available only porosity and permeability). Modelling of porosity and permeability was performed separately for individual sequences using the control procedure of the previously developed lithological model (petrophysical properties linked to lithofacies). The output of this task for the model of Ładzice DSA are the following properties: facies, porosity and permeability.

It is worth mentioning that the precision of the spatial mapping of the variability of reservoir formations and sealing layers developed for both analyzed geological models would certainly be improved by the availability of more data, including an additional well data, as well as the results of seismic data processing and interpretation.

The next step of work was an uncertainty study along with a risk analysis of modeling structural surfaces as well as comprehensive uncertainty analysis of facies and petrophysical properties, performed for the Ładzice DSA in Jurassic Czestochowa District.

The risk assessment of the quality of the 3D model in the Petrel software was performed within the module Uncertainty and optimization. It was used to calculate alternative, stochastic variants of the structural surfaces included in the 3D model (horizons).

Moreover, uncertainty workflow for facies and petrophysical properties was performed to determine the pore volumes, included 300 simulations of model with facies, porosity and permeability realizations. Developed realizations of petrophysical properties (porosity, permeability) closest to

P10, P50, P90 percentiles of the pore volume model will be used for the needs of flow simulations in further WP3 tasks.

The final step of task 3.1 was the process of upscaling of the grid to fit to the computational limitation of dynamic simulations of the CO_2 injection.

The initial model was constructed on the basis of a regular grid of 370 × 402 x 50 cells (7,437,000 cells) with surface dimensions of 50 × 50 m. The horizontal and vertical grid resolution were modified. This resulted in a model with a cell resolution of 72 × 65 × 20 (93,600 cells) with surface dimensions of 250 × 300 m. Amount of layers of the grid were reduced from 50 to 20 – part of layers were grouped together to create a reservoir mesh used for flow simulations.

Then, vertical and horizontal properties upscaling was performed to transfer the properties from the fine grid to the coarse grid. The results of scaling up the structure and properties are presented on stochastic realizations of porosity and permeability closest to P50 model of pore volume (Figure 4.60-4.61).

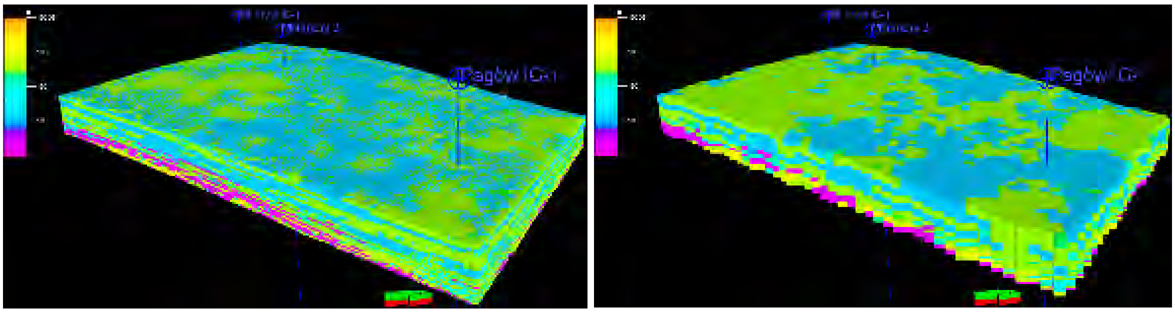

Figure 4.60: Stochastic realization of permeability closest to P50 model of pore volume: (left) initial model with resolution of grid of 370×402×50 - 7,437,000 cells; (right) upscaled model with resolution of grid of 72×65×20 - 93,600 cells

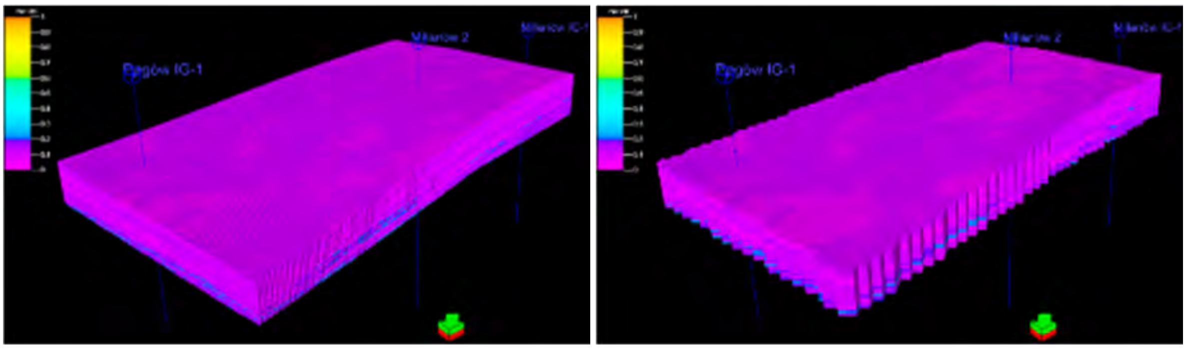

Figure 4.61: Stochastic realization of porosity closest to P50 model of pore volume: (left) initial model with resolution of grid of 370×402×50 - 7,437,000 cells; (right) upscaled model with resolution of grid of 72×65×20 - 93,600 cells

The PilotSTRATEGY project has received funding from the European Union's Horizon 2020 research and innovation programme under grant agreement No. 101022664

4.5 References

Deutsch, C. V.; Journel, A.G. (1992) GSLIB: Geostatist- ical Software Library and user's guide. Oxford University Press, New York.

Dommisse R., Structural and Stratigraphic Modeling Techniques in Shale and Tight Oil Basin Reservoir Studies. Bureau of Economic Geology, Jackson School of Geosciences, The University of Texas at Austin, 2022.

Górecki et al., 2002. Górecki W., Papiernik B., Małkowski T., Łapinkiewicz A. P., Riecher B., Kotarba M., Kosakowski P., Kowalski A., Smolarski L. & Śliż K. 2002 - Geologiczne i generacyjno-akumulacyjne uwarunkowania występowania złóż ropy naftowej i gazu ziemnego w niecce miechowskiej - analiza, reprocessing i reinterpretacja w systemie Promax i StrataModel. Arch. ZSE AGH (in Polish).

Jureczka, J.; Chećko, J.; Krieger, W.; Warzecha, R. Formacje i struktury solankowe perspektywiczne dla składowania CO_2 w regionie Górnośląskiego Zagłębia Węglowego (Feasibility study of CO_2 storage in saline formations and structures of the Upper Silesian Coal Basin). *Biul. Państw. Inst. Geol.* 2012, *448*, 47–56 (in Polish).

Koteras, A.; Chećko, J.; Urych, T.; Magdziarczyk, M.; Smolinski, A. An Assessment of the Formations and Structures Suitable for Safe CO_2 Geological Storage in the Upper Silesia Coal Basin in Poland in the Context of the Regulation Relating to the CCS. Energies 2020, 13, 195. https://doi.org/10.3390/en13010195

Schlumberger Information Solutions (SIS), 2010. Petrel Seismic-To-Simulation Software. New York, NY, USA: Schlumberger, version 2010.1.

STRATEGY CCUS, 2020. Key data for characterising sources, transport options, storage and uses in the promising regions, Deliverable D2.2, research project: STRATEGY CCUS (H2020-LC-SC3-2018-2019-2020/H2020-LC-SC3-2018-NZE-CC), October 2020.

Ślączka, A., 1985. Potrójna IG-1. Kambr, Prekambr. Profil litologiczno-stratygraficzny. Profile Głębokich Otworów Wiertniczych Instytutu Geologicznego, 59: 38-41 (in Polish).

Śliwińska, A.; Strugała-Wilczek, A.; Krawczyk, P.; Leśniak, A.; Urych, T.; Chećko, J.; Stańczyk, K. Carbon Capture Utilisation and Storage Technology Development in a Region with High CO_2 Emissions and Low Storage Potential - A Case Study of Upper Silesia in Poland. Energies 2022, 15, 4495. https://doi.org/10.3390/en15124495

Urych, T.; Smoliński, A. Numerical Modeling of CO_2 Migration in Saline Aquifers of Selected Areas in the Upper Silesian Coal Basin in Poland. Energies 2019, 12, 3093. https://doi.org/10.3390/en12163093

Wachowicz, J. Studium bezpiecznego składowania dwutlenku węgla na przykładzie aglomeracji śląskiej - Praca zbiorowa pod redakcją Jana Wachowicza. Wyd. Główny Instytut Górnictwa: Katowice, Poland, 2010. (in Polish)

Zawisza L., 1993. Simplified method of absolute permeability estimation of porous beds.

Złonkiewicz, 2001. Ewolucja basenu niecki miechowskiej w jurze jako rezultat regionalnych przemian tektonicznych (Evolution of the Miechów Depression basin in the Jurassic as a result of regional tectonical changes), PIG-PIB, Przegląd Geologiczny, 2006, Vol. 54, nr 6, pages: 534—540 (in Polish).

5 Portugal

5.1 Introduction

5.1.1 Dataset

The subsurface geo-characterization of the storage elements in the offshore Northern sector of the Lusitanian Basin was conducted in the WP2 – Geo-characterization studies (Wilkinson et al. 2023) using the available data, such as the legacy well information and 2D/3D seismic reflection data (Figure 5.1).

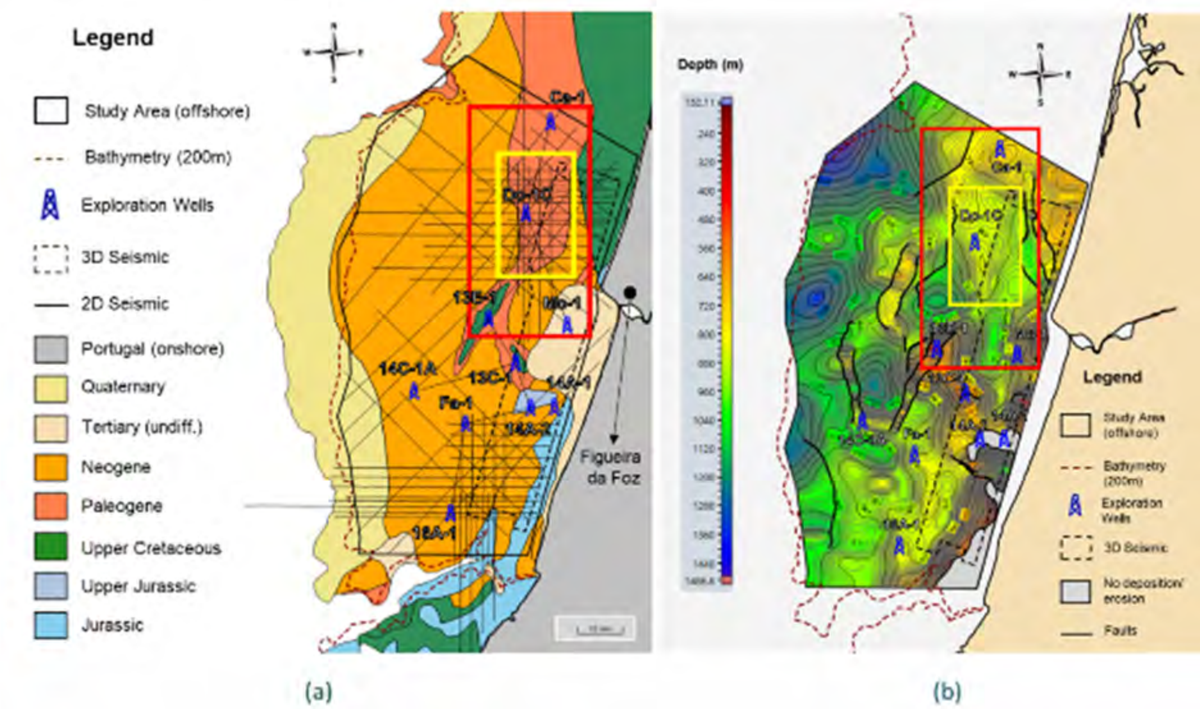

Figure 5.1: Maps of the (a) data availability in the study area and (b) top Torres Vedras Group reservoir structure, highlighting the boundary of the static model by the red rectangle, and the boundary of the reservoir model in yellow (adapted from Wilkinson et al., 2023).

The selection of the study area for building the static model is illustrated by the red rectangle in Figure 5.1. This area includes the selected prospect Q4-TV1 and covers a total area of approximately 1925 km^2. The reservoir model area, which is identified in yellow in Figure 5.1 and will input the dynamic simulation, encompasses the area of P10 scenario of the prospect Q4-TV1 (Wilkinson et al. 2023) and the legacy well Do-1C. The reservoir model area covers approximately 570 km^2 but lacks adequate well data coverage (only one well). Therefore, the static model accounts for a larger area to incorporate the log data of four wells, aiming to capture the reservoir heterogeneities area in a wider region.

The dataset transferred from WP2 to WP3 for building the static model is composed by a set of petroleum exploration legacy wells, the structural elements (i.e., horizons and faults) resulting from seismic interpretation and time-depth conversion studies, and the conceptual geological model:

i) Four wells (Mo-1, 13E-1, Do-1C and Ca-1) with the stratigraphic markers, and the log data from petrophysical analysis: volume of shale (Vshale), total and effective porosity (PHIT and PHIE) and water saturation (Sw). From these 4 petrophysical properties, only the Vshale and PHIE were used for the modelling studies, along with the lithofacies and permeability estimated during this task 3.1 and further detailed in the section of petrophysical analysis;

ii) Eight seismic horizons of the main geological formations (from bottom to top of static model): Top Dagorda Formation (~199 Ma), Top Brenha Formation (~160 Ma), Top Alcobaça Formation (~145 Ma), Top Torres Vedras Group (~100 Ma), Top Cacém Formation (93 Ma), Top Aveiro Group (~68 Ma), Top Espadarte Formation (50 Ma) and Seabed (0 Ma), presented in the section of the structural modelling;

iii) Six fault surfaces, in which 4 are normal faults (F1, F2, F3 and F6) and two are thrust faults (F4 and F5), presented in the section of the structural modelling;

iv) Conceptual geological model, mainly comprising the definition of the different stratigraphic units of the storage complex and the depositional environment insights of the reservoir unit, as further indicated in the section of the conceptual geological model.

The building of the static model with uncertainties was conducted in sequential sub-tasks: from the processing and analysis of the available data, followed by the structural, stratigraphic and property modelling, to the uncertainty analysis, volumetrics, and final reservoir models. This general workflow is illustrated in Figure 5.2.

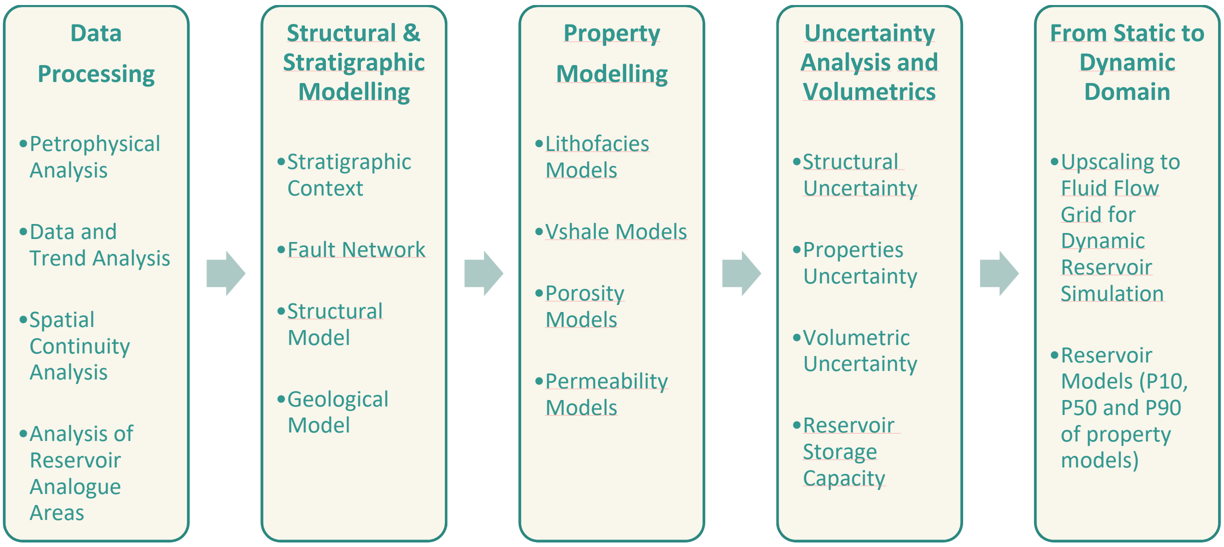

Figure 5.2: Workflow followed for building the static model with uncertainties.

5.1.2 Stratigraphic Context

The stratigraphic context of the static model was defined based on seven regions (from bottom to top):

1) the Middle Jurassic Carbonates, between the horizons of top Salt (Dagorda Formation) and top Brenha (Brenha Formation);

The PilotSTRATEGY project has received funding from the European Union's Horizon 2020 research and innovation programme under grant agreement No. 101022664

2) the Upper Jurassic Siliciclastics and Carbonates, between the horizons of top Secondary Reservoir (Alcobaça Formation) and the top Primary Reservoir (Torres Vedras Group);
3) the Lower Cretaceous Siliciclastics, between the horizons of top Primary Reservoir (Torres Vedras Group) and top Secondary Reservoir (Alcobaça Formation);
4) the Upper Cretaceous Limestones, between the horizons of top Primary Seal (Cacém Formation) and top Primary Reservoir (Torres Vedras Group);
5) the Upper Cretaceous Siliciclastics, between the horizons of top Secondary Seal (Aveiro Group) and top Primary Seal (Cacém Formation);
6) the Paleocene Dolomites, between the horizons of top Espadarte (Espadarte Formation) and top Secondary Seal (Aveiro Group); and
7) the Eocene-Miocene Siliciclastics, between the horizons of Seabed and top Overburden (Espadarte Formation).

The set of regions defined in the stratigraphic context are illustrated in Figure 5.3. All these regions are conformable between each other, except the eroded transition between the Jurassic and Cretaceous geological formations (the top region of the Upper Jurassic Siliciclastics and Carbonates), due to the existence of an unconformity, and at the top of the region Eocene-Miocene Siliciclastics delimited by the Seabed horizon.

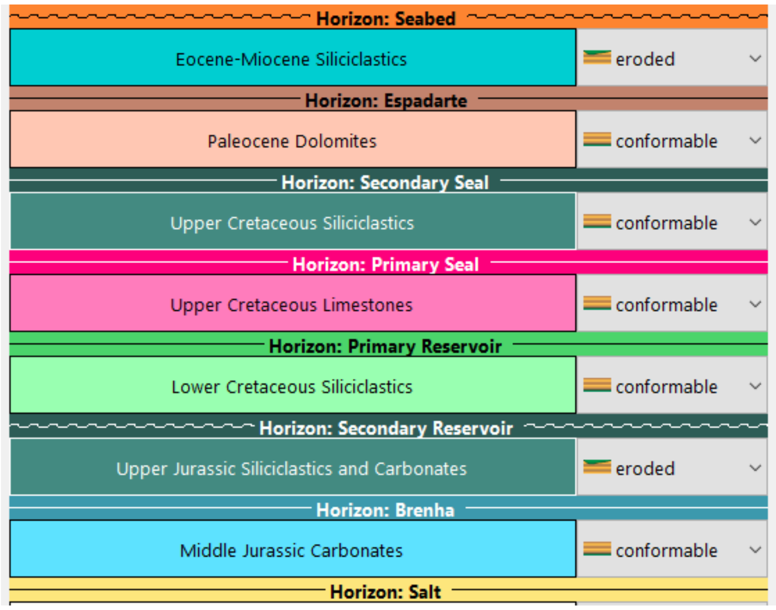

Figure 5.3: Stratigraphic context used in the static modelling studies.

Although the regions of the Lower Cretaceous Siliciclastics and the Upper Jurassic Siliciclastics and Carbonates are mentioned in Figure 5.3 as corresponding to the Primary Reservoir and Secondary Reservoir, respectively, only the Lower Cretaceous Siliciclastics (Primary Reservoir) is considered the reservoir target in this study. From now on in this report, the Primary Reservoir is designated as the Reservoir unit.

The PilotSTRATEGY project has received funding from the European Union's Horizon 2020 research and innovation programme under grant agreement No. 101022664

5.1.3 Conceptual Geological Model

Based on the storage complex information of the conceptual geological model (Wilkinson et al., 2023), and linking it to the stratigraphic context information, the Reservoir unit corresponds to the Torres Vedras Group (Lower Cretaceous Siliciclastics), capped by the Primary Seal (Upper Cretaceous Limestones of the Cacém Fm.), a potential Secondary Seal unit (Upper Cretaceous Siliciclastics of Aveiro Group), the overburden units of the Paleocene Dolomites and the Eocene-Miocene Siliciclastics. The underburden units of the reservoir are the Jurassic regions of the static model, such as the Upper Jurassic Siliciclastics and Carbonates and the Middle Jurassic Carbonates.

Additional information from the depositional model of the primary reservoir in the study area of the static model as well as from an analogue area in the offshore setting of the basin, is presented in the next sub-section.

5.1.3.1 Depositional Model

The depositional model of the reservoir (Lower Cretaceous Torres Vedras Group) is characterised by the deposition of shallow marine to fluvial sandstones in the northern sector of the offshore setting of the Lusitanian Basin. The study area for building the static model is identified in the paleoenvironmental sketch of the Figure 5.4, in which the main sedimentary flow directions in this sector of the basin and the reservoir thickness at each well location are also presented. There are significant thickness variations in the offshore setting of the basin, although the thickness variation of the four wells of the WP3 dataset is relatively similar with less than 100m of lateral variation (mainly in the two wells located in the southern part of the red rectangle).

Due to the lack of more detailed geological information on the depositional model, e.g., the existence of 2D cross-sections or 3D diagram models of the reservoir depositional environment, or further knowledge of the fluvial sandstones channels (length, width and thickness variations), the use of object-based simulation algorithms to reproduce the small- and large-scale reservoir internal architecture elements is not recommended here due to the high degree of uncertainty.

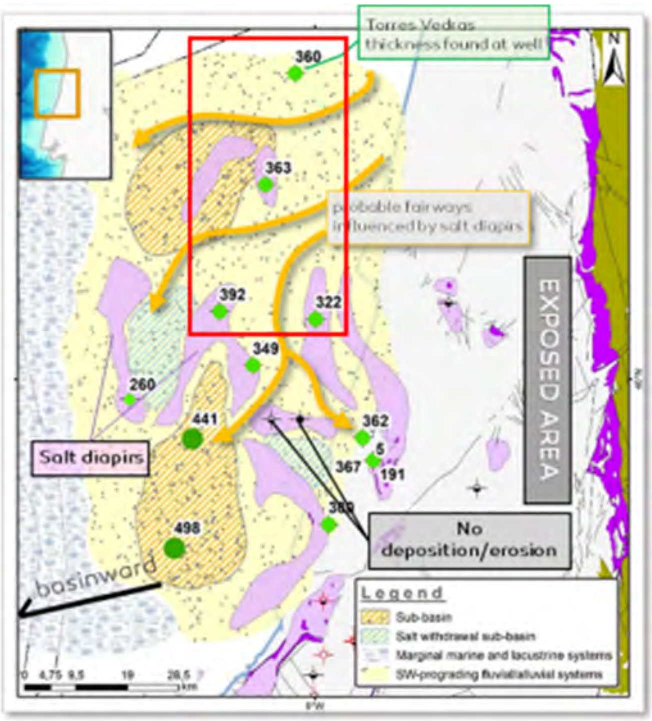

The PilotSTRATEGY project has received funding from the European Union's Horizon 2020 research and innovation programme under grant agreement No. 101022664

Figure 5.4: Paleoenvironmental sketch map at the Albian age illustrating the sub-basins, salt diapirs and the main sedimentary flow directions (from Wilkinson et al., 2023) in the study area. Static model area identified by the red rectangle.

The information available from the depositional model relates to the main sedimentary flow directions (Figure 5.4), in which for the study area of the static model are approximately 45º NE [-15º ; +15º]. The relevance of this azimuthal information of the reservoir depositional environment is significant for the horizontal variograms modelling due to the lack of well log data for such a large study area of the static model with the presence of only four wells only. The studies of the modelling of horizontal variograms, as well as a quantitative reservoir characterization using geostatistical seismic inversion, were conducted in analogue areas, and detailed in section 7.3.1 of the Annexes.

5.2 Data Processing

5.2.1 Petrophysical Analysis

This section presents the estimation of lithofacies and permeability reservoir properties at the location of the wells. The lithofacies were obtained for all the regions of the static model, while the permeability was only estimated for the reservoir unit.

The well Ca-1 was not initially considered for the petrophysical analysis conducted in the WP2 due to reservoir data only exists in the bottom zone, lacking in most of the reservoir. But, since this well locates inside the static model, and it is the only well in the northernmost area, the volume of shale (Vshale) and the effective porosity (PHIE) were also estimated for this well, even if it is limited to the bottom zone of the reservoir. Figure 5.5 illustrates the logs of these two properties not only for the well Ca-1 but also for the other three wells. Further details of the estimation of these petrophysical reservoir properties can be found in the petrophysics deliverable D2.6.

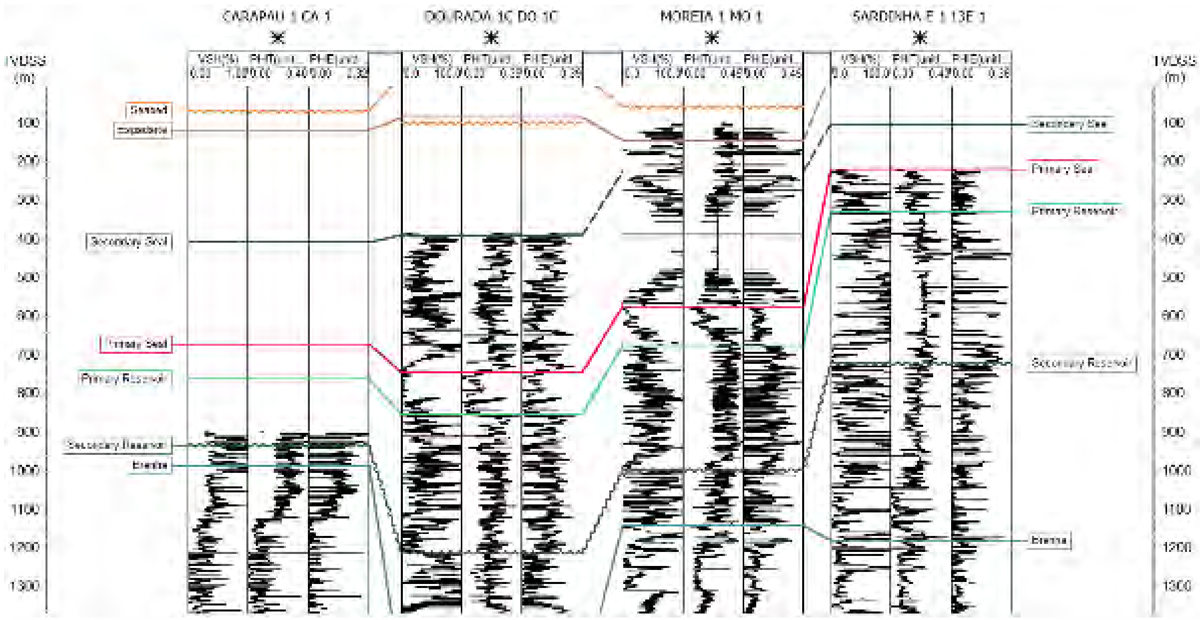

Figure 5.5: Volume of shale (Vshale), total porosity (PHIT) and effective porosity (PHIE) logs of the four wells considered for the static model.

The PilotSTRATEGY project has received funding from the European Union's Horizon 2020 research and innovation programme under grant agreement No. 101022664

5.2.1.1 Lithofacies

The lithofacies were estimated for the wells Mo-1, Do-1C, 13E-1 and Ca-1 using a petrophysical commercial software based on clusters to discriminate the electrofacies, which are numerical combinations of petrophysical log responses that reflect specific physical and compositional characteristics of a given rock interval. In this study, the electrofacies were determined from the composite logs (from WP2) such as gamma-ray (GR), sonic (DT) and density (DEN). The porosity estimated in the petrophysical analysis conducted in the WP2 was not used for lithofacies estimation due to being already a resulting log, as well as the resistivity log due to the reservoir (saline aquifers) at the location of the wells may be composed by different brine compositions.

Based on the well samples and the composite profile, it was possible to assign a set of electrofacies to different lithofacies using the clustering method "minimize the within-cluster sum of squares distance" to make this process supervised. From this process, 6 lithofacies resulted from the 15 electrofacies. Figure 5.6 illustrates the 6 lithofacies estimated for the set of wells of the static model, such as sandstone, limestone, dolomite, clay, halite, and anhydrite. This set of lithofacies estimated for the wells corresponds to the hard data used in the lithofacies modelling section, allowing the determination of the lithofacies for the regions of the static model.

The reservoir unit is only composed by sandstones and clays, while the primary seal is mainly composed by limestones, and a small percentage of sandstones and clays, and the secondary seal is also composed by these three lithofacies (sandstone, clay, and limestone).

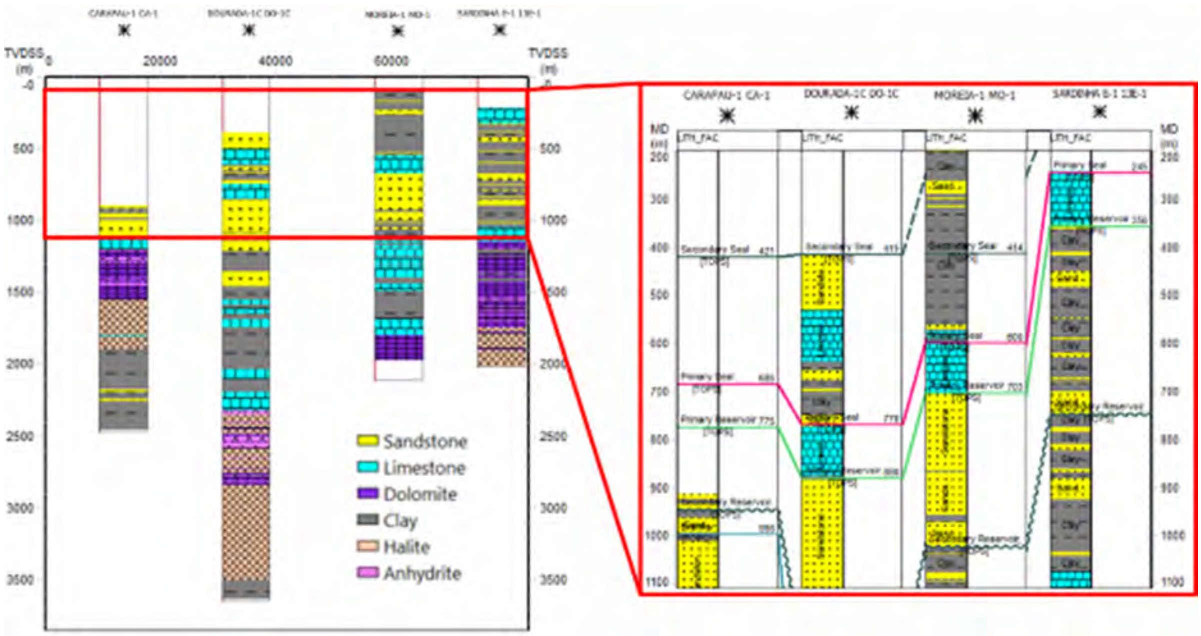

Figure 5.6: Lithofacies estimated for the set of wells of the static model. The zoom in of the lithofacies logs illustrate the three lithofacies composing the reservoir and both primary and secondary seals.

A further analysis of the lithofacies per well and per static model region is done in the section of the data trend analysis in the Annexes (section 7.3.2).

The PilotSTRATEGY project has received funding from the European Union's Horizon 2020 research and innovation programme under grant agreement No. 101022664

5.2.1.2 Permeability

The reservoir permeability is a petrophysical property generally difficult to determine, even if there exist some data measurements from the laboratory tests and analysis to allow the calibration of permeability estimates with those estimates based on the geophysical well-log data.

In this study, no permeability laboratory tests were conducted in WP2, relying only on the information available from a set of wells at shallower reservoir depths. These values of the Lower Cretaceous reservoir were determined in 7FP COMET project (Martínez, 2012) from several onshore aquifer systems, located in different geographical areas, and they present a significant dispersion for the considered average depth intervals.

Figure 5.7a presents the permeability values according to the corresponding average depth intervals from a set of 69 wells distributed in the following aquifer systems (Figure 5.7b): Aveiro (6 wells), Figueira da Foz-Gesteira (10 wells), Leirosa-Monte Real (5 wells), Alpedriz (8 wells), Ourém (13 wells), Pousos-Caranguejeira (2 wells) and Torres Vedras (25 wells).

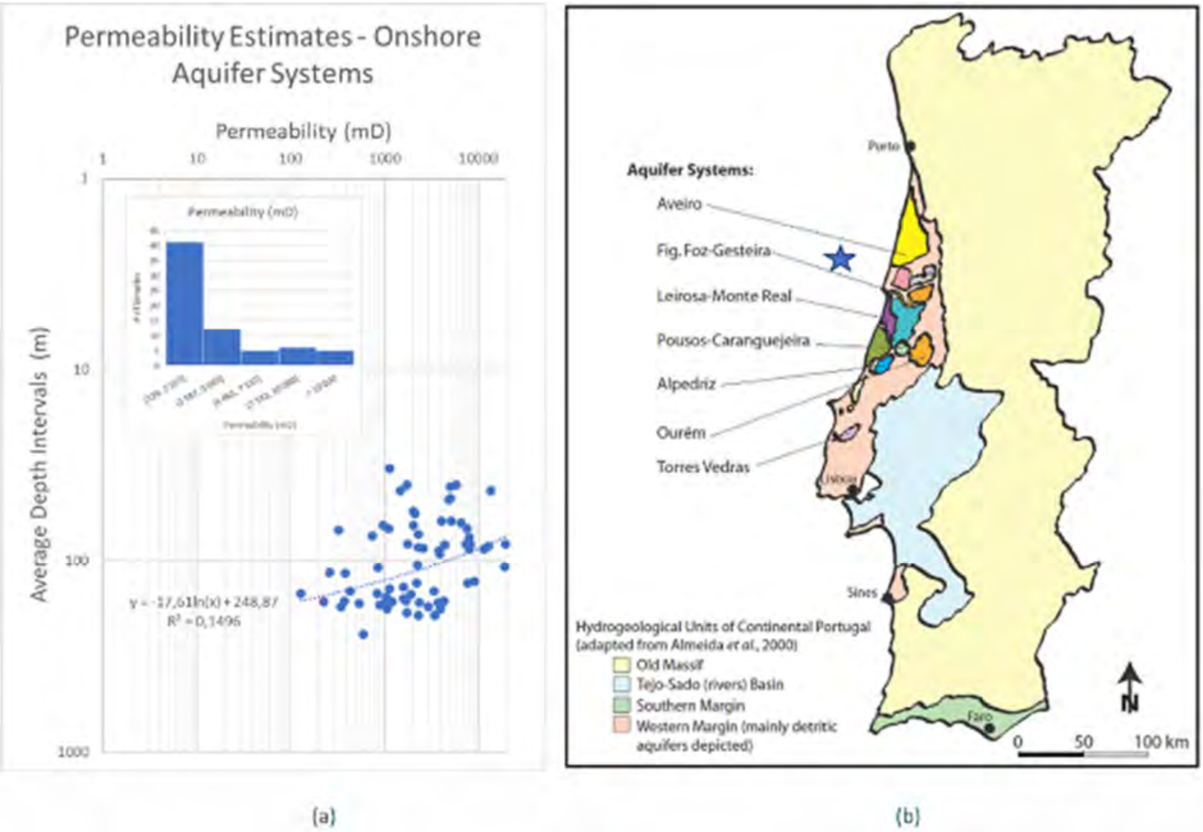

Figure 5.7: (a) Permeability estimates in the 7FP COMET project from a set of 69 wells of (b) onshore aquifer systems (Lower Cretaceous) located in the Lusitanian basin. The blue star illustrates the location of the Q4-TV1 prospect in the offshore area.

From the statistics of the data, the permeability values range from 129mD to 19570mD, with a median value of 2235mD and a mean value of 3718mD for depth intervals up to 250m. The variation of permeability values at similar average depth intervals confirms the significant lateral and vertical heterogeneity of the reservoir unit (Lower Cretaceous Torres Vedras Group) for the several aquifer systems. For this reason, the relationship between permeability and depth values may not be an adequate indicator to predict the reservoir permeability values at depth intervals deeper than 800m.

The PilotSTRATEGY project has received funding from the European Union's Horizon 2020 research and innovation programme under grant agreement No. 101022664

Considering a degradation model of the permeability values with depth, this information at shallower depths indicates that the reservoir unit should present adequate permeability and injectivity for the Q4-TV1 prospect (depths of about 850-1200m).

To determine the reservoir permeability values, the relationship presented in the work of Díaz-Curiel et al. (2016) between permeability (k in Darcy) and effective porosity (ϕ $[-]$), assuming a constant cementation exponent (m), was used (Equation 1):

$$k = 2.0 \,.\, 10^{9} . \phi^{7m} . (1 - \phi^{m})^{39} \qquad \text{(Equation 1)}$$

The main objective of the work of Díaz-Curiel et al. (2016) consisted in finding a relationship for the geophysical estimation of permeability in sedimentary media from porosity. The resulting Equation 1 was applied and compared with several data sets collected in the literature, in which its validation was consistent with the statistically expected values in sedimentary basins for consolidated and unconsolidated media.

The cementation exponents (or factors) have been accepted as measurements of the degree of cement and consolidation of the rock, and the tortuosity of the pore geometry of current flow. From the lithology reports of the four wells considered for the static modelling, the net-intervals of this siliciclastic reservoir are generally described as unconsolidated sands, although the presence of a argillaceous cement may be considered for the depth intervals between about 800-1200m, mainly due to the variation in the spatial distribution of the known permeability values of the aquifer systems in the onshore lateral equivalent geological formation (i.e., Lower Cretaceous reservoir). The effective porosity (PHIE) logs from WP2 were used in Equation 1 considering three cementation exponents (m =1.7, 1.8 and 1.9) due to the uncertainty associated to this reservoir parameter. Figure 5.8 illustrates the distribution intervals of permeability values of the wells Do-1C, Mo-1, 13E-1, and Ca-1 for the set of cementation exponents used.

The PilotSTRATEGY project has received funding from the European Union's Horizon 2020 research and innovation programme under grant agreement No. 101022664

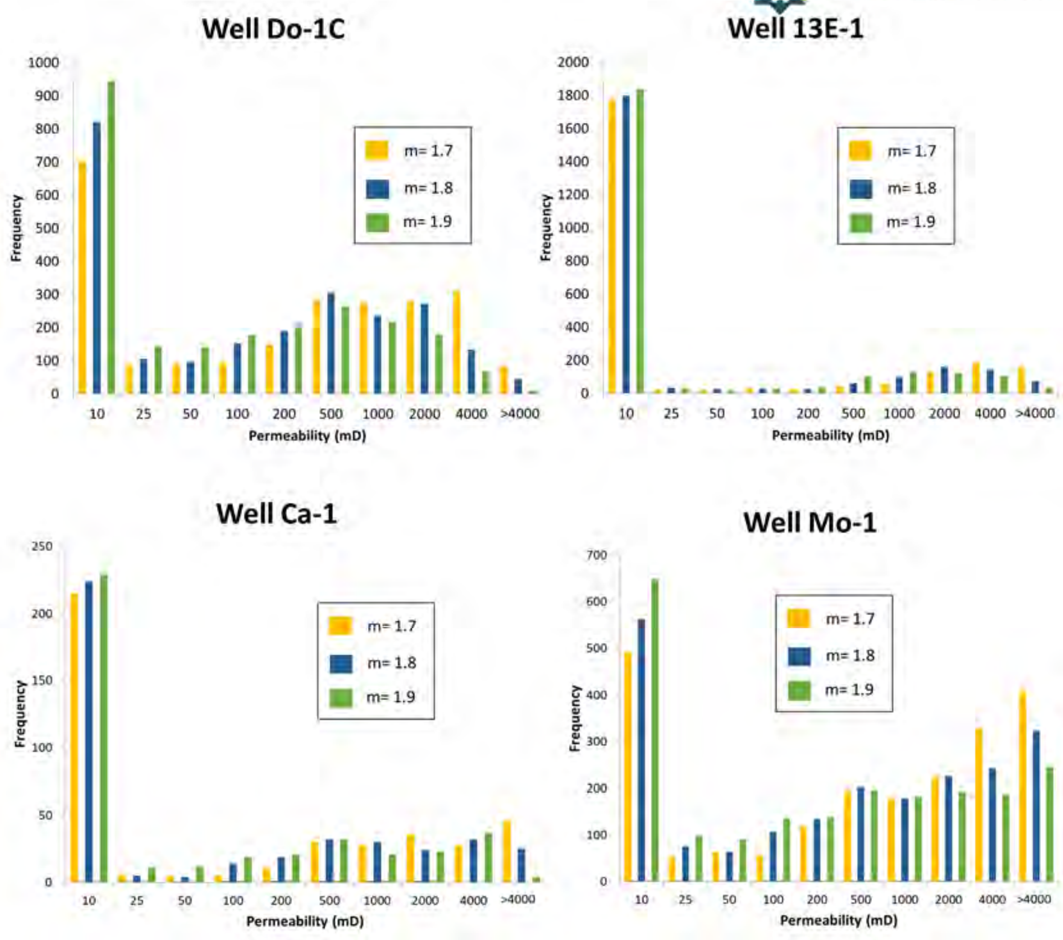

Figure 5.8: (a) Permeability estimates for the wells of the static model based on the variation of the cementation exponent (m).

The summary statistics of the permeability values for the three cementation exponents are listed in the Table 5.1. The Q4-TV1 prospect is located close to the well Do-1C with mean values of reservoir permeability from about 329mD (m=1.9) to about 862mD (m=1.7) and median values from about 39mD (m=1.9) to about 244mD (m=1.7). Although the cementation exponent m=1.7 corresponds to more unconsolidated sands, the resulting permeability values from the statistics seem too much optimistic for the reservoir depth intervals of this study. The magnitude order of the resulting mean and median permeability values, based on the cementation exponents m=1.8 and m=1.9, would be more adequate. For the petrophysical modelling, the permeability well log data corresponds to the permeability estimates based on the cementation exponent m=1.8.

Table 5.1: Summary statistics of the permeability estimates (mD) for the three cementation exponents.

Cementation exponents	Wells	Mean	Std. Deviation	Minimum	Median	Maximum	Number of Samples
1.7	Do-1C	862.064	1260.617	0.0001	243.509	6039.123	2355
	13E- 1	641.949	1410.349	0.0001	0.001	6041.770	2579

The PilotSTRATEGY project has received funding from the European Union's Horizon 2020 research and innovation programme under grant agreement No. 101022664

	Mo-1	1742.119	2035.459	0.0001	733.552	6044.713	2113
	Ca-1	981.387	1675.969	0.0001	0.029	6008.574	410
1.8	Do-1C	542.989	930.989	0.0001	100.570	6016.549	2355
	13E- 1	456.869	1106.026	0.0001	0.001	6044.433	2579
	Mo-1	1396.567	1895.320	0.0001	356.987	6044.712	2113
	Ca-1	697.482	1323.959	0.0001	0.005	5532.282	410
1.9	Do-1C	328.463	658.688	0.0001	39.263	5599.782	2355
	13E- 1	310.168	835.152	0.0001	0.001	5966.674	2579
	Mo-1	1099.818	1734.644	0.0001	163.138	6044.676	2113
	Ca-1	472.090	983.081	0.0001	0.001	4672.083	410

The permeability values were also estimated for both the primary and secondary seal regions of the static model. Contrarily to the reservoir unit, which is a rock formation composed of siliciclastic deposits mainly classified as two lithofacies only (sandstone and clay), the seal formations are also constituted by a given proportion of carbonates (in this case limestone lithofacies). While the primary seal is mostly composed of limestones (only a very few proportions of clays and sandstones estimated at the available wells), considered as a carbonate rock formation, the proportion of limestones present in the secondary seal is, in general, smaller than the other two lithofacies as estimated for the wells, being therefore mostly composed of siliciclastic rocks.

Considering the siliciclastic rocks of the secondary seal and the carbonate rocks of the primary seal, the permeability values were estimated, in this case, using the Timur-Coates equation. This equation (Equation 2), developed by M. Timur and G. R. Coates, is widely used to estimate the permeability (k) of porous media, particularly in siliciclastic environments, based on porosity (ϕ), water saturation (Sw) and empirical constants (a, b and c), and it is expressed as follows:

$$k = a \, . \frac{\phi^b}{Sw^c} \qquad \text{(Equation 2)}$$

These empirical constants are determined through regression analysis based on core data from the specific siliciclastic rock formation under consideration. Constant values of a = 8581, b = 4.4, and c = 2 were carefully chosen considering the available geological data and used for the siliciclastic rocks of the secondary seal. For the primary seal, the constant values of a = 10000, b = 4.5, and c = 2 were used based on literature values for tight carbonates rock formations (Mulyanto et al. 2020). While acknowledging the inherent variability in such estimates, the approach followed in this study demonstrates the adaptability of the Timur-Coates equation in situations where laboratory-derived constants are unavailable.

The permeability estimates and the main statistics from the available wells for both secondary and primary seals are presented in the Table 5.2. These values were used in the petrophysical modelling of the permeability for both model regions. The resulting distributions are represented by the histograms in the section 2.3.2.4 of the Annexes.

The PilotSTRATEGY project has received funding from the European Union's Horizon 2020 research and innovation programme under grant agreement No. 101022664

Table 5.2: Summary statistics of the permeability estimates (mD) for the secondary seal and primary seal regions of the static model.

Permeability (mD)	Wells	Mean	Std. Deviation	Minimum	Median	Maximum	Number of Samples
Secondary Seal	Do-1C	5.074	9.049	0.0001	0.864	73.206	2330
	13E- 1	3.125	4.927	0.0001	0.339	15.071	14
	Mo-1	7.614	27.744	0.0001	0.202	238.134	1397
Primary Seal	Do-1C	4.074	8.213	0.0001	0.322	88.145	722
	13E- 1	0.162	0.452	0.0001	0.006	5.095	721
	Mo-1	6.343	14.228	0.0001	0.916	133.266	676

5.2.2 Data and Trend Analysis

The analysis of the available well-log data was performed using the Data and Trend Analysis (DTA) workflow of the Aspen SKUA software. This task encompassed the exploratory data analysis of the rock properties is presented for all the regions of the static model, followed by the modelling of the spatial continuity analysis, the upscaling of the hard data and, at the end, the estimation of the soft data for simulation. Due to the extension of the information, the results of the data and trend analysis for each region of the static model and rock property are presented in the Annexes (sections 2.3.2, 2.3.3, 2.3.4 and 2.3.5).

The wells Do-1C and Mo-1 present the most adequate reservoir conditions, i.e., higher effective porosity and permeability layers, and lower presence of clayey layers as illustrated by the volume of clay and lithofacies logs of Figure 5.9, when compared to the well 13E-1.

It is important to note that the simulation of lithofacies and petrophysical properties were only conducted for the reservoir, primary and secondary seals. As the median and mean property values of PHIE and vshale from all the wells per model region do not differ significantly, the mean values are, in general, considered representative of the data. As such, they were used as constant values to parametrize the additional four static model regions where no simulation was performed: the reservoir overburden (Eocene-Miocene and Paleocene) and underburden (Upper and Middle Jurassic). The mean values of the volume of clay and effective porosity per well and model region are summarised in Table 5.3.

The PilotSTRATEGY project has received funding from the European Union's Horizon 2020 research and innovation programme under grant agreement No. 101022664

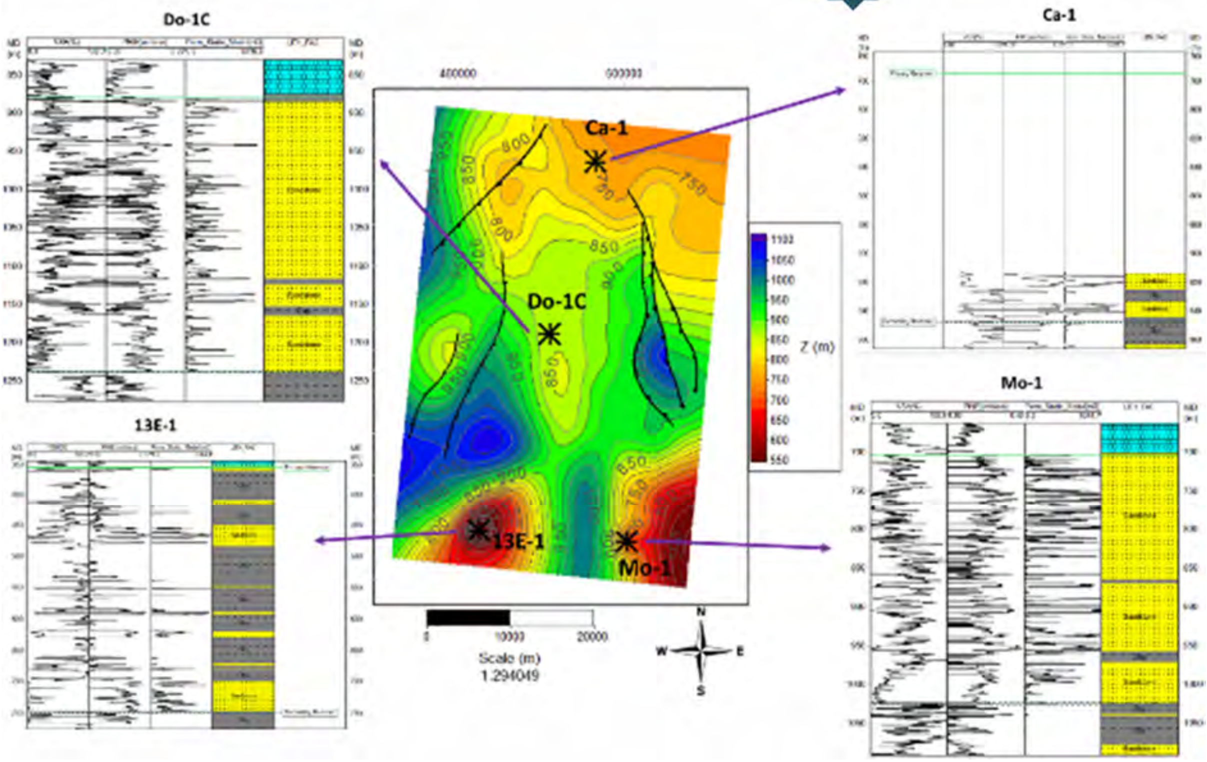

Figure 5.9: Structural map of reservoir top and the available log data in the well tracks: (from the left to the right) volume of clay, effective porosity, permeability and lithofacies. The light and dark green lines in the log tracks correspond to the top and bottom of the reservoir unit, respectively.

Table 5.3: Mean values of volume of shale and effective porosity of the model regions and wells.

Mean Values	Do-1C		Mo-1		Ca-1		13E - 1		All wells	
Property / Region	Vshale (%)	PHIE (%)	Vshale (%)	PHIE (%)	Vshale (%)	PHIE (%)	Vshale (%)	PHIE (%)	Vshale (%)	PHIE (%)
Eocene-Miocene	-		79	5	-		-		79	4
Paleocene	42	20	76	8					72	9
Secondary Seal	37	13	69	6			49	11	49	11
Primary Seal	20	11	33	13			28	5	28	10
Reservoir	41	15	40	17	60	12	47	8	47	13
Upper Jurassic	49	12	46	10	63	10	42	6	42	8
Middle Jurassic	42	3	24	4	26	4	26	2	26	3

The PilotSTRATEGY project has received funding from the European Union's Horizon 2020 research and innovation programme under grant agreement No. 101022664

5.3 Static Modelling

5.3.1 Structural Modelling

The structural modelling of this work was conducted in the Aspen SKUA software using the Structure & Stratigraphy (SnS) workflow. The building of the fault network, the structural model and the geological model and grid are presented in the next sub-sections.

5.3.1.1 Fault Network

The fault network was built using the six fault surfaces from seismic interpretation task of WP2. Distances of 600m and 60m were considered for the areal and vertical resolutions of the fault network, respectively. This fault network (Figure 5.10a) was performed based on the convex curve outline building method using a smooth approach of the data (fault surfaces), considering the connection of the available faults closer than 300m. This resulted in the connection between the surfaces of the faults F1 and F2 (Figure 5.10b). To create the fault blocks, inserting faults in the volume of interest, areal and vertical resolution distances of 600m and 60m, respectively, were considered.

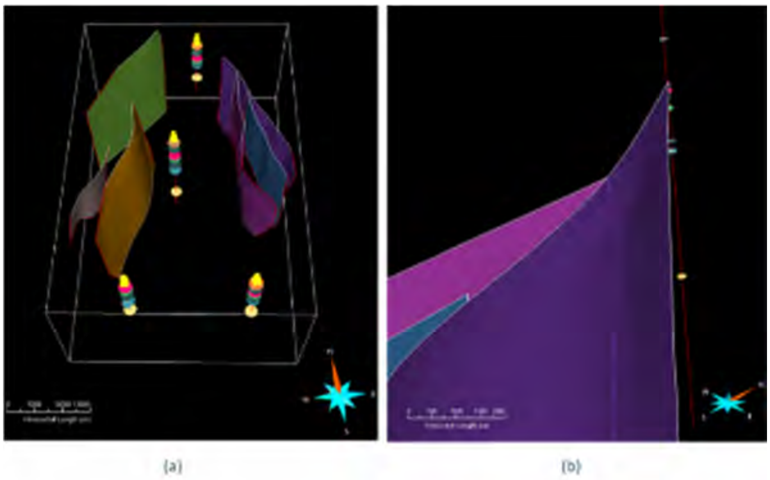

Figure 5.10: (a) Fault network of the structural model and (b) the connection between the faults F1 and F2.

5.3.1.2 Structural Model

The integration of the eight seismic horizons with the previous fault network to build the structural model (Figure 5.11) was performed by honouring of the stratigraphic well markers. The building of the horizons model was done using a global smooth approach to generate consistency between the available data. The refinement of the horizons was required to reproduce the fault displacements and the ties of each horizon to the corresponding stratigraphic markers. This required a data refinement of the horizons around the faults of 350m and around the markers of 700m (areal) and 40m (vertical). The final step of the structural modelling was the generation of the UVT model by computing the paleo-coordinates. This was based on the UVT transform technology to ensure the subsurface is modelled with no distortions from the depositional space (UVT coordinates) to the actual geological geometry space (XYZ coordinates). The resulting UVT model is illustrated in Figure 5.12a.

The PilotSTRATEGY project has received funding from the European Union's Horizon 2020 research and innovation programme under grant agreement No. 101022664

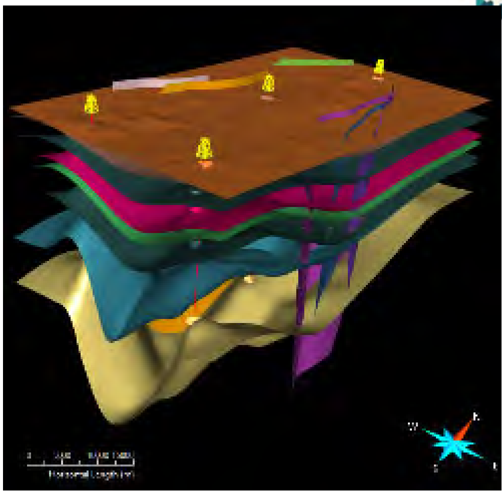

Figure 5.11: Structural model of the study area illustrating the fault network and the horizons honouring the stratigraphic well markers.

5.3.1.3 Geological Model

After building the structural model, seven model regions were defined based on the stratigraphic context and the well markers to create the geological model as shown in Figure 5.12. The thickness and gross-rock volumes of each model region (Table 5.4) were computed before building the final geological grid (Figure 5.13).

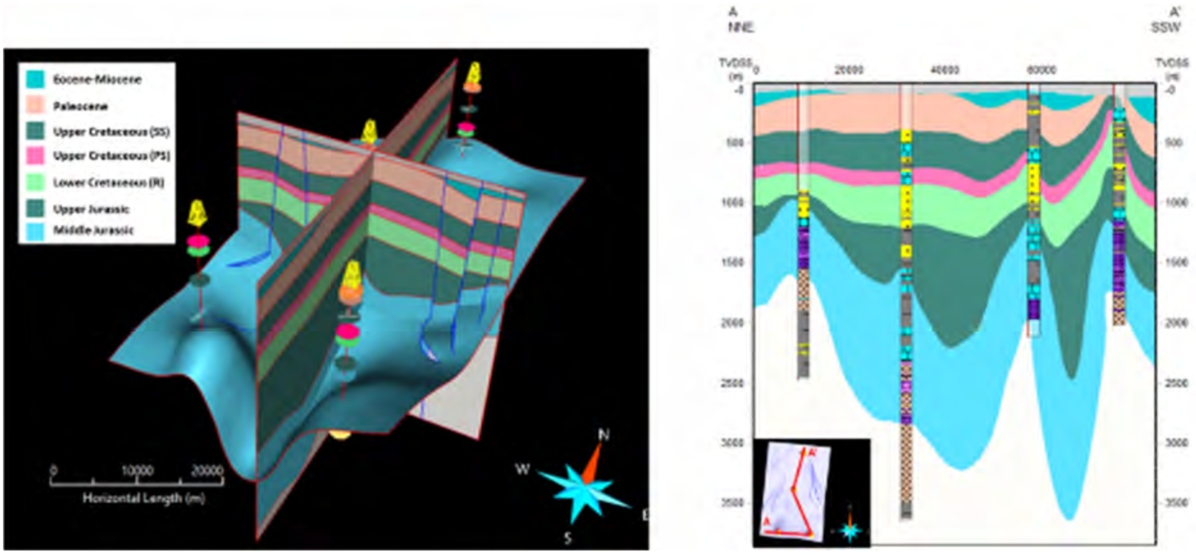

Figure 5.12: (a) UVT model and (b) a cross-section between the wells of the static model with the 7 geological regions defined in the geological modelling (SS – Secondary Seal, PS – Primary Seal, and R – Reservoir).

The areal extension of the geological model grid was defined as a cell size of 200m for both i- and j-directions, resulting in a total of 203 (i-axis) and 289 (j-axis) cells. Due to the computational time to simulate the rock properties presented in the next sections, only the main stratigraphic unit of the geological model (i.e., the reservoir, and primary and secondary seals) were defined with a fine-scale resolution in the vertical grid cell dimensions (Table 5.4). The dimension of the final geological grid is: 203x289x225 (13 200 075 cells).

The PilotSTRATEGY project has received funding from the European Union's Horizon 2020 research and innovation programme under grant agreement No. 101022664

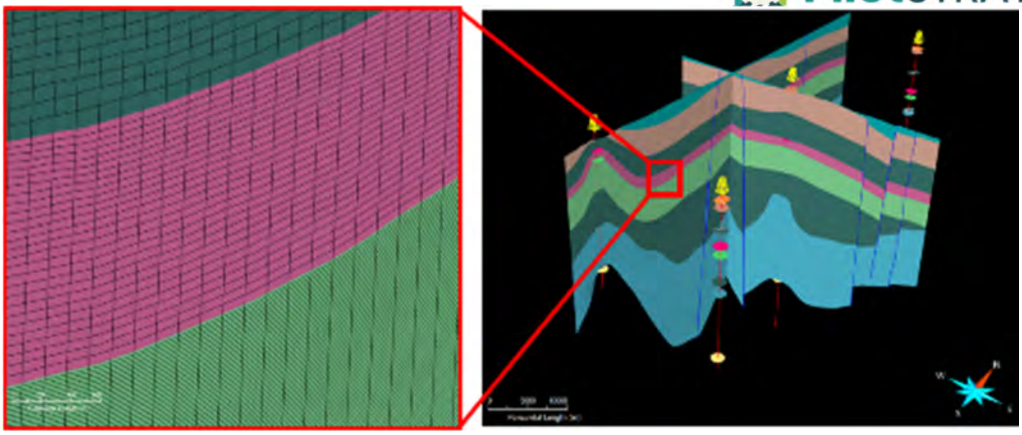

Figure 5.13: Comparison of the grid cell dimensions of the geological model for the three main regions: the secondary seal (dark green), the primary seal (pink) and the reservoir (light green).

Table 5.4: Gross-rock volume (GRV), number and thickness of vertical grid cells and thickness of the geological model regions.

Stratigraphic Units of the Geological Model	GRV (x10^9 m^3)	Number of Layers	Layer Thickness (m)	Unit Thickness (m)
Eocene-Miocene Siliciclastics	123.967	1	269.416	269.416
Paleocene Dolomites	558.661	1	295.393	295.393
Upper Cretaceous Siliciclastics (SS)	555.181	29	10	287.354
Upper Cretaceous Limestones (PS)	258.398	27	5	135.414
Lower Cretaceous Siliciclastics (R)	617.752	165	2	329.587
Upper Jurassic Siliciclastics and Carbonates	819.680	1	1338.88	1338.88
Middle Jurassic Carbonates	1824.900	1	985.457	985.457

5.3.2 Facies Modelling

5.3.2.1 Methodology

The simulation of lithofacies was performed recurring to pixel-based simulation algorithms (Deutsch & Journel, 1998) in the Aspen SKUA software. Two different algorithms for simulating discrete

The PilotSTRATEGY project has received funding from the European Union's Horizon 2020 research and innovation programme under grant agreement No. 101022664

properties were tested: Sequential Indicator Simulation (SIS) and Truncated Gaussian Simulation (TGS), using both the hard data and the generated soft data. SIS is a commonly used variogram-based categorical simulation technique, very useful when there is no clear geometry of the geological bodies. SIS is based on kriging but using a sequential stochastic method to draw Gaussian realization using an indicator transform (Ringrose & Bentley, 2015). The TGS is also a variogram-based technique used to simulate categorical variables based on the facies proportions (Beucher & Renard, 2016).

The application of SIS results in images that capture higher lateral and vertical variation of the facies, both for seals and reservoir units. In the TGS results, a more continues extension of the sandstones is observed. The interbedded clay layers observed on the lithology profiles of the wells, are better reproduced in the SIS models. TGS simulation method alone (i.e., with no soft data conditioning) poorly reproduces the expected lithofacies spatial distribution (not only for the reservoir lithofacies, but also for the seal unit), as well as the proportion data observed by the reservoir histogram from the wells. In addition, TGS method seems more adequate for sequential/ hierarchy lithofacies simulation (assuming, for instance, sand, clay, and clayey sand), as observed in the simulation models, lacking a more robust assessment of the model parameters space. Therefore, the selected simulation algorithm adopted to generate the final lithofacies models was the SIS with trend to incorporate the soft data into the simulation.

5.3.2.2 Lithofacies Models

At the scale of the geological model, the resulting lithofacies models can reproduce the conceptual geological information for the reservoir region. This include the interbedded clay layers within the reservoir unit and the potential stratigraphic trapping in the northern area of the structure, where the Q4-TV1 prospect is located, towards the well Ca-1. These results are illustrated in the several reservoir k-layers of Figure 5.14 and in the cross-section of Figure 5.15. In addition, it is important to mention that the clay layer at the bottom of the primary seal, verified at the location of the well Do-1C is also reproduced laterally at the top reservoir structure of the Q4-TV1 prospect (Figure 5.15).

The primary seal is mostly composed by limestones, presenting some small-scale layers of sandstones and clays lithofacies, which is conformable with the conceptual geological model.

The three lithofacies of the secondary seal, such as limestone, sandstone, and clay, are also reproduced in the lithofacies models. At the structure of the Q4-TV1 prospect (Figure 5.15), the spatial distribution of lithofacies (mostly sandstone and clay) for the top and bottom of the secondary seal are also reproduced according to the lithofacies logs of the well Do-1C.

The histograms of the lithofacies proportions for the three regions of the static model are shown in the Annexes (section 2.3.6). In general, the lithofacies proportions determined from the well data are reproduced in the resulting models: about 80% of limestone lithofacies in the primary seal, and about 65-70% of sandstone and 30-35% of clays for the reservoir region. However, the limestone lithofacies proportion for the secondary seal seems to be underestimated in the lithofacies models, when compared to those determined from the well data, and possibly overestimate the clay lithofacies proportions. This may be related to the coarser vertical resolution of the cells in this model region when compared to the finer vertical scale resolution of the cells in the primary seal and reservoir.

The PilotSTRATEGY project has received funding from the European Union's Horizon 2020 research and innovation programme under grant agreement No. 101022664

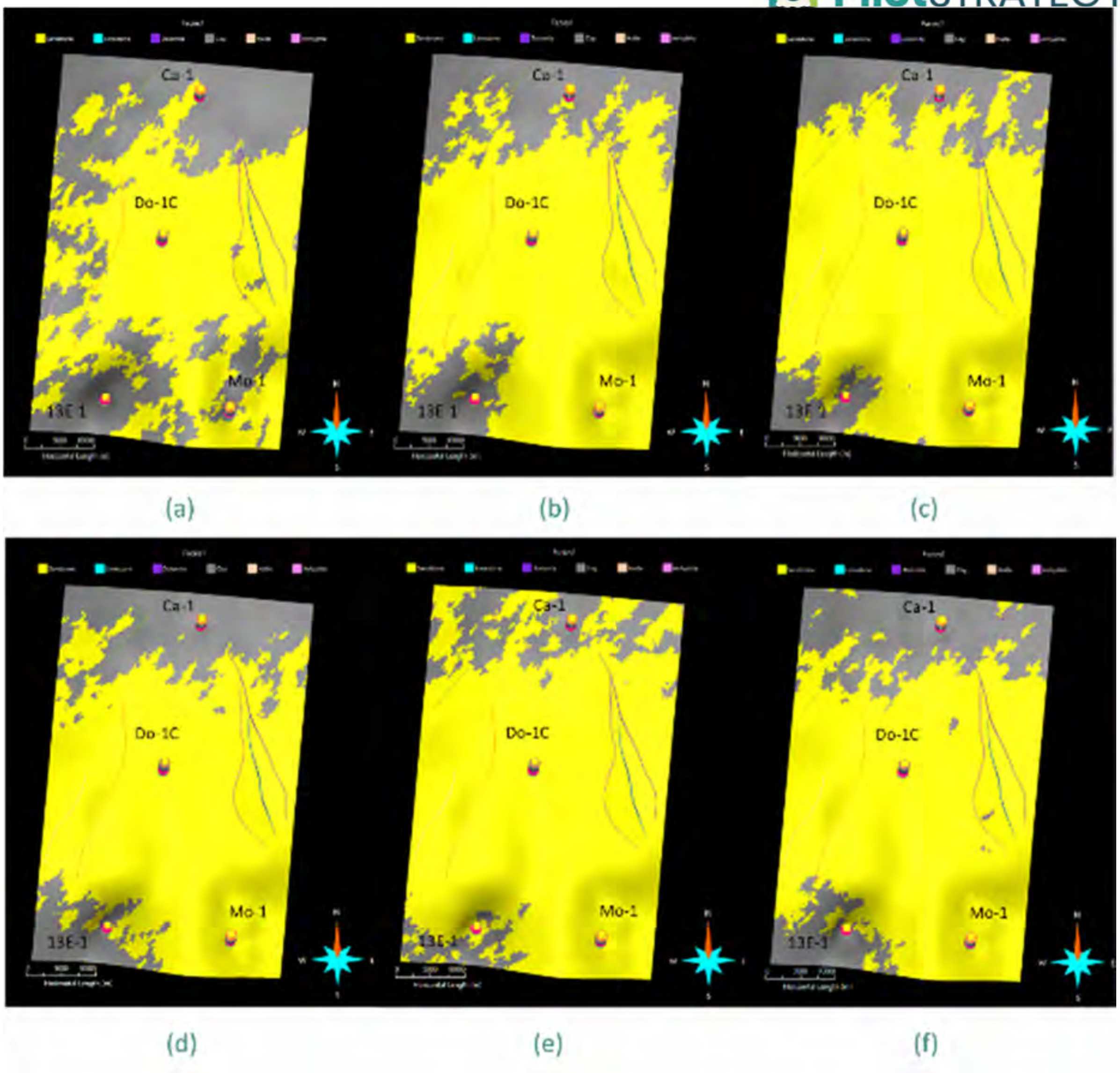

Figure 5.14: Realization of lithofacies for the reservoir (a) k-layer 70, (b) k-layer 90, (c) k-layer 110, (d) k-layer 130, (e) k-layer 150 and (f) k-layer 170.

The PilotSTRATEGY project has received funding from the European Union's Horizon 2020 research and innovation programme under grant agreement No. 101022664

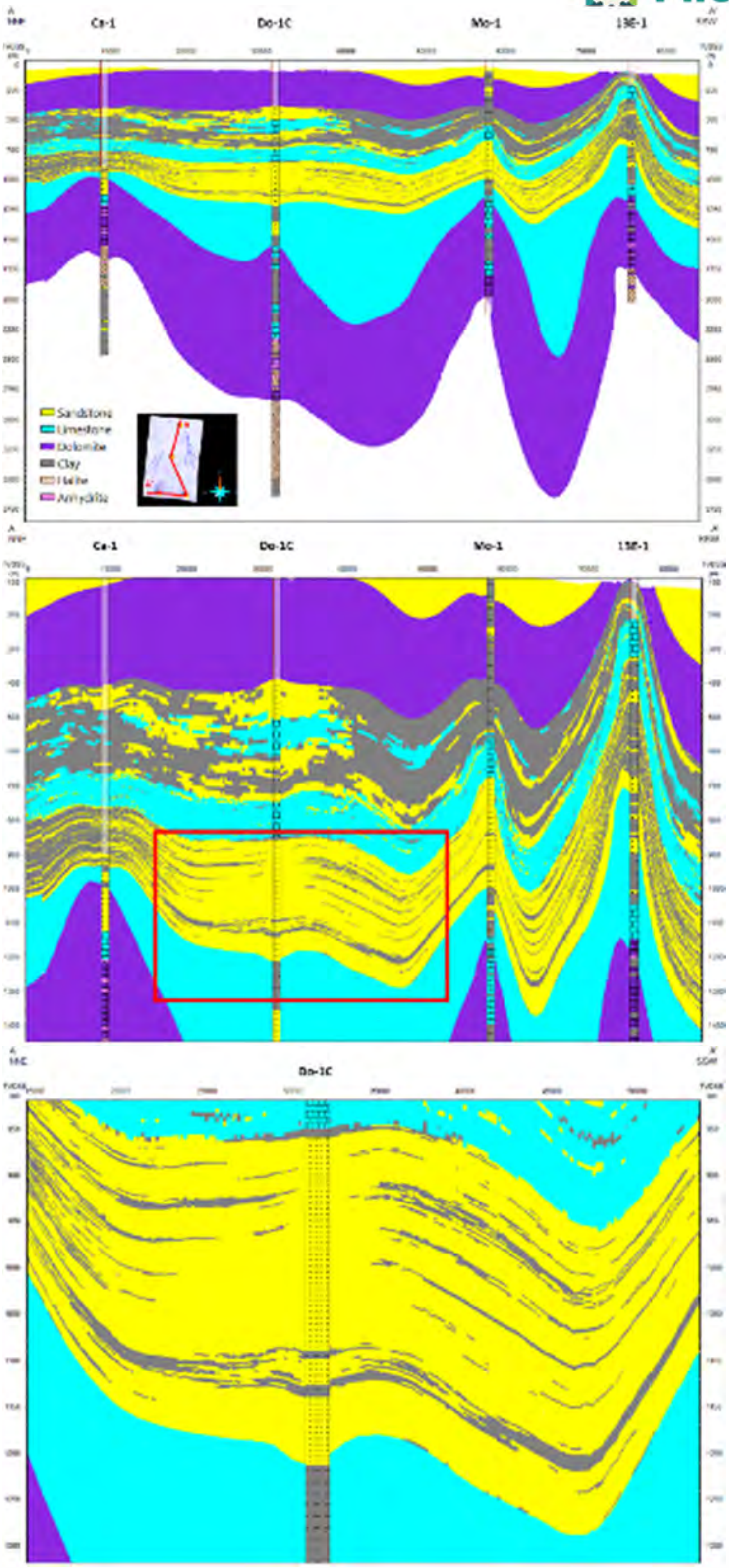

Figure 5.15: Realization of lithofacies shown in a cross-section of the static model, for the reservoir and seals regions, and for the structure of the Q4-TV1 prospect. The rectangle illustrates the location of thes Q4-TV1 prospect.

The PilotSTRATEGY project has received funding from the European Union's Horizon 2020 research and innovation programme under grant agreement No. 101022664

5.3.3 Petrophysical Modelling

5.3.3.1 Methodology

Similar as for the simulation of lithofacies, the simulation of the continuous properties for the petrophysical models was performed using pixel-based simulation algorithms in the Aspen SKUA software. The Sequential Gaussian Simulation (SGS) algorithm (Deutsch & Journel 1998) was adopted to generate the models of volume of clay, effective porosity, and permeability. In more detail, the simulation of volume of clay models were obtained using SGS with simple kriging, conditioned by the well data and subsequent to the lithofacies models; the effective porosity models were simulated using SGS with locally varying means, allowing the conditioning of both hard and soft data, and the permeability models were generated using SGS with collocated co-kriging (hard data: well log of permeability; soft data: effective porosity).

The starting point for the simulation of petrophysical models consisted in the equiprobable set of lithofacies realizations to constrain the simulation of the continuous properties according to the three lithofacies present in the geological model grid. This constraining process is guaranteed by firstly generating dynamic regions for each lithofacies in the Aspen SKUA software, which are being updated for each set of realizations during the simulation process. This cascade workflow is illustrated in Figure 5.16. With respect to the reservoir region only, in which sandstone and clay lithofacies are present, the simulation of effective porosity and permeability models will depend on the precedent spatial distribution of lithofacies and percentage of volume of clay that are simulated, to better constrain the values of these petrophysical properties. This approach was also followed to simulate the petrophysical properties for the primary and secondary seals.

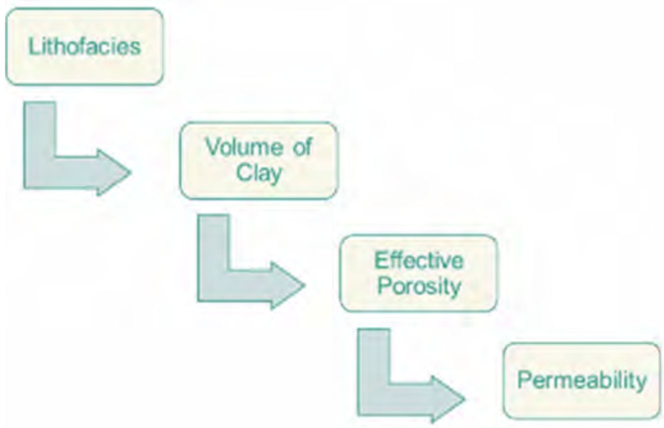

Figure 5.16: Workflow in cascade adopted for the simulation of petrophysical properties from lithofacies.

5.3.3.2 Petrophysical Models

The simulation of volume of clay, effective porosity and permeability properties was performed. The spatial continuity patterns and distributions of the values between the petrophysical models are geologically consistent with the conceptual information, as illustrated in Figure 5.18.

In the k-layers of the reservoir, presented in Figure 5.17, the higher values of effective porosity (>15%) and permeability (>500mD) are mainly located in the central area of the geological model , where the structure of the Q4-TV1 prospect is located, but also in the southernmost area of the model close to the well Mo-1, and between the wells Mo-1 and Do-1C. The lateral degradation of the reservoir properties is observed towards the northern section of the layer in the direction of well Ca-1, which is aligned with the conceptual understanding that there is a stratigraphic trapping mechanism in this

The PilotSTRATEGY project has received funding from the European Union's Horizon 2020 research and innovation programme under grant agreement No. 101022664

area. Although not observed a strong variation in the facies in both layers (mostly sands in both), nor in the volume of clay (showing low values) or porosity (high values), the central part of the layer in the top of the reservoir (layer 90) indicates higher permeability values, whereas at the middle of the reservoir (layer 130) the higher permeability values are located mostly in the southern part between wells 13E-1 and Mo-1. This is aligned with the vertical variation of permeability assumed at the wells.

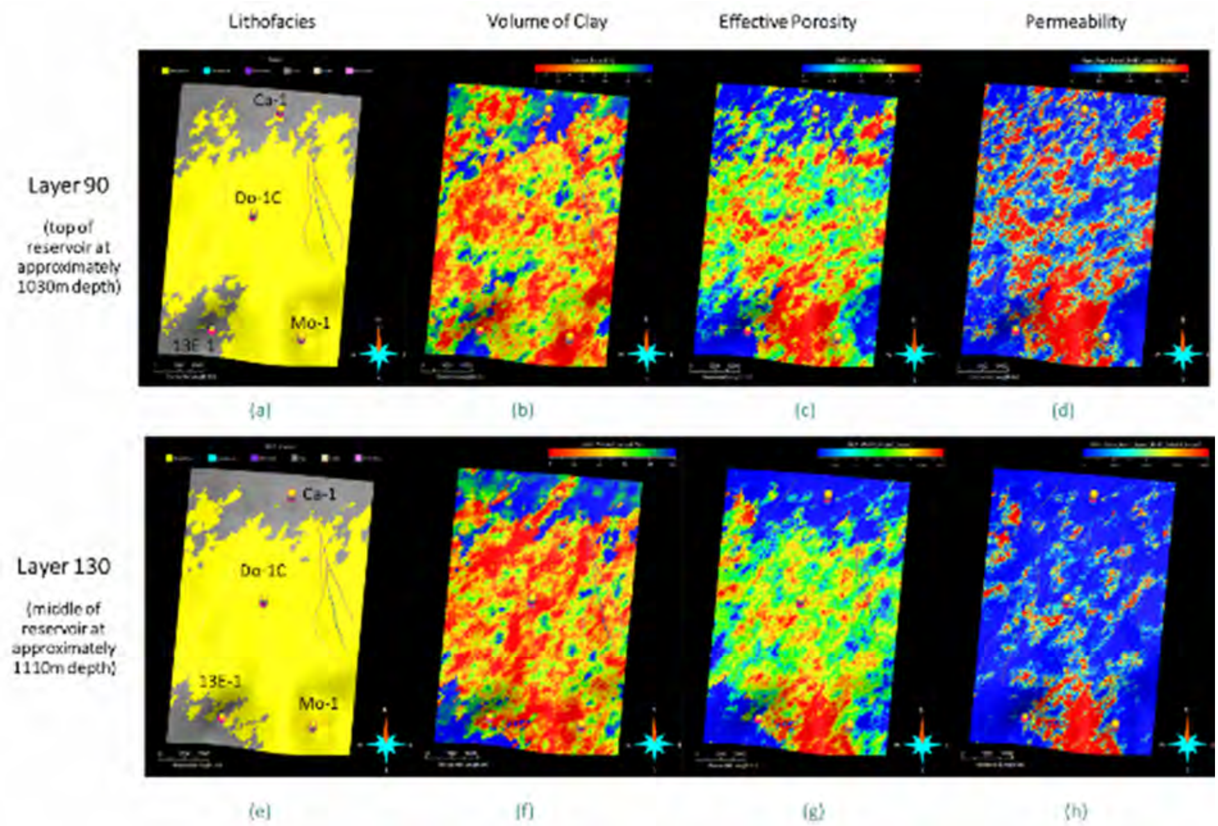

Figure 5.17: Realization of the reservoir k-layers 90 (top row) and 130 (bottom row): (a) and (e) correspond to lithofacies, (b) and (f) to volume of clay in %, (c) and (g) to effective porosity, and (d) and (h) to permeability (mD).

The cross-section between the wells for the volume of shale, effective porosity and permeability is shown in Figures 5.18, 5.19 and 5.20, respectively, illustrating the spatial distribution of the petrophysical properties for the static model regions and for the structure of the Q4-TV1 prospect.

The secondary seal is mainly presenting higher values (>50%) of volume of clay and lower values (<10%) of effective porosity at the locations close to the wells Ca-1, Mo-1, and 13E-1, while lower values (<50%) of volume of clay and higher values (>10%) of effective porosity were simulated close to the location of the well Do-1C (Figure 5.18 and 5.19). Despite the relatively high values of effective porosity, low permeability values are obtained in the simulated models close to the location of the target area (well Do-1C) as well as for the full area of the secondary seal in the static model, in general, as illustrated by the cross-section of Figure 5.20.

In general, the values of volume of clay are mostly low (close to 0%) for the primary seal for the entire model region, being consistent with the lithofacies models of this region (mainly limestone lithofacies). However, the effective porosity of the primary seal presents a higher variation depending on the geological model area: lower values (<15%) are presented in the areas close to the wells Ca-1 and

The PilotSTRATEGY project has received funding from the European Union's Horizon 2020 research and innovation programme under grant agreement No. 101022664

13E-1, and lower-medium values (about 15%) of effective porosity were simulated at the nearby locations of the wells Do-1C and Mo-1 (Figure 5.18 and 5.19). Similarly, as for the secondary seal, the permeability values of the primary seal are mostly low (close to 0mD) at the location of the well Do-1C, where the prospect Q4-TV1 is located, and in the other three wells present in the static model.

In the reservoir region, the locations close to the wells Ca-1 and 13E-1 mainly show higher values of volume of clay, generally between 80-100% (Figure 5.18), and lower values of effective porosity and permeability, such as <10% and <50-100mD, respectively (Figures 5.18 and 5.19). The reservoir areas that present more adequate conditions are located nearby the wells Do-1C and Mo-1. At these locations, most of the reservoir layers present volume of clay values lower then 30-40%, effective porosity values higher than 15% and permeability values higher than 100-500mD. It is important to note that the synclinal structure of the reservoir region, between the structural highs where the wells Mo-1 and 13E-1 are located (Figures 5.17, 5.19 and 5.20), presents several layers with high values of effective porosity (about 25-30%) and permeability (>1000mD).

The PilotSTRATEGY project has received funding from the European Union's Horizon 2020 research and innovation programme under grant agreement No. 101022664

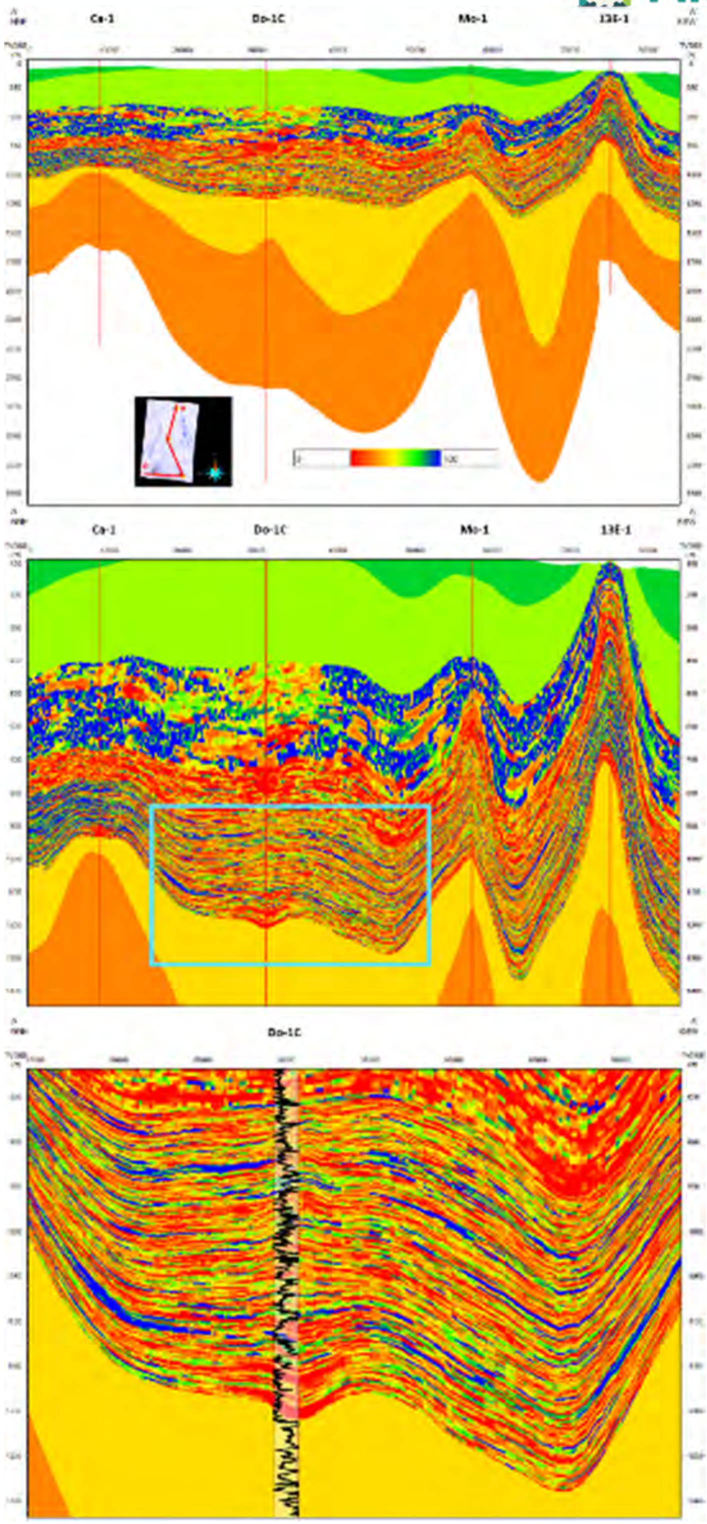

Figure 5.18: Realization of volume of clay shown in a cross-section of the static model, for the reservoir and seals regions, and for the structure of the Q4-TV1 prospect. The rectangle illustrates the location of the Q4-TV1 prospect.

The PilotSTRATEGY project has received funding from the European Union's Horizon 2020 research and innovation programme under grant agreement No. 101022664

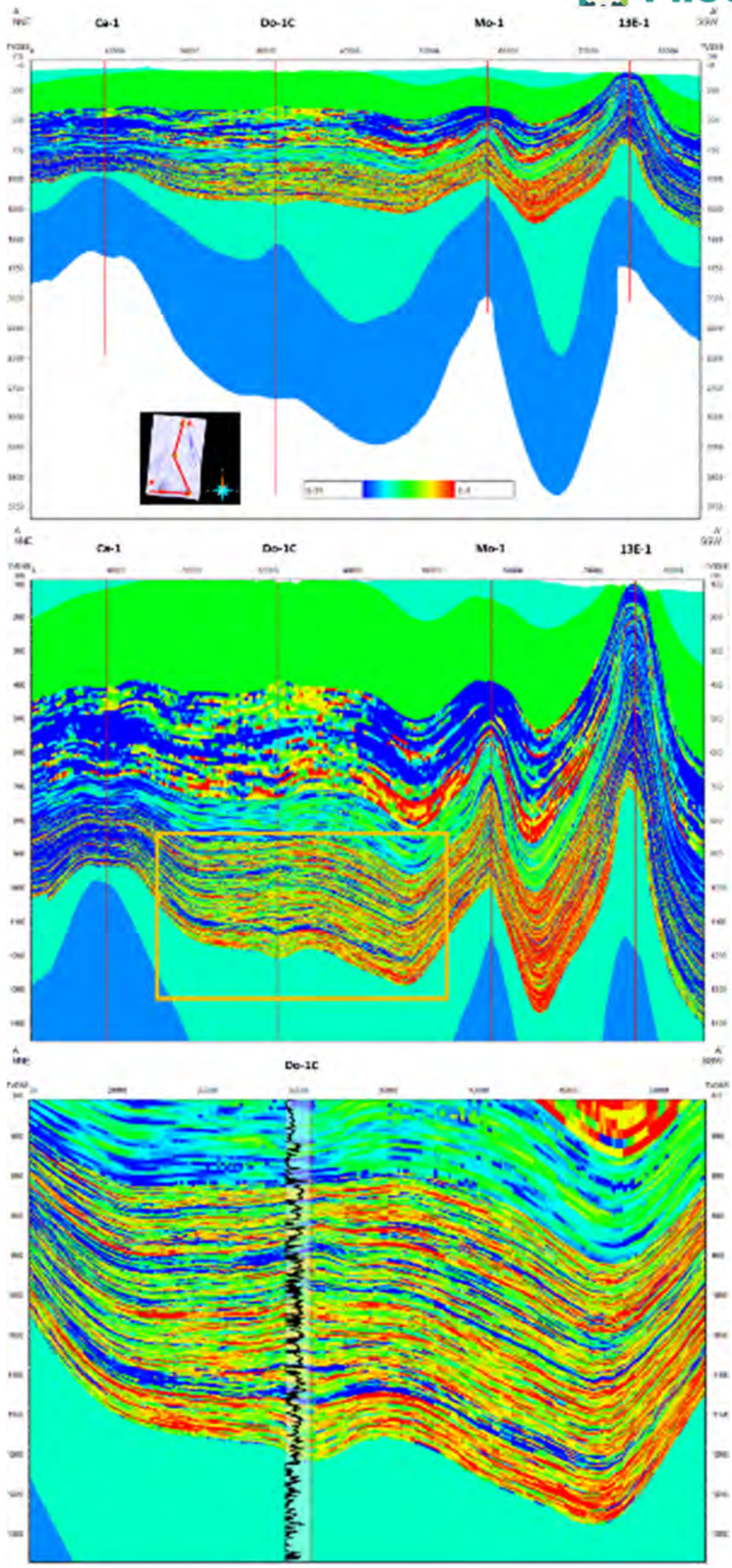

Figure 5.19: Realization of effective porosity shown in a cross-section of the static model, for the reservoir and seals regions, and for the structure of the Q4-TV1 prospect. The rectangle illustrates the location of the Q4-TV1 prospect.

The PilotSTRATEGY project has received funding from the European Union's Horizon 2020 research and innovation programme under grant agreement No. 101022664

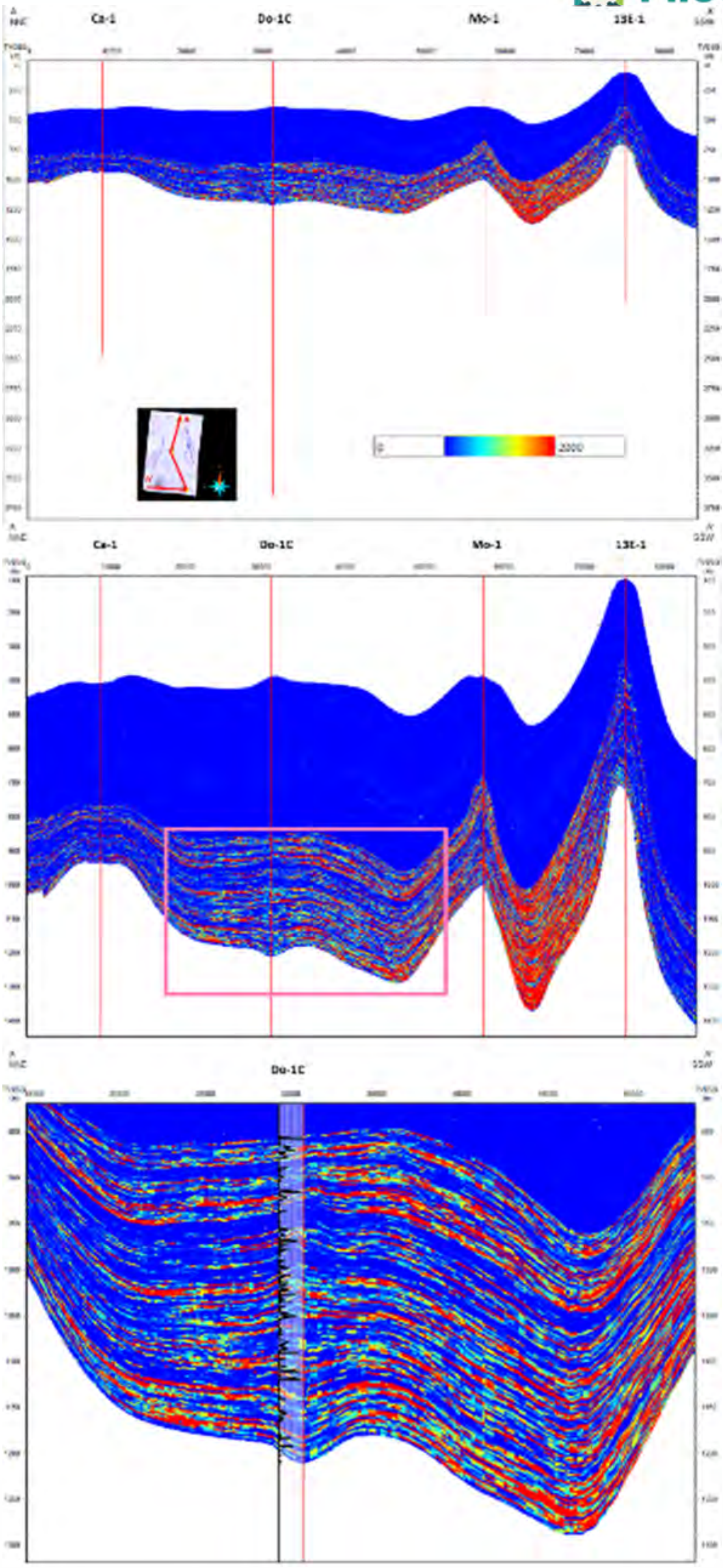

Figure 5.20: Realization of permeability shown in a cross-section of the static model, for the reservoir and seals regions, and for the structure of the Q4-TV1 prospect. The rectangle illustrates the location of the Q4-TV1 prospect.

The PilotSTRATEGY project has received funding from the European Union's Horizon 2020 research and innovation programme under grant agreement No. 101022664

At the location of the Q4-TV1 prospect, several reservoir layers with high percentage of volume of clay (Figure 5.18) and low effective porosity (Figure 5.19) are observed, such as at the depths of about 950m, 1000m and 1100m, which may correspond to the interbedded clay layers or sandstone layers with relatively low effective porosity. These no-flow (or relatively low-flow) reservoir units are also observed in the permeability model (Figure 5.20) for these depth locations. In general, five main reservoir flow units can be identified at the depth intervals between about 860-880m, 940-960m, 1020-1050m, 1080-1100m, and 1110-1170m. The first two depth intervals correspond to the main target depths, previously identified in the geo-characterization studies for the structure of the prospect Q4-TV1, and the last interval depth corresponds to the layers of coarse sandstones and conglomerates present in the bottom of the reservoir. Depending on the dispersion of the CO_2 plume over time within the reservoir, these deeper intervals would also be interesting to be considered in the dynamic simulation studies.

The histograms of the petrophysical properties of interest estimated from the well data and simulated in the models are shown in the Annexes (section 2.3.7), as well as the summary statistics for the secondary seal, primary seal, and reservoir regions of the static model. The probability distribution functions and the main statistics of the rock properties from the well data are, in general, accordingly honoured in the simulated models. It is important to highlight that, despite the high variations in effective porosity values at the Q4-TV1 prospect in both secondary and primary seals, the permeability values in the corresponding models remain significantly low. The permeability distributions for the secondary and primary seal, as shown in its histogram, indicate that approximately 80% of the values are below 1mD, with a median around 1.834mD. Similarly, the primary seal's histogram shows that about 86% of its permeability values fall below 1mD, with a median value close to 0.157mD. The low permeability categories derived from the hard data (well log data) histograms are accurately reflected in the generated models, and the principal statistical measures are generally reproduced (refer to section 2.3.7 in the Annexes). Furthermore, the substantial thickness of these sealing formations, combined with this data, implies the existence of a relatively sufficient retention capacity to inhibit CO_2 flow and prevent leakage through them.

5.4 Uncertainty Analysis

The uncertainty analysis of the static model was performed in three components. First, the uncertainty assessment of the structural elements of the model was conducted to evaluate the displacement of faults and horizons and its impact on the gross-rock volume of the static model and the reservoir unit (structural uncertainty). Then, the uncertainty assessment of the spatial distribution of the petrophysical models was done by retrieving the main statistics of the set of reservoir properties. The last approach consisted of the analysis of volumetrics considering simultaneously the uncertainty of structural and petrophysical information and several parameters used in the modelling of rock properties.

5.4.1 Structural Elements

The uncertainty modelling of the structural elements of the static model was performed by simulating 100 realizations for the full structural model using the “Uncertainty” module of the Aspen SKUA software.

The uncertainty of the horizons was conducted using the “constant” input parameter to define the position of horizons within an envelope with maximum displacement of 25m and 50m for top horizon

The PilotSTRATEGY project has received funding from the European Union’s Horizon 2020 research and innovation programme under grant agreement No. 101022664

of the static model (Seabed horizon) and the bottom horizon of the static model (Salt horizon), respectively. The “move with others” input parameter was selected for the intermediate horizons to follow the displacement of the top and bottom horizons of the static model, honouring the stratigraphic markers of the wells in the study area. The maximum displacement values used correspond to the uncertainties across the seismic interpretation and time-depth conversion studies.

From the simulation results of horizons, it is visible that the horizons present higher uncertainty (higher envelope) in the horizontal (or sub-horizontal) surface zones between the wells (Figure 5.21), when compared to other zones where the dip is steeper, as for instance in the last two horizons of the static model (Brenha and Salt horizons).

Uniform distributions were considered for the uncertainty of the faults with a maximum displacement distance to the original fault of 50 m for the first set of faults (F1, F2, F3) and 100 m for the second set of faults (F4, F5, F6). This difference was based on the confidence degree of the seismic interpretation of these structural elements with the respect to the geophysical data availability and quality. Indeed, the faults of set 1 were mostly interpreted from 3D seismic data and those from set 2 were interpreted from 2D seismic profiles. From the fault modelling results illustrated in the cross-section of Figure 5.22, the faults of the set 1 present a lower uncertainty (lower envelope) when compared to the faults of set 2, as expected from the defined uncertainty ranges (i.e., max. 50m vs. 100m). The summary statistics and histograms of the displacement of the faults are shown the Annexes (section 2.3.8).

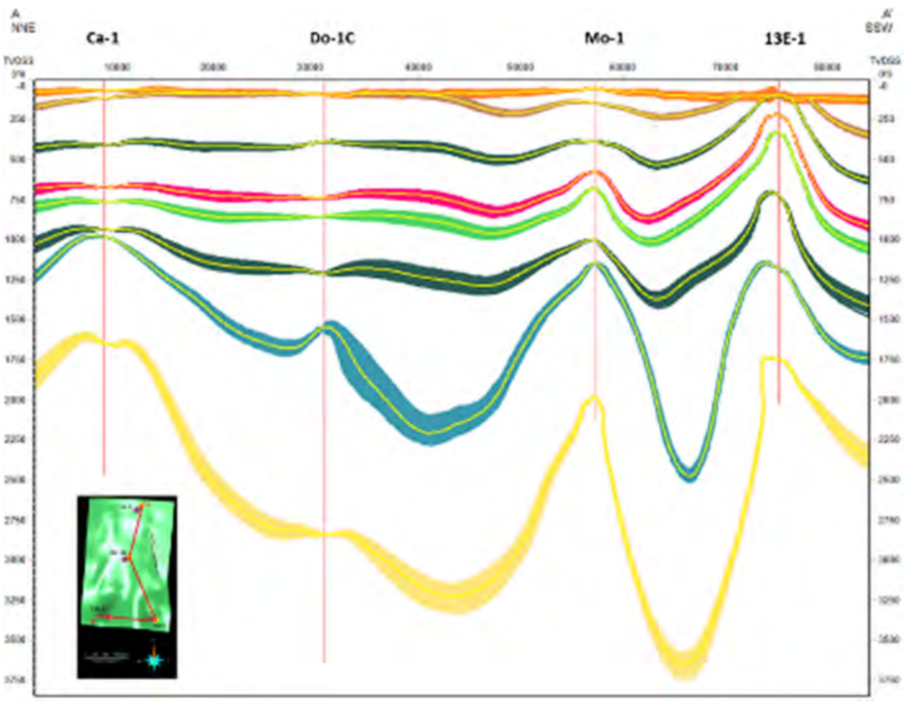

Figure 5.21: Cross-section between the wells illustrating the displacement uncertainty of the 8 horizons of the static model. The yellow horizon within the uncertainty envelopes corresponds to the original horizon surfaces.

The gross-rock volume for the seven regions of the static model and the full reservoir unit are shown by the resulting probability distribution functions (histograms) and cumulative distribution functions (CDFs) in the Annexes (section 2.3.8.1) and summarised in Table 5.5.

The PilotSTRATEGY project has received funding from the European Union’s Horizon 2020 research and innovation programme under grant agreement No. 101022664

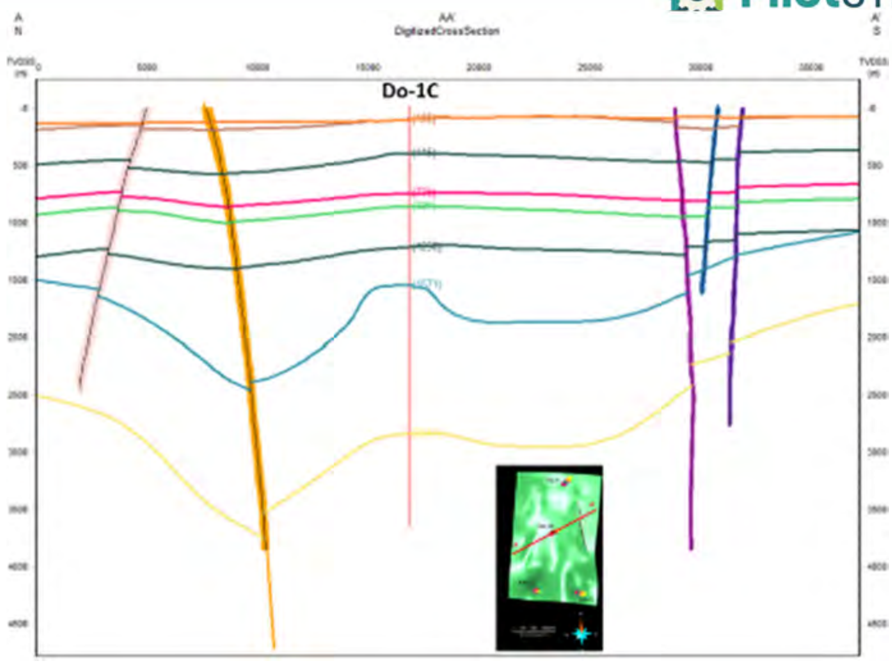

Figure 5.22: Cross-section illustrating the displacement uncertainty of 5 faults of the static model (only the fault F5 is missing in the cross-section). The black fault within the uncertainty envelopes corresponds to the original fault surfaces.

Table 5.5: Summary statistics of the gross-rock volume for the full static model (all regions) and reservoir unit.

Gross-rock volume (GRV)	Static Model (m^3)	Reservoir Unit (m^3)
Base Case	731.2×10^{10}	617.8×10^{9}
Lower Case (P_{10})	730.3×10^{10}	604.5×10^{9}
Most Likely (P_{50})	731.5×10^{10}	618.5×10^{9}
Higher Case (P_{90})	732.4×10^{10}	635.3×10^{9}
Minimum	729.8×10^{10}	588.7×10^{9}
Mean	731.4×10^{10}	618.9×10^{9}
Maximum	733.3×10^{10}	654.2×10^{9}
Standard Deviation	794.8×10^{7}	127.7×10^{8}
Variance	631.8×10^{17}	163.1×10^{18}
Number of Samples	100	

The PilotSTRATEGY project has received funding from the European Union's Horizon 2020 research and innovation programme under grant agreement No. 101022664

5.4.2 Petrophysical Properties

The uncertainty of the petrophysical properties of the reservoir model were evaluated based on the simulation of a set of 100 realizations of each rock property. From the set of simulated models, the main statistics of the dataset of models were computed using the post-processing tools in the Aspen SKUA software.

The reservoir lithofacies uncertainty models are illustrated in Figure 5.23 for the most frequent occurrence of lithofacies, statistically similar in this software to the set of data of the percentile 50, and for the percentiles 10, 25, 75 and 90. According to these models and the corresponding histograms of lithofacies proportions, illustrated in the Annexes (section 2.3.8.2), there is an increase of the clay lithofacies proportion in the models with the increase of the percentile that was computed, i.e., for the percentile 90 of the simulated dataset, the proportion of clay lithofacies increases about 20% comparing to the lithofacies most frequent occurrence model.

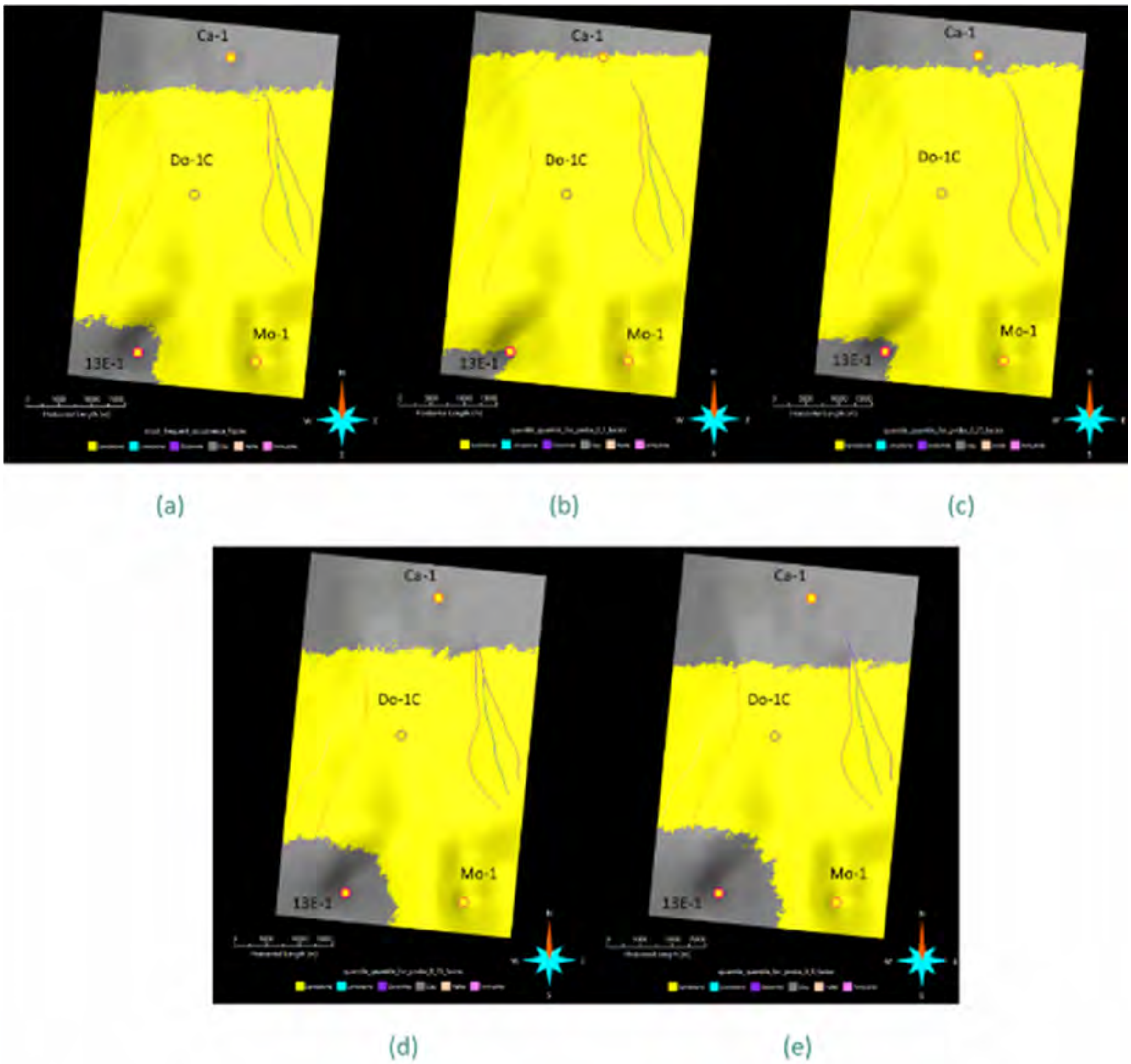

Figure 5.23: Reservoir k-layer 90 of lithofacies: (a) most frequent occurrence (percentile 50), (b) percentile 10, (c) percentile 25, (d) percentile 75, (e) percentile 90.

The main statistics from the set of models of petrophysical properties were also computed for the volume of clay, effective porosity, and permeability. Each petrophysical property is derived sequentially based on each lithofacies model that is simulated for a given realization number, following the cascade approach presented in Figure 5.16. The mean, median, standard deviation, and percentiles 10, 25, 75 and 90 are illustrated in Figures 5.24, 5.25 and 5.26 for the volume of clay, effective porosity, and permeability, respectively. Most of the property uncertainty values for the volume of clay and effective porosity are associated with the model areas close to the wells 13E-1 and Ca-1, corresponding to the clay lithofacies areas, but also in the transition zones between the two lithofacies present in the reservoir. Regarding the reservoir permeability, the uncertainty of the spatial distribution from the set of models of this property are in the central area of the model, in which the permeability values present higher variation. The histograms for the volume of clay, effective porosity and permeability are shown in the Annexes (section 2.3.8.2).

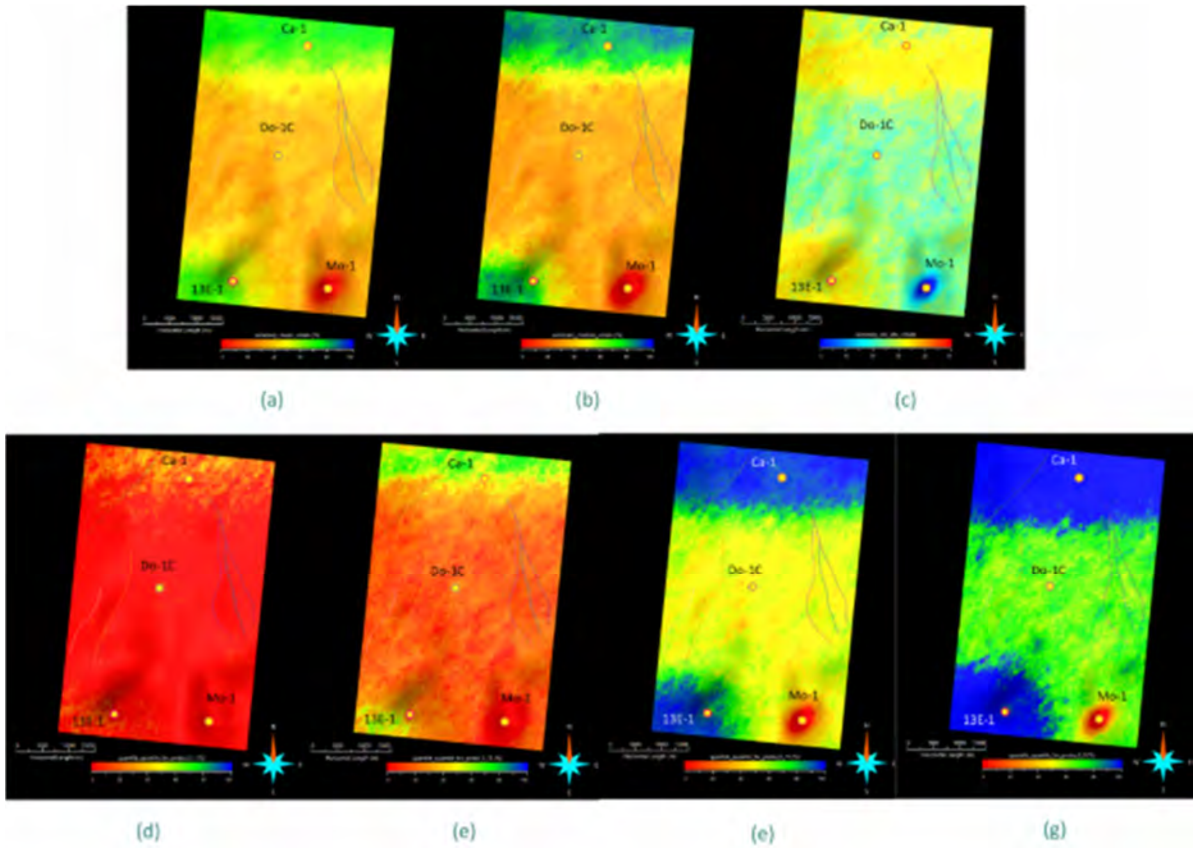

Figure 5.24: Volume of clay k-layer 90 of the reservoir region for the (a) mean, (b) median (percentile 50), (c) standard deviation, (d) percentile 10, (e) percentile 25, (f) percentile 75, and (g) percentile 90.

The PilotSTRATEGY project has received funding from the European Union's Horizon 2020 research and innovation programme under grant agreement No. 101022664

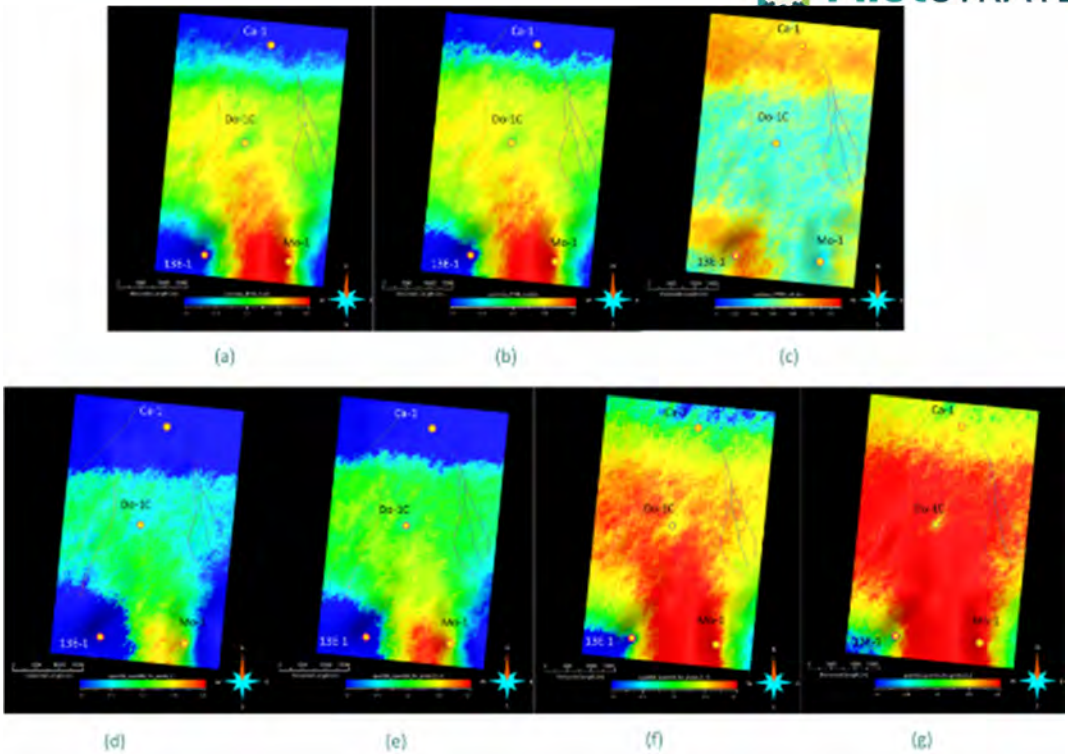

Figure 5.25: Reservoir k-layer 90 of effective porosity: (a) mean, (b) median (percentile 50), (c) standard deviation, (d) percentile 10, (e) percentile 25, (f) percentile 75, and (g) percentile 90.

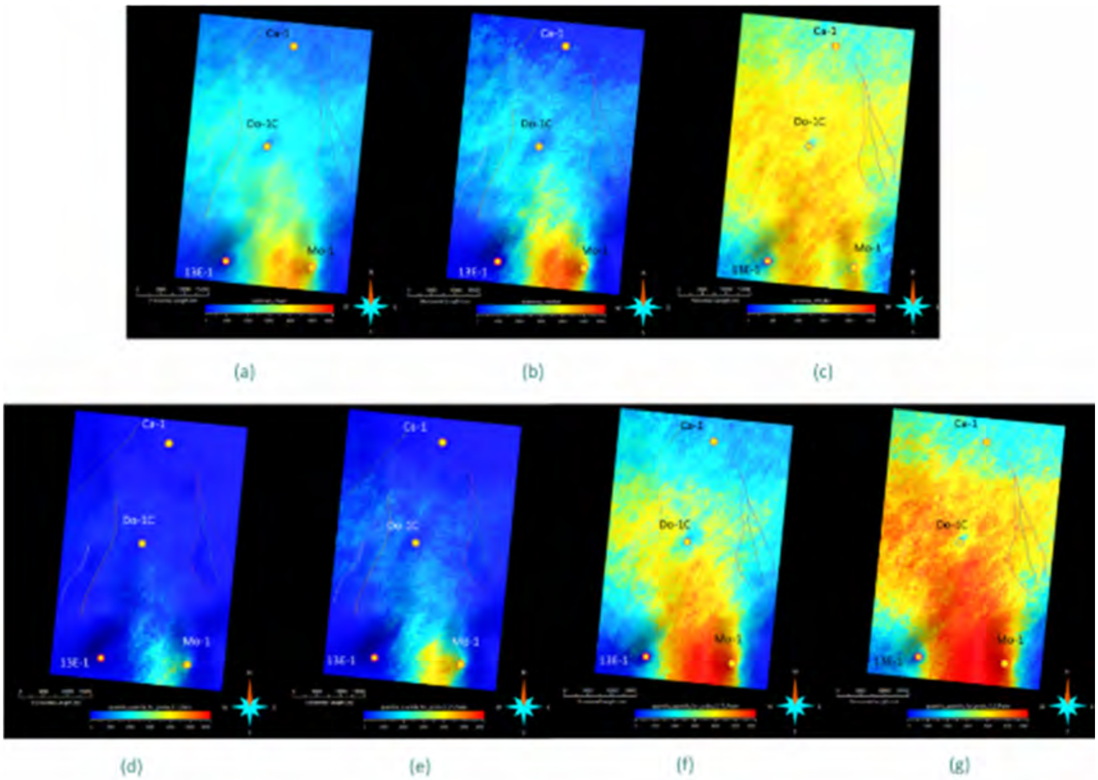

Figure 5.26: Reservoir k-layer 90 of permeability: (a) mean, (b) median (percentile 50), (c) standard deviation, (d) percentile 10, (e) percentile 25, (f) percentile 75, and (g) percentile 90.

The PilotSTRATEGY project has received funding from the European Union's Horizon 2020 research and innovation programme under grant agreement No. 101022664

5.4.3 Volumetrics uncertainty analysis

The uncertainty related with the volumes was conducted using the "Reservoir Risk Assessment" (JACTA) module of the Aspen SKUA software. In this uncertainty modelling study, 300 simulations of the reservoir unit of the static model were performed based on both structural and petrophysical parameters.

The uncertainty of the variogram model parameters (ranges and azimuth values) were also considered for all the petrophysical properties used in the volumetric analysis, such as lithofacies and effective porosity. Triangular distributions were defined to integrate the uncertain parameters, which are presented in the Table 5.6. To determine the net-to-gross reservoir value, a cut-off of 8% from the effective porosity property was set, defining the net-to-gross equal to 1 for effective porosity values higher or equal to 8% and equal to 0 for effective porosity values lower than 8%.

Table 5.6: Uncertain parameters used in the volumetric analysis of the gross-rock volume, net-rock volume, and net-porous volume of the reservoir region of the static model.

Uncertain Parameters		Minimum Values	Base Case Values	Maximum Values
Lithofacies and PHIE	Azimuths (º)	30	45	60
	Main Direction Ranges (m)	4500	6250	8000
	Minor Direction Ranges (m)	2500	3750	5000
Lithofacies	Vertical Direction Ranges (m)	5	35	50
PHIE		5	20	50

From the simulation results, the values of gross-rock volume, net-rock volume and net-porous volume were obtained for the reservoir unit as listed in Table 5.7. The uncertainty ranges of the reservoir volumes are also illustrated by the histograms in the Annexes (section 2.3.8.3).

Table 5.7: Summary statistics of the gross-rock volume, net-rock volume, and net-porous volume of the reservoir region of the static model.

Static Model	Gross-rock Volume (m^3)	Net-rock Volume (m^3)	Net-porous Volume (m^3)
Lower Case (P_{10})	$600x10^9$	$354x10^9$	$704x10^8$
Most Likely (P_{50})	$620x10^9$	$364x10^9$	$727x10^8$
Higher Case (P_{90})	$640x10^9$	$375x10^9$	$754x10^8$
Minimum	$590x10^9$	$342x10^9$	$671x10^8$

The PilotSTRATEGY project has received funding from the European Union's Horizon 2020 research and innovation programme under grant agreement No. 101022664

Mean	$620x10^9$	$364x10^9$	$728x10^8$
Maximum	$650x10^9$	$389x10^9$	$804x10^8$
Standard Deviation	$130x10^8$	$820x10^7$	$201x10^7$
Variance	$160x10^{18}$	$672x10^{17}$	$404x10^{16}$
Number of Samples	300		

The mean values from the set of 300 simulations are about $620x10^9$ m^3 for the reservoir gross-rock volume, about $364x10^9$ m^3 for the net-rock volume, and $728x10^8$ m^3 for the net-porous volume. It is important to note that the resulting volumes are representative for the full reservoir unit of the static model, considering the entire areal and vertical reservoir dimensions, i.e., the total area and thickness of the reservoir in the static model.

5.5 Final Remarks

The static geological model with uncertainties was successfully accomplished in the task 3.1 of WP3 for the offshore area of the Lusitanian Basin in Portugal.

The available data of the study area (wells and seismic data) was limited and the lack of detailed information about the reservoir depositional model were two main challenges for building the static model. To overcome these limitations, the study area of the static model was extended beyond the target area boundaries, to cover the closest three additional wells (Figure 5.1), and additional studies using the 3D seismic data from southern analogue areas (section 2.3.1 of the Annexes) was also considered. This allowed to retrieve information for modelling the variograms and increase the data representativeness of the study area (i.e., distribution and extreme values of the hard data) of lithofacies and petrophysical properties. Furthermore, this also allowed to provide additional insights about the spatial continuity patterns of the reservoir properties away from the wells control. Despite of these main challenges faced during the static model building, the resulting rock property models reproduce the main statistics from the hard data of the wells and the main spatial trends, as expected from the conceptual geological and depositional information of the reservoir in the study area.

The lack of permeability data at the required depths of interest increased the uncertainty in estimating this reservoir property, which required to be determined recurring to literature relationships, and no permeability analyses from the laboratory were available. This task of estimating the permeability values would clearly benefit if laboratory core-flooding analyses with CO_2 in reservoir samples could be conducted for calibrating the estimated values. Nevertheless, the resulting distributions of permeability for the available wells are consistent with the range of values determined from previous hydraulic tests in analogue areas of the onshore setting of this sedimentary basin and for the same reservoir formation, providing confidence in the resulting permeability models.

The PilotSTRATEGY project has received funding from the European Union's Horizon 2020 research and innovation programme under grant agreement No. 101022664

Based on the set of simulated models of lithofacies and petrophysical properties, conducted in the uncertainty analysis of volumetrics of the section 5.4.3, the resulting P10, P50 (median) and P90 models were considered to generate the reservoir models based on the net-porous volumes. In this way, P10, P50, and P90 scenarios for all the properties will be used for the next tasks of the WP3 (tasks 3.2, 3.3 and 3.4). Figure 5.27 illustrates the reservoir models for the P10, P50 P90 of effective porosity, and horizontal and vertical permeability.

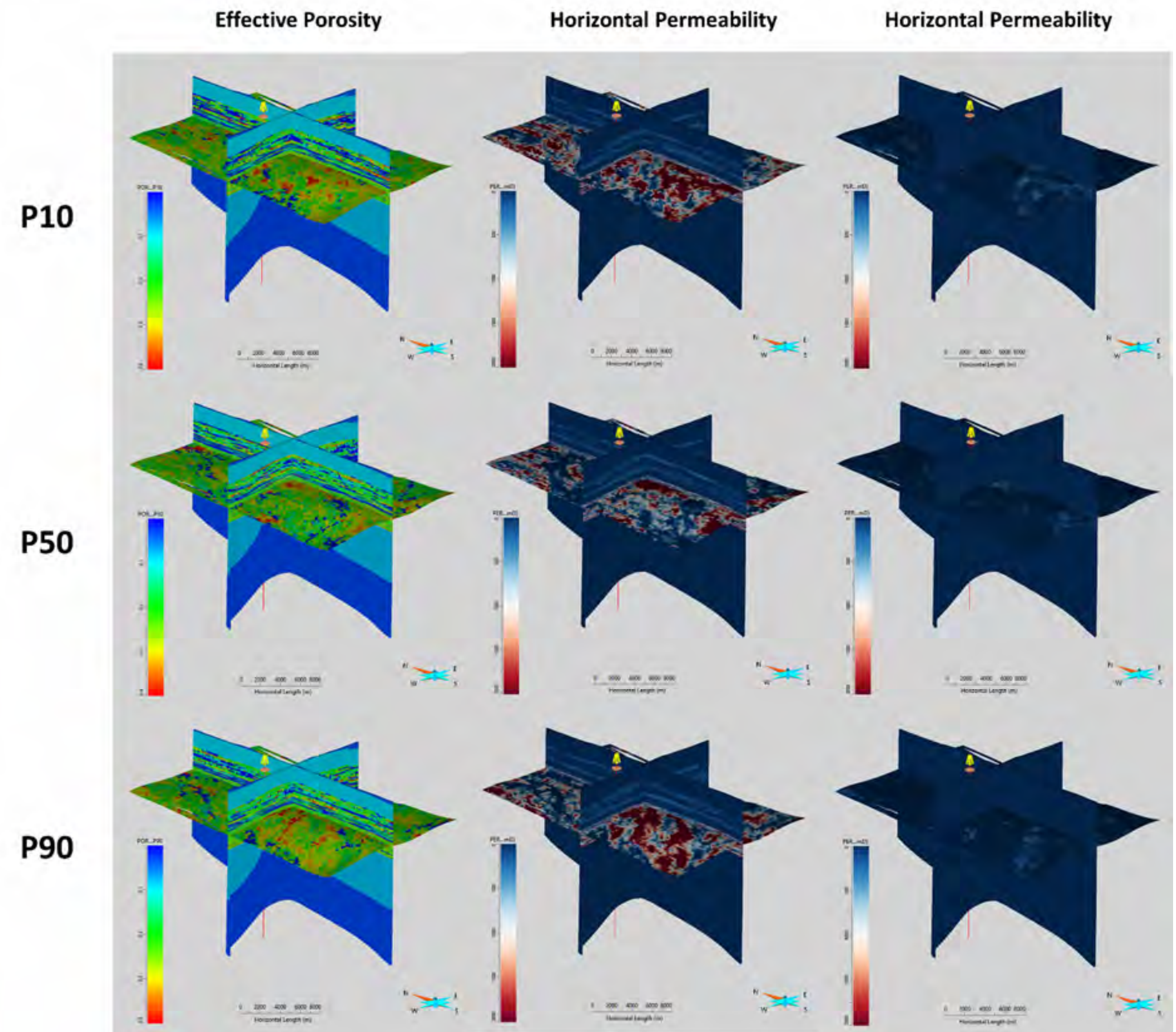

Figure 5.27: Reservoir models of P10, P50 and P90 corresponding to the net-porous volumes from the uncertainty studies for: (a) effective porosity, (b) horizontal permeability, and (c) vertical permeability. The reservoir models illustrate the k-layer 51.

The upscaling process from the static models to the reservoir models was performed for all the properties resulting in flow simulation grids of 89x135x108 cells, with areal dimensions of 200x200m and the following vertical dimensions: of 5m (reservoir), 10m (primary seal) and 20m (secondary seal). The overburden and underburden regions of the static model have only 1 layer (Figure 5.27) with the following dimensions: 191m (Eocene-Miocene), 330m (Paleocene), 1301m (Upper Jurassic) and 1061m (Middle Jurassic).

The PilotSTRATEGY project has received funding from the European Union's Horizon 2020 research and innovation programme under grant agreement No. 101022664

For CO_2 storage capacity optimization and determining the optimal well location (task 3.2), the recommended approach at this stage of research is as follows:

- For dynamic flow simulation, with the currently generated model design (reservoir model grid dimensions and cell thickness), executing the preliminary dynamic simulation runs using the P50 scenario of reservoir property models is recommended to check the required computational time and resources.
- If the results are satisfactory, the dynamic simulation should proceed with the same parametrization for the set of reservoir models of P10-P90 scenarios.
- If not, an iterative process between the static and dynamic domains should be conducted to update the reservoir model design, i.e., by adjusting the complexity of the models by decreasing the cells thickness and/ or grid dimensions, and apply the adequate local grid refinements in the reservoir models, such as at the well locations (CO_2 injection well and abandonment well Do-1C).

6 Ebro Region (Spain)

The study area is situated near the southern edge of the Ebro basin, which is interpreted as a foreland basin formed since the Paleocene over a Paleozoic basement affected by normal faults, oriented NW-SE and NE-SW, formed during two extension stages. Some of these faults, mainly in the southern border of the basin, were reactivated and inverted during the Alpine Orogeny.

The stratigraphic series is formed by an underlying basement of Paleozoic rocks with some degree of metamorphism. Above the basement, Triassic sediments display typical Germanic facies, including Buntsandstein red beds, Muschelkalk dolostones, limestones, and evaporites and Keuper evaporites and shales. Three different Triassic evaporitic sequences characterize the sedimentary pile at this sector: (i) a thin basal evaporite layer (Röt facies), (ii) a thick succession of Middle Triassic evaporites (M2, middle Muschelkalk facies), and (iii) a thick succession of continental evaporites and fine grained clastics of Late Triassic age. The oldest Jurassic rocks of the Ebro Basin are 50 m of dolomites overlain by a cyclic anhydrite unit bearing dolomitic interbeds (Lécera Fm) with a total thickness of 200 – 450 m.

This oldest sequence is overlaid by a maximum of 300 m of multiple shallow platform carbonate sequences (dolomites, limestones and limestones with interbedded marls). This is overlain by continental carbonate and detrital Cretaceous deposits. The base of the Cenozoic continental evaporitic and detrital rocks is unconformable. This erosional surface cuts the Cretaceous and Jurassic deposits.

The Buntsandstein (main reservoir) contact with the Permian is clear and slightly discordant and is divided by three formations, from bottom to top (Figure 6-1):

- Aranda Fm. (Lower Triassic): Sandstone, interbedded with thin (centimeter) shales, red and, occasionally, green.
- Carcalejos Fm. (Anisian age), it is formed by alternating red colored sandstones and shales, and sometimes contains levels of microconglomerates.
- Rané Fm. (Anisian age), it is formed by alternating shales and fine-grained red sandstones.

In log analysis Aranda formation is unit B-1, and unit B-2 corresponds to Carcalejos formation, as they are usually named in the oil and gas industry in this area. B-3 has also been defined in this report and correspond to the very top Röt/Rane formation, which is the primary seal of the Buntsandstein reservoir.

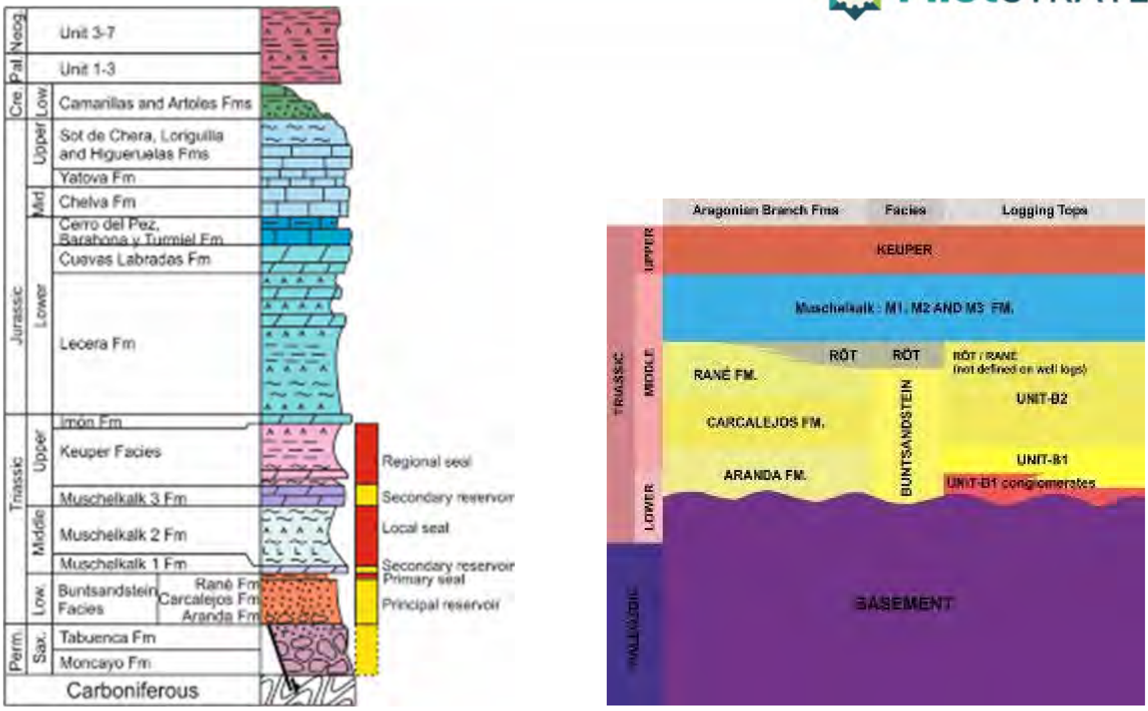

Figure 6-1: Simplified lithostratigraphic column of the area and correlation between Triassic formations.

For more detailed geological description and bibliographic references, see PilotStrategy Deliverable 2.7 (Wilkinson, M., 2023) on the conceptual geological model.

6.1 Available data presentation

In the Lopín area, the only available data is some 2D seismic sections from oil exploration surveys of the 80's. The nearest well is about 4 km southwards. Therefore, the area was enlarged to include it for calibration purposes. Petrophysical properties have been taken from other wells, which, although being further away from the study area, have useful information on the target storage formation. For detailed description of the sedimentary sequences and for sampling for laboratory analysis, two sites located at about 60 km southwards have been considered as field analogues.

Detailed information on used dataset is included in Deliverable 2.7 "Conceptual Geological Models". As a summary, the data sources were:

Seismic sections. 9 lines in SEG-Y format files vectorised from TIFF files for horizon and fault interpretation.

Gravimetric survey. For calibrating the interpretation and infer the geological structure where there is no other data.

Well data. A set of 12 wells were studied from which the two nearest ones, with well-log data of the storage formation, were analysed (EBRO-1 and EBRO-2).

Passive seismic survey. Passive seismic methods have provided constraints for the interpretation of seismic reflection sections and gravimetric model.

The PilotSTRATEGY project has received funding from the European Union's Horizon 2020 research and innovation programme under grant agreement No. 101022664

Field analogues. For detailed stratigraphic sequence description and petrophysical results from samples from stratigraphic sequences studied in natural outcrops (Torre de las Arcas section and Peñas Royas section).

Analogues from Europe and North Africa Buntsandstein facies were also studied for comparison.

Photogrammetry with Drone. Survey on Buntsandstein sandbodies geometries and amalgamation.

The general process for generating the geological static model is synthetized in Figure 6-2.

Figure 6-2: Workflow followed for the whole modelling process and tools available in Aspen SKUA software.

6.2 Data processing

6.2.1 Time to depth conversion

Prior to the seismic interpretation, time to depth conversion of the seismic lines was carried out. This approach was chosen due to the absence of information about the velocities in depth in the area. The only source of data were the average velocities used in the seismic processing for each line, therefore the conversion was only possible along these lines and could not be extended between lines. As a reference, the well Lopin-1, located southwards from the target area, was used. Initially, the extent of the study area was planned to be smaller, but it was widened in order to include more data from the gravimetric survey (see Deliverable 2.3) and the mentioned wellbore. This well did not reach the target Buntsandstein formation, so no well-log information was available. Fortunately, data of the overburden could be recovered, including the depths of the horizons.

Two seismic lines nearby the Lopin-1 well were converted from time to depth and some reflectors of the resulting lines were found to be coincident with the well markers. This way this methodology was validated and applied to the rest of the seismic lines.

The software used was Aspen SKUA, and the methodology is described in detail in the Deliverable 2.7.

The PilotSTRATEGY project has received funding from the European Union's Horizon 2020 research and innovation programme under grant agreement No. 101022664

6.2.2 Horizons and faults interpretation

Horizons and faults interpretation was made having in mind the source of error of both the low resolution of the seismic data and the time to depth conversion. Therefore, after this task, an uncertainty analysis has been done, as explained in the 6.3 Modelling section.

Horizons and faults were traced as usual in this kind of studies, except that no well markers were available to constrain the horizons interpretation. To overcome this problem, or at least to try to reduce the uncertainty in locating the reflectors corresponding to the stratigraphic horizons, the interpretation started in the seismic profiles nearest to the Lopin-1 Well. Despite the fact that there are no markers beyond the Buntsandstein Fm top in this well, the reflectors of the overburden could be followed in the seismic profiles and matched with the well markers. Then, the interpretation was continued in the remaining sections. Due to the low resolution of the reflectors, special care has been taken in parts with noise and in the intersections of the seismic profiles. The conceptual geological model and the geologic regional knowledge was important during the interpretation task.

After the analysis of the nearest wells and outcrops, it was found that the three members of the Buntsandstein formation could be differentiated by the porosity property (see next section), and an estimation of the thickness of each member was done. This was used as reference data for including such members as individual regions inside the storage formation. The thickness of the Buntsandstein was found to be very constant throughout the basin, so three horizons, corresponding to the tops of the three members, were built, parallel to the top of the formation (named B1, B2 and B3).

6.2.3 Well log analysis

In the Deliverable 2.7 there is a comprehensive explanation of the well log analysis procedures. Therefore, this chapter will be a simplified approach that will explain the main results and the data that have been used to feed the model.

Below are selected well log data that we considered critical in order to create the static model from.

- From Gamma Ray the Volume of Shales (Vsh from GR index),
- Tops and bottoms of each studied formation (markers mainly from GR),
- Estimated porosity from different analysis from Resistivity, Neutron/Density or Sonic logs.
- Net thickness vs Gross thickness of the reservoir (based in porosity cut-off, as later defined in this report).
- Histograms of the porosities.
- Vertical Variograms of the porosities.
- General vertical distribution of porous facies in each legacy well.
- Lateral facies variations in the basin, from legacy wells correlations.
- Facies/lithological interpretation of the wells based in reported cutting analysis and well logs, all of them from 60's to 80's final well reports.

Porosity to permeability relationships were obtained using cross plots from core and outcrops samples analysis (laboratory data).

In the Conceptual model defined in the Deliverable 2.7, the Ebro Basin main reservoir selected was the Buntsandstein facies sandstone. It has been finally divided in three parts from bottom to top:

- B1: from the Palaeozoic discordance to the bottom of the B2. It consists of siliciclastic sequences of Braided channels, with some intercalations of less permeable facies that vary

The PilotSTRATEGY project has received funding from the European Union's Horizon 2020 research and innovation programme under grant agreement No. 101022664

from silty to shaly beds. As per the bibliography, the fairway of these channels seems to be towards the NE.

- B2: Some channelized sand bodies more or less isolated into thick non-permeable lithologies (shaly to silty).
- B3: At the very top, it is the primary seal and consist of mainly argillaceous facies.

The Buntsandstein has been commonly interpreted in this area as slightly eastward tilted basin filled up by fluvial deposits. The present faults have been originated afterwards, during the alpine orogeny. B2 and B3 member mark a change in the sedimentation with less channels and more argillaceous sedimentation.

As already stated, the former wells are not in the ZOI (Zone of Interest). Anyway, their logs are consistent with the facies shown in the outcrops, which may indicate a quite homogeneous sedimentary environment in the Triassic. That said, it is very difficult to interpret different typical fluvial facies from these ancient logs. These logs show a quite homogeneous Gamma Ray signatures that are interpreted as mainly sandy formations with scarce shaly intercalations. Data from Neutron-Density logs, Sonic and Resistivity show a gradual increase in sandstones and porosities to the top, a gradual change to the B2 formation with more argillaceous intercalations up to a shale dominant facies characteristic of the B2 formation. Another formation has been described as B3, that is the primary seal of this reservoir, also known as Röt facies.

Porosities from Well-Logs

Porosity distribution histograms were generated for the Buntsandstein for the following offset wells (Figure 6-14):

- Fraga-1
- Mayals-1
- Caspe-1
- Ballobar-1
- Ebro-1
- Ebro-2
- Monegrillo-1

Differences between these wells are clear, in the mean data and the distributions. Are these differences due to facies variations, to diagenesis or other factors? The Buntsandstein sedimentology in this area seems to be quite homogeneous, so it may be due to the diagenesis. Figure 6-15 shows the relationship between porosity and Buntsandstein depth in the studied wells. Thus, decision was made to use the closest offset wells to ZOI in the range of depths similar to the planned Pilot area. Ebro-1 and Ebro-2 wells were therefore selected also because they have a comprehensive set of data (including pressure and temperature gradients).

Anyway, the porosities distributions in these wells shows a slight increase towards the B1 top, even if, in the last tens of meters on B1 top, they show a gradual decrease in porosities though (Figure 6-16).

In order to model this facies distribution, we perform numeric facies analysis. We have used the available data from well logs from the legacy wells, outcrops analysis and samples data.

The PilotSTRATEGY project has received funding from the European Union's Horizon 2020 research and innovation programme under grant agreement No. 101022664

Field analysis and Laboratory data

On the outcrops and rock samples is worthy to note that soft or initially interpreted "shaly" intercalations are mostly composed of very fine sands or silty formations with very low permeability but not null. Three stratigraphic columns were done: two in the Buntsandstein outcrops nearby the ZOI (70Km SW) and one in a Buntsandstein core from the Chiprana-1 well, stored in the IGME facilities in Peñarroya (Córdoba, Spain) (Figure 6-18). Those outcrops are interpreted as mainly braided channelized facies with floodplain facies, with little evidences of palaeosols or lacustrine facies within the B1 sections. There are aeolian facies in the Buntsandstein in this area, but we are unable to distinguish them in the logs, so they are absent in this interpretation. B2 is interpreted as mainly flooding plains with some channel facies isolated. These channels are probably link with meandering channels, but then again based on scarce data. B3 marks a sea flooding event that covers the Ebro Basin, and consist of siltstones, shales and evaporites that are the primary seal of the reservoir just below of the Muschelkalk formations. Muschelkalk formation are thick levels of dolomites (M1 and M3) with evaporites and shales in between them (M2) (Figure 6-1).

To model the sandbodies in the Buntsandstein, which should be the CO_2 storage target, we attempted several approaches. We try to correlate field and laboratory data with the offset wells logs. The interpreted facies are difficult to match with the well logs. Well logs have a quite homogeneous signature that makes tricky to split them in the number of facies interpreted on the field, rather than just differentiate sandstones and shales. There was an attempt to match porosities with different facies but, then again, it seems that porosities have not the typical multimode distribution meaning the presence of different facies (see Figure 6-14). In addition, in the Figure 6-18, we can see how the rock samples porosities are not clearly linked with the interpreted facies. This is likely due to the presence of other factors that control the porosities distributions.

Nevertheless, we have used stratigraphic data to compute the thickness and abundance of two facies:

- Facies with more than 8% porosity
- Facies with less than 8% porosity.

The reason to do so was to simplify the model in a more practical way, knowing than below 8% porosity the permeabilities are very low. In the Figure 6-17, we have plotted the whole set of rock samples porosities versus the reported laboratory permeabilities.

It made it easier to compare field data with the well logs data, since the porosities are indeed already found in each well and are used for the already cited histograms, Net to Gross calculations and vertical gradations in the wells. But from the field data we collected, the sandbodies thickness, lateral extensions (to some degree with the Photogrammetry survey) and vertical channel overlaps. All those data needed to fill up the FLUVSIM workflow in the Aspen SKUA software.

Data used to model facies

In the Aspen SKUA FLUVSIM workflow, it is needed to fill up several parameters to model a fluvial reservoir.

Channel Proportion: as said we have considered "Channel" facies to be above 8% porosity. We have defined channel in a similar way than Gibling (2006): all kind of facies inside the channel area/zone. So, in this report, several channels aggregated together in a single sandbody (even with some bars o levees included) are considered "channel facies" unless there are separated by a sealing level. The

The PilotSTRATEGY project has received funding from the European Union's Horizon 2020 research and innovation programme under grant agreement No. 101022664

FLUVSIM facies named “Shales” are here considered to be “outside” the channel area and they have porosities always below 8%. So, the Channel proportion will be in fact equal to the Net to Gross, as it is defined by the ratio of cumulated thickness of levels with porosity above 8% versus the total formation thickness.

Maximum Channel number (number of channel facies): This parameter has been set by trial and error. When modelling the facies with the FLUVSIM tool we regularly compare porosities histograms between the reference offset wells (Ebro-1 and Ebro-2) with the porosity histogram coming from the model. The idea was that Model histogram should be somehow similar to those 2 wells histograms. We had to increase the channel numbers until we got a similar porosity distribution. This method was also used for other parameters adjustments.

Orientation of the Channels: Authors in the area (Arche et al., 2004) have defined a general fairway for the channels towards the NE (about N45 ° E). This is consistent with the wells correlations described in the Deliverable 2.7.

Sinuosity parameters: the most of them are set as per Gibling (2006) and present-day braided rivers geometries (Brahmaptutra, Saskatchewan and Skeidarasandur rivers). Anastomosed channels (B2) seem to be complicated to model, so some adjustments have been made to have sound channels models, i.e. to get something river-like instead to have a high frequency wave-shape channel.

Thickness: channel thickness data have been interpreted from outcrops (stratigraphic columns and photogrammetry) and literature data (Gibling (2006)) with little adjustment to have porosity histograms similar to the reference wells. We should remember we are defining channel as all sediments inside the channel area, and this definition has also a vertical meaning.

Channels Width: To establish the channels width, we tried to use the outcrops data, but we immediately learned that channels are far wider than the outcrops expose. Instead, we used the studies of Gibling (2006) that collect a series of data from worldwide river systems research (Figure 6-19). Albeit this work is not counting the likely compaction of these levels in the geological record. Some of the figures are simplified (Width, Width ondulation and Width ondulation length Scale) or taken by the default figure in the Aspen SKUA FLUVSIM workflow.

Vertical Channel Overlap: it has been calculated considering the number of channelized bodies into every channel facies (considered all bodies to form a channel facies, as stated above). So, it is a ratio of a single channel facies over the number of Channelized bodies included in it, from outcrops stratigraphic columns.

6.3 Modelling

6.3.1 Structural modelling

For building the structural model, the SKUA Structure and Stratigraphy Workflow has been used. Horizon and fault interpretations are the main input features. The volume of interest has been defined for including the wider area considered in the gravimetric survey. The residual map of Bouguer anomaly revealed a structure with horst and grabens with a NW-SE orientation, which served as a guide in the interpretation and gave some clues for the location of the main faults.

The modelling task was made as a feedback process with the interpretation task where the inconsistencies detected in the model were fixed in the interpretation part.

The PilotSTRATEGY project has received funding from the European Union’s Horizon 2020 research and innovation programme under grant agreement No. 101022664

First, a fault structure was built and the spatial relationships between faults were checked and adjusted where needed. An important issue was to assess the actual or most probable extent of the faults, given the uncertainty when trying to follow up the faults planes between profiles. As a quality control, the fault length-throw relationship was used (Kim *et al.*, 2003). A plot of maximum displacement against fault length was drawn and compared with literature references for normal faults (see Figure 6-20). Displacement/Length ratios range from 1.3E-2 to 1.7E-1, which fit with the results of previous authors.

Once the structural model was finished an isobath map was made in order to check the proposed structure and it was seen a probable closure at about 1,650 mbsl (Figure 6-3**Erreur ! Source du renvoi introuvable.**).

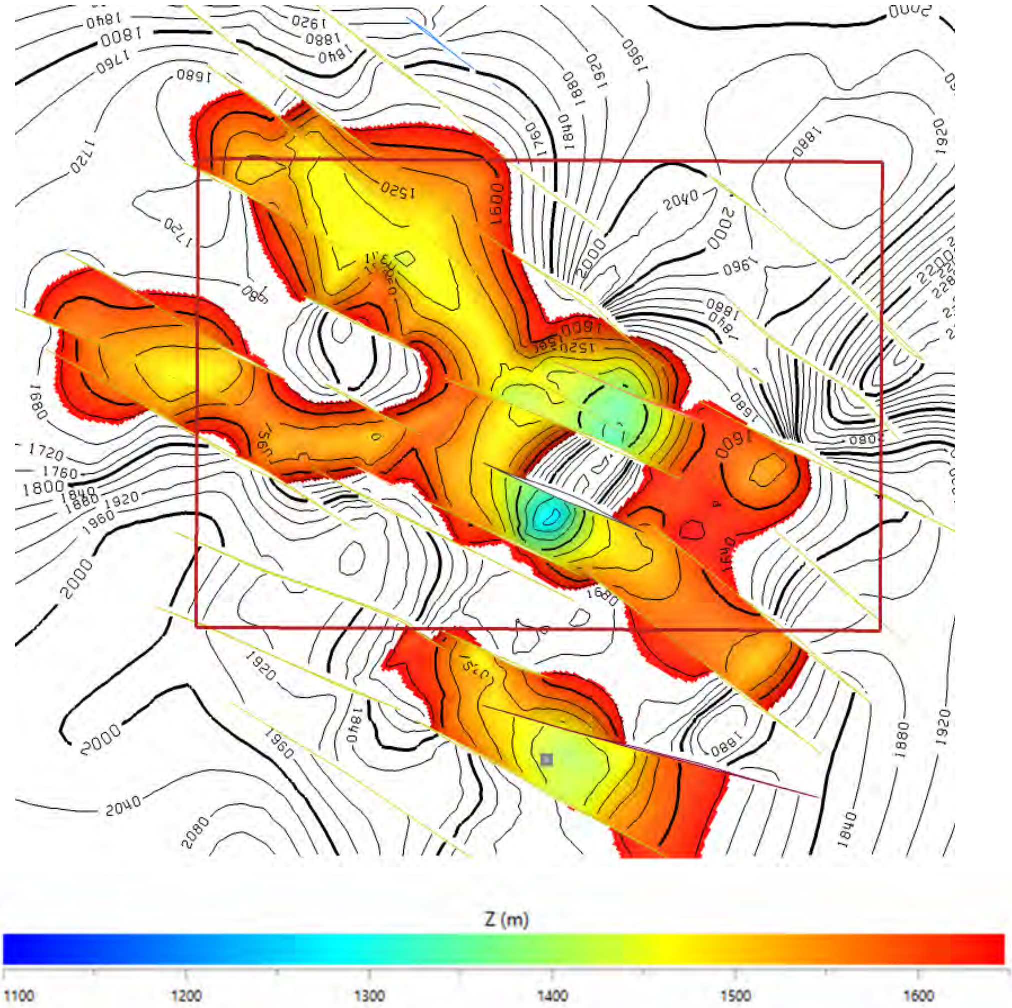

Figure 6-3: Isobath map of the top of the Buntsandstein formation. Coloured area is the possible closure at 1,650m. The red rectangle is the area initially proposed for investigation. Depth datum is the sea level.Grid

The geological grid was built from the structural model using the Aspen SKUA Grid Workflow, as a continuation of the previous one. The cell size is 200x200x2m for the model in the storage formation part, and 200x200 and one cell in depth per formation in the overburden and underburden. This size was decided taking into account the size of the model and the requirements the further flow model, and at the same time, trying to preserve the heterogeneity in the distribution of the properties.

The PilotSTRATEGY project has received funding from the European Union's Horizon 2020 research and innovation programme under grant agreement No. 101022664

The result was a model with 1,467,840 cells with a distribution of 132x139x80 cells, 70 only for the storage formation and the 10 remaining cells of the pillar for the overburden and overburden. See Figure 6-21 and Figure 7-22.

6.3.2 Subsurface properties

From the well logs of porosity, proportions of channels along the B1 and B2 regions were calculated (Figure 6-23 and Figure 6-24). Then, a vertical proportion curve for each region was derived from the wells and following the facies classification in channel and shale (Figure 6-25, Figure 6-26 and Figure 6-27) and it was transferred to the geological grid (Figure 6-28). In this way, a property group with channel and shale proportions was populated in the whole grid.

Given that each member has facies with different porosities, it was necessary to create distribution curves for populating the porosity independently. Four distribution curves were created from the porosity calculated in the wells (Figure 7-29, Figure 6-30 and Figure 6-31).

As mentioned before, the target formation was divided into two members, named B1 for the Aranda member, and B2 for the Carcalejos member on top. Both are composed of alternating sandstones and shales, corresponding to channel fills and floodplain deposits, although with different proportion and distribution of channels. As there was no information of the channel distribution, the approach used was trying to reproduce the heterogeneity of the alternating channel and shales facies (Figure 6-4).

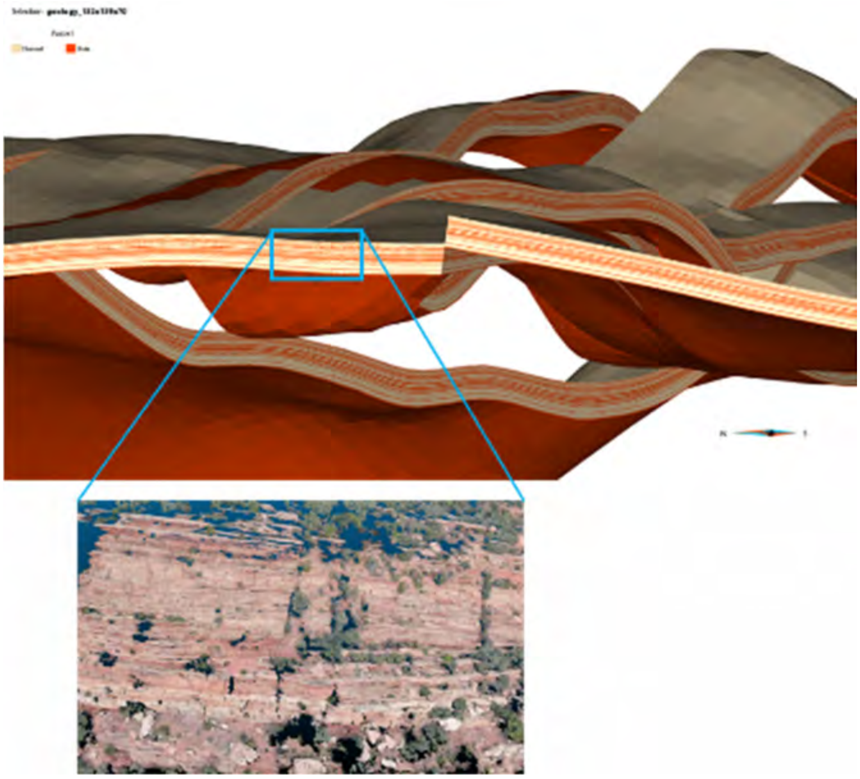

Figure 6-4: Example of the heterogeneity in the outcrop and representation in the model.

For the vertical heterogeneity, the information from the EBRO-1 and EBRO-2 wells was taken. For the horizontal and vertical heterogeneity, the object simulation FLUVSIM was chosen among the different options available in the Reservoir Properties Workflow in Aspen SKUA. Hence the channel distribution was the result of a stochastic estimation together with a more detailed vertical proportion estimation.

The population of the channel objects and the properties have been done in two steps for each member. First, the channels and shales were created as regions with the FLUVSIM simulator. The input data are the parameters of the channels geometry (see Table 6-1) and the vertical proportion distribution of channels and shales.

Table 6-1. Channel parameters estimated for the FLUVSIM channel distribution for each member.

Channel Proportion (%)	**Min**	**Mode**	**Max**
B1	50.00%	60.00%	70.00%
B2	6.00%	10.39%	18.00%
Maximum Channel (number of channel facies)			
B1	2450		
B2	100		
Orientation (deg)	**Min**	**Mode**	**Max**
B1	-25	-45	-65
B2	-25	-45	-65
Sinuosity Average departure (m)	**Min**	**Mode**	**Max**
B1	30	125	1500
B2	250	1250	2864
Sinuosity length scale (m)	**Min**	**Mode**	**Max**
B1	100	500	5000
B2	100	500	5000
Thickness (m)	**Min**	**Mode**	**Max**
B1	1.00	5.00	16.00
B2	0.52	2.86	10.29
Thickness undulation (m)	**Min**	**Mode**	**Max**
B1	0.50	2.00	7.00
B2	0.52	3.89	7.26
Thickness undulation length scale (m)	**Min**	**Mode**	**Max**
B1	13.00	1000.00	3000.00
B2	100.00	500.00	5000.00
Width Thickness Ratio	**Min**	**Mode**	**Max**
B1	50.00	200.00	400.00
B2	70.21	155.13	352.05
Width	**Min**	**Mode**	**Max**
B1	-1.00	-1.00	-1.00
B2	7.29	100.21	724.19
Width Undulation	**Min**	**Mode**	**Max**
B1	1.00	1.00	1.00
B2	7.30	20.00	100.00
Width Undulation length Scale	**Min**	**Mode**	**Max**
B1	250.00	400.00	450.00

B2	7.30	20.00	100.00
Vertical Channel Overlap			
B1		0.40	
B2		0.28	

The channel parameters were inferred from the examples of fluvial systems in literature (Gibling, 2006; Rhoads, B., 2020)

At the same time, the porosity for the channels was populated following the respective porosity distribution curve and variogram. The second step consisted in populating the porosity throughout the shale facies using the Sequential Gaussian Simulation (SGS) with the appropriate distribution curve and variogram. This workaround was chosen because the FLUVSIM workflow only allows the population of the porosity in the regions defined as channels. Figure 6-32 and Figure 6-33 show some screenshots with the steps followed and specified parameters. Figure 6-34 shows the panel ready for starting the simulation. Notice the two separate processes for facies and porosity which must be run once for each seed number.

A drawback of this method is that, at least with the version of the software and the license used, several iterations cannot be done for creating multiple scenarios for uncertainty evaluation. This issue is discussed in the next section.

A few simulations were run and the distributions of the porosity in the resulting scenarios were compared with the input distributions. The simulated porosity distribution in the geological grid model depends on the combination of four constraints, namely, the distribution curves of the porosity, the variograms, the vertical proportion of the facies and the channels parameters. The latter have high influence in the results. For this reason and, given the high uncertainty in the estimation of such values, several simulations were run for comparing the distribution curve of the simulated porosity with the initial one. The channel parameters of the FLUVSIM simulation workflow were changed in every iteration until the resulting porosity distribution matched the input distribution. (Figure 6-35). The parameters which finally allowed to accomplish this requirement are show in Table 6-1.

6.3.3 Uncertainties study

The uncertainty study was twofold. First, the structural uncertainty was assessed to estimate the variation of the volume of the storage formation in the structural model. Once the grid model was built and the petrophysical properties were populated, the properties uncertainty was assessed to evaluate the variation in the porous volume for different scenarios.

6.3.3.1 Structural uncertainty

Prior to the construction of the structural model, two main issues were detected. On one hand, the low resolution of the seismic data used could lead to misinterpretation of the horizons. On the other hand, the time to depth conversion of the seismic profiles also implies uncertainty, derived from the method used. Therefore, an uncertainty analysis was carried out, in order to assess how much a variation in depth of the interpreted horizons and faults could influence the volume of the storage formation and the shape of the geological structure. The structural uncertainty was calculated with the Aspen SKUA Uncertainty Workflow. It was considered a variation in depth of 100m for the Buntsandstein top and bottom horizons. This figure was estimated to be the average vertical distance between reflectors. Given that two intermediate divisions of this formation were established

The PilotSTRATEGY project has received funding from the European Union's Horizon 2020 research and innovation programme under grant agreement No. 101022664

(delimiting the B1, B2 and B3 facies), these additional horizons were left to follow the accommodation according with the change in depth of the main horizons. The rest of the horizons of the series were not conditioned.

All the faults were assigned a possible variation of 75m on both sides, perpendicular to the fault planes. This is a default distance used by the software. It was considered adequate after measuring the width of the zones where the discontinuities of the reflectors allowed to infer the faults.

A total of 1000 iterations were run, for which 1000 equiprobable models were created. Only the variation in volume for the B1 and B2 facies were considered. The statistical results show a variation in volume between 41,990 Mm^3 and 45,410 Mm^3 in comparison with a volume of 44,130 Mm^3 for the base case. See statistical results in Table 6-2 and graphic output in Figure 6-36.

The variation in volume of the simulated scenarios with respect to the base case ranges from -4.71% to 2.90% for the whole storage formation. By regions, it ranges from -4.04% to 2.19% for the B1 member and from -6.23% to 4.50% for the B2 member (Table 6-2).

When compared with the median value, the difference is -1.1% for the whole storage formation and -1.1% and -1.2 for the B1 and B2 member respectively.

Table 6-2. Statistical results for the structural uncertainty for 1000 realisations (base case, maximum and minimum, mean volume, and standard deviation values) and differences with respect to the base case. Gross Rock Volume in m3.

	Base case	**Min**	**Max**	**Mean**	**Std. Dev.**	**Min. Diff.**		**Max. Diff.**		**Median Diff.**	
B1+B2	4.41 10^{10}	4.20 10^{10}	4.54 10^{10}	4.37 10^{10}	5.12 10^{8}	-2.14 10^{9}	-4.71%	1.28 10^{9}	2.90%	-4.90 10^{8}	-1.11%
B1	2.88 10^{10}	2.76 10^{10}	2.94 10^{10}	2.85 10^{10}	2.71 10^{8}	-1.19 10^{9}	-4.04%	6.30 10^{8}	2.19%	-3.20 10^{8}	-1.11%
B2	1.54 10^{10}	1.44 10^{10}	1.60 10^{10}	1.52 10^{10}	2.48 10^{8}	-1.00 10^{9}	-6.23%	6.90 10^{8}	4.50%	-1.80 10^{8}	-1.17%

An example of the variation in depth for some of the realisations can be seen in Figure 6-5.

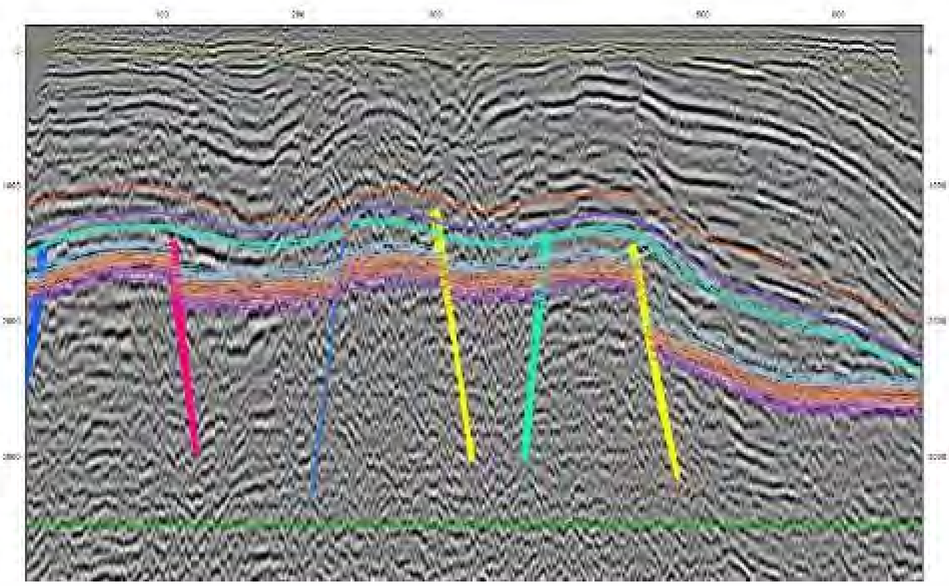

Figure 6-5: Cross-section showing several realisations with changes in depth of the horizons.

The PilotSTRATEGY project has received funding from the European Union's Horizon 2020 research and innovation programme under grant agreement No. 101022664

Different realisations produce different geometry of the trapping structure. Figure 6-37 shows some examples. Figure 6-38 shows the cumulative standard deviation of the gross rock volume for all the realizations.

For the next step, the building of the geological grid holding the petrophysical properties, only the geological structure of the base case is used.

6.3.3.2 Properties uncertainty

For the estimation of the properties uncertainty, the Aspen SKUA Reservoir Properties Workflow has been used. The purpose of this task is to generate several models with random channel geometries and porosity distributions constrained with channel parameters and distribution curves. The entry data have been the geological grid with the regions, the porosity, and the relationships between the porosity and the shale volume and the permeability. As mentioned before, the series of simulations have not been run in a single step but two: one step for the channel porosity and another step for the shale porosity. To repeat the simulation several times and consider random variability, the simulations have been run by mean of a macro, changing the seed parameter in each repetition. Therefore, a list of randomly generated seed number was supplied in an external text file with 1,000 random values (Figure 6-39).

This macro calls the previously created workflow and computes the statistics of the calculated porosity for the B1 and B2 regions in each loop.

Among all the statistical parameters, the porosity volume of the two members (B1 and B2) was chosen to compare the scenarios. Three scenarios were chosen from the percentiles P10, P50 and P90. Therefore, three different grid models were populated with the porosity property of each scenario. The chosen scenarios and their respective pore volumes and seed number are in Table 6-3. Figure 6-40 shows the cumulative standard deviation of the total porosity volume for all the realizations for the regions B1+B2.

Table 6-3. Summary of the total pore volume for the three final scenarios selected and seed number of their corresponding realization.

	Scenario P10	Scenario P50	Scenario P90
Total pore volume (Mm3)	2649.77	2811.46	2973.61
Seed number	628	360	451

The porosity values of the formation for the three scenarios are shown in the following tables (6-4 to 6-7).

Table 6-4. Statistics of the total porosity volume values of the Buntsandstein Fm. for each scenario (B1 and B2 members)

Statistic	Scenario P10	Scenario P50	Scenario P90
P10	0.00%	0.00%	0.00%
P50	6.38%	7.09%	8.03%
P90	12.80%	13.15%	13.35%
maximum	18.65%	18.65%	18.65%
mean	5.89%	6.24%	6.60%
minimum	0.00%	0.00%	0.00%

The PilotSTRATEGY project has received funding from the European Union's Horizon 2020 research and innovation programme under grant agreement No. 101022664

std_dev	0.0516	0.0525	0.0535

Table 6-5: Porosity statistical values for the Buntsandstein Fm. for its member B1

Statistic	Scenario P10	Scenario P50	Scenario P90
P10	0.02%	0.03%	1.54%
P50	8.45%	9.10%	9.77%
P90	13.54%	13.83%	14.04%
Maximum	18.65%	18.65%	18.65%
Mean	8.00%	8.49%	9.14%
Minimum	0.00%	0.00%	0.00%
std_dev	0.0457	0.0449	0.0430

Table 6-6: Porosity statistical values for the Buntsandstein Fm. for its member B2

Statistic	Scenario P10	Scenario P50	Scenario P90
P10	0.00%	0.00%	0.00%
P50	0.04%	0.04%	0.04%
P90	9.25%	9.40%	9.24%
Maximum	15.21%	15.21%	15.21%
Mean	1.98%	2.09%	1.90%
Minimum	0.00%	0.00%	0.00%
std_dev	0.0370	0.0382	0.0368

Table 6-7: Porosity statistical values only for channels for the B1 and B2 members

Region	Statistic	Scenario P10	Scenario P50	Scenario P90
B1 and B2	P10	8.653%	8.649%	8.652%
	P50	10.740%	10.742%	10.770%
	P90	14.516%	14.510%	14.530%
	maximum	18.654%	18.654%	18.654%
	Mean	11.246%	11.246%	11.292%
	minimum	8.006%	8.006%	8.006%
	std_dev	0.023	0.023	0.023
B1	P10	8.713%	8.716%	8.711%
	P50	10.968%	11.017%	10.975%
	P90	14.744%	14.744%	14.744%
	maximum	18.654%	18.654%	18.654%
	Mean	11.458%	11.469%	11.463%
	minimum	8.006%	8.006%	8.006%
	std_dev	0.023	0.023	0.023
B2	P10	8.352%	8.312%	8.320%
	P50	9.662%	9.610%	9.653%

	P90	11.310%	11.246%	11.397%
	maximum	15.212%	15.212%	15.212%
	Mean	9.876%	9.826%	9.882%
	minimum	8.041%	8.041%	8.041%
	std_dev	0.014	0.014	0.014

Finally, the porosity values of these scenarios for each region were calculated, *i.e.,* three porosity properties were created, one for each resulting scenario (Poro_10, Poro_50 and Poro_90) and calculated to the porosity values corresponding to the realization of the percentile. For the B3 region (primary seal) a value of 0% was assigned. The facies property was calculated to the facies values for the corresponding run by region (Facies_10, Facies_50, Facies_90). In Figure 6-41 there are screen captures of the facies distribution for regions B1 and B2 at different sampled grid levels.

The rest of the properties, *i.e.*, permeability and shale volume (Vsh), have been considered dependent of the porosity. The correlation between these properties, were estimated from the well and laboratory data (see 6.2.3 and 0 sections). For their calculation, simple scripts with the corresponding equations were applied. In Figure 6-6 and Figure 6-7 are screen captures and statistics graphs for the porosity, permeability and shale volume properties of the final model.

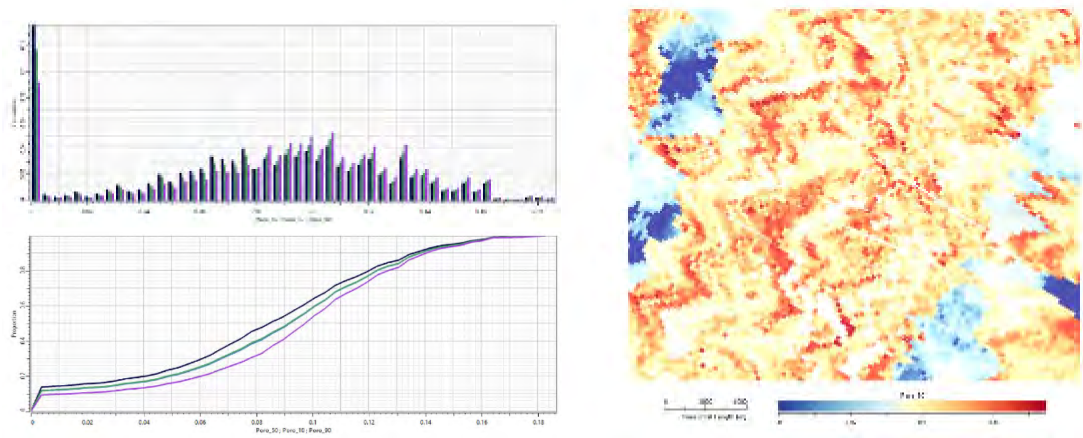

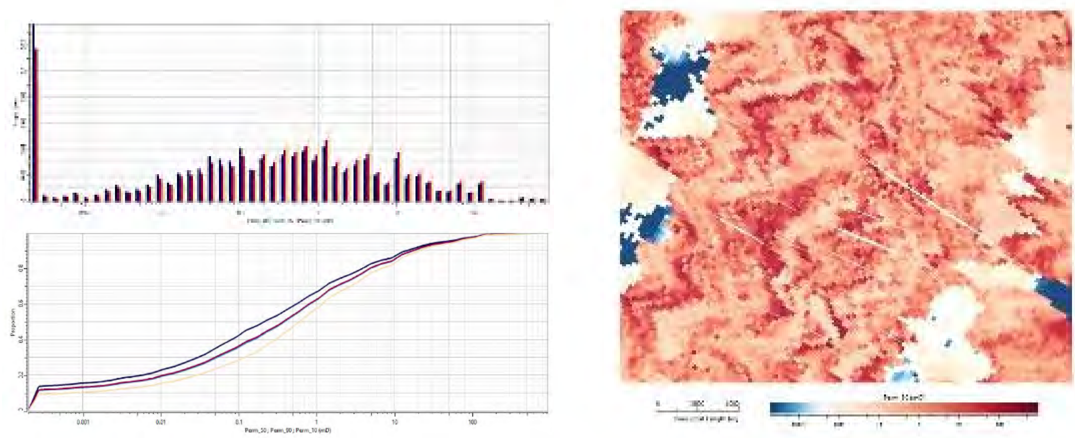

The PilotSTRATEGY project has received funding from the European Union's Horizon 2020 research and innovation programme under grant agreement No. 101022664

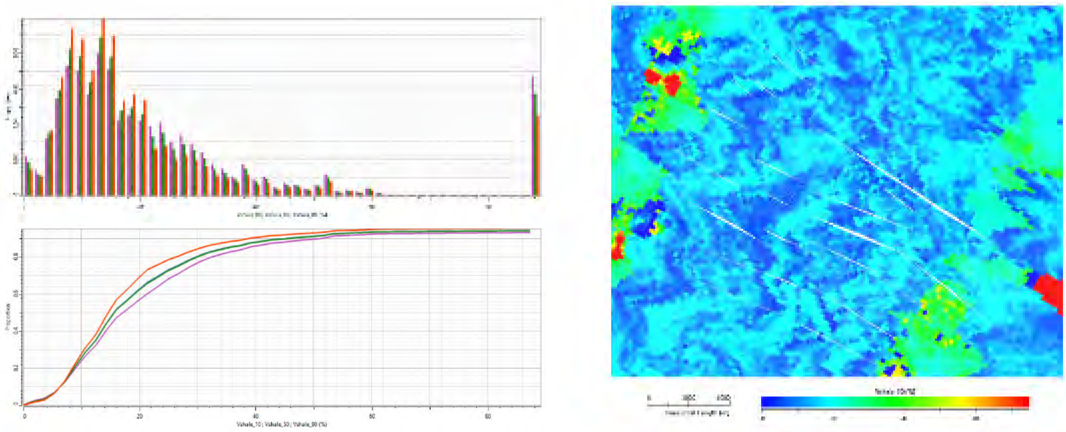

Figure 6-6: Examples of the porosity (top), permeability (middle) and sale volume (bottom) distributions of the P50 scenario for region B1 (right column) and histograms and cumulative curves (left column) for the P10, P50 and P90 scenarios.

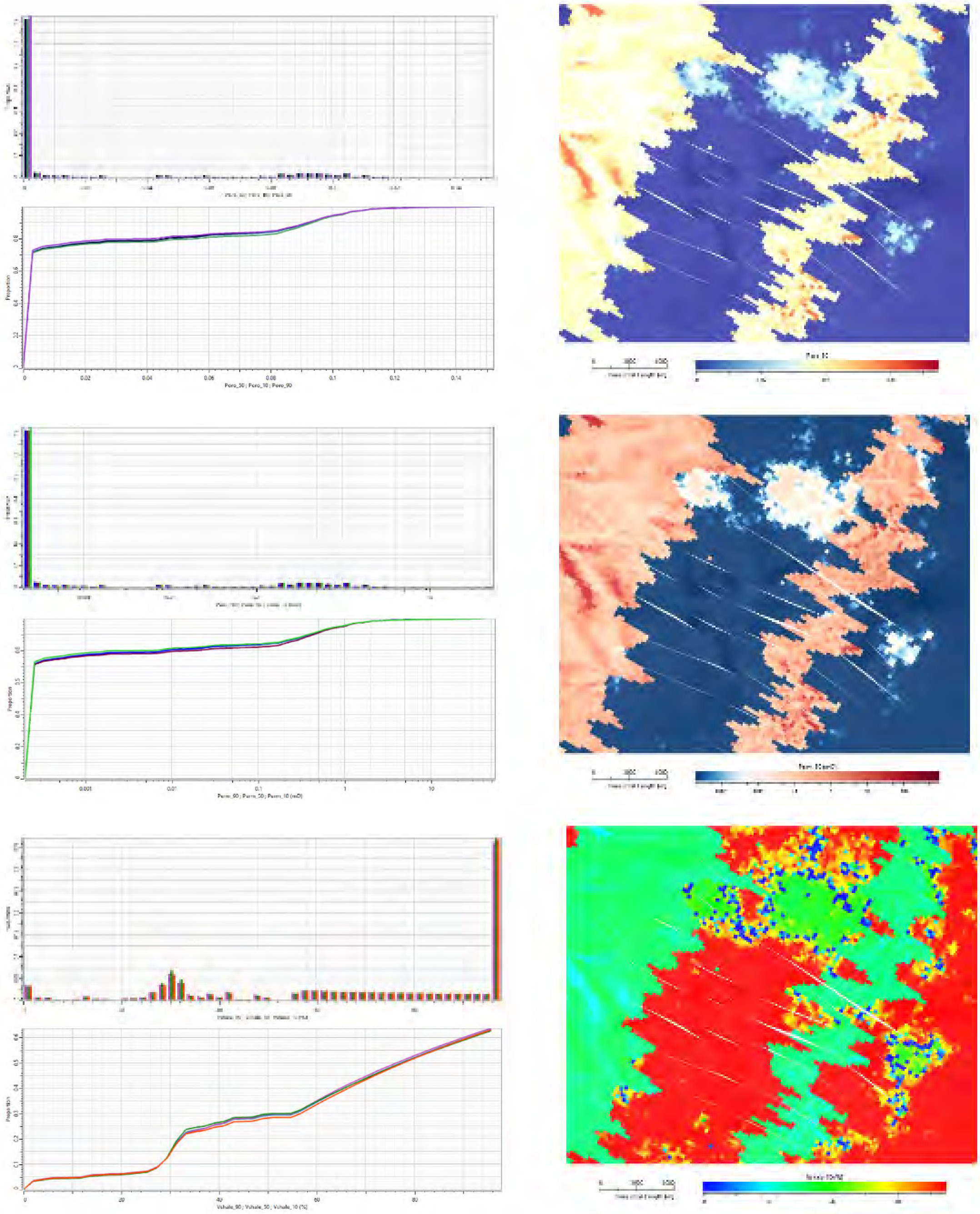

Figure 6-7: Examples of the porosity (top), permeability (middle) and sale volume (bottom) distributions of the P50 scenario for region B2 (right column) and histograms and cumulative curves (left column) for the P10, P50 and P90 scenarios.

6.3.3.3 Fault-seal analysis

The fault-seal analysis implied the creation of gridded faults and the computing of the juxtaposition and shale gouge ratio (SGR), by means of calculations involving fault geometries and petrophysical properties in the vicinity of the faults. All the faults present in the model were included. The resolution of the gridded fault surfaces was set 100m in the horizontal and 2m in the vertical direction, in order to approximately keep the same resolution of the geological grid model. The clay volume was read from the shale volume property and the maximum smear distance was supposed to be zero.

The outcome is a series of properties that will be used in the dynamic model: SGR, Vshale_minus, Vshale_plus and facies juxtaposition. In Figure 6-8Figure 6-7 three screen shots are shown with examples of the resulting properties.

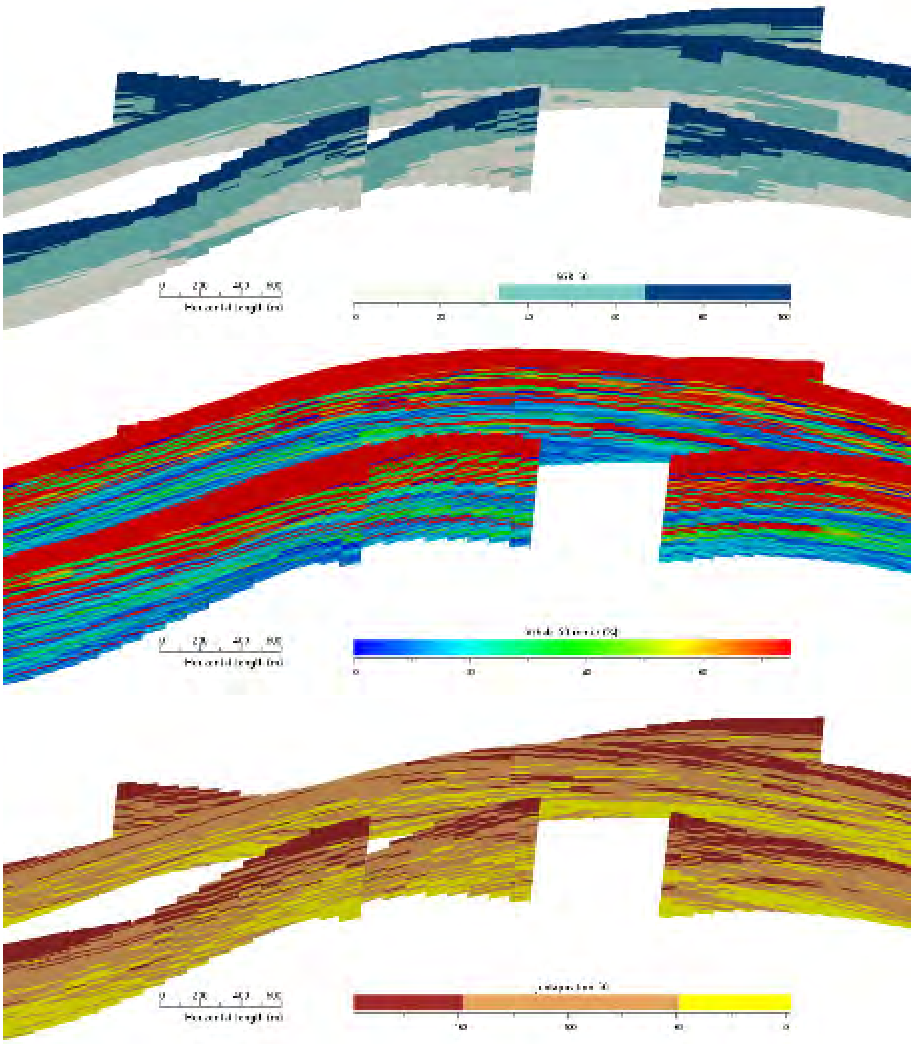

Figure 6-8: Examples of the Shale Gouge Ratio (SGR) (top), Shale Volume (Vsh) (middle) and juxtaposition (bottom) in some selected faults for the, P50 scenario.

These properties are used for evaluating the sealing potential of the faults. The result is a set of transmissibility multipliers in the flow simulation grid which can be exported to external flow simulators.

6.4 Modelling challenges

During the development of the model, two main challenges had to be faced, related with the scarcity of source data.

In the interpretation phase the main issue was the poor resolution of the seismic data and the lack of wells in the area which could have been used for correlating the horizons. This was overcome by extending the area of study to include the Lopin-1 well, located to the south, and the seismic lines

The PilotSTRATEGY project has received funding from the European Union's Horizon 2020 research and innovation programme under grant agreement No. 101022664

near it. The knowledge of the conceptual model and the regional geology, helped to interpret the geological structure and stratigraphy of the site.

The scarcity of data also made the characterisation of the facies a difficult task. From the study of the outcrops and other wellbores, two members with different facies sequences could be determined. In order to reproduce the variability in the rock properties, both horizontal and vertical, a statistical analysis of the porosity from cores, well logs and laboratory analysis was carried out. Given that no actual distribution of the facies in the site could be known, the goal was to obtain a model which reproduces the same spatial variability of the rock properties as seen in the statistical analysis. This way several equiprobable scenarios were obtained, from which three were chosen as representative of the most to least favourable in terms of capacity.

6.5 Recommendations

For future development of the proposed storage site in the Lopin area, we consider several important tasks to be accomplished.

Deploy a 3D seismic survey covering the whole area in order to obtain a seismic cube. Due to the scarcity of geophysical data in the site, this is considered as the main source of information for getting reliable information of the underground. It is necessary to remark that the presence of thick evaporitic layers could represent an important issue to consider.

Drill at least one well for characterising the stratigraphic series and take enough core samples for petrophysical analysis.

The study of the formations in the overburden is also advisable in order to include other suitable storage formations and characterize secondary seals.

6.6 Conclusions

The present static model has been built using data from former exploration campaigns in the area, mainly seismic sections and legacy well data (including one reservoir core). In addition to them, new set of data have been acquired: Gravimetric survey, passive seismic surveys, field analogues analysis/sampling, photogrammetry surveys of those outcrops.

The result was a model with 1,467,840 cells with a distribution of 132x139x80 cells, 70 only for the storage formation and the rest for the overburden and underburden. See Figure 6 11 and Figure 6 12.

The geological concept of the area was reported in previous reports (Deliverable 2.7) and this model tries to include those concepts. The reservoir (Buntsandstein) sedimentology has been described as fluvial system with wide braided channels and floodplain deposits.

The reservoir formation (Buntsandstein) is divided in this report into three parts, from bottom to top: B1, B2 and B3. B3 corresponds to argillaceous impermeable facies and it is considered the primary seal in this formation. B1 and B2 shows two different facies, the channel related facies (above 8% of porosity) and the floodplain facies (porosity below 8%).

To sum up, Tables 6-8 and 6-9 show the main numbers of the model.

The PilotSTRATEGY project has received funding from the European Union's Horizon 2020 research and innovation programme under grant agreement No. 101022664

Table 6-8: Gross Rock Volume in Mm3. (P90= pessimistic case / P10= optimistic case)

	Base case	P90	P50	P10	Std. Dev.
B1+B2	44,130	43,010	43,640	44,310	511.8
6.7 B1	28,790	28,120	28,470	28,830	270.8
B2	15,350	14,860	15,170	15,490	248.3

Table 6-9: Summary of the porosity, net go gross and total volume of the channel facies for the two members of the storage formation for the P50 scenario. (*) NtG: cumulated thickness of channel facies over total thickness

Channels	**Φ B1**	**Φ B2**	**NtG B1(*)**	**NtG B2 (*)**	**Vol B1 (Mm³)**	**Vol B2 (Mm³)**
Maximum	18.65%	15.21%	100.00%	63.51%	29,420	16,040
Mean	11.47%	9.83%	60.60%	14.88%	28,470	15,180
6.8 Minimum	8.01%	8.04%	0.00%	0.00%	27,600	14,350
P90	8.72%	8.31%	45.93%	5.01%	28,120	14,860
P50	11.02%	9.61%	59.72%	14.93%	28,470	15,170
P10	14.74%	11.76%	75.66%	25.07%	28,830	15,490
Std. Dev.	2.3%	1.4%	11.4%	7.9%	270.8	248.3

Considering only the NE structure of the ZOI, a likely site for the pilot injection has been estimated (Figure 6-9).

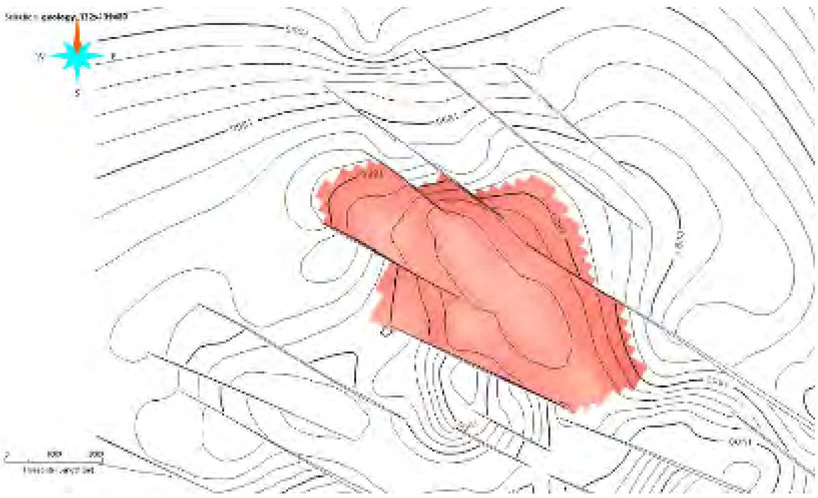

Figure 6-9: Likely site for the pilot injection. The top of the B2 member is shown. Closure isobath is about 1,650 mbsl.

The PilotSTRATEGY project has received funding from the European Union's Horizon 2020 research and innovation programme under grant agreement No. 101022664

Table 6-10: Gross volume and total pore volume in channel facies for B1 and B2 members for the P50 scenario in the pilot site (see Figure 6-9).

	Vol (Mm^3)	Vol x Φ P50 x NtG
B1	945	62.4
B2	693	9.99
Total	1,640	72.4

6.9 References

Arche, A., Gómez, J. L., Marzo, M., & Vargas, H., (2004). *The siliciclastic Permian-Triassic deposits in Central and northeastern Iberian Peninsula (Iberian, Ebro and Catalan basins): a proposal for correlation*. Geologica Acta, 305-305.

Gibling, M. R.(2006), *Width and thickness of fluvial channel bodies and valley fills in the geological record: a literature compilation and classification*; Journal of Sedimentary Research, v. 76, 731–770

Rhoads, B. (2020). Channel Planform – Controls on Development and Change. In *River Dynamics: Geomorphology to Support Management* (pp. 186-196). Cambridge: Cambridge University Press. doi:10.1017/9781108164108.008

Wilkinson, M. (2023). Deliverable 2.7 – Conceptual Geological Models of the Portugal, Spain and France. PilotSTRATEGY project, Grant Agreement: 101022664

Young-Seog Kim, David J. Sanderson (2005) *The relationship between displacement and length of faults: a review*, Earth-Science Reviews, Volume 68, Issues 3–4,2005, Pages 317-334,ISSN 0012-8252. doi.org/10.1016/j.earscirev.2004.06.003.

6.10 Acknowledgments

We appreciate the help provided by Aspen and its support team, who kindly have guided us in using the Aspen SKUA software tools to successfully complete this modelling task.

7 Appendix

7.1 Additional information, figures and tables for Paris Basin, French region (3)

The Aspen SKUA project (version 2022) was created with the following project settings:

- Projection RGF93 / Lambert-93
- Datum: Mean Sea level
- Area Units: Meters
- Depth Unit: Meters
- Time Unit: milliseconds
- Depth Axis Positive Values: Downward
- Preferred Z-axis: Depth

	BIS-1	BRM-1	CHM-3	CHN-1	CLF-1	ETC-1	IVY-1D	LSB-1	NSL-1	RAC-3	SVY-1	VIX-1
Top_Cenomanian	714	608.121	628	771.837	703	611.161	707.109	727.509	739.521	686	618.84	744.296
Top_Alb. Clay	787	707.05	710	851.926	801	702.415	811.15	786.408	835.755	779	678.575	846.544
Top_Alb. Sand	829	750.332	752	903.129	843	739.257	869.173	836.825	884.59	824	717.109	900.731
Top_Albo-Aptian	880	791.68	798	951.678	892	782.27	909.189	886.299	926.244	878	801.897	945.924
Top_Barremian	978	888	890	1058.03	987	879.134	1029.24	995.047	1026.27	962	873.955	1049.98
Top_Purbeckian	1138	1063	1059	1220.12	1152	1052.93	1246.34	1147.10	1196.72	1127	1027.15	1215.62
Top_Portlandian	1175	1105.80	1093	1262.67	1186	1087.25	1285.36	1186.12	1239.01	1162	1052.84	1253.40
Top_Kimmeridgian	1302	1249.47	1226	1388.09	1314	1227.74	1444.44	1304.85	1361.10	1296	1180.32	1379.30
Top_Oxfordian_Sup	1463	1433.62	1404	1547.25	1480.5	1406.12	1642.51	1457.66	1511.91	1469	1348.87	1530.55
Top_Oxfordian-Inf	1719	1725.51	1683	1798.83	1741	1693.69	1945.61	1701.59	1760.29	1741	1608.82	1776.26
Top_Marnes_Massigny	1802	1790	1753	1873	1820	1763	2028	1781	1832	1811	1682	1850
Top_Callovian-Upper	1817	1804.13		1891.98	1833.5	1772.30	2040.63	1797.08	1841.62	1822	1694.11	1867.46
Top_Callovian-Low	1846				1859		2070.64			1848		
Ca26	1841	1818.23	1783	1918	1853.04	1791	2068.44	1819	1873.03	1842.67	1721	1891.88
Ca24	1850	1829.75	1802	1930	1872.41	1806.66	2082.09	1832	1885	1858.53	1734	1909
SBComb	1877	1849.89	1842	1961	1888.22	1840	2105.96	1845	1911	1877.42	1756	1927
Bt10	1979.13	1988.08	1952	2059.21	2009.43	1967.49	2237.82	1960	1996.06	2005.52	1867.76	2024.88
Bj1	2046	2049.35	2013	2151	2075	2042.95	2314.19	2014	2069	2082.95	1918.14	2103
Top_Aalenian	2078	2088.81	2050	2175.10	2111	2072.70	2359.74	2042.93	2079.16	2117	1966.61	2131.77
Top_Toarcian	2091	2109.59	2068	2187.57	2119	2092.54	2377.74	2063.88	2098.00	2136	1984.55	2142.72
Top_Lias-Middle	2181	2237.20	2187	2287	2229	2218.31	2485.76	2114.86	2175.75	2254	2056.60	2221.66
Top_Rhetian	2368	2408	2357	2475.83	2423	2417.44		2260.93		2458	2218.52	2408.02

Table 3.20 Markers for all stratigraphic intervals in the static model (in MD).

The PilotSTRATEGY project has received funding from the European Union's Horizon 2020 research and innovation programme under grant agreement No. 101022664

	BIS-1	BRM-1	CHM-3	CHN-1	CLF-1	ETC-1	IVY-1D	LSB-1	NSL-1	RAC-3	SVY-1	VIX-1	average thickness	average thickness seismic area
Top_Cenomanian	73	98.929	82	80.089	98	91.254	104.041	58.899	96.234	93	59.735	102.248	86.45241667	92.01025
Top_Alb. Clay	42	43.282	42	51.203	42	36.842	58.023	50.417	48.835	45	38.534	54.187	46.02691667	46.75575
Top_Alb. Sand	51	41.348	46	48.549	49	43.013	40.016	49.474	41.654	54	84.788	45.193	49.50291667	48.504
Top_Albo-Aptian	98	96.32	92	106.353	95	96.864	120.052	108.748	100.034	84	72.058	104.062	97.79091667	99.263
Top_Barremian	160	175	169	162.097	165	173.804	217.105	152.059	170.446	165	153.197	165.634	169.0285	176.77625
Top_Purbeckian	37	42.804	34	42.542	34	34.317	39.02	39.014	42.291	35	25.692	37.784	36.95533333	36.255
Top_Portlandian	127	143.672	133	125.423	128	140.494	159.074	118.737	122.088	134	127.479	125.904	132.0725833	137.0185
Top_Kimmeridgian	161	184.144	178	159.163	166.5	178.378	198.076	152.806	150.814	173	168.553	151.245	168.47325	174.644
Top_Oxfordian_Sup	256	291.897	279	251.581	260.5	287.567	303.096	243.934	248.379	272	259.953	245.709	266.6346667	272.899
Top_Oxfordian-Inf	98	78.62		93.15	92.5	78.611	95.025	95.492	81.326	81	85.282	91.198	88.20036364	91.63125
Top_Marnes_Massigny	39	28.239	30	45	33.04	28	40.449	38	41.035	31.676	39	41.883	36.27683333	36.04125
Top_Callovian-Upper														0
Top_Callovian-Low														0
Ca26	9	11.512	19	12	19.37	15.667	13.644	13	11.965	15.863	13	17.117	14.2615	14.46925
Ca24	27	20.145	40	31	15.81	33.333	23.876	13	26	18.885	22	18	24.08741667	21.39275
SBComb	102.13	138.187	110	98.219	121.21	127.496	131.855	115	85.067	128.097	111.767	97.888	113.9096667	120.823
Bt10	66.87	61.268	61	91.781	65.57	75.455	76.367	54	72.933	77.429	50.38	78.112	69.26375	71.559
Bj1	32	39.46	37	24.107	36	29.757	45.549	28.933	10.161	34.05	48.467	28.771	32.85458333	36.89975
Top_Aalenian	13	20.785	18	12.469	8	19.838	18.006	20.953	18.848	19	17.942	10.953	16.48283333	14.5015
Top_Toarcian	90	127.608	119	99.424	110	125.768	108.018	50.98	77.745	118	72.047	78.942	98.12766667	106.5045
Top_Lias-Middle	187	170.796	170	188.83	194	199.131		146.069		204	161.921	186.361	180.8108	146.25
Top_Rhetian														

Table 3.21 Calculated thickness in stratigraphic intervals based on marker information.

The PilotSTRATEGY project has received funding from the European Union's Horizon 2020 research and innovation programme under grant agreement No. 101022664

	BIS-1_path	BRM-1	CHM-3	CHM-4	CHN-1	CLF-1	ETC-1	IVY 1D	LSB-1	NSL-1	RAC 3	SVY-1	VIX-1
DRHO	y	Y	y	n	y	y	y	y	y	n	y	y	y
DT	y	y	y	y	y	y	y	y	y	y	y	y	y
Electro Facies Nphi Rhob	y	y	y	n	y	y	y	y	n	y	y	y	y
Facies Pilot Strategy	n	y	n	n	y	n	y	n	y	y	n	y	y
GR	y	y	y	y	y	y	y	y	y	y	y	y	y
NPHI	y	y	y	y	y	y	y	y	n	y	y	y	y
PEF	n	y	y	y	y	y	y	n	y	n	n	y	y
PHIE	n	y	n	n	y	n	n	n	y	y	y	y	n
RHOB	y	y	y	y	y	y	y	y	y	y	n	y	y
RM	n	y	y	n	y	y	y	y	y	y	y	y	y
RT	n	y	y	n	y	y	y	y	y	y	n	y	y
RXO	n	n	y	n	y	y	n	n	n	n	n	y	n
SP	y	y	y	y	y	y	y	y	y	y	y	y	n
BS	y	n	y	n	n	y	n	y	n	n	y	n	n
CALI	y	n	y	y	n	y	n	y	n	n	y	n	n
ILD	y	n	n	y	n	n	n	n	n	n	n	n	n
ILM	y	n	n	y	n	n	n	n	n	n	n	n	n
THOR	n	n	n	n	n	y	n	n	n	n	n	n	n
URAN	n	n	n	n	n	y	n	n	n	n	n	n	n

Table 3.22 Compilation of available data for each well in the model area in the reservoir interval Ca26 to top Bj10.

DRHO = Bulk Density Correction [kg/m3]
DT = Delta T Sonic Transit Time [us/ft]
Electro Facies Nphi Rhob = some kind of facies
Facies Pilot Strategy = another facies log from 0 to 10
GR = Gamma Ray [gAPI]
NPHI = Thermal Neutron Porosity [m3/m3] ?
PEF [%] ? = photoelectric adsorption
PHIE = Effective Porosity [m3/m3] ?
RHOB = bulk density[.g/cm3]
RM = Medium Resistivity [.ohm.m];
RT = Deep Resistivity [.ohm.m];
RXO = Micro Resistivity [.ohm.m];?
SP = spontaneous potential [mV]
BS = Bit Size [IN]
CALI = Caliper [IN]
ILD = Deep Induction Standard Processed Resistivity [OHMM]
ILM = Medium Induction Standard Processed Resistivity [OHMM]
THOR = Thorium [PPM]
URAN = Uranium [PPM]

The PilotSTRATEGY project has received funding from the European Union's Horizon 2020 research and innovation programme under grant agreement No. 101022664

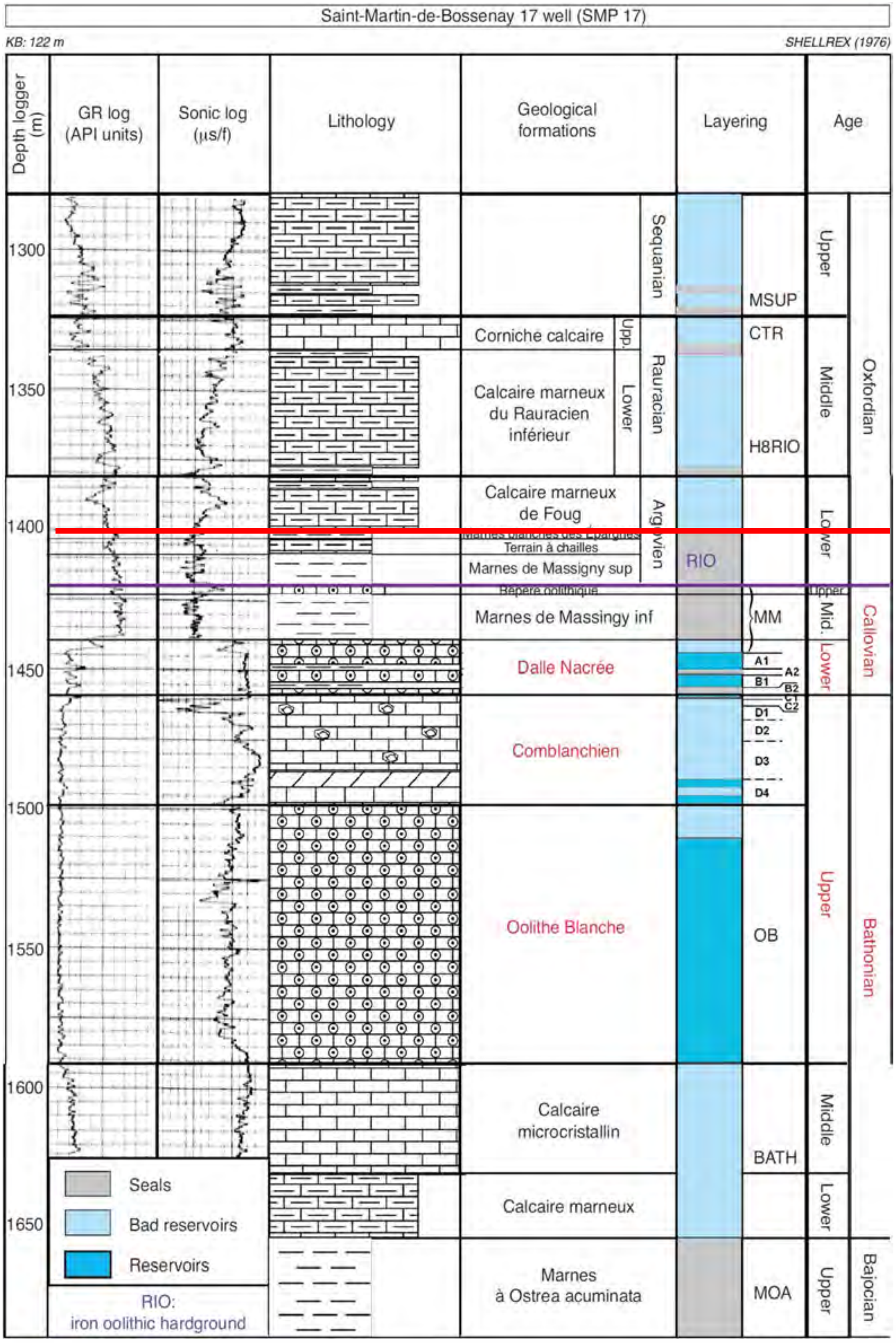

Figure 3.58 Formation interpretation in the well SMB-17. In red the interpretation of the top Marnes de Massingy. Modified from Delmas et al. 2012.

The PilotSTRATEGY project has received funding from the European Union's Horizon 2020 research and innovation programme under grant agreement No. 101022664

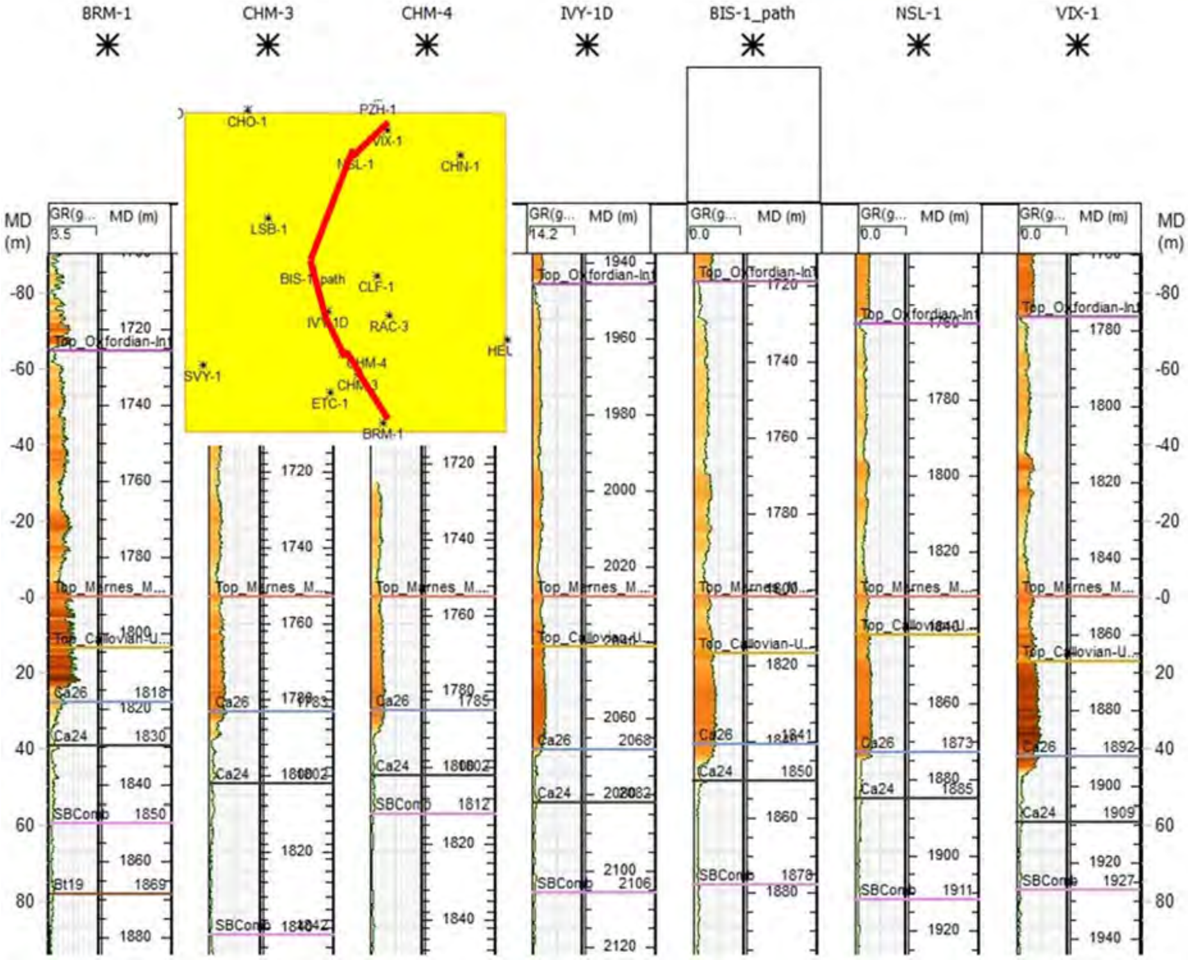

Figure 3.11 Interpretation result of the top Marnes de Massingy in North South direction.

The PilotSTRATEGY project has received funding from the European Union's Horizon 2020 research and innovation programme under grant agreement No. 101022664

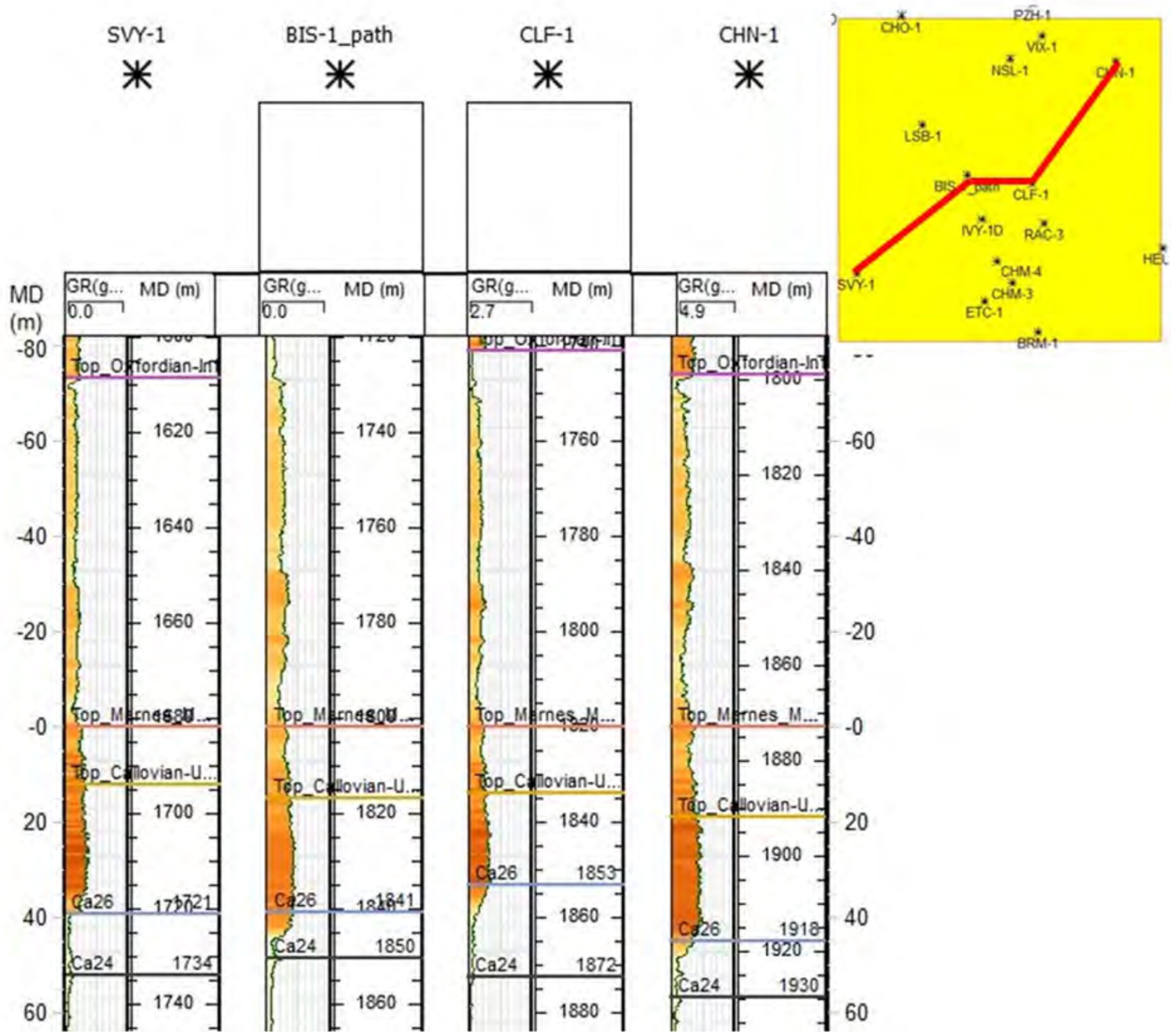

Figure 3.12 Interpretation result of the top Marnes de Massingy in East West direction.

The PilotSTRATEGY project has received funding from the European Union's Horizon 2020 research and innovation programme under grant agreement No. 101022664

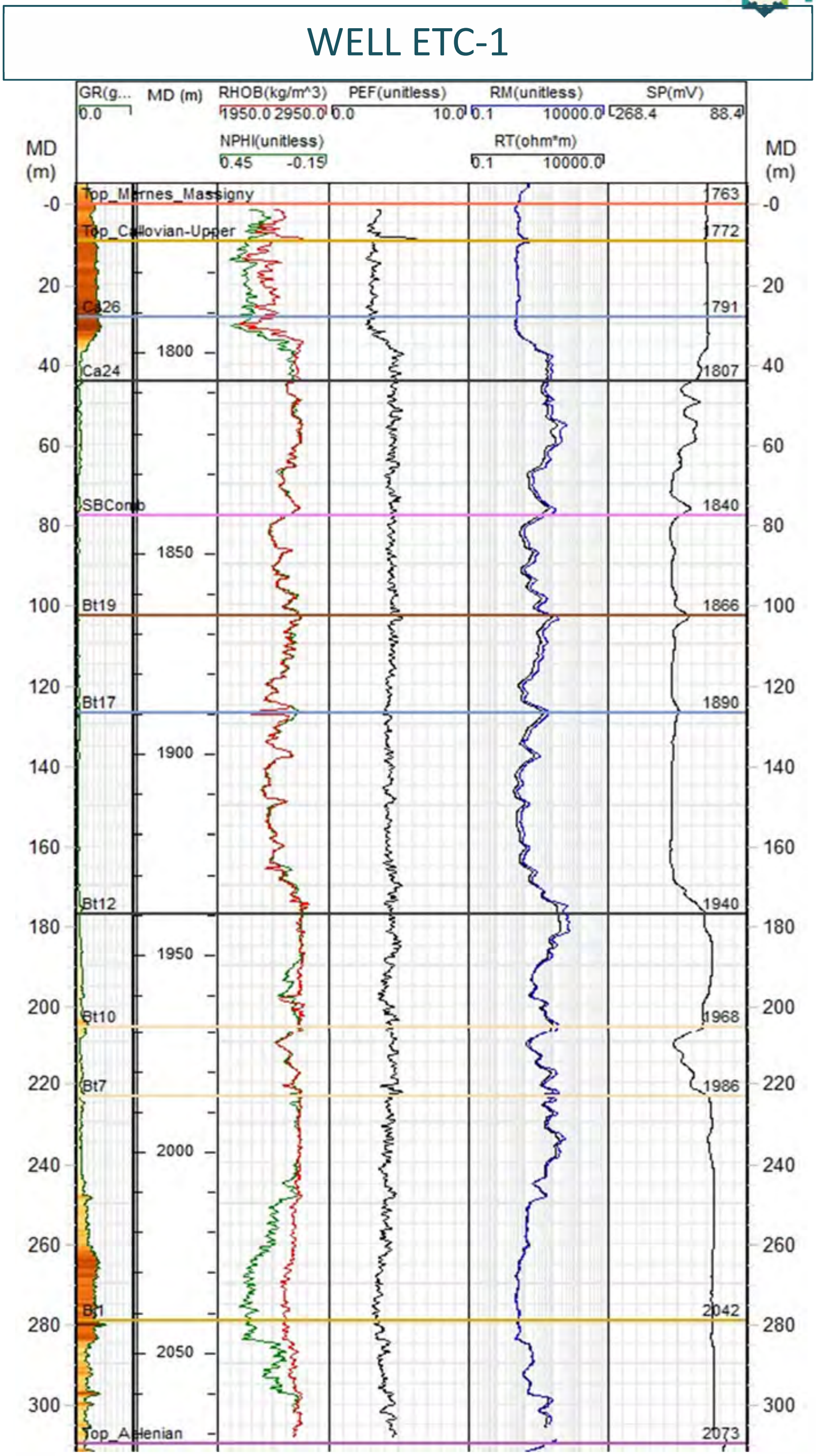

Figure 3.13 Petrophysical log set used for interpretation, example well ETC-1.

The PilotSTRATEGY project has received funding from the European Union's Horizon 2020 research and innovation programme under grant agreement No. 101022664

Well	GR max shale [API]	GR min shale [API]
ETC-1	140	10
CLF-1	120	20
IVY-1D	140	20
LSB-1	120	15
BIS-1	130	15
RAC-3	130	15
NSL-1	110	20
VIX-1	145	15
CHN-1	125	15
SVY-1	140	15
BRM-1	150	15
CHM-3	140	15
CHM-4	120	15
MLN-1	110	15

Table 3.23 GR values used to calculate the Vshale property

Well	NPHI max shale	Vshale cutoff
ETC-1	0,38	0,5
CLF-1	0,38	0,5
IVY-1D	0,40	0,5
LSB-1	No NPHI log	
BIS-1	0,38	0,5
RAC-3	0,38	0,4
NSL-1	0,38	0,5
VIX-1	0,35	0,5
CHN-1	0,38	0,4
SVY-1	0,38	0,5
BRM-1	0,38	0,5
CHM-3	0,41	0,4
CHM-4	0,38	0,4

Table 3.24 NPHI values and Vshale cut off values to calculate effective porosity

The PilotSTRATEGY project has received funding from the European Union's Horizon 2020 research and innovation programme under grant agreement No. 101022664

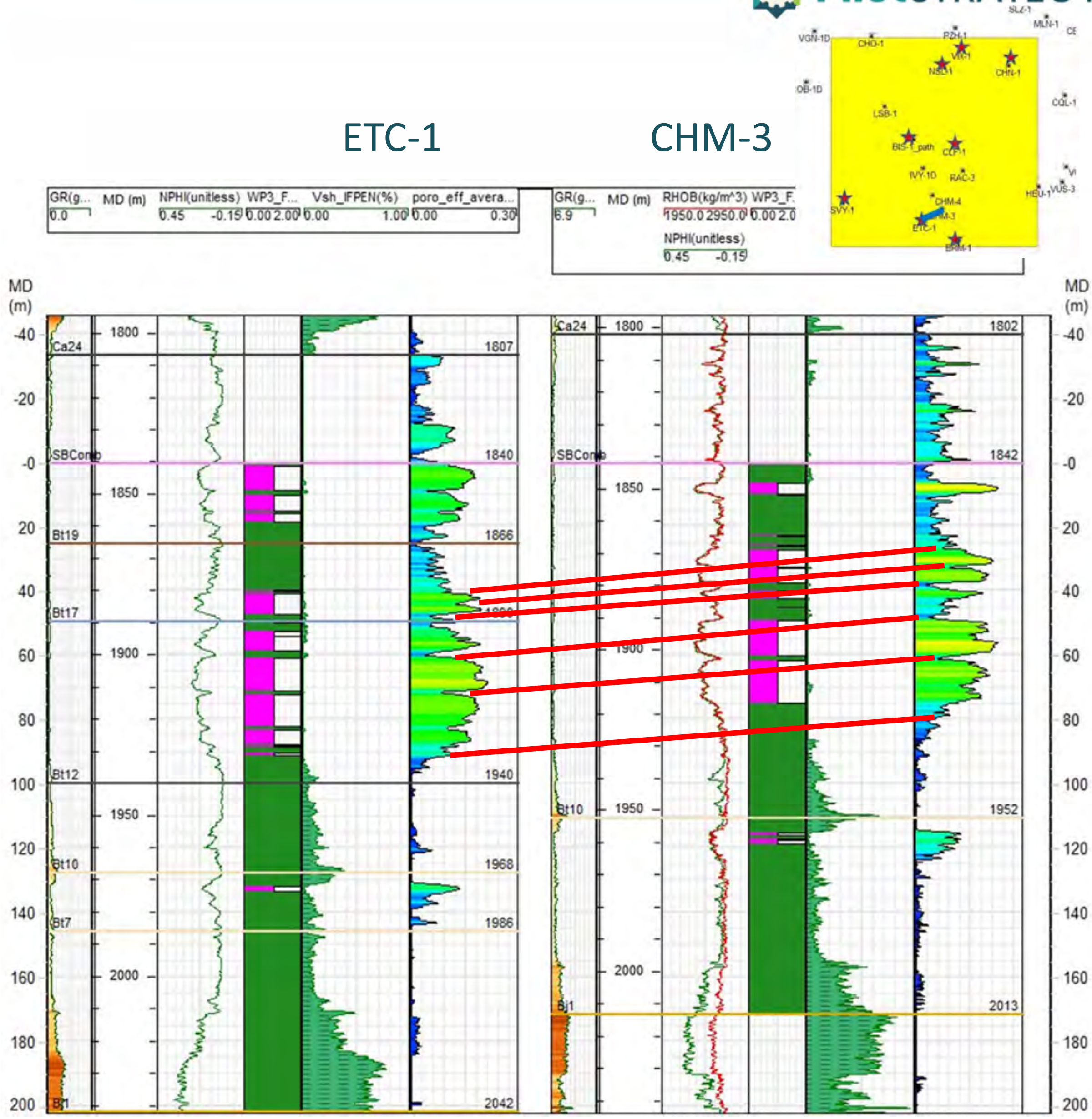

Figure 3.14 Peak-to-peak correlations to establish the extensions of the high porosity Oolithic bodies.

The PilotSTRATEGY project has received funding from the European Union's Horizon 2020 research and innovation programme under grant agreement No. 101022664

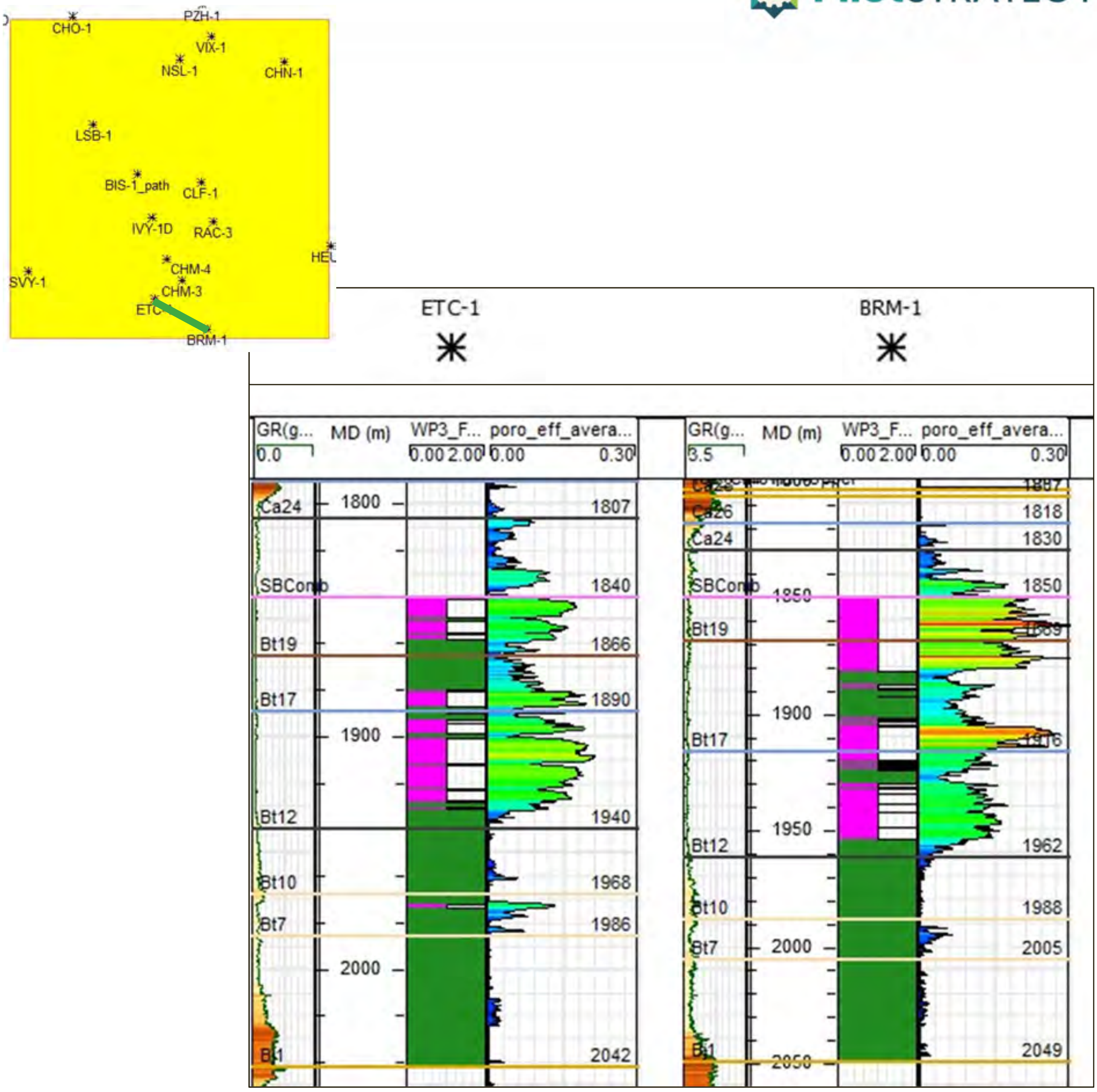

Figure 3.15 Peak-to-peak correlations to establish the extensions of the high porosity Oolithic bodies, a correlation in East West could not be established.

The PilotSTRATEGY project has received funding from the European Union's Horizon 2020 research and innovation programme under grant agreement No. 101022664

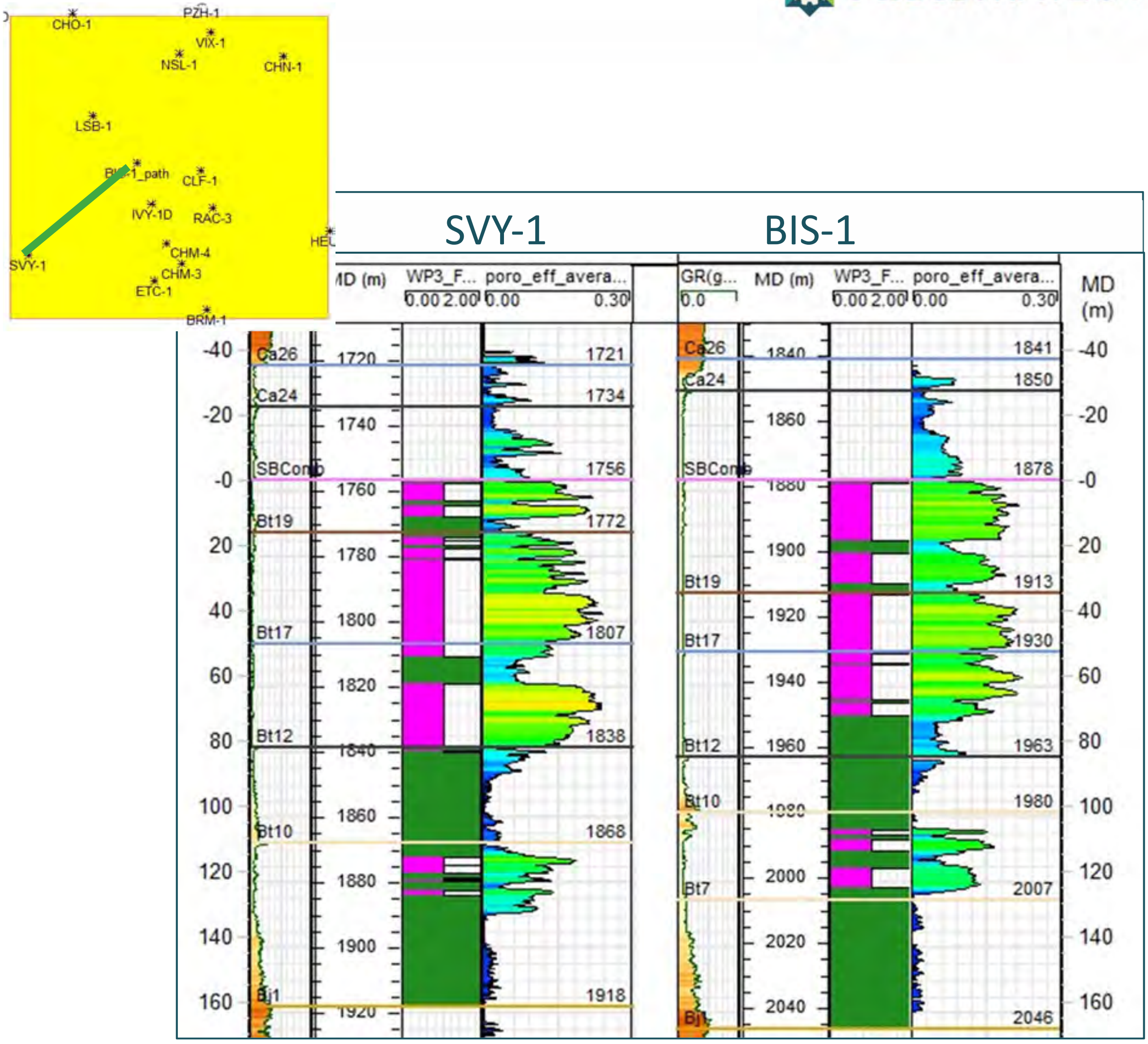

Figure 3.16 Peak-to-peak correlations to establish the extensions of the high porosity Oolithic bodies, a correlation in above 13.5 km could not be established.

The PilotSTRATEGY project has received funding from the European Union's Horizon 2020 research and innovation programme under grant agreement No. 101022664

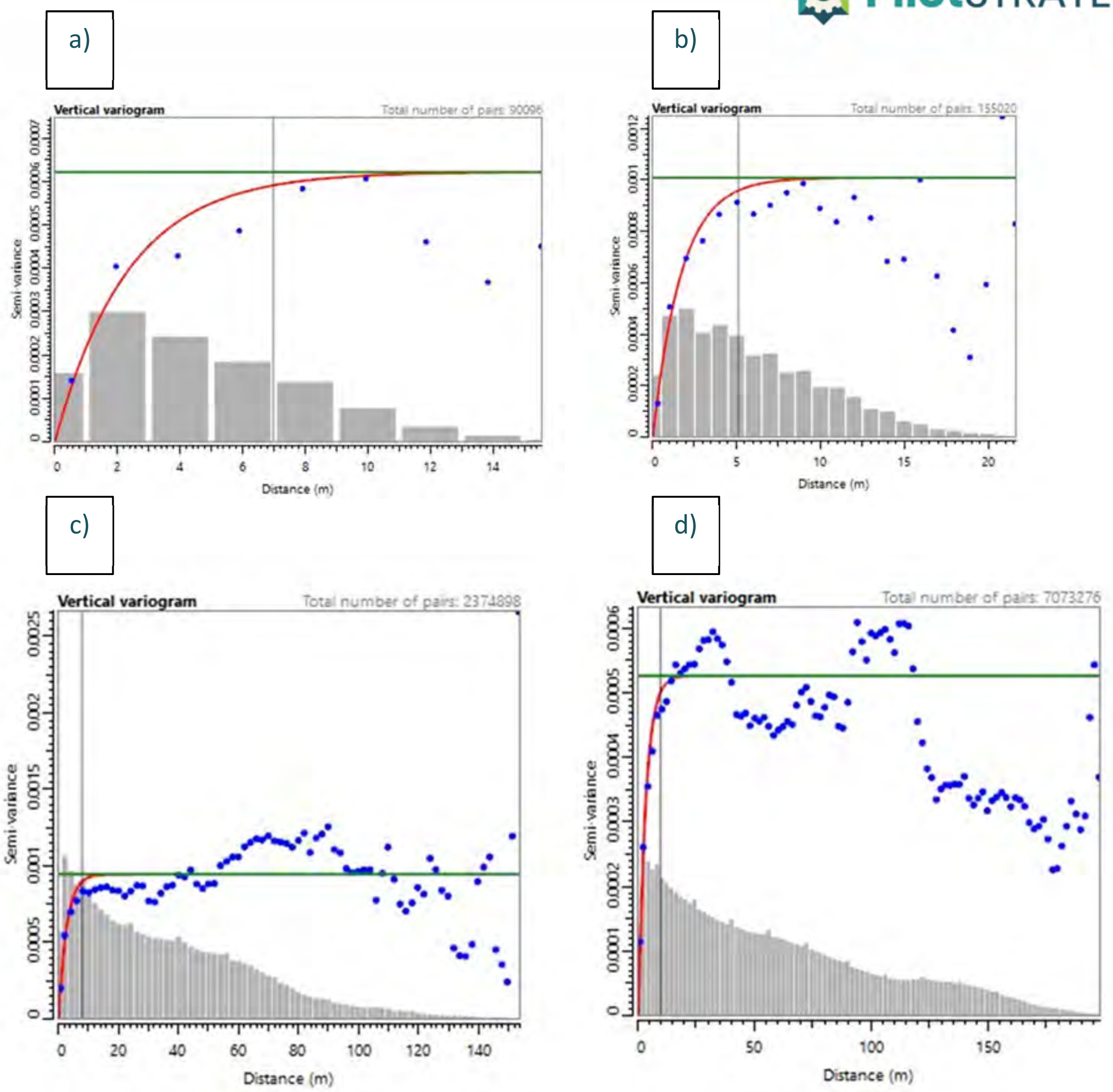

Figure 3.17 Porosity vertical experimental variograms and models for each formation. (a) Dalle Nacrée (b) Comblanchien (c) Oolithe blanche high porosity facies (d) Oolithe blanche low porosity facies

The PilotSTRATEGY project has received funding from the European Union's Horizon 2020 research and innovation programme under grant agreement No. 101022664

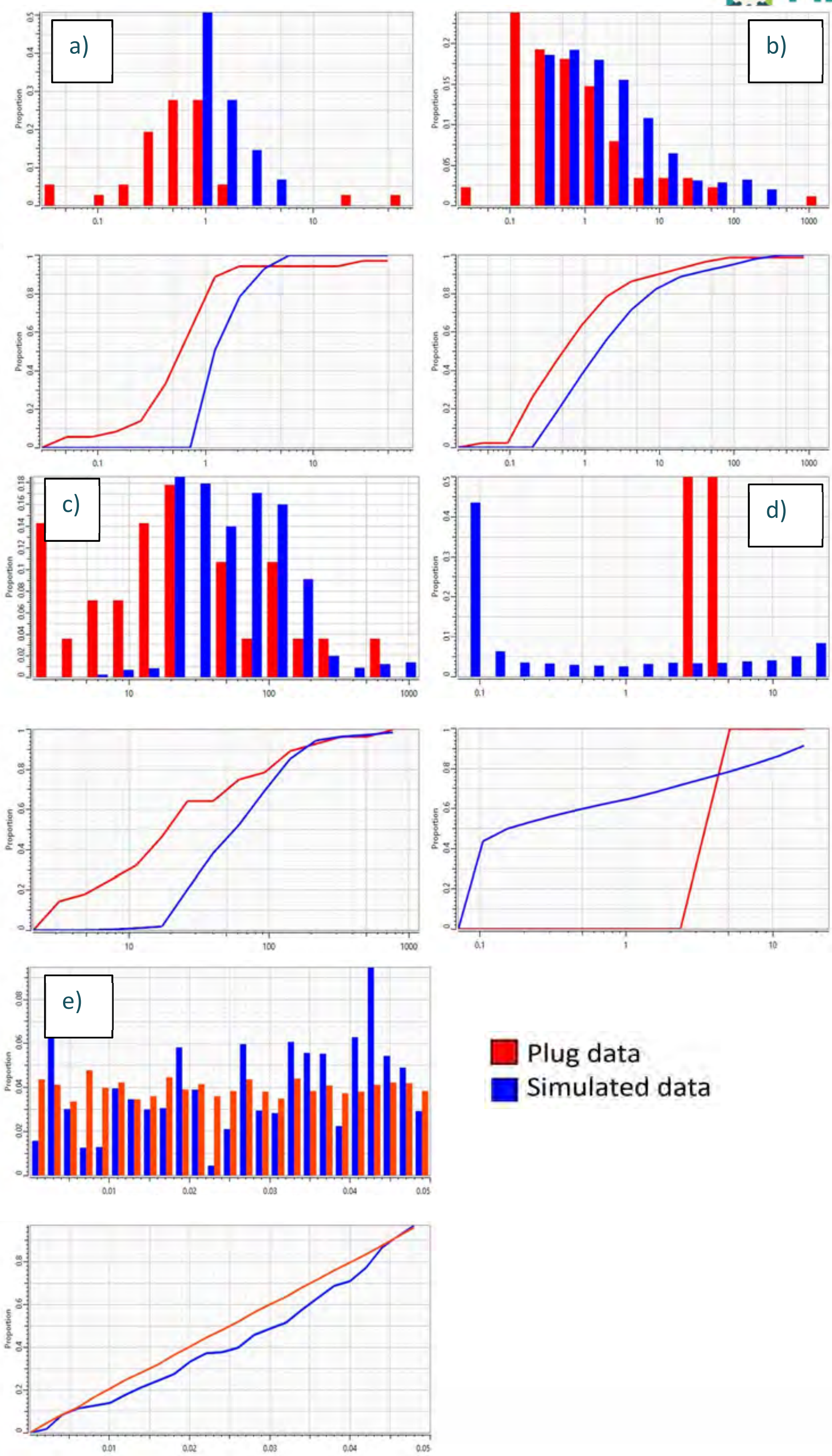

Figure 3.18 Comparison of permeability plug data from wells CHM-4, CHN-1, IVY-1D, VIX-1 and the simulated permeability with the K-Φ laws. For the Marnes de Massingy a permeability log was simulated based on a random distribution. a) Dalle Nacrée (b) Comblanchien (c) Oolithe blanche high porosity facies (d) Oolithe blanche low porosity facies, (e) Marnes de Massingy

The PilotSTRATEGY project has received funding from the European Union's Horizon 2020 research and innovation programme under grant agreement No. 101022664

System	Horizon	Region in Apen SKUA model	Φ Temis Model	K Temis Model
	Topography	X_Topo	Temis: Oligocene 42.86% Lutetian 45.83 % Ypresian 51.56% Average = 46.75%	Temis: Oligocene 185.44mD Lutetian 14.64mD Ypresian 40.41Md Average = 80mD
Cretaceous	Top Upper Cretaceous	69_5_Upper_Cretaceous	Maastrichtian 29.10%	Maastrichtian 0.39mD
	Top_Cenomanian	X_Top_Cenomanian_markers	Same as Maastrichtian	Same as Maastrichtian
	Top_Alb. Clay	X_Top_Alb_Clay_Markers	Gault shales 17.28%	Gault shales 0.01mD
	Top_Alb. Sand	X_Top_Alb_Sand_Markers	Albian 22.42%	Albian 1.17mD
	Top_Albo-Aptian	X_Top_Albo-Aptian_Markers	Aptian 12.63%	Aptian 0.01mD
	Top_Barremian	X_Top_Barremian_markers_AND_horizon	Barremian 11.28 %	Barremian 0.01mD
Jurassic	Top_Purbeckian	X_Top_Purbeckian_marker_AND_horizon	Tithonian 20.77%	Tithonian 5.23mD
	Top_Portlandian	X_Top_Portlandian_markers_AND_horizons	Tithonian 20.77%	Tithonian 5.23mD
	Top_Kimmeridgian	X_Top_Kimmeridgian_markers_AND_horizon	Kimmeridgian 15.89%	Kimmeridgian 1.13mD
	Top_Oxfordian_Sup	X_Top_Oxf_Sup_markers_AND_horizons	Oxfordian 12.74%	Oxfordian 0.01mD
	Top_Oxfordian-Inf	X_Top_Oxf_Inf_Horizons_AND_Markers	Sequanian 9.09%	Sequanian 0.01mD
	Top_Marnes_Massingy			
	Ca26_vf			
	Ca24_vf			
	Sb-Comb_vf			
	Bt10_vf			
	Bj1_vf	X_Top_Bajocian_Markers_AND_Horizons	Bajocian 13.2%	Bajocian 0.36mD
	Top_Aalenian	X_Top_Aalenian_Markers_AND_Horizons	Aalenian 12.94%	Aalenian 0.34mD

The PilotSTRATEGY project has received funding from the European Union's Horizon 2020 research and innovation programme under grant agreement No. 101022664

	Top_Toarcian	X_Top_Toarcian_Markers_AND_Horizons	Toarcian 12%	Toarcian 0.00mD
	Top_Lias-Middle	X_Top_Lias_Middle_Horizons_AND_Markers	Dommerian 5.61% Hettangian 5.47%	Dommerian 0.00mD Hettangian 0.00mD
Trias	Top_Trias	X_JMM_Top_Trias	Rhetian 9.26% Norian 5.75% Average = 7,51%	Rhetian 0.02mD Norian 0.0mD Average = 0.01mD
	Top Carnian	231_5_Carnian	Carnian 7.35%	Carnian 0.01mD
	Top Middle Trias	237_5_Middle_Trias	Ladinian 9.03% Anisian 15.84% Average = 12.44	Ladinian 0.05mD Anisian 2.66mD Average = 1.355

Table 3.25 Table listing porosity and permeability values used for the over-and underburden layers in the model

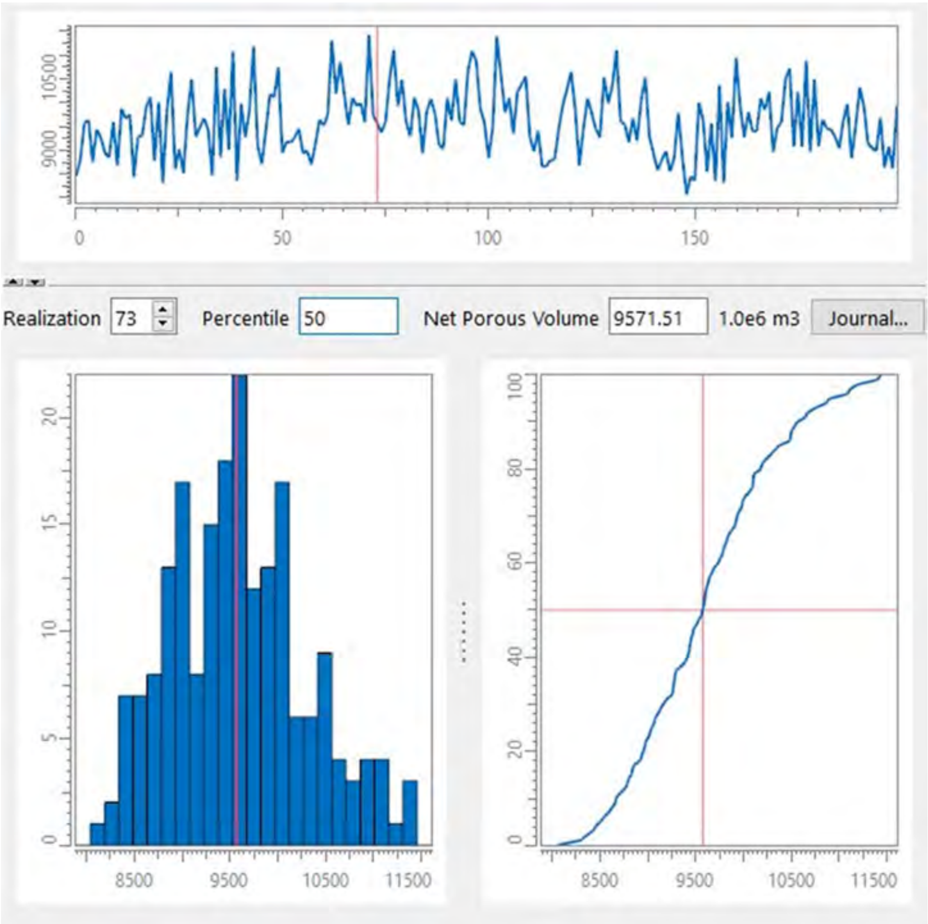

Figure 3.19: Net porous volume distribution for the Oolithe Blanche formation from the 200 realizations of the uncertainty study

The PilotSTRATEGY project has received funding from the European Union's Horizon 2020 research and innovation programme under grant agreement No. 101022664

		P10	P50	P90
Porosity (whole Oolithe Blanche formation)	**Samples:**	27200	27200	27200
	Minimum:	0.0054836	0.000636361	0.00720137
	Median:	0.0858697	0.0940968	0.103366
	Maximum:	0.228052	0.26352	0.275282
	Mean:	0.0860994	0.0946056	0.105158
	Std. deviation:	0.0368	0.0420141	0.0479113
	Variance:	0.00135424	0.00176518	0.00229549
Permeability X (whole Oolithe Blanche formation) [mD]	**Samples:**	27200	27200	27200
	Minimum:	0.0948915	0.0733755	0.103945
	Median:	17.7541	23.8976	38.2331
	Maximum:	640.398	715.204	897.8
	Mean:	24.0141	35.3118	61.5667
	Std. deviation:	27.2982	43.9901	78.4976
Permeability Z (whole Oolithe Blanche formation) [mD]	**Samples:**	27200	27200	27200
	Minimum:	0.0948915	0.0733755	0.103945
	Median:	1.097	1.16005	1.06046
	Maximum:	640.398	714.344	897.795
	Mean:	12.64	18.8103	27.571
	Std. deviation:	22.848	35.6661	65.5007

Table 3.26: Statistical variation for the Oolithe Blanche formation for porosity and permeability. Comparison of scenarios P10, P50, P90 after upscaling for the 500m resolution grid.

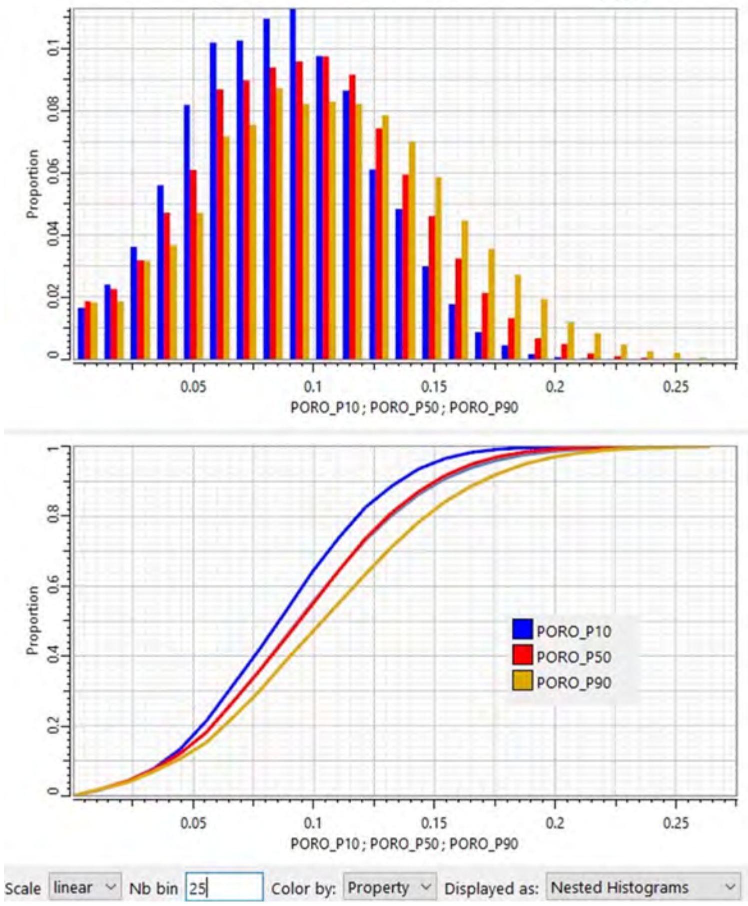

Figure 3.20 Porosity distribution for the P10, P50 and P90 scenarios after the upscaling process for the Oolithe Blanche formation. Shown is the distribution for the 500m grid resolution.

The PilotSTRATEGY project has received funding from the European Union's Horizon 2020 research and innovation programme under grant agreement No. 101022664

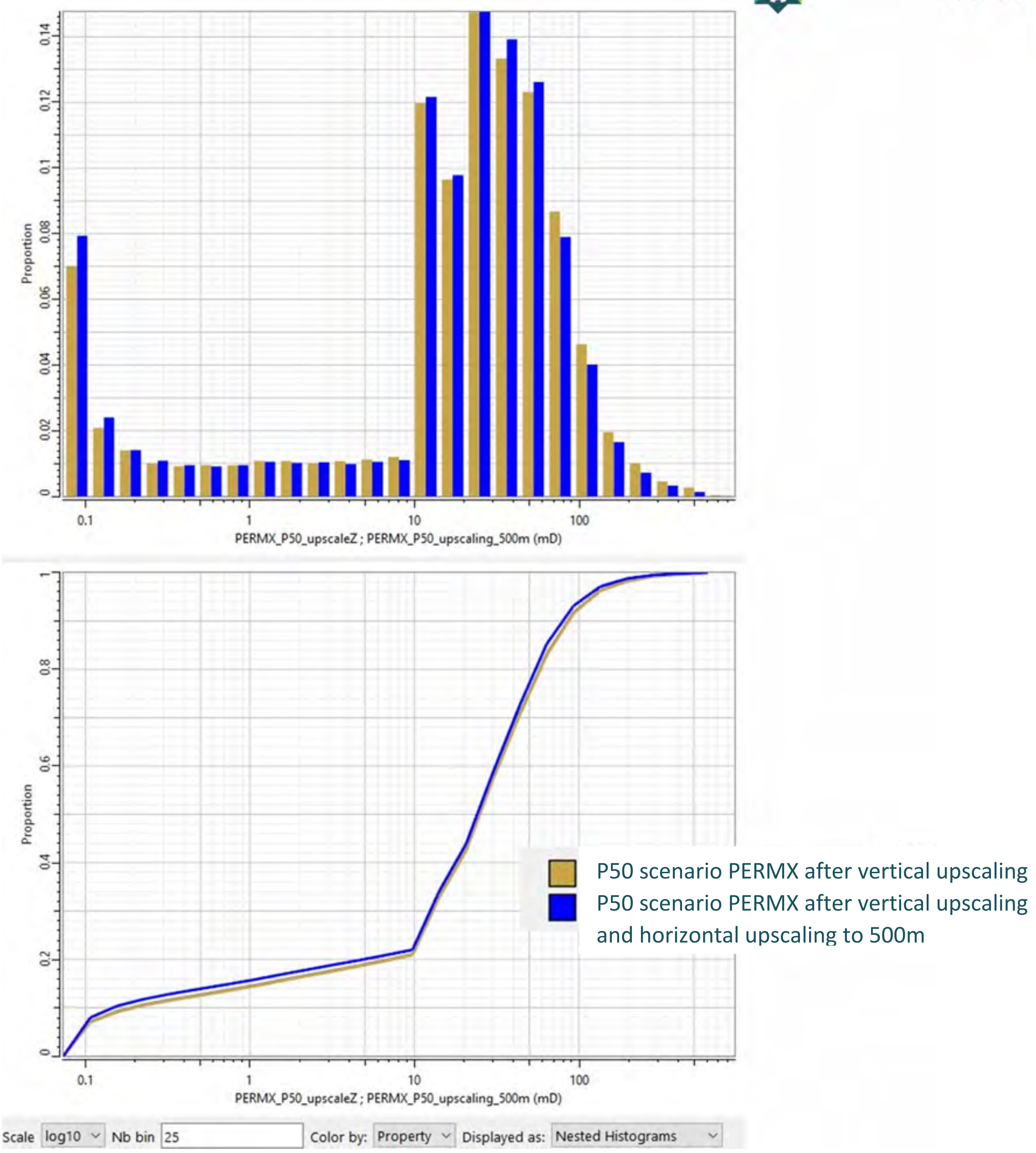

Figure 3.21: Comparison of the permeability in X direction after the vertical upscaling (brown) and after the additional upscaling to 500m cell size (blue) for the P50 scenario.

The PilotSTRATEGY project has received funding from the European Union's Horizon 2020 research and innovation programme under grant agreement No. 101022664

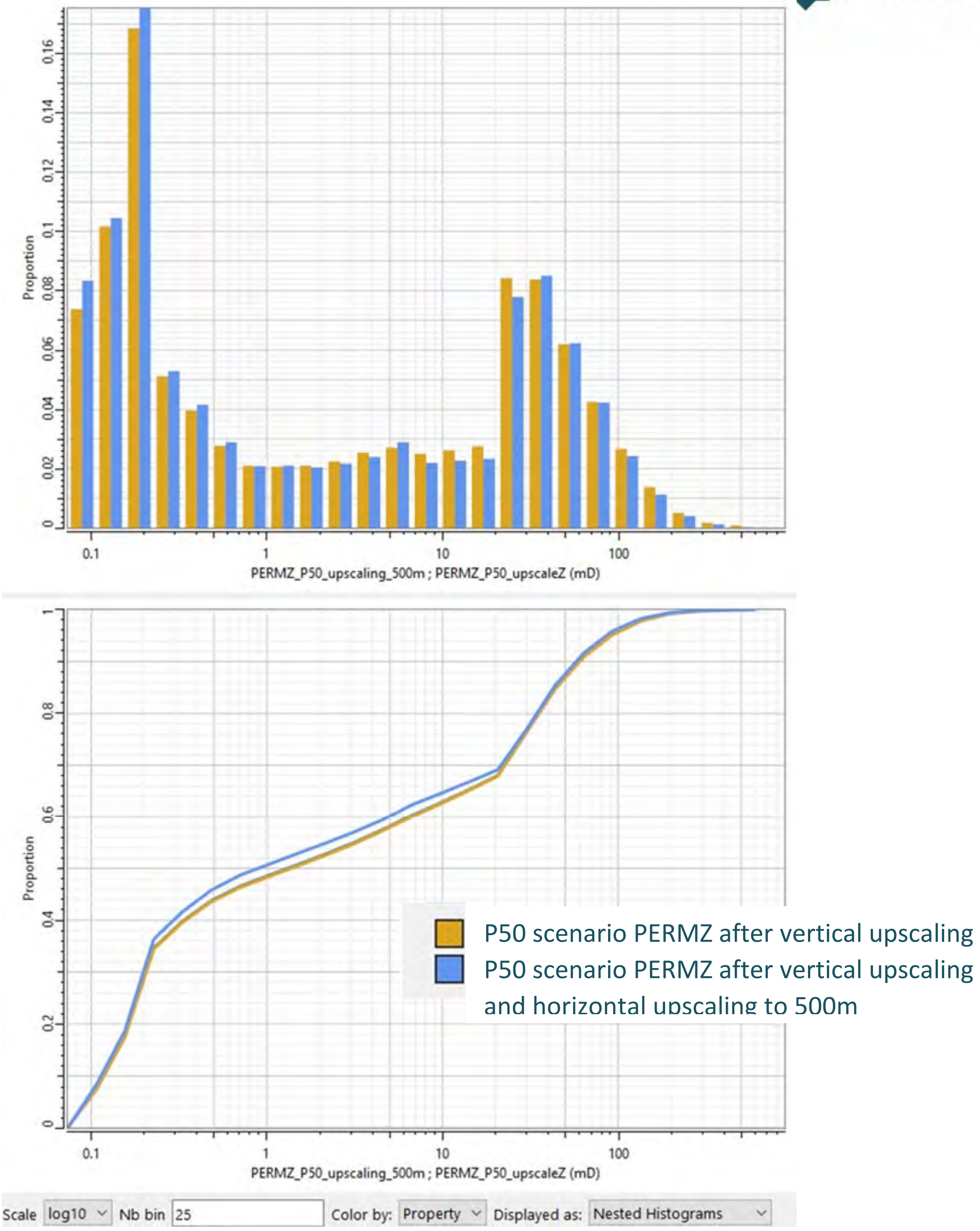

Figure 3.22: Comparison of the permeability in Z direction after the vertical upscaling (brown) and after the additional upscaling to 500m cell size (blue) for the P50 scenario.

7.2 Additional figures and tables for Upper Silesia, Poland region (4)

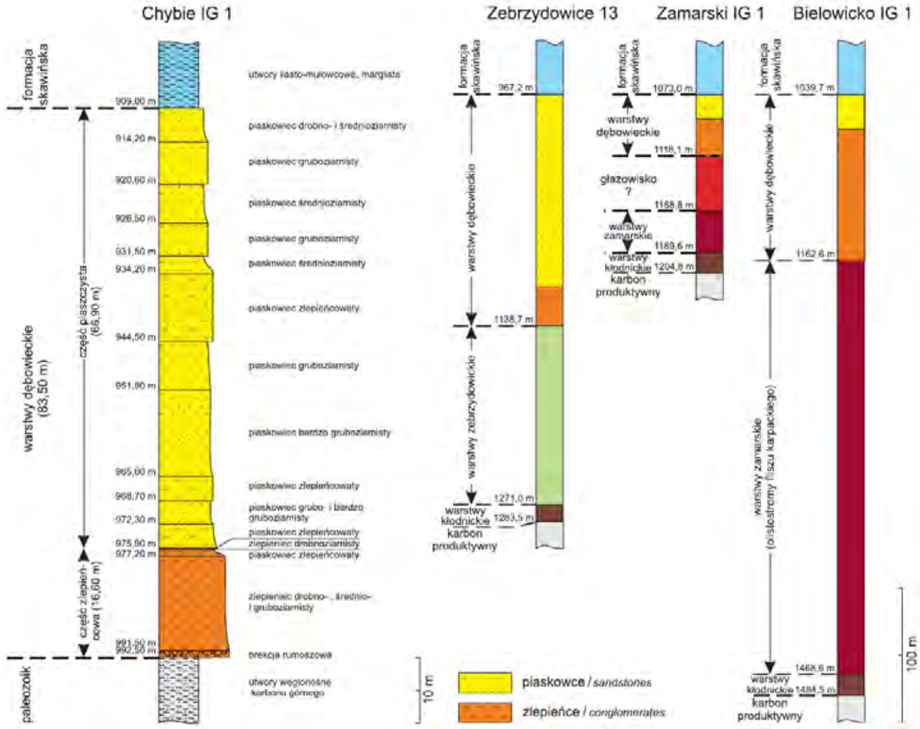

Figure 4.1: Profiles of Dębowiec Beds and Miocene strata basement (Jureczka et al., 2012)

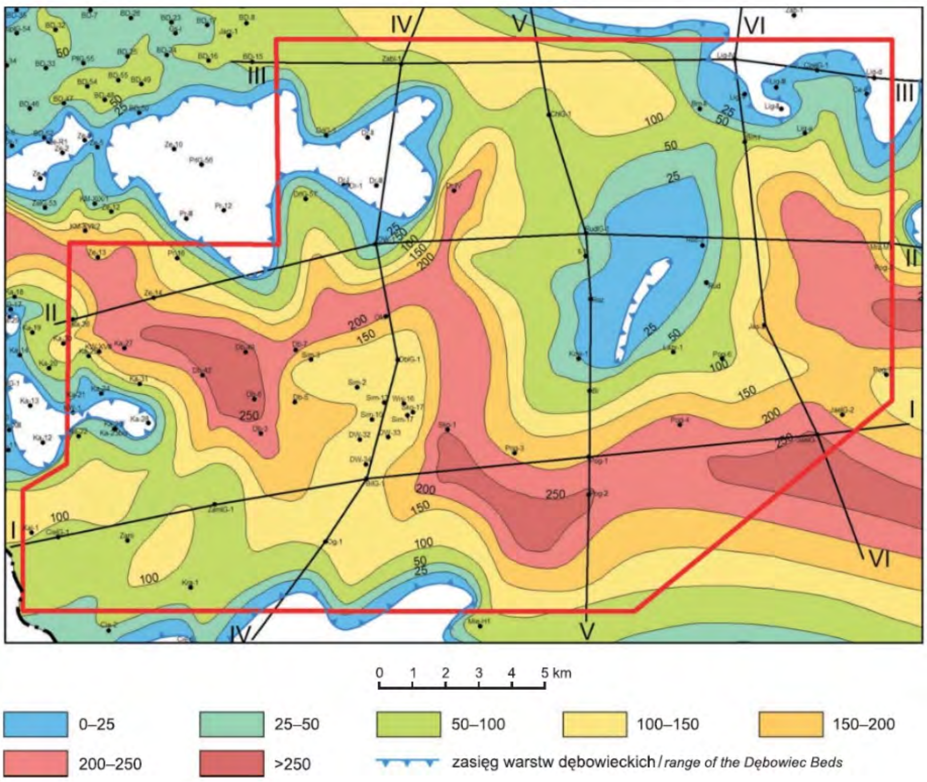

Figure 4.2: Thickness of Dębowiec Beds in the Cieszyn-Skoczów-Czechowice area (Jureczka et al., 2012)

The PilotSTRATEGY project has received funding from the European Union's Horizon 2020 research and innovation programme under grant agreement No. 101022664

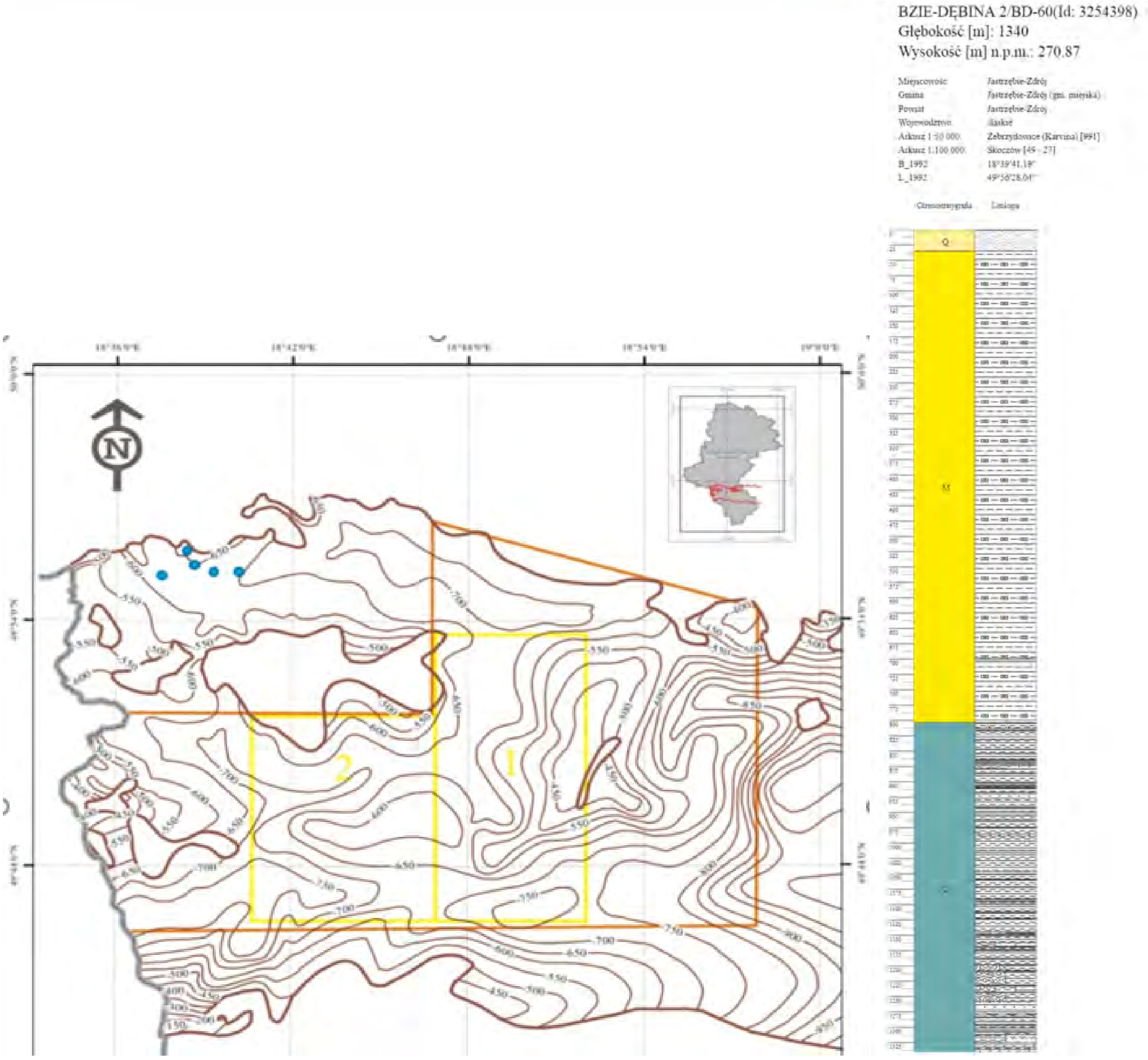

Figure 4.3: Location of new boreholes

The PilotSTRATEGY project has received funding from the European Union's Horizon 2020 research and innovation programme under grant agreement No. 101022664

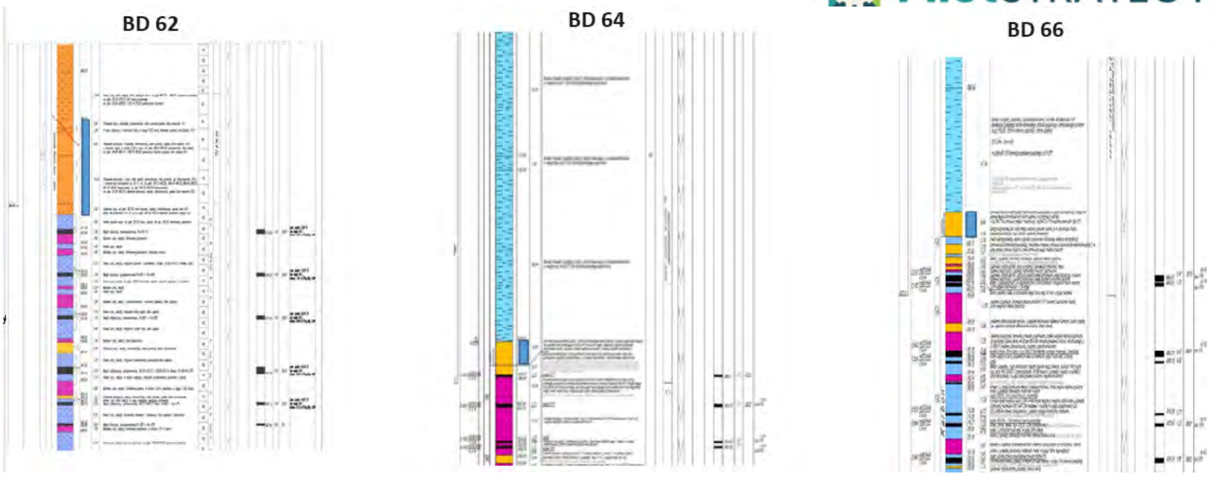

Figure 4.4: Example of well profiles with lithological data

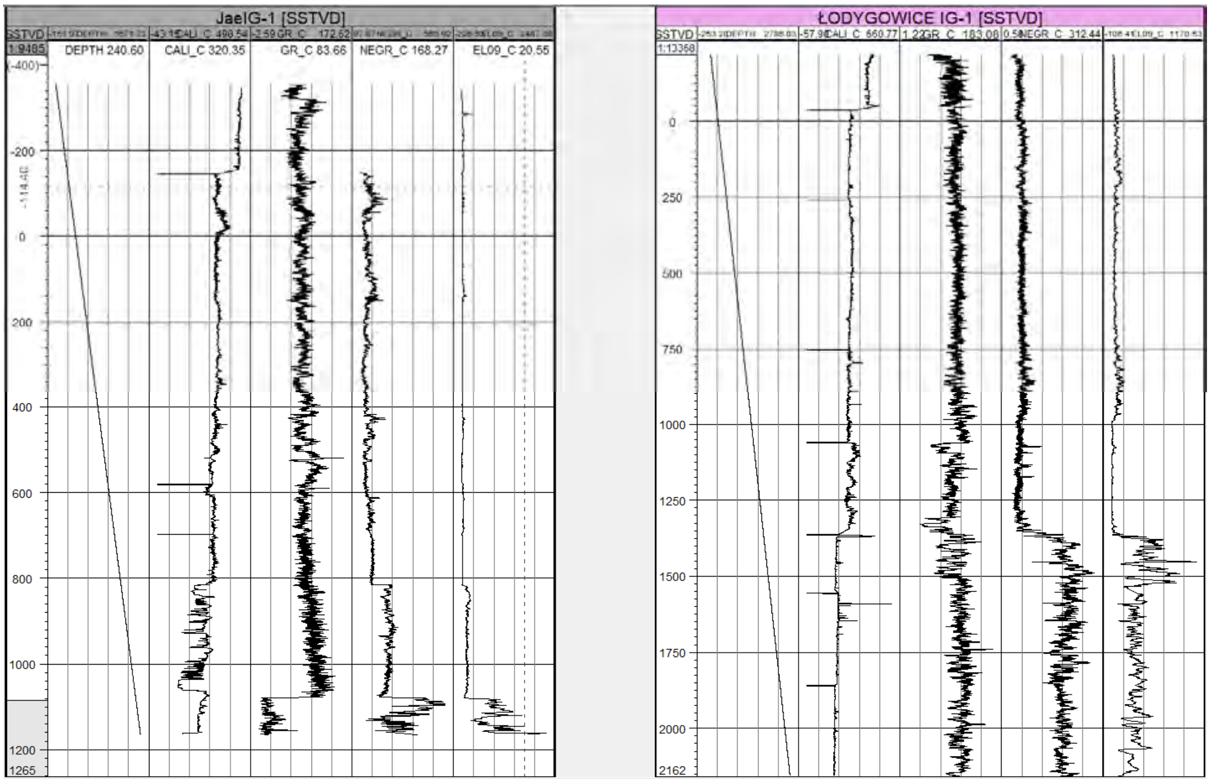

Figure 4.5: Example of well-log LAS data (Log ASCII)

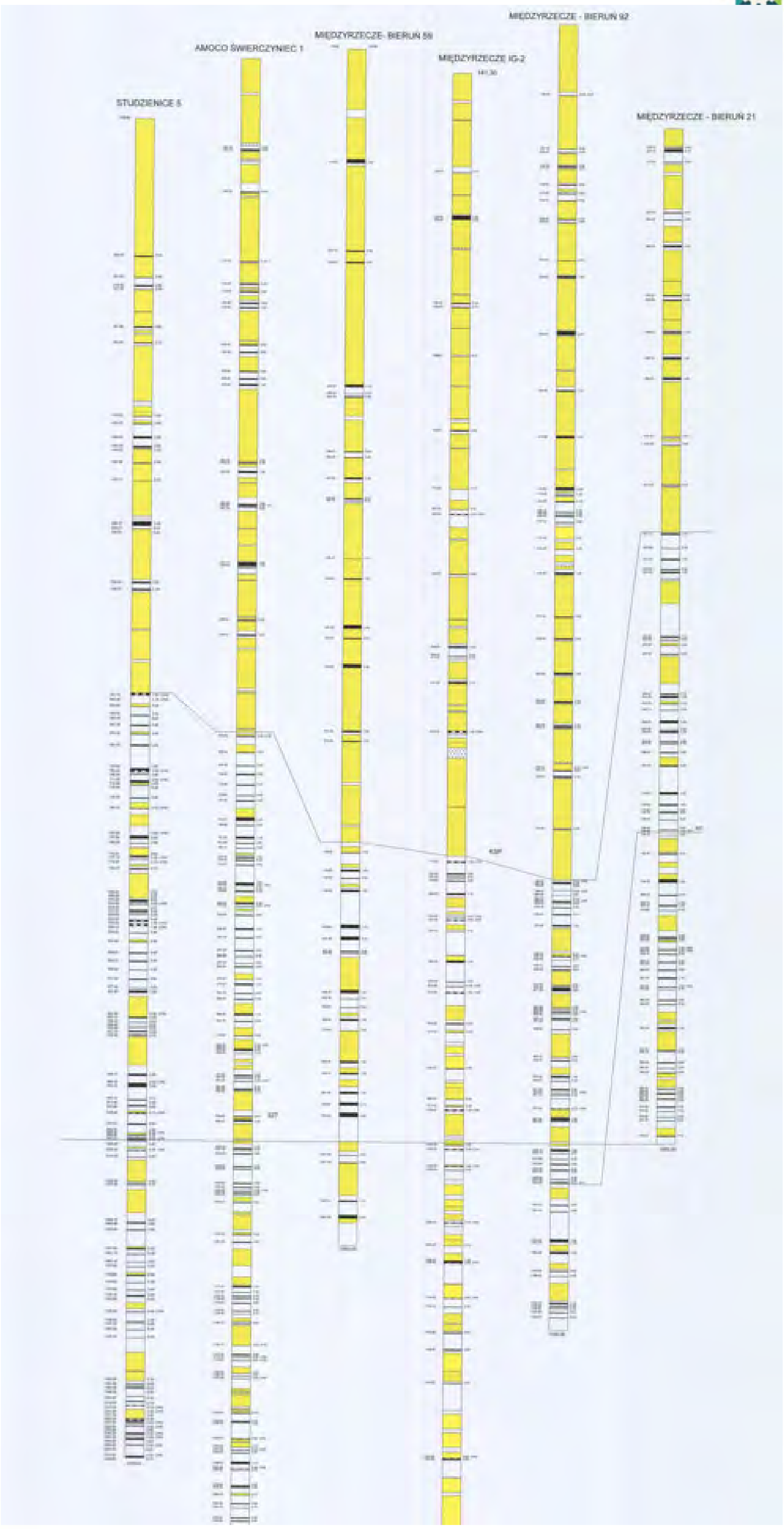

Figure 4.6: Example of stratigraphic inter-well correlations

The PilotSTRATEGY project has received funding from the European Union's Horizon 2020 research and innovation programme under grant agreement No. 101022664

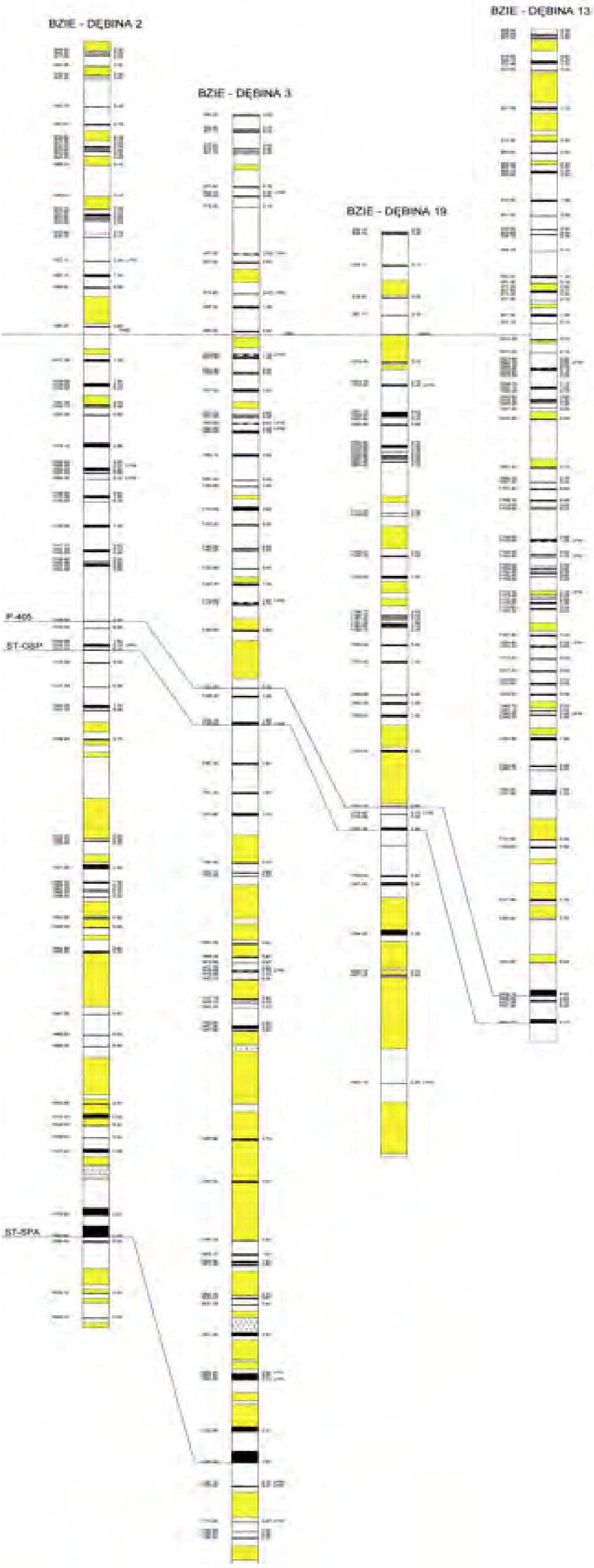

Figure 4.7: Example of stratigraphic inter-well correlations

The PilotSTRATEGY project has received funding from the European Union's Horizon 2020 research and innovation programme under grant agreement No. 101022664

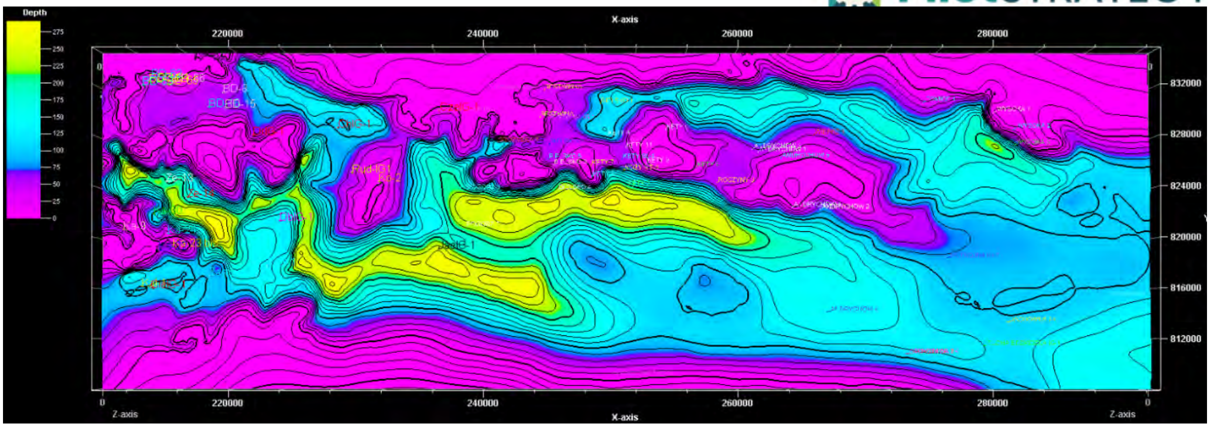

Figure 4.8: Structural map of the top of the Dębowiec layers in model

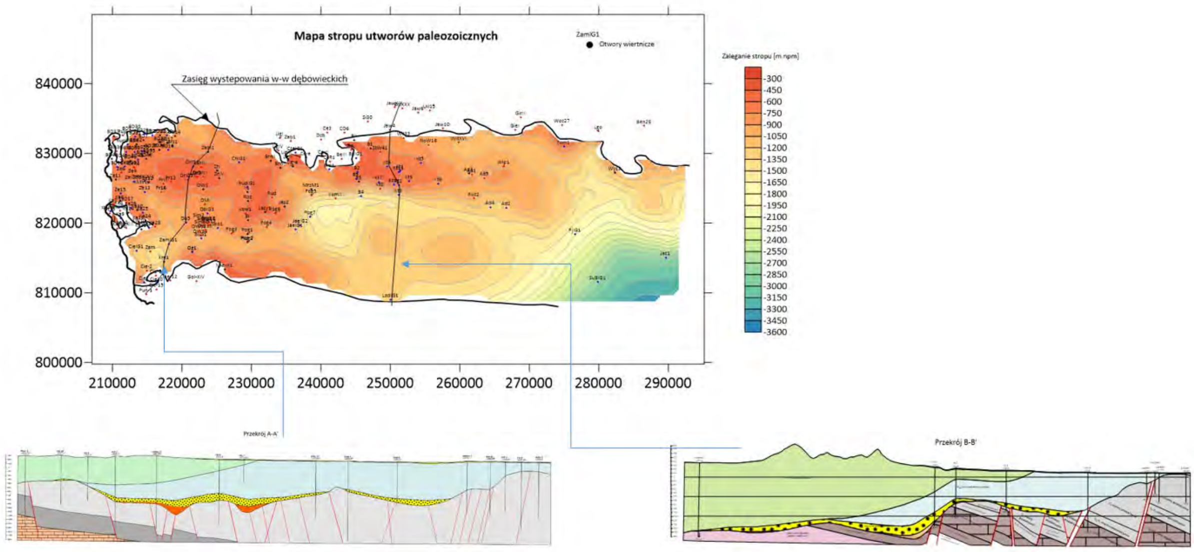

Figure 4.9: Structural map of the top of the Paleozoic formations with cross-sections

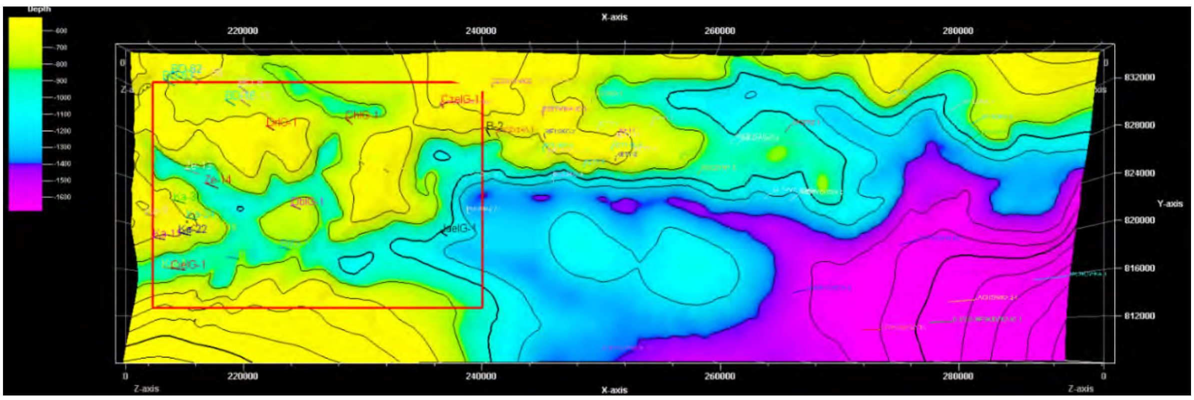

Figure 4.10: Structural map of the top of the Paleozoic formations with cross-sections in model

The PilotSTRATEGY project has received funding from the European Union's Horizon 2020 research and innovation programme under grant agreement No. 101022664

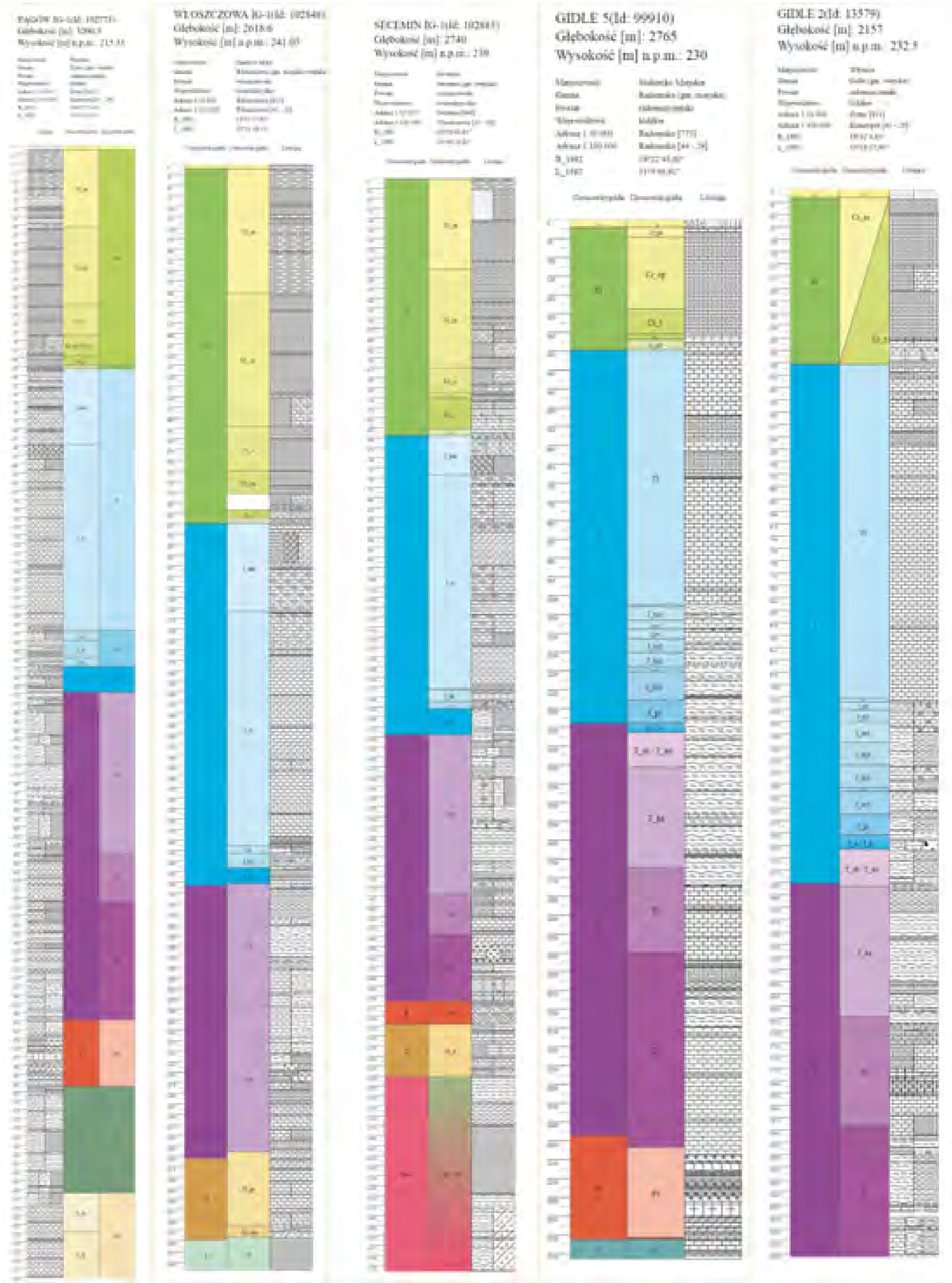

Figure 4.11: Compilation of lithologies in 10 boreholes

The PilotSTRATEGY project has received funding from the European Union's Horizon 2020 research and innovation programme under grant agreement No. 101022664

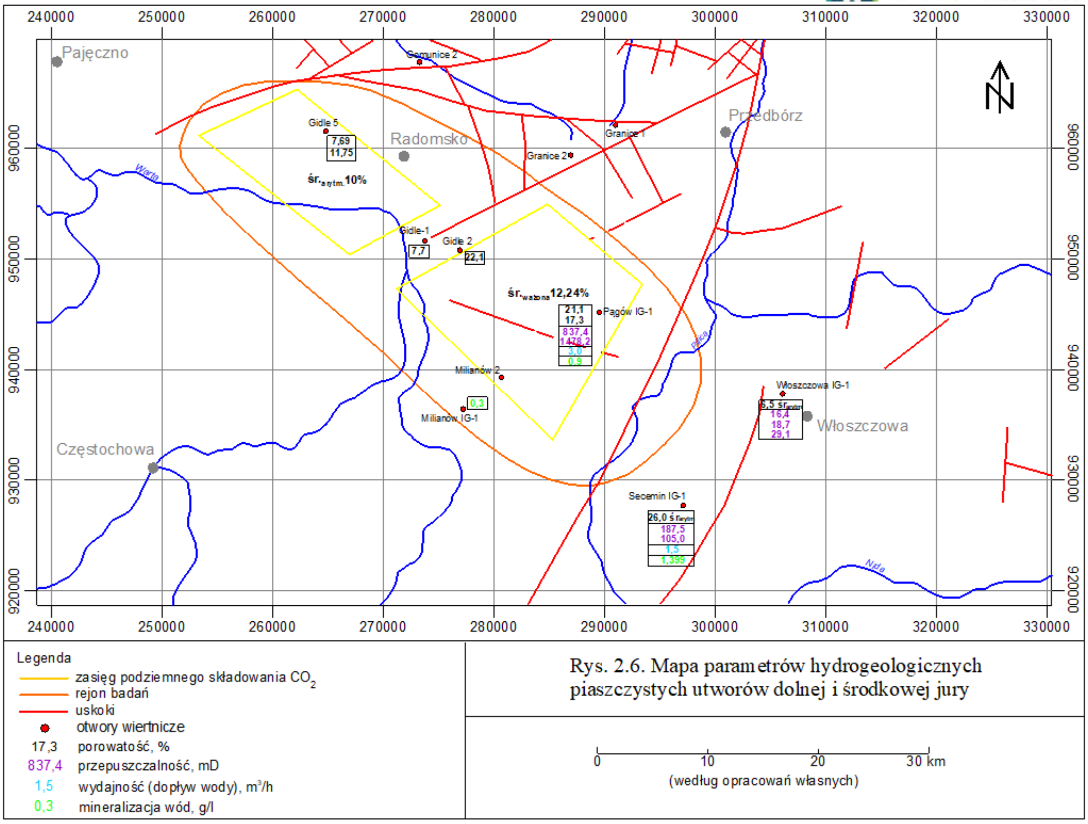

Figure 4.12: Map of hydrogeological properties of sandstones of Lower and Middle Jurassic - only part of wells with available petrophysical data (Wachowicz et al., 2010)

$$M^{1,399}\frac{Cl^{50,93}\ HCO_3{}^{39,82}\ SO_4{}^{5,59}}{Na^{96,91}\ Ca^{2,25}\ K^{1,15}\ Mg^{0,29}}$$

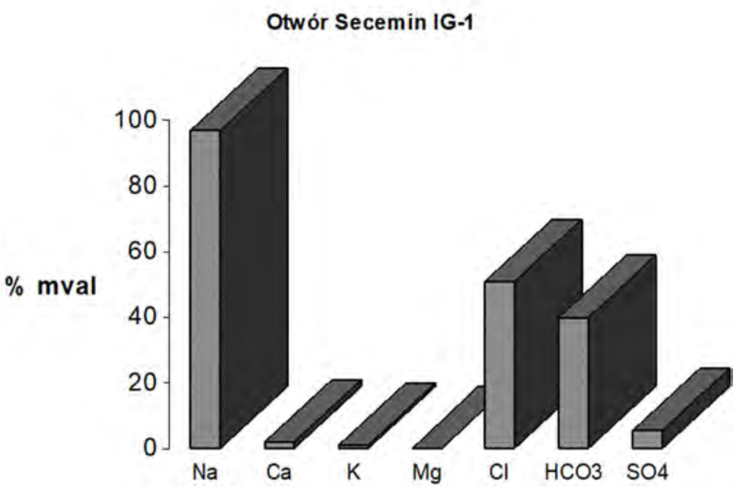

Figure 4.13: Physicochemical composition of Lower Jurassic waters (Wachowicz et al., 2010)

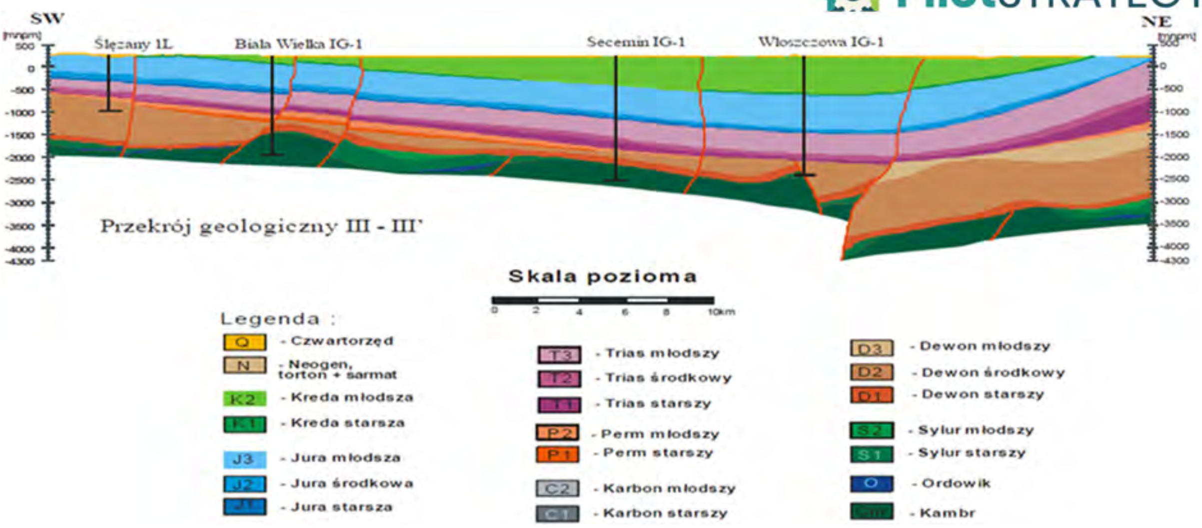

Figure 4.14: Analysis of geological cross-sections (Złonkiewicz, 2001, Górecki et al., 2002)

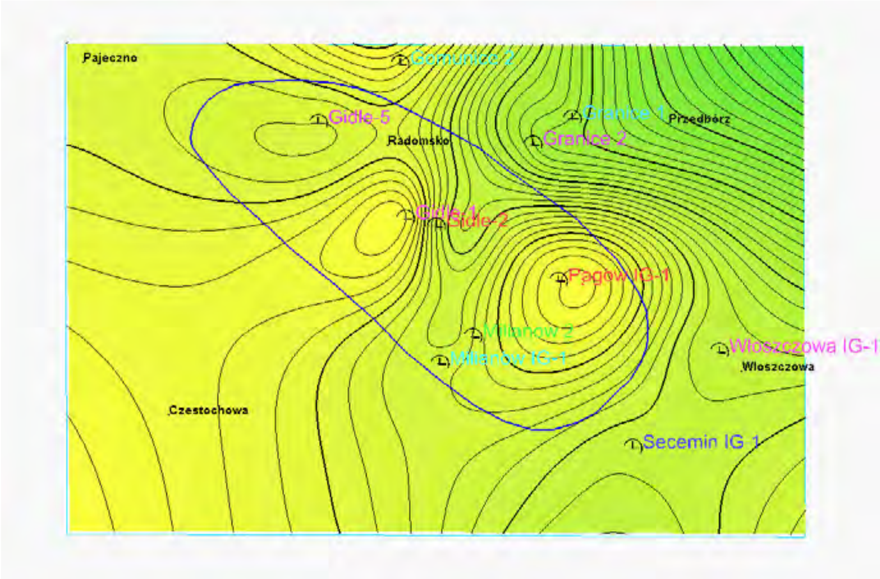

a)

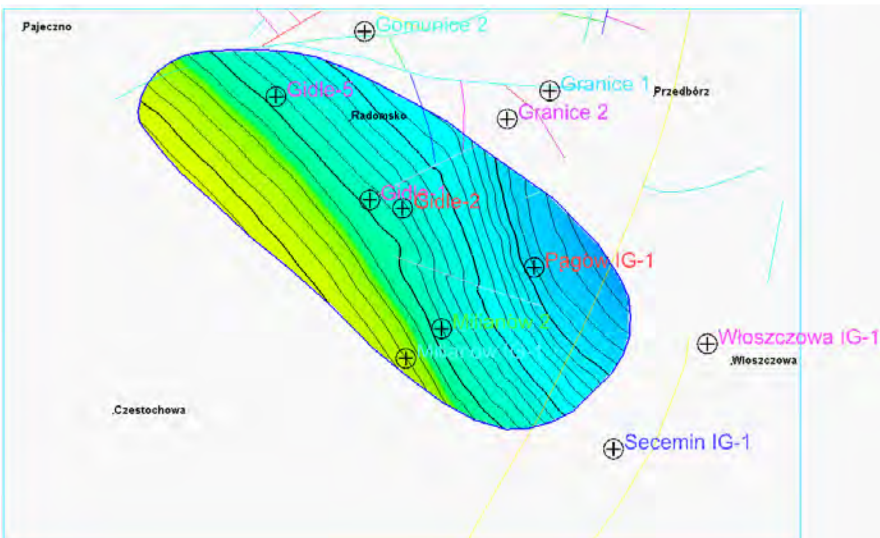

b)

Figure 4.15: Structural surfaces of the top (a) and the base (b) of reservoir layers in the area of the Jurassic structure

The PilotSTRATEGY project has received funding from the European Union's Horizon 2020 research and innovation programme under grant agreement No. 101022664

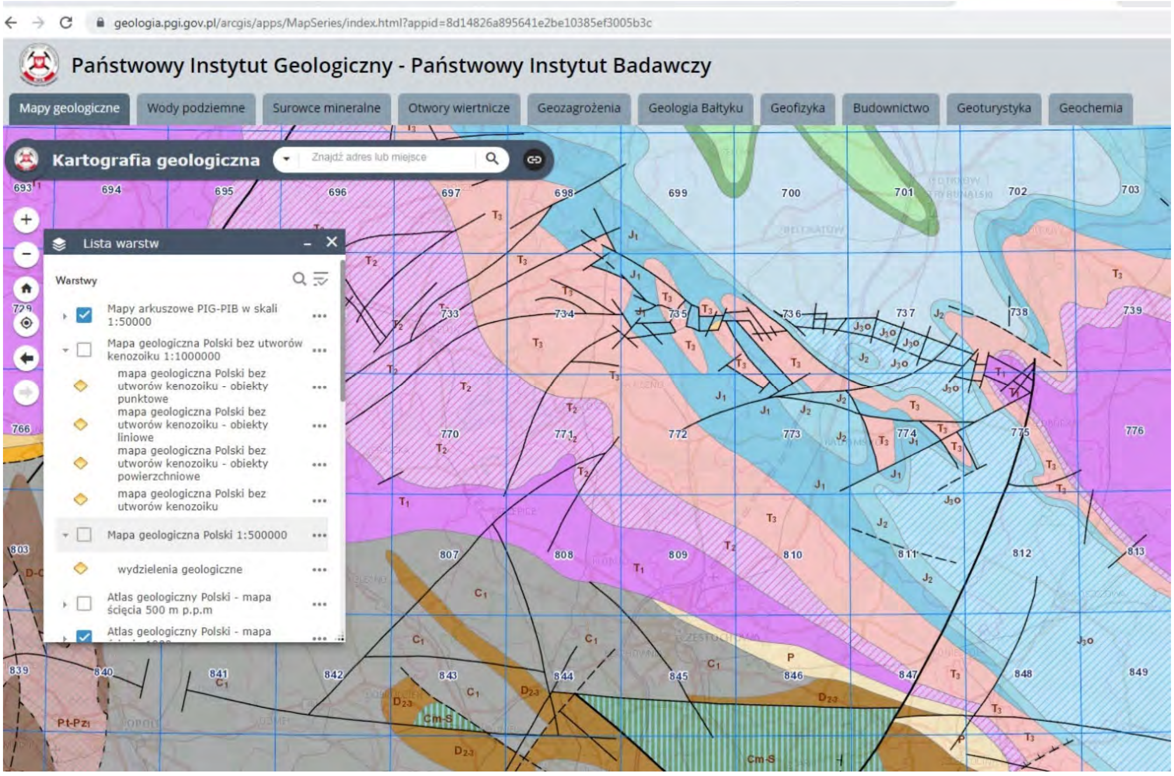

Figure 4.16: Geological map of the area of the Jurassic structure (Polish Geological Institute)

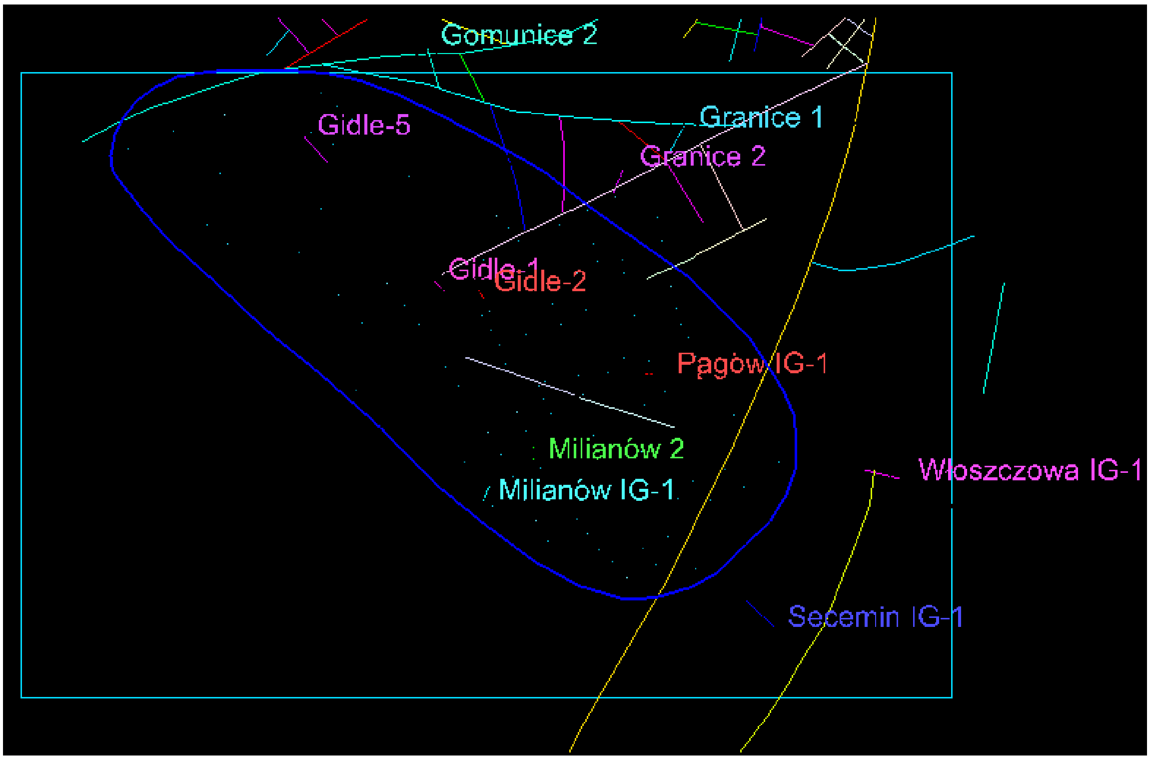

Figure 4.17: Fault lines in structural framework model in the area of the Jurassic structure

The PilotSTRATEGY project has received funding from the European Union's Horizon 2020 research and innovation programme under grant agreement No. 101022664

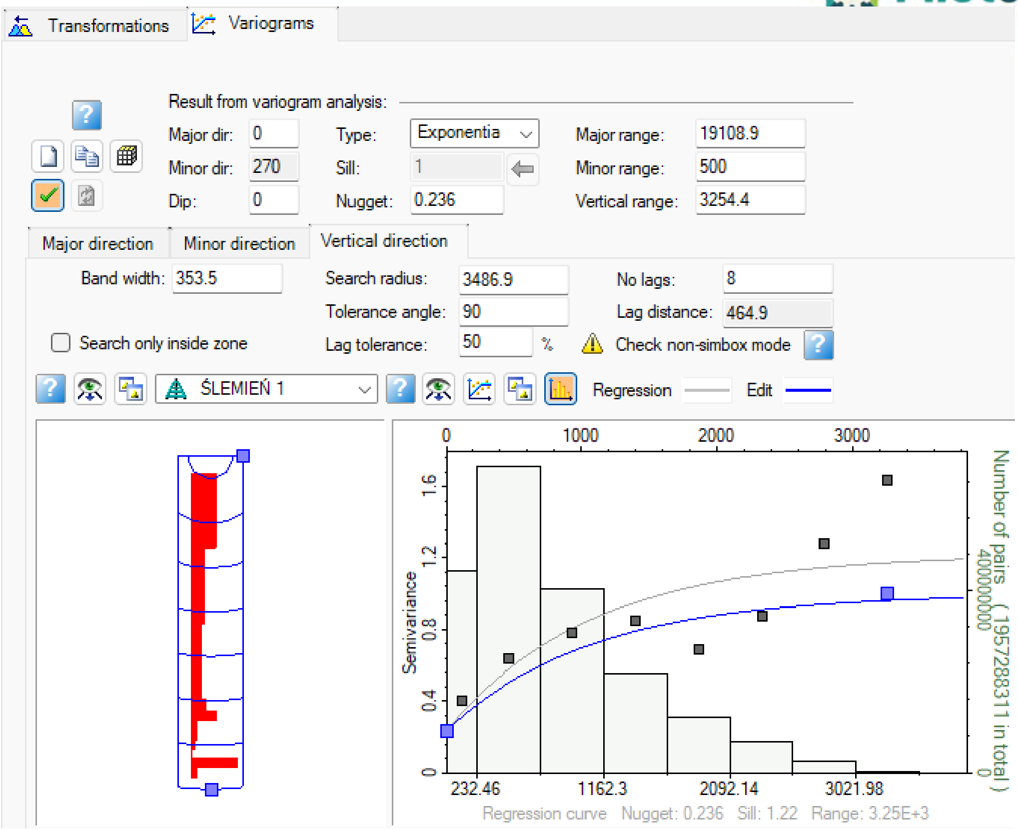

Figure 4.18: Results from variogram analysis – vertical direction of porosity (reservoir)

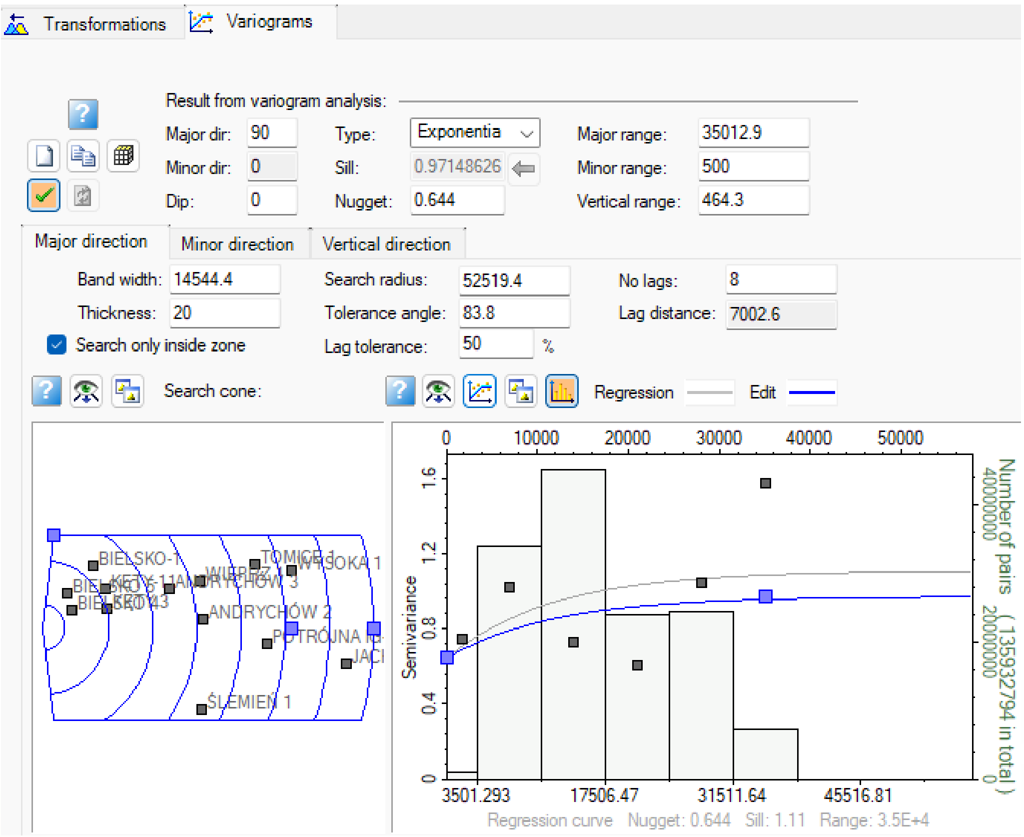

Figure 4.19: Results from variogram analysis – major direction of porosity (reservoir)

The PilotSTRATEGY project has received funding from the European Union's Horizon 2020 research and innovation programme under grant agreement No. 101022664

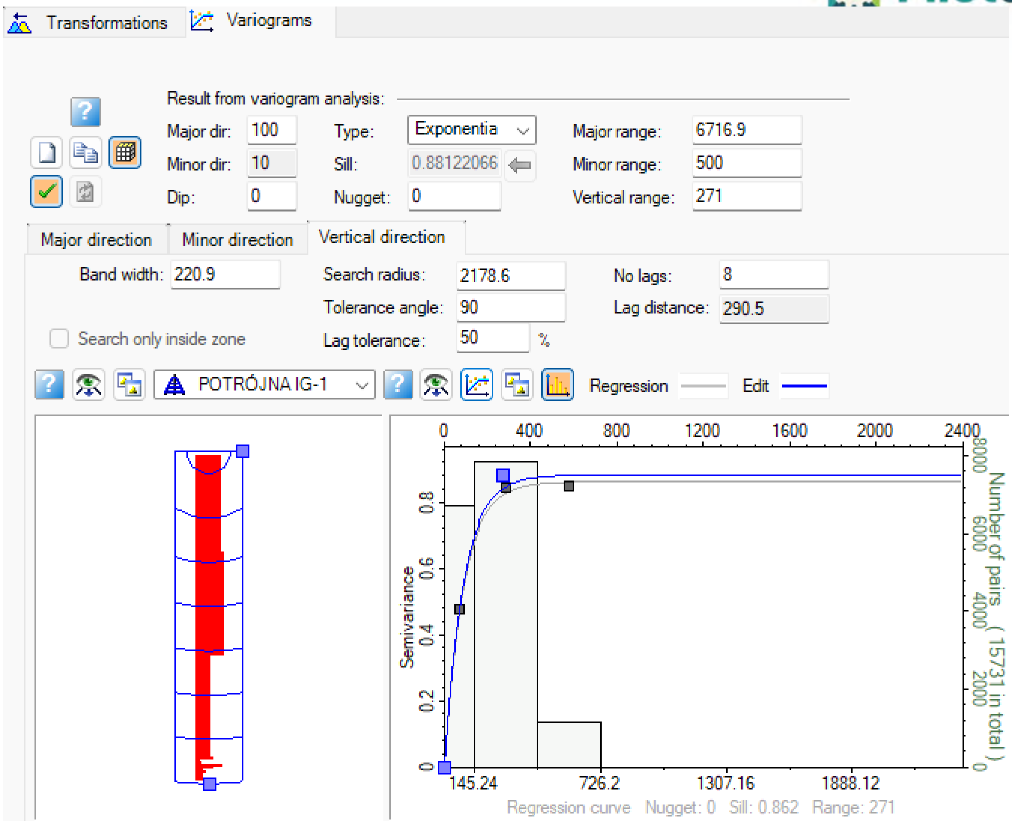

Figure 4.20: Results from variogram analysis – vertical direction of porosity (sealing layer)

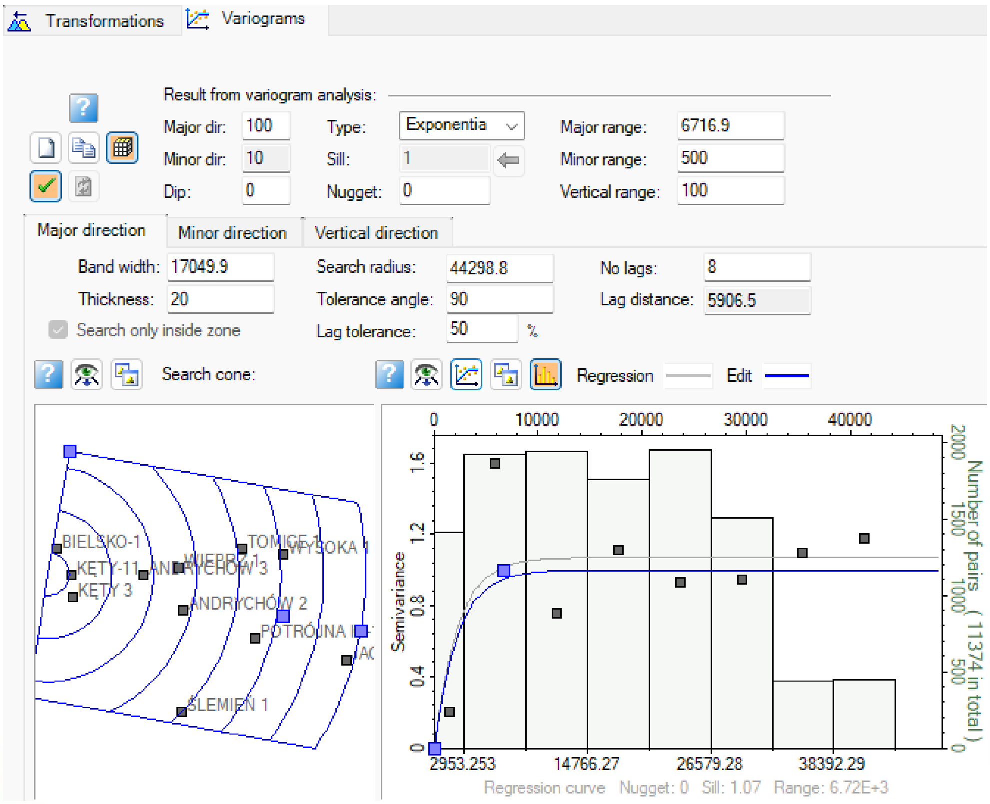

Figure 4.21: Results from variogram analysis – major direction of porosity (sealing layer)

The PilotSTRATEGY project has received funding from the European Union's Horizon 2020 research and innovation programme under grant agreement No. 101022664

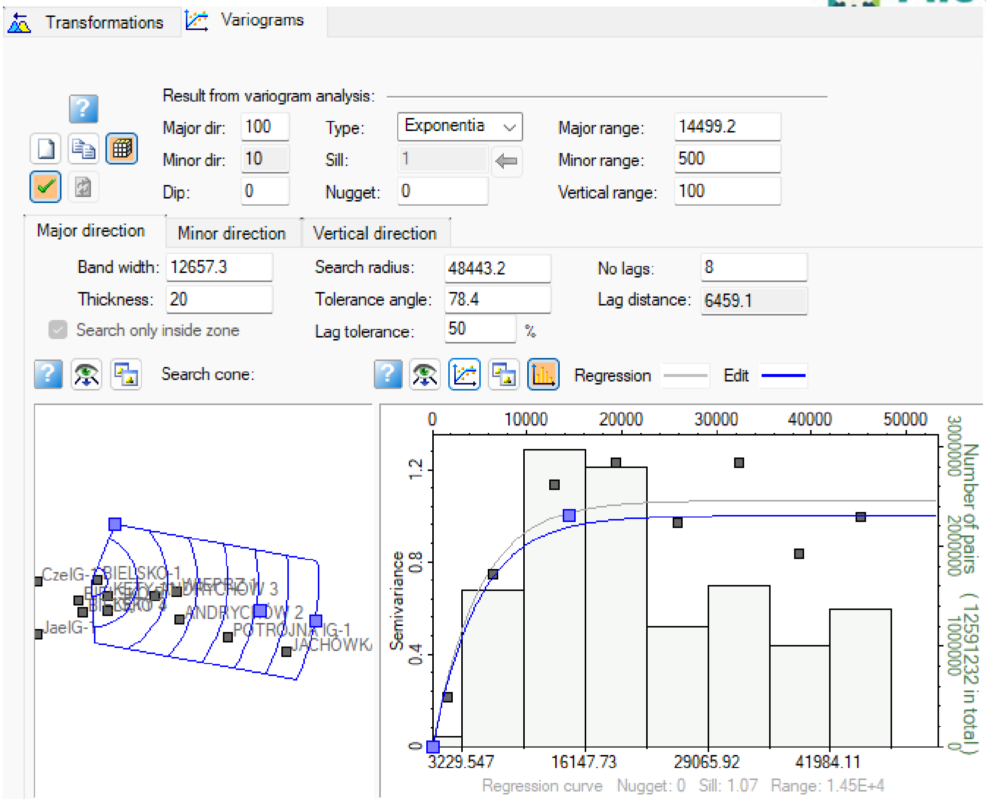

Figure 4.22: Results from variogram analysis – major direction of shale content (reservoir)

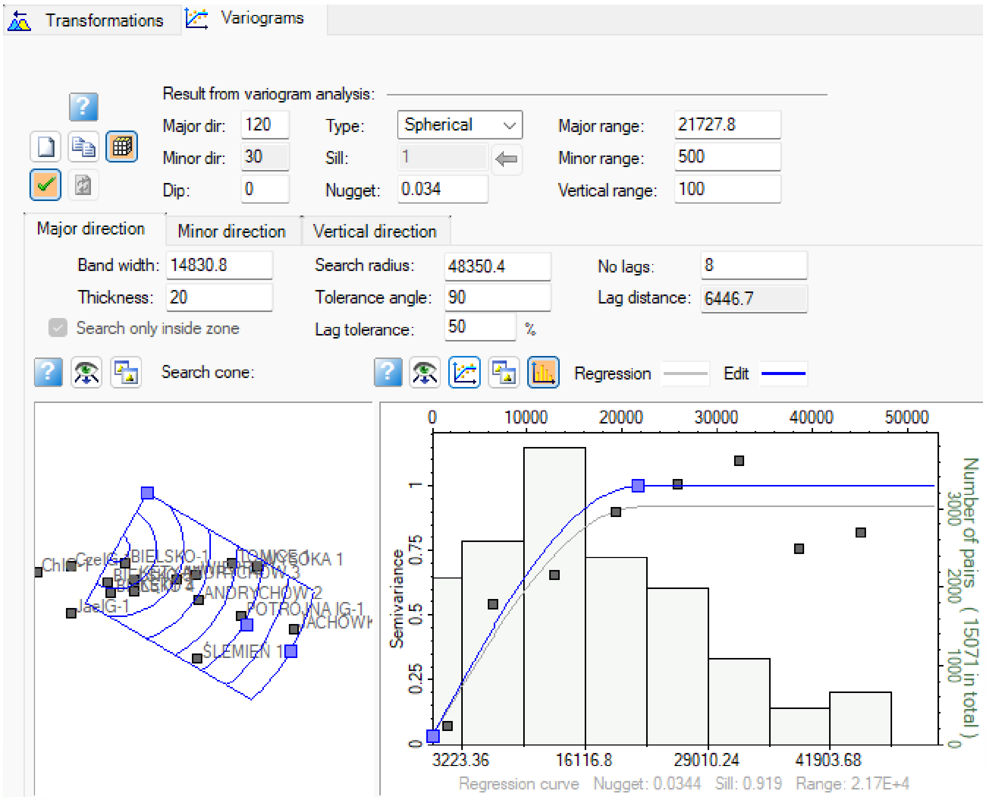

Figure 4.23: Results from variogram analysis – major direction of shale content (sealing layer)

The PilotSTRATEGY project has received funding from the European Union's Horizon 2020 research and innovation programme under grant agreement No. 101022664

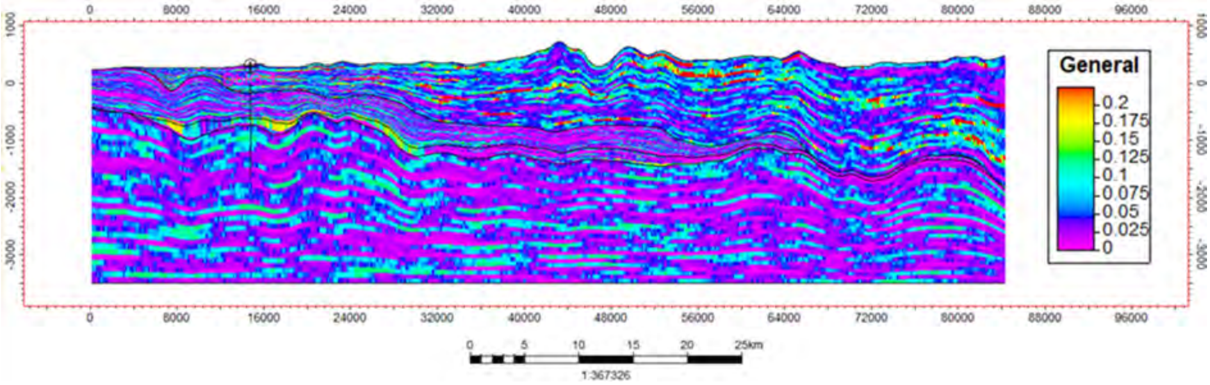

Figure 4.24: Porosity field (one realization, SGS) on the Z-cross-section

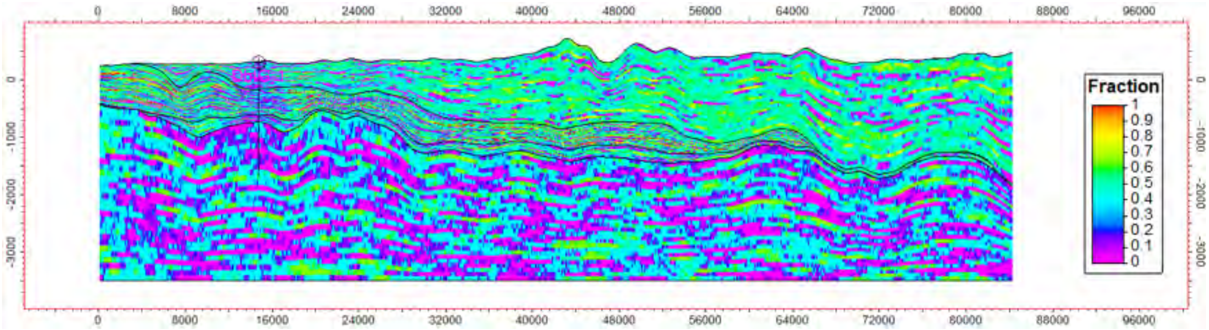

Figure 4.25: Vshale distribution on the Z-cross-section (SGS algorithm, one realization)

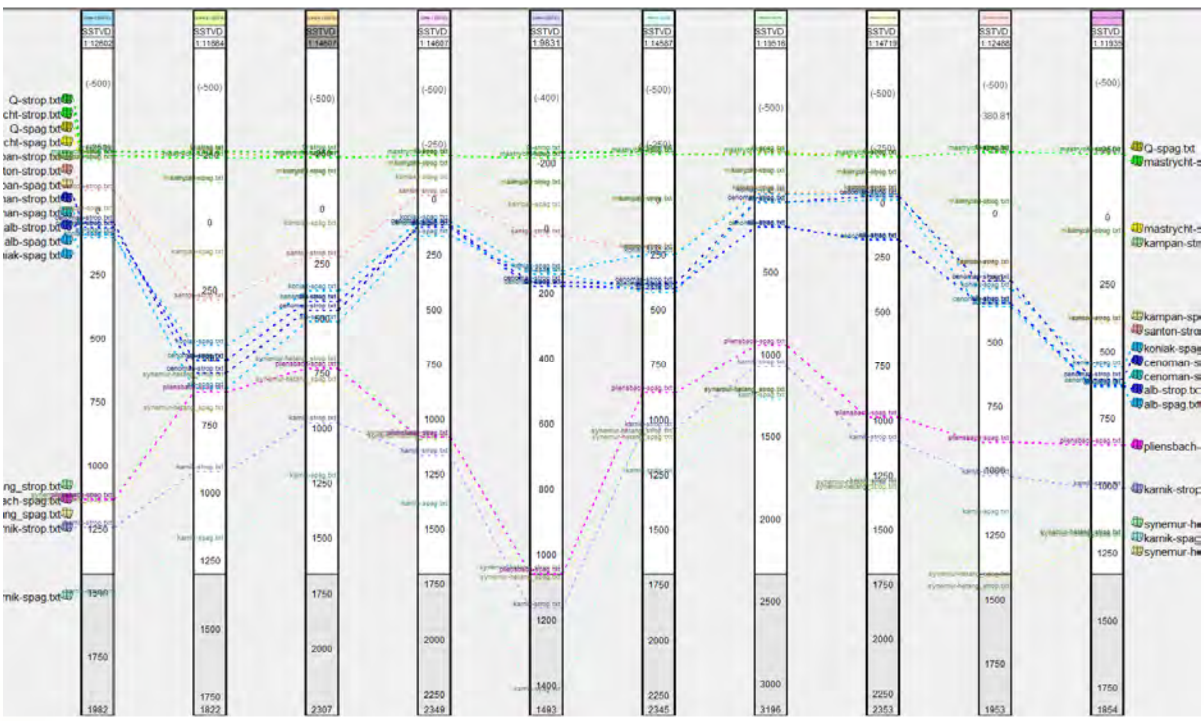

Figure 4.26: Well data correlation and development of structural surfaces in the area of the Jurassic structure

The PilotSTRATEGY project has received funding from the European Union's Horizon 2020 research and innovation programme under grant agreement No. 101022664

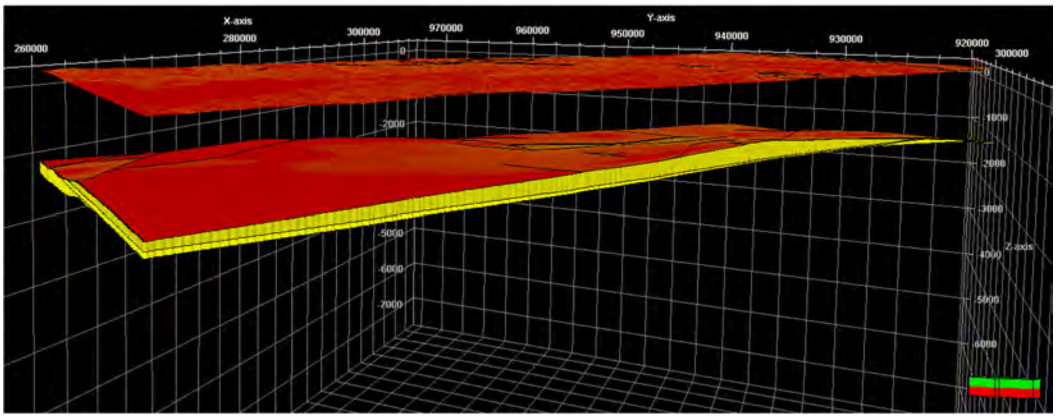

Figure 4.27: Surface area and reservoir layers

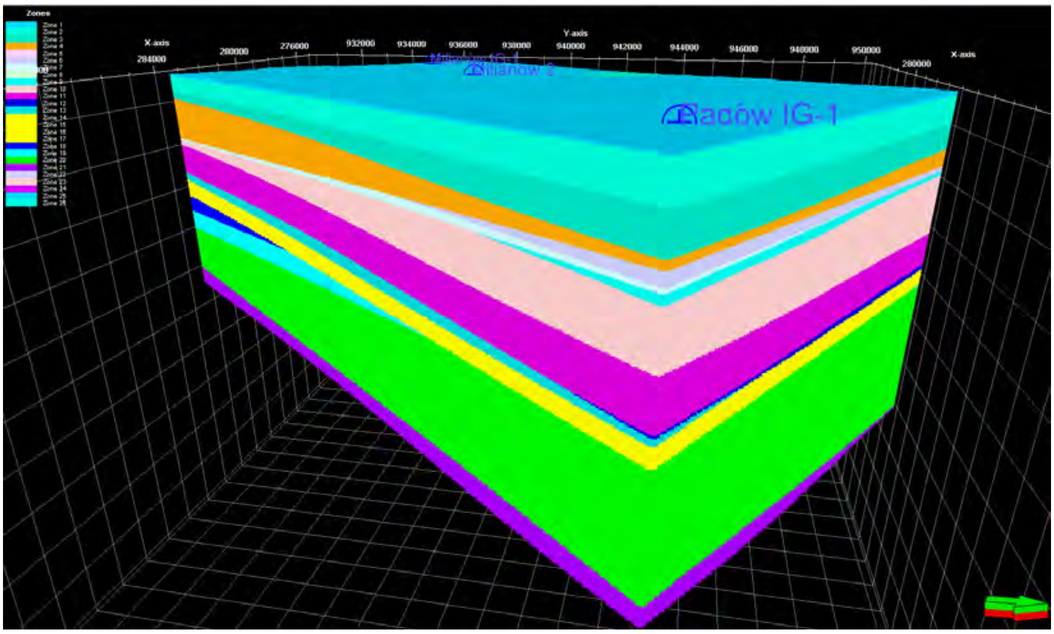

Figure 4.28: Zones model

The PilotSTRATEGY project has received funding from the European Union's Horizon 2020 research and innovation programme under grant agreement No. 101022664

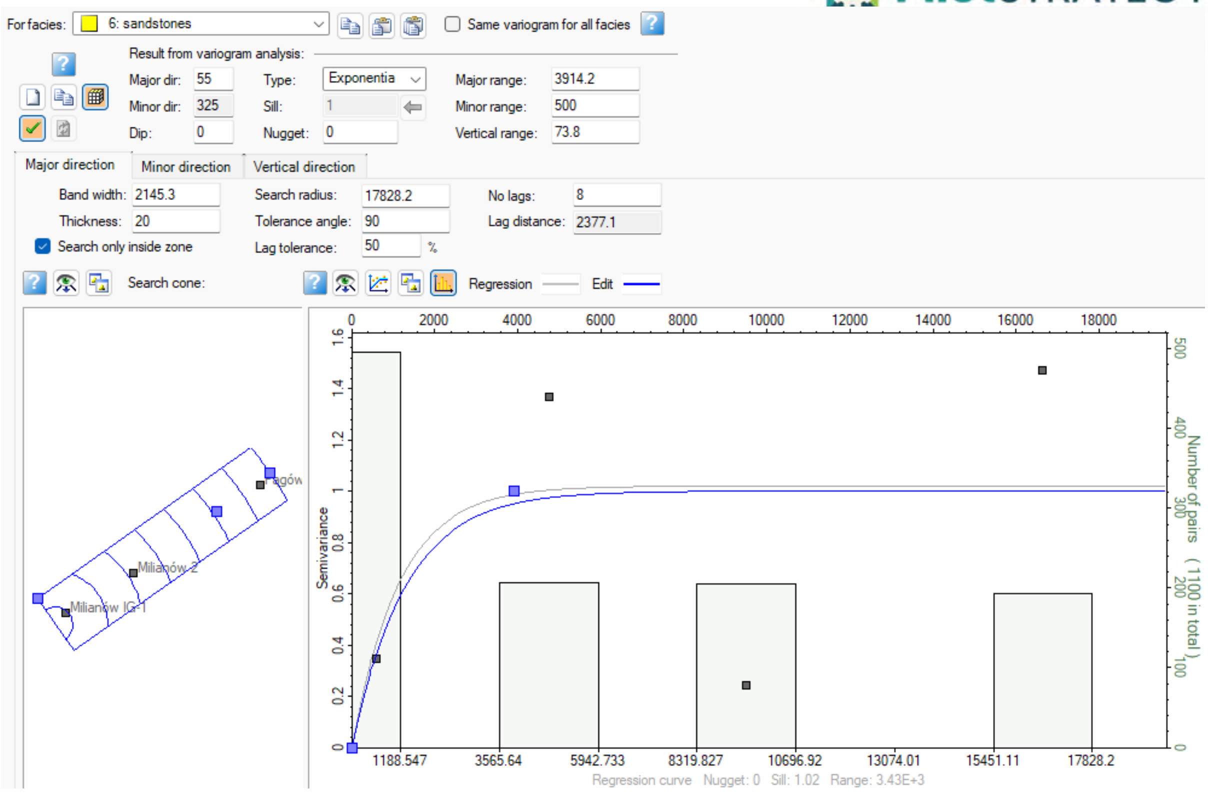

Figure 4.29: Variogram – major direction of sandstones

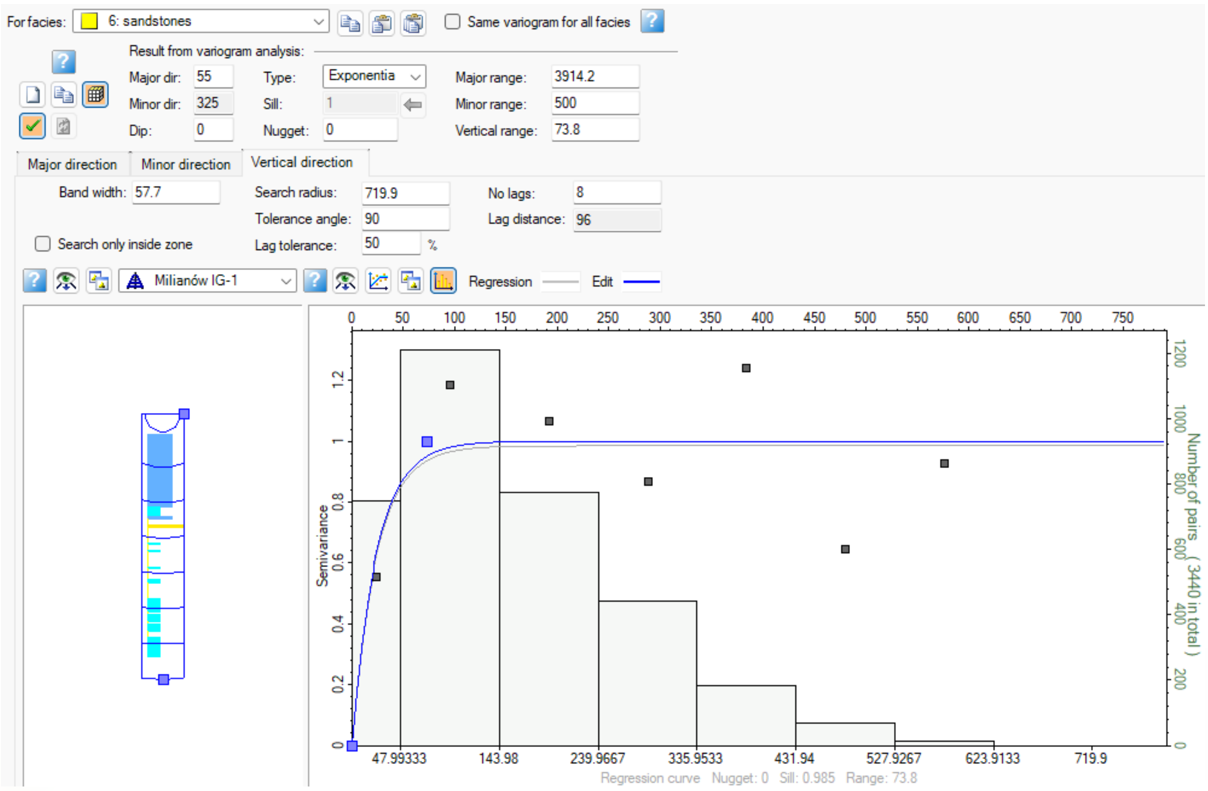

Figure 4.30: Variogram – vertical direction of sandstones

The PilotSTRATEGY project has received funding from the European Union's Horizon 2020 research and innovation programme under grant agreement No. 101022664

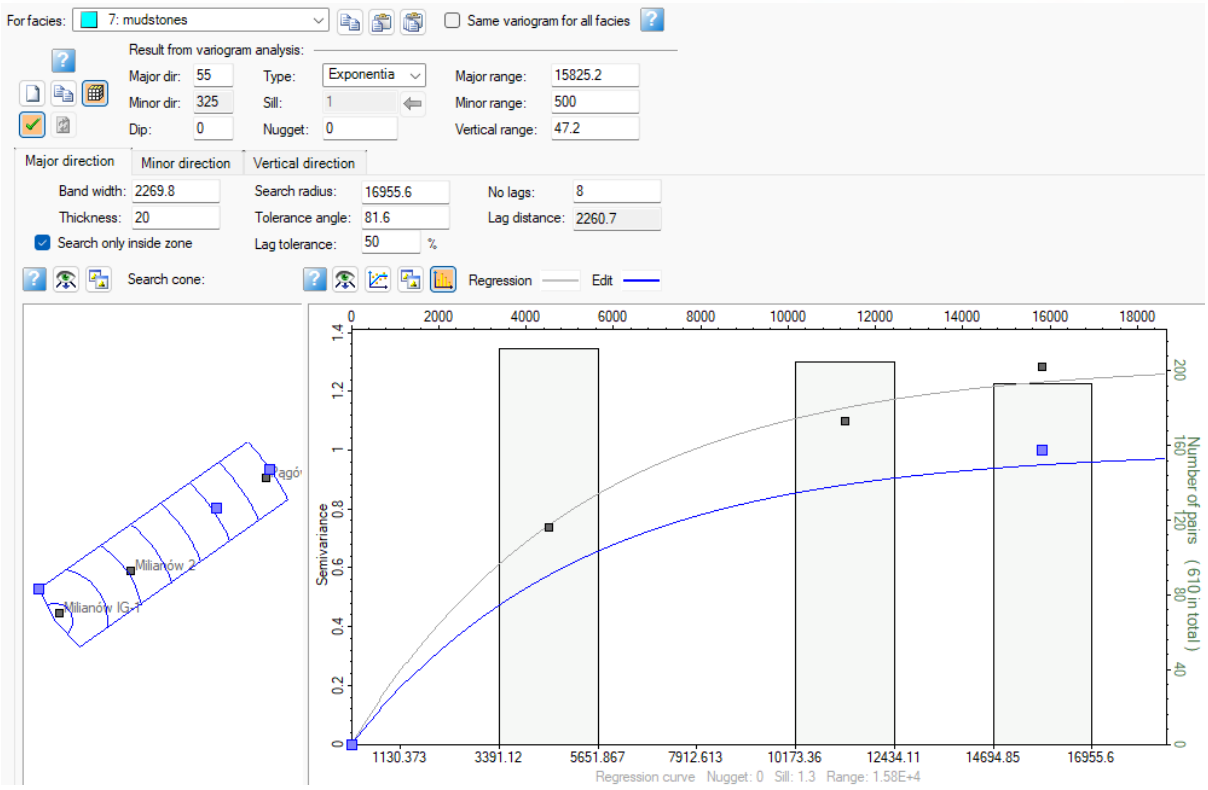

Figure 4.31: Variogram – major direction of mudstones

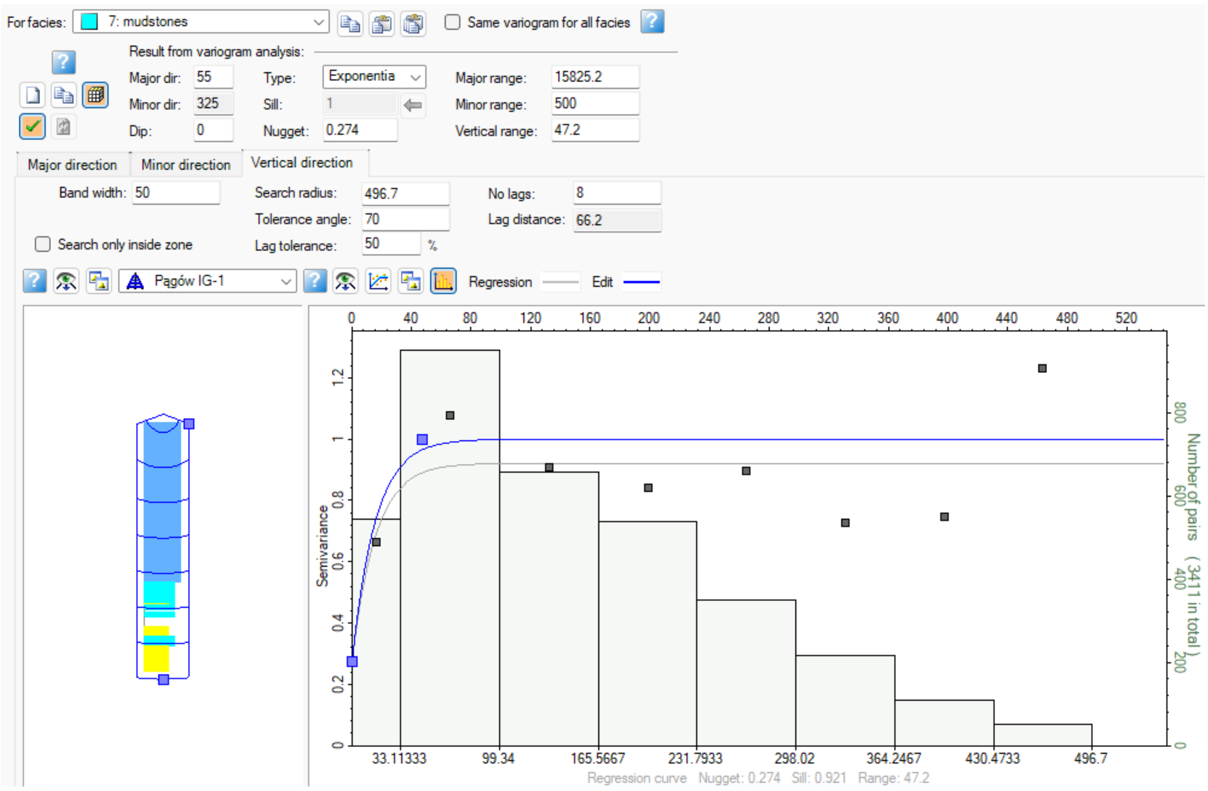

Figure 4.32: Variogram – vertical direction of mudstones

The PilotSTRATEGY project has received funding from the European Union's Horizon 2020 research and innovation programme under grant agreement No. 101022664

Table 4.1: Statistical characteristics of the facies model – sealing layers and reservoir

SEALING LAYER 1								
Code	**Name**	**%**	**N**	**Intervals**	**Min**	**Mean**	**Max**	**Std**
2	claystones	12.93	38906	34190	0.1 (1)	11.6 (1.14)	60.2 (4)	7.257
7	mudstones	79.49	239185	84576	0.1 (1)	28.0 (2.83)	106.1 (5)	21.76
8	limestones	7.58	22809	20847	0.1 (1)	11.2 (1.09)	57.4 (4)	6.49
SEALING LAYER 2								
Code	**Name**	**%**	**N**	**Intervals**	**Min**	**Mean**	**Max**	**Std**
2	claystones	29.11	208037	114222	0.0 (1)	7.3 (1.82)	67.6 (12)	7.16
6	sandstones	16.05	114694	64102	0.0 (1)	5.3 (1.79)	71.1 (10)	6.568
7	mudstones	49.53	353987	141356	0.0 (1)	19.2 (2.5)	110.0 (15)	20.77
8	limestones	3.19	22809	20847	0.1 (1)	11.2 (1.09)	57.4 (4)	6.49
9	conglomerate	2.12	15133	11279	0.0 (1)	3.8 (1.34)	39.1 (5)	4.17
RESERVOIR LAYER 1								
Code	**Name**	**%**	**N**	**Intervals**	**Min**	**Mean**	**Max**	**Std**
2	claystones	31.88	448301	262934	0.0 (1)	9.6 (1.7)	119.6 (18)	8.941
6	sandstones	37.12	521888	235800	0.0 (1)	14.2 (2.21)	150.4 (20)	16.64
7	mudstones	28.30	397899	180671	0.0 (1)	16.8 (2.2)	110.0 (15)	19.12
8	limestones	1.62	22809	20847	0.1 (1)	11.2 (1.09)	57.4 (4)	6.49
9	conglomerate	1.08	15133	11279	0.0 (1)	3.8 (1.34)	39.1 (5)	4.17
RESERVOIR LAYER 1								
Code	**Name**	**%**	**N**	**Intervals**	**Min**	**Mean**	**Max**	**Std**
2	claystones	30.10	497364	301639	0.0 (1)	10.7 (1.65)	173.6 (18)	11.8
6	sandstones	39.15	646977	299072	0.0 (1)	17.0 (2.16)	286.4 (22)	22.86
7	mudstones	28.46	470239	236409	0.0 (1)	17.4 (1.99)	256.4 (15)	20.73
8	limestones	1.38	22809	20847	0.1 (1)	11.2 (1.09)	57.4 (4)	6.49
9	conglomerate	0.92	15133	11279	0.0 (1)	3.8 (1.34)	39.1 (5)	4.17

Table 4.2: Statistical characteristics of the facies model

Statistics for Lithologies								
Entire property statistics:								
Code	**Name**	**%**	**N**	**Intervals**	**Min**	**Mean**	**Max**	**Std**
0	clays	0.44	33177	29112	0.0 (1)	12.1 (1.14)	49.7 (2)	6.716
2	claystones	14.32	1075680	698847	0.0 (1)	37.4 (1.54)	530.3 (18)	39.89
3	shales	3.60	270066	195141	0.0 (1)	73.4 (1.38)	587.8 (9)	46.46
4	marlstones	21.04	1580228	628631	0.1 (1)	44.3 (2.51)	485.2 (25)	39.67
5	sands	1.83	137206	93038	0.0 (1)	19.2 (1.47)	74.5 (3)	10.28
6	sandstones	15.50	1163798	669321	0.0 (1)	35.5 (1.74)	576.6 (21)	40.61
7	mudstones	14.44	1084558	519472	0.0 (1)	40.1 (2.09)	523.6 (18)	46.85
8	limestones	28.55	2144233	689108	0.1 (1)	70.6 (3.11)	806.9 (28)	106.9
9	conglomerate	0.27	20409	14077	0.0 (1)	4.2 (1.45)	36.9 (6)	4.869
Upscaled cells statistics:								
Code	**Name**	**%**	**N**	**Intervals**	**Min**	**Mean**	**Max**	**Std**
0	clays	0.34	1	1	5.6 (1)	5.6 (1)	5.6 (1)	0
2	claystones	14.43	43	5	4.9 (1)	106.5 (8.6)	430.5 (18)	164.2
3	shales	0.67	2	2	48.6 (1)	51.5 (1)	54.3 (1)	2.865
4	marlstones	19.46	58	7	8.6 (1)	123.1 (8.29)	309.5 (23)	122.2
5	sands	1.68	5	3	12.5 (1)	25.9 (1.67)	38.3 (2)	10.58
6	sandstones	14.77	44	13	2.6 (1)	40.3 (3.38)	108.7 (7)	30.68
7	mudstones	17.45	52	9	4.9 (1)	95.0 (5.78)	353.1 (18)	138.4
8	limestones	30.87	92	8	33.7 (1)	250.6 (11.5)	744.7 (26)	226
9	conglomerate	0.34	1	1	7.3 (1)	7.3 (1)	7.3 (1)	0

The PilotSTRATEGY project has received funding from the European Union's Horizon 2020 research and innovation programme under grant agreement No. 101022664

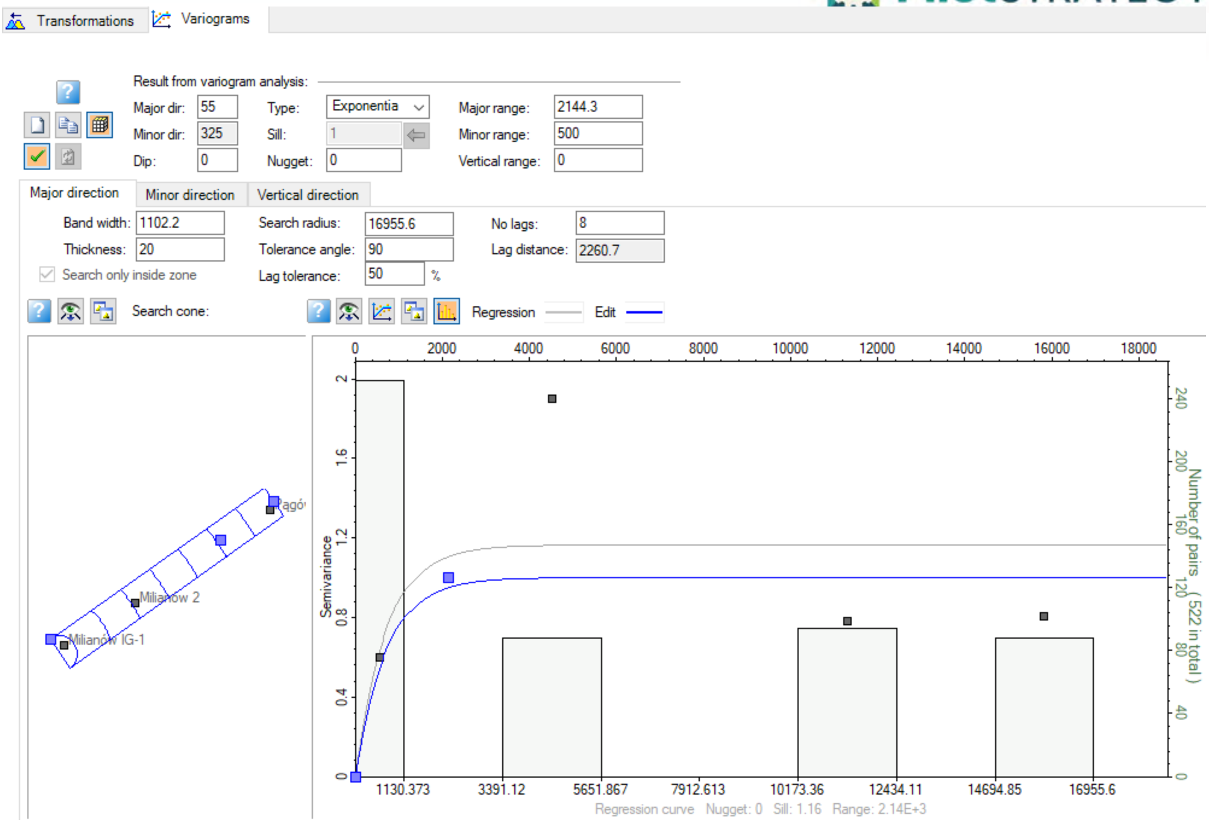

Figure 4.33: Results from variogram analysis – major direction of porosity (the layer of primary seal)

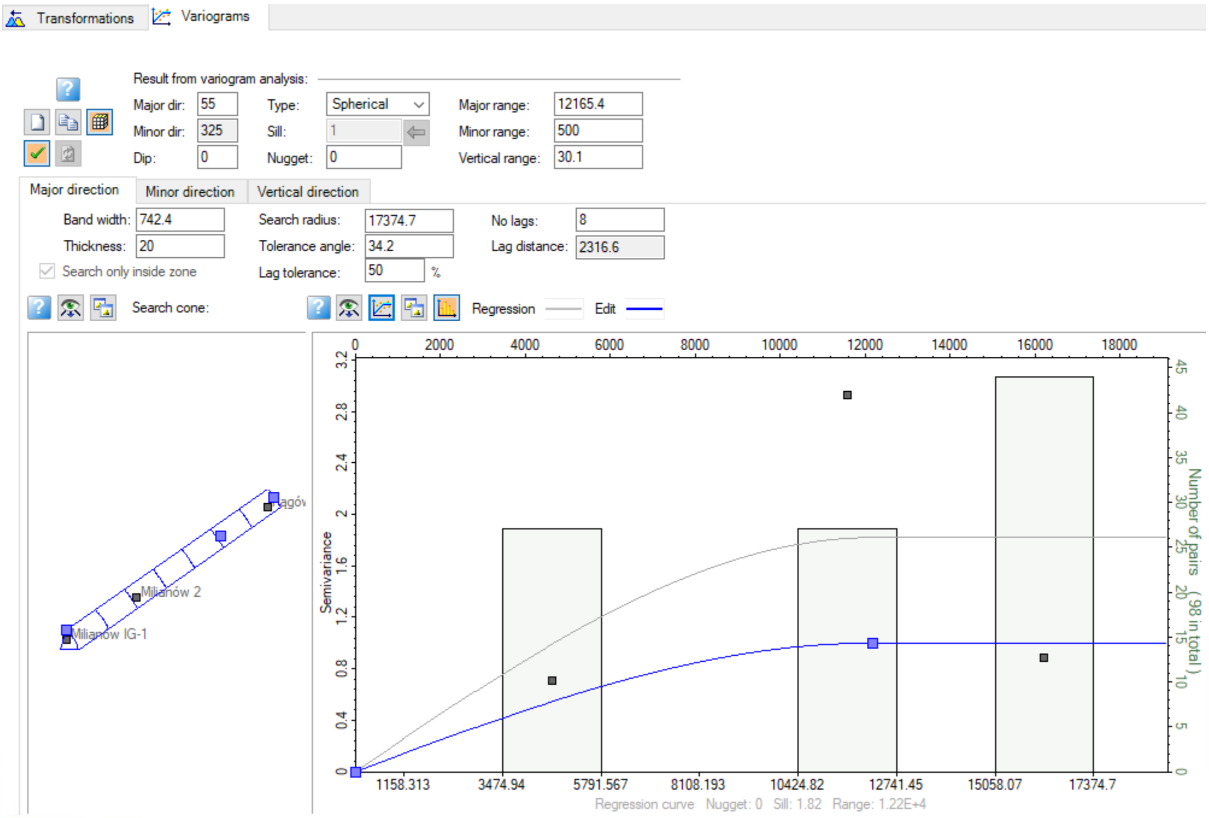

Figure 4.34: Results from variogram analysis – major direction of porosity (the layer of reservoir)

The PilotSTRATEGY project has received funding from the European Union's Horizon 2020 research and innovation programme under grant agreement No. 101022664

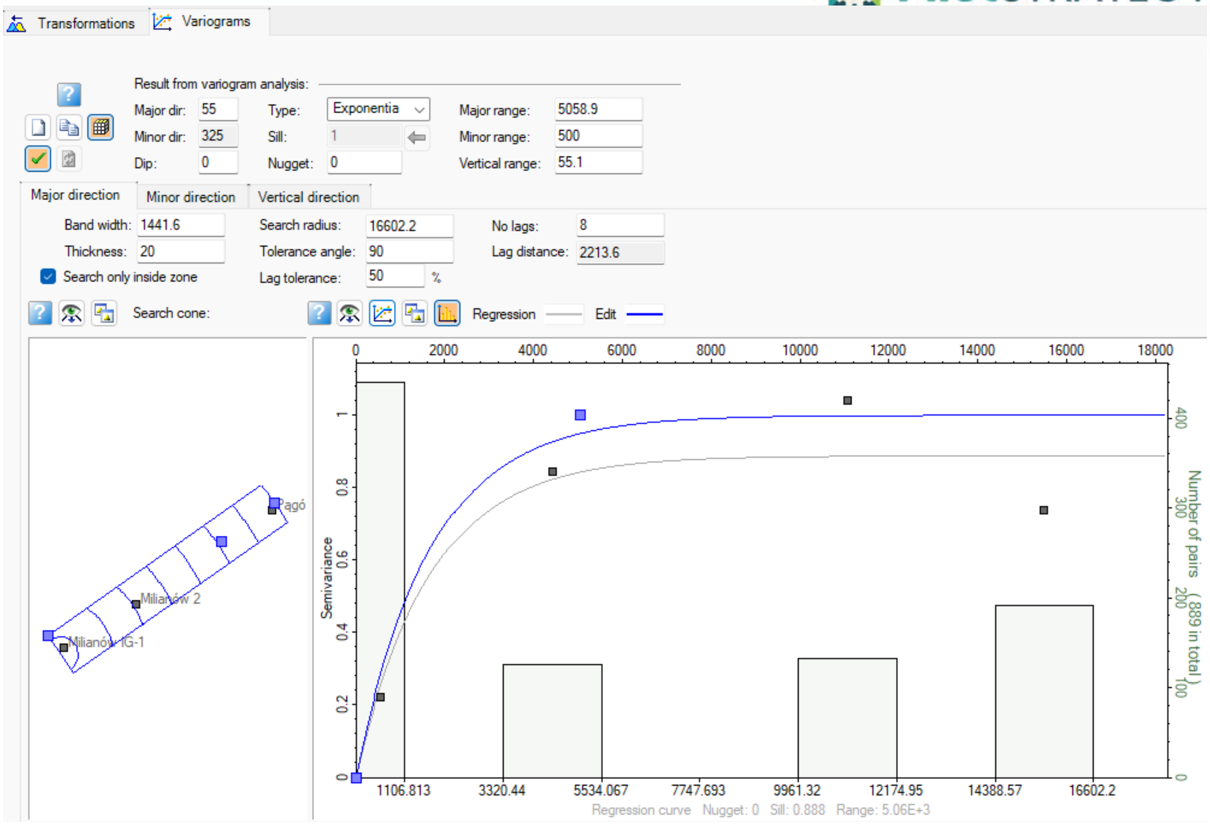

Figure 4.35: Results from variogram analysis – major direction of porosity

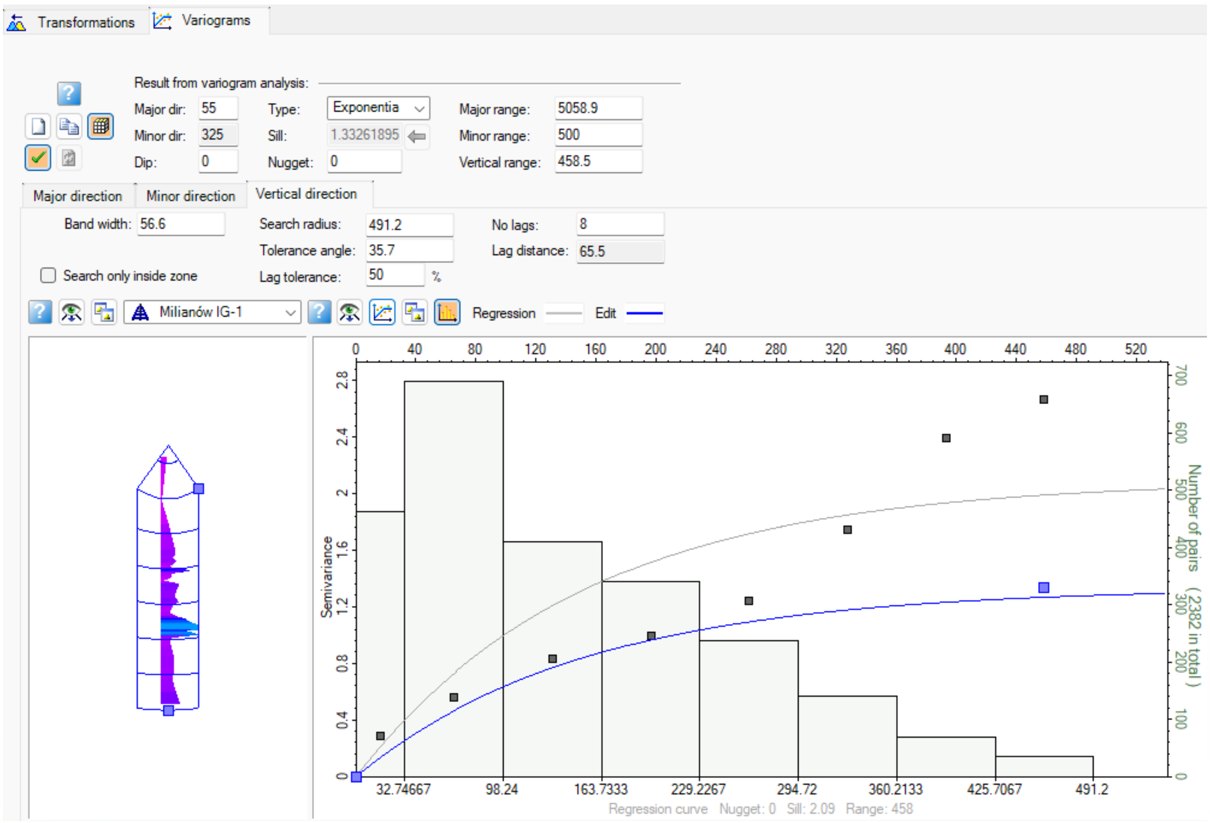

Figure 4.36: Results from variogram analysis – vertical direction of porosity

The PilotSTRATEGY project has received funding from the European Union's Horizon 2020 research and innovation programme under grant agreement No. 101022664

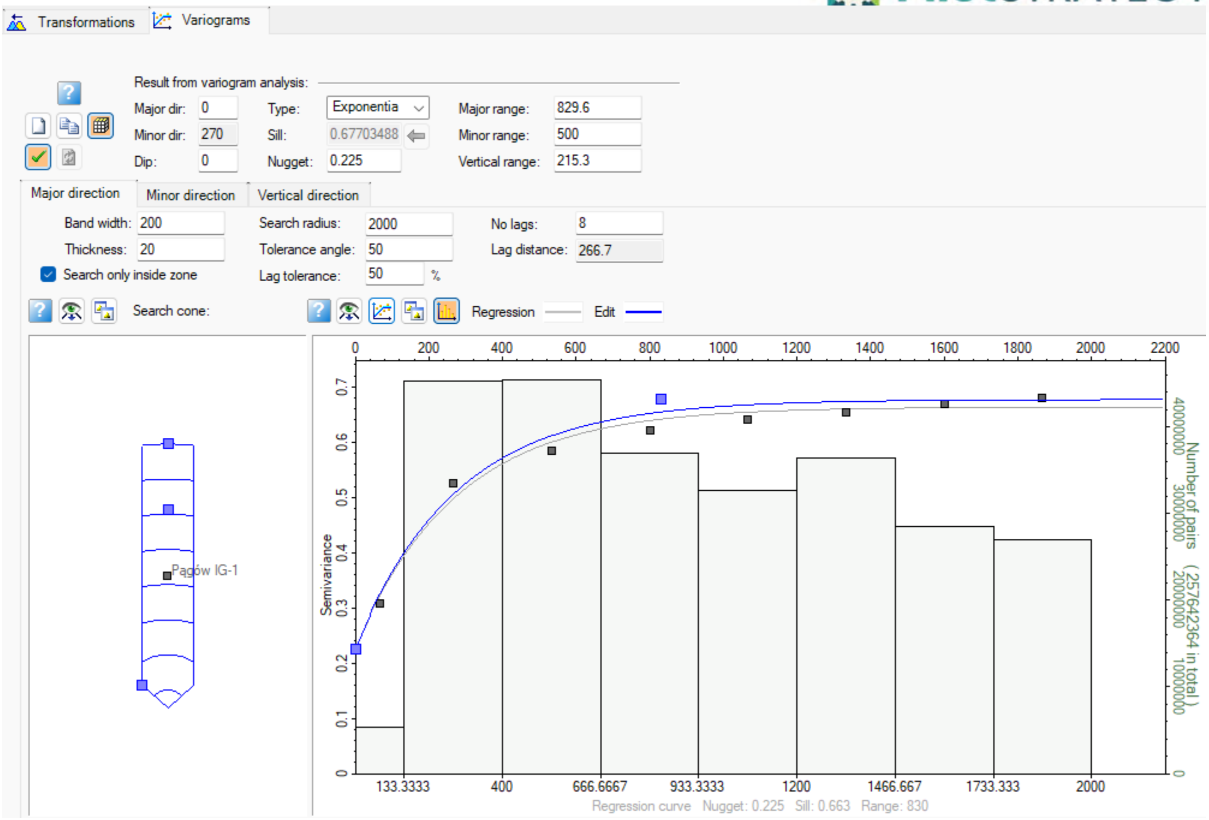

Figure 4.37: Results from variogram analysis – major direction of permeability

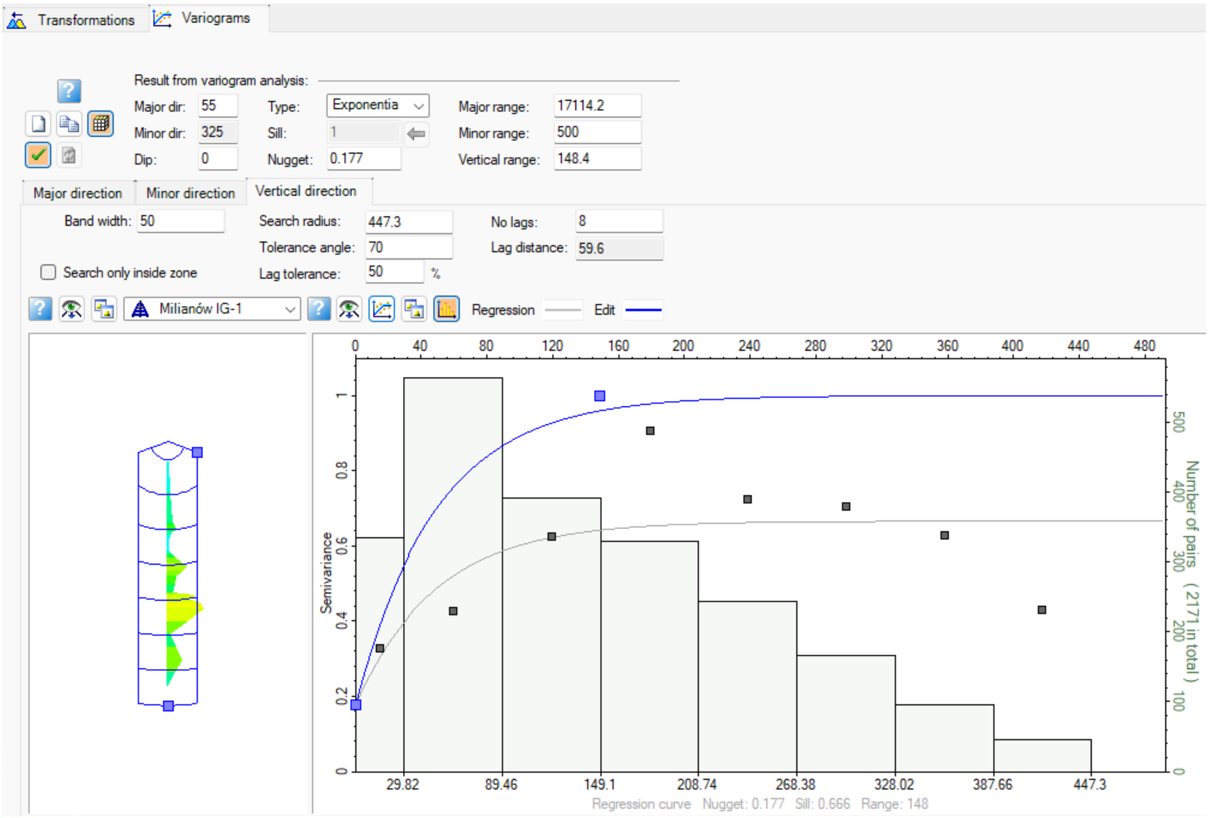

Figure 4.38: Results from variogram analysis – vertical direction of permeability

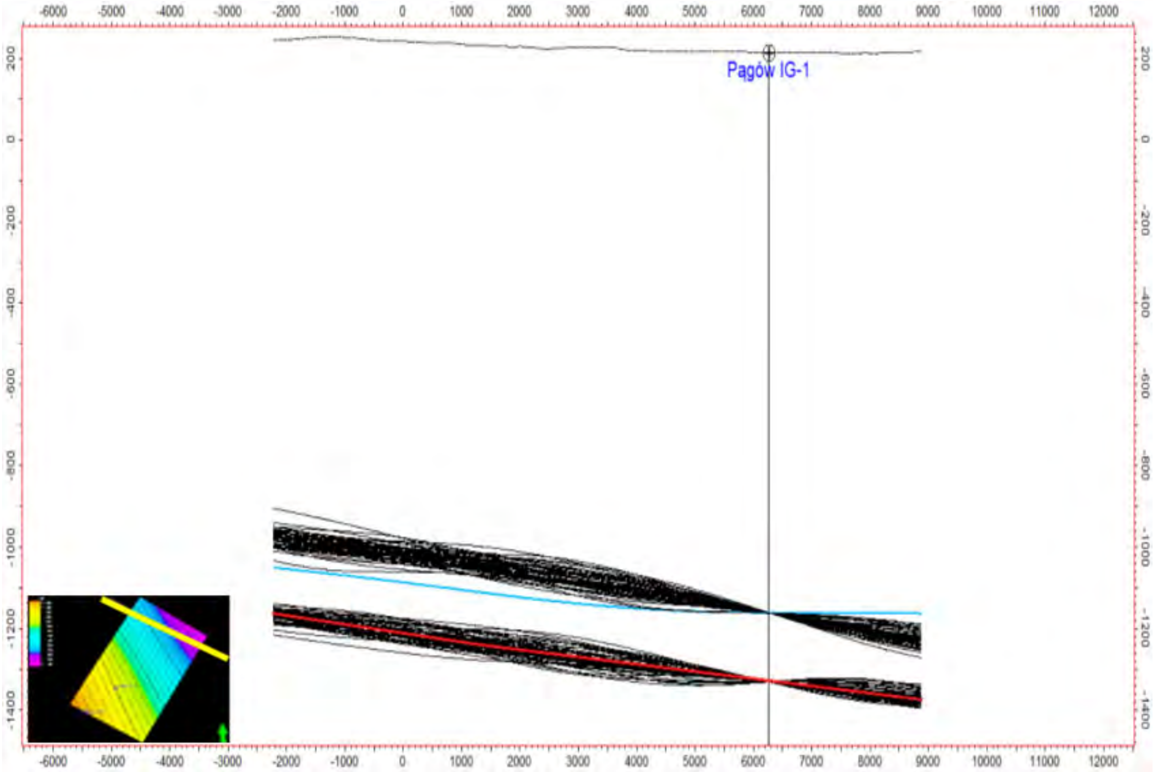

Figure 4.39: Surfaces of the Lower Jurassic floor (red line) and Middle Jurassic top (blue line) and 50 stochastic variants (black lines) on cross-section

7.3 Additional information, figures and tables for Lusitanian Basin (Portugal) (5)

7.3.1 Conceptual Geological Model

7.3.1.1 Additional Insights and Information (analogue areas)

The potential Q4-TV1 prospect, located close to the well Do-1C (Figure 5.1), is partially covered by a 3D offshore volume of seismic reflection data (fullstack) available in its southeast area. However, it is possible to retrieve relevant information from this geophysical data for the prospect property modelling based on analogue areas where the seismic data has a better areal coverage. The location of these analogue areas of the 3D seismic data are illustrated in Figure 5.1a, in which quantitative reservoir characterization studies (geostatistical seismic inversion) were conducted, and in Figure 5.1b, in which this part of the 3D seismic data was considered for the horizontal variogram modelling for the reservoir unit and both primary and secondary seal regions.

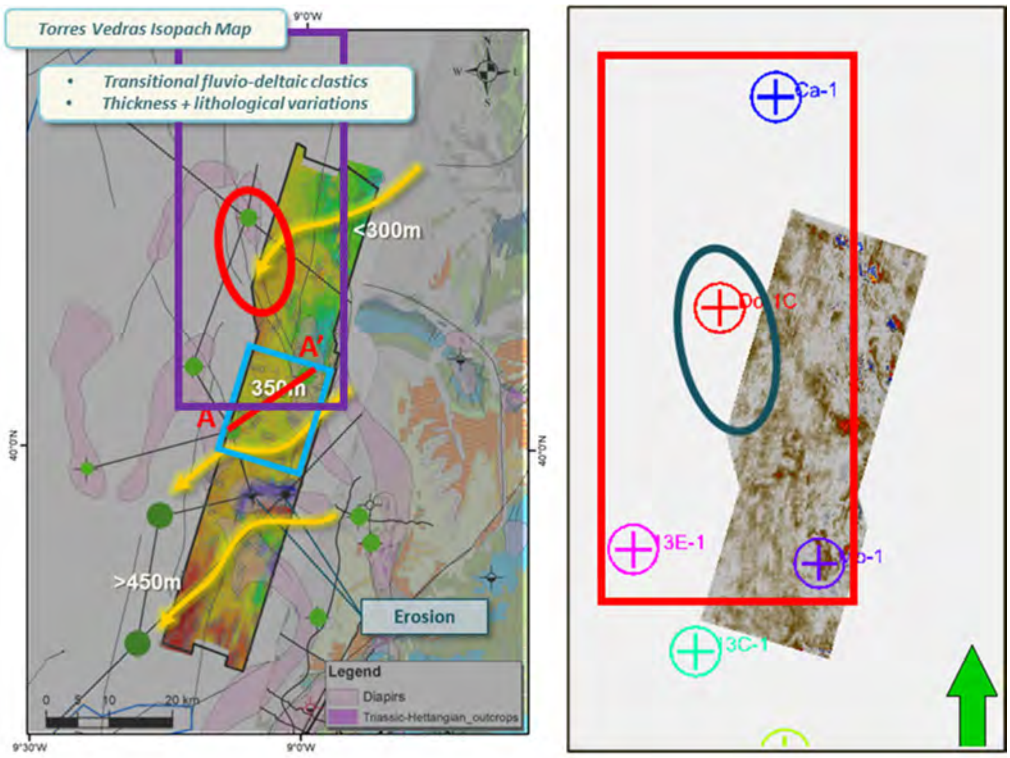

(a) (b)

Figure 5.1: (a) Simplified sedimentary fairways for the Torres Vedras Group reservoir (adapted from Wilkinson et al. 2023), the location of the offshore 3D seismic volume, and the cross-section (red) between the wells 13C-1 and Mo-1 at the analogue area (blue) considered to apply the quantitative characterization methods; (b) part of the 3D seismic volume used for the horizontal variogram modelling. The Q4-TV1 prospect location is illustrated by the red ellipse (a) and the blue ellipse (b), and the static model boundaries by the purple rectangle (a) and the red rectangle (b).

7.3.1.2 Spatial Continuity Analysis

For the horizontal variogram modelling, different azimuths were firstly analysed for both main and minor horizontal directions from the 3D seismic volume of the analogue area using Petrel® software. Due to the lack of a good well data coverage of the study area, the horizontal variogram ranges

The PilotSTRATEGY project has received funding from the European Union's Horizon 2020 research and innovation programme under grant agreement No. 101022664

computed from the seismic data were used for the simulation of the lithofacies and petrophysical models.

The searching parameters used are listed in the Table 5.1 and were kept the same for the variogram analysis of the three main regions of the static model: the reservoir unit and the primary and secondary seal. It is important to mention that before performing the variogram modelling analysis and fitting, the seismic resampling of the original seismic data of this analogue area was conducted to the static model according to the resolution (i.e., the grid cell dimensions) of the reservoir and primary and secondary seal regions. More details about the areal and vertical grid cell dimensions for each of these static model regions are presented in the structural modelling section.

Table 5.1: Searching parameters for the horizontal variogram modelling at the analogue area of the 3D seismic volume for all the three static model regions: reservoir and primary and secondary seals.

Number Lags	Lag Distance (m)	Search Radius (m)	Band width (m)	Tolerance Angle (º)	Lag Tolerance
20	500	10 000	2500	45	100

The seismic data for the reservoir unit presents an anisotropic spatial behaviour, ranging the preferential directions between 30º NE-SW and 60º NE-SW. This is consistent with the information of the reservoir depositional model, in which the main sedimentary fairways at the location of the static model (Figure 5.1) and for the potential Q4-TV1 prospect are also within this range of azimuth values, with an average value of about 45º NE-SW. This is the azimuth value used for the main horizontal direction, while the orthogonal azimuth value of 135º NW-SE was used for the minor horizontal direction.

The experimental variograms for the reservoir were fitted by exponential models of one structure as illustrated in Figure 5.2 and the variogram parameters are presented in Table 5.2.

(a)

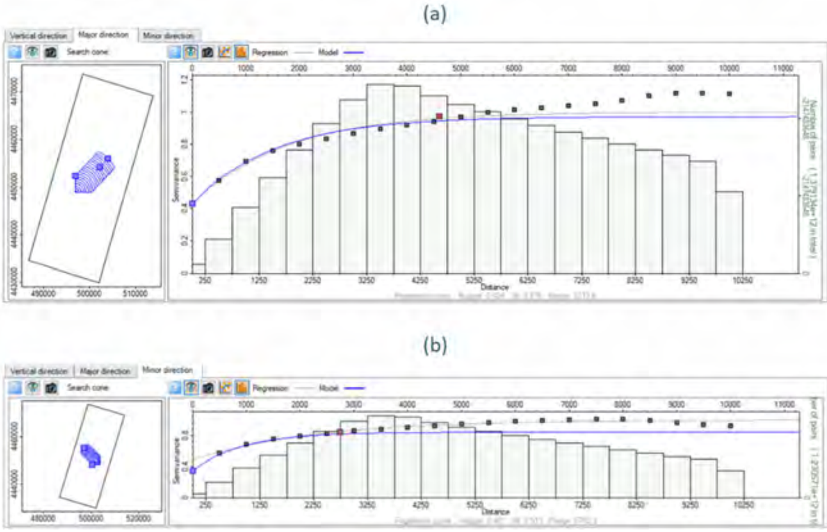

(b)

Figure 5.2: Experimental variogram model fitting for the Reservoir region (Torres Vedras Group) at the analogue area: (a) main horizontal direction of 45º and (b) minor horizontal direction of 135º.

Table 5.2: Variogram parameters for the Reservoir region (Torres Vedras Group).

The PilotSTRATEGY project has received funding from the European Union's Horizon 2020 research and innovation programme under grant agreement No. 101022664

Variogram Model	Azimuth (º)	Main Direction Range (m)	Minor Direction Range (m)
Exponential	45 [+15,-15]	6250 [4500, 8000]	3750 [2500,5000]

The experimental data presents a nugget effect of about 0.3-0.4 due to the existence of small-scale variability of the seismic data. Interval ranges between 4500-8000m and 2500-5000m were considered for the main and minor horizontal directions, respectively, presenting a horizontal anisotropy ratio of 1.8.

The experimental variograms for the primary seal were fitted by exponential models of one structure as illustrated in Figure 5.3 and the variogram parameters are presented in Table 5.3. The azimuth analysis was conducted for the primary seal presenting the preferential direction (anisotropy) within the range of 30-60º NE-SW, therefore an average azimuth of 45º NE-SW was considered for the variogram modelling. The experimental data presents a nugget effect of about 0.3-0.4 and the interval ranges between 2000-4500m and 1500-3000m were considered for the main and minor horizontal directions, respectively, presenting an anisotropy ratio of about 1.5-2.5.

(a)

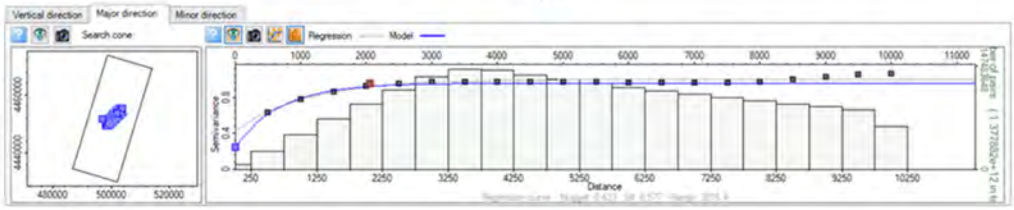

(b)

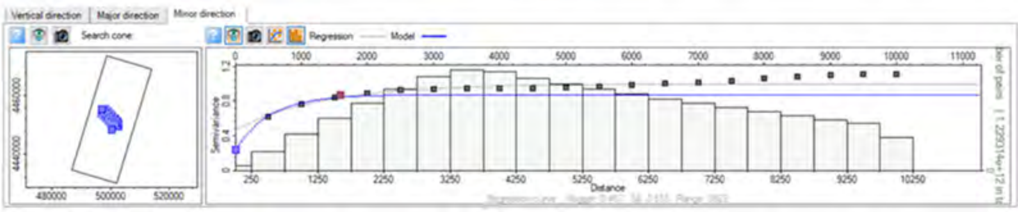

Figure 5.3: Experimental variogram model fitting for the Primary Seal region (Cacém Fm.) at the analogue area: (a) main horizontal direction of 45º and (b) minor horizontal direction of 135º.

Table 5.3: Variogram parameters for the Primary Seal region (Cacém Fm.).

Variogram Model	Azimuth (º)	Main Direction Range (m)	Minor Direction Range (m)
Exponential	45 [+15,-15]	3250 [2000,4500]	2250 [1500,3000]

Figure 5.4 illustrates the experimental variograms of the secondary seal for the main and minor horizontal directions, considering the average azimuth values of 45º NE-SW. The variogram parameters are presented in Table 5.4.

The PilotSTRATEGY project has received funding from the European Union's Horizon 2020 research and innovation programme under grant agreement No. 101022664

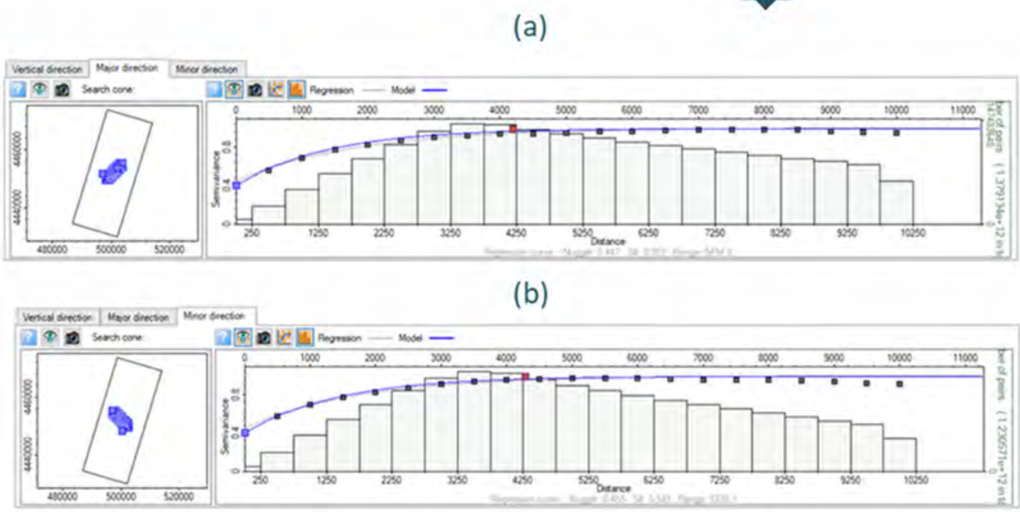

Figure 5.4: Experimental variogram model fitting for the Secondary Seal region (Aveiro Group) at the analogue area: (a) main horizontal direction and (b) minor horizontal direction: (a) main horizontal direction of 45º and (b) minor horizontal direction of 135º.

Table 5.4: Variogram parameters for the Secondary Seal region (Aveiro Group).

Variogram Model	Azimuth (º)	Main Direction Range (m)	Minor Direction Range (m)
Exponential	45 [+15,-15]	6250 [4000,8500]	5000 [4000,6000]

These horizontal variogram models from the seismic data for the three static model regions were used in the facies and petrophysical modelling workflow to reproduce the areal spatial distribution of the rock properties due to the lack of enough well data.

7.3.1.3 Seismic Inversion

Besides the variogram modelling, quantitative seismic characterisation studies of other analogue area located within the 3D seismic volume and south of the Q4-TV1 prospect (Figure 5.1) have been conducted for further insights about the depositional (lithofacies) model and reservoir properties.

Iterative geostatistical seismic inversion methods (GSI; Soares 2007, Pereira et al. 2020) and stochastic simulation and co-simulation algorithms (Soares 2001, Horta & Soares 2010) have been used to infer the acoustic and petrophysical properties of the reservoir unit.

The geo-modelling workflow of this seismic inversion method allows to generate acoustic impedance models conditioned to the well-log data (wells 13C-1 and Mo-1) and derived from the 3D fullstack seismic data of the analogue area. From the seismic inversion process, a set of acoustic impedance models were simulated using stochastic sequential simulation. From these models, effective porosity models were co-simulated, allowing to obtain a lithofacies volume of this analogue area. Due to the quality and resolution of the 3D fullstack seismic data, the identification of small-scale reservoir features is difficult to retrieve, requiring further analysis.

Figure 5.5 illustrates a cross-section of effective porosity for the reservoir and seal. It is visible the presence of intercalations between low to high porosity values in the area between the wells, but also close to the well Mo-1, corresponding to reservoir interbedded clays and sands layers. This vertical layering must be reproduced in the reservoir unit of the static model. The low porosity values nearby

The PilotSTRATEGY project has received funding from the European Union's Horizon 2020 research and innovation programme under grant agreement No. 101022664

the area of the well 13C-1 suggests a presence of a high shaly reservoir area, that can also be verified by the reservoir lithofacies model of Figure 5.6, while the area surrounding the Mo-1 is mainly composed by sands. In addition, the resulting lithofacies proportions of the reservoir in this analogue area, such as about 80% sands and 20% of clays, can also be used to compare with the proportions distribution of the reservoir region of the static model, although the clay content of the reservoir area in the static model is expected to be higher (about 40%) than in this analogue area, which the sand proportion is high mainly due to the high net-to-gross value (about 82%) of the well Mo-1. This information is relevant to deepen the geological understanding that can be transferred from the analogue area to the static model as the well Mo-1 locates inside the area of the static model and the well 13C-1, despite it is outside, it locates in a structural high and presents similar reservoir properties compared to the well 13E-1, which is in the southern area of the static model (Figure 5.1).

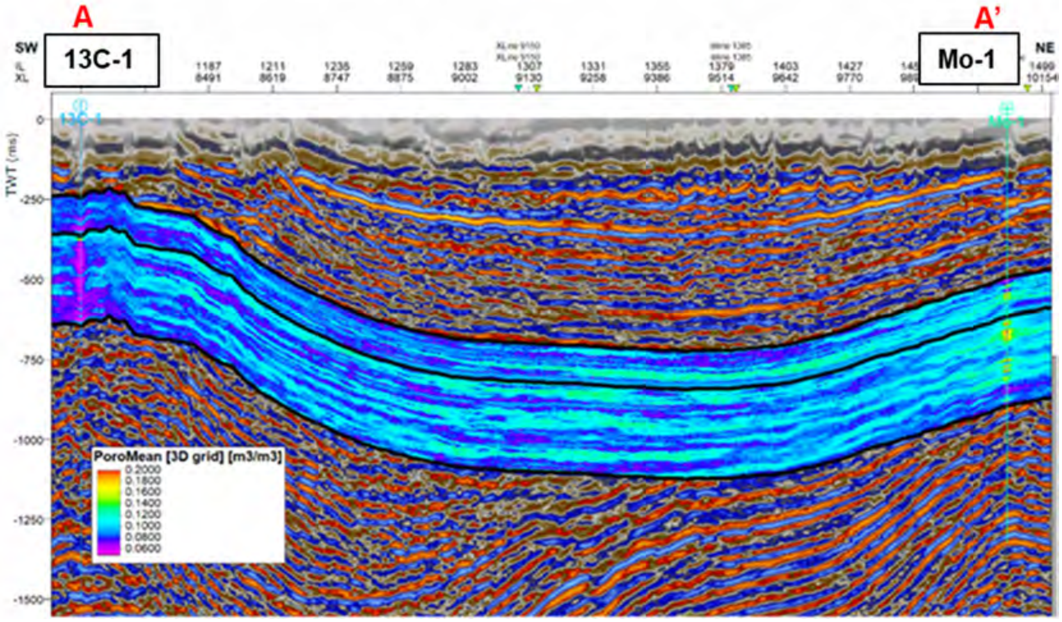

Figure 5.5: Cross-section of the reservoir effective porosity of the analogue area with the 3D fullstack seismic data in the background.

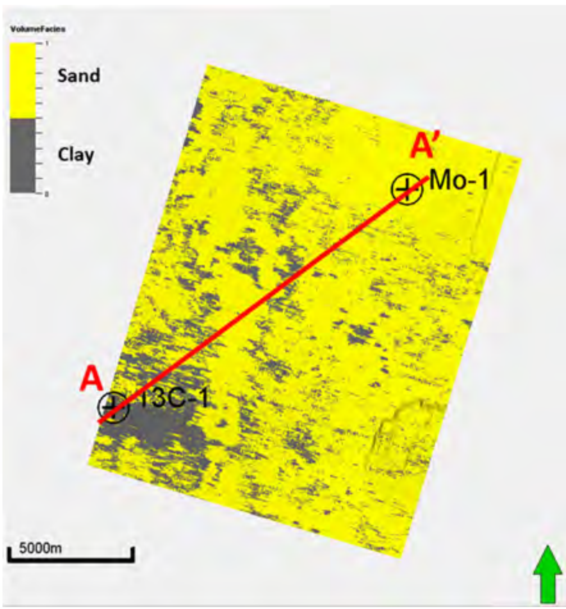

The PilotSTRATEGY project has received funding from the European Union's Horizon 2020 research and innovation programme under grant agreement No. 101022664

Figure 5.6: Reservoir layer of the lithofacies model in the analogue area. The red line indicates the cross-section between the wells of Figure 5.5.

7.3.2 Exploratory Data Analysis

7.3.2.1 Lithofacies

7.3.2.1.1 Eocene-Miocene

The Eocene-Miocene region is intercepted by the well Mo-1 only, as illustrated by the histogram of Figure 5.7, presenting the clay lithofacies for the entire unit of the model.

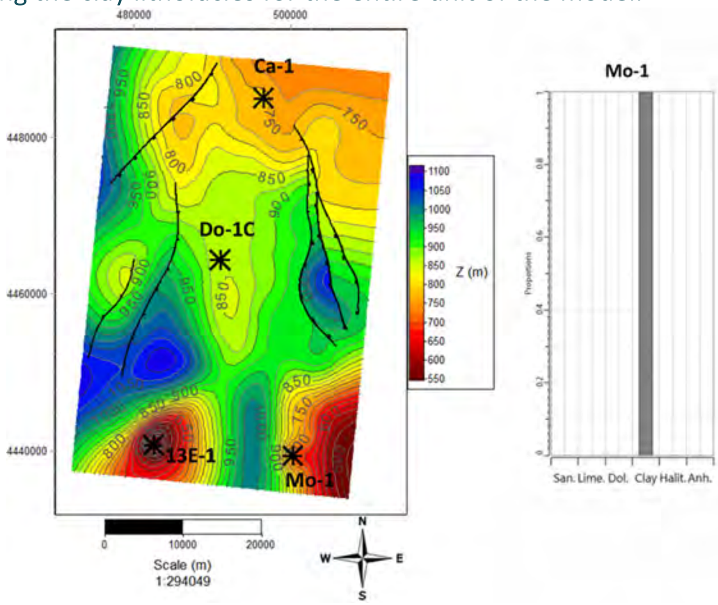

Figure 5.7: Histograms of the available well-log lithofacies of the Eocene-Miocene region.

7.3.2.1.2 Paleocene

Similar as for the Eocene-Miocene region, the well Mo-1 is the only well that intercepts the Paleocene region of the model, presenting a proportion higher than 80% of clay lithofacies and less than 20% of sandstone lithofacies (Figure 5.8).

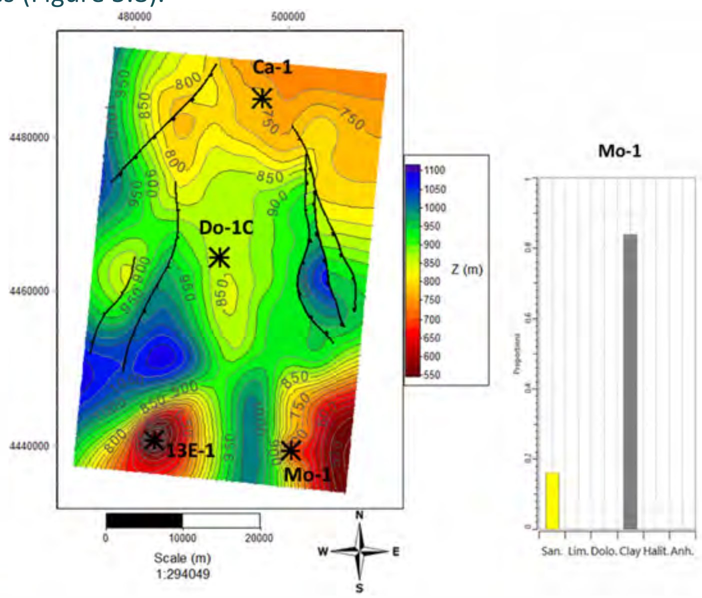

The PilotSTRATEGY project has received funding from the European Union's Horizon 2020 research and innovation programme under grant agreement No. 101022664

Figure 5.8: Histograms of the available well-log lithofacies of the Paleocene region.

7.3.2.1.3 Upper Cretaceous – Secondary Seal

Three wells of the available dataset contain data in the secondary seal unit (Upper Cretaceous), as illustrated in Figure 5.9, in which the well Do-1C presents a more uniform lithofacies proportion distribution of sandstone, limestone and clay (with a higher proportion of sandstone), the well 13E-1 is classified as limestone only, and the well Mo-1 presents mostly clay (although a small percentage of sandstone and limestone is also present). The well Ca-1 also intercepts this region; however, the full set of composite logs were not available to allow the lithofacies classification for this unit.

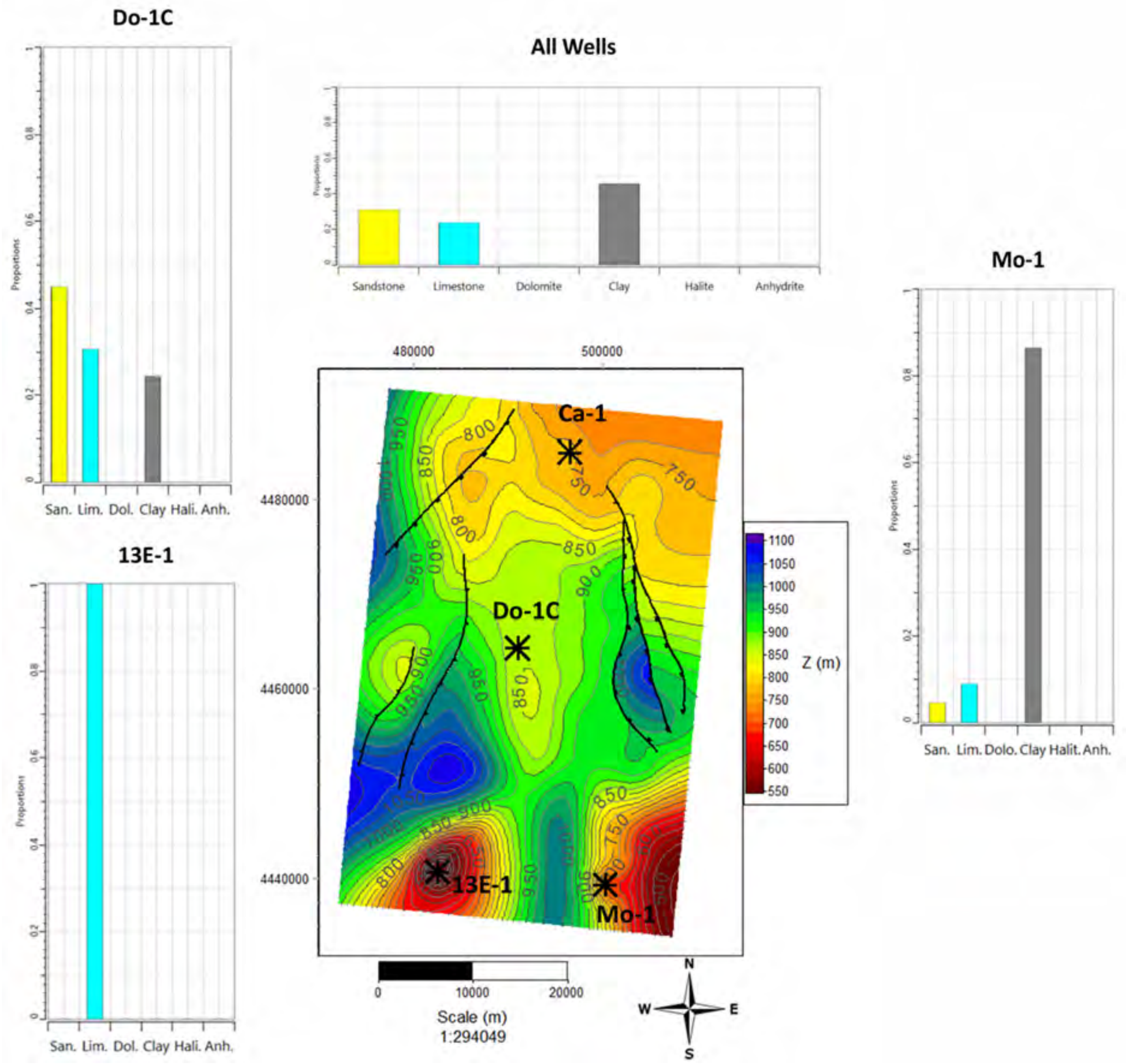

Figure 5.9: Histograms of the available well-log lithofacies of the Upper Cretaceous – Secondary Seal region.

7.3.2.1.4 Upper Cretaceous – Primary Seal

The primary seal unit (Upper Cretaceous region) is mainly composed by limestone lithofacies, representing more than 90% of the total lithofacies proportions of the wells Do-1C, 13E-1 and Mo-1

The PilotSTRATEGY project has received funding from the European Union's Horizon 2020 research and innovation programme under grant agreement No. 101022664

as illustrated in Figure 5.10. Similar as for the secondary seal unit, there was no data available for the lithofacies classification of the primary seal in the location of the well Ca-1.

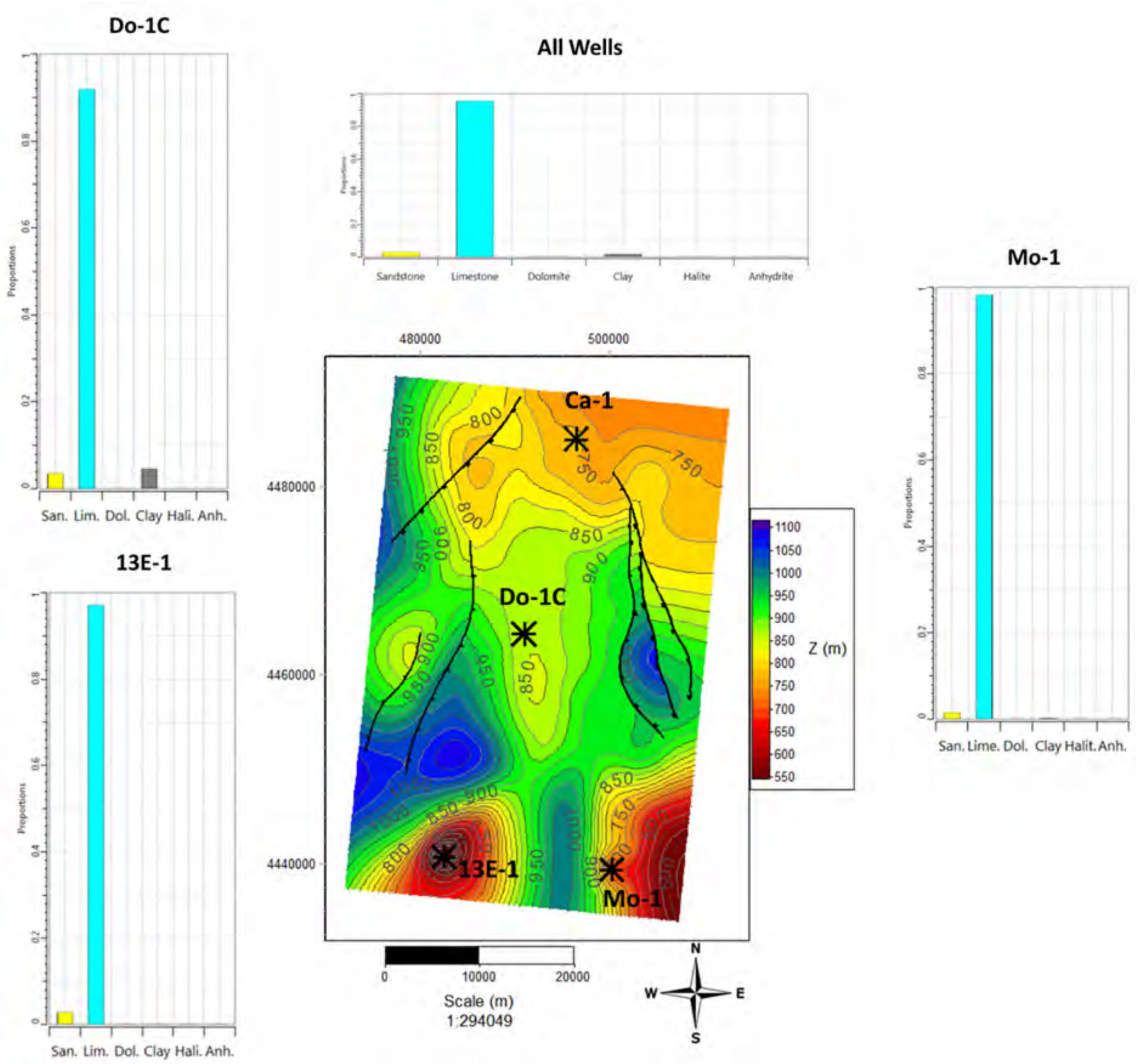

Figure 5.10: Histograms of the available well-log lithofacies of the Upper Cretaceous – Primary Seal region.

7.3.2.1.5 Lower Cretaceous – Reservoir

The reservoir unit (Lower Cretaceous) is the first model region that was possible to classify the lithofacies for all the four wells and determine the lithofacies proportions (Figure 5.11). Apart from the well 13E-1, which presents about 70% of clay lithofacies, the sandstone lithofacies are mostly present in the other reservoir locations intercepted by the 3 wells. It is important to mention that although the lithofacies classification for the well Ca-1 was only possible for the bottom reservoir layers, where the reservoir presents coarse sandstones/ conglomerates; however, the reservoir units present much higher intercalations of clays in the central and top reservoir areas and the overall lithofacies proportions may be close to the lithofacies proportion of the well 13E-1.

The PilotSTRATEGY project has received funding from the European Union's Horizon 2020 research and innovation programme under grant agreement No. 101022664

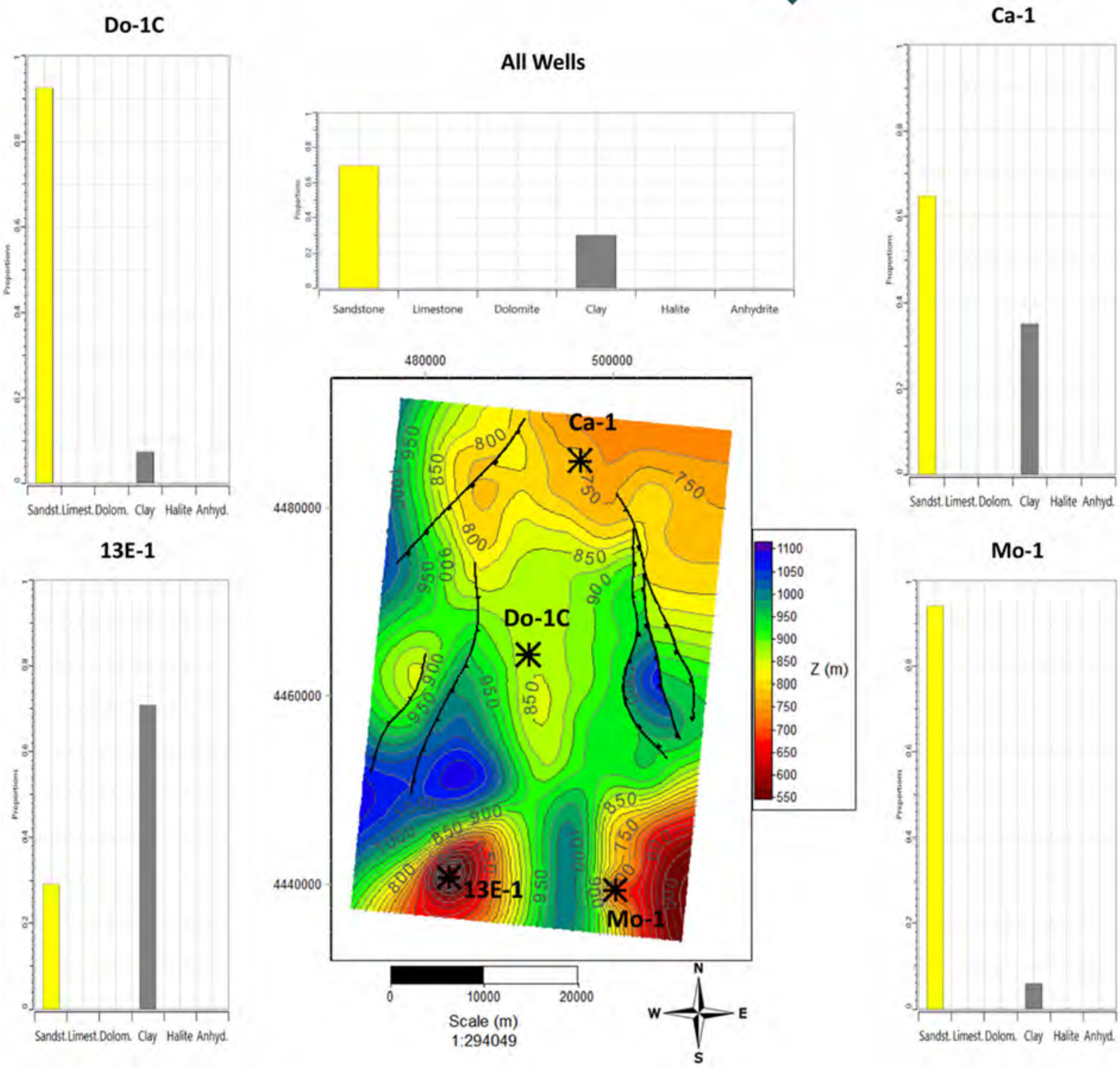

Figure 5.11: Histograms of the available well-log lithofacies of the Lower Cretaceous – Reservoir region.

7.3.2.1.6 Upper Jurassic

The lithofacies proportions of the Upper Jurassic unit are mainly classified as clay lithofacies, although at the location of the wells Ca-1 and Do-1C there is a significant presence of sandstone lithofacies as well. In addition, Figure 5.12 also illustrates the presence of some carbonates in this model region, such as around 20% of limestone lithofacies and less than 10% of dolomite lithofacies.

The PilotSTRATEGY project has received funding from the European Union's Horizon 2020 research and innovation programme under grant agreement No. 101022664

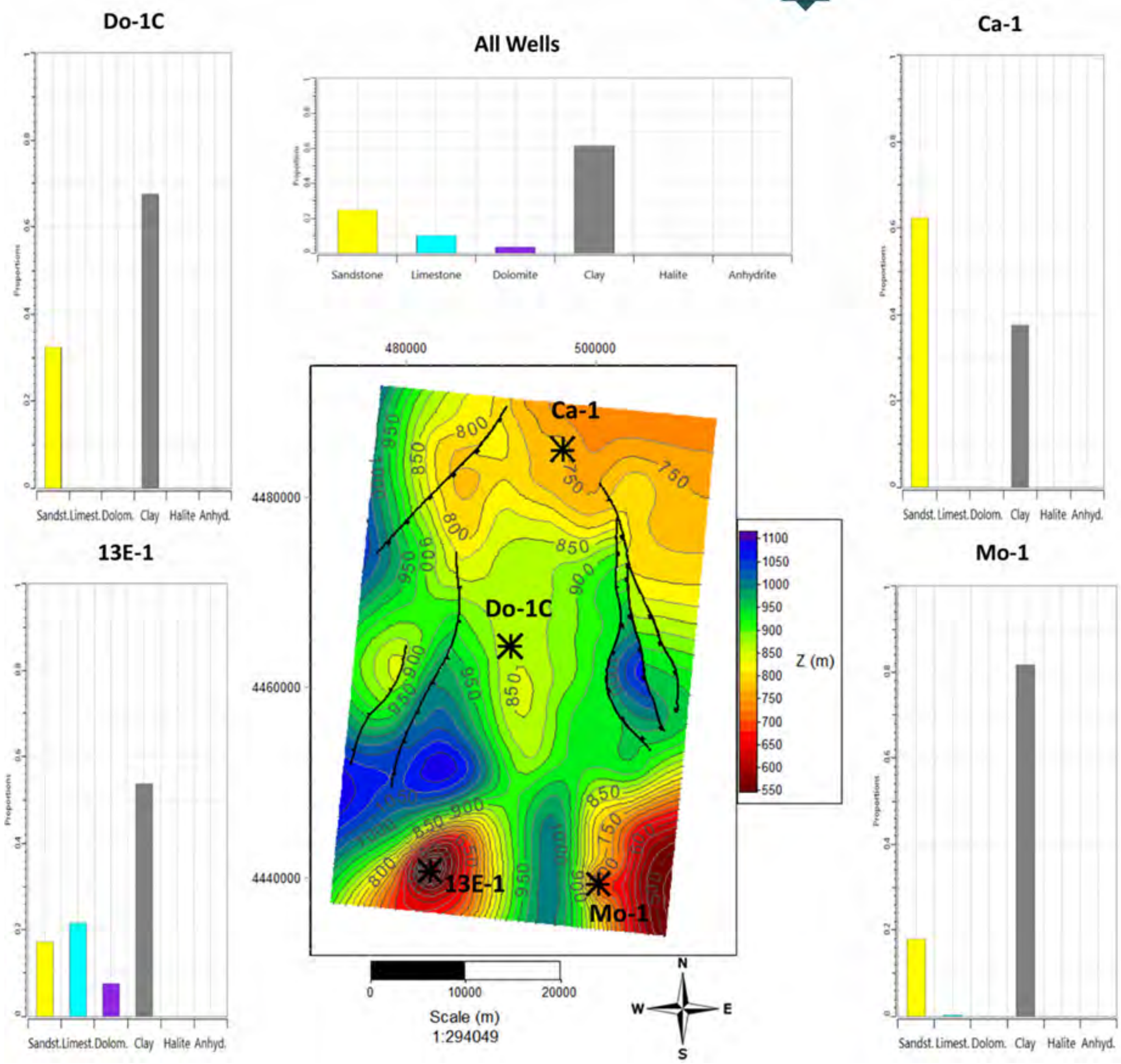

Figure 5.12: Histograms of the available well-log lithofacies of the Upper Jurassic region.

7.3.2.1.7 Middle Jurassic

The last model region (Middle Jurassic unit) is the most heterogeneous in terms of lithofacies proportions (Figure 5.13). Besides the presence of a small proportion of siliciclastics, i.e., sandstones but mainly clay lithofacies represented in the wells Mo-1 and Do-1C, there is also a presence of carbonates (dolomites and limestones) and evaporites (anhydrite and halite totalizing of about 30-35% of lithofacies proportions in the wells Ca-1 and Do-1C).

The PilotSTRATEGY project has received funding from the European Union's Horizon 2020 research and innovation programme under grant agreement No. 101022664

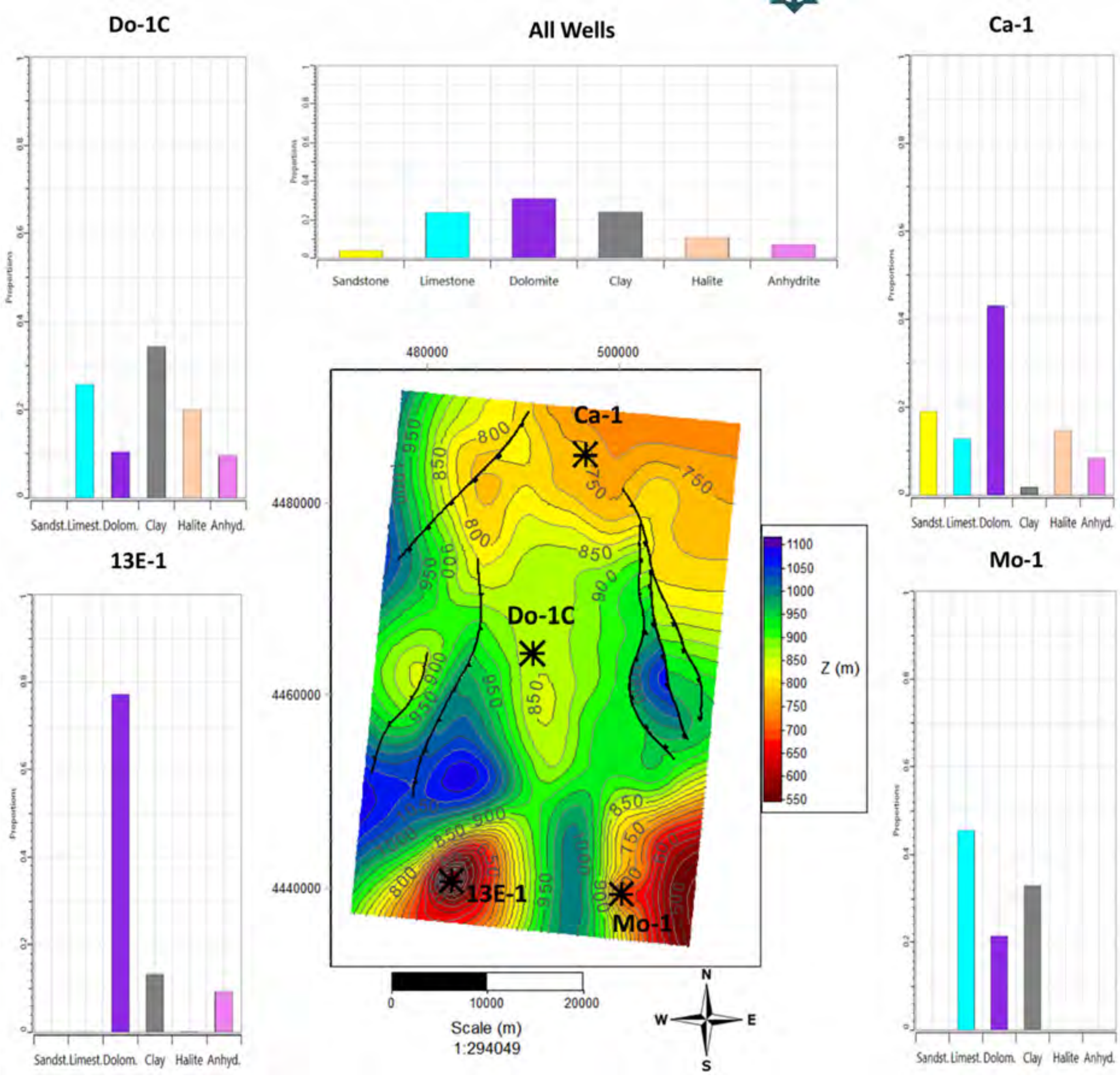

Figure 5.13: Histograms of the available well-log lithofacies of the Middle Jurassic region.

7.3.2.2 Volume of Clay

7.3.2.2.1 Eocene-Miocene

The analysis of the volume of clay (continuous property) for the Eocene-Miocene region considers the well Mo-1 only. The histogram is illustrated in Figure 5.14, in which most of the data shows high percentage of presence of clay (30% of the data is 100% of clay), being consistent with the lithofacies classified for the region.

The PilotSTRATEGY project has received funding from the European Union's Horizon 2020 research and innovation programme under grant agreement No. 101022664

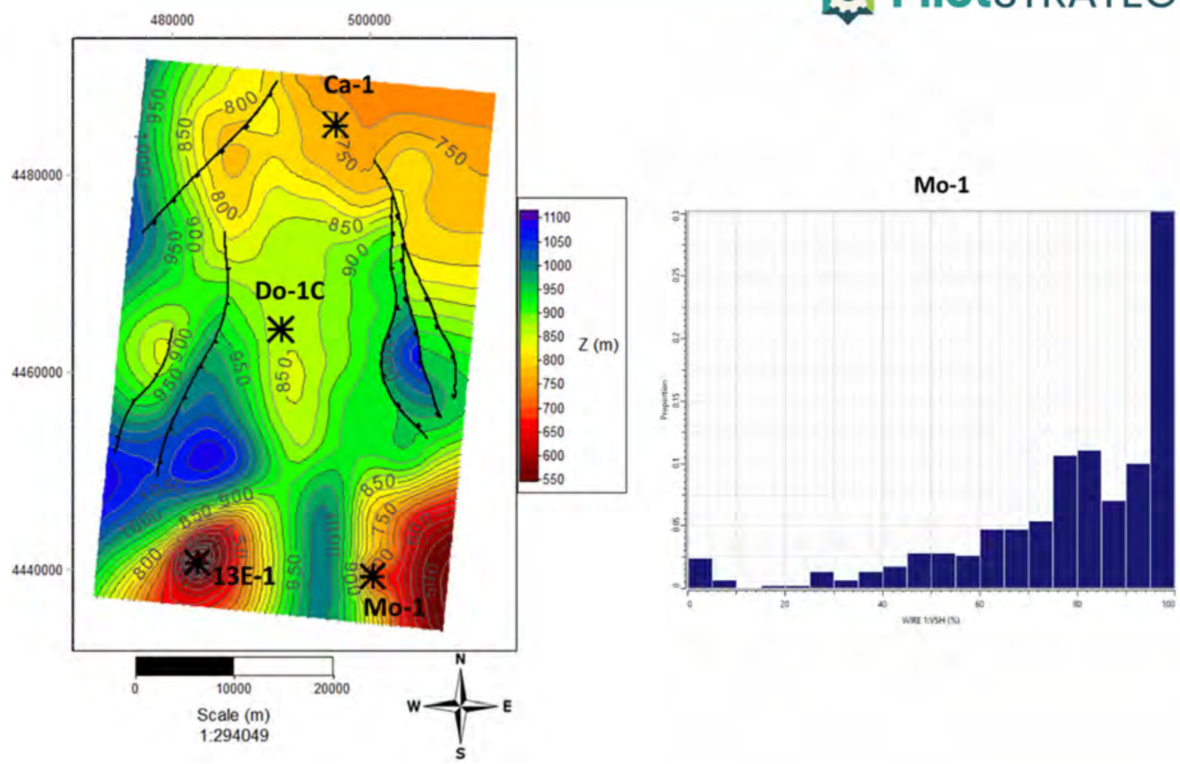

Figure 5.14: Histograms of the available well-log volume of clay of the Eocene-Miocene region.

7.3.2.2.2 Paleocene

In the Paleocene model region, the volume of clay was determined from the wells Do-1C and Mo-1, presenting a different distribution interval of values from one well to the other (Figure 5.15): the well Do-1C presents high proportion (more than 15%) in the histogram of the volume of clay of about 40%, while in the well Mo-1 more than 45% of the data corresponds to a high probability of volume of clay.

The PilotSTRATEGY project has received funding from the European Union's Horizon 2020 research and innovation programme under grant agreement No. 101022664

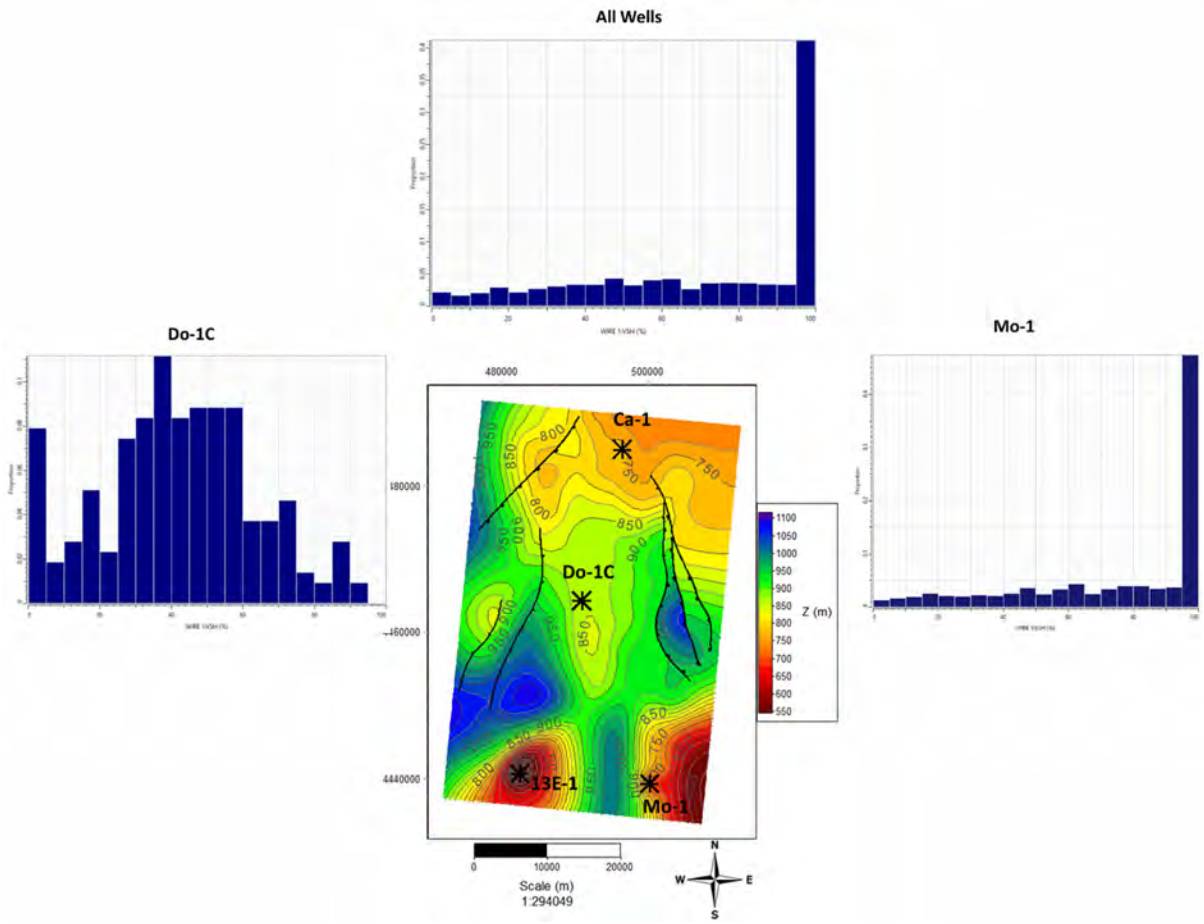

Figure 5.15: Histograms of the available well-log volume of clay of the Paleocene region.

7.3.2.2.3 Upper Cretaceous – Secondary Seal

The volume of clay of the three available wells (Figure 5.16) consists in the presence of mainly clays for the wells 13E-1 and Mo-1 in the secondary seal (Upper Cretaceous), while most of the values from the well Do-1C are lower than 50% of the volume of clay property.

The PilotSTRATEGY project has received funding from the European Union's Horizon 2020 research and innovation programme under grant agreement No. 101022664

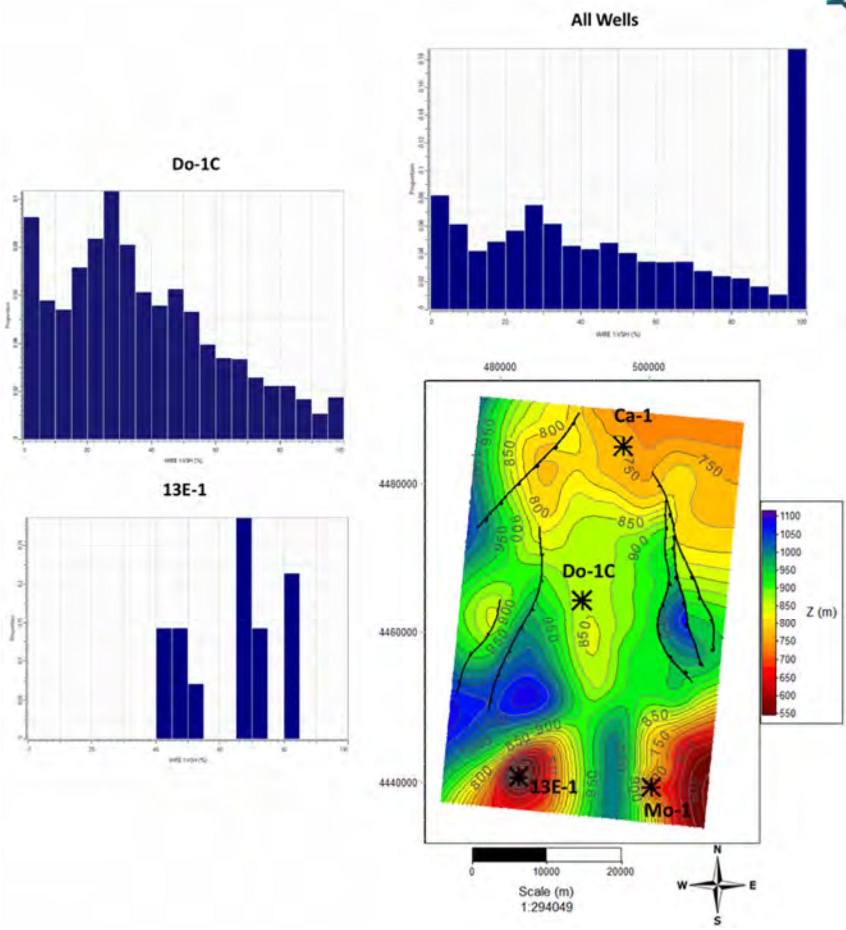

Figure 5.16: Histograms of the available well-log volume of clay of the Upper Cretaceous – Secondary Seal region.

7.3.2.2.4 Upper Cretaceous – Primary Seal

The expected volume of clay in the primary seal unit (Upper Cretaceous) is relatively small according to the data available illustrated in the histograms of the three wells (Figure 5.17) due to the lithofacies present, which is mainly limestone. Nonetheless, the presence of small percentage of clays and sands (clayey sands) are also expected in the primary seal interval at and nearby the location of these wells.

The PilotSTRATEGY project has received funding from the European Union's Horizon 2020 research and innovation programme under grant agreement No. 101022664

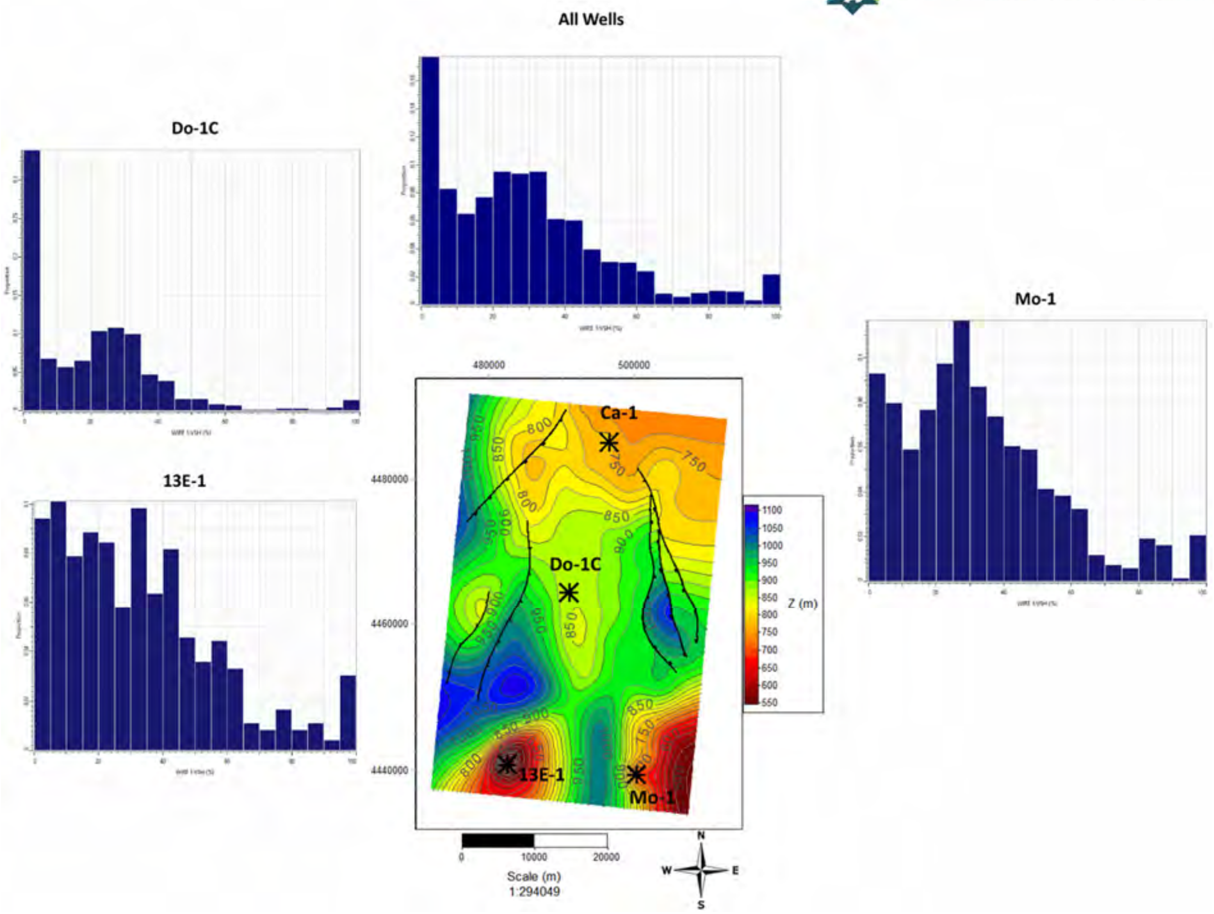

Figure 5.17: Histograms of the available well-log volume of clay of the Upper Cretaceous – Primary Seal region.

7.3.2.2.5 Lower Cretaceous – Reservoir

The reservoir unit (Lower Cretaceous) presents mainly sandstone lithofacies, but interbedded clay layers are also expected to exist. This analysis is also illustrated in the histograms of volume of clay of Figure 5.18, in which higher proportions of clay are mainly present in the reservoir at the location of the wells Ca-1 and 13E-1, and a smaller amount, traduced by lower proportions in the volume of clay, at the location of the wells Mo-1 and Do-1C, where the reservoir quality is expected to be more adequate (and where the Q4-TV1 prospect is also located in between these two wells).

The PilotSTRATEGY project has received funding from the European Union's Horizon 2020 research and innovation programme under grant agreement No. 101022664

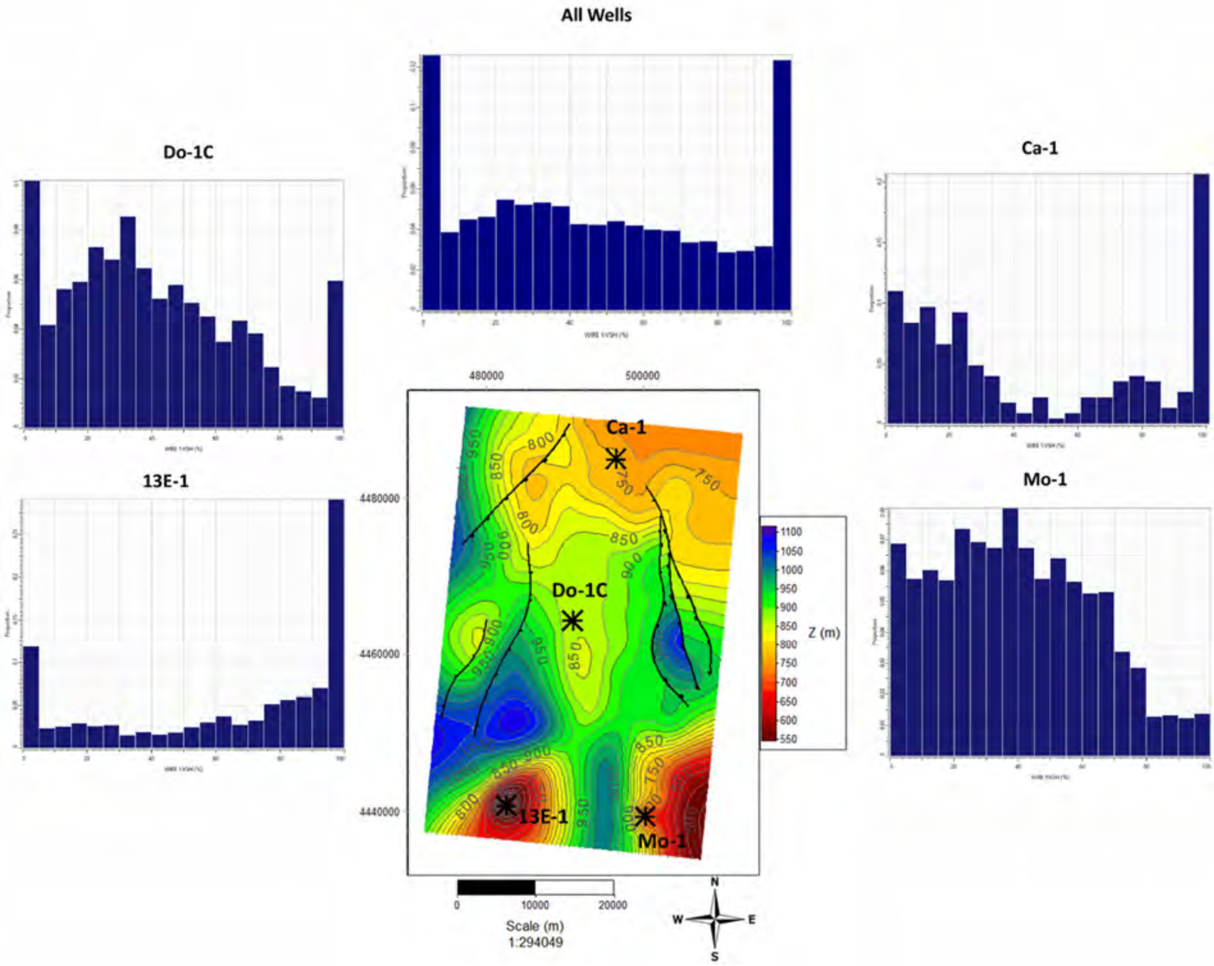

Figure 5.18: Histograms of the available well-log volume of clay of the Lower Cretaceous – Reservoir region.

7.3.2.2.6 Upper Jurassic

The histograms of the volume of clay determined for the wells in the Upper Jurassic region (underburden reservoir unit) are presented in Figure 5.19. Higher proportions of volume of clay are present in the wells Ca-1, Do-1C and 13E-1, while the lower proportions are present in the well Mo-1 but also in the wells Do-1C and 13E-1. It is important to mention that the most uncertainty in the volume of clay is associated with the well Mo-1, in which the higher percentage values are present in the histogram classes between 40-50%.

The PilotSTRATEGY project has received funding from the European Union's Horizon 2020 research and innovation programme under grant agreement No. 101022664

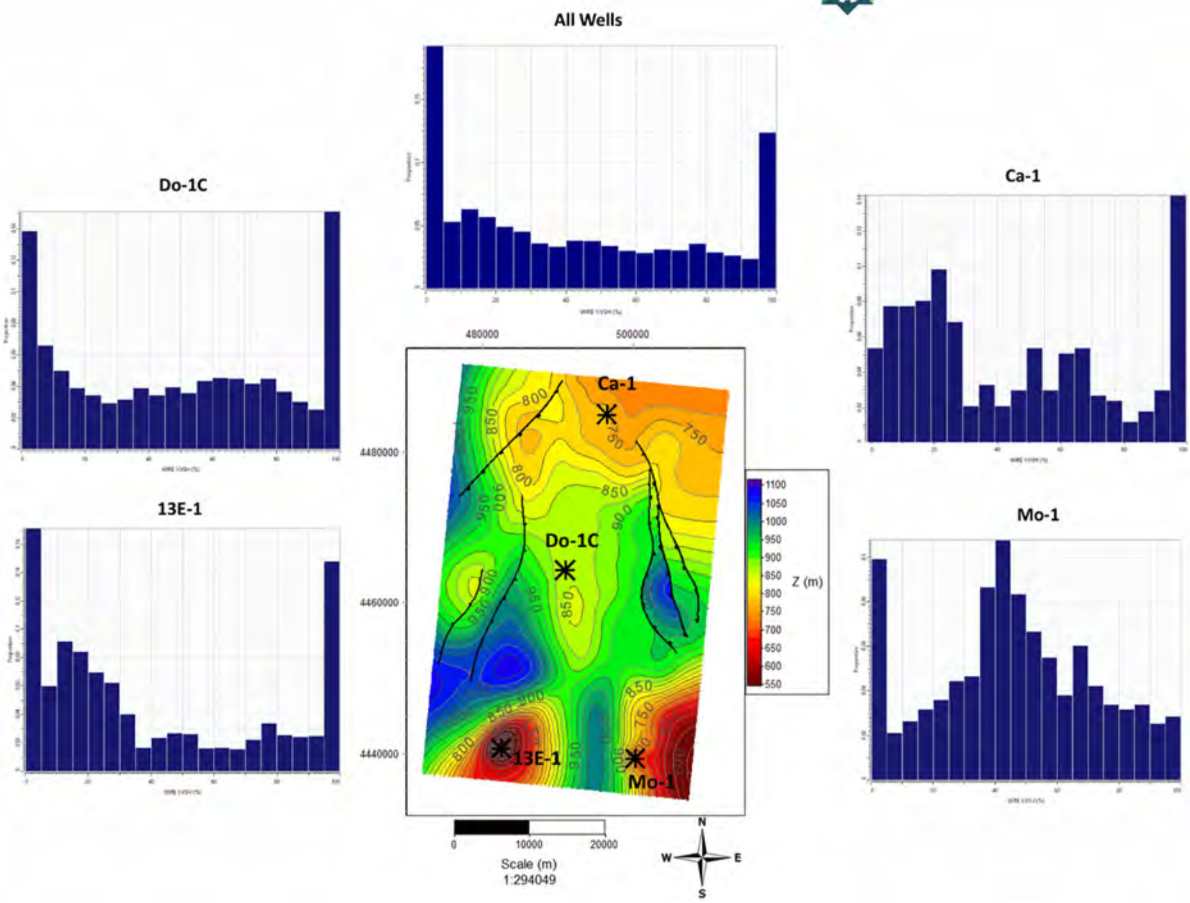

Figure 5.19: Histograms of the available well-log volume of clay of the Upper Jurassic region.

7.3.2.2.7 Middle Jurassic

In the Middle Jurassic unit, small amounts of volume of clay are present in all the available wells as this model region is mainly composed by carbonates and evaporites (as confirmed by the lithofacies classification). Nonetheless, the histograms of the wells illustrated in Figure 5.20 present values in the intermediate histogram classes of the four wells and some layers of clay may be expected to be present in this model region.

The PilotSTRATEGY project has received funding from the European Union's Horizon 2020 research and innovation programme under grant agreement No. 101022664

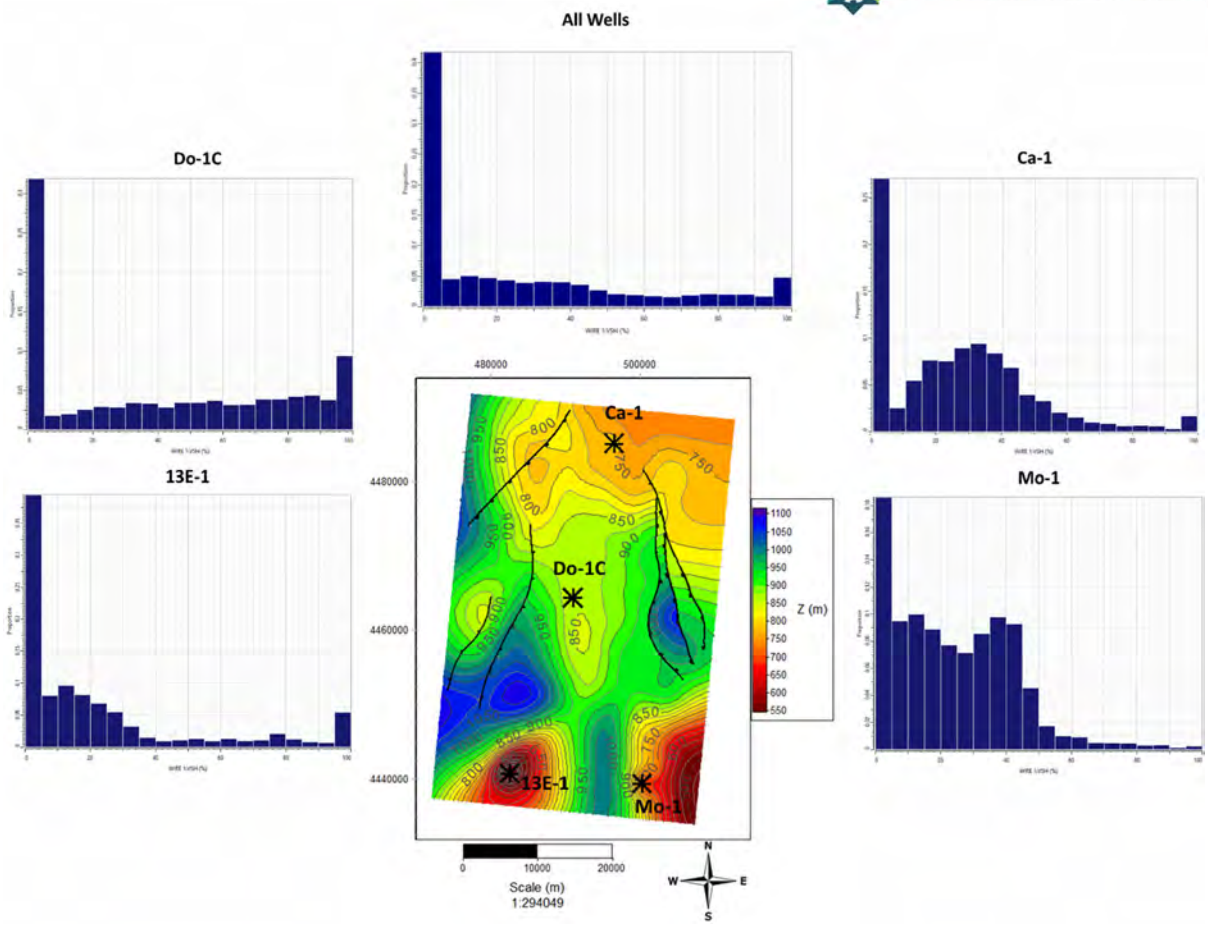

Figure 5.20: Histograms of the available well-log volume of clay of the Middle Jurassic region.

The main statistics of the volume of clay for all the regions of the static model are listed in Table 5.5.

Table 5.5: Summary statistics of volume of clay for all the wells per each region of the static model.

Region / Property	Volume of Clay (%) - All Wells					
	Minimum	Median	Maximum	Mean	Std. Deviation	Number of Samples
Eocene-Miocene	0.001	83.49	99.99	78.88	22.65	470
Paleocene	0.001	82.18	99.99	71.59	30.81	1639
Sedondary Seal	0.001	42.78	99.99	48.68	33.25	3741
Primary Seal	0.001	25.10	99.99	28.18	23.02	2119
Reservoir	0.001	43.70	99.99	47.09	32.69	7122
Upper Jurassic	0.001	35.57	99.99	42.26	34.64	6480
Middle Jurassic	0.001	13.78	99.99	26.39	31.28	21330

The PilotSTRATEGY project has received funding from the European Union's Horizon 2020 research and innovation programme under grant agreement No. 101022664

7.3.2.3 *Effective Porosity*

7.3.2.3.1 Eocene-Miocene

The effective porosity histogram of the Eocene-Miocene region is presented in Figure 5.21. As mentioned previously, the information available corresponds to the well Mo-1, in which most of the effective porosity values are low due to the presence of clay lithofacies.

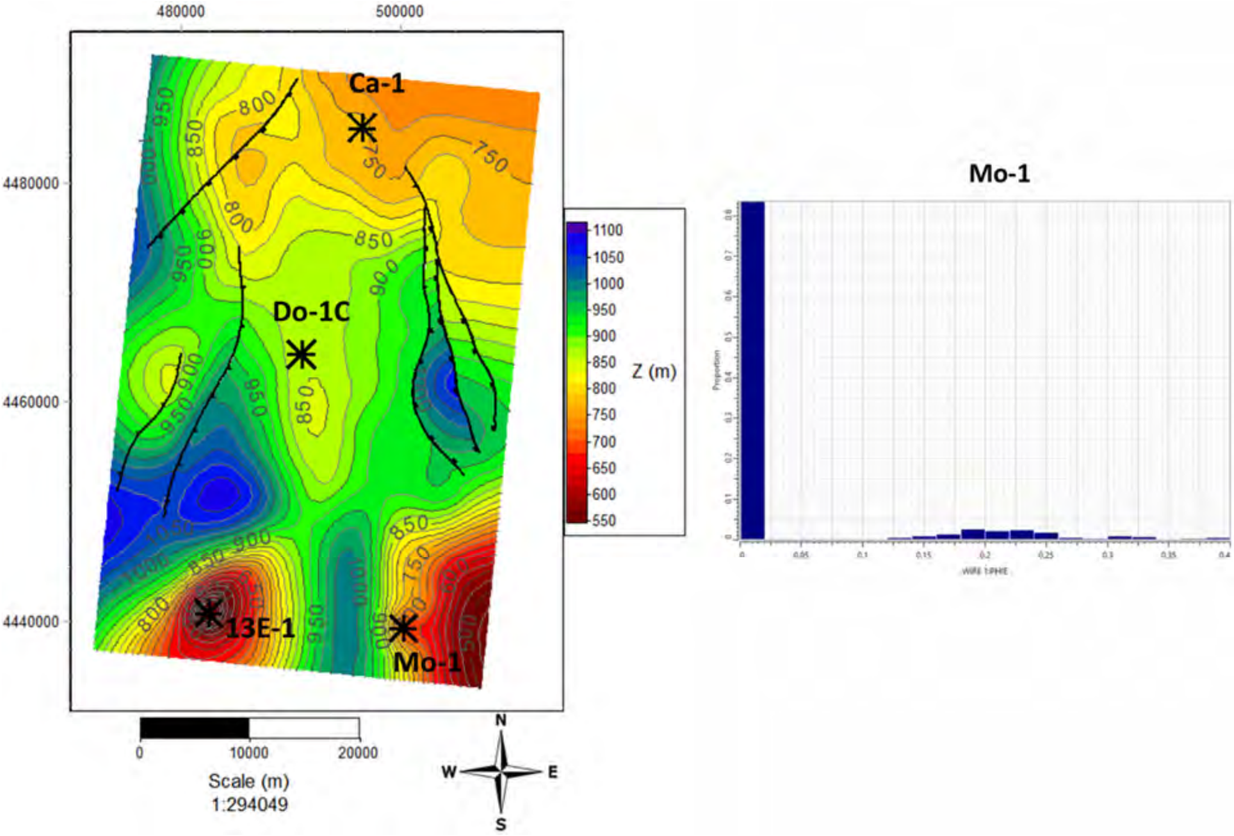

Figure 5.21: Histograms of the available well-log effective porosity of the Eocene-Miocene region.

7.3.2.3.2 Paleocene

The effective porosity of the Paleocene region was analysed in the wells Do-1C and Mo-1 (Figure 5.22). While the values are mainly low in the well Mo-1 (more than 70% of the data), the values in the well Do-1C are mainly distributed in the central classes of the histogram property where less clay lithofacies are expected to be found.

The PilotSTRATEGY project has received funding from the European Union's Horizon 2020 research and innovation programme under grant agreement No. 101022664

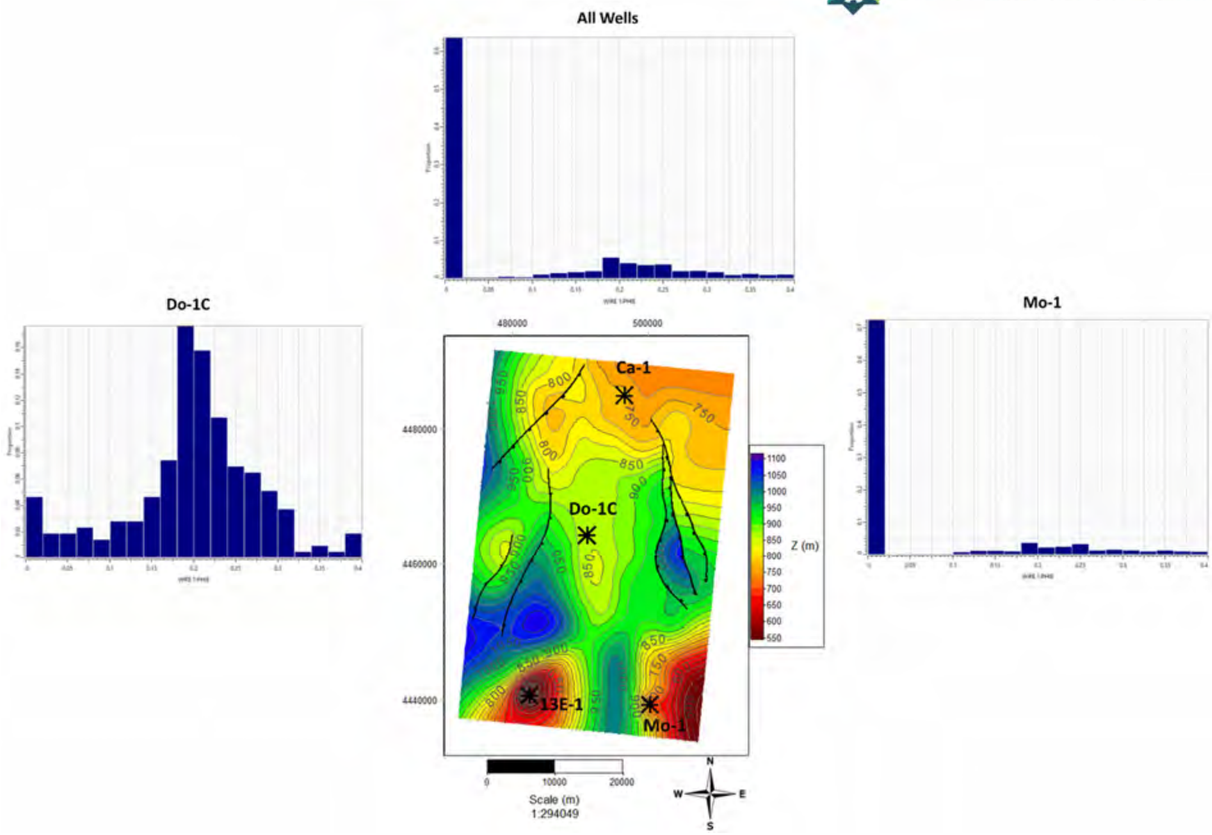

Figure 5.22: Histograms of the available well-log effective porosity of the Paleocene region.

7.3.2.3.3 Upper Cretaceous – Secondary Seal

The analysis of the effective porosity of the secondary seal region (Upper Cretaceous) was conducted from three wells and the histograms are illustrated in Figure 5.23. The lateral and vertical spatial distribution of this model region, confirmed by the lithofacies data, is also supported by the distinct distribution of effective porosity values of the wells. The lithofacies classification of the well 13E-1 resulted in limestone lithofacies, presenting different effective porosity values (more than 20% are close to zero and almost 80% range from about 5-25%). For the well Do-1C, 10% of the effective porosity (low values) correspond to the clay lithofacies while the other histogram classes are associated to both sandstone and limestone, while for the well Mo-1 almost 70% of the effective porosity values are low due to the dominant clay lithofacies (and a small percentage of medium-to-high values for the sandstone and limestone lithofacies).

The PilotSTRATEGY project has received funding from the European Union's Horizon 2020 research and innovation programme under grant agreement No. 101022664

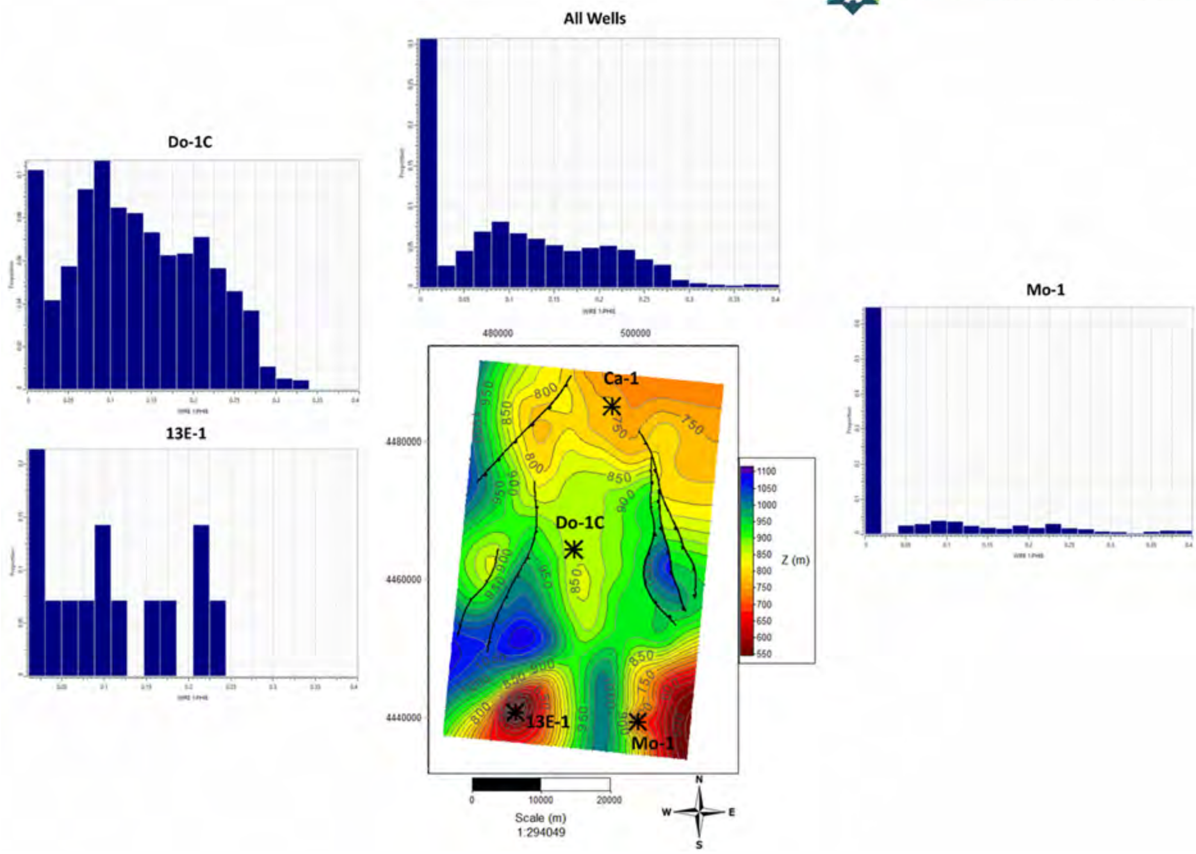

Figure 5.23: Histograms of the available well-log effective porosity of the Upper Cretaceous – Secondary Seal region.

7.3.2.3.4 Upper Cretaceous – Primary Seal

From the lithofacies classification of the primary seal unit (Upper Cretaceous), more than 90% of the data from the wells corresponds to limestone lithofacies. However, and like the volume of clay, the effective porosity of these limestones presents high variation from well to well as illustrated in Figure 5.24. The primary seal limestones can be sub-divided in two groups: the crystalline and argillaceous limestones, which are mainly responsible for the medium-to-high and lower effective porosity values, respectively, besides the small amounts of sandstones and clays also present (specially for the well Do-1C).

The PilotSTRATEGY project has received funding from the European Union's Horizon 2020 research and innovation programme under grant agreement No. 101022664

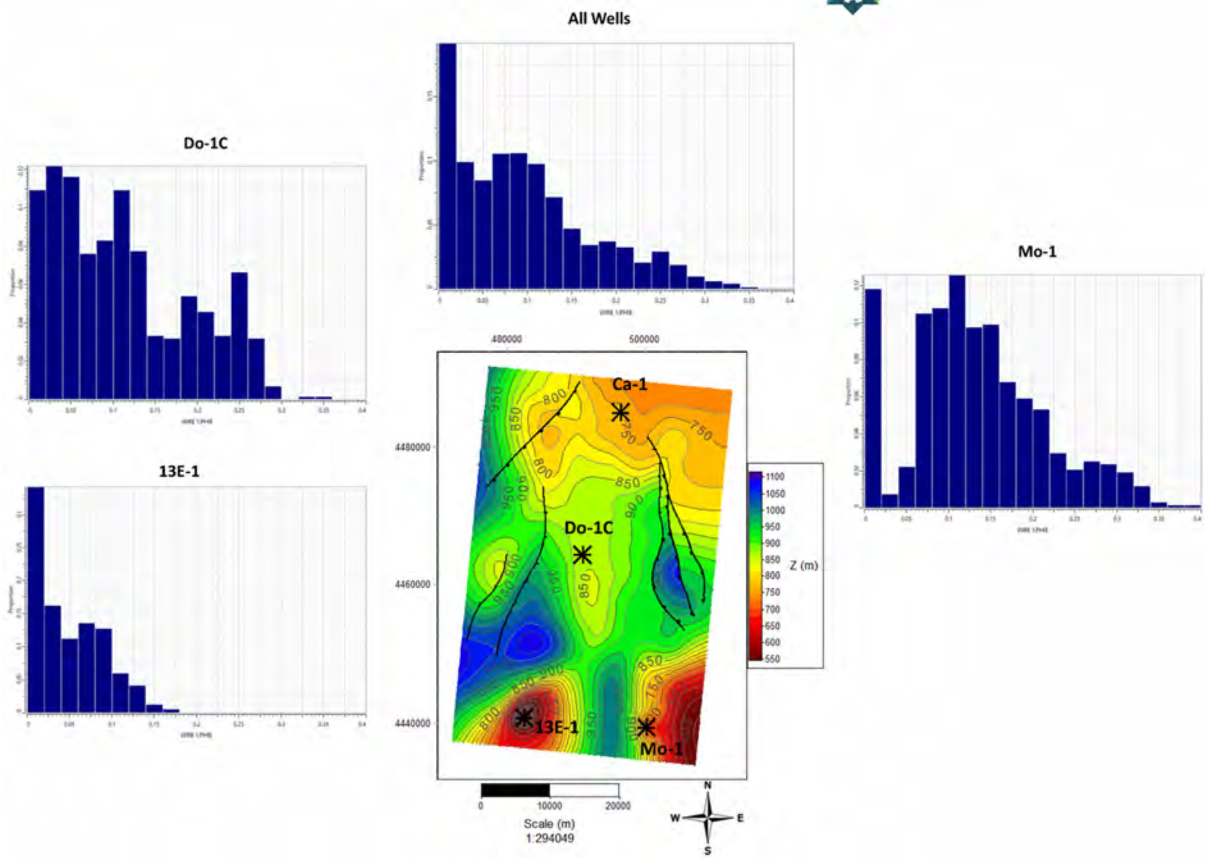

Figure 5.24: Histograms of the available well-log effective porosity of the Upper Cretaceous – Primary Seal region.

7.3.2.3.5 Lower Cretaceous – Reservoir

The histograms of the effective porosity for each well in the reservoir unit (Lower Cretaceous) are illustrated in Figure 5.25. As the lithofacies classification resulted in two lithofacies, such as sandstone and clay, the medium-to-high values of effective porosity correspond to the sandstone lithofacies, while the low effective porosity corresponds to the clay lithofacies (or clayey sand layers), in which about 50% of the data of the wells Ca-1 and 13E-1 are close to zero, and about 12% and more than 20% for the wells Do-1C and Mo-1, respectively.

The PilotSTRATEGY project has received funding from the European Union's Horizon 2020 research and innovation programme under grant agreement No. 101022664

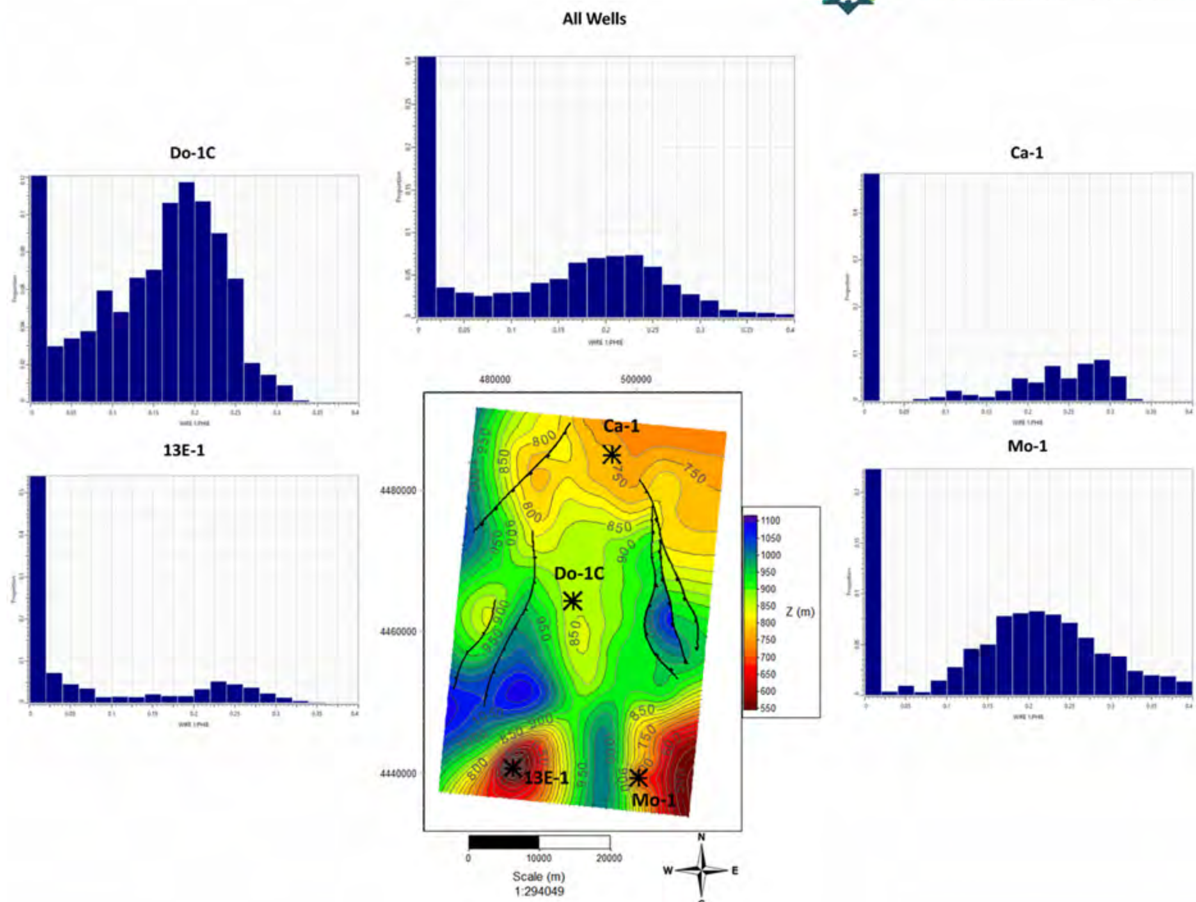

Figure 5.25: Histograms of the available well-log effective porosity in the Lower Cretaceous – Reservoir region.

7.3.2.3.6 Upper Jurassic

The effective porosity histograms of the Upper Jurassic region for the four wells are shown in Figure 5.26. Although the distribution between the wells 13E-1 and Mo-1 is similar, they present relatively different lithofacies classifications: despite the clay is the dominant lithofacies in this region of the wells, traduced by the high percentage of low effective porosity values, the well 13E-1 also presents sandstone and carbonate lithofacies (limestone and dolomite layers), while the well Mo-1 presents mostly sandstones only.

The PilotSTRATEGY project has received funding from the European Union's Horizon 2020 research and innovation programme under grant agreement No. 101022664

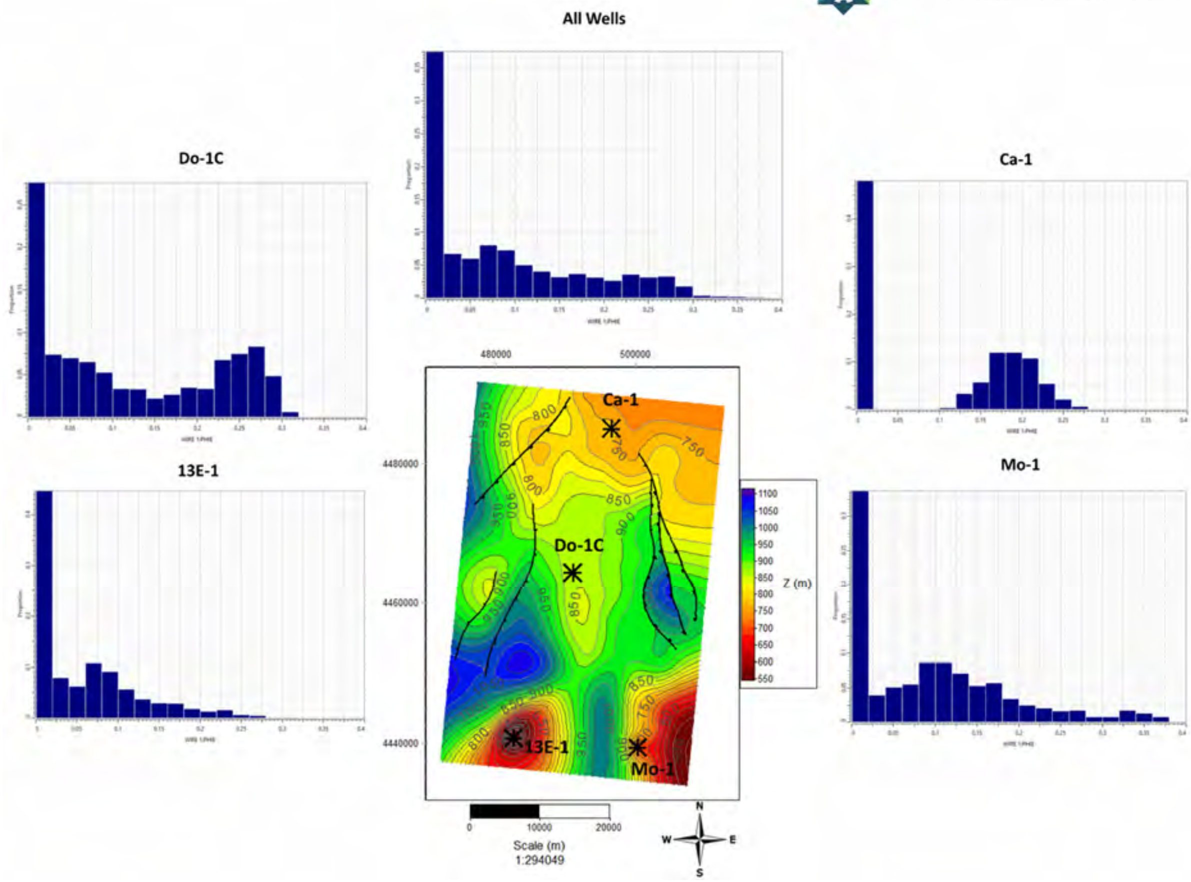

Figure 5.26: Histograms of the available well-log effective porosity of the Upper Jurassic region.

7.3.2.3.7 Middle Jurassic

The histograms of effective porosity in the Middle Jurassic region are illustrated in Figure 5.27, presenting, in general, similar distribution values. However, the well Ca-1 is the only one presenting the existence of the six lithofacies (siliciclastics, carbonates and evaporites) simultaneously in the same region, while the other wells do not present sandstone lithofacies, being mainly composed by carbonates and clays. This justifies the low effective porosity values (more than 50-60% of the data) in these wells, while the low effective porosity values of the well Ca-1 resulted from the carbonates and evaporites present in this unit.

The PilotSTRATEGY project has received funding from the European Union's Horizon 2020 research and innovation programme under grant agreement No. 101022664

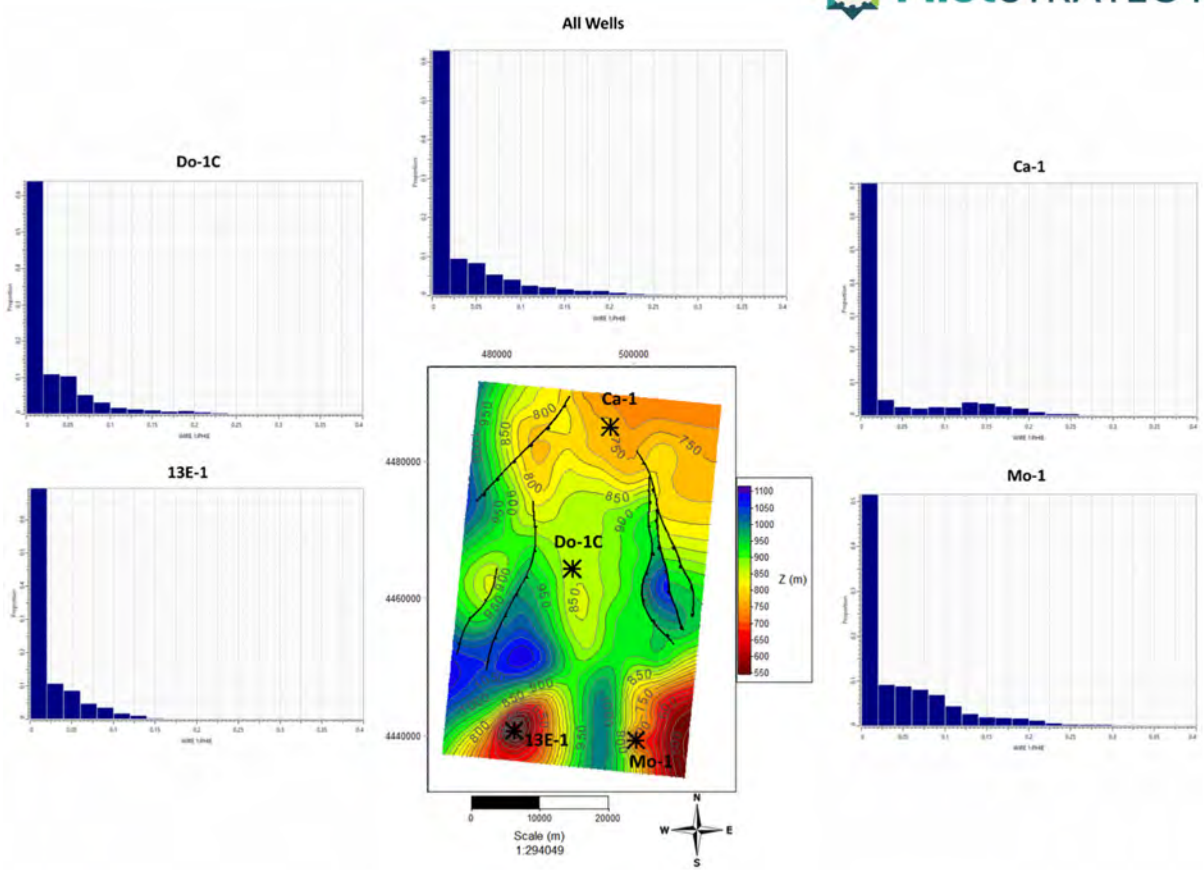

Figure 5.27: Histograms of the available well-log effective porosity of the Middle Jurassic region.

The main statistics of the effective porosity for all the regions of the static model are listed in Table 5.6.

Table 5.6: Summary statistics of effective porosity for all the wells per each region of the static model.

Region / Property	Effective Porosity (%) - All Wells					
	Minimum	Median	Maximum	Mean	Std. Deviation	Number of Samples
Eocene-Miocene	0.01	0.04	45.00	4.22	10.20	470
Paleocene	0.01	0.05	45.00	8.79	12.78	1639
Sedondary Seal	0.01	9.26	43.68	10.47	9.57	3741
Primary Seal	0.01	8.26	38.81	9.57	7.89	2119
Reservoir	0.01	14.10	43.48	12.96	10.93	7112
Upper Jurassic	0.01	5.90	37.79	8.43	9.06	6480
Middle Jurassic	0.01	0.03	36.12	3.00	5.04	21330

7.3.2.4 Permeability

7.3.2.4.1 Upper Cretaceous – Secondary Seal

The permeability histograms of the secondary seal unit (Upper Cretaceous) are illustrated in Figure 5.28. More details and the summary statistics were presented in the section of the petrophysical analysis of the main deliverable (section 5.2.1.2). The correlation coefficient between effective porosity and permeability for all the wells is 96.98%, therefore a value of 97% was used in the petrophysical modelling to generate the permeability models.

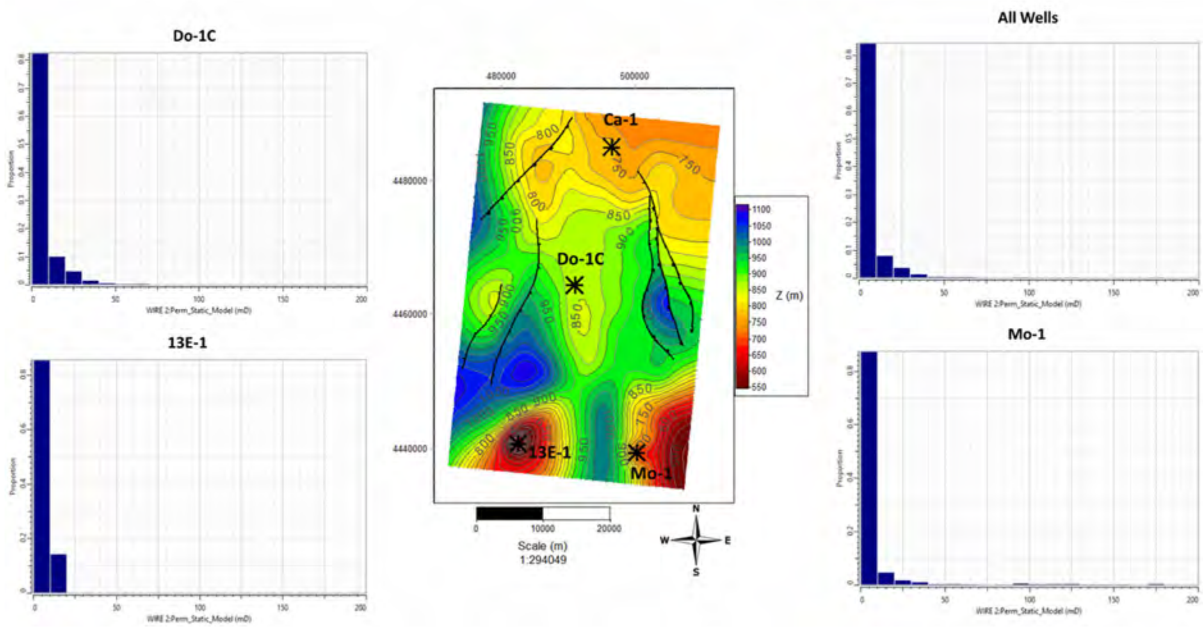

Figure 5.28: Histograms of the available well-log permeability of the Upper Cretaceous – Secondary Seal region.

7.3.2.4.2 Upper Cretaceous – Primary Seal

The permeability histograms of the primary seal unit (Upper Cretaceous) are illustrated in Figure 5.29. More details and the summary statistics were presented in the section of the petrophysical analysis of the main deliverable (section 5.2.1.2). The correlation coefficient between effective porosity and permeability for all the wells is 93.70%, therefore a value of 94% was used in the petrophysical modelling to generate the permeability models.

The PilotSTRATEGY project has received funding from the European Union's Horizon 2020 research and innovation programme under grant agreement No. 101022664

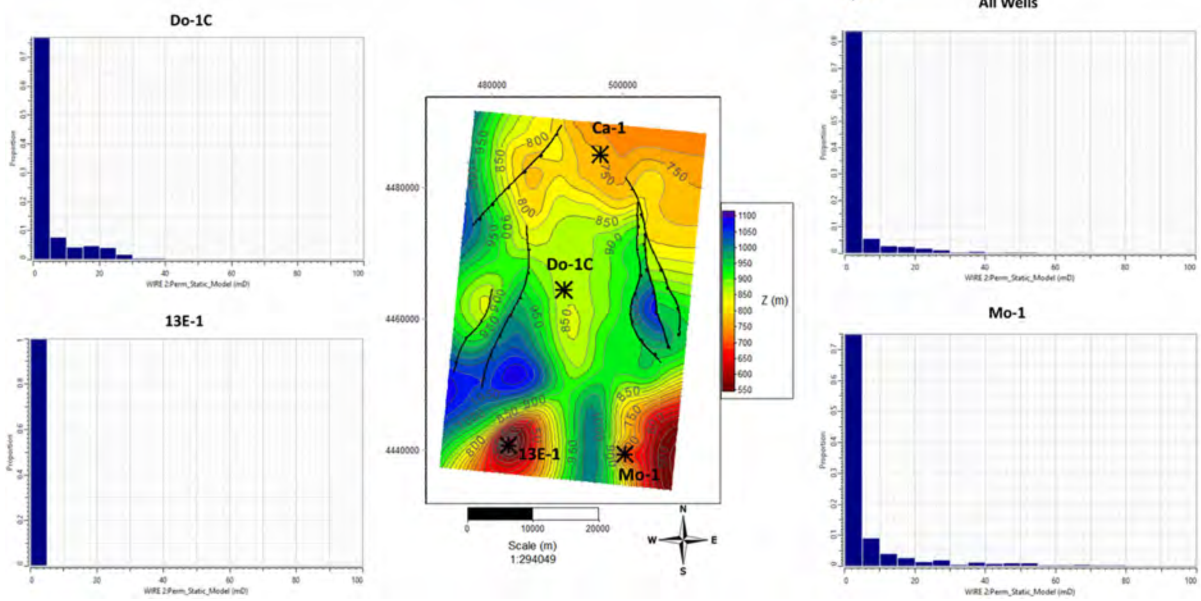

Figure 5.29: Histograms of the available well-log permeability of the Upper Cretaceous – Primary Seal region.

7.3.2.4.3 *Lower Cretaceous – Reservoir*

The permeability histograms of the reservoir unit (Lower Cretaceous) are illustrated in Figure 5.30. More details and the summary statistics were presented in the section of the petrophysical analysis of the main deliverable (section 5.2.1.2). The correlation coefficient between effective porosity and permeability for all the wells is 90.74%, therefore a value of 91% was used in the petrophysical modelling to generate the permeability models.

The PilotSTRATEGY project has received funding from the European Union's Horizon 2020 research and innovation programme under grant agreement No. 101022664

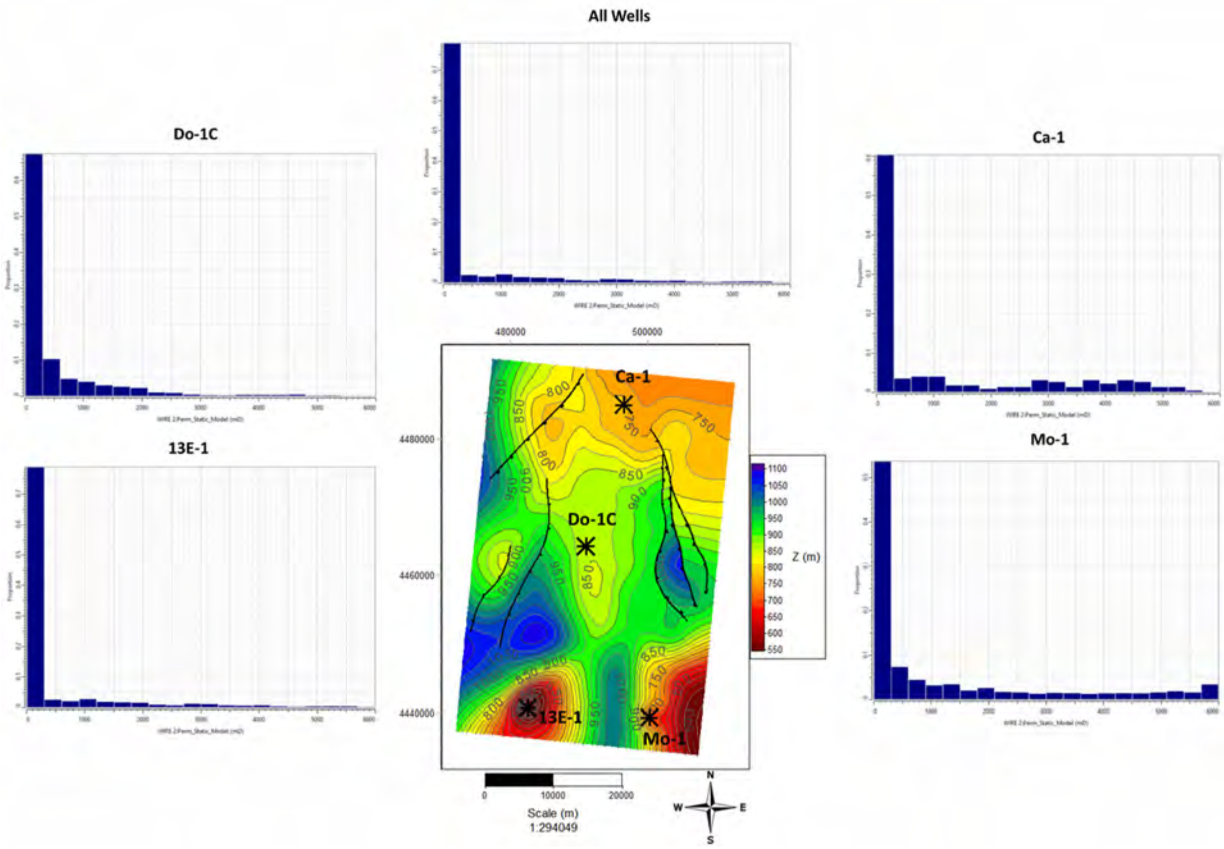

Figure 5.30: Histograms of the available well-log permeability of the Lower Cretaceous – Reservoir region.

7.3.3 Spatial Continuity Analysis

This sub-section presents the estimation of the spatial continuity patterns of the rock properties, conducted by the variogram modelling study, for the three model regions considered for simulation: the reservoir, and the primary and secondary seals.

The variogram ranges of the main and minor horizontal directions, as well as the azimuth values, were taken from the mean values estimated based on the 3D seismic data (analogue area) as presented in the first section. The variogram ranges of the vertical direction of each property were determined from the available well-log data for each model region using one structure for fitting the experimental variograms with mathematical models.

7.3.3.1 Lithofacies

7.3.3.1.1 Upper Cretaceous – Secondary Seal

The vertical experimental variogram of the lithofacies for the secondary seal (Upper Cretaceous) is illustrated in Figure 5.31 and the variogram parameters are presented in Table 5.7.

The PilotSTRATEGY project has received funding from the European Union's Horizon 2020 research and innovation programme under grant agreement No. 101022664

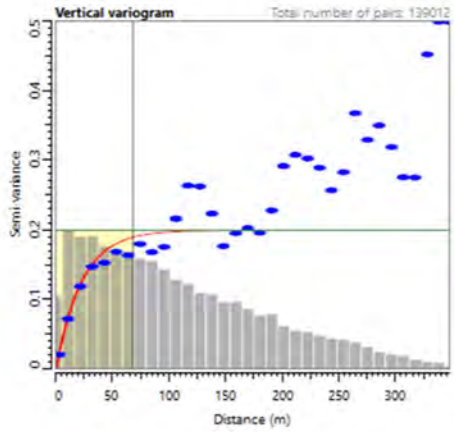

Figure 5.31: Vertical variogram of the available well-log lithofacies of the Upper Cretaceous – Secondary Seal region.

Table 5.7: Variogram modelling parameters for lithofacies simulation of the secondary seal region (Upper Cretaceous).

Variogram Model	Azimuth (º)	Vertical Direction Range (m)	Main Direction Range (m)	Minor Direction Range (m)
Exponential	45	68	6250	5000

7.3.3.1.2 Upper Cretaceous – Primary Seal

The vertical experimental variogram of the lithofacies for the secondary seal (Upper Cretaceous) is illustrated in Figure 5.32 and the variogram parameters are presented in Table 5.8.

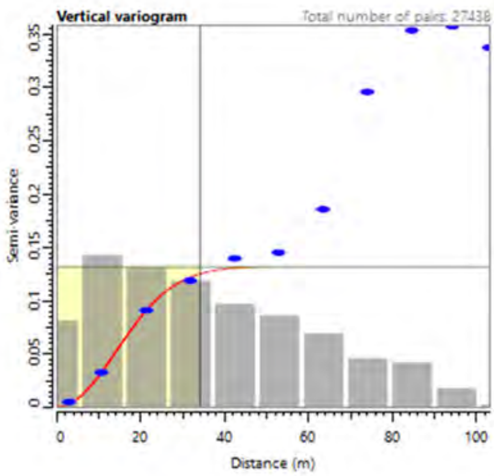

Figure 5.32: Vertical variogram of the available well-log lithofacies of the Upper Cretaceous – Primary Seal region.

Table 5.8: Variogram modelling parameters for lithofacies simulation of the primary seal region (Upper Cretaceous).

Variogram Model	Azimuth (º)	Vertical Direction Range (m)	Main Direction Range (m)	Minor Direction Range (m)

The PilotSTRATEGY project has received funding from the European Union's Horizon 2020 research and innovation programme under grant agreement No. 101022664

Gaussian	45	34	3250	2250

7.3.3.1.3 Lower Cretaceous – Reservoir

The vertical experimental variogram of the lithofacies for the secondary seal (Upper Cretaceous) is illustrated in Figure 5.33 and the variogram parameters are presented in Table 5.9.

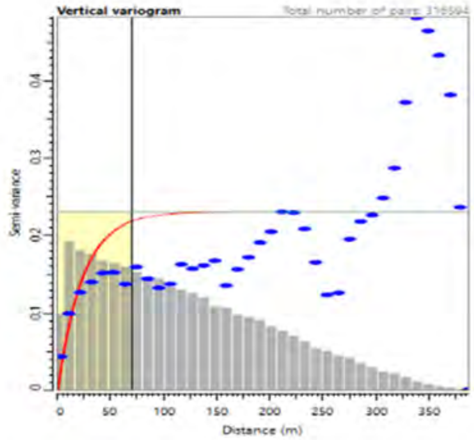

Figure 5.33: Vertical variogram of the available well-log facies of the Lower Cretaceous – Reservoir region.

Table 5.9: Variogram modelling parameters for lithofacies simulation of the reservoir region (Lower Cretaceous).

Variogram Model	Azimuth (º)	Vertical Direction Range (m)	Main Direction Range (m)	Minor Direction Range (m)
Exponential	45	35	6250	3750

7.3.3.2 Volume of Clay

7.3.3.2.1 Upper Cretaceous – Secondary Seal

The vertical experimental variogram of the volume of clay for the secondary seal (Upper Cretaceous) is illustrated in Figure 5.34 and the variogram parameters are presented in Table 5.10.

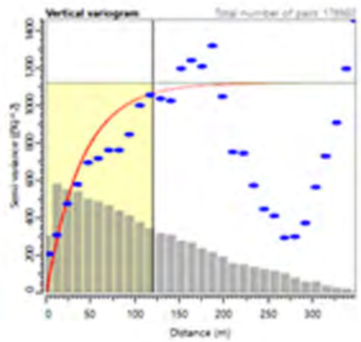

The PilotSTRATEGY project has received funding from the European Union's Horizon 2020 research and innovation programme under grant agreement No. 101022664

Figure 5.34: Vertical variogram of the available well-log volume of clay of the Upper Cretaceous – Secondary Seal region.

Table 5.10: Variogram modelling parameters for volume of clay simulation of the secondary seal region (Upper Cretaceous).

Variogram Model	Azimuth (º)	Vertical Direction Range (m)	Main Direction Range (m)	Minor Direction Range (m)
Exponential	45	120	6250	5000

7.3.3.2.2 Upper Cretaceous – Primary Seal

The vertical experimental variogram of the volume of clay for the primary seal (Upper Cretaceous) is illustrated in Figure 5.35 and the variogram parameters are presented in Table 5.11.

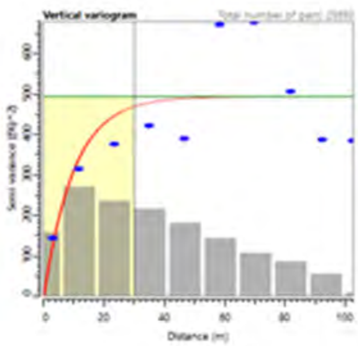

Figure 5.35: Vertical variogram of the available well-log volume of clay of the Upper Cretaceous – Primary Seal region.

Table 5.11: Variogram modelling parameters for volume of clay simulation of the primary seal region (Upper Cretaceous).

Variogram Model	Azimuth (º)	Vertical Direction Range (m)	Main Direction Range (m)	Minor Direction Range (m)
Exponential	45	30	3250	2250

7.3.3.2.3 Lower Cretaceous – Reservoir

The vertical experimental variogram of the volume of clay for the reservoir (Lower Cretaceous) is illustrated in Figure 5.36 and the variogram parameters are presented in Table 5.12.

The PilotSTRATEGY project has received funding from the European Union's Horizon 2020 research and innovation programme under grant agreement No. 101022664

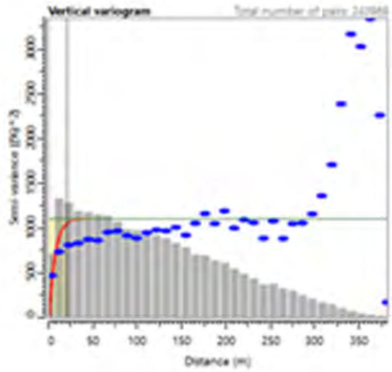

Figure 5.36: Vertical variogram of the available well-log volume of clay of the Lower Cretaceous – Reservoir region.

Table 5.12: Variogram modelling parameters for volume of clay simulation of the reservoir region (Lower Cretaceous).

Variogram Model	Azimuth (º)	Vertical Direction Range (m)	Main Direction Range (m)	Minor Direction Range (m)
Exponential	45	20	6250	3750

7.3.3.3 Effective Porosity

7.3.3.3.1 Upper Cretaceous – Secondary Seal

The vertical experimental variogram of the effective porosity for the secondary seal (Upper Cretaceous) is illustrated in Figure 5.37 and the variogram parameters are presented in Table 5.13.

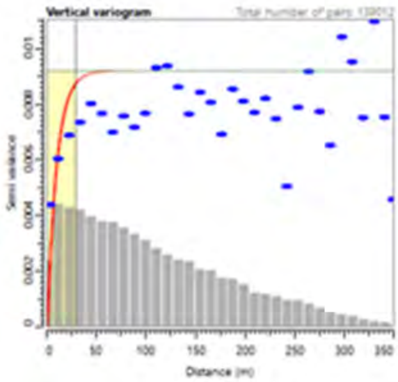

Figure 5.37: Vertical variogram of the available well-log effective porosity of the Upper Cretaceous – Secondary Seal region.

Table 5.13: Variogram modelling parameters for effective porosity simulation of the secondary seal region (Upper Cretaceous).

Variogram Model	Azimuth (º)	Vertical Direction Range (m)	Main Direction Range (m)	Minor Direction Range (m)

The PilotSTRATEGY project has received funding from the European Union's Horizon 2020 research and innovation programme under grant agreement No. 101022664

Exponential	45	29	6250	5000

7.3.3.3.2 Upper Cretaceous – Primary Seal

The vertical experimental variogram of the effective porosity for the primary seal (Upper Cretaceous) is illustrated in Figure 5.38 and the variogram parameters are presented in Table 5.14.

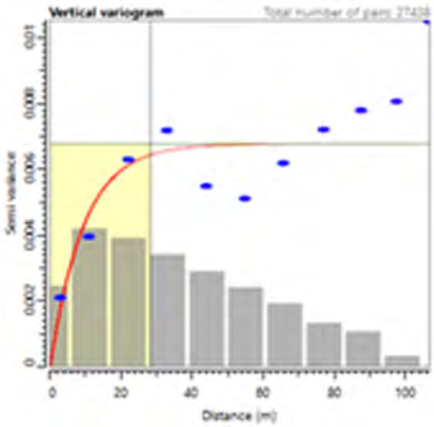

Figure 5.38: Vertical variogram of the available well-log effective porosity of the Upper Cretaceous – Primary Seal region.

Table 5.14: Variogram modelling parameters for effective porosity simulation of the primary seal region (Upper Cretaceous).

Variogram Model	Azimuth (º)	Vertical Direction Range (m)	Main Direction Range (m)	Minor Direction Range (m)
Exponential	45	28	3250	2250

7.3.3.3.3 Lower Cretaceous – Reservoir

The vertical experimental variogram of the effective porosity for the reservoir (Lower Cretaceous) is illustrated in Figure 5.39 and the variogram parameters are presented in Table 5.15.

The PilotSTRATEGY project has received funding from the European Union's Horizon 2020 research and innovation programme under grant agreement No. 101022664

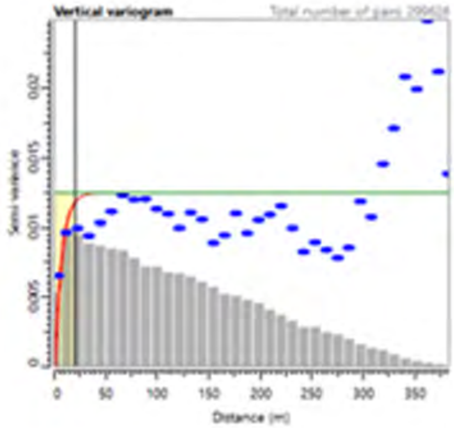

Figure 5.39: Vertical variogram of the available well-log effective porosity of the Lower Cretaceous – Reservoir region.

Table 5.15: Variogram modelling parameters for effective porosity simulation of the reservoir region (Lower Cretaceous).

Variogram Model	Azimuth (º)	Vertical Direction Range (m)	Main Direction Range (m)	Minor Direction Range (m)
Exponential	45	20	6250	3750

7.3.3.4 Permeability

7.3.3.4.1 Upper Cretaceous – Secondary Seal

The vertical experimental variogram of the permeability for the secondary seal (Upper Cretaceous) is illustrated in Figure 5.40 and the variogram parameters are presented in Table 5.16.

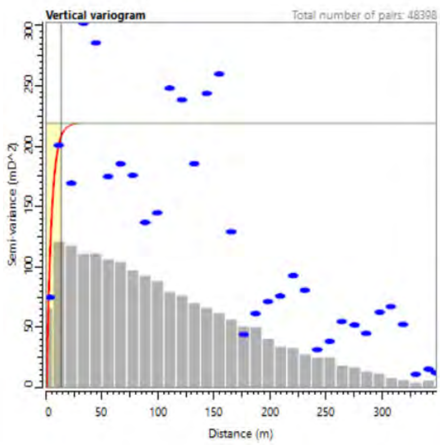

Figure 5.40: Vertical variogram of the available well-log permeability of the Upper Cretaceous – Secondary Seal region.

Table 5.16: Variogram modelling parameters for permeability simulation of the secondary seal region (Upper Cretaceous).

Variogram Model	Azimuth (º)	Vertical Direction Range (m)	Main Direction Range (m)	Minor Direction Range (m)
Exponential	45	17	6250	5000

7.3.3.4.2 Upper Cretaceous – Primary Seal

The vertical experimental variogram of the permeability for the primary seal (Upper Cretaceous) is illustrated in Figure 5.41 and the variogram parameters are presented in Table 5.17.

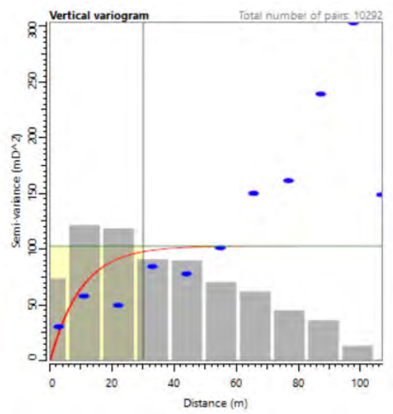

Figure 5.41: Vertical variogram of the available well-log permeability of the Upper Cretaceous – Primary Seal region.

Table 5.17: Variogram modelling parameters for permeability simulation of the primary seal region (Upper Cretaceous).

Variogram Model	Azimuth (º)	Vertical Direction Range (m)	Main Direction Range (m)	Minor Direction Range (m)
Exponential	45	30	3250	2250

7.3.3.4.3 Lower Cretaceous – Reservoir

The vertical experimental variogram of the permeability for the reservoir (Lower Cretaceous) is illustrated in Figure 5.42 and the variogram parameters are presented in Table 5.18.

The PilotSTRATEGY project has received funding from the European Union's Horizon 2020 research and innovation programme under grant agreement No. 101022664

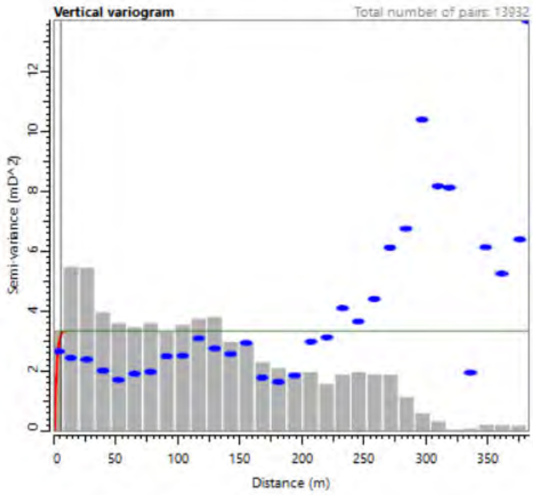

Figure 5.42: Vertical variogram of the available well-log permeability of the Lower Cretaceous – Reservoir region.

Table 5.18: Variogram modelling parameters for permeability simulation of the reservoir region (Lower Cretaceous).

Variogram Model	Azimuth (º)	Vertical Direction Range (m)	Main Direction Range (m)	Minor Direction Range (m)
Exponential	45	9	6250	3750

7.3.4 Upscaling of Hard Data

Due to the differences in the resolution of the well-log data and the vertical cell thickness of the static model, the upscaling process is required before conducting the lithofacies and petrophysical modelling. The hard data (raw) of the rock properties of the wells is converted into blocked data to complete the transferring of the data to the geological model grid.

Different methods were tested, such as nearest-to-cell-center, arithmetic mean, harmonic mean, and geometric mean, to check the accuracy of the upscaling process and to preserve the small-scale vertical heterogeneities of the well-log data. From the tested methods, the nearest-to-cell-center method matches with relative accuracy (comparing to the other methods) not only the heterogeneities of the model regions, but also the main statistics were preserved from the high-resolution well-logs to the blocked data of the grid. Nonetheless, and valid for all the upscaling methods, the proportion of the minimum and/ or maximum values struggles to be exactly preserved due to the skewed nature of the histograms of permeability and, in some cases, the volume of shale and effective porosity.

The next sub-sections present the comparison between the raw vs. blocked data for all the rock properties according to the three model regions of interest.

7.3.4.1 Upper Cretaceous – Secondary Seal

The PilotSTRATEGY project has received funding from the European Union's Horizon 2020 research and innovation programme under grant agreement No. 101022664

The histograms of the rock properties for the secondary seal region (Upper Cretaceous), as illustrated in Figure 5.43, comparing the raw data and the upscaled blocked data.

It is important to note that the permeability values required a transformation from logarithmic scale to linear scale before performing the simulation (and vice-versa after simulation).

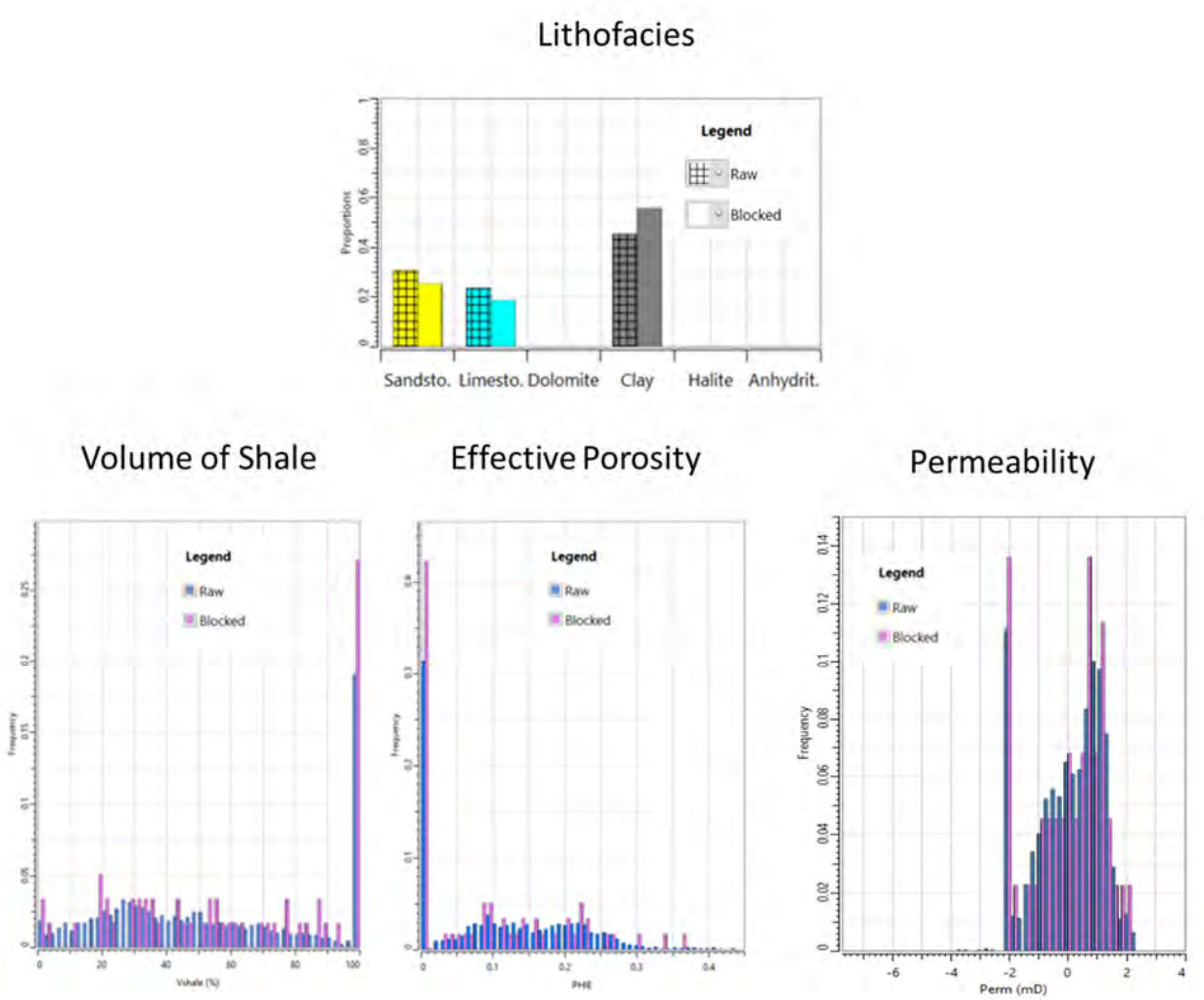

Figure 5.43: Raw vs. blocked histograms of the available well-log data of the Upper Cretaceous – Secondary Seal region.

7.3.4.2 Upper Cretaceous – Primary Seal

The histograms of the rock properties for the primary seal region (Upper Cretaceous), as illustrated in Figure 5.44, comparing the raw data and the upscaled blocked data.

It is important to note that the permeability values required a transformation from logarithmic scale to linear scale before performing the simulation (and vice-versa after simulation).

The PilotSTRATEGY project has received funding from the European Union's Horizon 2020 research and innovation programme under grant agreement No. 101022664

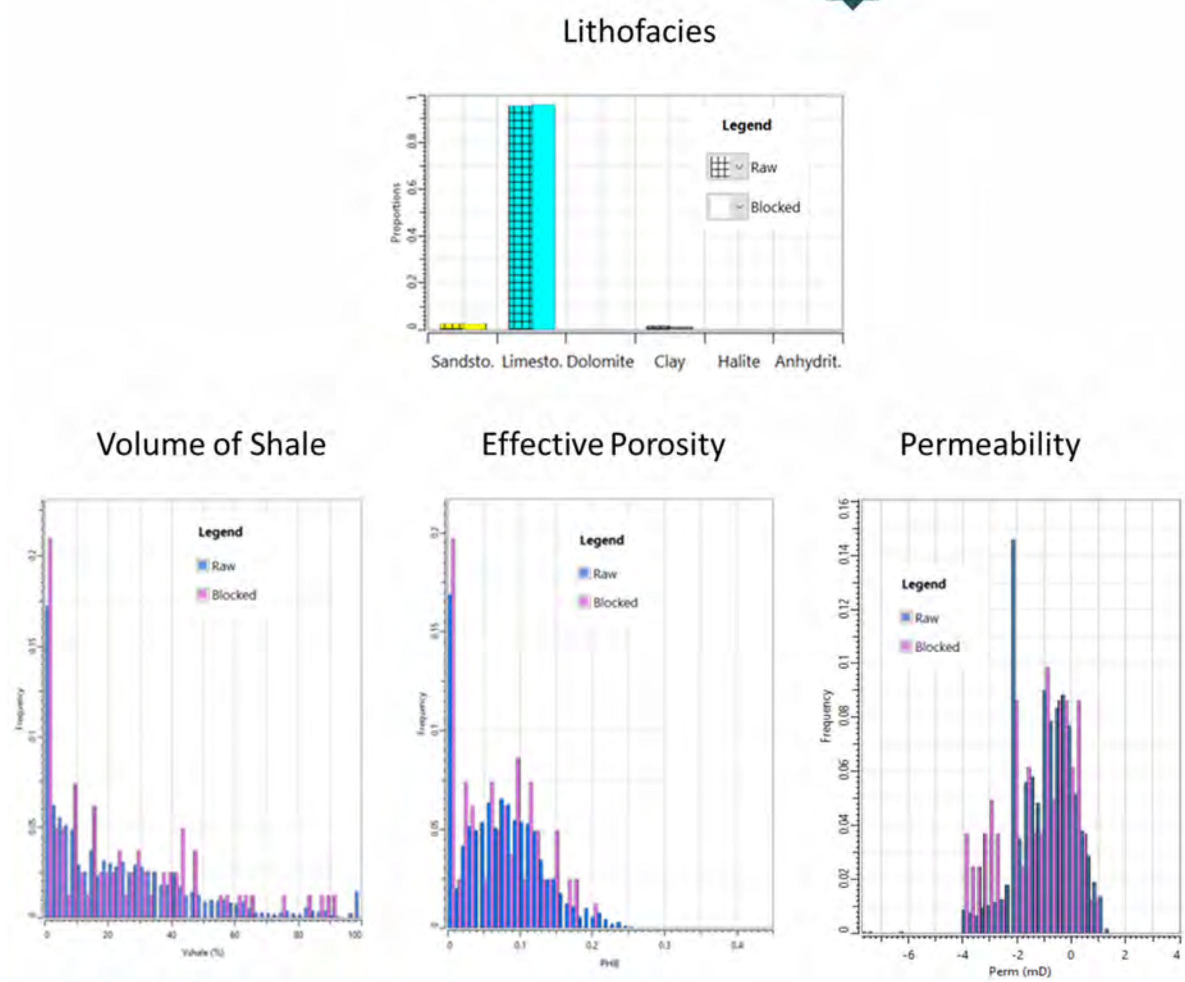

Figure 5.44: Raw vs. blocked histograms of the available well-log data of the Upper Cretaceous – Primary Seal region.

7.3.4.3 Lower Cretaceous – Reservoir

The histograms of the rock properties for the reservoir region (Lower Cretaceous), as illustrated in Figure 5.45, comparing the raw data and the upscaled blocked data.

It is important to note that the permeability values required a transformation from logarithmic scale to linear scale before performing the simulation (and vice-versa after simulation).

The PilotSTRATEGY project has received funding from the European Union's Horizon 2020 research and innovation programme under grant agreement No. 101022664

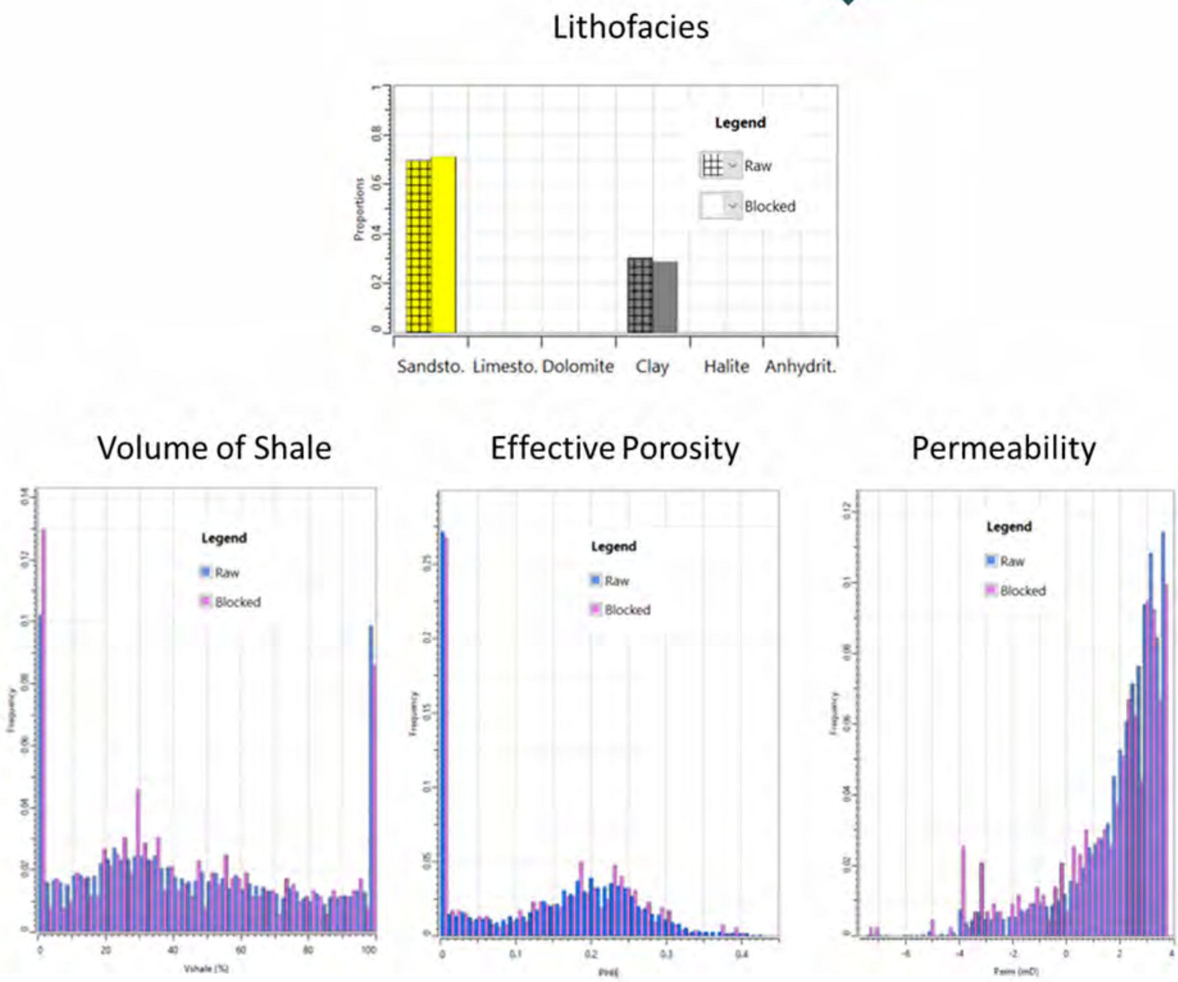

Figure 5.45: Raw vs. blocked histograms of the available well-log data of the Lower Cretaceous – Reservoir region.

7.3.5 Soft Data for Simulations

The inference of rock properties using geostatistical simulation and co-simulation algorithms is achieved relying on the well-log data (hard data) and conditioning of soft data. The resulting models honour the reproduction of the properties at the location of the wells, the univariate statistics (i.e., the probability distribution function of the property of interest, represented by the histogram), the bi-variate statistics (i.e., the joint distribution between the primary and secondary variables, represented by the cross-plot) and the spatial continuity patterns (represented by the variogram models). However, when the hard data spatial coverage lacks in the area under study, the integration of additional conditioning data (soft data) may be advantageous to improve the simulation models according to a prior knowledge or conceptual information available. It is important to mention that the use of soft data in the simulation must be handled carefully to avoid over-constraints of the simulation results, limiting the uncertainty exploration of the model parameters space.

The next sub-section presents the soft data considered for the simulation of discrete and continuous properties, such as lithofacies and effective porosity, respectively.

7.3.5.1 Lithofacies

The PilotSTRATEGY project has received funding from the European Union's Horizon 2020 research and innovation programme under grant agreement No. 101022664

The soft data for the lithofacies modelling was firstly conducted by estimating the 1D vertical proportion curves (VPCs) from the raw data of the wells. Figure 5.46 illustrates the VPCs of lithofacies simultaneously for the four available wells.

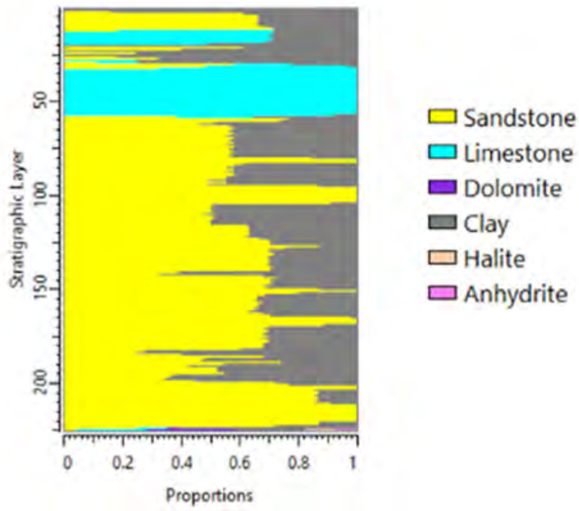

Figure 5.46: Vertical proportion curves (VPCs) of lithofacies of the available well data.

From the 1D VPCs of lithofacies, the spatial VPCs were generated based on a spatial matrix approach. This matrix dimensions should be defined according to the conceptual geological knowledge of the study area away from the well data, which in this case corresponds to the existence of interbedded clay layers within the sandstone reservoir. These conceptual VPCs of lithofacies were generated for the reservoir, and secondary and primary seals. Different dimensions of VPCs spatial matrices were tested for the i- and j-directions of the grid, such as 3x5, 5x7 and 6x8, respectively.

Due to the lack of more accurate knowledge from the conceptual model, and in order to avoid an over-constraint in the simulation of the lithofacies soft data, the VPCs spatial matrix of 3x5 was adopted, in which the matrix squares where the wells are located were conditioned by the VPCs of the wells (hard data) and the remaining locations by the conceptual VPCs that were edited manually for this purpose as illustrated in Figure 5.43. These VPCs away from the wells were edited manually according to the conceptual knowledge of the reservoir and the available well data, i.e., sandstones with interbedded clays, establishing different proportions for both sandstone and clay lithofacies across the grid layers of the reservoir unit.

The PilotSTRATEGY project has received funding from the European Union's Horizon 2020 research and innovation programme under grant agreement No. 101022664

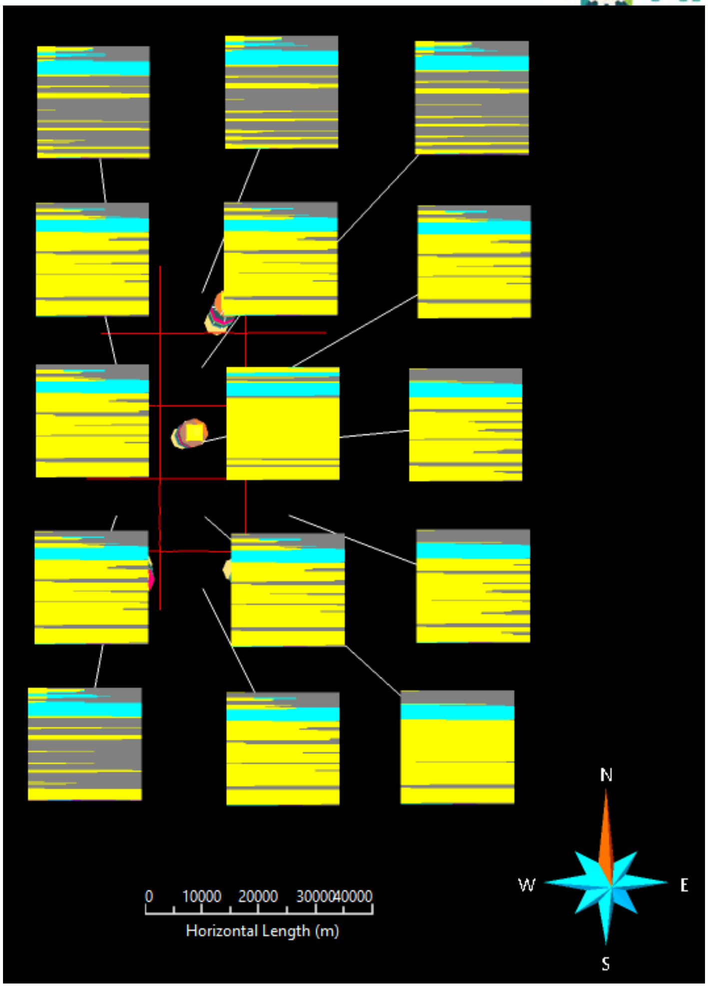

Figure 5.47: Spatial VPCs matrix of lithofacies with a dimension of 3x5.

The final step of determining the soft data of lithofacies consisted in building the 3D proportion cube by interpolating the information of the VPCs spatial matrix, using simple kriging, and transferring the soft data to the geological model grid. The final soft data of lithofacies resulted in 3D proportion cubes for the lithofacies of sandstone (Figure 5.48a), limestone (Figure 5.48b) and clay (Figure 5.48c).

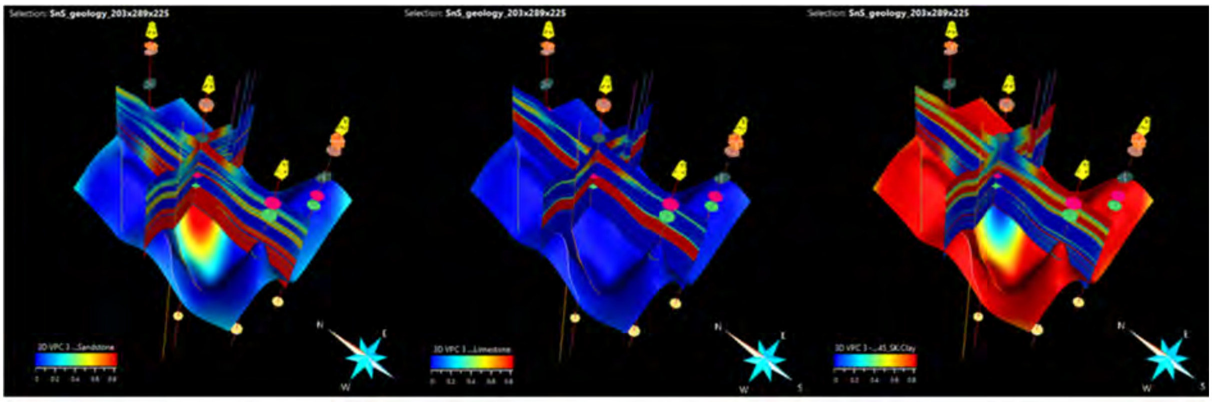

(a) (b) (c)

The PilotSTRATEGY project has received funding from the European Union's Horizon 2020 research and innovation programme under grant agreement No. 101022664

Figure 5.48: 3D VPCs cubes of lithofacies soft data for (a) sandstone, (b) limestone and (c) clay.

7.3.5.2 Effective Porosity

The soft data for continuous properties was also determined for the volume of clay and effective porosity, although only the soft data for the latter was kept due to inconsistencies in the final soft data results of the former, which may bring higher spatial uncertainty in the simulation models.

Similar as for the lithofacies, 1D vertical trend curves (VTCs) were estimated for the three model regions and considering the effective porosity data simultaneously for the available wells as shown in Figure 5.49.

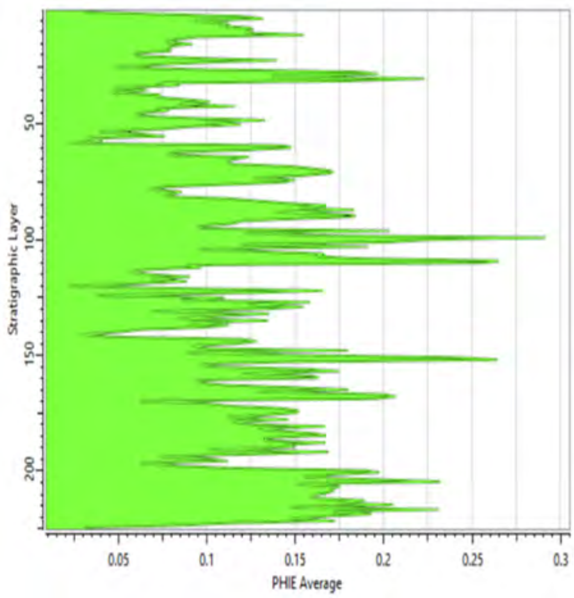

Figure 5.49: Vertical trend curves (VTCs) of effective porosity of the available well data.

After determining the VTCs from the raw well data (hard data), 2D trend maps of effective porosity were generated according to each lithofacies. These maps resulted from the interpolation of the VTCs using the discrete smooth interpolation (DSI) method for the lithofacies of sandstone (Figure 5.50a), limestone (Figure 5.50b) and clay (Figure 5.50c).

The PilotSTRATEGY project has received funding from the European Union's Horizon 2020 research and innovation programme under grant agreement No. 101022664

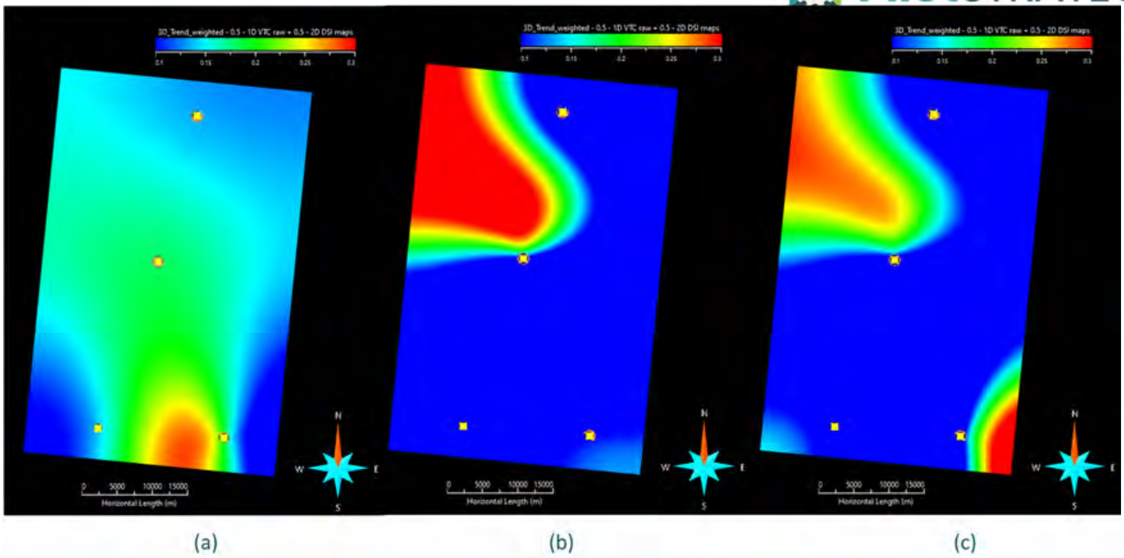

Figure 5.50: 2D trend maps of effective porosity according to the lithofacies (a) sandstone, (b) limestone, and (c) clay.

The 3D trend cube of effective porosity was calculated and transferred to the geological model grid using both the 1D VTCs and the 2D trend maps using a weighted average method. Different weights assigned to the VTCs and 2D trend maps were tested and a final weighting of 50% for each soft data was defined as a compromise of do not assign a high importance neither to the high-resolution log data nor to the smooth spatial trend maps. The resulting 3D trend cube is illustrated in Figure 5.51.

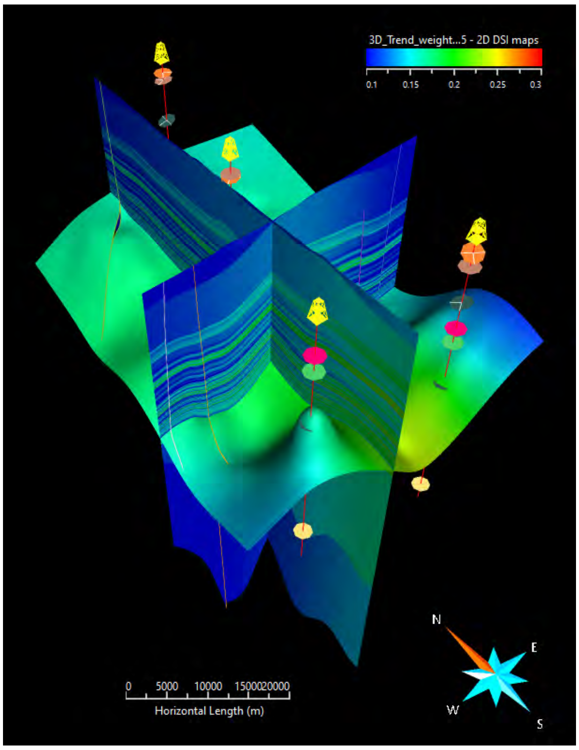

Figure 5.51: 3D trend cube of effective porosity in the geological model grid to condition the simulation as soft data.

The PilotSTRATEGY project has received funding from the European Union's Horizon 2020 research and innovation programme under grant agreement No. 101022664

7.3.6 Facies Modelling

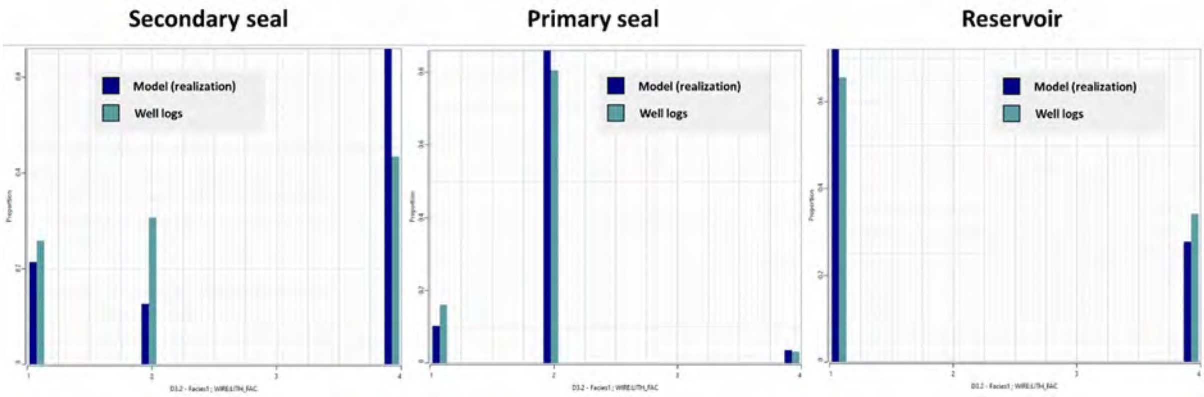

Figure 5.52: Histograms of lithofacies from the well data and the simulated models. Lithofacies 1 – sandstone, lithofacies 2 – limestone and lithofacies 4 – clay.

7.3.7 Petrophysical Modelling

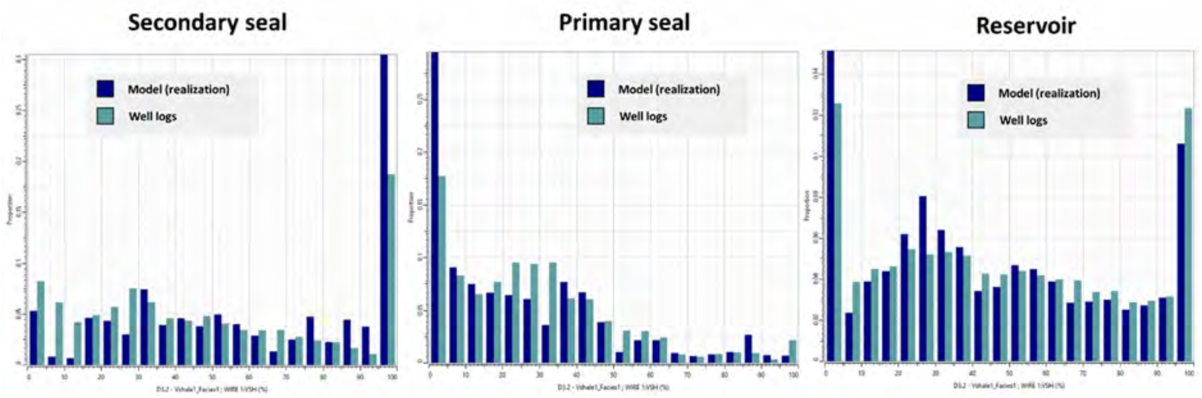

Figure 5.53: Histograms of volume of clay from the well data and the simulated models.

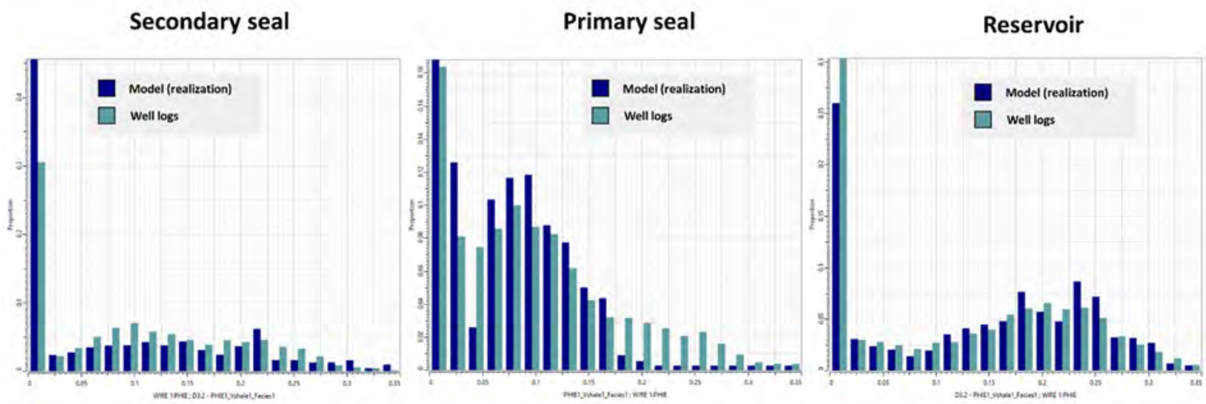

Figure 5.54: Histograms of effective porosity from the well data and the simulated models.

The PilotSTRATEGY project has received funding from the European Union's Horizon 2020 research and innovation programme under grant agreement No. 101022664

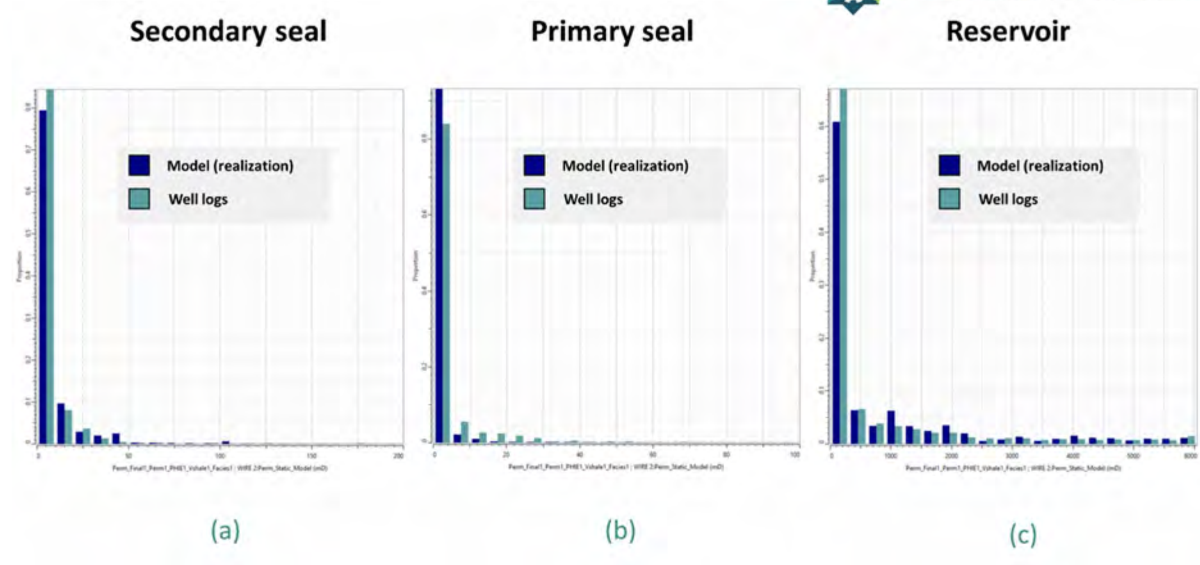

Figure 5.55: Histograms of permeability from the well data and the simulated models.

Table 5.19: Statistics of the Secondary seal rock properties.

Secondary Seal		Well logs (hard data)	Models
Volume of clay (%)	Number of Samples	59	1417698
	Minimum	0.0001	0.0001
	Median	59	64
	Maximum	99.99	99.99
	Mean	61	63
	Std. Deviation	32	33
Effective porosity (%)	Number of Samples	59	1417698
	Minimum	0.0001	0.0001
	Median	7	5
	Maximum	37	37
	Mean	9	9
	Std. Deviation	10	11
Permeability (mD)	Number of Samples	44	1417698
	Minimum	0.0001	0.0001
	Median	1.783	1.834
	Maximum	238	238
	Mean	9	10
	Std. Deviation	18	29

Table 5.20: Statistics of the Primary seal rock properties.

Primary Seal		Well logs (hard data)	Models
Volume of clay (%)	Number of Samples	81	1319797
	Minimum	0.0001	0.0001

The PilotSTRATEGY project has received funding from the European Union's Horizon 2020 research and innovation programme under grant agreement No. 101022664

	Median	16	18
	Maximum	99.99	99.99
	Mean	24	25
	Std. Deviation	24	24
Effective porosity (%)	Number of Samples	81	1319797
	Minimum	0.0001	0.0001
	Median	8	8
	Maximum	35	35
	Mean	7	9
	Std. Deviation	5	8
Permeability (mD)	Number of Samples	81	1319797
	Minimum	0.0001	0.0001
	Median	0.104	0.157
	Maximum	133	133
	Mean	4	4
	Std. Deviation	10	18

Table 5.21: Statistics of the Reservoir rock properties.

Reservoir		Well logs (hard data)	Models
Volume of clay (%)	Number of Samples	523	8063445
	Minimum	0.0001	0.0001
	Median	38	38
	Maximum	99.99	99.99
	Mean	44	44
	Std. Deviation	32	33
Effective porosity (%)	Number of Samples	523	8063445
	Minimum	0.0001	0.0001
	Median	14	16
	Maximum	41	41
	Mean	13	14
	Std. Deviation	11	11
Permeability (mD)	Number of Samples	432	8063445
	Minimum	0.0001	0.0001
	Median	176	116
	Maximum	6045	6045
	Mean	970	852
	Std. Deviation	1495	1432

7.3.8 Uncertainty Analysis

7.3.8.1 Structural Elements

The summary statistics and histograms of the displacement of each fault of the static model are shown in Table 5.22 and Figure 5.56, respectively. The summary statistics and histograms for the six faults simultaneously and for the two sets of faults are presented in Table 5.23 and Figure 5.57, respectively.

The PilotSTRATEGY project has received funding from the European Union's Horizon 2020 research and innovation programme under grant agreement No. 101022664

The negative values of faults displacements correspond to the simulated values from the left side of the fault surface while the positive values from the right side of the fault surface.

The faults F1 and F2 present lower values of the mean absolute displacements when compared to the fault F2, even assigning the same input value of maximum displacement of 50m. Similarly, the fault F4 also results in a higher uncertainty value of the mean absolute displacements comparing to the faults F5 and F6.

Table 5.22: Summary statistics of the fault displacement (relative to the base case) for each fault.

Fault Displacement (m)	F1	F2	F3	F4	F5	F6
Base Case	0					
Lower Case (P_{10})	-32.262	-34.075	-38.584	-73.626	-67.760	-80.470
Most Likely (P_{50})	7.470	7.559	-5.930	12.550	6.975	-21.785
Higher Case (P_{90})	35.359	34.181	40.139	75.808	76.796	73.941
Minimum	-47.118	-47.992	-55.213	-96.879	-92.550	-92.616
Mean	2.762	2.658	-0.380	0.470	4.138	-12.032
Maximum	43.490	42.478	49.235	93.509	89.006	85.758
Standard Deviation	26.335	25.701	29.242	56.036	56.1695	54.000
Variance	693.540	660.531	855.114	3140.070	3155.020	2916.020
Mean of Absolute Displacements	45.304	45.235	52.224	95.194	90.778	89.187
Number of Samples	100					

The PilotSTRATEGY project has received funding from the European Union's Horizon 2020 research and innovation programme under grant agreement No. 101022664

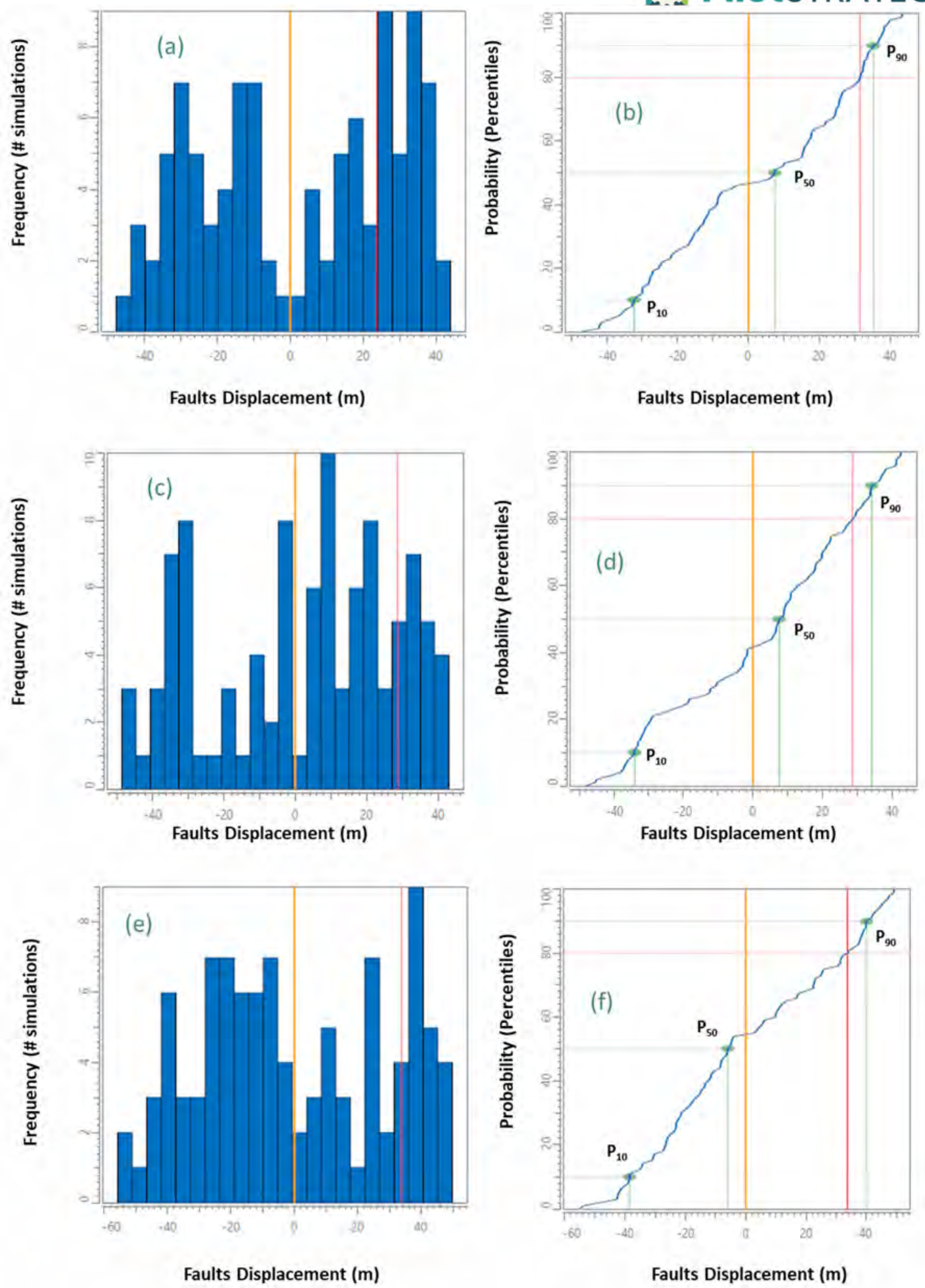
(a)
Frequency (# simulations)
Faults Displacement (m)
(b)
Probability (Percentiles)
P_{10}
P_{50}
P_{90}
Faults Displacement (m)
(c)
Frequency (# simulations)
Faults Displacement (m)
(d)
Probability (Percentiles)
P_{10}
P_{50}
P_{90}
Faults Displacement (m)
(e)
Frequency (# simulations)
Faults Displacement (m)
(f)
Probability (Percentiles)
P_{10}
P_{50}
P_{90}
Faults Displacement (m)

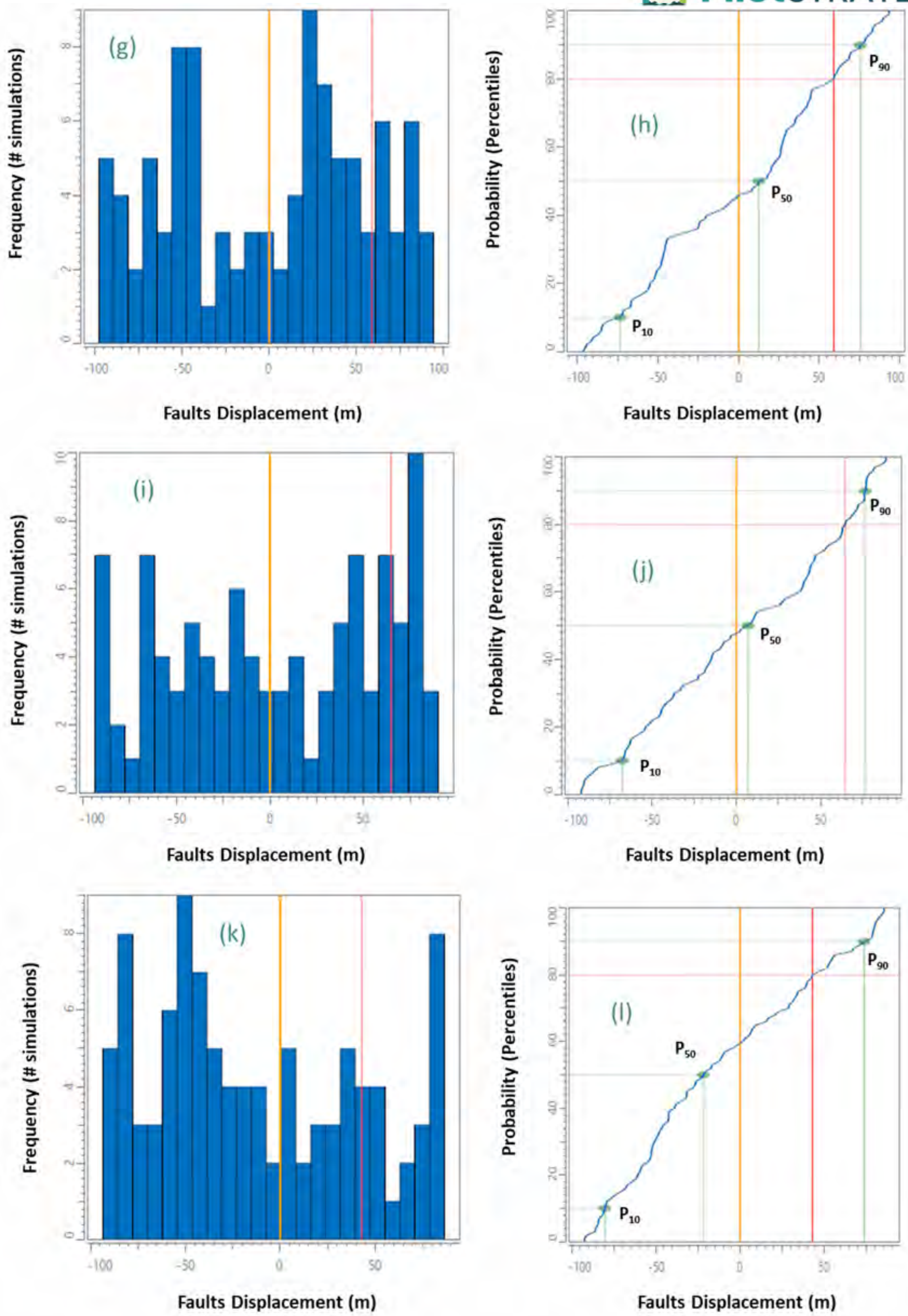

Figure 5.56: Histograms of the fault displacement for the faults: (a) F1, (c) F2, (e) F3, (g) F4, (i) F5 and (k) F6; and the corresponding cumulative distribution functions of the faults (b) F1, (d) F2, (f) F3, (h) F4, (j) F5 and (l) F6. The orange lines correspond to the base case scenarios (before the simulations) and the red lines correspond to a given selected simulation percentile.

The PilotSTRATEGY project has received funding from the European Union's Horizon 2020 research and innovation programme under grant agreement No. 101022664

Table 5.23: Summary statistics of the fault displacement (relative to the base case) for the 6 faults and fault sets 1 and 2.

Fault Displacement (m)	6 Faults	Set 1 (F1, F2, F3)	Set 2 (F4, F5, F6)
Base Case		0	
Lower Case (P_{10})	-137.154	-72.576	-128.981
Most Likely (P_{50})	-6.979	7.328	-2.214
Higher Case (P_{90})	144.198	75.831	126.460
Minimum	-290.205	-108.907	-204.581
Mean	-2.384	5.040	-7.4241
Maximum	272.258	122.524	196.350
Standard Deviation	107.688	54.810	92.505
Variance	11596.700	3004.090	8557.240
Mean of Absolute Displacements	281.232	115.716	200.466
Number of Samples		100	

The PilotSTRATEGY project has received funding from the European Union's Horizon 2020 research and innovation programme under grant agreement No. 101022664

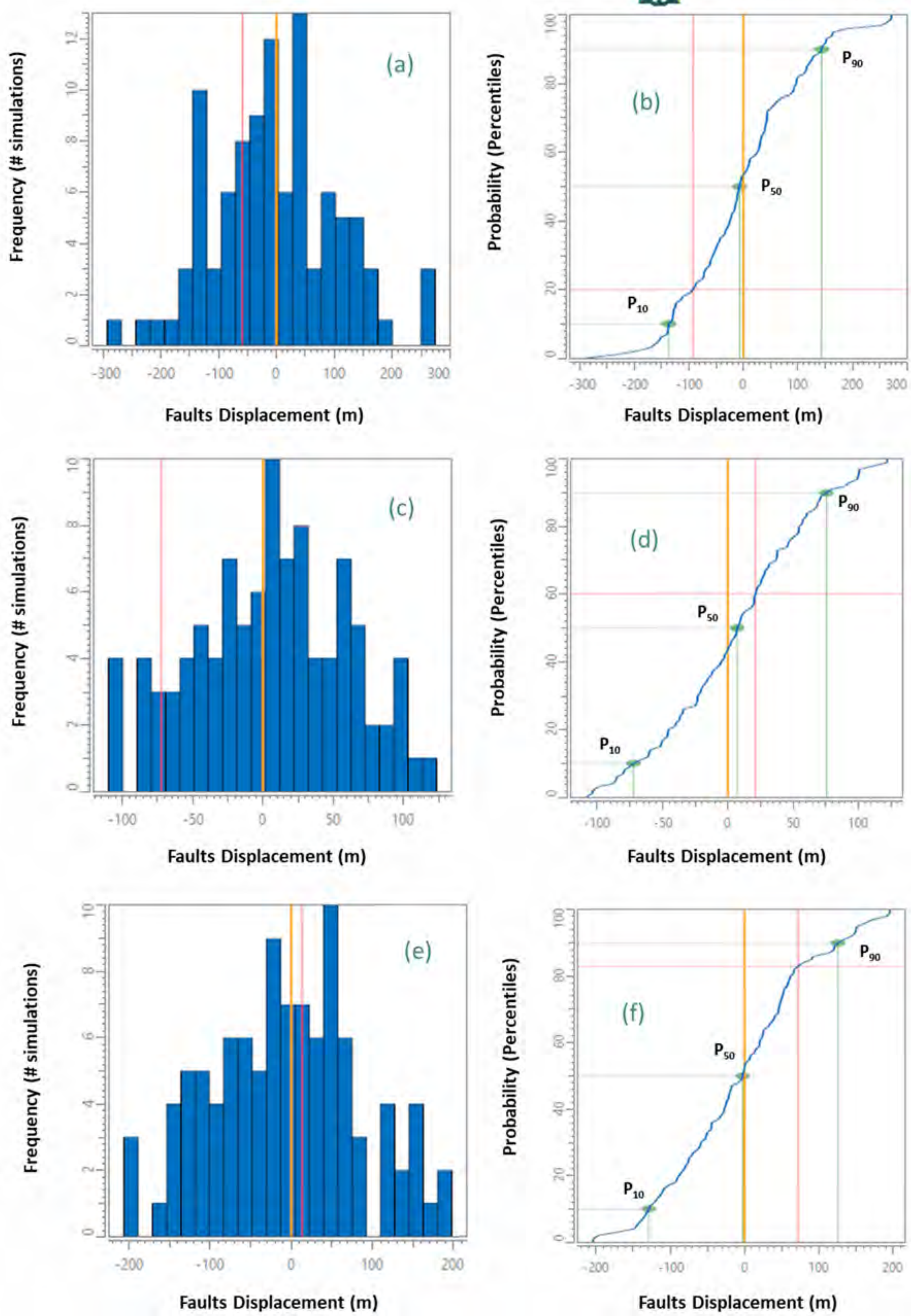

Figure 5.57: Histograms of the fault displacement for the (a) 6 faults, (c) fault set 1 and (e) fault set 2, and the corresponding cumulative distribution functions for the (b) 6 faults, (d) fault set 1 and (f) fault set 2. The orange lines correspond to the base case scenarios (before the simulations) and the red lines correspond to a given selected simulation percentile.

The PilotSTRATEGY project has received funding from the European Union's Horizon 2020 research and innovation programme under grant agreement No. 101022664

Figure 5.58 shows the histograms of the gross-rock volume for the static model (all regions) and reservoir region.

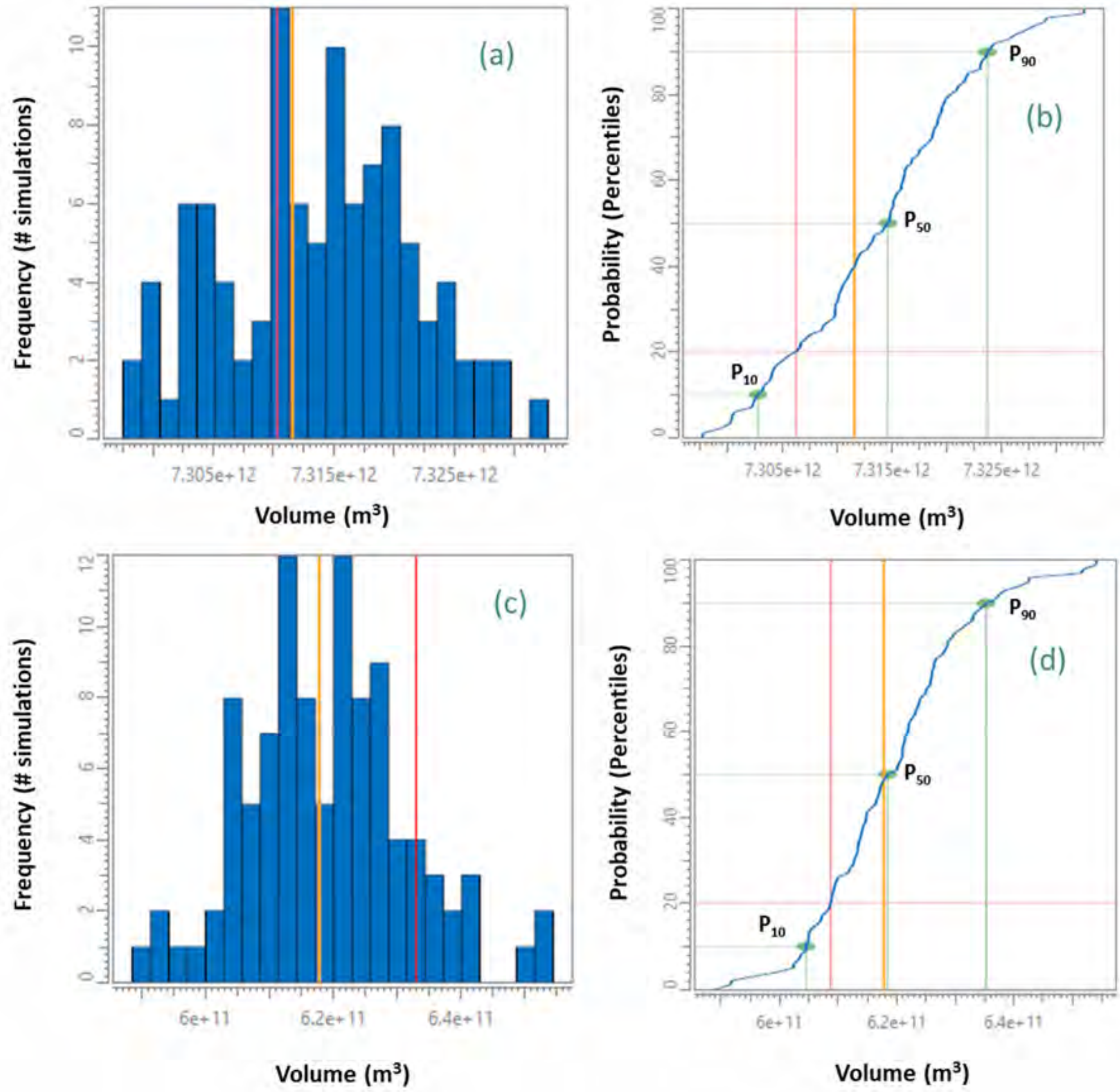

Figure 5.58: Histograms of the gross-rock volume for the (a) static model and (c) reservoir unit and the corresponding cumulative distribution functions for the (b) static model and (d) reservoir region. The orange lines correspond to the base case scenarios (before the simulations) and the red lines correspond to a given selected simulation percentile.

The PilotSTRATEGY project has received funding from the European Union's Horizon 2020 research and innovation programme under grant agreement No. 101022664

7.3.8.2 Petrophysical Properties

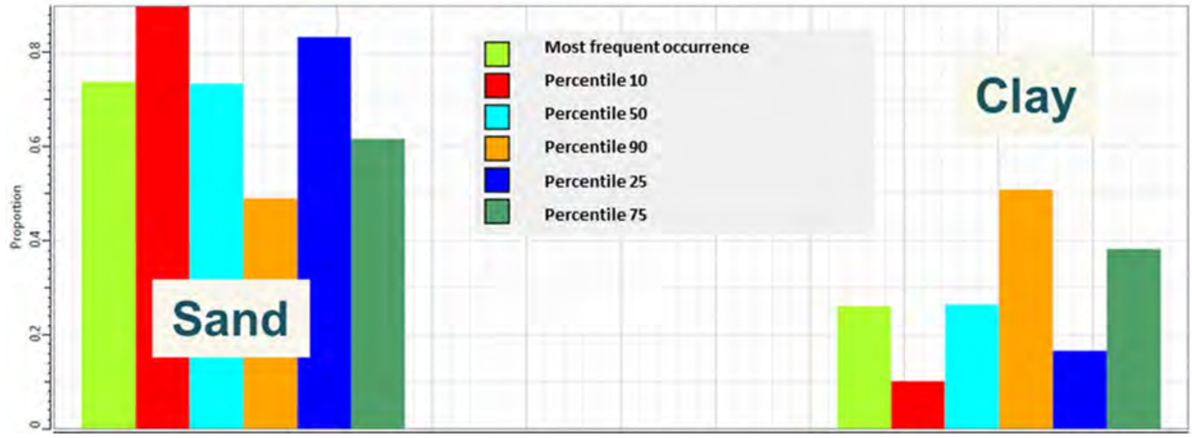

Figure 5.59: Histogram of lithofacies for the reservoir region.

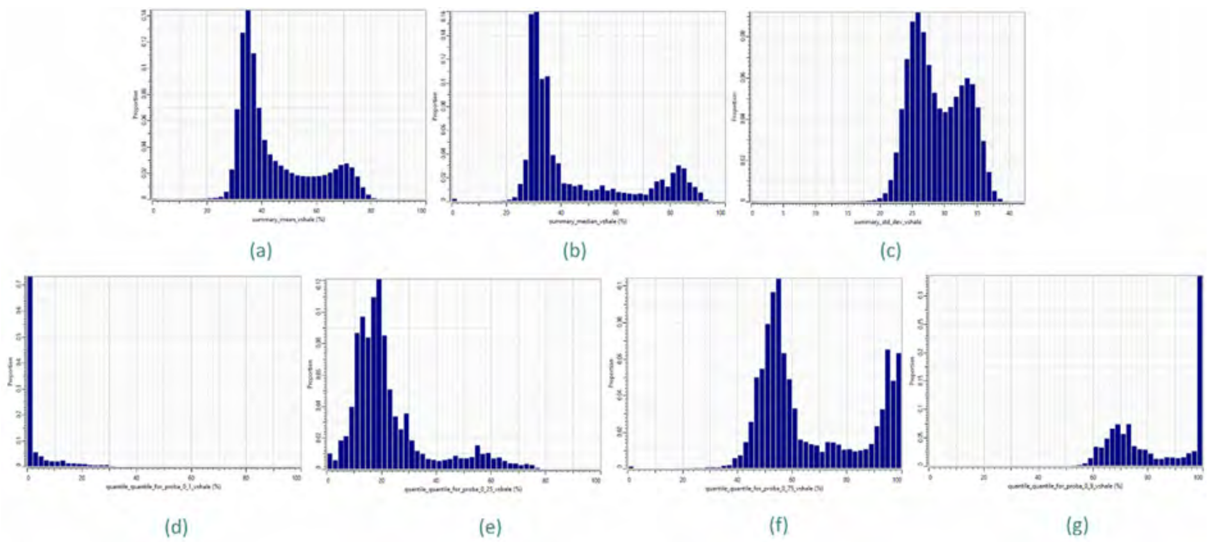

Figure 5.60: Histograms of volume of clay: (a) mean, (b) median (percentile 50), (c) standard deviation, (d) percentile 10, (e) percentile 25, (f) percentile 75, and (g) percentile 90 for the reservoir region (Lower Cretaceous)

The PilotSTRATEGY project has received funding from the European Union’s Horizon 2020 research and innovation programme under grant agreement No. 101022664

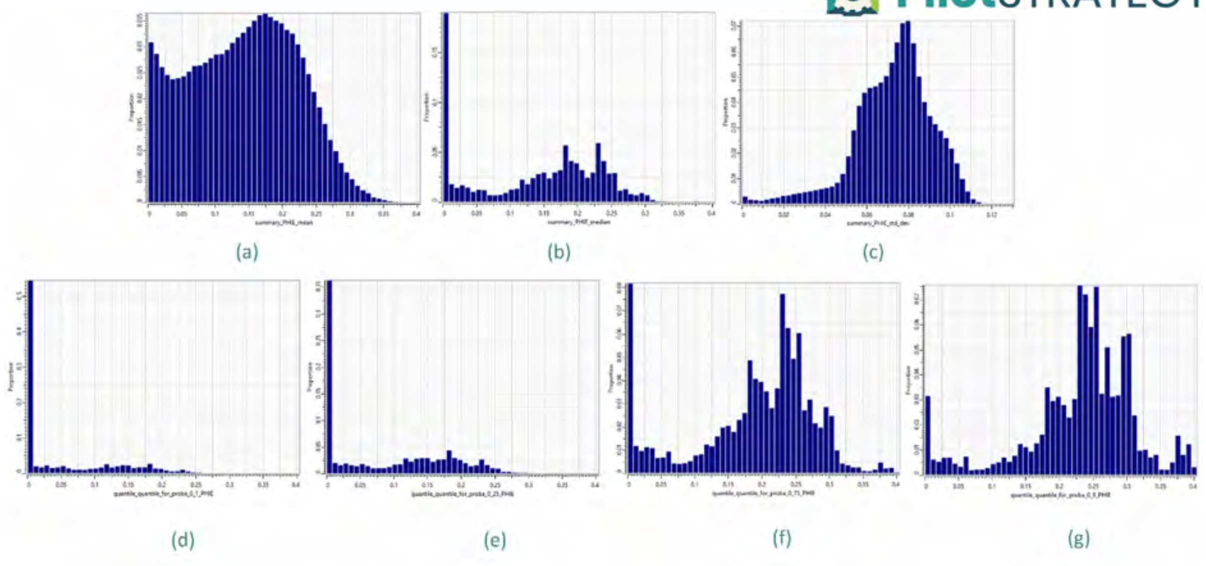

Figure 5.61: Histograms of effective porosity: (a) mean, (b) median (percentile 50), (c) standard deviation, (d) percentile 10, (e) percentile 25, (f) percentile 75, and (g) percentile 90 for the reservoir region (Lower Cretaceous).

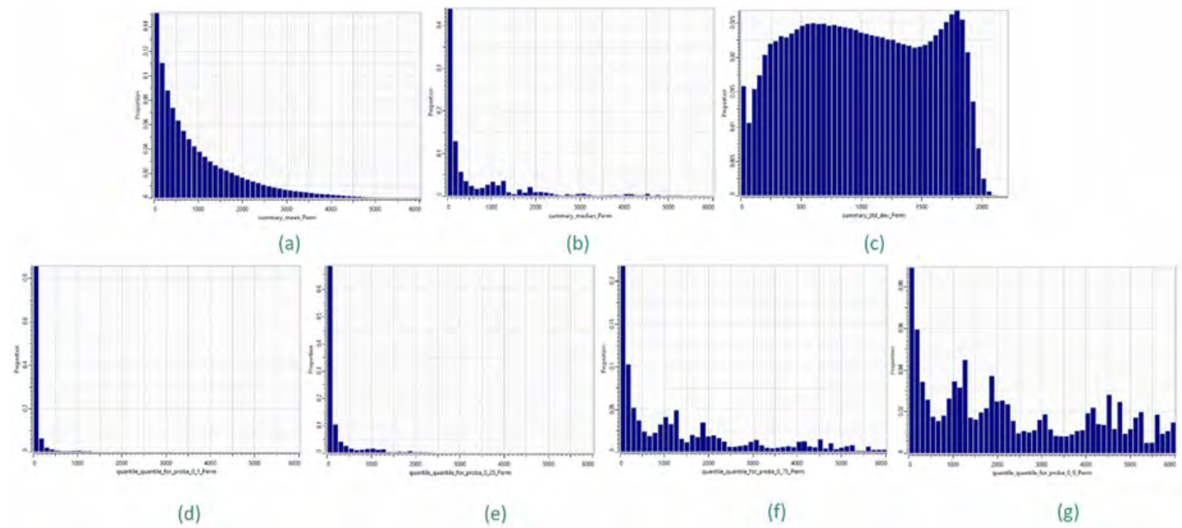

Figure 5.62: Histograms of permeability: (a) mean, (b) median (percentile 50), (c) standard deviation, (d) percentile 10, (e) percentile 25, (f) percentile 75, and (g) percentile 90 for the reservoir region (Lower Cretaceous).

The PilotSTRATEGY project has received funding from the European Union's Horizon 2020 research and innovation programme under grant agreement No. 101022664

7.3.8.3 Volumetrics

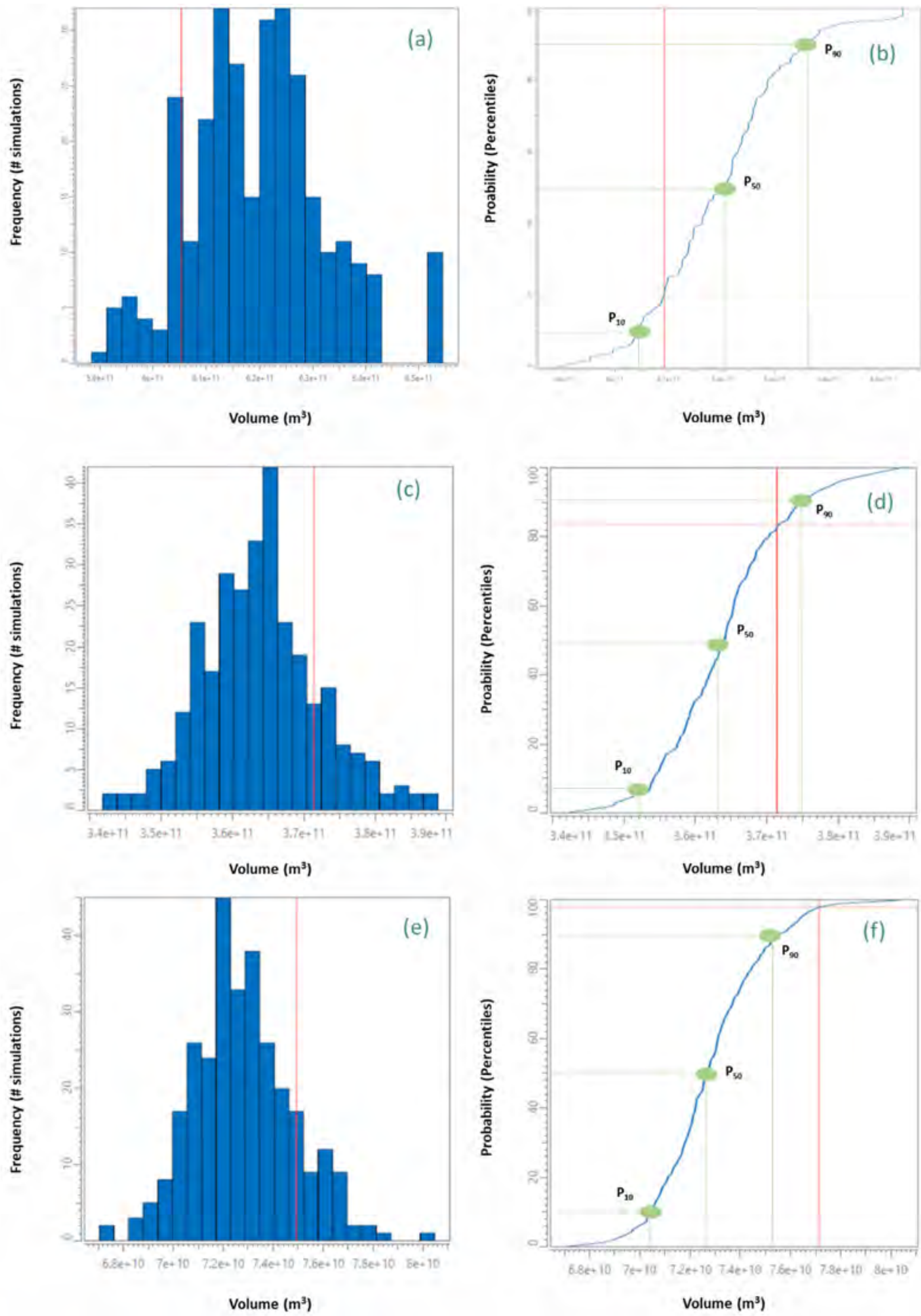

Figure 5.63: Histograms of the reservoir volumes for the reservoir region (Lower Cretaceous) of the static model: (a) gross-rock volume, (c) net-rock volume and (e) net-porous volume; and the corresponding cumulative distribution functions for the (b) gross-rock volume, (d) net-rock volume and (f) net-porous volume. The red lines correspond to a given selected simulation percentile.

The PilotSTRATEGY project has received funding from the European Union's Horizon 2020 research and innovation programme under grant agreement No. 101022664

7.4 Additional figures and tables for Ebro Basin, Spain region (6)

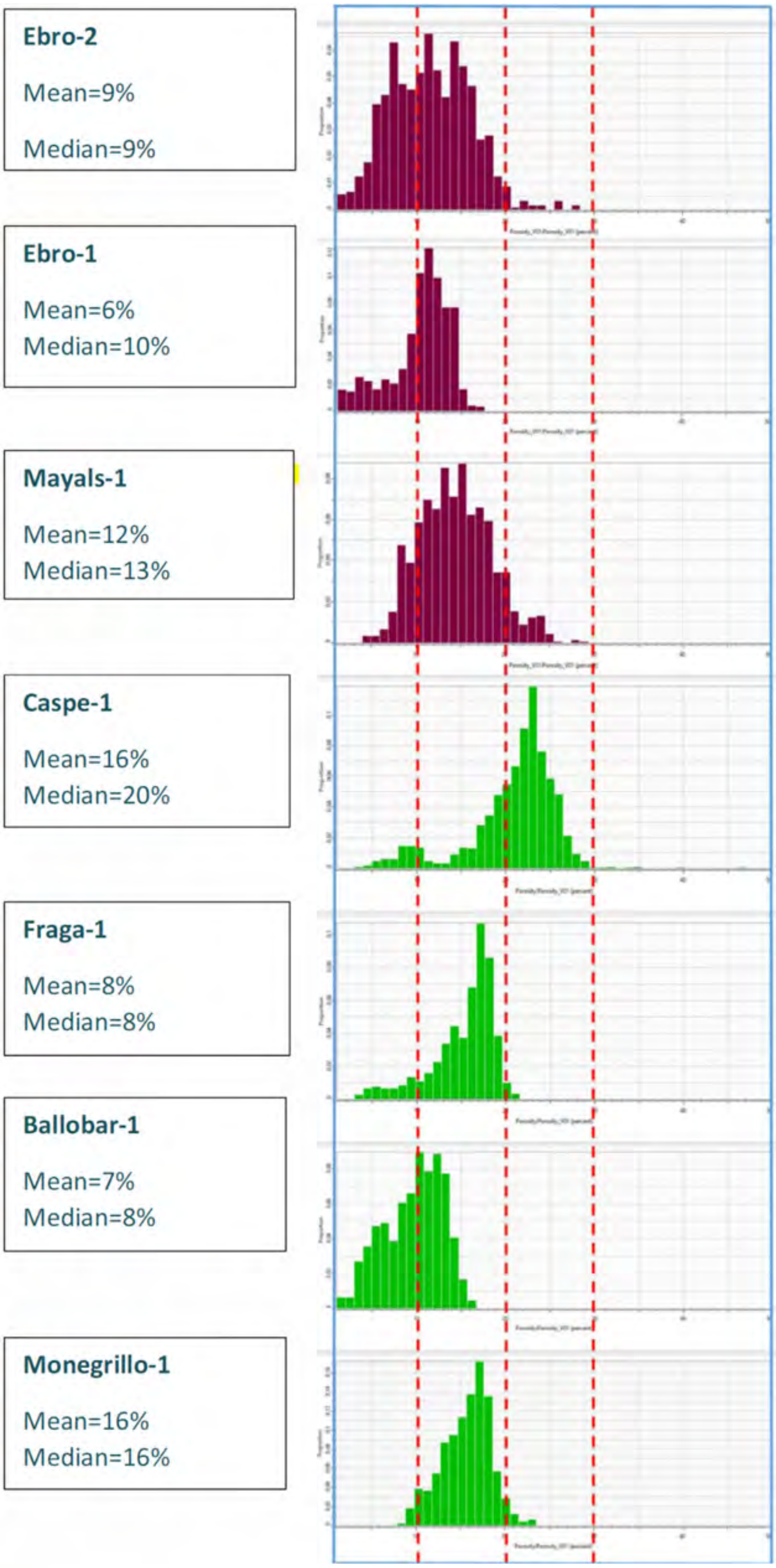

Figure 6-14: Porosity histograms of available offset wells in the area. Red dashed lines mark 10, 20 or 30% porosities.

The PilotSTRATEGY project has received funding from the European Union's Horizon 2020 research and innovation programme under grant agreement No. 101022664

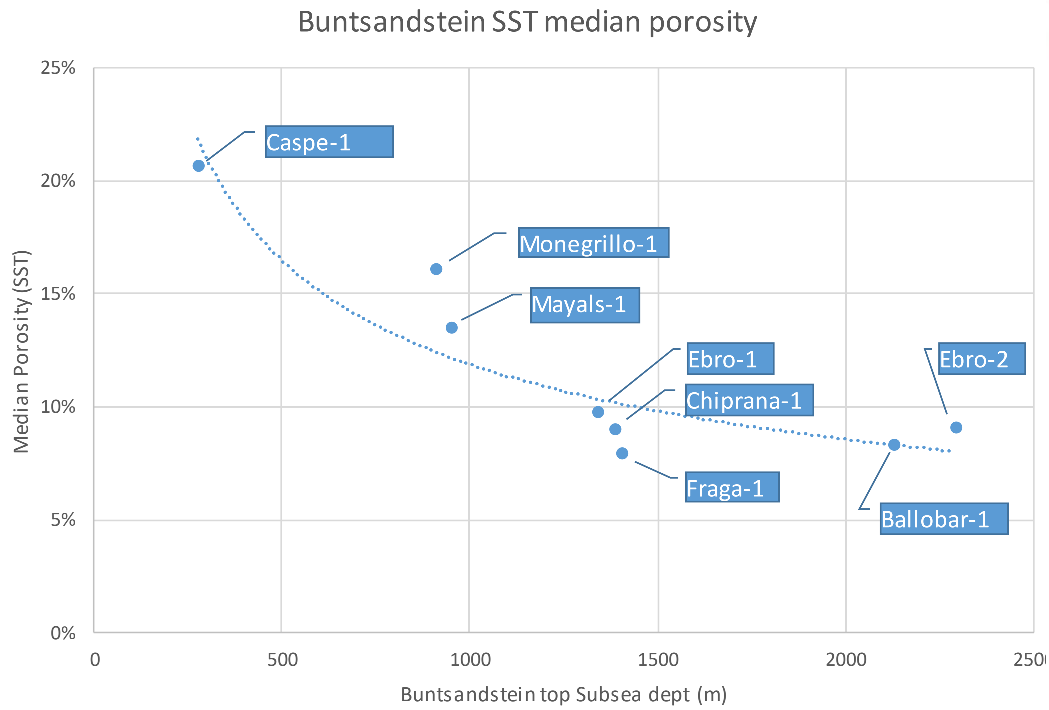

Figure 6-15: Crossplot of median porosities in the Buntsandstein sandstones versus Buntsandstein top depth (bmsl).

The PilotSTRATEGY project has received funding from the European Union's Horizon 2020 research and innovation programme under grant agreement No. 101022664

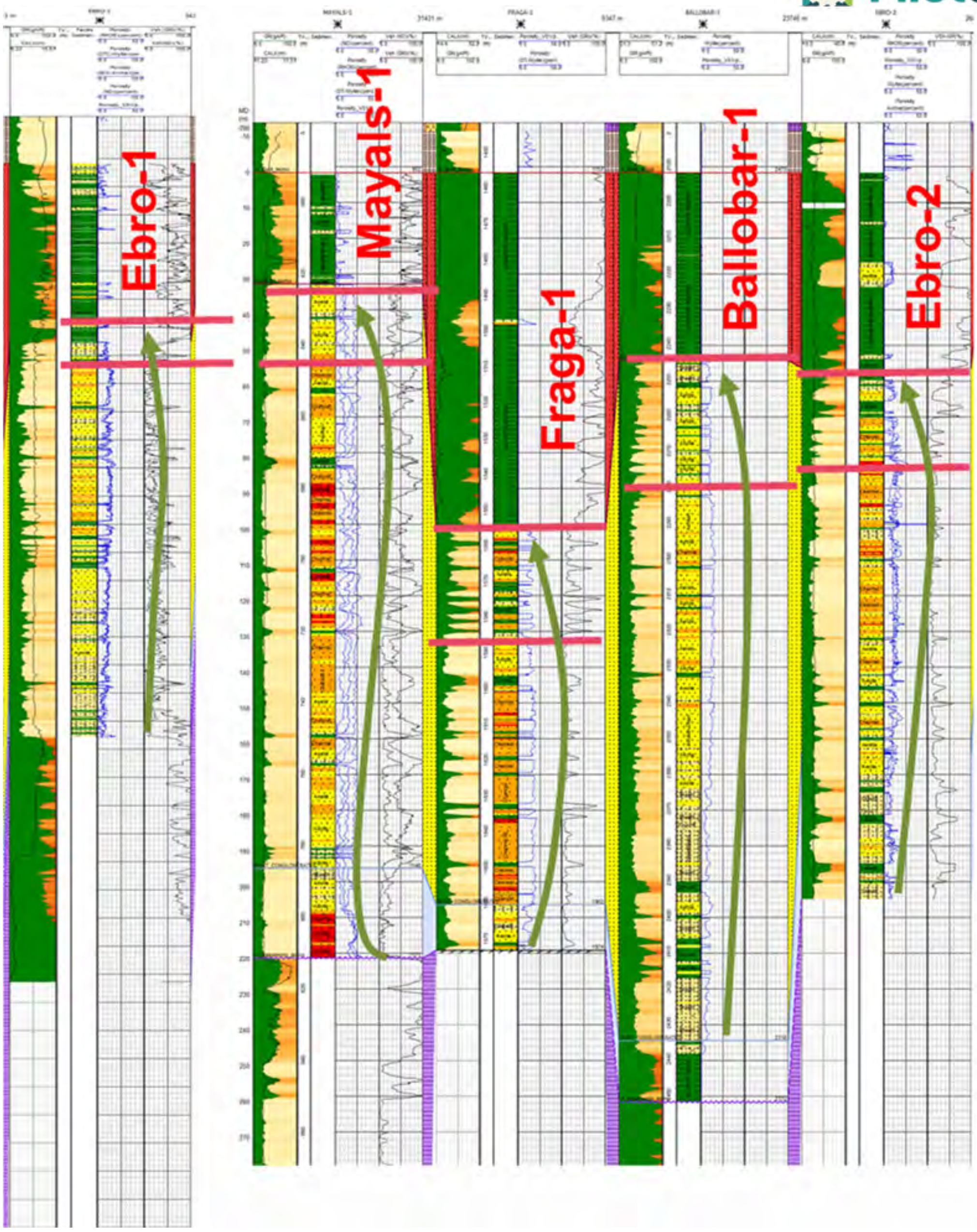

Figure 6-16: Porosities on some offset wells showing slight increase towards the B1 top, between the two horizontal red lines they gradually decrease until B2 formation.

The PilotSTRATEGY project has received funding from the European Union's Horizon 2020 research and innovation programme under grant agreement No. 101022664

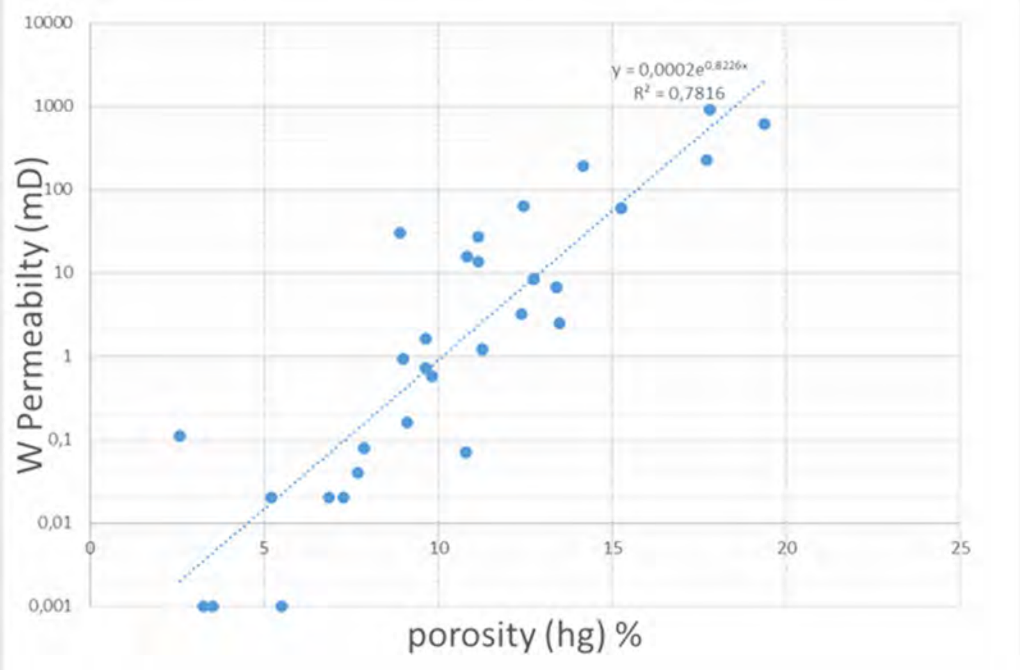

Figure 6-17: porosities from all rock samples from outcrops and core (Chiprana-1) versus the reported permeabilities from the laboratory. Below 8% porosity the permeabilities for water will be below 1 mD.

The PilotSTRATEGY project has received funding from the European Union's Horizon 2020 research and innovation programme under grant agreement No. 101022664

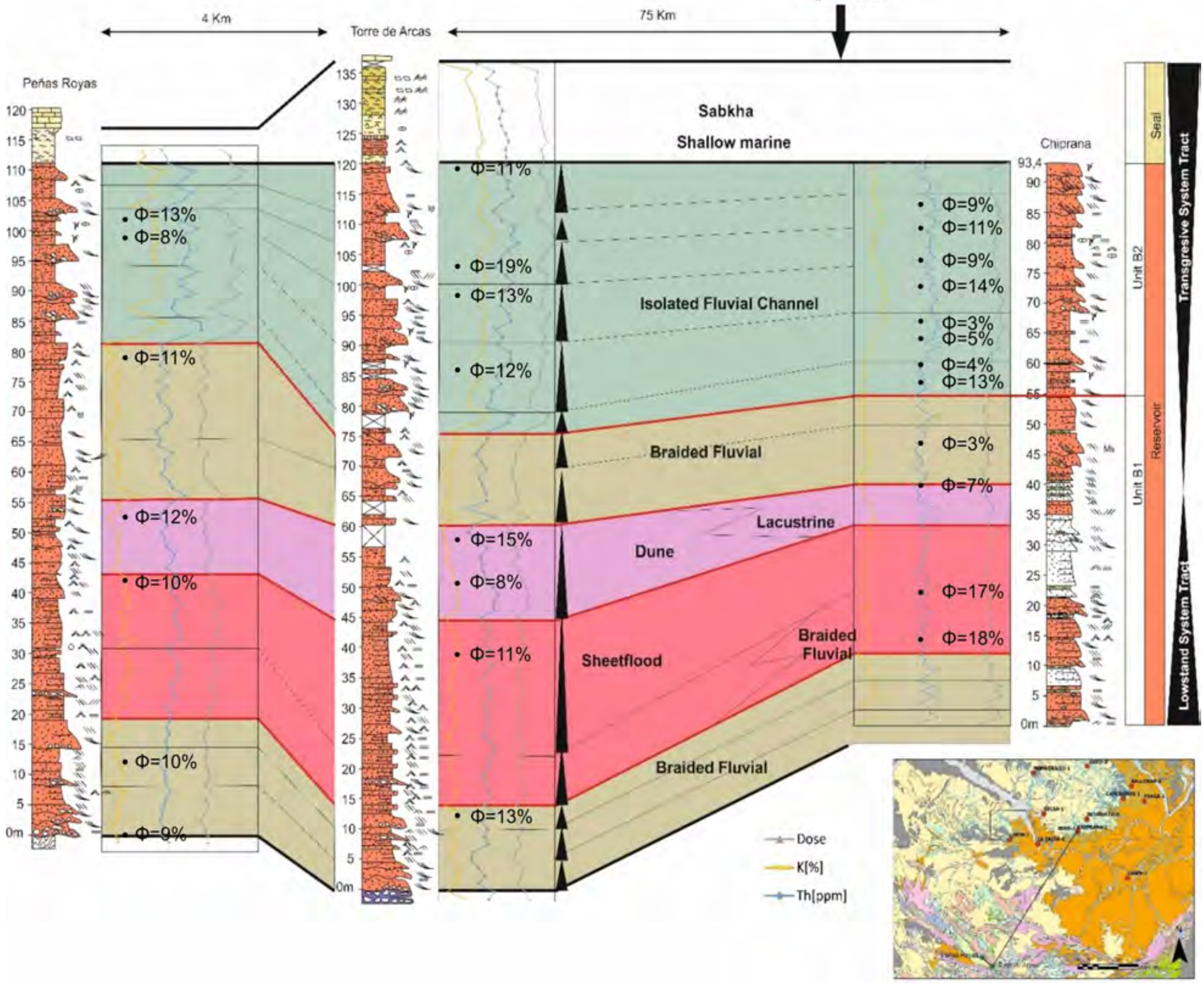

Figure 6-18: stratigraphic and sedimentological interpretation of outcrops and core (Chiprana-1) of the Buntsandstein in the Ebro Basin, with the field Spectral GR readings. Black balls mark the rock samples took and their porosities from laboratory test.

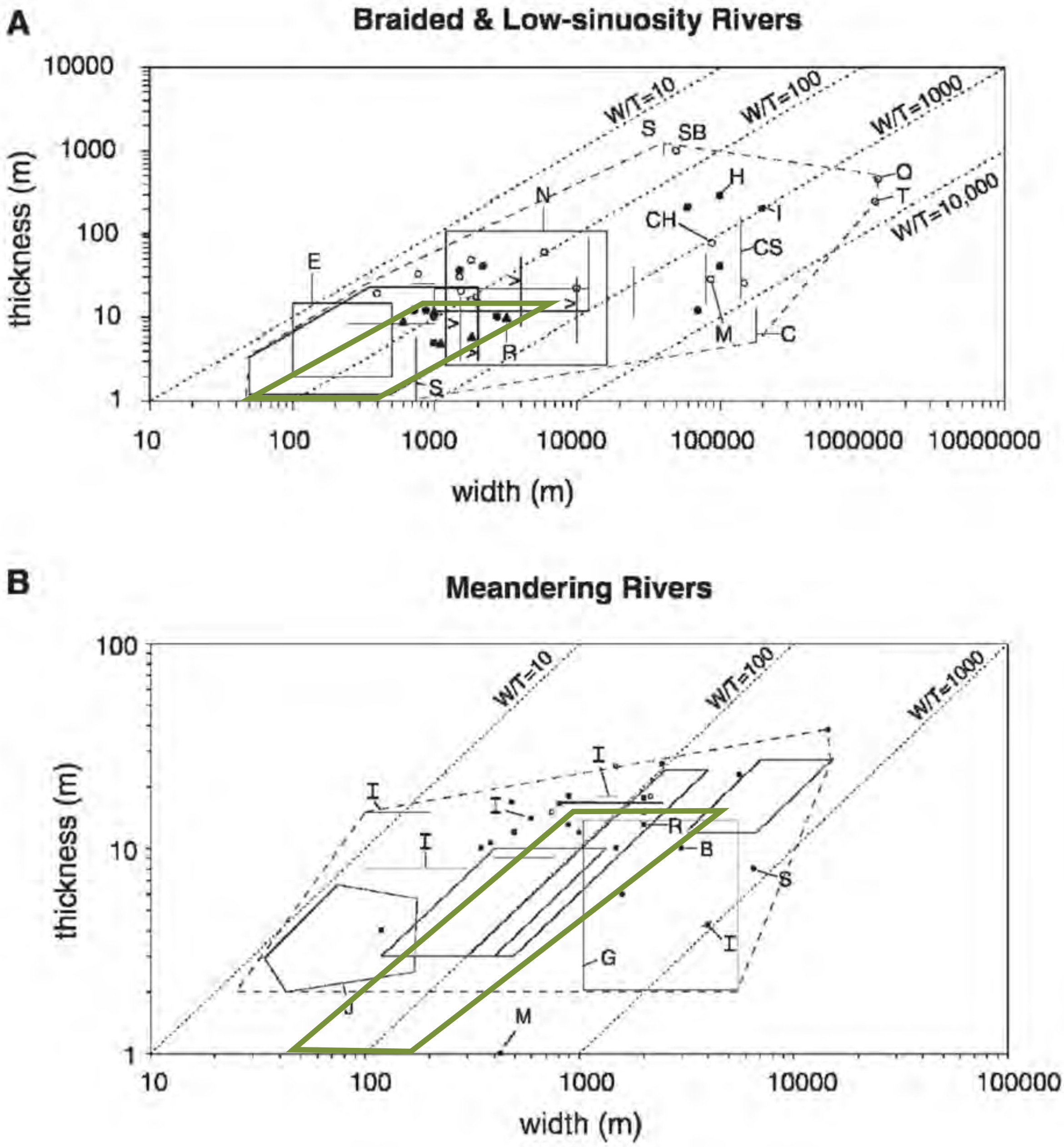

*Figure 6-19: **A**: Braided and low-sinuosity rivers; C= Cadomin formation; CH=Cypress Hills Formation; CS= Castlegate Sandstone; E=Escanilla Group; H=Hawkesbury Sandstone; I=Ivishak Sandstone; M=Mesa Rica Formation; N= Newcastle Coal Measures; O= Ogalalla Group; R= Quaternary, Riverina, Australia; S= Siwalik Group; SB= South Bar Formation; T= Tuscarora Formation. **B**: Meandering rivers; B= Beaufort Group; G= German Creek Formation; J= Jogging Formation; M= Miocene, Spain (Murillo el Fruto); I= Indonesian Cenocoiz; R= Rangal Coal Measures (solid squares); S= Scalby Formation (Gibling 2006). Outlined in green the areas with the Ebro Basin channels thickness/width modelled relationships.*

The PilotSTRATEGY project has received funding from the European Union's Horizon 2020 research and innovation programme under grant agreement No. 101022664

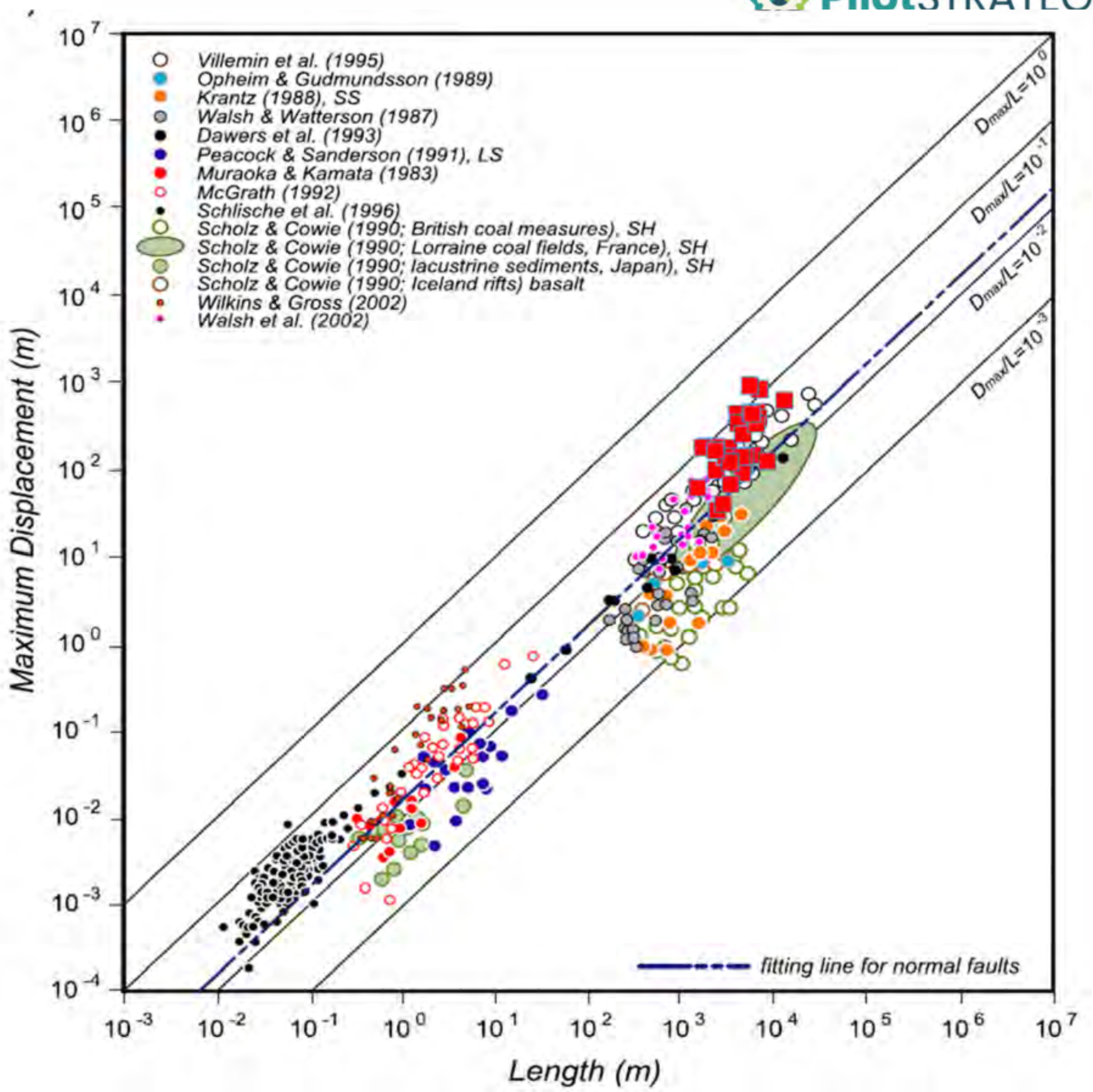

Figure 6-20: Maximum fault displacement vs fault length for the faults in the Lopín area (red squares) plotted over data from several authors for normal faults. Modified from Kim et al., 2003.

The PilotSTRATEGY project has received funding from the European Union's Horizon 2020 research and innovation programme under grant agreement No. 101022664

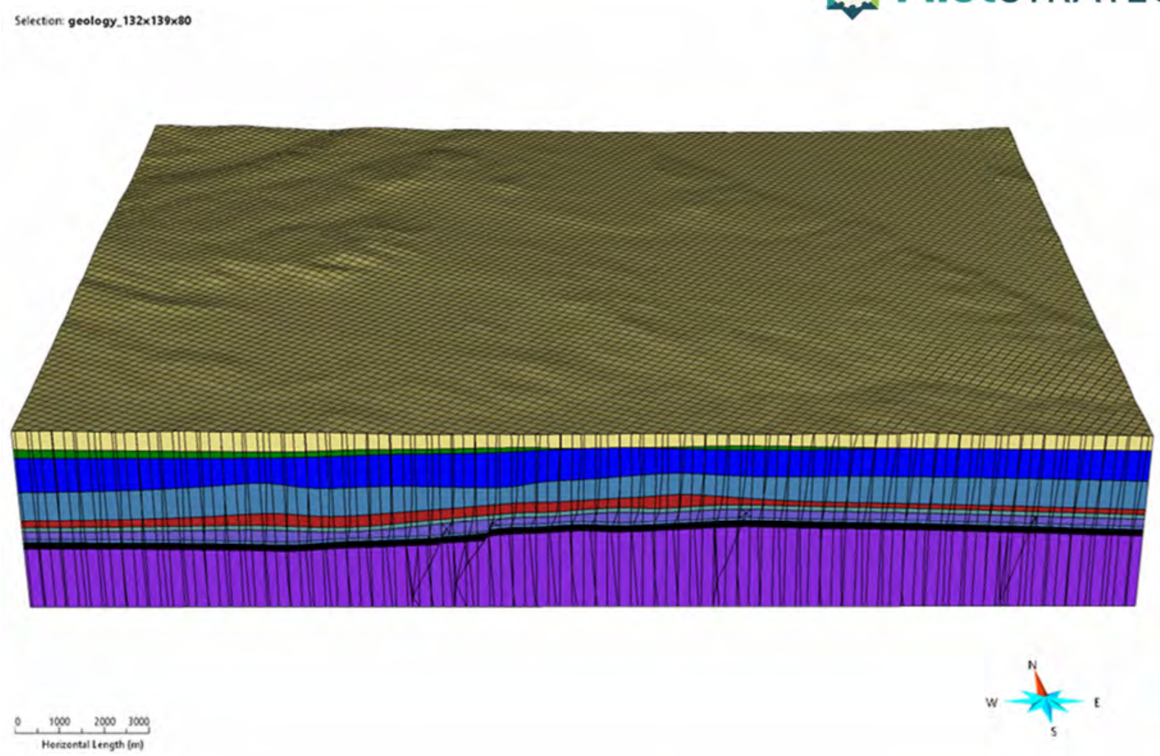

Figure 6-21: Grid model of the interpreted area. Over the basement, a layer corresponding to the storage formation, with a denser grid. The overburden and the underburden have only one cell in depth per formation.

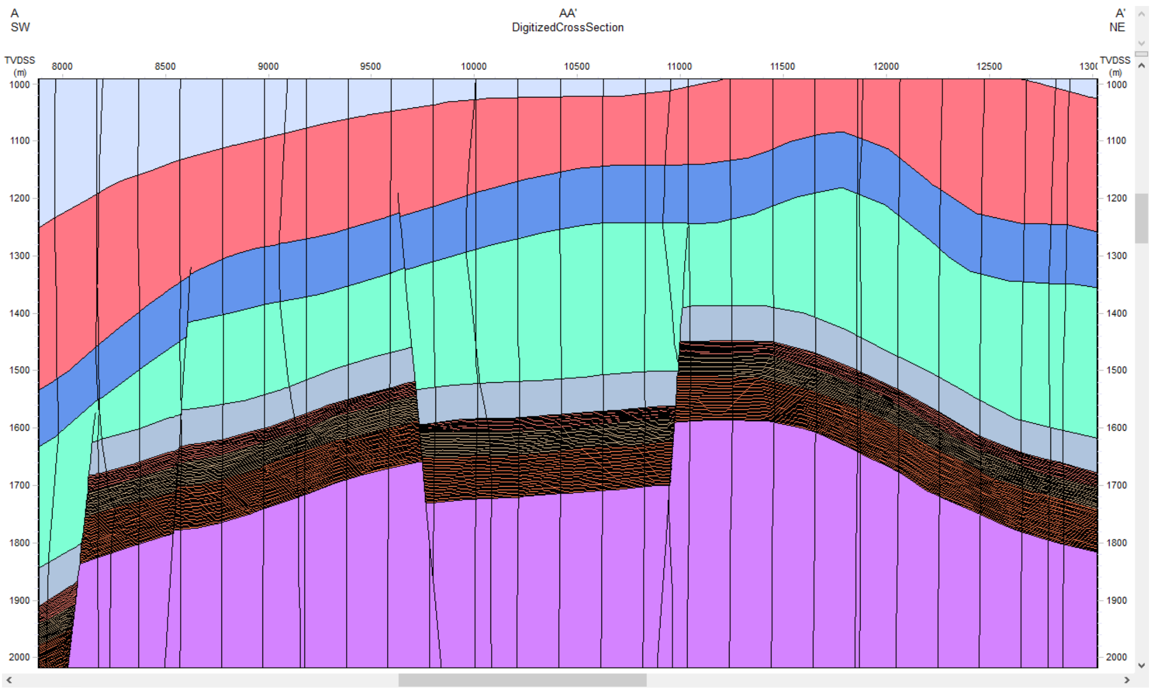

Figure 7-22: Cross section showing the denser discretization in the Buntsandstein formation. Vertical scale x3.

The PilotSTRATEGY project has received funding from the European Union's Horizon 2020 research and innovation programme under grant agreement No. 101022664

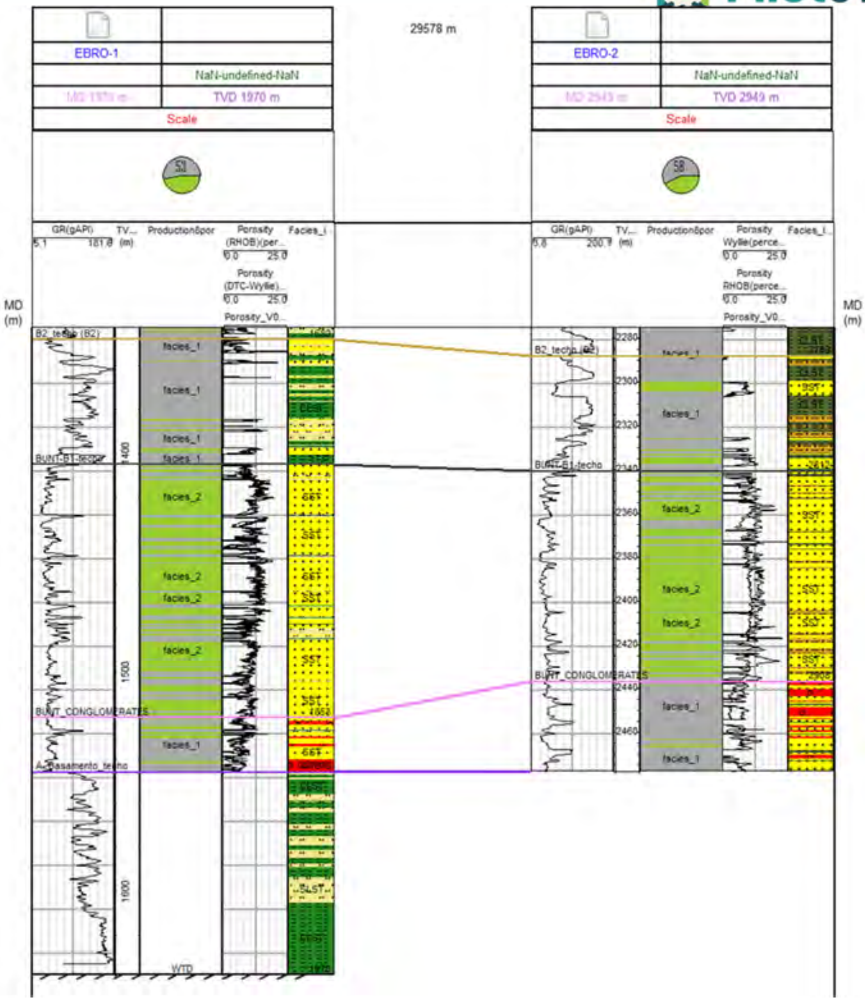

Figure 6-23: EBRO-1 (left) and EBRO-2 (right) correlation showing the logs used for the porosity estimation and the channel and shale facies defined from 8% porosity cut-off.

The PilotSTRATEGY project has received funding from the European Union's Horizon 2020 research and innovation programme under grant agreement No. 101022664

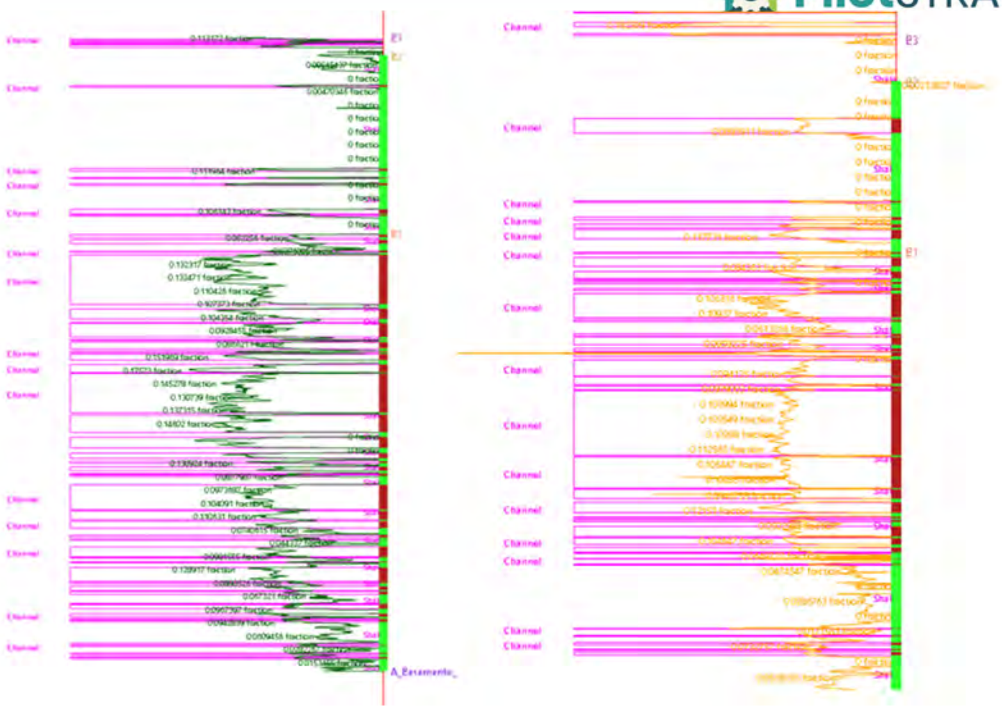

Figure 6-24: Regions defined in wells EBRO-1 (left) and EBRO-2 (right) from porosity ranges.

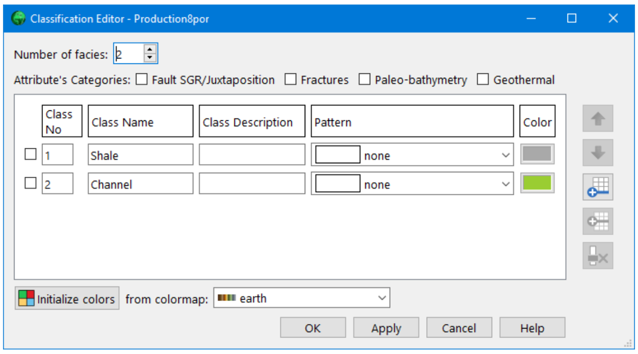

Figure 6-25: Classification for channel and shale.

The PilotSTRATEGY project has received funding from the European Union's Horizon 2020 research and innovation programme under grant agreement No. 101022664

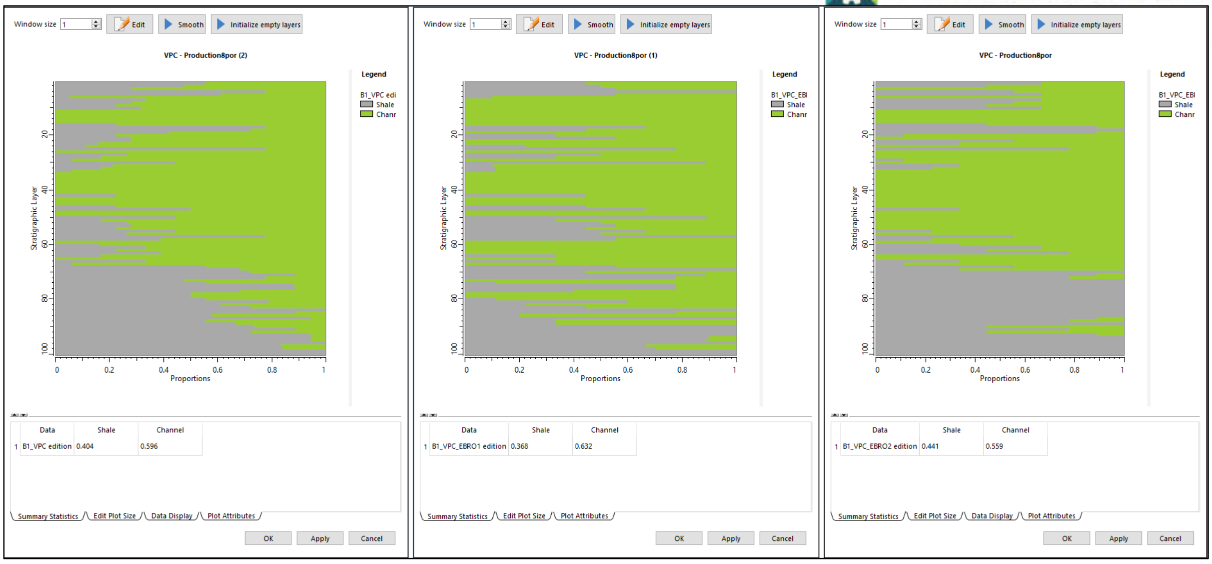

Figure 6-26: Vertical proportion curves (VPC) from well rock classification in B1 region. VPC for EBRO-1 and EBRO-2 wells (middle and right) and common VPC calculation used for the grid (left)

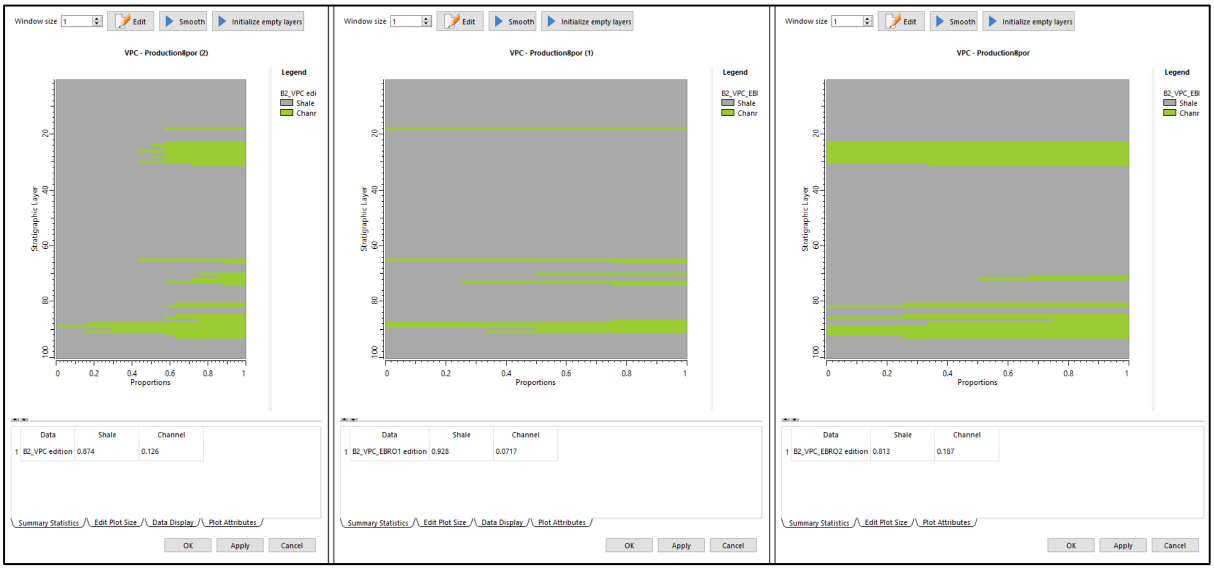

Figure 6-27: Vertical proportion curves (VPC) from well rock classification in B2 region. VPC for EBRO-1 and EBRO-2 wells (middle and right) and common VPC calculation used for the grid (left)

The PilotSTRATEGY project has received funding from the European Union's Horizon 2020 research and innovation programme under grant agreement No. 101022664

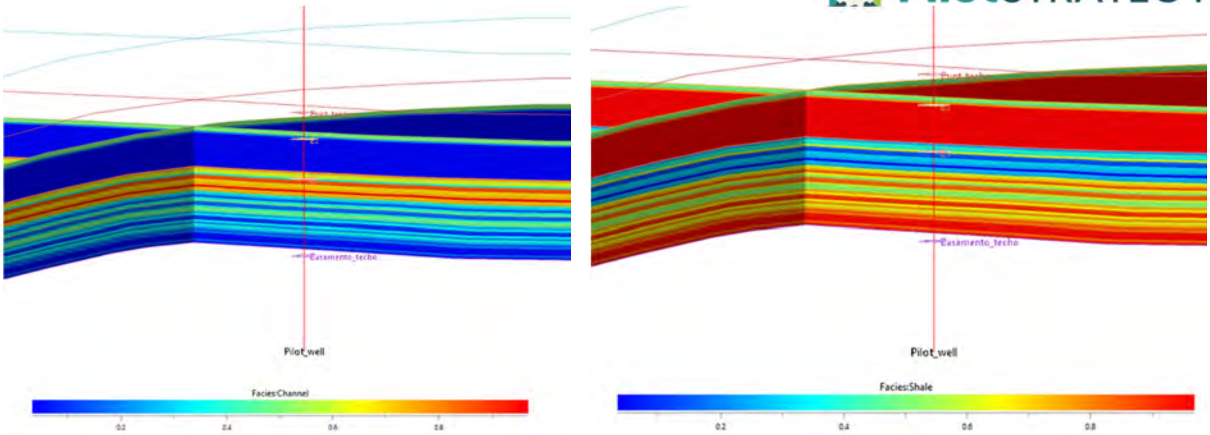

Figure 6-28: VPC transferred to the geological grid model by region. Channel facies proportion (left) and shale facies proportion (right) for the B1 member (lower part) and B2 member (upper part).

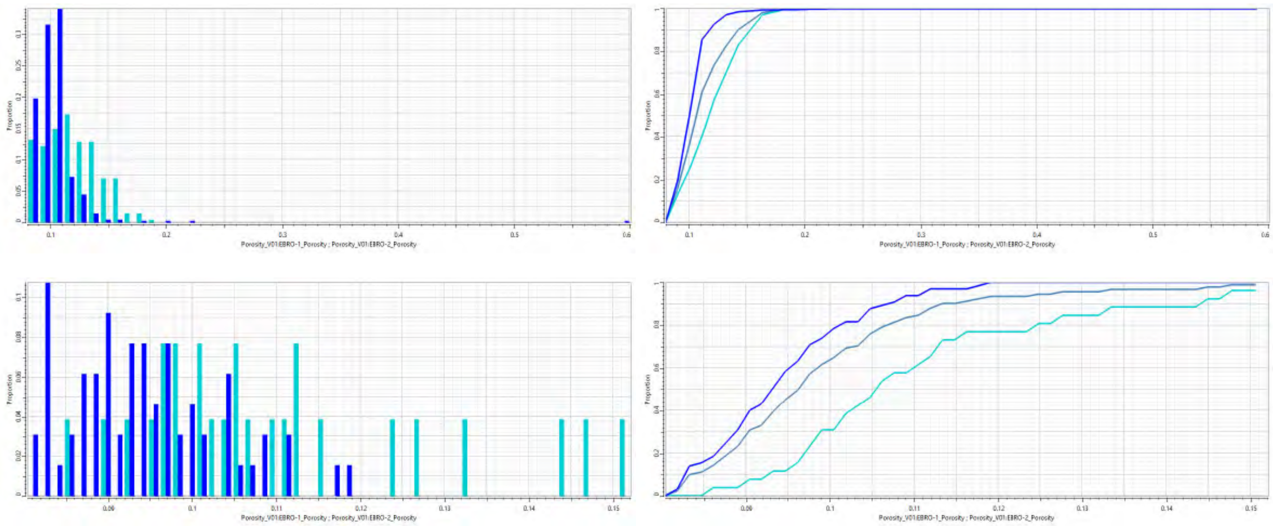

Figure 7-29: Porosity values distribution for the channel facies in EBRO-1 well (top) and EBRO-2 well (bottom).

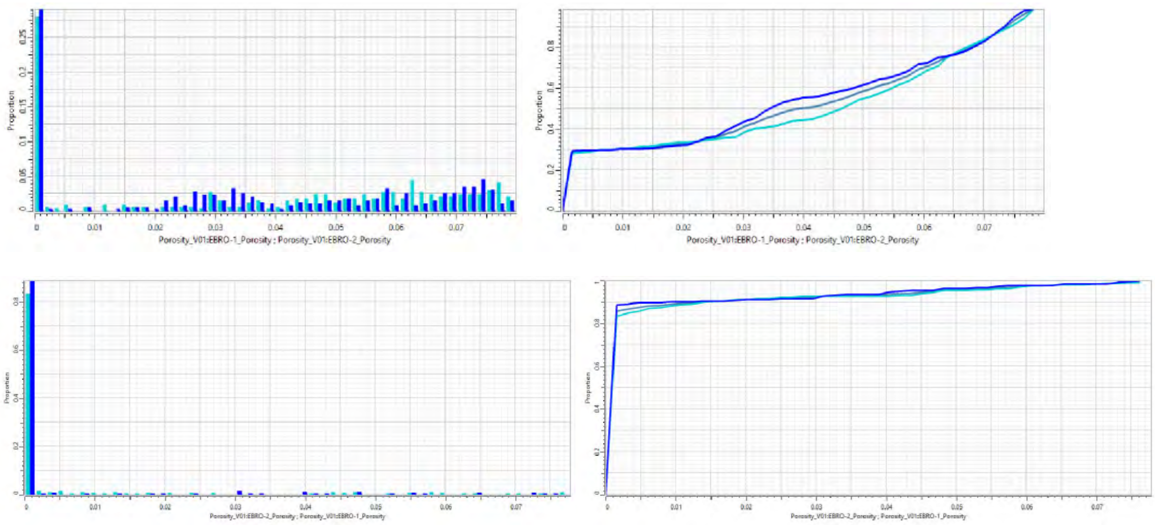

Figure 6-30: Porosity values distribution for the shale facies in EBRO-1 well (top) and EBRO-2 well (bottom).

The PilotSTRATEGY project has received funding from the European Union's Horizon 2020 research and innovation programme under grant agreement No. 101022664

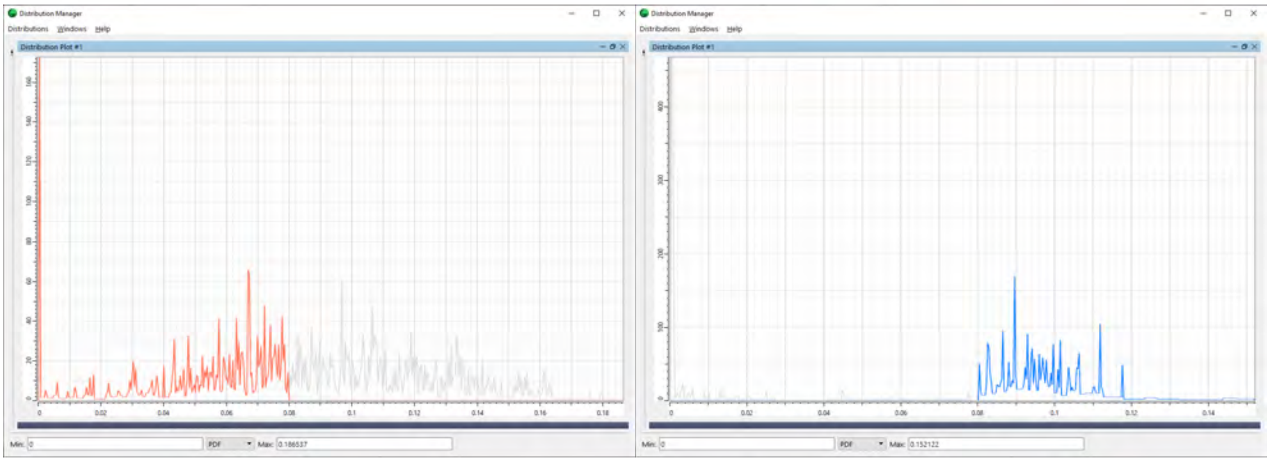

Figure 6-31: Resulting porosity distribution curves for the B1 member (left) and the B2 member (right). The curves have been split by the 8% of porosity value for distinguishing between shales and channels.

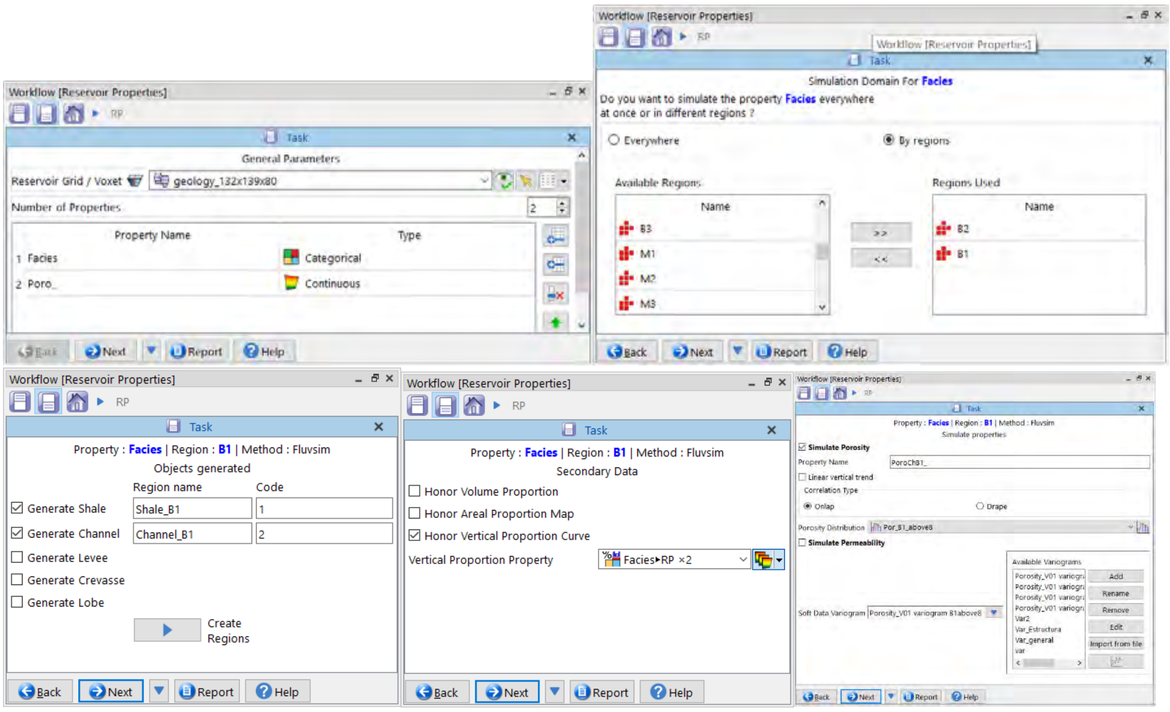

Figure 6-32: Steps followed to set up the parameters in the workflow for the channel facies. Definition of the properties and the channel subregions for each member region. For constraining the properties distribution VPC, distribution curves and variograms are provided.

The PilotSTRATEGY project has received funding from the European Union's Horizon 2020 research and innovation programme under grant agreement No. 101022664

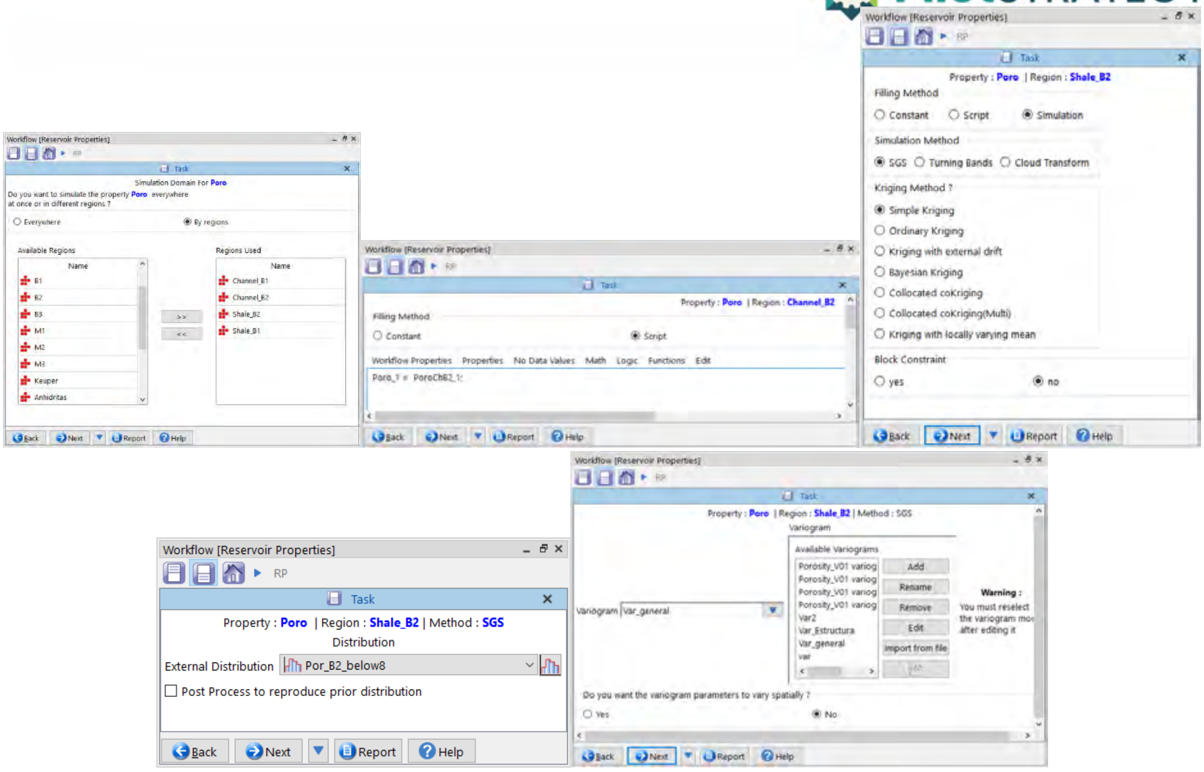

Figure 6-33: Calculation of the porosity of the channel facies and shales facies.

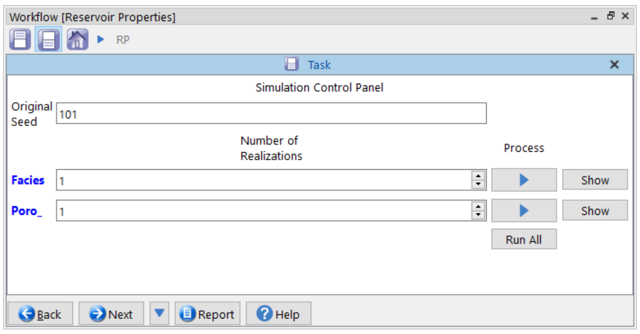

Figure 6-34: Simulation control panel ready for starting the simulations. Only one simulation will be run at a time.

The PilotSTRATEGY project has received funding from the European Union's Horizon 2020 research and innovation programme under grant agreement No. 101022664

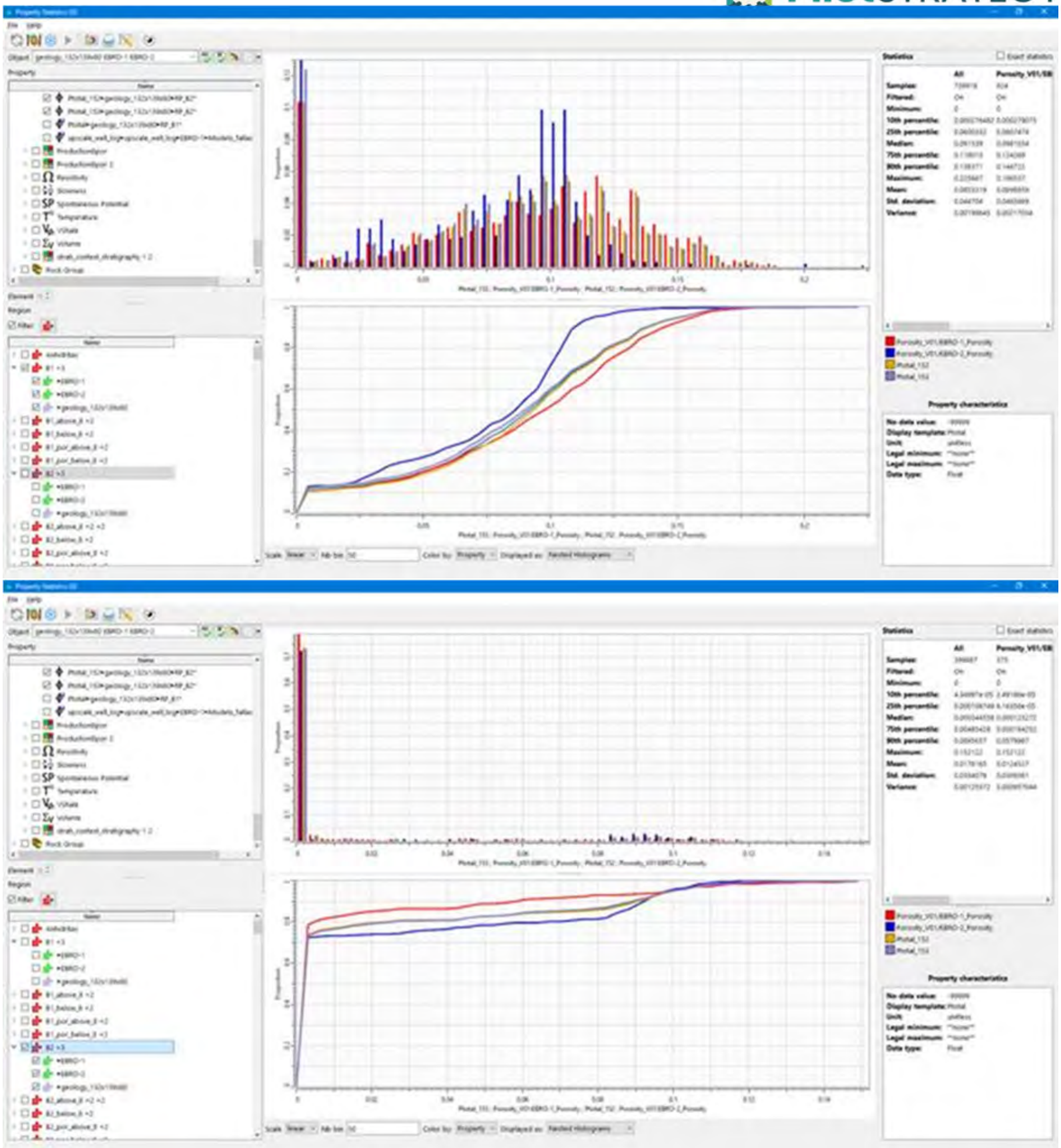

Figure 6-35: Statistical results of porosity distribution of the B1 (above) and B2 (below) members compared with the distributions in the wells, after adjusting the FLUVSIM parameters.

The PilotSTRATEGY project has received funding from the European Union's Horizon 2020 research and innovation programme under grant agreement No. 101022664

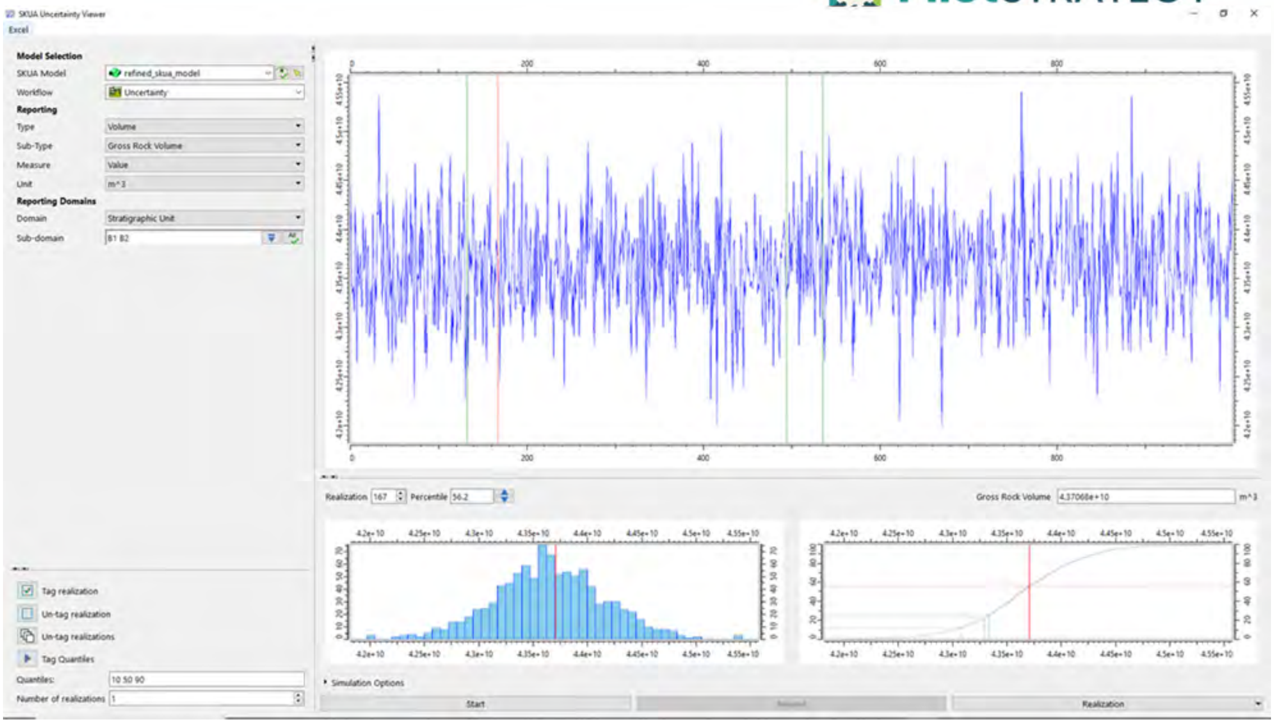

Figure 6-36: Statistical results with the change in volume of the B1 and B2 members for 1,000 realisations.

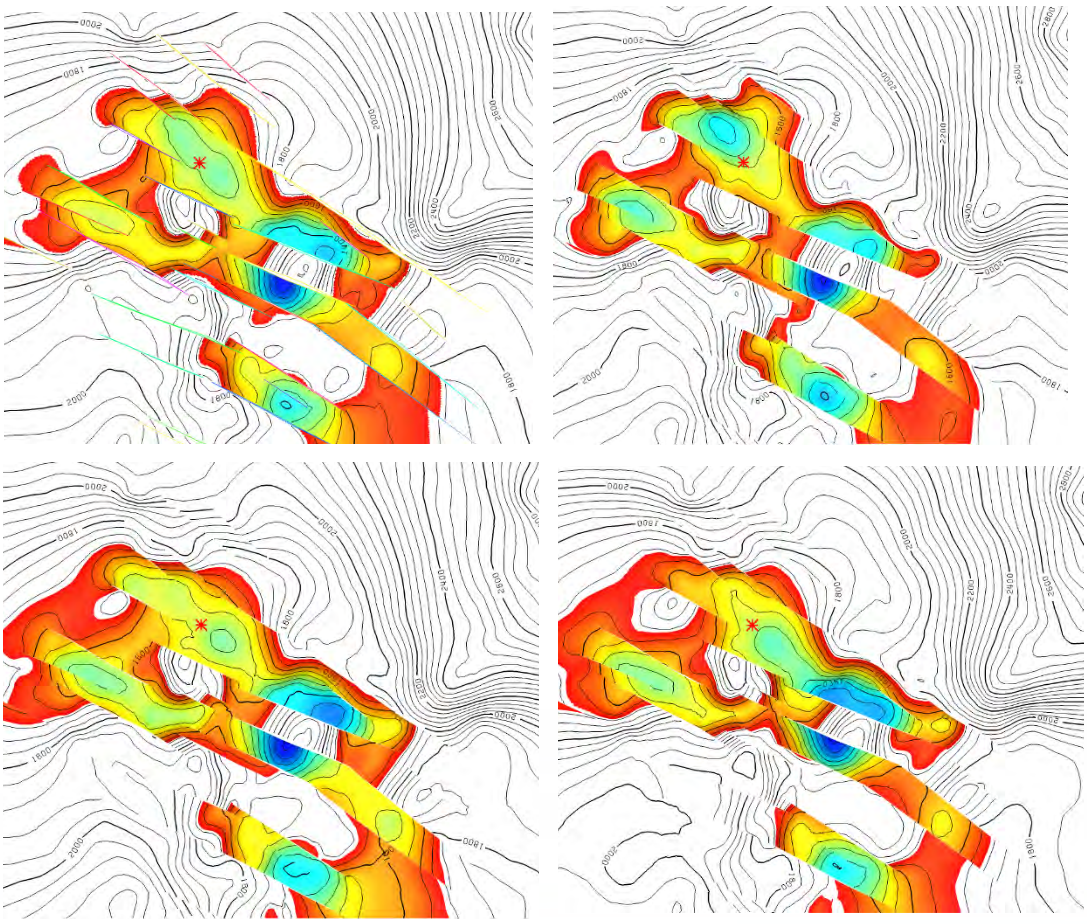

Figure 6-37: Examples of different realisations to compare the variation in the geometry of the trapping structure over the top of the Buntsandstein formation. Coloured area is the possible closure at 1,650m (red: deeper; blue: shallower). Depth datum is the sea level.

Figure 6-38: Cumulative standard deviation of the gross rock volume for 1,000 realizations for the structural uncertainty.

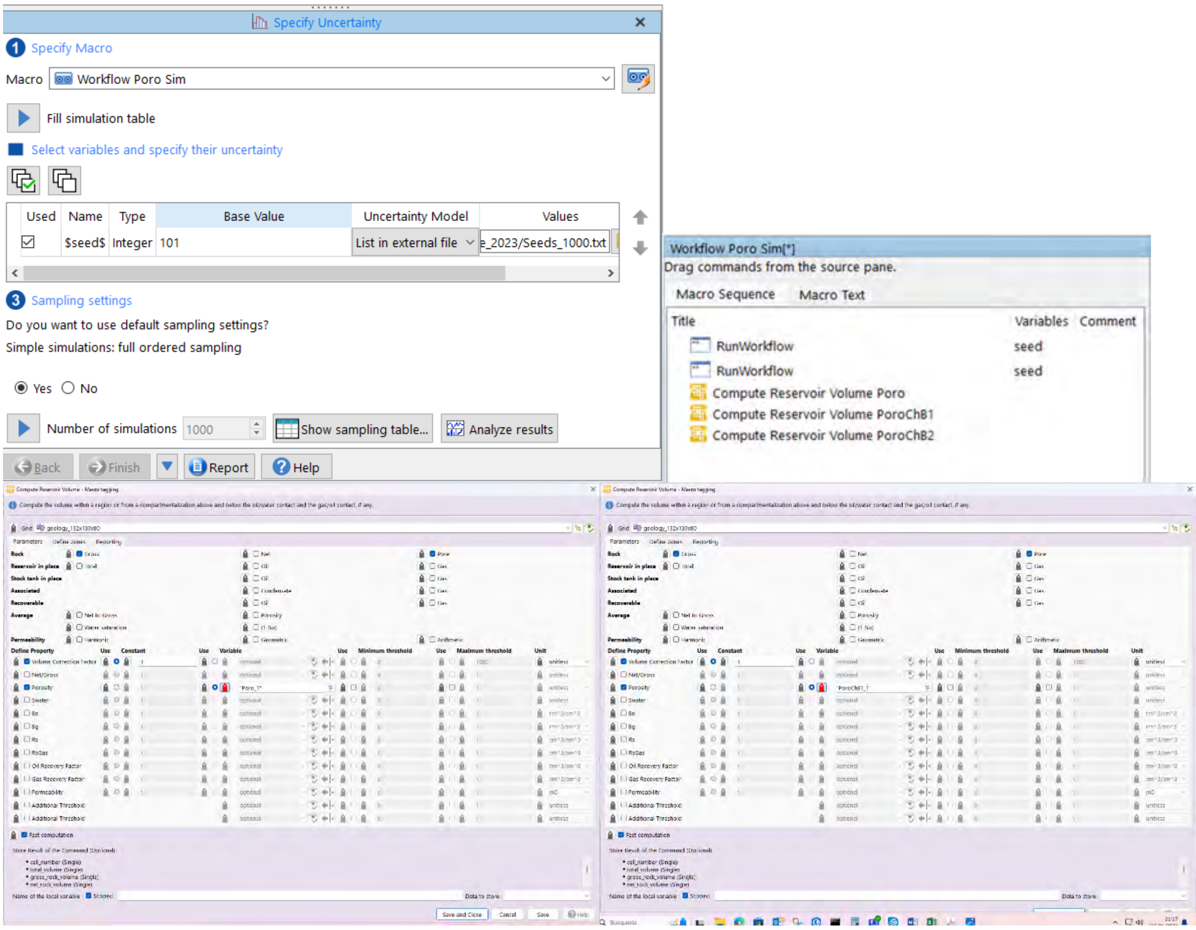

Figure 6-39: Macro created for running the Properties Workflow and computing the statistics for the porosity volume values.

The PilotSTRATEGY project has received funding from the European Union's Horizon 2020 research and innovation programme under grant agreement No. 101022664

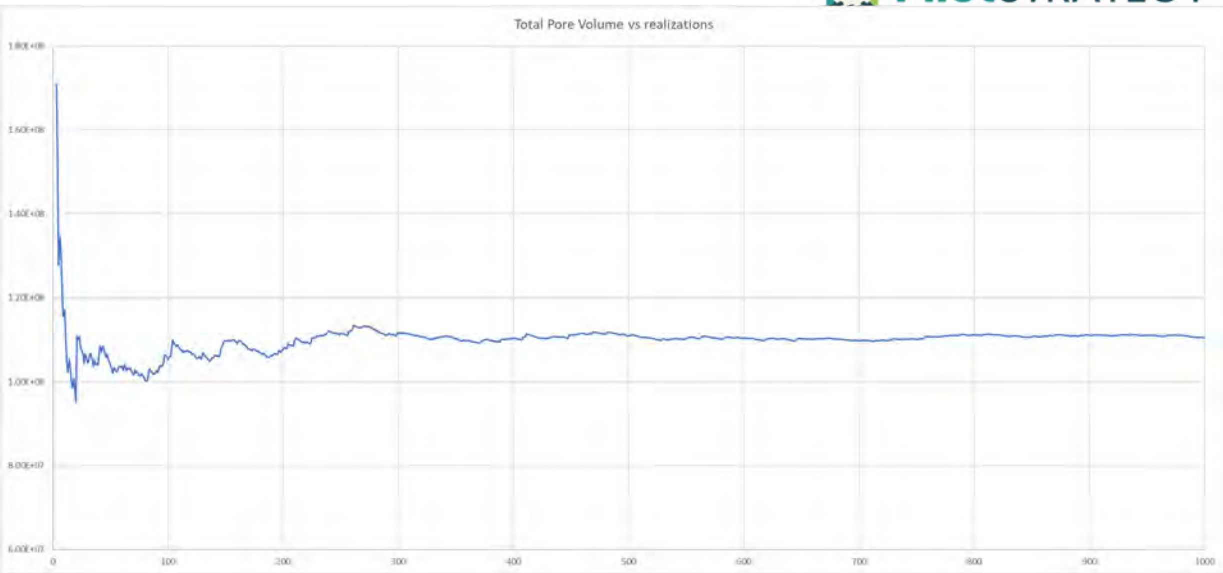

Figure 6-40: Cumulative standard deviation of total porosity volume for 1,000 realizations for the property uncertainty in B1 and B2 regions.

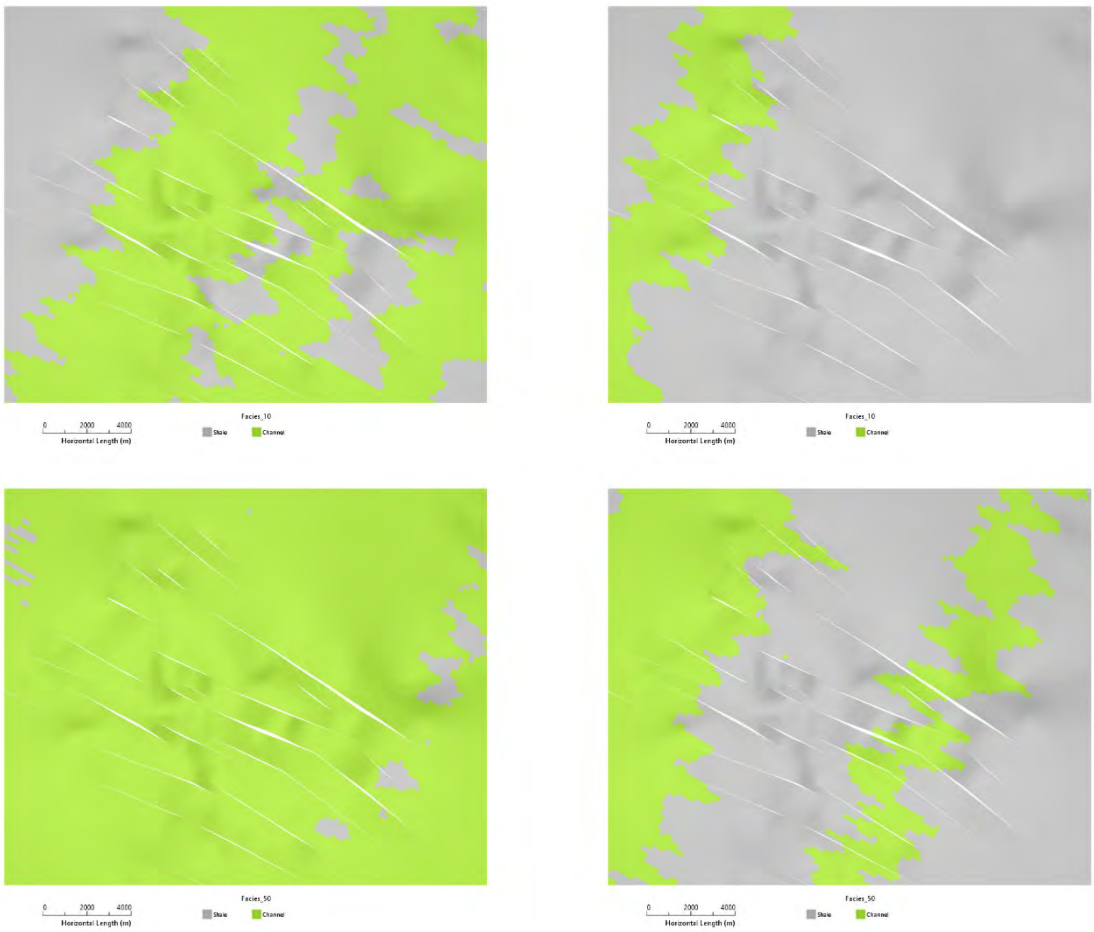

The PilotSTRATEGY project has received funding from the European Union's Horizon 2020 research and innovation programme under grant agreement No. 101022664

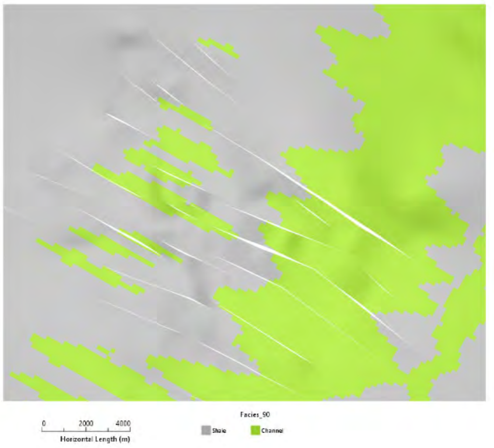

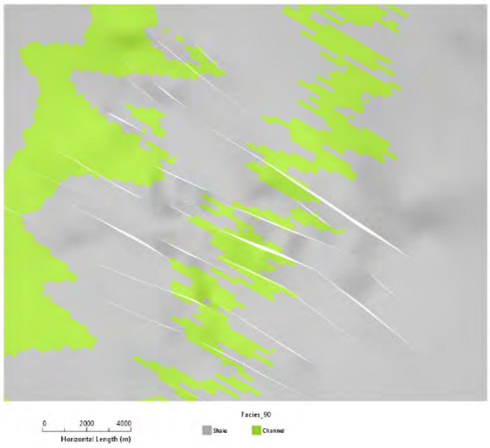

Figure 6-41: Examples of the facies distribution for the resulting model for region B1 (left) and B2 (right) and for scenarios corresponding to the percentiles P10 (top), P50 (middle) and P90 (bottom).

The PilotSTRATEGY project has received funding from the European Union's Horizon 2020 research and innovation programme under grant agreement No. 101022664